Renata Sofia Araújo da Silva

Screening of P-glycoprotein inducers and activators as effective antidotes against its toxic substrates in Caco-2 cells. The example of paraquat.

Tese do 3º Ciclo de Estudos Conducente ao grau de Doutoramento em Ciências Farmacêuticas, na especialidade de Toxicologia

PhD thesis of the 3rd Cycle of Studies in Pharmaceutical Sciences on the Specialty of Toxicology

Trabalho realizado sob a orientação de
Elaborated under supervision of

Professor Doutor Fernando Manuel Gomes Remião

Professora Doutora Helena Maria Ferreira da Costa Ferreira Carmo

Novembro 2013

I've learned....

" That everyone wants to live on top of the mountain, but all the happiness and growth occurs while you're climbing it."

William Shakespeare

Aos meus Pais

Ao Nuno

À Mariana

Por tudo.

AGRADECIMENTOS

O espaço limitado desta secção de agradecimentos, seguramente, não me permite agradecer, como devia, a todas as pessoas que, ao longo "da minha escalada" me ajudaram, direta ou indiretamente, a cumprir os meus objetivos e atingir o "cume de mais uma montanha". De facto, embora uma tese seja, pela sua finalidade académica, um trabalho individual, há contributos de natureza diversa que não podem e nem devem deixar de ser realçados. Por essa razão, desejo expressar um sentido e profundo sentimento de reconhecido agradecimento, nomeadamente:

- Ao Professor Fernando Remião, orientador desta tese, agradeço o constante estímulo e coragem para superar as adversidades inerentes à realização desta etapa, apesar de saber que a sorte não me assistia logo à primeira caminhada de cada percurso. Agradeço ainda a sua total disponibilidade, confiança e o apoio científico prestado. Acredito que as dificuldades por que passamos durante esta caminhada nos fazem valorizar e acreditar que, com esforço, é possível atingir os objetivos.

- À Professora Helena Carmo, coorientadora desta tese, agradeço o enorme apoio prestado que ultrapassou largamente a fronteira do relacionamento de cariz profissional. Obrigada pela partilha, pelas gargalhadas, pela amizade, assim como pelo apoio científico prestado em cada momento deste percurso. Muito mais do que uma orientadora…és para mim uma **AMIGA**!

- À Dr.ª Lourdes agradeço pela forma brilhante com que comanda as inúmeras expedições iniciadas no laboratório de Toxicologia. Obrigada pelo carinho e apoio científico prestado. Mais uma vez reitero a minha opinião de que a sua dedicação e postura são prova viva que à frente de grandes descobertas e acontecimentos está sempre uma "Grande Mulher"!

- À Engenheira Maria Elisa Soares, agradeço o papel de "Mãe do laboratório". A ela, do fundo do meu coração, agradeço o imenso carinho, o amor e a preocupação constante, e peço desculpa por, muitas vezes, não corresponder na mesma medida.

- Ao Dr. Félix Carvalho agradeço o incomparável entusiasmo e apoio científico prestado durante a realização deste trabalho. A forma como positiva com que encara a ciência é uma fonte de inspiração para aqueles que o rodeiam.

- À Drª Emília Sousa e à Drª Andreia Palmeira, agradeço a enorme dedicação e o importante contributo científico que permitiu aumentar a qualidade do trabalho realizado.

- À Dr.ª Paula gradeço a amizade e a disponibilidade demonstrada, e a importante contribuição para a realização deste trabalho
- À Márcia Carvalho e à Sónia, agradeço a amizade, o carinho e o importante incentivo. A dedicação que têm pela ciência e a forma positiva como a encaram são um exemplo para aqueles que a cada dia iniciam a sua caminhada.
- Ao Professor Francisco Amado, agradeço o importante contributo ciêntifico e a oportunidade de aumentar grandemente os meus conhecimento ao abrir as portas do seu laboratório e ao me tratar como um dos seus colaboradores.
- Agradeço aos elementos do Centro de espectrometria de massa da Universidade de Aveiro - Rui, Rita, Armando, Miguel, Catarina, Sofia, Ana Isabel, Renato, Cláudia, Zita - pela amizade e carinho, e pela forma familiar com que sempre me receberam e que sempre me fez sentir em casa. Agradeço ainda ao Rui pelo importante contributo ciêntífico e pela forma entusiasmante com que encara a ciência.
- À Bridge e ao Ricardo, agradeço o enorme carinho e amizade, as cantorias e coreografias, as gargalhadas e todos os bons momentos que me ajudaram a ultrapassar os dias difíceis desta caminhada. Apesar da maior distância estarão sempre no meu coração e nas minhas boas memórias.
- À Vera e ao João, agradeço o companheirismo e a amizade. A sua dedicação à ciência e o seu rigor científico são também um excelente exemplo. À Vera, agradeço ainda o enorme incentivo e as palavras de apoio que ajudaram imenso na fase final desta “escalada”.
- À Luciana, agradeço o enorme carinho e amizade, e os bons momentos por que passamos durante a sua estadia em Portugal. Apesar da distância sei que a nossa amizade se irá manter. Desculpa algumas ausências, talvez porque assombrada nos meus problemas não conseguia ver os teus. Obrigada por tudo.
- À Ana Oliveira e à Teresa Baltasar, agradeço o enorme companheirismo e amizade. De facto, a alegria ilumina a vida e os nossos bons momentos de diversão ajudaram a ultrapassar todos os maus momentos.
- Aos companheiros desta caminhada - Diana, Márcia, Juliana, Cátia, Ana Margarida, Mª João, Marcelo, Rita, Mariline, Margarida - agradeço o carinho e amizade, e as longas horas de brincadeiras... tudo é mais fácil a sorrir!!!

- Ao Daniel, agradeço do fundo do coração pela dedicação desmesurada que me prestou ao longo desta caminhada. Sem ti ao meu lado tudo teria sido muito mais difícil. Obrigada pelo carinho, pela amizade sem limites e pelo apoio incondicional. Desculpa a forma talvez um pouco invasiva com que fui descobrindo a tua beleza de ser, beleza essa que é imensurável e que teimas em manter escondida pela forma reservada com que encaras a vida. Obrigada por me fazeres ver que as verdadeiras alegrias e surpresas sabem muito melhor quando nos dão luta para alcançar! Espero que, a partir de agora, estejas ao meu lado em todas as caminhadas…e espero que juntos possamos escalar muitas montanhas!!!
- À Vânia, agradeço o enorme carinho, amizade e sentimento de entreajuda. Tudo começou com uma simples partilha de naturalidade e acabou numa enorme amizade. Obrigada pela forma contagiante e positiva com que alegras a vida daqueles que te rodeiam. De facto, agora tenho a certeza de que as pessoas entram na nossa vida por acaso, mas não é por acaso que elas permanecem! Obrigada por tudo!
- À Cristina Catarino, agradeço o enorme carinho e amizade, e o constante incentivo para ultrapassar esta difícil etapa.
- À Guida e à Marta, agradeço a enorme amizade, carinho e incentivo, e peço imensas desculpas pelas inúmeras ausências.

Ao longo deste tempo foi indispensável o apoio da família sem o qual, muito provavelmente, não teria sido possível chegar ao termo desta caminhada e manter o equilíbrio emocional indispensável para poder trabalhar. Assim:

- Aos meus pais agradeço o incomensurável incentivo recebido ao longo de todos estes anos. Agradeço pelos valores, pelos exemplos e pelo apoio incondicional na decisão de me dedicar à investigação. Sem o vosso apoio este trabalho não teria sido possível…Obrigado por tudo!
- À Mariana… sei que *"… a **infância** é um tempo de sonho e de descoberta, de interrogação e assombro".* Desculpa a falta de atenção, dedicação e de tempo para te mimar com histórias e brincadeiras. Obrigada pelo carinho, pela tua inocência de criança e pelo enorme sorriso que me ilumina sempre que chego a casa. Prometo que te vou recompensar e que sempre que quiseres agora "**a mamã conta**"**!**

- Agradeço ao Nuno, que me encorajou na decisão de encetar, prosseguir e concluir este doutoramento, e me fez saborear a verdadeira solidariedade, quando se mostrou complexo o desafio de assegurar a articulação entre a função de Mãe e de investigadora. Obrigada pelo incansável apoio e por em muitos momentos seres pai e mãe! Desculpa algumas ausências e silêncios.
- Agradeço à Liana pelo amor, carinho e incentivo, e por acreditar sempre que eu ia conseguir chegar ao fim.
- Ao João, agradeço a lufada de ar fresco e de serenidade que trouxeste àqueles que te rodeiam.

A quantidade de agradecimentos tem uma tendência a ser proporcional ao tempo do percurso. E quando este tempo se alonga, juntamente com os agradecimentos, devem vir algumas desculpas. Deste modo, termino pedindo desculpa a todos aqueles a quem eu me esqueci de agradecer.

This work was supported by the Fundação para a Ciência e Tecnologia (FCT)-project PTDC/SAU-OSM/101437/2008 - QREN initiative with EU/FEDER funded through COMPETE - Operational Programme for Competitiveness Factors. The work was also supported by FCT within the framework of Strategic Projects for Scientific Research Units of R&D (project PEst-C/EQB/LA0006/2011).

Renata Silva acknowledges FCT for her PhD grant [SFRH/BD/29559/2006].

PUBLICATIONS

Manuscripts in international peer-review journals

1. Silva R, Carmo H, Dinis-Oliveira R, Cordeiro-da-Silva A, Lima S C, Carvalho F, Bastos M L, Remião F (2010). In vitro study of P-glycoprotein induction as an antidotal pathway to prevent cytotoxicity in Caco-2 cells. *Archives of Toxicology,* 85(4):315-326.

2. Silva R, Carmo H, Vilas-Boas V, Guedes-de-Pinho P, Dinis-Oliveira R, Carvalho F, Silva I, Correia-de-Sá P, Remião F (2013). Doxorubicin decreases Paraquat accumulation and toxicity in Caco-2 cells. *Toxicology Letters*, 217(1):34-41.

Manuscripts submitted to international peer-review journals

1. Silva R, Carmo H, Vilas-Boas V, Barbosa D J, Palmeira A, Sousa E, Carvalho F, Bastos M L, Remião F (2013). Colchicine effect on P-glycoprotein expression and activity: *in silico* and *in vitro* studies. *Submitted for publication.*

2. Silva R, Carmo H, Vilas-Boas V; Barbosa D J, Monteiro M, Guedes-de-Pinho P, Bastos M L, Remião F (2013). Several transport systems contribute to the intestinal uptake of Paraquat, modulating its cytotoxic effects. *Submitted for publication.*

3. Silva R, Palmeira A, Carmo H, Barbosa D J, Gameiro M, Gomes A, A M Paiva, Sousa E, Pinto M, Bastos M L, Remião F (2013). P-glycoprotein induction in Caco-2 cells by newly synthetized thioxanthones prevents Paraquat cytotoxicity. *Submitted for publication.*

4. Silva R, Sousa E, Carmo H, Palmeira A, Barbosa D J, Gameiro M, Pinto M, Bastos M L, Remião F (2013). Induction and activation of P-glycoprotein by dihydroxylated xanthones protect against the cytotoxicity of the P-gp substrate paraquat. *Submitted for publication.*

Unsubmitted Manuscripts

1. Silva R, Carmo H, Vilas-Boas V, Barbosa D J, Bastos M L, Remião F. Hypericin protects Caco-2 cells against Paraquat toxicity through P-glycoprotein induction.

Abstracts in international peer-review journals

1. Silva R, Cordeiro-da-Silva A, Lima S A C, Carvalho F, Bastos M L, Carmo H, Remião F (2008). Effect of P-Glycoprotein inducers on its expression and activity in Caco-2 cells. Toxicology Letters, 180 (1): S116.

2. Silva R, Cordeiro-da-Silva A, Carvalho F, Bastos M L, Carmo H, Remião F (2009). P-glycoprotein induction as a cellular protection tool against xenobiotics toxicity. *Toxicology Letters*, 189 (1): S213.

3. Silva R, Carmo H, Guedes-de-Pinho P, Dinis-Oliveira R, Carvalho F, Bastos M L, Remião F (2010). The paraquat-induced toxicity is reversed with the co-exposure to doxorubicin in caco-2 cells. *Toxicology Letters*, 196 (1): S110.

4. Houdkova T, **Silva R**, Cordeiro-Da-Silva A, Carmo H, Remião F (2010). Effect of colchicine on P-glycoprotein expression and activity in Caco2 cells. *Toxicology Letters*, 196 (1): *S108-S109*.

5. Silva R, Vilas-Boas V, Carmo H, Dinis-Oliveira R J, Carvalho F, Bastos M L, Remião F (2011). P-glycoprotein induction by hypericin protects Caco-2 cells against paraquat toxicity. *Toxicology Letters*, 205 (1): S93-S94.

6. Remião F, **Silva R**, Vilas-Boas V, Barbosa D J, Palmeira A, Sousa E, Carvalho F, Bastos M L, Carmo H (2013). P-glycoprotein expression and activity are differently modulated by Colchicine in Caco-2 cells: In vitro and in silico studies. *Toxicology Letters*, 221 (1): S179-S180.

Poster Communications

1. Silva R, Cordeiro-da-Silva A, Carvalho F, Bastos M L, Carmo H, Remião F (2008). Exploring therapeutical pathways with an in vitro model of P-gp induction. *In* 1st National Meeting on Medicinal Chemistry, Porto, Portugal.

2. Silva R, Cordeiro-da-Silva A, Lima S A C, Carvalho F, Bastos M L, Carmo H, Remião F (2008). Effect of P-Glycoprotein inducers on its expression and activity in Caco-2 cells. *In* 45th Congress of European Societies of Toxicology (EUROTOX 2008), Rhodes, Greece.

3. Silva R, Cordeiro-da-Silva A, Carvalho F, Bastos M L, Carmo H, Remião F (2009). P-glycoprotein induction as a cellular protection tool against xenobiotics toxicity. *In* 46st Congress of European Societies of Toxicology (EUROTOX 2009), Dresden, Germany.

4. HoudKova T, **Silva R**, Cordeiro A, Carmo H, Remião F (2010). Effect of colchicine on p-glycoprotein expression and activity in Caco–2 cells. *In* 3rd Meeting of young researchers at UP (IJUP 2010), Porto, Portugal.

5. Silva R, Carmo H, Guedes-de-Pinho P, Dinis-Oliveira R, Carvalho F, Bastos M L, Remião F (2010). The paraquat-induced toxicity is reversed with the co-exposure to doxorubicin in caco-2 cells. *In* XII International Congress of Toxicology (IUTOX 2010), Barcelona, Spain.

6. Houdkova T, **Silva R**, Cordeiro-Da-Silva A, Carmo H, Remião F (2010). Effect of colchicine on P-glycoprotein expression and activity in Caco2 cells. *In* XII International Congress of Toxicology (IUTOX 2010), Barcelona, Spain.

7. Silva R, Vilas-Boas V, Carmo H, Dinis-Oliveira R J, Carvalho F, Bastos M L, Remião F (2011). P-glycoprotein induction by hypericin protects Caco-2 cells against paraquat toxicity. *In* 47st Congress of European Societies of Toxicology (EUROTOX 2011), Paris, France.

8. Silva R, Vitorino R, Carmo H, Vilas-Boas V, Amado F, Bastos M L, Remião F (2012). Comparative analysis of two-dimensional polyacrylamide gel electrophoresis (2-DE) and Liquid Chromatography/SDS-PAGE electrophoresis (LC/SDS-PAGE) for the separation and identification of proteins from a nuclear-enriched protein fraction. *In* Proteomics Workshop 2012, Aveiro, Portugal.

9. Remião F, **Silva R**, Vilas-Boas V, Barbosa D J, Palmeira A, Sousa E, Carvalho F, Bastos M L, Carmo H (2013). P-glycoprotein expression and activity are differently modulated by Colchicine in Caco-2 cells: *In vitro* and *in silico* studies. *In* 49st Congress of European Societies of Toxicology (EUROTOX 2013), Interlaken, Switzerland.

Oral communications in scientific meetings

1. Silva R, Cordeiro-da-Silva A, Carvalho F, Bastos M L, Carmo H, Remião F (2008). Effect of p-glycoprotein inducers on its expression and activity in caco-2 cells. *In* XXXIX Reunião Anual da Sociedade Portuguesa de Farmacologia, XXV Reunião de Farmacologia Clínica e VIII Reunião de Toxicologia, Lisboa, Portugal.

2. Silva R, Dinis-Oliveira R, Cordeiro-da-Silva A, Carvalho F, Bastos M L, Carmo H, Remião F (2009). Induction of p-glycoprotein expression by doxorubicin protects caco-2 cells against paraquat-induced toxicity. *In* XL Reunião Anual da Sociedade Portuguesa de

Farmacologia, XXVIII Reunião de Farmacologia Clínica e IX Reunião de Toxicologia, Porto, Portugal.

Oral communications by invitation

1. **Silva R**, Cordeiro-da-Silva A, Carvalho F, Bastos M L, Carmo H, Remião F (2009). P-glycoprotein induction as a cellular protection tool against xenobiotics toxicity. *In* 46st Congress of European Society of Toxicology (EUROTOX 2009), Dresden, Germany.

RESUMO

RESUMO

A glicoproteína P (P-gp) é uma bomba de efluxo dependente de ATP, codificada pelo gene *MDR1* em humanos, a qual está envolvida na resistência de células neoplásicas a múltiplos fármacos anticancerígenos, dada a capacidade que estas células apresentam de sobreexpressar esta proteína. No entanto, a P-gp encontra-se igualmente expressa em tecidos epiteliais humanos não neoplásicos, onde apresenta uma expressão celular polarizada. Considerando o seu largo espetro de substratos e a sua elevada capacidade de efluxo, a P-gp pode, assim, desempenhar um papel crucial na diminuição da absorção de xenobióticos, reduzindo a sua acumulação intracelular. De facto, este mecanismo de defesa pode ser de particular importância a nível intestinal, diminuindo significativamente a absorção intestinal de xenobióticos e, consequentemente, evitando o seu acesso aos órgãos-alvo. Deste modo, os estudos incluídos nesta tese tiveram como objetivo a pesquisa e desenvolvimento de indutores e/ou ativadores da P-gp seguros, específicos e potentes, para potencial uso como antídotos em intoxicações causadas por substratos tóxicos desta bomba de efluxo.

No presente trabalho, as células Caco-2 foram usadas como modelo *in vitro* do epitélio intestinal humano. Este modelo celular tem ampla aceitação na previsão da absorção e excreção intestinal de fármacos e apresenta uma boa correlação entre os níveis de expressão da P-gp e os níveis normalmente expressos no jejuno humano. Como modelo de substrato tóxico da P-gp foi utilizado o paraquato (PQ), um herbicida cuja toxicidade pulmonar, em ratos intoxicados, foi revertida pelo aumento dos níveis de expressão da P-gp no pulmão, após administração de um fármaco indutor da P-gp. Na presente tese, foram estudados os mecanismos de entrada do PQ nas células Caco-2, os quais parecem envolver mais do que um sistema de transporte, incluindo o sistema de captação da colina, o transportador das poliaminas e o sistema de transporte y^+ para aminoácidos básicos, sendo este um processo sensível ao sistema cálcio/calmodulina e à N-etilmaleimida. Com o propósito de desenvolver antídotos para promover o efluxo do PQ, foram utilizados indutores da P-gp, já descritos, como a doxorubicina (DOX), colchicina e hipericina (HYP), assim como compostos recentemente sintetizados, nomeadamente derivados (tio)xantónicos. Foram, assim, avaliados os seus efeitos na expressão e atividade da P-gp, bem como o seu potencial efeito na redução da citotoxicidade do PQ.

Os resultados obtidos demonstraram que as células Caco-2 são um modelo *in vitro* adequado à pesquisa de indutores da P-gp, apresentando uma rápida capacidade de resposta a um estímulo indutor, tal como demonstrado pelo aumento significativo na expressão desta proteína 6 h após a exposição à DOX. Foi igualmente possível observar, neste modelo *in vitro*, que, tal como a DOX, também a HYP aumentou significativamente tanto a expressão como a atividade da P-gp, em função da concentração e do tempo de exposição testados, resultando numa significativa proteção contra a citotoxicidade induzida pelo PQ. De realçar que a redução da citotoxicidade do PQ mediada pela DOX

foi mais pronunciada quando este indutor foi adicionado 6 h após o início da exposição ao PQ, o que foi explicado pela simultânea inibição da entrada do PQ (através da inibição do sistema de captação da colina) e pelo aumento da sua excreção (através do aumento da expressão/atividade da P-gp). Consequentemente foi observada uma redução notável na acumulação intracelular do PQ, explicando a marcada redução na sua citotoxicidade. Estes dados demonstram que a indução da P-gp é uma abordagem terapêutica valiosa em cenários de intoxicação real, em que o antídoto exerce seus efeitos protetores após o contacto do tóxico com as células-alvo.

Com a colchicina, observou-se um aumento significativo na expressão da P-gp, apesar da capacidade de efluxo se manter inalterada, o que se explica pela sua ação como inibidor competitivo da P-gp, o que foi confirmado pelos estudos realizados in *silico*. Os resultados dos estudos computacionais e biológicos obtidos para a colchicina, HYP e DOX salientam a importância da avaliação simultânea da expressão e atividade da P-gp na pesquisa de indutores, uma vez que estes parâmetros podem ser regulados de forma distinta. Na verdade, o sucesso de um indutor da P-gp contra xenobióticos tóxicos dependerá essencialmente do aumento da função da bomba, sem o qual não é possível reduzir a acumulação intracelular desses xenobióticos .

Derivados (tio)xantónicos recentemente sintetizados foram também avaliados como potenciais indutores e ativadores da P-gp, verificando-se, pela primeira vez, a capacidade destes compostos para aumentar significativamente quer a expressão quer a atividade da P-gp, e proteger as células Caco-2 contra a citotoxicidade do PQ. Estes compostos demonstraram igualmente a capacidade de aumentar a atividade da P-gp na ausência de aumento da sua expressão, um efeito compatível com um fenómeno de ativação da P-gp. Com base nestes resultados, foi proposto um mecanismo de co-transporte entre (tio)xantonas e PQ, o qual foi suportado por estudos de *docking*. Estes compostos representam, assim, uma nova fonte promissora de antídotos contra intoxicações por substratos tóxicos da P-gp, tais como o PQ. Além disso, foram desenvolvidos e validados, pela primeira vez, farmacóforos para indutores e activadores da P-gp, que podem ser de grande importância, no futuro, para prever novos ligandos, tal como tem sido descrito para substratos e inibidores. Adicionalmente foi criado um modelo de 2D QSAR para ativadores da P-gp, o qual demonstra que a carga parcial máxima de átomos de oxigénio está relacionada com a capacidade das xantonas dihidroxiladas para ativação da P-gp.

Em conclusão, nesta tese, foi demonstrado que vias antidotais eficazes podem ser alcançadas através da promoção do efluxo de xenobióticos tóxicos, tal como o PQ, resultando numa redução significativa dos seus níveis intracelulares e, consequentemente, numa significativa redução da sua toxicidade. Além disso, a redundância e/ou multiplicidade de sistemas de transporte deve ser tida em consideração para obter uma ação antidotal mais eficaz.

PALAVRAS-CHAVE: Glicoproteína P; Indução; Ativação; Células Caco-2; Paraquato.

ABSTRACT

ABSTRACT

P-glycoprotein (P-gp) is an ATP-dependent efflux pump encoded by the *MDR1* gene in humans, which is known to mediate multidrug resistance of neoplastic cells to cancer therapy. However, P-gp is also constitutively expressed in normal human epithelial tissues with a cellular polarized expression. Therefore, due to its broad substrate specificity and its great efflux capacity, P-gp can play a crucial role in limiting the absorption of harmful xenobiotics, decreasing their intracellular accumulation. In fact, such a defence mechanism can be of particular relevance at the intestinal level, by significantly reducing the intestinal absorption of the xenobiotic and, consequently, avoiding its access to the target organs. Thus, the studies included in this thesis aimed to develop and screen safe, specific and potent P-gp inducers and/or activators, which could be used as potential antidotes in intoxications elicited by toxic P-gp substrates.

In the present work, Caco-2 cells were used as an *in vitro* model of the human intestinal epithelium, considering their wide acceptance for predicting drug intestinal absorption and excretion in humans, and the good correlation between the expressed levels of the P-gp protein as compared to those of the normal jejunum. Furthermore, paraquat (PQ) was used as a model of a toxic P-gp substrate, since the pulmonary toxicity of this extremely toxic herbicide was reverted, *in vivo*, upon administration of a P-gp inducer to intoxicated rats. We observed that more than one transport system is involved in PQ uptake into Caco-2 cells, including the choline uptake system, the polyamine transporter and the y^+ basic amino acids transport system, being a Calcium/calmodulin- and N-ethylmaleimide- sensitive process. In order to induce and/or activate P-gp, described P-gp inducers, such as doxorubicin (DOX), colchicine, and hypericin (HYP), as well as newly syntethized (thio)xanthones were used, and their effects on P-gp expression and activity were assessed. Furthermore, their potential protective effects in reducing the cytotoxic effects of PQ were evaluated.

Our results demonstrated that Caco-2 cells are a suitable *in vitro* model for the screening of P-gp inducers, showing prompt responsiveness to the induction stimulus, with significant increases in P-gp expression observed as soon as 6 h after DOX exposure. Furthermore, in this *in vitro* model, we also observed that HYP, like DOX, significantly increased both P-gp expression and activity according to the concentration and time of exposure tested, resulting in a significant protection against PQ-induced cytotoxicity. Noteworthy, DOX-mediated reduction in PQ cytotoxicity was more pronounced when the inducer was added 6 h after the beginning of PQ exposure, which was attributed to a dual role in both the inhibition of PQ entrance (through the inhibition of the choline uptake system) and the increase in its excretion (through increased P-gp expression/activity). Consequently, a remarkable reduction in PQ intracellular accumulation was observed, which explains the astonishing reduction in its cytotoxicity. These data demonstrated that P-gp induction is a valuable therapeutic approach in real-

life intoxication scenarios, where the antidote exerts its protective effects well after the intoxicant contacts with the target cells.

When evaluating colchicine, a significant increase in P-gp expression occurred, while no significant change in P-gp efflux capacity was observed, which can be explained by its action as a competitive inhibitor as supported by the performed *in silico* studies. Noteworthy, both computational and biological data obtained for colchicine, HYP and DOX emphasize the importance of simultaneously evaluating P-gp expression and activity for the screening of P-gp inducers, since these features may be differentially regulated. In fact, the success of a P-gp inducer against harmful xenobiotics is dependent on the increase in the pump function, without which it is not possible to reduce the intracellular accumulation of toxic P-gp substrates.

Newly synthetized (thio)xanthonic derivatives were also screened and, for the first time, the ability of these compounds to significantly increase P-gp expression and protect Caco-2 cells against PQ cytotoxicity was reported. Furthermore, these compounds demonstrated the ability to immediately increase P-gp activity, even in the absence of increased P-gp expression, an effect compatible with a P-gp activation phenomenon. The possibility of a co-transport mechanism between (thio)xanthones and PQ was further supported by docking studies. Therefore, these compounds represent a promising new source of antidotes against intoxications by harmful P-gp substrates, such as PQ. Furthermore, for the first time, pharmacophores for P-gp inducers and activators were developed and validated, which can be of utmost importance, in the future, in predicting new ligands, as has been long made for P-gp substrates and inhibitors. Additionally, a 2D QSAR model was created for P-gp activators, which demonstrated that the maximal partial charge for oxygen atoms is related with the ability of dihydroxylated xanthones for P-gp activation.

In conclusion, in this thesis, it was demonstrated that effective antidotal pathways can be achieved by efficiently promoting the P-gp-mediated efflux of deleterious xenobiotics, such as PQ, resulting in a significant reduction in their intracellular levels and, consequently, in a significant reduction in their toxicity. Also, the redundancy and/or multiplicity of transports systems needs to be addressed for an effective antidotal action.

KEYWORDS: P-glycoprotein; Induction; Activation; Caco-2 cells; Paraquat.

TABLE OF CONTENTS

TABLE OF CONTENTS

INDEX OF FIGURES

INDEX OF FIGURES

INDEX OF TABLES

INDEX OF TABLES

ABBREVIATIONS LIST

ABBREVIATIONS LIST

2-AAF - 2-acetylaminofluorene

5′-AMP - Adenosine 5′-monophosphate

ABC - ATP-binding cassette

ABCB1 - ATP-binding cassette sub-family B member 1

ADME - Absorption, distribution, metabolism and excretion

ADP - Adenosine 5’-diphosphate

ADP_L - Loosely bound ADP

AhR - Aryl hydrocarbon receptor

ALL - Acute lymphoblastic leukaemia

AML - Acute myelogenous leukaemia

AMP-PNP - 5'-adenylyl-β,γ-imidodiphosphate

AP-1- Activator protein 1

APC - *Adenomatous polyposis coli* gene

AR - Androgen receptor

ARG - L-Arginine

ATP - Adenosine 5'-triphosphate

ATP_L - Loosely bound ATP

ATP_T - Tightly bound ATP

ATPγS - Adenosine 5′-(γ-thio)triphosphate

AUC - Area under the plasma concentration-time profile curve

BA - Bioavailability

BBB - Blood brain barrier

Bcl-2 - B-cell lymphoma 2 protein

BCRP - Breast cancer resistance protein (ABCG2)

bp - base pair

C/EBP - CCAAT-box/enhancer binding proteins

C/EBPβ - CCAAT/enhancer-binding protein beta (also called NF-IL-6)

Ca^{2+}/CaM - Calcium/calmodulin

CAAT - CAAT element

cAMP - Cyclic adenosine monophosphate

CAR - Constitutive androstane receptor

CAT - Chloramphenicol acetyltransferase

Cmax - Maximum (or peak) concentration

CML - Chronic myeloid leukemia

CNS – Central nervous system

CRE - cAMP responsive element
CREB - cAMP-response element-binding protein
CtBP1 - C-terminal-binding protein 1
CYP P450 - Cytochrome P450
Cys - Cysteine
DC - Dendritic cells
DG - 2-Deoxyglucose
DME - Drug metabolizing enzyme
DNA - Deoxyribonucleic acid
DOX - Doxorubicin
EGF - Epidermal growth factor
EGR-1 - Early growth response protein 1
EM - Electron microscopy
EMSA - Electrophoretic mobility shift assay
ERKs - Extracellular signal-regulated kinases
ERM - Ezrin/radixin/moesin protein family
ET-1 - Endothelin-1
ETP - Etoposide
ETS - ‘E twenty-six’ proteins
ETS-1 - ‘E twenty-six’ protein 1
FRET - Fluorescence resonance energy transfer
FXR - Secondary farnesoid X receptor
FZD1- Frizzled-1 Wnt receptor
GC-Box - GC-rich region
GIT - Gastrointestinal tract
GlcCer - Glucosylceramide
GR - Glucocorticoid receptor
GRE - Glucocorticoid response element
GST - Glutathione-S-transferases
GTP - Guanosine triphosphate
Gy - Gray (unit of absorbed dose according to the international system of units)
HA - Hyaluronan
HAT - Histone acetyltransferase
Hb - Hydrogen bond
HC-3 - Hemicholinium-3
HDAC - Histone deacetylase
HIF-1α - Hypoxia-inducible factor-1α

h*MDR1* - Human *MDR1* gene
HNF1α - Hepatocyte nuclear factor 1 α
hPXR - Human pregnane X receptor
HRE - Hypoxia responsive element
HRS - Hyper-radiosensitivity
HSE - Heat shock element
HSF - Heat-shock transcription factor
HSF-1 - Heat-shock transcription factor 1
Hsp - Heat shock protein
HT - Head-to-tail element
HYP - Hypericin
i.p. - Intraperitoneal
IkB - Inhibitor-κB
IKK - IκB kinase
IL - Interleukin
INR - Initiator element
invMED1 - Inverted mediator-1 element (multiple start site element downstream 1)
IRR - Induced radiation resistance
JNK - c-Jun NH2-terminal protein kinase
LDA - Linear discriminant analysis
LDFRT - Low-dose fractionated radiation therapy
LPS - Bacterial lipopolysaccharide
LSCC - Human laryngeal squamous cell carcinoma
LXR - Liver X receptor
LYS - L-Lysine
MAPK - Mitogen-activated protein kinase
MDR - Multidrug resistance
MDR1 - Multi-Drug Resistance 1 gene (ABCB1)
MED1 - multiple start site element downstream 1
MEF-1 - *MDR1* promoter-enhancing factor 1
MLR - Multiple linear regression
mRNA - Messenger RNA (ribonucleic acid)
MRP - Multidrug resistance protein (ABCC family, MRP 1-6)
MTS - Methanethiosulfonate
MTT - (4,5-dimethylthiazol-2-yl)-2,5-diphenyl tetrazolium bromide
NB - Neuroblastoma
NBD - Nucleotide binding domain

NEM - N-ethylmalemide
NF-IL-6 - Nuclear factor for IL-6 expression
NF-Y - Nuclear factor Y
NF-κB - Nuclear factor-κB
NK - Natural killer cells
NLS - NF-κB nuclear localization signal
NRs - Nuclear receptors
NSAIDs - Nonsteroidal anti-inflammatory drugs
NSCLC - Human non-small cell lung cancer cells
P/CAF - p300/CREB binding protein-associated factor
p53 - p53 tumor suppressor protein
PAF - Platelet-activating factor
PBMC - Peripheral blood mononuclear cells
PC - Phosphatidylcholine
PE - Phosphatidylethanolamine
p-ERM - Phosphorylated ERM
P-gp - P-glycoprotein
Pi - Inorganic phosphate
PI3K - Phosphoinositide-3-kinase
PIP_3 - Phosphatidylinositol 3,4,5-triphosphate
PKA - Protein kinase A
PKB - protein kinase B or Akt
PKC - Protein kinase C
PLSD - Partial least square discriminant analysis
Pol II - RNA polymerase II
PPAR - Peroxisome proliferator activated receptor
PQ - Paraquat
PR - Progesterone receptor
PUT - Putrescine
PXDLS - Pro-X-Asp-Leu-Ser motifs
PXR - Pregnane X receptor (also termed steroid xenobiotic receptor, SXR)
QSAR - Quantitative structure-activity relationship
RAR -Retinoic acid receptor
RHO 123 - Rhodamine 123
RhoA - Ras homolog gene family member A
RNA - Ribonucleic acid
ROCK - RhoA-associated coiled-coil containing kinase

ROS - Reactive oxygen species

RT-PCR - Reverse transcription polymerase chain reaction

RXR - Retinoid xenobiotic receptor

shRNAmir - Micro-adapted short hairpin RNA

SM - Sphingomyelin

SNP - Single nucleotide polymorphism

Sp1 - Specificity protein 1

Sp3 - Specificity protein 3

SRE - Serum response elemento

SRF - Serum response factor

SULTS - Sulphotransferases

SXR - Steroid xenobiotic receptor

TAP - Transporter associated with antigen processing

TCF - T cell factor elements

TCF/LEF - T-cell factor/lymphoid enhancer factor complex

TFIID - Transcription factor II D

TFP - Trifluoperazine

TGF-α - Transforming growth factor α

TM - Transmembrane

TMD - Transmembrane domains

TMHs - Transmembrane α-helices

TNF-α -Tumor necrosis factor alpha

TPA - 12-*O*-tetradecanoylphorbol-13-acetate

TR - thyroid hormone receptor

TRAIL - TNF-related apoptosis-inducing ligand

TUNEL - Terminal nucleotidyl transferase–mediated nick end labeling assay

TXs - Thioxanthones

UDPGT - UDP-glucuronosyltransferase

UV - Ultraviolet

VAL - L-Valine

VDR - Vitamin D receptor

VEGF - vascular endothelial growth factor

V_i - Orthovanadate

VLCFA - Very long chain fatty acids

WT-1 - Wilms' tumor (WT) suppressor 1

Xs - Xanthones

YB-1 - Y-box binding protein 1

Y-Box - inverted CCAAT element

ZnRD1 - Zinc ribbon domain containing protein 1

OUTLINE OF THE DISSERTATION

OUTLINE OF THE DISSERTATION

The present dissertation is divided into four main sections:

- **Part I – General Introduction on P-glycoprotein**

In this section, a review on the existing literature on P-glycoprotein is presented, in order to provide a good basis for understanding the objectives and the obtained results of the experimental studies. The general objectives are also included in this section.

- **Part II – Experimental section**

In part II, the manuscripts published or submitted for publication in the scope of this dissertation are presented. Also, a brief consideration on the experimental *in vitro* model and on the model of the toxic P-gp substrate used in the studies is also included in this section.

- **Part III – Discussion and Conclusions**

In this section, an integrated discussion of the results obtained in the scope of this dissertation is presented. The discussion of their potential relevance and their connection with existing scientific reports is also addressed here. Moreover, part III includes the main conclusions taken from the work of the present dissertation.

- **Part IV – References**

In this final part, all the literature references that were used in the introduction and discussion sections are listed.

PART I

I. GENERAL INTRODUCTION ON P-GLYCOPROTEIN

I.1. Overview of the ABC Transporters

The bioavailability of a wide variety of compounds, including endogenous substances, drugs and xenobiotics, is determined by the balance between uptake and efflux transporters that facilitate their movement across the membranes. These transporters are important to maintain the cellular homeostasis, as well as to detoxify potentially toxic substances (DeGorter et al. 2012). Among the efflux transporters, the ATP-binding cassette (ABC) transporters are the most extensively studied. The name "ABC transporters" was introduced in 1992 by Chris Higgins based on the reference to the highly conserved ATP-binding cassette, the most characteristic feature of this superfamily of proteins (Higgins 1992).

The ABC family of transport proteins represents one of the largest families of proteins in living organisms (Dean et al. 2001; Gottesman and Ambudkar 2001) and members of this family play a central role in cellular physiology. In fact, this superfamily comprises more than 100 membrane transporters/channels, which are involved in diverse functions, including the extrusion of harmful compounds, uptake of nutrients, transport of ions and peptides, and cell signalling (Chang 2003; DeGorter et al. 2012; Gottesman and Ambudkar 2001). Mutations in the ABC transporters have been linked with several human diseases, including cystic fibrosis, persistent hyperinsulinemic hypoglycemia of infancy, the Dubin-Johnson syndrome, Stargardt disease and Tangier disease (Gottesman and Ambudkar 2001).

These transporters are universally expressed across genera, ranging from bacteria and plants to mammals (Higgins 1992). In humans, 49 ABC transporters have been identified (Table 1), and classified on the basis of phylogenetic analysis into 7 subfamilies: ABCA (12 members; previously ABC1), ABCB (11 members; previously MDR/TAP), ABCC (13 members; previously MRP/CFTR), ABCD (4 members; previously ALD), ABCE (1 member; previously OABP), ABCF (3 members; previously GCN20) and ABCG (5 members; previously White) (Table 1) (Couture et al. 2006; Dean et al. 2001; Sharom 2008; Vasiliou et al. 2009).

Table 1. List of human ABC genes, chromosomal location, expression and function

Symbol	Alias	Location	Expression	Function
ABCA				
ABCA1	ABC1	9q31.1	Ubiquitous	Cholesterol efflux onto HDL
ABCA2	ABC2	9q34	Brain	Drug resistance
ABCA3	ABC3, ABCC	16p13.3	Lung	Multidrug resistance
ABCA4	ABCR	1p22	Rod photoreceptors	N-retinylidene-PE efflux

Table 1. (cont.) List of human ABC genes, chromosomal location, expression and function.

Symbol	Alias	Location	Expression	Function
ABCA5		17q24.3	Muscle, heart, testes	
ABCA6		17q24.3	Liver	Multidrug resistance
ABCA7		19p13.3	Spleen, thymus	Cholesterol efflux
ABCA8		17q24	Ovary, heart, skeletal muscle, liver	Transports certain lipophilic drugs
ABCA9		17q24.2	Heart	Might play a role in monocyte differentiation and macrophage lipid homeostasis
ABCA10		17q24	Muscle, heart	
ABCA12		2q34	Stomach	
ABCA13		7p12.3	Low in all tissues	Involved in an Inherited disorder affecting the pancreas
ABCB				
ABCB1	P-gp,PGY1, MDR1	7q21.12	Liver, kidney, intestine, brain, testis, adrenal gland, uterus, ovary, placenta, pancreas	Multidrug resistance
ABCB2	TAP1	6p21.3	All cells	Peptide transport
ABCB3	TAP2	6p21.3	All cells	Peptide transport
ABCB4	PGY3, MDR2/3	7q21.1	Liver	PC transport
ABCB5		7p21.1	Ubiquitous	Melanogenesis
ABCB6	MTABC3	2q36	Mitochondria	Iron transport
ABCB7	ABC7	Xq13.3	Mitochondria	Fe/S cluster transport
ABCB8	MABC1	7q36	Mitochondria	Intracellular peptide trafficking across membranes
ABCB9		12q24	Heart, brain	
ABCB10	MTABC2	1q42.13	Mitochondria	Export of peptides derived from proteolysis of inner-membrane proteins
ABCB11	SPGP	2q24	Liver , intestine	Bile salt transport
ABCC				
ABCC1	MRP1	16p13.1	Lung, PBMC, intestine, brain, kidney, testis	Drug resistance
ABCC2	MRP2	10q24	Liver, intestine, kidney	Organic anion efflux
ABCC3	MRP3	17q22	Lung, intestine, liver, kidney, pancreas, placenta,	Drug resistance
ABCC4	MRP4	13q32	Prostate, lung, adrenal gland, ovary, testis	Nucleoside transport
ABCC5	MRP5	3q27	Skeletal muscle, heart, brain	Nucleoside transport
ABCC6	MRP6	16p13.1	Kidney, liver	
CFTR	ABCC7	7q31.2	Exocrine tissues	Chloride ion channel
ABCC8	SUR1	11p15.1	Pancreas	Sulfonylurea receptor
ABCC9	SUR2	12p12.1	Heart, muscle	Encodes the regulatory SUR2A subunit of the cardiac K^+(ATP) channel
ABCC10	MRP7	6p21.1	Heart, skeletal, muscle, spleen, liver	Multidrug resistance
ABCC11	MRP8	16q12.1	Breast, testis	Drug resistance in breast cancer
ABCC12	MRP9	16q12.1	Breast, testis, brain, ovary, skeletal muscle	Multidrug resistance

Table 1. (cont.) List of human ABC genes, chromosomal location, expression and function.

Symbol	Alias	Location	Expression	Function
ABCC13		21q11.2	Fetal liver, bone marrow	
ABCD				
ABCD1	ALD	Xq28	Peroxisomes	VLCFA transport
ABCD2	ALDL1, ALDR	12q12	Peroxisomes	Major modifier locus for clinical diversity in X-linked ALD (X-ALD)
ABCD3	PXMP1, PMP70	1p21.3	Peroxisomes	Involved in import of fatty acids and/or fatty acyl-coenzyme A into the peroxisome
ABCD4	PMP69, P70R	14q24.3	Peroxisomes	May modify the ALD phenotype
ABCE				
ABCE1	OABP, RNS4I	4q31	Ovary, testes, spleen	Oligoadenylate binding protein
ABCF				
ABCF1	ABC50	6p21.33	Ubiquitous	Involved in susceptibility to autoimmune pancreatitis
ABCF2		7q36	Ubiquitous	Tumour suppression at metastatic sites and in endocrine pathway for breast cancer/drug resistance
ABCF3		3q27.1	Ubiquitous	
ABCG				
ABCG1	ABC8, White	21q22.3	Ubiquitous	Cholesterol transport
ABCG2	ABCP, MXR, BCRP	4q22	Placenta, brain, intestine	Toxin efflux, drug resistance
ABCG4	White2	11q23.3	Liver, spleen, eye, brain and macrophage	
ABCG5	White3	2p21	Liver, intestine	Sterol transport
ABCG8		2p21	Liver, intestine	Sterol transport

ALD, adrenoleukodystrophy; ATP, adenosine triphosphate; CFTR, cysticfibrosis transmembrane conductance regulator gene; HDL, high density lipoprotein; PBMC, peripheral blood mononuclear cells; PC, Phosphatidylcholine; PE, phosphatidylethanolamine; PIN, prostatic intraepithelial neoplasia; VLCFA, very long chain fatty acids [adapted from (Couture et al. 2006; Dean et al. 2001; Vasiliou et al. 2009)].

The ABC-transporters use energy from ATP hydrolysis to move their substrates across biological membranes (plasma membrane, as well as intracellular membranes of the endoplasmic reticulum, peroxisome, and mitochondria) and against their concentration gradients, thereby limiting the cellular accumulation of their substrates (Borst and Elferink 2002; Chang 2003; DeGorter et al. 2012). Moreover, they are characterized by the presence of a highly conserved ATP-binding motif (DeGorter et al. 2012). ABC transporters typically contain a pair of ATP-binding domains, also known as nucleotide binding domains (NBD), and two sets of transmembrane domains (TMD), normally containing six membrane-spanning α-helices. The NBD contain three conserved domains: Walker A and B domains, found in all ATP-binding proteins, and a signature C motif (LSGGQ signature C), located upstream of the Walker B site (Hyde et al. 1990). The C domain is specific to ABC transporters and distinguishes them from other ATP-binding

proteins. The prototype ABC protein contains, as mentioned, two NBD and two TMD, with the NBDs located in the cytoplasm, and this topology will be discussed in detail in section I.3. These proteins pump substrates in a single direction, typically out of the cytoplasm. For hydrophobic compounds, this movement is often from the inner leaf of the phospholipid membrane bilayer to the outer layer or to an acceptor molecule (Dean et al. 2001).

The previously described typical topology of an ABC transporter is not applicable to all members. Indeed, ABC genes are organized into either full transporters, containing (at least) two TMD and two NBD, or half transporters, containing one of each domain. The half transporters assemble as either homodimers or heterodimers to create a functional transporter (Hyde et al. 1990). BCRP is a half-transporter containing 6 transmembrane regions and 1 NBD; P-gp, MRP4, MRP5, MRP8, and MRP9 proteins contain 12 transmembrane regions, split into two halves forming TMDs, each with a NBD (prototype ABC proteins); MRP1,MRP2, MRP3, MRP6, and MRP7 have an extra TMD towards the N-terminus comprising 5 extra transmembrane regions (Couture et al. 2006).

The genes that encode ABC genes are widely dispersed in the genome and show a high degree of amino acid sequence identity among eukaryotes (Dean et al. 2001). Members of this large superfamily important in drug efficacy and toxicity, include P-glycoprotein (MDR1/ABCB1; P-gp), breast cancer resistance protein (BCRP/ABCG2), and transporters of the multidrug resistance-associated protein (MRP/ABCC) family (DeGorter et al. 2012). From the previously referred transporters, the present thesis will focus on P-gp.

I.2. P-glycoprotein tissue distribution and physiological role

I.2.1. P-gp tissue distribution and main physiological role

P-glycoprotein is a member of the ABCB [multidrug resistance (MDR)/(TAP)] subfamily of transporters. The ABCB subfamily is composed of four full transporters and seven half transporters, being the only human subfamily having both types of transporters (Dean et al. 2001).

P-gp exists in a number of different isoforms, which have more than 70% sequence homology and are encoded by a small family of closely related genes. In humans, P-gp is encoded by two MDR genes, *MDR1/ABCB1* and *MDR3*/*ABCB*4 (also designated *MDR2*), which arose from a duplication event, and are located, adjacent to each, on the long arm of chromosome 7 (7q21) (Callen et al. 1987; Chin et al. 1989). The MDR phenotype is associated with the MDR1 isoform (Hennessy and Spiers 2007). Additionally, the human MDR3 isoform functions as a phosphatidylcholine (PC) translocase, or “flippase”,

exporting this phospholipid into the bile (Ruetz and Gros 1994). However, under certain conditions, the human MDR3 demonstrated to transport some MDR1 substrates, albeit inefficiently (Smith et al. 2000). Therefore, since the drug transporting isoform shares 78% amino acid sequence identity with the PC-exporting isoform, it has been suggested that they may share similar structures and mechanisms of action (Sharom 2007). In rodents, P-gp is encoded by three genes: *Abcb1a/Mdr1a/mdr3* and *Abcb1b/Mdr1b/mdr*1, which encode drug transporters, and *mdr2/Abcb4*, that encode for a protein that carries out PC export into the bile (Sharom 2007). In the following sections of this dissertation, the term P-gp will be used to indicate the *ABCB1* gene product (or *abcb1a*/*abcb1b* gene products in studies performed in rodents).

P-gp, expressed as a result of the transcription of the *ABCB1*/*MDR1* gene, is the most extensively studied mammalian ABC transporter and is often regarded as the prototype for understanding their biochemical mechanisms (Gottesman et al. 2002; Gottesman et al. 1996; Sharom 2011; Zhou 2008). Moreover, P-gp was the first ABC transporter to be cloned and, as already mentioned, is the best characterized protein of the ABC transporter superfamily due in part to its significant role in conferring a MDR phenotype to cancer cells that develop intrinsic or acquired cross-resistance to diverse chemotherapeutic agents, resulting in the failure of chemotherapy for many cancers (Ambudkar et al., 1999). In fact, this efflux pump was firstly isolated from colchicine-resistant Chinese hamster ovary cells, where it modulated drug permeability by reducing their apparent cellular permeability (Juliano and Ling 1976) and, therefore associated with this resistance phenotype.

The expression of this efflux pump was afterwards identified in normal tissues (Thiebaut et al. 1987), as well as in many cultured cells of mammalian and human origin, including 39 of 60 tumour cell lines used by the U.S. National Cancer Institute in the discovery of new anti-cancer drugs (Alvarez et al. 1995). Although P-gp was found expressed in most human (Thiebaut et al. 1987) and rodent tissues (Croop et al. 1989) at low levels, it was found at much higher levels at the apical surface of epithelial cells of the large and small intestine, liver bile ductules and kidney proximal tubules (Figure 1) (Chin et al. 1989; Fojo et al. 1987; Thiebaut et al. 1987). Therefore, having all these organs excretory roles, it suggests that the pump may have a physiological role in the elimination of xenobiotics or some endogenous metabolites. P-gp was also found in the pancreatic ductules, adrenal gland, placenta, testis (blood testis barrier) and in the apical membrane of endothelial cells lining the capillaries of the brain (Chin et al. 1989; Cordon-Cardo et al. 1990; Cordon-Cardo et al. 1989; Fojo et al. 1987; Schinkel 1999; Thiebaut et al. 1987). These lastly mentioned endothelial cells form a continuous monolayer, the so-called blood-brain barrier (BBB), which prevents blood components from crossing into the central

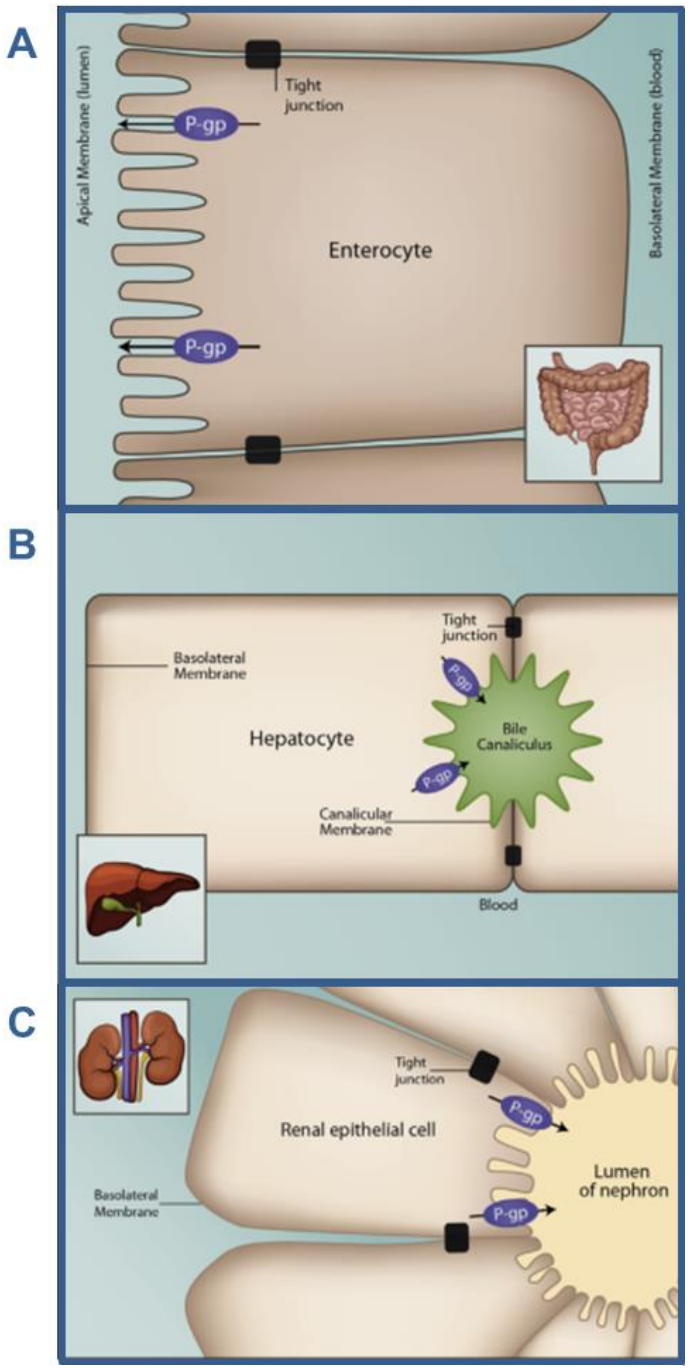

Figure 1. P-gp cellular localization in the intestine, liver and kidney.

P-gp is found on the apical/luminal membrane of intestinal epithelial cells (A), the canalicular membrane of human hepatocytes (B), and the apical/luminal membrane of renal proximal tubule cells (C) [taken from (Wessler et al. 2013)].

nervous system. P-gp was found oriented in these cells to transport substrates towards the blood, constituting a major factor in limiting their entry into the brain, thus protecting against the noxious effects of P-gp substrates (Schinkel 1999; Schinkel et al. 1994; Schinkel et al. 1996; Schinkel et al. 1995). P-gp has also been found to play a role in the blood-inner ear barrier, where it was found expressed in the capillary endothelial cells of the cochlea and vestibule (Saito et al. 1997). Accordingly, the main role of P-gp in the blood-brain and blood-tissue barriers is likely the protection of these organs from toxic compounds that gain entry into the circulatory system. Additionally, high levels of P-gp expression were identified at the luminal surface of secretory epithelial cells in the pregnant endometrium (Arceci et al. 1988), as well as in the placenta (Gil et al. 2005), where it appears to play a central role in protecting the fetus from the toxicity of a variety of endogenous and exogenous molecules (Kalabis et al. 2005). Interestingly, besides being expressed in a stage-specific manner in the placenta, P-gp has also restricted expression in the developing embryo (MacFarland et al. 1994; van Kalken et al. 1992). P-gp present in the apical border of fetus-derived epithelial cells facing the maternal circulation is optimally oriented to protect the fetus against incoming amphipathic toxins (Lankas et al. 1998).

Additionally, this efflux protein was also found on the surface of hematopoietic cells, albeit its function remains enigmatic (Eckford and Sharom 2009). However, it was demonstrated, *in vivo,* that its presence in hematopoietic progenitor cells of the bone

marrow protects these vital cells from toxic drugs during chemotherapy (van Tellingen et al. 2003).

Altogether, the P-gp tissue localizations suggests that the protein plays a physiological role in the protection of susceptible organs like the brain, testis and inner ear from toxic xenobiotics, in the secretion of metabolites and xenobiotics into bile, urine, and the lumen of the gastrointestinal tract, and possibly in the transport of hormones from the adrenal gland and the uterine epithelium. In fact, this physiological role has been strongly supported by studies with transgenic knockout mice lacking one or both of the genes encoding the drug-transporting P-gps, *Abcb1a* and *Abcb1b* (Schinkel et al. 1994). Both the single and double knockout mice demonstrated a normal lifespan and appeared healthy, were fertile, viable, and phenotypically indistinguishable from wild-type mice under normal conditions (Schinkel et al. 1994). However, P-gp knockout mice showed radical changes in the susceptibility to many drugs. Specifically, when P-gp substrates were administered, the drugs were accumulated at very high levels in the brain, when compared with wild-type mice, resulting in neurotoxicity (Schinkel et al. 1994). For example, *Abcb1a* knockout mice displayed a disrupted blood-brain barrier and an increased sensitivity to the centrally neurotoxic pesticide ivermectin (100-fold) and to the carcinostatic drug vinblastine (3-fold) (Schinkel et al. 1994). Thus, this P-gp isoform appears to play the major role in preventing accumulation of drugs in the brain (Jette et al. 1995; Schinkel et al. 1994). Moreover, the double-knockout mouse also proved to be a valuable tool for the evaluation of P-gp-mediated transport of drugs that are targeted to the central nervous system (Doran et al. 2005).

Finally, in what concerns to the ABCB4 protein, it is expressed at high levels on the bile canalicular membrane of hepatocytes, in accordance with its proposed role in transport of PC into the bile (Smit et al. 1994; Smith et al. 1994).

I.2.2. Other proposed roles of P-glycoprotein in cell physiology

Apart from its important role in the cellular protection against harmful xenobiotics, *in vivo*, P-gp functions may also include the transport of endogenous molecules and metabolites (Eckford and Sharom 2009). In fact, possible endogenous substrates include phospholipids and glycolipids, platelet-activating factors (PAF), β-amyloid peptides, small cytokines, such as interleukins, and steroid hormones, such as aldosterone and β-estradiol-17β-D-glucuronide (Eckford and Sharom 2009; Sharom 2011). However, the information on the extent of P-gp-mediated transport of these endogenous molecules *in vivo* is scarce (Sharom 2011). Noteworthy, a putative P-gp role in hormone/cytokine transport could explain its expression in tissues such as the adrenal gland, hematopoietic cells, and lymphocytes (Eckford and Sharom 2009). Daleke et al. described that P-gp is

capable of transporting a wide variety of lipids, including NBD [(7-nitro-2,1,3-benzoxadiazol-4-yl)-aminododecanoyl] glycerol PL (a NBD-phospholipid), sphingolipids and PAF (Daleke 2007). P-gp is also able to translocate fluorescent derivatives of simple glycosphingolipids such as glucosylceramide (Eckford and Sharom 2005; Lala et al. 2000). Therefore, the pump present in the Golgi apparatus may have a relevant role in flipping glucosylceramide from the cytoplasmic leaflet into the luminal leaflet, which is required during the biosynthesis of more complex glycosphingolipids (Lala et al. 2000). However, although P-gp can act as a phospholipid flippase (see section I.4.2.1), it is unlikely that this is its primary *in vivo* function, since the rate of flipping is relatively low (Romsicki and Sharom 2001).

As previously referred, P-gp is also expressed in the adrenal gland, on hematopoietic stem cells, natural killer (NK) cells, antigen-presenting dendritic cells (DC), and T and B lymphocytes (Klimecki et al. 1994; Randolph et al. 1998). Although the mdr1a/1b knockout mice displayed a seemingly complete immune-cell repertoire (Schinkel et al. 1997), the capacity of these mice to produce an efficient immune response against pathogens or tumours, and their relative susceptibility to autoimmunity, is not yet fully understood (Johnstone et al. 2000). Therefore, although P-gp expression on blood-tissue barriers and on epithelial cells of the gastrointestinal or urinary system is consistent with a drug-removal role, the selective expression on adrenal and hematopoietic cells led some researchers to propose additional functions for P-gp.

In fact, several review articles reported additional P-gp roles in cell physiology, and among these proposed P-gp functions are its roles in immunology and apoptosis. Johnstone et al. (2000) summarized various P-gp physiological functions, such as the translocation of cytokines by P-gp in hemotopoietic stem cells, the inhibition of apoptosis by P-gp-mediated translocation of sphingomyelin, its involvement in cholesterol metabolism and phospholipid translocation, and its role as volume activated chloride channel regulator (Johnstone et al. 2000). It was also described that P-gp might play a fundamental role in regulating cell differentiation, proliferation and survival (Johnstone et al. 2000). Effects of functional P-gp on chloride channel activity, phospholipid transport and cholesterol esterification are summarized in Table 2 (Johnstone et al. 2000).

Additionally, van Meer (2005), in a study of cellular lipidomics showed the vital role of lipids in cell signalling, and also reviewed ABC lipid transporters as extruders, flippases, or flopless activators (van Meer 2005). Moreover, it was shown that the lipid composition of normal cell organelles, membranes, locations of lipid synthesis and lipid rafts is related with the translocation of lipids by P-gp (van Meer 2005). It was proposed that if a lipid originates from the cytosolic membrane surface, this represents lipid flop and is probably a side activity of transporters (van Meer et al. 2006).

Table 2. Proposed roles for P-gp in cell physiology.

Proposed function	Cells[1]	Inhibitors	Conclusions
Volume activated chloride channel regulator	● *MDR1* transfected cells: NIH3T3 cells (Bond et al. 1998; Gill et al. 1992; Hardy et al. 1995; Valverde et al. 1992), S1 cells (Valverde et al. 1992), HeLa cells (Hardy et al. 1995), CHO cells (Bond et al. 1998), BALB/c-3T3 cells (Vanoye et al. 1999). ● MDR1–MM transfected[2]: S1 cells (Gill et al. 1992). ● MDR1-8A, MDR1-8E transfected[3]: HeLa cells (Hardy et al. 1995). ● MDR1-3SA transfected: BALB/c-3T3 cells (Vanoye et al. 1999). ● mdr1a transfected: CHO cells (Bond et al. 1998; Valverde et al. 1996). ● mdr1b transfected: CHO cells (Bond et al. 1998; Valverde et al. 1996).	Forskolin (Valverde et al. 1992), verapamil (Valverde et al. 1992), dideoxyforskolin (Bond et al. 1998; Valverde et al. 1992), quinine (Valverde et al. 1992), antisense oligonucleotides (Valverde et al. 1992), doxorubicin (Gill et al. 1992), vincristine (Gill et al. 1992), TPA (Bond et al. 1998; Hardy et al. 1995), PKC (Bond et al. 1998; Hardy et al. 1995; Vanoye et al. 1999), tamoxifen (Valverde et al. 1996).	● MDR1 transfected-cells (Bond et al. 1998; Gill et al. 1992; Hardy et al. 1995; Valverde et al. 1992; Vanoye et al. 1999) and mdr1a (Bond et al. 1998; Valverde et al. 1996) P-gp can regulate the activity of volume-activated chloride channels. ● mdr1b P-gp does not regulate chloride channel activity (Bond et al. 1998; Valverde et al. 1996). ● Chloride channel regulation is inhibited by phosphorylation of P-gp by PKC (Bond et al. 1998; Hardy et al. 1995; Vanoye et al. 1999).
Phospholipid translocase	● *mdr1a* transfected: yeast (Ruetz and Gros 1994), LLC-PK1 cells (van Helvoort et al. 1996) ● mdr1b transfected yeast (Ruetz and Gros 1994) ● mdr2 transfected yeast (Ruetz and Gros 1994) ● MDR1 transfected LLC-PK1 cells (van Helvoort et al. 1996) ● MDR3 transfected LLC-PK1 cells (van Helvoort et al. 1996) ● CEM/VBL300 cells (Bosch et al. 1997)	Vanadate (Ruetz and Gros 1994), verapamil (Ruetz and Gros 1994; van Helvoort et al. 1996), PSC833 (Bosch et al. 1997), UIC2 antibody (Bosch et al. 1997), cyclosporin A (Sugawara et al. 2005)	● mdr1a and mdr1b P-gp do not translocate lipids (Ruetz and Gros 1994) ● mdr2 P-gp can function as a PC translocase (Ruetz and Gros 1994) ● mdr2 P-gp flippase activity is ATP-dependent (Ruetz and Gros 1994) ● MDR3 P-gp can function as a PC translocase (van Helvoort et al. 1996) ● MDR3 P-gp flippase activity is ATP-dependent (van Helvoort et al. 1996) ● MDR1 (Bosch et al. 1997; van Helvoort et al. 1996) and mdr1a (van Helvoort et al. 1996) P-gp can translocate a range of short chain phospholipid analogs

Table 2. (cont.) Proposed roles for P-gp in cell physiology.

Proposed function	Cells[1]	Inhibitors	Conclusions
Cholesterol metabolism	● CHO, HeLa, Caco-2 and HepG2 cells (Debry et al. 1997); 8226/DOX6 cells (Luker et al. 1999) ● MDR1 transfected NIH3T3 cells (Luker et al. 1999)	Steroid hormones (Debry et al. 1997; Luker et al. 1999), verapamil (Debry et al. 1997; Luker et al. 1999), PSC833 (Debry et al. 1997)	● MDR inhibitors block esterification of plasma membrane cholesterol (Debry et al. 1997; Luker et al. 1999) ● Expression of MDR1 P-gp correlates with increased esterification of plasma membrane cholesterol (Luker et al. 1999)

Adapted from (Johnstone et al. 2000)

[1]Transfected cell lines used in each study with the cDNAs expressed by each plasmid shown in italics.

[2]*MDR1-MM* is an expression plasmid encoding P-gp with Lys to Met mutations at positions 433 and 1076, which has defective ATP hydrolysis.

[3]*MDR1-8A* and *MDR1-8E* are expression plasmids encoding P-gp with replacement of eight Ser/Thr residues within the P-gp linker region with Ala (8A) or Glu acid (8E). The MDR1-8A product mimics non-phosphorylated P-gp, whereas the MDR1-8E product mimics phosphorylated P-gp. *MDR1-3SA* is an expression plasmid for P-gp with Ser to Ala mutations within the linker region at positions 661, 667 and 671.

PC - phosphatidylcholine

PKC - Protein kinase C

More recently, a detailed review on several P-gp physiological functions was made according to the corresponding substrates, except for drug excretion, being these functions summarized in Table 3 (Mizutani et al. 2008)

Table 3. Summary of physiological functions of P-gp (ABCB1, MDR1)

Substrates/Functions	Function	References
Platelet-activating factor (PAF)	Translocation of PAF across the plasma membrane PAF inhibition of drug transport by P-gp Phospholipid flippases	(Ernest and Bello-Reuss 1999) (Raggers et al. 2001) (Daleke 2007)
Sphingomyelin (SM) and glucosylceramide (GlcCer)	Translocation of SM and GlcCer Translocation of C_6-NBD-GlcCer in the apical medium	(Slotte and Bierman 1988) (van Helvoort et al. 1996)
Apoptosis	P-gp prevents stem-cell differentiation P-gp prevents programmed cell death, apoptosis P-gp protect cells from death	(Robinson et al. 1997) (Smyth et al. 1998) (Johnstone et al. 1999)
Phosphatidylcholine (PC)	Translocation of C_6-NBD-PC across the apical membrane Translocation of natural PC to the cell surface	(Bosch et al. 1997) (Kalin et al. 2004)
Cholesterol and its esterification	Transport of a variety of steroids Transport of glucocorticoids P-gp esterified more cholesterol Direct interaction of cholesterol with the substrate binding site Increase of esterified cholesterol according to the level of P-gp	(Barnes et al. 1996) (Gruol et al. 1999) (Luker et al. 1999) (Wang et al. 2000) (Gayet et al. 2005)
Cytokines	Transport of cytokines, IL-1β, IL-2, IL-4 and IFN ɣ Release of IL-2	(Raghu et al. 1996) (Drach et al. 1996)
Chloride channel regulator	Associated with a volume-activated chloride channel Bifunctional with both transport and channel regulator	(Hardy et al. 1995) (Bond et al. 1998)
Others	Subunit twisting "Gate" opens in transmembrane domains of other ABC transporters	(Hollenstein et al. 2007) (Ivetac et al. 2007)

NBD - [(7-nitro-2,1,3benzoxadiazol-4-yl)-aminododecanoyl] glycerol PL. Adapted from (Mizutani et al. 2008)

I.3. P-glycoprotein topology, structure and synthesis

Human P-gp is a single 170 kDa polypeptide (Juliano and Ling 1976) consisting of 1280 amino acids organised in two tandem repeats of 610 amino acids joined by a linker region of ~60 amino acids (Chen et al. 1986). As previously referred, the protein appears to have arisen by a gene duplication event, by fusing two homologous halves, each consisting of six highly hydrophobic transmembrane α-helices (TMHs) and one nucleotide binding domain (NBD) located on the cytoplasmic side of the membrane, which binds and hydrolyses ATP (Figure 2A) (Hennessy and Spiers 2007; Sharom 2008; Sharom 2011).

The two half molecules are separated by a highly charged cytoplasmic 'linker region', which is phosphorylated at several sites by protein kinase C (PKC) (Higgins et al. 1997). The TMHs are considered to form the pathway through which the drug molecules cross the membrane (see below). The NH_2- and COOH-termini, as well as the NBDs, are located intracellularly, and the first extracellular loop is N-glycosylated (Zhou 2008). Each NBD consists of two core consensus motifs, referred to as the Walker A and B motifs, which are found in many proteins that bind and hydrolyse ATP and GTP, and a LSGGQ signature C motif, which, as previously referred, is unique to the ABC superfamily (Figure 2A) (Walker et al. 1982). These motifs are directly involved in the binding and hydrolysis of nucleotides (Sharom 2008; Sharom 2011; Zhou 2008).

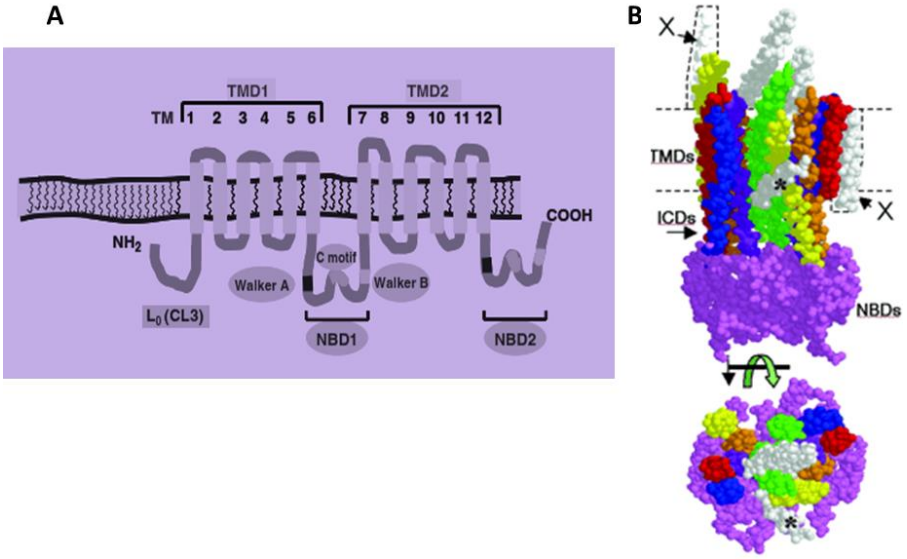

Figure 2. Topology and structure of P-gp
(A) Topological model of P-gp, showing the two homologous halves, each with one TMD, containing six TMHs, and one NBD. Taken from (Zhou 2008)**. (B)** Medium-resolution cryoelectron microscopy structure of hamster P-gp bound to the non-hydrolysable nucleotide analogue AMP-PNP (adenosine 5′-[β,γ-imido]triphosphate) and with all residues modelled as alanine. A side view of the protein with the NBDs (violet) at the bottom with a top view below. The 12 putative membrane-spanning α-helices have been colored in pairs to indicate the two halves of the transporter. A pseudo-symmetry relationship is seen. Four additional gray-colored helices do not show an obvious symmetry relationship; one (*) is intracellular, tilted, and too short to cross a membrane; another (shown in the side view by X) is ambiguous in its location; the other two are at the extracellular side of the protein (the dashed lines indicate the putative bounds of a 4.5-nm-thick lipid bilayer). ICD, intracytoplasmic domain. Taken from (Rosenberg et al. 2005).

P-gp is synthesised in the endoplasmic reticulum as a core-glycosylated intermediate with a molecular weight of 150 kDa, being the carbohydrate moiety subsequently modified in the Golgi apparatus prior to the export to the cell surface (Loo and Clarke 1999b). Although P-gp is glycosylated on its first extracellular loop, the role of glycosylation is unclear. Experiments using P-gp mutants lacking the N-terminal glycosylation sites showed that substrate transport was unaffected (Schinkel et al. 1993). However, glycosylation may alter trafficking and stability of P-gp within the plasma membrane (Hennessy and Spiers 2007).

The previously referred P-gp topology has been established and confirmed by cysteine (cys) mutagenesis and epitope-insertion experiments (Kast et al. 1996; Loo and Clarke 1995b). Earlier studies using various heterologous expression systems suggested other topologies in which putative transmembrane (TM) segments were displaced outside the membrane, however, it seems likely that these arrangements were the result of misfolding, and do not reflect the true topology of the transporter *in vivo* (Linton and Higgins 2002). The TM regions from both P-gp halves form the drug-binding region of the protein and drugs enter this binding pocket from the lipid bilayer (Loo and Clarke 1999c).

Early work by Rosenberg et al. using electron microscopy (EM) single particle image analysis of purified P-gp produced a very low resolution structure, which suggested the existence of a large, 5 nm diameter, central pore in the protein (Rosenberg et al. 1997). This pore was closed at the cytoplasmic face of the membrane, forming an aqueous chamber within the membrane from which entry points to the membrane lipid were observed. Two widely-separated 3 nm lobes on the cytoplasmic side of the membrane were thought to represent the NBDs (Rosenberg et al. 1997). This structure was in disagreement with both biochemical studies, which suggested kinetic cooperativity between the two catalytic sites, and with the high-resolution X-ray crystal structures of other ABC proteins, which showed close physical association of the two NBDs. Fluorescence resonance energy transfer (FRET) studies, in which two different fluorescent probes were covalently linked to each Walker A motif Cys residue also indicated that the positioning of the two NBDs is compatible with a sandwich dimer model (see I.4.3) (Qu and Sharom 2001), and Urbatsch et al. found that the two Walker A Cys residues could readily crosslink spontaneously (Urbatsch et al. 2001). Additionally, it was also demonstrated that Cys residues in the Walker A motifs could be crosslinked at low temperatures to Cys residues in the LSGGQ motif (signature C), indicating that the signature sequences in one NBD are adjacent to the Walker A site in the other NBD (Loo et al. 2002). Moreover, it was later shown that nucleotide binding causes a repacking of the P-gp TM regions (Rosenberg et al. 2001), which could open the central pore to allow access of hydrophobic drugs directly from the lipid bilayer (Rosenberg et al. 2003). It was proposed from this reorganization that ATP binding, not hydrolysis, drives the conformational changes associated with transport (Rosenberg et al. 2001) (see I.4.3). The vanadate-trapped complex of P-gp displayed a third distinct conformation of the protein, suggesting that rotation of TM α-helices had taken place (Rosenberg et al. 2001). Mouse P-gp has also been studied by EM and image analysis of 2D crystals of purified protein in a lipid bilayer, and the resulting low resolution projection structure (22 Å) was compact, and suggested that the two cytoplasmic NBDs interact closely (Lee et al. 2002).

The structure of hamster P-gp was then studied by a higher resolution EM, and the highest resolution structure [8 Å, (1 Å=0.1 nm); Figure 2B], confirmed the presence of two closely associated NBDs (Rosenberg et al. 2005), being this the first three-dimensional structure characterized for an intact eukaryotic ABC transporter. Moreover, this structure bears a much greater resemblance to the mouse P-gp structure, so it seems likely that the NBDs indeed form the "sandwich dimer" observed for other ABC proteins (Rosenberg et al. 2005) (see I.4.3). Additionally, this structure also clearly showed the existence of 12 TMHs, supporting the proposed topology of the protein, but the resolution was not high enough to discern further details. The packing arrangement of the P-gp TMHs was systematically explored by Loo and co-workers, who introduced Cys residues into defined positions within a Cys-less P-gp construct, and then carried out cross-linking studies (Loo and Clarke 2000). The observed pattern suggested that TMH 6 is close to TMH 10, 11, and 12, whereas TMH 12 is close to TMH 4, 5, and 6. Subsequent work showed that the ends of TMH 2 and TMH 11 are close together on the cytoplasmic side of the membrane (Loo et al. 2004c), as are the cytoplasmic ends of TMH 5 and TMH 8 (Loo et al. 2004a).

While the structures of bacterial ABC importers and exporters have been established (Dawson and Locher 2006; Hollenstein et al. 2007; Oldham et al. 2007; Pinkett et al. 2007; Ward et al. 2007) and P-gp characterized at low resolution by EM (Lee et al. 2008; Rosenberg et al. 2003), an x-ray structure of P-gp would be of particular interest because of the clinical relevance of this transporter. In 2009, Aller *et*.al reported x-ray crystal structures (3.8 - 4.4 Å) of mouse P-gp, both in the absence of substrate, and with two stereoisomeric cyclic hexapeptide inhibitors bound to the transporter (Aller et al. 2009). The authors fully described the structure of mouse P-gp, which has 87% sequence identity to human P-gp in a drug-binding competent state. In this report, the structure of P-gp (Figure 3) represents a nucleotide-free inward-facing conformation arranged as two "halves" with pseudo two-fold molecular symmetry, spanning ~136 Å perpendicular to and ~70 Å in the plane of the bilayer. The NBDs are separated by ~30 Å. In fact, two interdigitated bundles of α-helices were observed, each made up of portions from both the N-terminal and C-terminal halves (TMHs 1 - 3, 6, 10 and 11, and TMHs 4, 5, 7 - 9 and 12). The long intracellular loops of one helix bundle contact the opposing NBD. The inward facing conformation formed from the two bundles of six helices results in a large internal cavity open to both the cytoplasm and the inner leaflet of the membrane. Also, two portals seem to allow the access for entry of hydrophobic molecules directly from the membrane. The portals are formed by TMHs 4/6 and 10/12, each of which have smaller side chains that could allow tight packing during NBD dimerization. At the widest point within the bilayer, the portals are ~9 Å wide and each are formed by an intertwined interface in which TMHs 4/5 (and 10/11) crossover to make extensive contacts with the opposite α-helical

bundle (Figure 3) (Aller et al. 2009). Each intertwined interface buries ~6,900 Å^2 to stabilize the dimer interface (Aller et al. 2009) and is a conserved motif in bacterial exporters (Dawson and Locher 2006; Ward et al. 2007). In fact, this crossover between the two halves of the transporter was also previously seen in the crystal structure of the bacterial transporters Sav1866 (Dawson and Locher 2006) and MsbA (Ward et al. 2007).

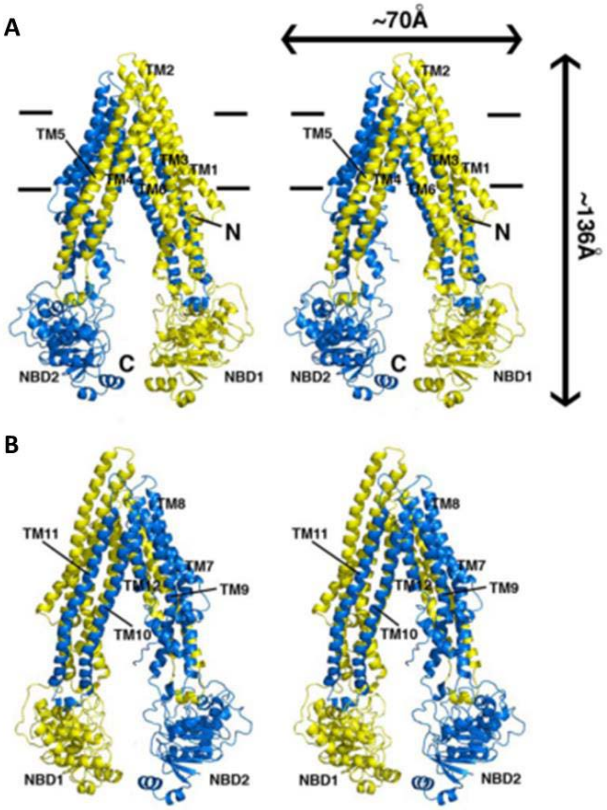

Figure 3. Structure of P-gp.
(A) Front and **(B)** back stereo views of P-gp. TM1-12 are labelled. The N and C-terminal half of the molecule are colored yellow and blue, respectively. TM4-5 and TM10-11 cross over to form intertwined interfaces that stabilize the inward facing conformation. Horizontal bars represent the approximate positioning of the lipid bilayer. The N- and C-termini are labelled in panel A. Transmembrane (TM) α-helices and nucleotide binding domains (NBD) are also labelled. Taken from (Aller et al. 2009).

This mouse P-gp crystal structure greatly increased the potential for improved structure-based approaches for modulation of P-gp activity, in spite of the highly flexible and complex nature of the protein (Klepsch and Ecker 2010).

I.3.1. The drug-substrate binding sites – substrate binding pocket

P-gp-mediated transport demonstrated, *in vitro*, to be saturable, osmotically sensitive and to require ATP hydrolysis to generate a substrate concentration gradient (Sharom 1997). While drug binding is known to occur within the TMD of P-gp, the understanding of where and how substrates bind to this protein is improving. Using ATPase inhibition as a measure, Borgnia et al. suggested a single binding site in P-gp for all substrates (Borgnia et al. 1996). However, evidence suggests that P-g has multiple binding sites divided evenly into two categories: transport and regulation (Martin et al. 2000; Shilling et al. 2006). These distinct sites may interact as demonstrated by the stimulation of Hoechst 33342 transport by rhodamine 123 (Shapiro and Ling 1997c), acting by a cooperative mode of action. Results obtained from radioligand-binding studies

indicated that there are between two (Homolya et al. 1993; Loo and Clarke 1999c; Raviv et al. 1990; Shapiro et al. 1999; Shapiro and Ling 1997c; van Veen et al. 1998) to at least four (Martin et al. 2000) substrate-binding sites within the P-gp TMDs. Shapiro and Ling proposed the existence of at least two interacting binding sites that display positive cooperativity in drug transport (Shapiro and Ling 1997c). One site was suggested to bind rhodamine 123, other rhodamine drugs, and anthracyclines (the R-site), and a second site was proposed to bind Hoechst 33342 and colchicine (the H-site) (Shapiro and Ling 1997c). Later, they identified a third binding site in P-gp that binds prazosin and progesterone (Shapiro et al. 1999). Martin and co-workers suggested the existence of multiple drug binding sites that interact allosterically, based on measurements of radiolabeled drug binding to P-gp (Martin et al. 2000). It was also proposed that both the N- and C-terminal halves of P-gp contain binding sites, and these two sites may generate a single region in the overall protein structure (Loo et al. 2003c; Morris et al. 1994), being this drug-binding pocket large enough to accommodate more than one substrate (Loo and Clarke 2001c). Indeed, several research studies have demonstrated, both by fluorescence methods (Lugo and Sharom 2005a) as well as through binding of a thiol-reactive substrate (Loo et al. 2003b), that two different substrates can bind to P-gp at the same time. Also, there are relevant data indicating that substrate binding sites may overlap or be allosterically coupled (Ayesh et al. 1996; Dey et al. 1997; Ferry et al. 1995), raising the possibility that there is only a single common site (Borgnia et al. 1996). However, there is evidence for P-gp allosteric sites distinct from transport sites, as compounds such as the indolizin sulfone SR33557 and the 1,4-dihydropyridines confer allosteric control to the P-gp binding site for the transport of vinblastine (Martin et al. 1997). Therefore, the binding sites can be classified as both transport and modulating sites (Martin et al. 2000), and have the ability to switch between high and low affinity states to accommodate substrates/inhibitors (Wang et al. 2003). This switch between high- and low-affinity conformations might be caused by stimuli such as substrate binding and/or ATP hydrolysis (Zhou 2008). Additionally, conformational changes in P-gp have been demonstrated using proteolytic accessibility, and changes in antibody epitope recognition (Mechetner et al. 1997; Sonveaux et al. 1999).

Given the ability of P-gp to transport a diverse range of substrates/modulators (Table 4 and Table 5), several studies were conducted to set the key features of the P-gp-binding site(s). Moreover, the presence of multiple drug binding sites on P-gp could provide an explanation for the wide range of compounds known to interact with this protein. In early attempts to identify the location of the drug binding sites, P-gp was labelled with photoactive analogues of a variety of drug substrates (Bruggemann et al. 1992; Demeule et al. 1998; Demmer et al. 1997; Greenberger 1993). Identification of the

labelled peptides following proteolytic cleavage showed that labelling took place in the TMD of both halves of the protein.

More recent work using Cys-reactive substrate analogues and Cys mutations has localized the drug-binding pocket to the regions of P-gp bounded by TMH 4-6 and 10-12, as residues from these helices are important for drug binding (Loo and Clarke 1999a; Loo and Clarke 1999b; Loo and Clarke 1999c; Loo and Clarke 2000). Thiol cross-linking data clearly indicated that substrate binding is closely associated with TMH 1, 4, 5, 6, 9, 10, 11 and 12 (Bruggemann et al. 1992; Germann 1996; Loo et al. 2006a; Loo and Clarke 1997; Loo and Clarke 1999a; Loo and Clarke 2001b; Loo and Clarke 2002; Morris et al. 1994; Wang et al. 2003). Also, cys-scanning mutagenesis, reaction with an MTS (methanethiosulfonate) thiol-reactive analogue of verapamil (termed MTS–verapamil) and cross-linking analysis were conducted to test whether the TMH 7, in the C-terminal-half of P-gp, also contributes to drug binding. According to the obtained results, TMH 7 also forms part of the P-gp drug-binding pocket (Loo et al. 2006b). Moreover, the reported data are in agreement with that derived from both photoaffinity labelling (Ecker et al. 2002; Isenberg et al. 2001) and mutational analysis experiments [for review see (Frelet and Klein 2006; Peer et al. 2005; Shilling et al. 2006)]. Additionally, targeted mutagenesis of these TMHs altered drug resistance (Kajiji et al. 1993; Loo and Clarke 1993), supporting their involvement in drug binding. Moreover, mapping of the drug-binding pocket using thiol specific cross-linkers with spacer arms, in conjunction with P-gp mutants (cys residues introduced), points towards the presence of a central pore being funnel shaped, narrow at the cytosolic side, at least 0.9 - 2.5 nm wide in the middle and wider again at its extracellular surface (Loo and Clarke 2001c) (Figure 4) Moreover, this central pore is accessible to the aqueous medium (Loo et al. 2004b) and located at the interface of the two halves of the protein (Loo and Clarke 2005b). This configuration is consistent with the EM and image analysis data reported by Rosenberg et al. (Rosenberg et al. 1997; Rosenberg et al. 2005). Additionally, this interfacial localization was confirmed using propafenone photoaffinity ligands and mass spectrometry, where peptides from TMH 3, 5, 8, and 11 were specifically labelled (Pleban et al. 2005). When drugs bind, the packing of helices is altered in P-gp relative to the drug-free state, as shown by Cys cross-linking of pairs of residues (Loo et al. 2003d). The packing changes are specific to each substrate, which supports an induced-fit model of drug binding (Loo et al. 2003d).

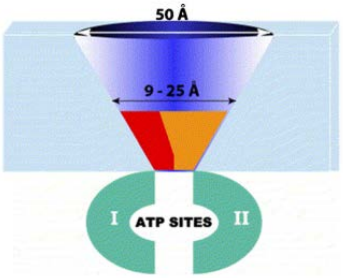

Figure 4. Cross-sectional schematic showing the approximate dimensions and shape of the drug-substrate-binding pocket and the central pore of P-gp.
Two drugs (depicted in red and orange) are shown to be simultaneously bound in the binding pocket. Taken from (Ambudkar et al. 2006).

Current models of P-gp drug binding thus suggest that, rather than one or a few discrete drug-binding sites, there is a large, flexible drug-binding region, which the high-resolution crystal structure appears to confirm. According to the X-ray crystal structure of mouse P-gp reported by Aller et al. (2009), the volume of the internal cavity within the lipid bilayer is substantial (6000 $Å^3$), and could accommodate at least two substrate molecules simultaneously (Aller et al. 2009). This cavity is open to the inner leaflet of the membrane via portals, probably to allow drug entry from the lipid bilayer. It is also open to the cytosol, suggesting that an inward-facing conformation of the protein has been captured. The presumptive drug binding pocket comprises mostly hydrophobic and aromatic residues. Of the 73 solvent accessible residues in the internal cavity, 15 are polar and only two (His60 and Glu871), located in the N-terminal half of the TMD, are charged or potentially charged (Aller et al. 2009). Additionally, in this study, P-gp was able to distinguish between the stereoisomers of cyclic peptides (QZ59-RRR and QZ59-SSS) (Figure 5) resulting in different binding locations, orientation and stoichiometry (Aller et al. 2009). Indeed, the most important aspect of the P-gp crystal-structure determination was this successful elucidation of two different structures with novel peptide inhibitors bound to the drug-binding region. QZ59-RRR and QZ59-SSS peptide stereoisomers bind to distinct sub-sites in the binding cavity in different orientations, and make different sets of contacts with amino acid side chains of the protein. QZ59-RRR binds one site per transporter located at the center of the molecule between TMH 6 and TMH 12. The binding of QZ59-RRR to the 'middle' site is mediated by mostly hydrophobic residues on TMHs 1,5,6,7,11, and 12 (e.g. held in place by favourable hydrophobic interactions with phenylalanine, tyrosine, leucine and isoleucine residues) (Figure 5). On the other hand, two molecules of QZ5-SSS are found at different locations, 'upper' and 'lower' sites, within the binding pocket (Figure 5A), and some polar residues are involved in interactions with the latter. Indeed, the QZ59-SSS molecule occupying the "upper" site is surrounded by hydrophobic aromatic residues on TMHs 1,2,6,7,11, and 12. The ligand in the "lower" site that binds to the C-terminal half of the TMD is in close proximity to TMHs 1,5,6,7,8,9,11, and 12 and surrounded by three polar residues (Gln721, Gln986, and Ser989) (Aller et al. 2009). Thus, this crystal

structure of P-gp shows overlapping binding sites for the two stereoisomers of the same drug, and demonstrated that two molecules of the same drug may be located in different regions of the cavity (Figure 5B). Comparison with the QZ59-RRR-bound structure allowed visualization for the first time of P-gp's ability to bind substrate stereoisomers and multiple molecules of the same substrate simultaneously, as previously indicated by substantial biochemical evidence (Loo et al. 2003c; Lugo and Sharom 2005a) (Dey et al. 1997; Loo et al. 2003b). Moreover, QZ59-RRR and QZ59-SSS bind to overlapping regions of the substrate-binding site, and in different orientations, by interacting with a different subset of amino acid residues in the protein. The binding of QZ59 to P-gp also confirmed the anticipated importance of TMH 5-6 and 9-12 in substrate binding, as predicted by cross-linking studies (Loo and Clarke 2005a).

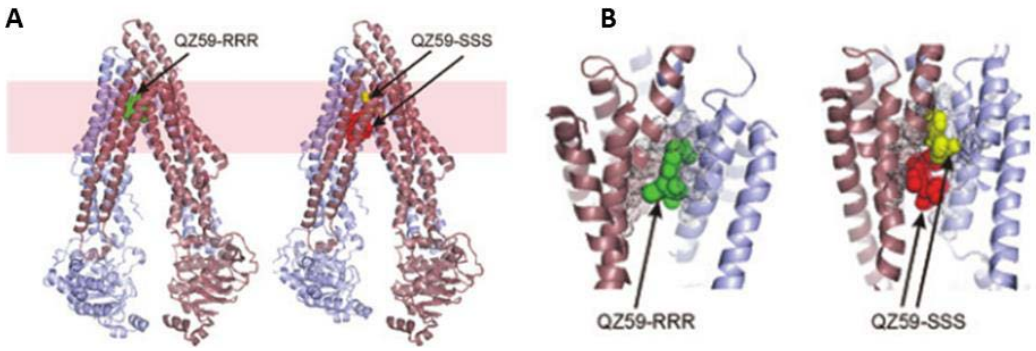

Figure 5. Binding of novel cyclic peptide P-gp inhibitors
(A) High-resolution X-ray structures of mouse P-gp bound to a single molecule of the cyclic peptide substrate QZ59-RRR (left-hand panel, peptide in green) and two molecules of its stereoisomer QZ59-SSS (right-hand panel, peptides in red and yellow). The approximate location of the membrane is indicated by the coloured bar. **(B)** Close-up views of the peptides inside the substrate-binding pocket; QZ59-RRR interacting with the middle site (left), and two molecules of QZ59-SSS occupying the upper and lower sites (right). Taken from (Aller et al. 2009).

Also, the co-crystal structures of P-gp with the QZ59 compounds demonstrated that the inward facing conformation is competent to bind drugs (Aller et al. 2009). Thus, this crystal structure suggests that, upon ATP binding/hydrolysis, the drug-binding cavity becomes closed to the inner leaflet and opens to either the outer membrane leaflet or the extracellular media, in support of the "vacuum cleaner" and "flippase" mechanisms of action (see I.4.2.1). Moreover, according to previous studies that have identified residues that interact with verapamil (Loo et al. 2006b; Loo and Clarke 1997), many of these residues faced the drug binding pocket in this crystal structure, and were highly conserved, suggesting a common mechanism of drug recognition (Aller et al. 2009). For both QZ59 compounds, isopropyl groups pointed in the same direction, toward TMH 9-12, and although certain residues in P-gp contact both compounds, the specific functional roles of the residues binding each inhibitor were different. For example: Phe332 contacts

the molecules in the “upper” but not “lower” sites of QZ59-SSS, but does contact the inhibitor in the “middle” site (QZ59-RRR); Phe724 was near both the “middle” and “lower”, but was much closer to a selenium atom in QZ59-SSS; Val978 plays an important role having close proximity to all three QZ59 sites. Interestingly, both Phe724 (human Phe728) and Val978 (human Val982) are protected from labelling by MTS-verapamil (Loo et al. 2006b; Loo and Clarke 1997), indicating that both are important for drug binding. While the upper half of the drug binding pocket contains predominantly hydrophobic/aromatic residues, the lower half of the chamber has more polar and charged residues (Aller et al. 2009) and, therefore, hydrophobic substrates that are positively charged may bind to these residues. The inward facing conformation of P-gp demonstrated to provide access to the internal chamber *via* portals that were open wide enough to accommodate hydrophobic molecules and phospholipids. The portals formed a contiguous space spanning the width of the molecule that allow P-gp to “scan” the inner leaflet to select and bind specific lipids and hydrophobic drugs prior to transport. Lipids and substrates may thus remain together during initial entry into the internal cavity (Aller et al. 2009). Also, mouse P-gp protein exhibited typical basal ATPase activity that was stimulated by drugs like verapamil and colchicine, and P-gp recovered from washed crystals retained near full ATPase activity. Moreover, both QZ59 compounds inhibited the verapamil-stimulated ATPase activity in a concentration-dependent manner.

Therefore, P-gp appears to bind multiple drugs by having a large highly flexible binding cavity which can accommodate several compounds in different locations by an ‘induced fit’ type of mechanism. Biochemical cross-linking and fluorescence studies had already pointed to a substrate-binding region with these properties (Loo and Clarke 2005a). The polyspecific nature of the P-gp-binding pocket and its ability to bind more than one drug molecule simultaneously makes the rational design of specific high-affinity inhibitors a challenging problem.

I.4. P-glycoprotein substrates and mechanism of drug efflux

I.4.1. P-gp substrates

P-gp can transport out of the cell a vast array of compounds, which are chemically, structurally and pharmacologically unrelated, including natural products, chemotherapeutic drugs, calcium channel blockers, steroids, linear and cyclic peptides, fluorescent dyes and pesticides, among many others (Table 4) (Hennessy and Spiers 2007; Kim 2002; Seelig 1998; Sharom 2011; Ueda et al. 1997; Varma et al. 2003; Zhou 2008). However, direct measurement of transport has been carried out for only a few of these putative substrates, and most have been identified on the basis of resistance of P-

gp-overexpressing cell lines to their cytotoxic effects (Sharom 2011). Most of these substrates are weakly amphipathic and relatively hydrophobic, often (but not always) containing aromatic rings and a positively charged N atom (Sharom 2011).

Table 4. Different classes of known P-gp substrates

Class	Examples
Analgesic Opioids	Morphine, pentazocine, fentanyl
Antiarrhythmics	Quinidine, verapamil, digoxin
Anticancer agents	**Antibiotics:** Anthracyclines (doxorubicin, daunorubicin), Actinomycines (actinomycin D), mytomicin C, mitoxantrone **Camptothecins**: topotecan, irinotecan (CPT-11) **Antimetabolites:** methotrexate, cytarabine, 5-fluorouracil, hydroxyurea **Epipodophyllotoxins**: etoposide, teniposide **Taxanes**: paclitaxel, docetaxel **Vinca alkaloids**: vinblastine, vincristine **Alkylating agents:** chlorambucil, cisplatin **Tyrosine kinase inhibitors**: imatinib mesylate, gefitinib **Others:** tamoxifen, bisantrene
Antidepressants	Amitriptyline, nortriptyline, doxepin
Anti-diarrheal agents	Loperamide (opioid), octreotide
Antiemetics	Ondansetron, domperidone
Antiepileptics and Anticonvulsants	Topiramate, phenytoin, carbamazepine, phenobarbital
Antigout agentes	Colchicine
Antihelmintics	Ivermectin
Antihistaminics	Terfenadine, fexofenadine
Anti-human immunodeficiency virus (HIV) agents	Nelfinavir, ritonavir, saquinavir, amprenavir, indinavir
Antihypertensives	Reserpine, debrisoquine, celiprolol, losartan, talinolol, prazosin
Antimicrobial agents	Erythromycin, doxycycline, itraconazole, ketoconazole, levofloxacin, rifampicin, sparfloxacin, tetracycline, grepafloxacin, clarithromycin, gramicidin A, valinomycin
Calcium channel blockers	Nifedipine, diltiazem, verapamil, azidopine, nicardipine
Calmodulin antagonists	Trifluoperazine, trans-flupentixol
Cardiac glycosides	Digoxin, digitoxin
Cholesterol-lowering agents	Lovastatin, simvastatin
Cyclic peptides	PSC833, beauvericin
Fluorescent dyes	Rhodamine 123, hoechst 33342, calcein AM (calcein acetoxymethylester)
Histamine H_2-receptor antagonists	Cimetidine, ranitidine
Immunosuppressive agents	Cyclosporin A, tacrolimus,sirolimus, valspodar
Linear peptides	ALLN (N-acetyl-L-leucyl-L-leucylnorleucinal),leupeptin, pepstatin A
Muscle relaxant agents	Vecuronium
Natural products	Flavonoids, curcuminoids
Neuroleptics	Chlorpromazine, phenothiazine
Pesticides	Methylparathion, endosulfan, paraquat
Steroid hormones	Aldosterone, corticosterone, dexamethasone, cortisol, methylprednisolone

Data are compiled from (Matheny et al. 2001), (Kim 2002), (Zhou 2008), (Sharom 2011) and http://www.tp-search.jp.

Due to the nature of P-gp (an efflux pump protecting against a wide variety of substances), P-gp substrates vary greatly in size, structure, and function, ranging from small molecules, such as organic cations, carbohydrates, amino acids, and some antibiotics, to macromolecules such as polysaccharides and proteins (Zhou 2008). Given the important role of this efflux pump in drug pharmacokinetics and in drug resistance, extensive studies have been undertaken to elucidate the molecular attributes required for interaction between this efflux protein and its small substrates, and to identify P-gp substrates or develop more potent, selective and specific P-gp inhibitors to overcome the problem of MDR. Therefore, the knowledge of the factors that determine substrate specificity is crucial for successful drug targeting and for the rational design of new drugs (Seelig 1998). Different attempts have been made to find a common set of structural and functional features required for a substrate to interact with P-gp. However, the P-gp poly-specificity (i.e. promiscuity) in substrate and inhibitor recognition makes the designing of effective candidate compounds difficult.

Rather than developing computational models based on complicated statistical techniques, earlier attempts were made to find a set of simple rules based on structural and functional features that can characterize the interactions between a substrate or inhibitor and P-gp. It was initially suggested that the minimum set of structural features includes a basic nitrogen atom and two planar aromatic domains (Zamora et al. 1988). Later, using a series of reserpine and yohimbine analogs, Pearce et al. (1989) demonstrated that these domains must adopt a well-defined conformation (Pearce et al. 1989). However, the screening of a broader range of compounds, including for example steroid hormones, revealed that compounds lacking a basic nitrogen can still interact with P-gp (Schinkel et al. 1996; Ueda et al. 1992). Therefore, it was suggested that the only common property of P-gp substrates was their relative hydrophobic and amphiphilic nature (Gottesman and Pastan 1993; Schinkel et al. 1996). Moreover, the study of the hydrophobic and amphiphilic nature of several P-gp substrates, such as domperidone, loperamide, and terfenadine, through the evaluation of their surface activity (Seelig et al. 1994), corroborated the previous assumption. However, the investigation of the surface activity of a broader range of P-gp substrates showed that even rather hydrophilic compounds, such as morphine, can function as weak P-glycoprotein substrates (Seelig 1998). The screening of the structures of a hundred chemically diverse compounds, previously tested as P-gp substrates was later performed to find potential elements responsible for substrate-P-gp interaction and for P-gp over-expression (Seelig 1998). It was demonstrated that a compound can interact with P-gp if it contains (a) either two electron donor groups with a spatial separation of 2.5±0.3 Å or (b) two electron donor groups with a spatial separation of 4.6±0.6 Å or (c) three electron donor groups with a

spatial separation of the outer two groups of 4.6±0.6 Å (Seelig 1998). Furthermore, these latter features (b and c) appeared to be responsible for P-gp over-expression Therefore, it was demonstrated that most P-gp substrates possess two or three electron-donor groups with a fixed spatial separation, with an increased number of these elements increasing the affinity for drug binding (Seelig 1998). Correspondingly, there is a high percentage of amino acids with hydrogen bonding donor side-chains in the transmembrane sequences of P-gp responsible for substrate recognition (Zhou 2008). Further studies have also found that partitioning into the lipid membrane is the rate-limiting step for the interaction of a substrate with P-gp and that dissociation of the P-gp-substrate complex is determined by the number and strength of the hydrogen bonds formed between the substrate and P-gp (Seelig and Landwojtowicz 2000)**.** Other studies have also suggested that there may exist some physicochemical characteristic features, such as lipophilicity, hydrogen-bonding ability, molecular weight, and surface area, that contribute to a drug's binding ability to P-gp (Bain et al. 1997; Wang et al. 2003).

Traditionally, experimental *in vitro* assays were used to assess the transport and interactions with P-gp of new chemical entities (Polli et al. 2001). However, these experimental assays are expensive, laborious and time-consuming. Moreover, the simple set of rules initially stated, although easily understood and used by laboratory scientists as well as computational chemists, are too simple to effectively characterize P-gp substrates or inhibitors. Therefore, *in silico* models that provide rapid and cheap screening platforms for identifying P-gp substrates or inhibitors have been recognized to be valuable tools (Ekins et al. 2007; Hou and Xu 2004). Extensive computational models, based on quantitative structure-activity relationship (QSAR) analyses (2D-QSAR and 3D-QSAR), pharmacophore modeling and molecular docking techniques, have thus been developed to predict P-gp substrates, as well as inhibitors [for a review see (Chen et al. 2012a)]. Moreover, a variety of statistical techniques as well as machine learning approaches, including for example multiple linear regression (MLR), partial least square discriminant analysis (PLSD) and linear discriminant analysis (LDA), have been employed to develop the theoretical models (Chen et al. 2012a). A multiple-pharmacophore model that can discriminate between substrates and non-substrates of P-gp was identified from a large data set of compounds obtained from the literature, and the application of this filter allows large virtual libraries to be screened efficiently for compounds less likely to be transported by P-gp (Penzotti et al. 2002). Another more general QSAR model was established based on a monolayer efflux classification as substrates or non-substrates (Ekins et al. 2002). It was later described a pharmacophore model based on the efflux ratios (obtained from Caco-2 permeability measurements) and on P-gp inhibition data (using a calcein-AM assay) of a diverse set of 129 compounds (Cianchetta et al. 2005). Accordingly to the

obtained pharmacophore, it was concluded that the P-gp recognition elements are two hydrophobic groups, 16.5 Å apart, and two hydrogen bond-acceptor groups, 11.5 Å apart, and that the dimensions of the molecule also play a role in its recognition as a substrate (Cianchetta et al. 2005). A QSAR model for discriminating P-gp substrates and non-substrates was also set up based on calculated molecular descriptors and multivariate analysis using a set of 53 diverse drugs (previously classified as substrates and non-substrates on the basis of the efflux ratio from Caco-2 permeability measurements) (Crivori et al. 2006). The model had an accuracy of 88.7% for the training set, but it only achieved an accuracy of 72.4% for the external set of 272 compounds (Crivori et al. 2006). Also, a linear discriminant model was developed to classify a larger data set of 163 compounds as P-gp substrates or non-substrates (91 substrates and 72 non-substrates) (Cabrera et al. 2006). The model was validated through the use of an external validation set (40 compounds, 22 substrates and 18 non-substrates), with a 77.50% accuracy prediction (Cabrera et al. 2006). More recently, more efficient models have been set up for prediction of P-gp substrates with an accuracy greater than 90% (Huang et al. 2007).

In the earlier stages of the in *silico* P-gp study, the QSAR and pharmacophore modeling techniques were the methods used to predict P-gp substrates (or inhibitors), given the lack of available crystal P-gp structures. In 2009, the X-ray structures of mouse P-gp were reported by Aller *et al.*, and the crystal P-gp structures provided good starting points for molecular docking studies (Aller et al. 2009). In many studies, the homology models were developed to characterize the putative ligand-binding sites or to investigate the possible conformations of P-gp in different states, and some publications showed the P-gp models used to dock compounds into the putative ligand-binding sites (Becker et al. 2009; Pajeva et al. 2009).

It is noteworthy that there is an overlap of the P-gp substrate specificity, particularly of cytostatic drugs, with other ABC transporters, such as ABCC1, ABCC2, and ABCG2 (Cascorbi 2006). Also, there is a broad range of overlapping substrate specificities and tissue distribution for P-gp and the CYP3A metabolizing enzymes, particularly CYP3A4 (Cascorbi 2006). Those substrates are known as CYP/P-gp bi-substrates, making P-gp and CYP3A a synergistic defence mechanism against the intrusion of xenobiotics. Specifically, both P-gp and CYP3A4 act synergistically as a protective barrier in the bioavailability of orally administered drugs (Cummins et al. 2002). The localization of P-gp and CYP3A proteins indicates that the amount of substrates metabolized by the CYP3A enzyme may be controlled by P-gp (Cummins et al. 2002). P-gp is also involved in the counteracting active transport of drugs back to the lumen after passive absorption into the enterocytes (Cummins et al. 2002). The drug is continuously moved between the lumen and enterocytes, thus allowing CYP3A4 to constantly access to the drug molecule. As a

consequence, the counter transportation of P-gp and metabolism mediated by CYP3A in the intestine reduces the oral bioavailability of a drug by controlling the concentration of molecules entering the systemic circulation. Therefore, P-gp influences the extent of drug metabolism in the intestine via prolonging the access of drugs to CYP3A4 near the apical membrane and decreasing their transport across the cells (Cummins et al. 2002).

Knowing whether a new compound is a P-gp substrate can thus provide important information on its tissue distribution (e.g. to brain) and elimination, which might be a useful criterion during drug candidate selection. For example, given that most anti-human immunodeficiency virus drugs are P-gp substrates, modification of their chemical structures leading to less recognition by P-gp will lead to improved penetration to the central nervous system and, thus, a better antiviral profile can be achieved (Zhou 2008).

I.4.2. Mechanism of drug efflux - P-gp models of pump function

Early in the study of MDR, it became evident that classical models for membrane protein solute transport (such as lactose transport by lactose permease) are not a reasonable description for drug efflux processes. Most membrane transporters sequester hydrophilic substrates (sugars, ions, etc.) from the hydrophobic bilayer core and shuttle them across the membrane via a hydrophilic protein pathway that is lined with polar and charged residues (Eckford and Sharom 2009). One feature that is shared, especially for P-gp and ABCG2, is the relative hydrophobicity of their transport substrates. Thus, many drugs that are substrates for these drug efflux pumps can readily cross lipid bilayers by passive diffusion. The exact mechanism by which P-gp couples the ATP hydrolysis to the movement of drugs across the plasma membrane, as well as the exact site of substrate interaction with the protein, are not well defined. However, several models have been advanced to account for the available experimental data, namely the “hydrophobic vacuum cleaner”, “flippase” and “pore” models (Figure 6) (Hennessy and Spiers 2007; Varma et al. 2003). Additionally, a “two cylinder engine” model has also been suggested (Jones and George 1998; Jones and George 2000). The first two models are the most widely accepted (Hennessy and Spiers 2007; Sharom 2011; Varma et al. 2003) and will be discussed with further detail. Moreover, both the “hydrophobic vacuum cleaner” and “flippase” models are consistent with the tertiary structural data for P-gp, indicating that substrates gain access to the pore from the lipid phase of the membrane (Rosenberg et al. 1997; Rosenberg et al. 2001).

I.4.2.1. "Hydrophobic vacuum cleaner" versus "flippase" models of function

The compounds that interact with P-gp are relatively hydrophobic and readily soluble in lipid bilayers, and it is now widely accepted that they partition into the membrane before interacting with the protein (Seelig and Landwojtowicz 2000). Moreover, the P-gp substrate binding sites appear to be, as previously mentioned, contained within its TMDs, and drugs gain access to these sites after partitioning into the lipid bilayer (Raviv et al. 1990). Thus, the idea that P-gp acts a "hydrophobic vacuum cleaner", that expels lipophilic molecules from the membrane into the extracellular medium, was firstly suggested by Higgins and Gottesman to account for the lipophilic nature of P-gp substrates (Higgins and Gottesman 1992) and has found widespread acceptance.

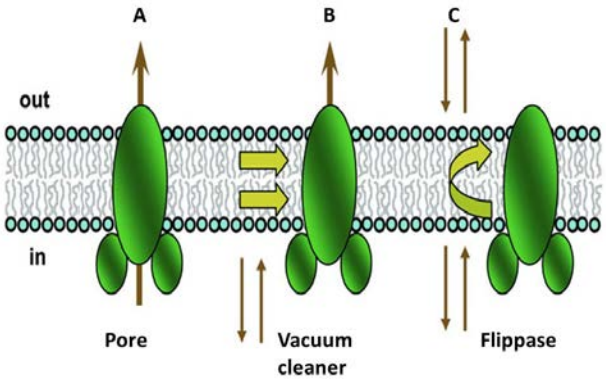

Figure 6. Models proposed to explain P-gp mechanism of drug efflux **(A)** Pore model, **(B)** Hydrophobic vacuum cleaner model and **(C)** Flippase model.
In pore model, drugs associate with P-gp in the cytosolic compartment and are transported out of the cell through a protein channel. In flippase model, drugs embed in the inner leaflet of the plasma membrane, bind to P-gp within the plane of membrane and are translocated to the outer leaflet of the bilayer from which they passively diffuse into extracellular fluid. The hydrophobic vacuum cleaner model combines the features of 'pore' and 'flippase' models. Adapted from (Varma et al. 2003).

The general consensus of the "hydrophobic vacuum cleaner" model (Figure 6B) relies on the principle that P-gp recognizes hydrophobic compounds embedded in the inner leaf of the plasma membrane (after they have partitioned into the bilayer), and pumps them out of the membrane directly to the external aqueous medium (Higgins and Gottesman 1992). This pumping action gives rise to a concentration gradient across the plasma membrane, with a higher drug concentration in the external aqueous phase. The transporter is able to intercept substrates before they have an opportunity to enter the cytosol, thus protecting the cell from exposure to potentially toxic molecules (Sharom 2011). In this model, structural data indicates that substrates could gain access to their binding sites through "gates" formed between TMHs 5/8 and 2/11 (Loo et al. 2003d). There is substantial experimental evidence to support this model. When the lipophilic probe iodonaphthalene-1-azide was used to photolabel P-gp, fluorescence resonance energy transfer data showed that the substrate doxorubicin was present within the membrane in close proximity to the transporter, rather than inside the cell (Raviv et al. 1990). This suggested that P-gp may bind doxorubicin from within the membrane and extrude it to the cell exterior. When acetoxymethylesters of fluorescent dyes are added to

intact cells, P-gp intercepts them before they can come into contact with cytosolic esterases and expels them into the extracellular medium (Homolya et al. 1993). This model is also strengthened by data demonstrating unidirectional transport of fluorescent P-gp substrates from the cytoplasmic leaflet of the plasma membrane to the external aqueous environment (Shapiro et al. 1997; Shapiro and Ling 1997b; Shapiro and Ling 1998b). Indeed, the dye Hoechst 33342 only becomes fluorescent after partitioning into the hydrophobic membrane interior, and kinetic measurements showed that its rate of transport by P-gp was directly proportional to its concentration in the lipid phase, rather than in the aqueous medium (Shapiro and Ling 1997b). Rosenberg et al. (2003) reported that 3D conformation of P-gp changes upon nucleotide binding to the intracellular NBD (Rosenberg et al. 2003). In the absence of nucleotide, the two transmembrane domains form a single barrel with a central pore that is open to the extracellular surface and spans much of the membrane depth, while upon binding nucleotides the TMDs reorganize into three compact domains that open the central pore along its length in a manner that could allow access of hydrophobic drugs directly from the lipid bilayer to the central pore of the transporter (Rosenberg et al. 2003). This model is also supported by the recent P-gp X-ray crystal structures, which, as previously mentioned, demonstrated that two peptide stereoisomers are bound deep within the TMDs, also suggesting that they may gain access to the protein from within the lipid bilayer (Aller et al. 2009).

The alternative proposal, the “flippase” model (Figure 6C), assumes that P-gp substrates are flipped from the inner leaflet of the lipid bilayer, to either the outer leaflet of the plasma membrane or directly to the extracellular environment (Higgins and Gottesman 1992). Therefore, the flippase model requires that drug substrates localize to one leaflet of the bilayer, rather than to the hydrophobic core of the membrane. In accordance, a panel of 9 molecules that bind to P-gp were shown to distribute discretely in one membrane leaflet, where they were localized to the interfacial region in a similar orientation to phospholipids (Siarheyeva et al. 2006). According to this model, it is also necessary a low rate of spontaneous movement of substrates between the two bilayer leaflets to allow P-gp to generate a drug concentration gradient. Indeed, the rate of movement of many P-gp substrates across a lipid bilayer ranges from minutes to hours (Eytan et al. 1996), whereas lipids have a flip-flop half-time of hours to days (Eckford and Sharom 2009). To reinforce this model, P-gp has the ability to bind lipid-like drugs and platelet-activating factors (Eckford and Sharom 2006), apart from also translocating fluorescently-labelled phospholipids across the membrane in an ATP-dependent fashion (Romsicki and Sharom 2001). Therefore, this protein may function as a translocase or ‘flippase’ for lipophilic molecules (Higgins and Gottesman 1992), moving them from the cytoplasm to the extracellular membrane leaflet. Moreover, this model of pump function may perhaps be

strengthened by the high level of sequence similarity between P-gp and its close relative ABCB4, which is a phosphatidylcholine flippase (Ruetz and Gros 1994) and, thus, they may share some functional attributes. The rate of spontaneous transbilayer movement of many P-gp substrates is relatively low and, as they appear to be discretely localized in one membrane leaflet, the transporter would be able to maintain a higher substrate concentration in the outer leaflet (Sharom 2011). Indeed, this flippase activity would also give rise to a substrate concentration gradient across the membrane, since the substrate in the outer leaflet would rapidly equilibrate with the external medium (Sharom 2011). However, because of the rapid partitioning equilibria involved, it is very difficult to distinguish between flippase activity and direct transport of a substrate from the membrane to the extracellular aqueous phase (Sharom 2011).

Several groups argued that colchicine, vinblastine and acetoxymethyl esters are pumped or “vacuumed” from the plasma membrane to the extracellular space (Hollo et al. 1994; Homolya et al. 1993; Stein et al. 1994). In support of this, electron spin paramagnetic resonance studies based on a model system (P-gp containing proteoliposomes obtained from *Saccharomyces cerevisiae*) indicated that P-gp concentrates (25-fold) spin-labelled verapamil in the aqueous phase (Omote and Al-Shawi 2002). These data agree with P-gp functioning as a “hydrophobic vacuum cleaner”. Controversially, a few studies have provided evidence supporting a “flippase” mechanism, by demonstrating altered distributions of fluorescent phosphatidylcholine, phosphatidylethanolamine, and sphingomyelin derivatives in cells expressing recombinant P-gp (van Helvoort et al. 1996) or in drug-selected cells overexpressing the protein (Abulrob and Gumbleton 1999). Also, both short-chain (van Helvoort et al. 1996) and long-chain (Bosch et al. 1997) fluorescent phospholipids were found to accumulate to a lesser extent in P-gp-expressing cells, and accumulation was increased upon treatment with a P-gp inhibitor. In accordance, using purified P-gp reconstituted into proteoliposomes, it was directly shown that the protein can flip, between the inner and outer leaflets of the plasma membrane, a variety of fluorescently labelled phospholipids and glycosphingolipids in an ATP-dependent, vanadate-sensitive fashion (Eckford and Sharom 2005; Romsicki and Sharom 2001). Phospholipid and glycosphingolipid translocation was inhibited in a concentration-dependent manner by known P-gp substrates, and the inhibitory potency was highly correlated with their P-gp binding affinity (Eckford and Sharom 2005; Romsicki and Sharom 2001). Conversely, if these labelled lipids were “vacuumed” into the aqueous phase, they would rapidly redistribute into the outer leaflet of the lipid membrane by virtue of their hydrophobic nature. This would give them the appearance of being transported by a “flippase”.

Noteworthy, both these models described above assume that P-gp substrates partition into the lipid phase prior to interacting with the protein. In fact, this may help to explain the P-gp unusually broad substrate specificity, since the primary determinant of specificity would be the ability of a substrate to appropriately intercalate into the lipid bilayer, with the subsequent interaction with the substrate-binding site being of secondary importance (Hennessy and Spiers 2007). Also, and as previously mentioned, both biochemical and structural data indicate that the P-gp substrate binding pocket is located within the TM regions of the protein that contact the cytoplasmic membrane leaflet (Aller et al. 2009; Lugo and Sharom 2005b; Qu and Sharom 2002; Shapiro and Ling 1997b), which is consistent with it acting as either a vacuum cleaner or a flippase model. However, experimentally it is difficult to distinguish between the “hydrophobic vacuum cleaner” and “flippase” models (Hennessy and Spiers 2007).

I.4.3. P-gp catalytical and transport cycle

ATP binding and hydrolysis was found to be essential for P-gp-mediated transport (Gottesman and Pastan 1993). The drug transport mediated by P-gp is powered by hydrolysis of ATP at the two cytoplasmic NBDs (Oswald et al. 2006). Site-directed mutagenesis approaches have demonstrated that the three NBDs highly conserved motifs (Walker A, Walker B and signature C) are important for the P-gp catalytic function (Frelet and Klein 2006). Structural studies on bacterial ABC proteins have yielded useful information on their catalytical cycle, leading to the now generally accepted concept that the NBDs must dimerize in order to hydrolyse ATP (Smith et al. 2002). According to this so-called ‘ATP sandwich dimer’, the NBDs are arranged in a head-to-tail arrangement, with two ATP molecules bound along the interface. Each nucleotide is held in place by the Walker A and B motifs of one NBD and the signature C motif of the other NBD, which thus form a composite binding site (Jones and George 1999). Therefore, each ATP-binding site is formed from the Walker A and B motifs of one NBD subunit and the signature C motif of the partner NBD motif, and two molecules of ATP are bound in these sites at the dimer interface (Sharom 2008). Moreover, these NBDs form a stable dimer in the presence of ATP when the catalytical activity is inactivated by mutation, thus supporting the critical role of NBD dimerization in the catalytical cycle of all ABC proteins (Hanekop et al. 2006; Smith et al. 2002). Nevertheless, the recently described mouse crystal structure of P-gp, as it does not contain a bounded nucleotide and since the two NBDs are separated by 30 Å (Aller et al. 2009), does not help in understanding the putative P-gp dimerization process. However, data obtained from cross-linking studies indicate that the signature C and Walker A motifs are close to each other (Loo et al. 2002).

The exact mechanism through which ATP hydrolysis is coordinated between the two NBDs, or how this energy is used to drive drug transport is still not completely understood (Callaghan et al. 2006). P-gp displays a constitutive ATPase activity (3-5 µmol/min/mg of purified protein), which is atypical for an ATP-driven transporter. This basal ATPase activity takes place in the absence of substrates, and depends on the presence of detergents, lipids and drugs (Liu and Sharom 1997; Sharom 2008). Moreover, the Km value for ATP hydrolysis is high (0.2-0.5 mM), indicating a relatively low affinity of P-gp for nucleotides (Sharom et al. 1995; Urbatsch et al. 1994). Moreover, this high level of basal ATPase activity in the absence of substrate (Shapiro and Ling 1994; Sharom et al. 1995; Urbatsch et al. 1994) was suggested to be due to uncoupling of ATPase from drug transport (Al-Shawi et al. 2003). Upon substrate binding, ATPase activity is increased by 3-4-fold (Martin et al. 1997; Senior et al. 1995), and in some cases up to 20-fold (Ambudkar et al. 1992). However, the modulation of P-gp ATPase activity by substrates and modulators occurs in a complex manner (Sharom 2008; Sharom 2011). In fact, some drugs stimulate P-gp ATPase activity, whereas others inhibit it, and a biphasic pattern of stimulation at low concentrations and inhibition at higher concentrations is also common (Garrigos et al. 1997; Litman et al. 1997a). The explanation for these effects is not completely understood, although the biphasic pattern might be a consequence of the presence of two drug-binding sites, a high-affinity stimulatory site and a low-affinity inhibitory site (Litman et al. 1997b). Moreover, since drug transport is driven by ATP hydrolysis, there must be conformational communication between the drug-binding pocket and the catalytic site. This was demonstrated by a study in which a fluorescent probe located close to the site of ATP binding displayed a change in its local environment following drug binding to the TM regions of the protein (Liu and Sharom 1996). Moreover, the increase in ATPase activity (and presumably transport) in the presence of a drug was negatively correlated with the predictive degree of hydrogen bonding of substrate in the drug-binding pocket (Omote and Al-Shawi 2006). Substrates with extensive H-bonding (daunorubicin) showed low ATPase stimulation and low transport rates, whereas substrates with low levels of H-bonding (e.g. spin-labelled verapamil) caused high ATPase stimulation and high transport rates. Furthermore, substrate mediated ATPase activity is both cell and species dependent. For example, vinblastine inhibits P-gp-mediated ATPase activity in Chinese hamsters (Shapiro and Ling 1994; Sharom et al. 1995; Urbatsch et al. 1994), but increases it in human KB cells (an epithelial carcinoma cell line) (Shapiro and Ling 1994; Sharom et al. 1995; Urbatsch et al. 1994). This may reflect differences in the amino acid sequences of P-gp in hamster and human cells, or differences in the lipid composition of their plasma membranes. With regard to the latter, P-gp localization and function are indeed critically dependent on their lipid environment (Doige et al. 1993;

Kamau et al. 2005) and, thus, the presence of different lipids and detergents on the membrane also affects the drug interaction pattern (Doige et al. 1993; Urbatsch and Senior 1995).

Additionally, the stoichiometry of ATP hydrolysis relative to substrate transport is a controversial issue, and it is still not known whether P-gp hydrolyses one or two molecules of ATP for each drug molecule it transports (Sharom 2011). Indeed, it was initially proposed that one molecule of substrate is effluxed at the expense of two ATP molecules (Gottesman and Pastan 1993). Some important mechanistic insights, into the catalytic cycle of the protein, were provided by the use of ortho-vanadate (V_i), an inorganic phosphate analogue (Sharom 2008; Sharom 2011). Addition of V_i in the presence of ATP leads to very rapid loss of ATPase activity, thus inhibiting P-gp catalytic activity. After a single catalytic turnover, Pi dissociates, and V_i takes its place, leading to 'trapping' of the stable complex $ADP{\cdot}V_i{\cdot}Mg^{2+}$ in one NBD (Urbatsch et al. 1995b). The V_i-trapped complex is very stable, and its structure is thought to resemble that of the catalytic transition state (Smith and Rayment 1996). Thus, the V_i-trapped state represents a post-hydrolysis conformation of P-gp. Since trapping of V_i in one NBD abolishes the catalytic activity at the other (Urbatsch et al. 1995b), as does the inactivation of one active site by mutation or covalent modification (Loo and Clarke 1995b), it is suggested that both active sites must be functional for ATP hydrolysis to occur (Sharom 2011). This observation led to the proposal that P-gp operates by an 'alternating sites' mechanism, in which only one NBD is catalytically active at any instant in time, and the two active sites take turns in hydrolysing ATP, thus alternating in catalysis (Senior et al. 1995). Thus, if one site is inactivated, catalysis halts after a single round of ATP turnover. Moreover, the NBDs have a similar affinity for ATP, and hydrolyse it at comparable rates (Loo and Clarke 1995a; Urbatsch et al. 1995a; van Veen et al. 1998). In the absence of a P-gp substrate, both NBDs are occupied with either ATP or ADP in the resting and transition states (Qu et al. 2003). Thus, the "vacant" active site in the vanadate-trapped complex of P-gp can bind ATP despite its lack of catalytic turnover (Qu et al. 2003).

Sauna et al. described the catalytic cycle of P-gp as comprising two cycles where substrate and nucleotide binding sites co-ordinately function to efflux the substrates by an ATP driven energy-dependent process. The drug and ATP initially bind to the protein at their own binding sites, where nucleotide hydrolyses to ADP occurs, yielding energy for the drug extrusion. The release of ADP from nucleotide binding site ends the first catalytic cycle, which is followed by a conformational change that reduces affinity for both substrate and nucleotide. The second catalytic cycle starts with the hydrolysis of another molecule of ATP and the released energy is used to reorient the protein to its native conformation. Subsequent release of ADP completes another catalytic cycle, returning the P-gp

molecule back to the original state, where it again binds to both substrate and nucleotide to initiate the next cycle (Sauna and Ambudkar 2001).

It was also shown that ATP binding, rather than ATP hydrolysis, induces a conformational change in the tertiary structure of P-gp (Rosenberg et al. 2003), bringing TMHs 1 and 11 into close proximity (Loo et al. 2005). As this interaction does not occur in the presence of ADP or AMP-PNP (5'-adenylyl-β,γ-imidodiphosphate, a competitive inhibitor of most ATP-dependent systems), it was proposed that this conformational change may be involved in the release of substrates following ATP hydrolysis (Loo et al. 2005). ATP binding also reduces the binding affinity of P-gp for its substrate (Martin et al. 2001; Rosenberg et al. 2001). Despite this, the general, but not unanimous consensus would be that ATP hydrolysis rather than ATP binding is required for substrate transport across the cell membrane (Al-Shawi et al. 2003; Hyde et al. 1990; Omote and Al-Shawi 2006; Senior et al. 1995), and that ATP hydrolysis promotes rotation of one or more transmembrane α-helices (Loo and Clarke 2001a).

There is unequivocal biochemical evidence to support a conformational change in P-gp upon substrate binding, including changes in epitope accessibility (Druley et al. 2001; Mechetner et al. 1997; Ruth et al. 2001; Sonveaux et al. 1999) and vulnerability to protease degradation (Julien and Gros 2000; Wang et al. 1998a). Liu and Sharom eloquently associated substrate binding to quench fluorescence within the NBDs (fluorescently tagged P-gp), thus linking the drug-binding pocket to a conformational change in the catalytic site of the NBD (Liu and Sharom 1996). Indeed, and as mentioned, substrate binding brings the Walker A sequences of one NBD close to the signature C motif of the other NBD (Loo et al. 2003a), such that the two NBDs interlock, with ATP interposed along the dimer interface. Interestingly, the conformational change, which leads to drug-mediated ATP hydrolysis, appears to be co-ordinated through residue 339 within TMH 6 (Rothnie et al. 2005). These studies are consistent with the low resolution electron crystallographic data showing a significant conformational change in the 3D structure of P-gp in the presence of the non-hydrolysable ATP analogue, AMP-PNP. In effect, binding of the ATP analogue caused the cylindrical, barrel-like structure of P-gp to reorganise into three compact domains, each with a diameter of 2-3 nm and a depth of 5–6 nm (Rosenberg et al. 2003).

Moreover, the stable nucleotide sandwich dimer structures reported for various ABC proteins and isolated NBDs have only been observed when ATP hydrolysis is blocked by either mutation of an essential catalytic residue or the absence of Mg^{2+}, not in situations where the proteins are catalytically active (Eckford and Sharom 2009). However, both mutational studies (Loo and Clarke 1995a) and the presence of trapped V_i at a single active site (Urbatsch et al. 1995b), suggest that the two NBDs of P-gp alternate in

hydrolysis. This, in turn, implies that the protein must always form asymmetrical structures during catalytic cycling, or the “memory” of which of the two active sites last hydrolysed ATP would be lost (Eckford and Sharom 2009). Tombline and co-workers were the first to isolate an asymmetric nucleotide-bound structure of P-gp by employing the catalytically inactive mutant E552A/E1197A (Tombline et al. 2004; Tombline et al. 2005). They found that this protein retained a single molecule of ATP where the binding affinity is approximately 50-fold higher than normally observed. This nucleotide is observed to be tightly “occluded” within the active site and, unlike loosely bound ATP, cannot be removed by washing or column chromatography. It was later reported that a single molecule of the non-hydrolysable nucleotide adenosine 5′-(γ-thio)triphosphate (ATPγS) is occluded within wild-type catalytically active P-gp (Sauna et al. 2007), again suggesting the existence of an asymmetric nucleotide-bound state. More recently, fluorescence spectroscopic approaches were used to characterize an asymmetric nucleotide-bound state of wild-type P-gp where two molecules of ATPγS are bound, one with the normally observed low affinity and one with 100-fold higher binding affinity (Siarheyeva et al. 2010). ADP and other non-hydrolysable analogues, including AMP-PNP, are not able to induce the asymmetric state, and both nucleotide molecules are bound with low affinity (Siarheyeva et al. 2010). The asymmetric intermediate is thought to exist transiently during the normal catalytic cycle, but the tightly bound ATP molecule is committed to hydrolysis and rapidly enters the transition state. It only appears possible to trap the asymmetric intermediate in stable form using ATPγS, or by inactivating an amino acid residue that is required for catalysis (Eckford and Sharom 2009). Moreover, this P-gp intermediate with one very tightly bound nucleotide (‘occluded’) and one loosely bound nucleotide (Sauna et al. 2007; Siarheyeva et al. 2010; Tombline et al. 2004; Tombline et al. 2005), probably represents an E•S (enzyme•substrate) intermediate normally present immediately before occurring the ATP hydrolysis (Siarheyeva et al. 2010).

According to what was described until now, many studies have been focused on fully clarifying the mechanistic details of how the P-gp NBDs hydrolyse ATP, and how drug transport is powered. Moreover, the crystal structures determined for mouse (Aller et al. 2009) and C. elegans (Jin et al. 2012) P-gp and other ABC transporters (Zolnerciks et al. 2011) have provided structural information about several aspects of substrate binding, transport, and ATP hydrolysis (Al-Shawi 2011; Callaghan et al. 2006). However, the drug transport mechanism of P-gp still remains controversial. Figure 7 shows a proposed catalytic cycle for P-gp that incorporates what is known about ATP binding, stoichiometry and affinity, NBD dimerization, and the occluded state where nucleotide is tightly bound at one of the active sites. The catalytic cycle starts with P-gp containing two ATP molecules, both bound with low affinity (ATP_L) (Figure 7, A). This state is stable and has been

observed in situations where catalysis is blocked, such as in fluorescently modified P-gp with no catalytic activity bound to native ATP (Liu and Sharom 1996) and in native active P-gp bound to fluorescent (Qu et al. 2003) or to spin-labelled (Delannoy et al. 2005) nucleotide analogues that are very poor substrates for hydrolysis by the protein. In this conformation, both halves of the NBD dimer interface are “open”, resulting in low ATP binding affinity (Km of 0.2-0.5 mM) (Figure 7, A) (Eckford and Sharom 2009). In catalytically active P-gp, the dimer interface rapidly closes around one of the bound ATP molecules, which becomes occluded (ATP_T), resulting in 50- to 100-fold higher binding affinity (Km of 5-10 µM) (Figure 7, B). This asymmetric nucleotide-bound state of P-gp is normally transient but can be stabilized by the use of the non-hydrolysable analogue, ATPγS (Sauna et al. 2007) and by mutation of an essential Glu residue in the catalytic sites (Tombline et al. 2004; Tombline et al. 2005). In native P-gp, the tightly bound ATP molecule is committed to be hydrolysed and rapidly enters the transition state. The drug to be transported binds to the substrate-binding pocket of P-gp, which is located within the cytoplasmic leaflet of the membrane (Figure 7, C). This step is arbitrarily shown as occurring after ATP loading and formation of the asymmetric occluded state, but it is known that ATP binding and drug binding can take place in any order, and (uncoupled) ATP hydrolysis can take place in the absence of transport substrate (Liu and Sharom 1996). The tightly bound ATP is then hydrolysed to ADP and Pi, and the transport substrate is moved to either the opposite side of the membrane or the outer leaflet of the bilayer (Figure 7, D). (see I.4.2.1). Hydrolysis of ATP at the occluded site results in opening of the dimer interface in that half (Figure 7, D), likely as a result of electrostatic repulsion between ADP bound to the Walker A motif in one NBD, and Pi bound to the signature C motif of the opposing NBD (Sauna et al. 2007). Opening of one-half of the NBD dimer interface results in simultaneous “site switching”, so that the other half of the dimer interface now becomes closed (Figure 7, D). The product (ADP) is thus loosely bound, and the second ATP molecule now interacts with high affinity and becomes occluded (Figure 7, D). Pi leaves from the open half of the dimer interface, and nucleotide exchange takes place, so that ADP is replaced by ATP, both loosely bound (Figure 7, E). At this stage, the protein has attained the asymmetric nucleotide-bound state once again (Figure 7, F). It reloads with drug, and the steps repeat, with ATP hydrolysis taking place at the other catalytic site (Figure 7, G - I). During active cycling, all the reaction intermediates are asymmetric, thus providing “memory”. The simultaneous ATP site affinity switch ensures that catalysis alternates between the two NBDs (Figure 7) (Siarheyeva et al. 2010). Movement of drug across the membrane may be driven by the energy released during ATP hydrolysis, and would involve switching from an inward-facing conformation with high drug-binding affinity to an outward-facing conformation with

low drug-binding affinity (Figure 7) (Siarheyeva et al. 2010). Other models for the mechanism of ABC transporters function have also been proposed, in which ATP binding alone drives drug transport [ATP switch model (Higgins and Linton 2004)], or two ATP molecules are hydrolysed sequentially to open both halves of the NBD dimer interface [processive clamp model (Janas et al. 2003)].

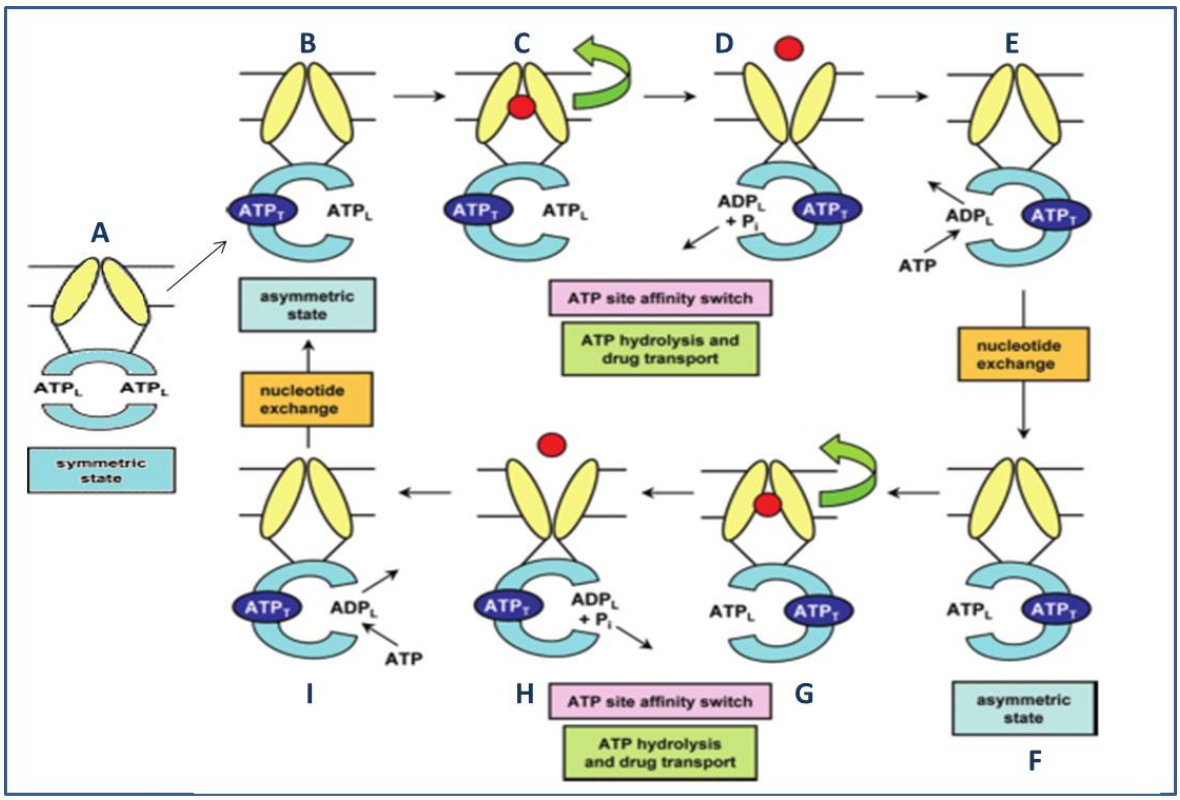

Figure 7. The P-gp catalytic and transport cycle - proposed cycle of ATP-driven NBD dimerization, ATP occlusion and hydrolysis, site-switching of nucleotide binding affinity, and drug transport across the membrane.

The cycle starts with binding of two molecules of ATP to the pump. If the protein is catalytically inactive, or a non-hydrolysable ATP analogue such as AMP-PNP is employed, this binding is of relatively low affinity (loosely bound ATP is indicated by ATP_L). In this symmetric state, both halves of the dimer interface are 'open', with each binding or occluding an ATP_L. If the pump is catalytically active, this state rapidly progresses to the asymmetric state, in which one ATP molecule is tightly bound or occluded (ATP_T) in one NBD, where the dimer interface is 'closed'. The tightly bound ATP molecule is committed to enter the catalytical transition state and undergoes hydrolysis, which provides the energy for drug (red sphere) movement from the binding pocket within the transporter to the extracellular space. Binding of the drug is shown after ATP binding, but these events can take place in a random order. ATP hydrolysis converts the tightly bound ATP to ADP and Pi, which are now loosely bound (ADP_L), resulting in opening of the dimer interface, and the drug is transported to the extracellular environment (or possibly the outer leaflet of the membrane). Drug transport probably involves a conformational change from an inward-facing to an outward-facing protein conformation. The other catalytic site simultaneously switches to the high-affinity state, resulting in tight binding of the second ATP molecule and closure of the dimer interface in the other NBD. In fact, the presence of ADP and Pi leads to opening of the closed dimer interface and simultaneous site switching, so that the opposing half of the dimer interface closes around the second ATP molecule, which is now occluded. It is known that Pi leaves the catalytic site first, after which the loosely bound ADP (ADP_L) dissociates and is replaced by another molecule of loosely bound ATP (nucleotide exchange). The asymmetric nucleotide-bound state is thus attained again, but with the tightly bound ATP in the opposing active site committed to hydrolysis. A second round of ATP hydrolysis and drug transport then takes place at the other NBD. P-gp exists in an asymmetric state at all stages of the catalytic cycle, thus requiring that the two NBDs alternate in hydrolysing ATP. Moreover, during catalytic cycling, at no point does P-gp exist in a symmetric nucleotide-bound state, thus providing "memory" and ensuring that the two active sites alternate in catalysis. Adapted from (Siarheyeva et al. 2010).

In agreement, the recently reported mouse P-gp apo crystal structure (nucleotide-free state) assumes that large openings to the cytoplasm and the inner leaflet of the lipid bilayer are used for compound entry, but substrate access is blocked from the outer membrane leaflet and the extracellular compartment (Aller et al. 2009) (Figure 8). This inward-facing conformation represents the molecule in a pre-transport state since it was demonstrated drug binding to an internal cavity open to the inner leaflet/cytoplasm. Therefore, compounds must be sufficiently membrane permeable to be accessed by P-gp, which scans for substrates by sampling a wide cross section of conformations. Once bound to the protein, the substrate (such as QZ59 compounds and verapamil used in the study) then induces binding of two molecules of ATP triggering a large conformational shift resulting in an outward-facing cavity and ejection of the substrate into the extracellular space. Hydrolysis of ATP then returns the protein back to its inward facing drug binding conformation and reinitiates the transport cycle (Figure 8). Moreover, this conformation likely represents an active state of P-gp because protein recovered from crystals had significant drug-stimulated ATPase activity (Aller et al. 2009).

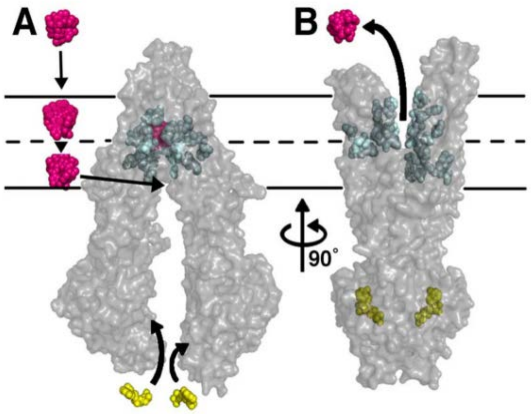

Figure 8. Model of substrate transport by P-gp **(A)** Substrate (magenta) partitions into the bilayer from outside of the cell to the inner leaflet and enters the internal drug-binding pocket through an open portal. The residues in the drug binding pocket (cyan spheres) interact with QZ59 compounds and verapamil in the inward facing conformation. **(B)** ATP (yellow) binds to the NBDs causing a large conformational change presenting the substrate and drug-binding site(s) to the outer leaflet/extracellular space. In this model of P-gp, which is based on the outward facing conformation of MsbA and Sav1866, exit of the substrate to the inner leaflet is sterically occluded providing unidirectional transport to the outside. Taken from (Aller et al. 2009).

In accordance, the putative drug transport route in the recently reported X-ray crystal structure of *Caenorhabditis elegans* also proposed that P-gp is open to the cytoplasmic side of the membrane, thus also suggesting that drugs can enter the pocket from the inner membrane leaflet (Jin et al. 2012). This intimate connection with the membrane suggests that the transporter may be profoundly affected by the physicochemical properties of the host bilayer. Indeed, and as previously mentioned, membrane composition and biophysical properties are known to affect P-gp function. For example, P-gp ATPase activity is modulated by both membrane lipids and detergents (Doige et al. 1993; Li-Blatter et al. 2009; Urbatsch and Senior 1995). The binding affinity of reconstituted P-gp for drug substrates is sensitive to phospholipid headgroup, acyl chain length, and lipid fluidity (Romsicki and Sharom 1999). Inclusion of cholesterol in the

host bilayers was also found to affect drug binding, drug transport, and ATPase activity (Eckford and Sharom 2008). Also, a decrease in the lateral packing density of the bilayer has been proposed to influence the thermodynamics of ATP hydrolysis (Aanismaa et al. 2008).

Early work showed that P-gp transport function in plasma membrane vesicles and intact cells could be altered by changes in membrane fluidity induced by small molecule fluidizers, surfactants, and amphiphiles (Callaghan et al. 1993; Sinicrope et al. 1992; Woodcock et al. 1992). The mechanism of MDR reversal in this case does not appear to involve direct interaction between these agents and P-gp and may be linked to increases in membrane permeability (Drori et al. 1995) (see I.6.1.2.3). From these studies, it has been proposed that changing the properties of the membrane may be a useful approach for clinical MDR reversal (Regev et al. 1999). If such a strategy is to be successful, it is clearly important to have a good understanding of how the properties of the lipid environment affect all aspects of the P-gp catalytic cycle.

In a very recent study, using purified P-gp reconstituted into phospholipid bilayers with defined gel to liquid-crystalline melting transitions, the authors aimed to investigate the effect of membrane environment on the transporter, as well as three of its substrates. Although several studies demonstrated that membrane phase state, composition, and fluidity appear to be important parameters in the ability of P-gp to bind and transport drugs, the means by which membrane properties affect P-gp function are not fully understood. The obtained results demonstrated that Hoechst 33342, LDS-751, and MK-571 partitioned much more readily into liquid-crystalline phase bilayers than into gel phase bilayers, although drug binding affinities revealed that P-gp bound the three substrates more tightly when the lipid bilayer was in the gel phase. The binding affinity of the transporter for substrates within the bilayer was low, suggesting that it interacts with them weakly. Thermodynamic analysis revealed that both drug-P-gp and drug-lipid interactions contribute to binding affinity. Moreover, transport rates were found to be sensitive to both drug structure and lipid environment. It was also suggested that the rate of drug transport depends on both the affinity of P-gp for substrate and protein conformational changes (Clay and Sharom 2013). Therefore, transport rates do not appear to be limited exclusively by the rate of ATP hydrolysis and may be partially controlled by the rate of drug dissociation.

In conclusion, in spite of the controversy, it is generally believed that P-gp exists in at least two major conformations during the catalytic cycle, an “inward-facing” conformation with the high affinity drug binding pocket exposed to the cytoplasmic leaflet of the membrane and an “outward-facing” conformation in which the drug binding site has a lower affinity and is exposed to the outer leaflet or extracellular space. Conversion of the

inward-facing conformation to the outward-facing conformation requires hydrolysis of ATP, whereas subsequent nucleotide exchange and/or product release involving one (or both) NBD(s) is presumed to reset the transporter to the transport (Verhalen et al. 2012).

I.5. Role of P-glycoprotein in drug pharmacokinetics - importance in drug therapy and disease

As previously referred, P-gp interacts with many drugs in widespread clinical use (Table 4). Therefore, the clinical effectiveness of these drugs is greatly affected by P-gp, which alters their absorption and tissue distribution (Zhou 2008). As expected, P-gp-knockout mice displayed increased uptake of substrates from the digestive tract and markedly slower elimination from the circulation, which, for some drugs or xenobiotics, leads to dramatically increased toxicity (Liu et al. 2002a). Noteworthy, P-gp-knockout mice have proved to be very useful in the study of the role of mdr1-type P-gp in tissue accumulation and toxicity of various compounds, as well as in identifying or confirming drugs as P-gp substrates *in vivo* (Johnson et al. 2001a; Jonker et al. 1999; Liu et al. 2002a; Rao et al. 1999; Schinkel et al. 1997; Schinkel et al. 1994; Schinkel et al. 1996; Smit et al. 1998; Tsuruoka et al. 2001). Additionally, species differences between mouse and human P-gp with respect to substrate specificity appear to be small (Sharom 2011).

Interaction of a drug with P-gp can cause poor uptake in the intestine, thus reducing oral bioavailability, and prevent delivery of drugs to the target organs, such as the brain, which is a severe problem in the treatment of brain diseases. Overcoming the presence of P-gp in the intestinal epithelium is a serious problem in drug discovery, since new drug candidates may be poorly absorbed, making them ineffective clinically. Additionally, it is especially important to screen out P-gp substrates when developing drugs targeted to the brain, since, in most cases, their efficacy depends on their ability to cross the BBB (Sharom 2011). The BBB is formed by the tight junctions that connect the brain endothelial cells, thus restricting the entry of compounds from the circulating blood to the brain via paracellular and transcellular routes (de Boer and Gaillard 2007a; de Boer and Gaillard 2007b). Moreover, it is well established that P-gp, as well as BCRP, localized in the apical/luminal membrane of the brain capillary endothelial cells are a major barrier for brain penetration of drugs (Terasaki and Ohtsuki 2005). Since a vast number of drugs are P-gp substrates (e.g. cancer and antiviral drugs), it is quite hard to achieve drug concentrations in therapeutic levels for certain central nervous system conditions such as brain tumours and HIV (Zhou 2008). To circumvent the limited access of drugs into the brain, different approaches have been investigated, including not only the use of P-gp modulators, but also the use of drug delivery systems such as liposomes, nanoparticles,

peptide-vector strategies, modulators of endothelial tight junctions, or osmotic pressure modification (Zhou 2008). Also, it is important to keep in mind that oxidative stress can change P-gp expression in brain capillary-endothelial cells, as well as diseases can up- or down-regulate P-gp and other active transcellular transport systems in the BBB (de Boer et al. 2003). Apart from brain and intestinal P-gp, the protein localized in the apical membrane of renal epithelial cells exports compounds from the cytoplasm of renal tubular cells to the urine and, consequently, its substrates are expected to have a higher renal elimination than that expected by glomerular filtration (Zhou 2008).

Many studies have been undertaken to investigate the effects resulting from the co-administration of a P-gp inhibitor and a known P-gp substrate on blood plasma concentrations (Mealey 2004). Studies have been performed using P-gp knockout mice that were orally administered with P-gp substrates such as digoxin, opioids, paclitaxel, cyclosporine, and many others, and the obtained results have consistently shown that, in P-gp knockout mice, the plasma levels of these P-gp substrates are greatly enhanced. Similarly, in human studies, the administration of a P-gp inhibitor before taking an oral dose of morphine showed a 2-fold increase in blood plasma levels of morphine, when compared with those receiving an oral morphine dose alone (Mealey 2004). Therefore, this evidence indicates that P-gp activity in intestinal epithelial cells greatly influences the bioavailability of many drugs and highlights that: (i) P-gp seems to have a substantial role in pumping drugs out of epithelial cells after absorption and back into the intestine for excretion; (ii) decreased P-gp activity in the intestine can lead to dramatically increased drug bioavailability; and (iii) increased P-gp activity, due to a variety of factors such as drug interactions or genetic mutations of the *MDR1* gene, could possibly lead to therapeutic failure for a wide range of drugs that are P-gp substrates (Zhou 2008).

The co-administration of two drugs that are both P-gp substrates can also lead to major pharmacokinetic effects as they compete for the transporter (Staud et al. 2010). Plasma drug levels remain higher for longer periods of time, and a reduction in drug dose is often necessary to avoid toxicity. In patients, these drug-drug interactions are indeed very frequently a risk and can result in side-effects as simple as minor discomfort to the patient, or in extreme cases of life-threatening toxicities (Zhou 2008). Similar effects are observed when a P-gp substrate drug is used with foods or herbal supplements containing natural products that are also P-gp substrates, such as plant flavonoids or St John's wort (Borrelli and Izzo 2009). Therefore, the importance of P-gp in drug-drug interactions is increasingly being identified and it is generally accepted that co-administration of drugs that interact with this transporter not only as a substrate, but also as inhibitor or inducer, can result in drug-drug interactions that affect the pharmacokinetics and pharmacodynamics of the co-administered drugs. For these reasons, it is now

recommended, in the process of drug development and approval, the testing for P-gp interactions (Giacomini et al. 2010). These tests usually use polarized monolayers of epithelial cell lines either transfected with human P-gp, or naturally expressing the pump, and the movement of the test compound from the medium on the basolateral side of the monolayer to the medium on the apical side (B→A, passive diffusion plus P-gp-mediated efflux) is compared with the movement in the opposite direction (A→B, passive diffusion only). Also, other *in vitro* assays that assess the effect of a compound on P-gp ATPase or transport activity in membrane vesicles are also frequently used (Sharom 2011).

It should be also reinforced the role of P-gp in the cancer treatment, which will be further detailed in section I.6.1. For several cancers, including AML (acute myelogenous leukaemia), ALL (acute lymphoblastic leukaemia) and ovarian tumours, high P-gp expression levels are strongly linked to a weak response to chemotherapy treatment, since many anticancer drugs are P-gp substrates, and, consequently to a poor overall disease prognosis (Polgar and Bates 2005; Steinbach and Legrand 2007). However, in other cases, it has proved difficult to link MDR in cancer to P-gp expression, probably because there are multiple mechanisms by which some tumours can develop drug resistance. Furthermore, there has been much interest in combining P-gp modulators with chemotherapy drugs to improve the outcome of cancer treatment (Szakacs et al. 2006).

In conclusion, P-gp affects the disposition of many clinically administered drugs, having a major contribution to their ADME (absorption, distribution, metabolism and excretion) and, consequently, being implicated in potential pharmacokinetic drug-drug interactions (Lin and Yamazaki 2003a; Lin and Yamazaki 2003b; Mealey 2004; Zhou 2008). P-gp is of particular importance at the intestinal epithelium where it plays an important role in the extrusion of drugs from the blood into the intestinal lumen, and in preventing drugs in the intestinal lumen from entering the bloodstream, thus reducing their absorption and oral bioavailability (Zhou 2008).

I.6. P-glycoprotein inhibition, induction and activation

I.6.1. P-gp inhibition

As previously mentioned, drug resistance is considered the major cause of failure in anticancer therapy (Lage 2008). In fact, in spite of all the progress made in this field, only approximately 50% of all cancers are susceptible to chemotherapy and, of these, more than 50% rapidly develop drug resistance (Higgins 2007). Multidrug resistance (MDR) may be defined as a phenomenon whereby cancer cells that have been exposed to one type of drug develop cross resistance to other drugs that are structurally and functionally very dissimilar (Pauwels et al. 2007)

Several mechanisms were reported to play an important role in the complex phenomenon of MDR such as: induction of the efflux systems (P-gp); altered expression or function of target proteins (e.g. topoisomerase and tubulin; induction of detoxification pathways (e.g. glutathione-S-transferase that catalyse the conjugation of glutathione and drugs); enhanced DNA repair; and alterations in the apoptotic signal pathway (e.g. p53 mutation and bcl-2 overexpression) (Baguley 2002; Higgins 2007; Lage 2008; Lehnert 1996; Merino et al. 2004; Modok et al. 2006; Pauwels et al. 2007; Perez-Tomas 2006; Szakacs et al. 2006; Wu et al. 2008). Some of these mechanisms may coexist, rendering the cells refractory to treatment with drugs acting on a single target. Noteworthy, among the mechanisms of MDR reversal, the direct inhibition of P-gp is one of the best studied, and emerged, in 1981, with the demonstration that verapamil could reverse MDR (Tsuruo et al. 1981). In fact, over the past years, the therapeutic use of P-gp inhibitors to improve drug bioavailability by inhibiting P-gp in intestine, brain, liver and kidneys has gained considerable interest. Since this recognition that P-gp-mediated drug resistance is clinically important, a concerted research effort to screen for P-gp inhibitors or modulators has been extensively carried out, indicating the possibility of identifying clinically useful reversing agents for MDR. In the following section, an overview on the different generations of P-gp inhibitors, and on their corresponding mechanisms of action, will be presented.

I.6.1.1. Mechanisms of P-gp inhibition

A P-gp inhibitor may act by **(a)** blocking the substrate binding-site(s), either competitively, non-competitively or allosterically (Varma et al. 2003); **(b)** interfering with ATP hydrolysis (Shapiro and Ling 1997a) or **(c)** altering the integrity of cell membrane lipids (Drori et al. 1995) (Figure 9). There are currently many drugs that act as P-gp inhibitors, some of which are in use as therapeutic agents for other clinical indications (Table 5).

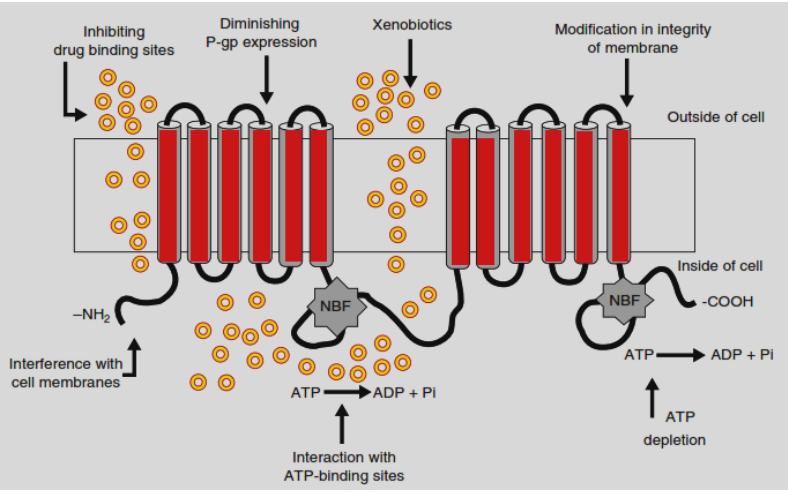

Figure 9. Mechanisms of P-gp inhibition.
Adapted from (Akhtar et al. 2011).

The calcium channel blocker, verapamil, and the immunosuppressant, cyclosporine A, are P-gp substrates that competitively inhibit the efflux pump (Miller et al. 1991; Slater et al. 1986; Tsuruo et al. 1981). Although these drugs inhibit the pump function by blocking the drug binding sites, the presence of multiple binding sites complicates the understanding, as well as hampers the development of conclusive structure-activity relation studies for substrates or inhibitors. On the other hand, compounds that inhibit ATP hydrolysis could perform better as P-gp inhibitors, since they are unlikely to be transported by P-gp, and will require a lower dose, for instance, locally at the gut lumen (Varma et al. 2003). For example, quercetin, a naturally occurring flavonoid, demonstrated to block P-gp function by, at least in part, interfering with the P-gp ATPase activity required for transport (Shapiro and Ling 1997a). Moreover, since none of the P-gp substrates had, until recently, demonstrated to interact with the nucleotide binding sites, thus not interfering with the P-gp ATPase catalytic cycle (Varma et al. 2003), further research in exploring the mechanism of ATP hydrolysis inhibition will likely provide newer and better inhibitors with potent and specific activity.

Finally, many commonly used pharmaceutical surfactants, such as sodium dodecyl sulphate, Tween-20 and Span-80, are emerging as a different class of P-gp inhibitors, which act by altering integrity of membrane lipids, thus interfering with membrane fluidity (Prakash 2010). This alteration in the membrane's microviscosity may, in fact, contribute to the alteration of the conformation of most transmembrane proteins and, therefore, modifications in secondary and tertiary structure were found to be the reason for loss of P-gp function due to disturbance in hydrophobic environment caused by surfactants (Varma et al. 2003). In the next section, a detailed overview will be made on the different generations of P-gp inhibitors, which greatly differ on their corresponding mechanism of action.

I.6.1.2. P-gp inhibitors

P-gp inhibitors are classified into four generations according to their potency, selectivity and drug-drug interaction potential, and not according to a chronologic development (Table 5) (Palmeira et al. 2012a).

Table 5. Known P-gp inhibitors

Class	Examples
First-generation	
Analgesics	Meperidine, Pentazocine
Anesthetics	Chloroform, Benzyl alcohol, Diethyl ether, Propofol
Antibiotics:	Cefoperazone, Ceftriaxone, Salinomycin, Nigericin, Erythromycin, Azithromycin, Brefeldin A, Bafilomycin, Clarithromycin, Valinomycin

Table 5. Known P-gp inhibitors

Class	Examples
Anticancer Drugs	Tamoxifen, Bicalutamide, Mitotane, Gefitinib, Lapatinib, Erlotinib, Lonafarnib (SCH 66336), Tipifarnib, Vinblastine
Antifungals	Itraconazole, Ketoconazole, Econazole, Dihydroptychantol A, Aureobasidin A
Antihistaminics	Benzquinamide, Azelastine, Tesmilifene, Astemizole, Terfenadine
Anti-inflammatory drugs	Zomepirac, Indomethacin, SC236, Curcumin, Ibuprofen, NS-398
Antidepressants	Amoxapine, Loxapine, Sertraline, Paroxetine, Fluoxetine
Antimalarial drugs	Quinine
Antiprotozoal drugs	Hycanthone, Monensin, Metronidazole
Antiviral drugs	Concanamycin A, Ritonavir, Nelfinavir, Saquinavir
Anxiolytics and sedative-hypnotics	Midazolam
Cardiac/circulation drugs	**Antiarrhythmics:** Amiodarone, Propafenone, Quinidine **Calcium channel blockers**: Verapamil, Deverapamil, Emopmil, Nifedipine, Nicardipine, Niguldipine, Nitrendipine, Nimodipine, Felodipine, Isradipine, Lomerizine, Tetrandrine, Mibefradil, Diltiazem, Bepridil **Antiplatelet drug:** Dipyridamole **Antihypertensives**: Reserpine, Prazosin, Doxazosin, Carvedilol
Central nervous system stimulators	Caffeine, Pentoxifylline, Nicotine, Cotinine,
Cholesterol-lowering drugs	Atorvastatin
Immunosuppressive drugs	Cyclosporin A, Tacrolimus, Sirolimus
Neuroleptics and Anti-psychotics	Trans-Flupentixol, Perphenazine, Prochlorpromazine, Chlorpromazine, Trifluoperazine, Perospirone, Haloperidol
Phosphodiesterase inhibitors	Vardenafil
Steroid Hormones	Progesterone, Medroxiprogesterone, Cortisol, Methylprednisolone, Medroxiprogesterone 17-acetate, Mifepristone, Tirilazad, U-74389F, SB4723, SB4769
Others	Tetrabenazine, Bromocriptine, Disulfiram, Methadone,
Second-generation	Dexverapamil, MM36, KR-30031, RO44-5912, PAK-104P, Dexniguldipine, Cinchonine, Hydro-cinchonine, Quinine homodimer Q2, BIBW22BS, Valspodar (PSC-833), Biricodar (VX-710), Timcodar (VX-853), Toremifene, SB-RA-31012 (tRA96023), CGP 42700, WK-X-34, Dofequidar (MS-209), Stipiamide homodimer, S9788
Third-generation	Zosuquidar (LY335979), Tariquidar (XR9576), Elacridar (GF120918), Laniquidar (R101933), Ontogen (OC144-093), DP7, PGP-4008, CBT-1
Fourth-generation	
Natural products	**Flavonoids** (quercetin, tangeretin, nobiletin, sinensetin, baicalein heptamethoxyflavone) **Alkaloids** (pervilleine F, ellipticine) **Coumarins** (cnidiadin, conferone, praeruptorin A, rivulobirin A, DCK) **Cannabinoids** (cannabidiol) **Taccalonolides** (taccalonolides A) **Diterpenes** (jolkinol B, portlanquinol, euphodendroidin D, pepluanin A)

Table 5. Known P-gp inhibitors

Class	Examples
Natural products (cont.)	**Sesquiterpenes** (dihydro-β-agarofuran sesquiterpenes) **Triterpenes** (sipholenone E, uvaol, sipholenol A, oleanolic acid) **Ginsenosides** (20S-ginsenoside) **Polyenes** [pentadeca-(8,13)-dien-11-yn-2-one] **Lignans** (schisandrin A, silibinin, nirtetralin)
Peptidomimetics	Reversin 121, Reversin 205, Peptide 15, XR9051
Surfactants and Lipids	Pluronic P85, tween-20, triton X-100, cremophor EL, poly(ethylene glycol)-300 (PEG-300), Nonidet P40
Dual ligands	Dual inhibitors of P-gp and tumor cell growth [aminated thioxanthones such as 1-[2-(1H-benzimidazol-2yl)ethanamine]-4-propoxy-9H-thioxanthen-9-one]

Data are compiled from (Matheny et al. 2001), (Kim 2002), (Zhou 2008), (Sharom 2011) and (Palmeira et al. 2012a).

I.6.1.2.1. First- and second-generation P-gp inhibitors

First-generation inhibitors are pharmacological active compounds, which are already in clinical use or compounds under investigation for other therapeutic indications, but also showing the ability to inhibit P-gp (Palmeira et al. 2012a; Varma et al. 2003). These include calcium channel blockers, such as verapamil; immunosuppressants, like cyclosporin A; anti-hypertensives, like reserpine, antiarrhythmics, such as quinidine; and antiestrogens, like tamoxifen and toremifen. Therefore, included in this class are not only the classic P-gp inhibitors (verapamil or cyclosporine A) but all compounds that had previously been described as having other main therapeutic applications, other than P-gp inhibition, irrespective of the date of discovery (Palmeira et al. 2012a). Many of these agents are themselves P-gp substrates and, thus, act by competing with the cytotoxic compounds for efflux by P-gp (Figure 10, competitive inhibition) (Varma et al. 2003). However, the clinical use of these compounds is limited by their toxicity, since high serum concentrations are achieved with the dose required for P-gp inhibition, given the low binding affinity for the pump (Varma et al. 2003). For example, the plasma concentrations of 2-6 μM of verapamil required to inhibit P-gp, are associated with serious cardiovascular effects in humans (Ford and Hait 1990).

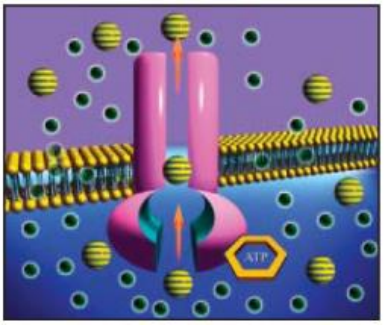

Figure 10. P-glycoprotein inhibition by first- and second-generation inhibitors (competitive inhibition)
First and second-generation inhibitors compete as a substrate with the cytotoxic agent for transport by the pump, limiting their efflux and increasing its intracellular concentration. Adapted from (Thomas and Coley 2003).

Second- and third-generation inhibitors, that specifically modulate P-gp, were then developed to improve the toxicity profile of the first-generation inhibitors. Second-generation inhibitors are analogues of the initial agents (Fox and Bates 2007; Palmeira et al. 2012a), that were developed from compounds with another recognized activity, but which were subjected to structural modifications in order to decrease their main therapeutic activity and increase P-gp inhibitory activity (specifically inhibit P-gp, with less toxicity and greater potency, when compared to the corresponding first-generation inhibitors) (Palmeira et al. 2012a). Therefore, these compounds lack the pharmacological activity of the first-generation compounds, and usually, possess a higher P-gp affinity (Varma et al. 2003). Non-immunosuppresive analogues of cyclosporin A, valspodar (PSC 833); D-isomer of verapamil, dexverapamil; and other compounds such as biricodar (VX-710), timcodar (VX-853) and dofequidar (MS-209), are some of the second-generation inhibitors. The best characterized and most studied of these agents is valspodar, a non-immunosuppressive derivative of cyclosporin A, that inhibits P-gp with 5- to 20-fold greater activity than cyclosporin A (Kusunoki et al. 1998; te Boekhorst et al. 1992; Twentyman and Bleehen 1991). Valspodar has been studied in numerous clinical trials in combination with cytotoxic agents, including etoposide, doxorubicin, mitoxantrone or paclitaxel (Advani et al. 2001; Baekelandt et al. 2001; Baer et al. 2002; Bates et al. 2001; Bates et al. 2004; Bauer et al. 2005; Carlson et al. 2006; Chauncey et al. 2000; Chico et al. 2001; Dorr et al. 2001; Fracasso et al. 2005; Fracasso et al. 2001; Gruber et al. 2003; Kang et al. 2001; O'Brien et al. 2010; Sonneveld et al. 2000).

However, complex and unpredictable drug-drug interactions may be observed for this class of second-generation compounds since they may inhibit two or more ABC transporters (Varma et al. 2003). Therefore, these compounds lack P-gp selectivity, as the compounds from the first-generation. For example, the pipecolinate derivative biricodar citrate (VX-710), which has also undergone extensive clinical development, interferes with drug efflux by directly binding with high affinity to P-gp (Germann et al. 1997a; Germann et al. 1997b) and also by inhibiting the ABC transporter MRP1 (Yanagisawa et al. 1999). Also, S9788 is 1.5 to 30 times more active than verapamil and 1.2 to 120 times more active than cyclosporine A but was also found to inhibit BCRP (Merlin et al. 1994; Merlin et al. 1995). This interaction of many second-generation modulators with other transporters, particularly those of the ABC transporter family, can lead to a decreased cell capacity to extrude toxic compounds or xenobiotics in the liver, kidney, or gastrointestinal tract (Sharma et al. 2003). For example, the inhibition of BCRP, a functional regulator of hematopoietic stem cells, may lead to serious adverse effects, including neutropenia and other myelotoxic effects (Bunting 2002).

Although second-generation P-gp inhibitors have a better pharmacologic profile, when compared to the first-generation compounds, they retain some characteristics that limit their clinical usefulness. Specifically, these compounds may significantly inhibit the metabolism and excretion of cytotoxic agents leading to unacceptable toxicity, thus requiring chemotherapy dose reductions in clinical trials. In particular, many of these compounds, such as valspodar and biricodar, are substrates for cytochrome P450 (CYP P450), and the competition between chemotherapeutic agents and these P-gp modulators for CYP P450 activity has given rise to unpredictable pharmacokinetic interactions. For example, valspodar demonstrated to inhibit CYP P450 enzymes, resulting in decreased clearance and increased systemic exposure to many cytotoxic agents (Fischer et al. 1998; Wandel et al. 1999), and this pharmacokinetic interaction hampered the clinical use of this P-gp inhibitor. In fact, this interaction with the pharmacokinetics of the associate chemotherapeutic drugs, which results in the chemotherapeutic drug toxicity, may require a dose reduction of the anticancer drug of 30-50% (Chico et al. 2001). Moreover, since the pharmacokinetic interactions between P-gp inhibitors and cytotoxic agents are unpredictable and cannot be determined in advance, reducing the dose of a cytotoxic agent may result in under-dosing, thus limiting the use of these second-generation modulators in the treatment of MDR cancers (Gottesman et al. 2002).

I.6.1.2.2. Third-generation P-gp inhibitors

To overcome the limitations of the first- and second-generation of P-gp modulators, several novel third-generation P-gp blockers were developed by using quantitative structure-activity relationships (QSAR) and combinatorial chemistry (Palmeira et al. 2012a). These P-gp inhibitors were developed primarily with the purpose of improving the treatment of MDR tumours and to inhibit P-gp with high specificity and potency. Among them, zosuquidar (LY335979), elacridar (GF120918), laniquidar (R101933), ontogen (OC144093), tariquidar (XR9576), DP7, PGP-4008 and CBT-1 are the most studied (Palmeira et al. 2012a; Varma et al. 2003). This class of compounds is composed by the most selective and potent P-gp inhibitors known to date, which were obtained by design, and many of them entered in clinical trials (Palmeira et al. 2012a). In fact, these compounds demonstrated a potency approximately 10-fold higher than the first- and second-generation inhibitors (Varma et al. 2003).

Among the most promising third-generation P-gp inhibitors is tariquidar (XR9576), an anthranilamide derivative long described as a specific P-gp inhibitor, which binds to P-gp by a non-competitive mechanism and with an affinity that greatly exceeds that of the transported substrates (Figure 11) (Fox and Bates 2007). In fact, this compound inhibits P-gp ATPase activity, although it is not clear whether its binding on P-gp is directed to the

ATP binding site or to an allosteric location, thus indirectly blocking the P-gp catalytic cycle (Martin et al. 1999). Moreover, it was described that tariquidar binds to the same P-gp site of the P-gp substrate Hoechst 33342 (Martin et al. 2000), located within the inner leaflet of the membrane (Qu and Sharom 2002; Shapiro et al. 1999; Shapiro and Ling 1997c), thus combining both transport and regulatory functions (Qu and Sharom 2002). The P-gp inhibitory effect of this compound largely exceeds those of first- and second-generation P-gp modulators in what concerns to potency and duration of action. In fact, the *in vitro* effect of tariquidar was evaluated using a panel of human (H69/LX4, 2780AD) and murine (EMT6 AR1.0, MC26) MDR cell lines and it potentiated the cytotoxicity of several drugs, including doxorubicin, paclitaxel, etoposide, and vincristine; with a complete reversal of resistance achieved in the presence of 25-80 nM tariquidar (Mistry et al. 2001). Moreover, inhibition of P-gp function was reversible, but the effects persisted for longer than 22 h after its removal, in contrast to P-gp substrates, such as cyclosporin A and verapamil, which lose their activity within 60 min, suggesting that tariquidar is not transported by P-gp (Mistry et al. 2001). Additionally, pharmacokinetic studies in healthy subjects demonstrated that single doses of tariquidar, up to 2 mg/kg intravenously or 750 mg orally, were well tolerated and provided complete P-gp inhibition for at least 24 h, as evaluated by rhodamine 123 accumulation in $CD56^+$ lymphocytes (Stewart et al. 2000). It was also described that nanoparticles or liposomes delivering a combination of this P-gp inhibitor and an anticancer drug (paclitaxel) are a very promising approach to overcome tumor drug resistance (Patel et al. 2011; Patil et al. 2009), which could be correlated with an increased accumulation of paclitaxel in tumor cells.

Elacridar, an acridone-carboxamide derivative, is another third-generation P-gp inhibitor and was initially described as a multi-drug resistance reversal agent (Hyafil et al. 1993), restoring the sensitivity of multidrug resistant tumours to doxorubicin. This compound acts by binding to the allosteric site of P-gp and reverses the drug resistance at the nanomolar range (Akhtar et al. 2011). Moreover, when co-administered with P-gp substrates, such as topotecan and paclitaxel, elacridar improved their oral absorption by inhibiting intestinal P-gp, thereby preventing efflux of substrate drugs into the intestinal lumen (Bardelmeijer et al. 2000; Bardelmeijer et al. 2004; Kruijtzer et al. 2002).

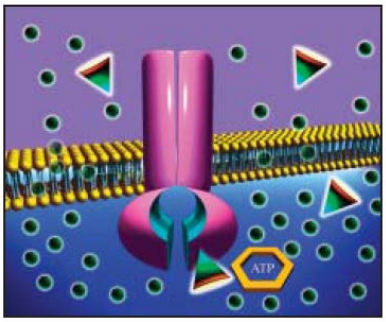

Figure 11. P-glycoprotein inhibition by third-generation inhibitors (non-competitive inhibition).

Third-generation P-gp inhibitors, such as tariquidar, bind with high affinity to the pump, but are not themselves substrates. This induces a conformational change in the protein, thereby preventing ATP hydrolysis and transport of the cytotoxic agent out of the cell, resulting in an increased intracellular concentration. Adapted from (Thomas and Coley 2003)].

However, tariquidar, as well as elacridar, were reported to also bind and inhibit the BCRP transporter (de Bruin et al. 1999; Kelly et al. 2011; Kruijtzer et al. 2002; Robey et al. 2004), thus increasing the potential for pharmacokinetic interactions. In fact, elacridar was reported to enhance the cytotoxicity of anticancer drugs in cells expressing BCRP at a similar potency to that of P-gp (de Bruin et al. 1999; Hyafil et al. 1993). On the other hand, other third-generation agents, such as zosuquidar and laniquidar, demonstrated to be more specific for P-gp, rather than for other ABC transporters, avoiding the risk of blocking other pumps, which might result in altered bioavailability or excretion of the chemotherapeutic agents (Palmeira et al. 2012a). Zosuquidar, which is among the most potent P-gp modulators known to date, inhibits the pump at nanomolar concentrations, both *in vitro* and *in vivo* (Dantzig et al. 2001; Green et al. 2001), and no evidence exist that it may act as a MRP or BCRP inhibitor (Palmeira et al. 2012a). However, its mechanism of P-gp inhibition is still unclear, although a non-competitive inhibitory mechanism has already been suggested, since it is not a substrate and cannot be transported by the pump (Dantzig et al. 1996).

One important feature of the third-generation P-gp inhibitors is that these compounds do not affect cytochrome P450 3A4 at relevant concentrations (Coley 2010a). For example, zosuquidar was demonstrated, *in vivo,* to have a significantly lower affinity for CYP3A than for P-gp, and to lack modulation of MRP1 or MRP2 (Dantzig et al. 1999). As a consequence, changes in the pharmacokinetics of the simultaneously administered antitumor agent are not expected, at least not to the extent verified with the previous generations, and, consequently, a chemotherapy dose reduction is not necessary (Takara et al. 2006).

However, the main disappointing aspect of the third-generation P-gp inhibitors was the unexpected toxic effects observed in several clinical trials [for review see (Palmeira et al. 2012a)]. For example, tariquidar was tested on phase III clinical trials on non-small-cell lung cancer patients but had to be stopped due to the high toxicity observed (Palmeira et al. 2012a). Therefore, in spite of all the progress made in the field of multidrug resistance with the discovery of these MDR modulators (suggested to be more potent and more specific than their precursors) they are still far from being considered perfect MDR modulators capable of effectively and safely overcoming resistance in cancer cells.

I.6.1.2.3. Fourth-generation P-gp inhibitors

Random and focused screening, systematic chemical modifications and combinatorial chemistry performed over the last three decades have given rise to the first three generations of P-gp inhibitors, some of them highly specific and potent. However,

given the several side effects and the pharmacokinetic interactions observed, their clinical use was limited. For this reason, new strategies were employed to find new P-gp inhibitors, such as compounds extracted from natural origins and their derivatives, surfactants and lipids, peptidomimetics and agents with dual activity, which constitute the fourth generation of P-gp inhibitors (Table 5) (Palmeira et al. 2012a).

The products of natural origin obtained for the first time from natural sources and specifically tested for P-gp inhibition are classified by some authors as belonging to the fourth-generation of P-gp inhibitors (Coley 2010b; Palmeira et al. 2012a). This "return" to the research for natural products results from the knowledge that some food components, such as orange, grapefruit, and strawberry, interfere with the oral bioavailability of many drugs, and that these drug-food interactions may involve P-gp. Moreover, starting from the active components of food and plant extracts already identified, several chemical modifications have been performed to generate novel, selective, and high affinity P-gp inhibitors. Among these new natural products, several flavonoids, alkaloids, coumarins, cannabinoids, ginsenosides, diterpenes, sesquiterpenes and triterpenes, among others, have been identified and tested for P-gp inhibition, with very promising results having been obtained [for a review see (Coley 2010b; Palmeira et al. 2012a)]. For example, several methoxyflavones present in orange juice (tangeretin, nobiletin, 3,3',4',5,6,7,8-heptamethoxyflavone) demonstrated to increase the accumulation of [^{3}H]vinblastine in Caco-2 cells, in a concentration-dependent manner, by specifically inhibiting the drug efflux *via* P-gp, and none of these methoxyflavones inhibited CYP3A4 (Takanaga et al. 2000). Also, in another study, tangeretin and nobiletin demonstrated to significantly inhibit P-gp function in human T lymphoblastoid leukemia MOLT-4 and its daunorubicin-resistant cells (Ishii et al. 2010)

Many commonly used pharmaceutical surfactants, such as sodium dodecyl sulphate, Tween-20 and Span-80, are emerging as a different class of P-gp inhibitors, which act by altering the integrity of membrane lipids, thus interfering with membrane fluidity (Prakash 2010). In fact, they seem to cause modifications in P-gp secondary and tertiary structure, resulting in the loss of P-gp functionality function due to interruption in hydrophobic environment by the surfactant molecule (Hugger et al. 2002b). Noteworthy, surfactants such as Pluronic P85, Tween-20, Triton X-100 and Cremophor EL can modulate MDR by inhibiting P-gp-mediated efflux, with no appreciable effect on the transbilayer movement of drugs (Palmeira et al. 2012a). Therefore, surfactants demonstrate a transporter-specific interaction rather than unspecific membrane permeabilization (Regev et al. 2007). Several *in vitro* studies performed in Caco-2 cells and MDR1-MDCK cells have demonstrated that changes in the membrane's microviscosity caused by surfactants, like poly(ethylene glycol)-300 (PEG-300),

cremophor EL and Tween 80, resulted in a significant inhibition of the pump activity (Hugger et al. 2002a; Hugger et al. 2002b; Rege et al. 2002). In those studies, PEG-300 caused an almost complete inhibition of P-gp activity in both Caco-2 and MDR1-MDCK cell monolayers, whereas Cremophor EL and Tween 80 only partially inhibited P-gp activity in Caco-2 cells (Hugger et al. 2002b). PEG induced changes in P-gp activity are probably related to changes in the fluidity of the polar head group regions of cell membranes (Hugger et al. 2002b). Moreover, since many surfactants are already approved for routine use in pharmaceutical formulations, the use of such compounds seems to be an intelligent choice for P-gp modulation. Although, in most of the studies, these compounds were tested *in vitro*, some animal studies are now emerging. For example, Eedara and co-workers performed *ex vivo*, *in situ* and *in vivo* studies to evaluate the dissolution, permeability and oral bioavailability of fexofenadine hydrochloride by preparing lipid surfactant based dispersions. The conducted *ex vivo* permeation studies, using the intestinal gut sac technique, resulted in reduced efflux of the drug by inhibiting intestinal P-gp and the *in situ* perfusion and the *in vivo* pharmacokinetic studies in male wistar rats demonstrated an improved absorption and oral bioavailability from the prepared dispersions, when compared to the pure drug (Eedara et al. 2013). Also, in rats dosed with raloxifene and tocopheryl polyethylene glycol succinate 1000 (TPPG 1000) it was observed an increase in raloxifene oral bioavailability, when compared to control rats (Wempe et al. 2009)

Recently, a growing attention has arisen for the development of multifunctional drugs, with the ability to interact with multiple targets related to a specific pathological condition (Morphy and Rankovic 2009). In a study performed by Palmeira et al. (2012) several aminated thioxanthones were reported as dual inhibitors of cell growth and P-gp (Palmeira et al. 2012c), setting a new opportunity for MDR reversal. According to the obtained results, 1-[2-(1H-benzimidazol-2yl)ethanamine]-4-propoxy-9H-thioxanthen-9-one was the most potent P-gp inhibitor causing, in a P-gp overexpressing cell line (K562Dox cells), an accumulation rate of rhodamine123 similar to verapamil. Additionally, other strategies have been adopted, such as the design of dual ligands to inhibit P-gp and stimulate nitric oxide synthase, as well as inhibitors of more than one transporter from the ABC superfamily (Palmeira et al. 2012a). The first strategy has arisen from the observed reversal of doxorubicin resistance when HT29-dx resistant cells were incubated with inducers of nitric oxide synthesis (Riganti et al. 2005). It was postulated than nitric oxide reduces the number of functionally active P-gp, perhaps by altering the proper conformation of the transporter (Riganti et al. 2005). In what concerns to the development of inhibitors of more than one ABC superfamily transporter, controversial opinions exist. In fact, several P-gp inhibitors, such as elacridar and tariquidar, two of the most potent P-gp

inhibitors found to date, were reported to interact with other ABC transporters, like the BCRP transporter (de Bruin et al. 1999; Kelly et al. 2011; Kruijtzer et al. 2002; Robey et al. 2004). Therefore, this aspect was faced as a disadvantage since it can increase the potential for pharmacokinetic interactions. However, the attempts to develop more effective MDR reversers by discovering P-gp selective compounds have, unsurprisingly, been unsuccessful. Therefore, an alternative targeting multiple efflux pumps, in some instances, may possess a higher therapeutic efficacy than a specific drug (Roth et al. 2004). A selective P-gp inhibitor would be effective if the tumor to be treated is resistant to chemotherapy through P-gp overexpression only. However, if the tumor overexpresses both P-gp and MRP1, for example, it would be of great advantage if a “promiscuous” dual activity drug targeting both transporters is available.

In conclusion, although more than 40 years have passed since the isolation of the first MDR cells (in 1968) and 32 years since the discovery of the first P-gp inhibitor (in 1981), an intense search for a “perfect” P-gp inhibitor, that can efficiently modulate the pump and restore the efficacy of chemotherapy, continues being performed. The demonstrated improved clinical efficacy of various drugs due to P-gp inhibition, especially drugs subjected to MDR, led to the design and development of modulators that more potent and specifically block P-gp efflux, resulting in improved toxicity profiles (Varma et al. 2003). A variety of compounds have been shown to reverse P-gp-mediated MDR and some MDR modulators have been undergoing clinical trials. Table 6 illustrates some examples of improved pharmacokinetics of P-gp substrates obtained with co-administration of P-gp inhibitors. The efforts of several investigators and laboratories spread all over the world, together with the adoption of new strategies, such as using computational techniques as pharmacophore construction or QSAR studies, thus have led to an increasing number of new P-gp inhibitors, many of them derivatives of known P-gp inhibitors, which have been synthetized according to the features that seem to be necessary for P-gp inhibition. However, further clinical investigations are still required to accomplish with the clinical reversal of P-gp-mediated MDR.

Table 6. Examples of improved pharmacokinetics of P-gp substrates with co-administration of P-gp inhibitors.

P-gp substrate	P-gp inhibitor	Experimental model	Pharmacokinetic effect	Literature Reference
First-generation inhibitors				
Etoposide	Cyclosporine A	Cancer patients	When used with a high-dose of cyclosporine A, etoposide doses should be reduced by approximately 50% to compensate the pharmacokinetic effects of cyclosporine A on etoposide;	(Lum et al. 1992)
Daunorubicin	Cyclosporine A	Cancer patients	Interference with daunorubicin pharmacokinetics	(List et al. 1993)
Doxorubicin	Cyclosporine A	Cancer patients	Inhibitor dose-dependent permeability enhancement	(Erlichman et al. 1993)
Mitoxantrone	Quinine	Cancer patients	No life-threatening toxicity was observed with quinine and it was capable of reverting MDR phenotype. Quinine increased the complete remission rate and survival in P-gp-positive myelodysplastic syndromes cases treated with intensive chemotherapy	(Wattel et al. 1998)
Digoxin[a]	Verapamil	Single-pass perfusion in rats	Increase in absorption rate	(Sababi et al. 2001)
Second-generation inhibitors				
Paclitaxel	R-verapamil	Cancer patients	Delayed mean paclitaxel clearance and increased peak concentration	(Tolcher et al. 1996)
Doxorubicin	Valspodar (PSC 833)[b]	Cancer patients	~50% increase in AUC	(Giaccone et al. 1997)
Paclitaxel[c]	Biricodar (VX-710)	Cancer patients	More than 50% decrease in paclitaxel clearance	(Rowinsky et al. 1998)
Paclitaxel	Dofequidar (MS-209)	Rats and mice	1.9- and 4.5-fold increase in BA in rats and mice, respectively	(Kimura et al. 2002)
Docetaxel	Dofequidar (MS-209)	Cancer patients	At the highest dose levels, an increase of docetaxel AUC when this agent is given in combination with MS209 was observed	(Diéras et al. 2005)
Third-generation inhibitors				
Paclitaxel[d]	Elacridar (GF120918)	mdr1ab(−/−) knockout mice and wild-type mice	Increased oral BA	(Bardelmeijer et al. 2000)
Doxorubicin	Zosuquidar (LY335979)	Cancer patients	~25% increase in BA at doxorubicin dose of 60 mg/m^2 and ~15% increase at a dose of 75 mg/m2	(Callies et al. 2003)
Paclitaxel	Ontogen (OC144093)	Cancer patients	~1.5-fold increase in AUC and ~2-fold increase in Cmax	(Guns et al. 2002)
Docetaxel[e]	R101933	Cancer patients	Pharmacokinetics did not alter in the presence of inhibitor but the faecal excretion of docetaxel decreased significantly	(van Zuylen et al. 2002)
Docetaxel	Tariquidar	Cancer patients	Tariquidar was well-tolerated and had less observed systemic pharmacokinetic interaction than previous P-gp inhibitors. Pharmacokinetic and pharmacodynamic trial using tariquidar showed it increased the retention of co-administered docetaxel	(Kelly et al. 2011)
Docetaxel	Ontogen (OC144093)	Cancer patients	The safety of the oral combination of ontogen and docetaxel was good and the relative apparent bioavailability was most likely caused by a significant effect of ontogen on the oral uptake of docetaxel	(Kuppens et al. 2005)

BA, bioavailability; AUC, area under the plasma concentration-time profile curve. [a] Absorption rate of digoxin varied at different segments of GIT (gastrointestinal tract) at different concentrations of verapamil.[b] Drugs like doxorubicin are transported by P-gp and MRP2, thus non-specific inhibitors (second-generation compounds) when co-administered largely increase Cmax (maximum concentration) and AUC. [c] VX-710 showed a decrease in paclitaxel clearance with a maximum tolerated dose of paclitaxel (<80 mg/m^2) that is roughly half of standard dose of 175 mg/m^2.[d] Pharmacokinetics of paclitaxel in mdr1ab(−/−) knockout mice was not altered by GF120918, whereas a significant increase in oral bioavailability (8.5–40.2%) was observed in wild-type mice. [e] Docetaxel clearance decreased from 2.5% to less than 1%. Adapted from (Varma et al. 2003).

I.6.2. P-gp induction

Through the up-regulation of drug efflux pumps, such as P-gp, cells can adapt to the presence of toxic xenobiotics, providing a long-term survival advantage. In fact, after a short-term exposure of cells to a variety of environmental insults, the *MDR1* gene is activated and a stable MDR phenotype is induced (Sharom 2007; Zhou 2008). It is recognized that there are multiple mechanisms by which mRNA synthesis can be regulated (splicing, transport, mRNA stability), and some of these mechanisms have already been described for the regulation of drug transporters (Lamba et al. 2003; Sharom 2007; Yague et al. 2003). However, the focus of this dissertation will be limited to those situations in which the regulation of expression has been shown to be mediated at the level of transcription. In what concerns specifically to the *MDR1* expression, it may be up-regulated by an increase in the amount of *MDR1* mRNA through transcriptional regulation, or stabilization of the mRNA (Sharom 2007; Yague et al. 2003). The first mechanism will be discussed in detail.

Transcription initiation involves a series of events leading to the formation of the first phosphodiester bond in the nascent RNA transcript. Early in the studies of transcription by RNA polymerase II (Pol II), the enzyme responsible for the synthesis of protein coding RNAs, it became clear that the polymerase alone was not sufficient for specific initiation from a DNA template (Scotto and Egan 1998). During the past decade, a tremendous effort has been directed at the purification and characterization of the additional protein factors required for basal transcription.

A considerable knowledge on the transcriptional regulation of the *MDR1* gene now exists (Callaghan et al. 2008; Labialle et al. 2002a; Labialle et al. 2002b; Scotto 2003; Scotto and Egan 1998; Shtil and Azare 2005). In general, the transcription of a gene is determined by myriad of response elements present within the promoter sequence, by their accessibility and complexity, and by transcription factors available to interact with these elements (Scotto 2003). The composition of these transcription factors is influenced by both the intracellular environment and extracellular signals, which can vary tremendously during the life of the cell. Moreover, the multi-protein complexes that assemble on the promoter sequence are also dynamic in nature, and influenced by the chromatin structure (Scotto 2003). Thus, the nature of these dynamic multiprotein complexes is grossly dictated by promoter architecture, yet subtly influenced by different signals, leading to profound regulatory switches. Additionally, multiple interacting pathways for activation of *MDR1* gene appear to be present (Sharom 2007), and this redundant network of *MDR1* regulation ensures the rapid emergence of resistance in cells subjected to chemical stress. Moreover, it appears that the *MDR1* gene is regulated by

specialized multiprotein complexes that include both common basic components (the basal or general transcription factors), as well as unique components that tailor a complex for the transduction of signals initiated by particular developmental, metabolic or environmental stimuli (Scotto 2003).

By more fully understanding the molecular mechanisms through which the *MDR1* gene is activated, it may be possible to intervene clinically to increase or prevent its transcriptional activation and, consequently, to reduce the intracellular concentration of harmful xenobiotics, or to overcome the MDR phenomenon, respectively.

I.6.2.1. P-gp inducers

Although P-gp is constitutively expressed in a cell- and tissue-specific manner, it may be induced by many drugs, including dexamethasone, rifampicin, the herbal antidepressant St John's wort and chemotherapeutic agents namely, doxorubicin, daunorubicin and vinblastine (Chaudhary and Roninson 1993; Chin et al. 1990a; Fardel et al. 1997; Harmsen et al. 2009; Hu et al. 1999; Kageyama et al. 2006; Kim et al. 2008; Nielsen et al. 1998; Tian et al. 2005; Zhou 2008). Table 7 compiles known P-gp inducers reported in the literature, as well as the experimental models and the methods used in each study, and highlights the enormous structural diversity of the reported inducers. Moreover, P-gp is induced not only by a number of chemical compounds, but also by other environmental factors, such as X-irradiation, UV-irradiation, cytokines, oxygen free radicals, tumor suppressor genes and heat shock (Chin et al. 1990b; Hu et al. 2000; Kioka et al. 1992b; Miyazaki et al. 1992; Ohga et al. 1998; Uchiumi et al. 1993; Wartenberg et al. 2005; Zastawny et al. 1993; Zhou 2008).

I.6.2.2. Regulation of P-gp expression at the transcription level

It is generally accepted that, in many cell lines and human metastatic sarcomas, P-gp expression is increased through the up-regulation of human *MDR1* (h*MDR1*) mRNA levels, (Hennessy and Spiers 2007). The increased h*MDR1* mRNA level can be linked either to gene amplification and/or increased gene transcription (Fojo et al. 1985; Roninson 1992; Scotto et al. 1986; Shen et al. 1986). The *MDR1* gene amplification seems to involve four to five neighbouring genes, which are not related to MDR and that are organized in amplicon (de Bruijn et al. 1986).

The human *MDR1* promoter region is atypical, as it does not contain a TATA promoter sequence (TATA-less promoter), and has multiple response elements (Figure 12), supporting the complex regulatory pattern controlling P-gp expression (Hennessy and Spiers 2007; Labialle et al. 2002b).

Table 7. Known P-gp inducers

Inducer	Experimental Model	Experimental Method	Literature Reference
2-Acetylaminofluorene	Sprague-Dawley rats (Liver)	Western blot	(Tateishi et al. 1999)
	Human hepatic epithelial Hep G2 cells (hepatocellular carcinoma) and human embryonic kidney 293T cells	RNase protection assay	(Kuo et al. 2002)
Abacavir	Human brain microvessel endothelial hCMEC/D3 cells	Western blot	(Chan et al. 2013a)
Actinomycin	Human epidermoid cancer KB cells (carcinoma, papilloma)	[a]CAT activity assay (*MDR1* promoter activity)	(Asakuno et al. 1994)
	Human T lymphoblastoid cell line CCRF-CEM	Northern blot	(Gekeler et al. 1988)
Aldosterone	Human epithelial renal HK2 cells	Western blot	(Romiti et al. 2002)
Ambrisentan	Human intestinal epithelial LS180 cells (Dukes' type B, colorectal adenocarcinoma)	Western blot and RT-PCR	(Weiss et al. 2013)
Amiodarone	Human intestinal epithelial LS180 cells (Dukes' type B, colorectal adenocarcinoma)	Western blot	(Schuetz et al. 1996a)
	Wistar rats (Liver, and kidney)	Western blot	(Cermanova et al. 2009)
Amprenavir	Human intestinal epithelial LS180V cells (LS180 cells selected for elevated P-gp levels with increasing concentrations of vinblastine) (Dukes' type B, colorectal adenocarcinoma)	Western blot	(Perloff et al. 2000)
	Human intestinal epithelial T84 cells (colorectal adenocarcinoma)	RT-PCR	(Haslam et al. 2008a)
	Human brain microvessel endothelial hCMEC/D3 cells	Western blot	(Chan et al. 2013a)
m-Amsacrine	Rat PC12 cells (pheochromocytoma), rat L6 cells (skeletal muscle myocyte), rat NRK-52E cells (normal kidney), rat IEC-18 cells (ileum), rat H4IIEC cells (liver) and mouse NIH 3T3 cells (fibroblast)	Slot blot and Northern blot	(Chin et al. 1990a)
Apigenin	Human intestinal epithelial Caco-2 cells (colorectal adenocarcinoma)	RT-PCR	(Lohner et al. 2007)
Artemisinine	Human intestinal epithelial HT29 cells (colorectal adenocarcinoma)	Western blot and RT-PCR	(Riganti et al. 2009b)
Asiatic acid	Human intestinal epithelial LS180 cells (Dukes' type B, colorectal adenocarcinoma)	Western blot and Immunocytochemistry	(Abuznait et al. 2011b)
Atazanavir	Human brain microvessel endothelial hCMEC/D3 cells	Western blot and Immunocytochemistry	(Zastre et al. 2009)
Atorvastatin	Human intestinal epithelial T84 cells (colorectal adenocarcinoma)	RT-PCR	(Haslam et al. 2008a)
Avermectin	Drosophila Schneider 2 (S2) cells	Western blot and Immunocytochemistry	(Luo et al. 2013)
Beclomethasone	Human intestinal epithelial Caco-2 cells, sub-clone CLEFF 9 (colorectal adenocarcinoma)	Western blot	(Crowe and Tan 2012)
Benzo(a)pyrene	Human intestinal epithelial Caco-2 cells (colorectal adenocarcinoma)	Western blot and RT-PCR	(Sugihara et al. 2007)
Benzo(e)pyrene	Human intestinal epithelial Caco-2 cells (colorectal adenocarcinoma)	Western blot and RT-PCR	(Sugihara et al. 2007)

Table 7. (cont.) Known P-gp inducers

Inducer	Experimental Model	Experimental Method	Literature Reference
Berberine	Human Hep3B, HepG2, and HA22T/VGH cells (hepatoma cell lines)	Flow cytometry	(Lin et al. 1999a)
Betamethasone	Cytotrophoblasts isolated from normal human full-term placentas	RT-PCR	(Manceau et al. 2012)
Bilirubin	Human intestinal epithelial T84 cells (colorectal adenocarcinoma) and human intestinal epithelial Caco-2 cells (colorectal adenocarcinoma)	RT-PCR	(Naruhashi et al. 2011)
Bosentan	Human intestinal epithelial LS180 cells (Dukes' type B, colorectal adenocarcinoma)	Western blot and RT-PCR	(Weiss et al. 2013)
Bromocriptine	Rat hepatoma Reuber H-35 cells	Western blot, RT-PCR and Northern blot	(Furuya et al. 1997)
Budesonide	Human intestinal epithelial LS180 cells (Dukes' type B, colorectal adenocarcinoma)	Western blot and RT-PCR	(Maier et al. 2007)
	Human intestinal epithelial Caco-2 cells (colorectal adenocarcinoma) , sub-clone CLEFF 9	Western blot	(Crowe and Tan 2012)
Caffeine	Human intestinal epithelial LS180 cells (Dukes' type B, colorectal adenocarcinoma)	Western blot and RT-PCR	(Abuznait et al. 2011a)
Cadmium chloride	Human intestinal epithelial Caco-2 cells clone TC7 (colorectal adenocarcinoma)	Western blot	(Huynh-Delerme et al. 2005)
Capsaicin	Human intestinal epithelial Caco-2 cells (colorectal adenocarcinoma)	Western blot and RT-PCR	(Han et al. 2006)
Carbamazepine	Human intestinal epithelial LS 174T cells (Dukes' type B, colorectal adenocarcinoma)	Northern blot	(Geick et al. 2001)
	Healthy humans (biopsy of tissue specimens from the lower duodenum)	RT-PCR	(Giessmann et al. 2004)
	Healthy humans (lymphocytes)	Western blot and RT-PCR	(Owen et al. 2006)
	Sprague–Dawley rats (capillary endothelial vessels, brain cortex and hippocampus)	Western blot and Immunohistochemistry	(Wen et al. 2008)
Catechin	Human intestinal epithelial Caco-2 cells (colorectal adenocarcinoma)	Western blot and RT-PCR	(Lohner et al. 2007)
Celiprolol	Human intestinal epithelial Caco-2 cells (colorectal adenocarcinoma)	Flow cytometry	(Anderle et al. 1998)
Cembratriene	Human intestinal epithelial LS180 cells (Dukes' type B, colorectal adenocarcinoma)	Western blot and Immunocytochemistry	(Abuznait et al. 2011b)
R-Cetirizine[b]	Human intestinal epithelial Caco-2 cells (colorectal adenocarcinoma)	Flow cytometry and RT-PCR	(Shen et al. 2007)
Cytarabine	Human leukaemia cell lines: K562 (bone marrow lymphoblast; chronic myelogenous leukaemia), KG1 cells (bone marrow myeloblast; acute myelogenous leukaemia) and H9 cells (cutaneous T lymphocyte;lymphoma)	Flow cytometry and cDNA-PCR	(Chaudhary and Roninson 1993)
	Human carcinoma cell lines: KB-3-1 (cervix carcinoma) and EJ cells (bladder carcinoma)		

Table 7. (cont.) Known P-gp inducers

Inducer	Experimental Model	Experimental Method	Literature Reference
Chlorambucil	Human leukaemia K562 cells (bone marrow lymphoblast; chronic myelogenous leukaemia	cDNA-PCR	(Chaudhary and Roninson 1993)
Cholate	Human intestinal epithelial T84 cells (colorectal adenocarcinoma) and human intestinal epithelial Caco-2 cells (colorectal adenocarcinoma)	RT-PCR	(Naruhashi et al. 2011)
Chrysin	Human intestinal epithelial Caco-2 cells (colorectal adenocarcinoma)	Western blot, Flow cytometry and RT-PCR	(Lohner et al. 2007)
Ciclosenide	Human intestinal epithelial Caco-2 cells (colorectal adenocarcinoma) , sub-clone CLEFF 9	Western blot	(Crowe and Tan 2012)
Cisplatin	Human leukaemia K562 cells (bone marrow lymphoblast; chronic myelogenous leukaemia	cDNA-PCR	(Chaudhary and Roninson 1993)
	Human KB epidermoid carcinoma Kst-6 cells[c]	[a]CAT activity assay (*MDR1* promoter activity)	(Ohga et al. 1998)
	Sprague-Dawley rats (Liver, kidney and intestine)	Western blot	(Demeule et al. 1999)
	Porcine kidney epithelial LLC-PK1 cells	RT-PCR	(Takara et al. 2003b)
Clotrimazole	Human intestinal epithelial LS 180 cells and the adriamycin-resistant subline, LS1 80/AD5O cells (Dukes' type B, colorectal adenocarcinoma)	Western blot	(Schuetz et al. 1996a)
	Human intestinal epithelial LS 174T cells (Dukes' type B, colorectal adenocarcinoma)	Northern blot	(Geick et al. 2001)
Colchicine	Wistar rats (Liver)	Northern blot	(Vollrath et al. 1994)
	Human peripheral blood promyeloblasts, HL-60 cells (acute promyelocytic leukaemia)	Flow cytometry	(Decleves et al. 1998)
Corticosterone	Human intestinal epithelial LS 174T cells (Dukes' type B, colorectal adenocarcinoma)	Northern blot	(Geick et al. 2001)
Curcuma extracts	Human intestinal epithelial Caco-2 cells (colorectal adenocarcinoma)	Western blot and RT-PCR	(Hou et al. 2008)
Cyanidin	Human intestinal epithelial Caco-2 cells (colorectal adenocarcinoma)	Western blot, Flow cytometry and RT-PCR	(Lohner et al. 2007)
Cycloheximide[d]	Primary rat hepatocytes, Human Hep G2 cells (hepatocellular carcinoma), Mouse Hepa 1 cells (mouse hepatoma cells) and Rat RC3 cells (a single cell clone of the rat H4-II-E hepatoma cell line)	Northern blot	(Gant et al. 1992)
Cyclophosphamide	Human intestinal epithelial LS180 cells (Dukes' type B, colorectal adenocarcinoma)	Western blot	(Harmsen et al. 2009)

Table 7. (cont.) Known P-gp inducers

Inducer	Experimental Model	Experimental Method	Literature Reference
Cyclosporine A	Sprague-Dawley rats (tubular cells of the kidney)	Western blot and Immunohistochemistry	(del Moral et al. 1997)
	Human epithelial renal HK2 cells	Western blot and RT-PCR	(Romiti et al. 2002)
Cytarabine	Human peripheral blood promyeloblasts, HL-60S cells (sensitive to doxorubicin) and the sub-lines HL-60 R0.5 and HL-60 R5, resistant to 0.5 μM and 5 μM doxorubicin, respectively (acute promyelocytic leukaemia)	Western blot and RT-PCR	(Prenkert et al. 2009)
Daidzein	Human intestinal epithelial Caco-2 cells (colorectal adenocarcinoma)	Western blot and RT-PCR	(Lohner et al. 2007)
Daunorubicin	Rat PC12 cells (pheochromocytoma), rat L6 cells (skeletal muscle myocyte), rat NRK-52E cells (normal kidney), rat IEC-18 cells (ileum), rat H4IIEC cells (liver) and mouse NIH 3T3 cells (fibroblast)	Slot blot and Northern blot	(Chin et al. 1990a)
	Human leukaemia K562 cells (bone marrow lymphoblast; chronic myelogenous leukaemia	cDNA-PCR	(Chaudhary and Roninson 1993)
	Human CEM/A7R cells (a variant of CCRF-CEM cells -human peripheral blood T lymphoblasts derived from acute lymphoblastic leukaemia)	Flow cytometry and Northern blot	(Hu et al. 1995)
	Murine Ehrlich ascites tumour EHR2 cells	Western blot and Immunocytochemistry	(Nielsen et al. 1998)
	Human T lymphoblasts MOLT-4 cells (acute lymphoblastic leukaemia)	Flow cytometry and RT-PCR	(Liu et al. 2002b)
Daurunavir	Human brain microvessel endothelial hCMEC/D3 cells	Western blot	(Chan et al. 2013a)
Depsipeptide (FK228)	Human peripheral blood mononuclear cells (normal and malignant)	RT-PCR	(Robey et al. 2006)
	108, 121, 127, and 143 renal carcinoma cell lines	RT-PCR	
	Human intestinal epithelial SW620 cells (Dukes' type C, colorectal adenocarcinoma	Flow cytometry	(Robey et al. 2006)
Desvenlafaxine	Friend Virus B-Type (FVB) mice (intestine)	ELISA	(Bachmeier et al. 2013)
Dexamethasone	Mouse hepatoma Hepa1c1c cells and Human hepatic HepG2 cells (hepatocellular carcinoma)	Western blot and RNase protection assay	(Zhao et al. 1993)
	Human intestinal epithelial LS 180 cells and the adriamycin-resistant subline, LS1 80/AD5O cells (Dukes' type B, colorectal adenocarcinoma)	Western blot and RT-PCR	(Abuznait et al. 2011a; Schuetz et al. 1996a)
	Sprague-Dawley rats (liver)	Western blot and RNase protection assay	(Salphati and Benet 1998)
	Human hepatic HepG2 cells (hepatocellular carcinoma) and NMRI mice (liver, heart, brain, and colon)	RT-PCR	(Sérée et al. 1998)
	Sprague-Dawley rats (liver and intestine)	Western blot	(Lin et al. 1999b)

Table 7. (cont.) Known P-gp inducers

Inducer	Experimental Model	Experimental Method	Literature Reference
Dexamethasone (cont.)	Sprague–Dawley rats (brain)	Western blot	(Aquilante et al. 2000)
	Human intestinal epithelial LS 174T cells (Dukes' type B, colorectal adenocarcinoma)	Northern blot	(Geick et al. 2001)
	Human epithelial renal HK2 cells	Western blot and RT-PCR	(Romiti et al. 2002)
	CD-1 rats (intestinal microsomes and brain microvessel endothelial cells)	Western blot	(Perloff et al. 2004)
	Wistar rats (lung)	Western blot	(Dinis-Oliveira et al. 2006c)
	Wistar rats (Liver and intestine)	Western blot	(Kageyama et al. 2006)
	Primary rat brain microvascular endothelial cells	Western blot	(Narang et al. 2008)
	Pregnant FVB mice (placenta)	Western blot and RT-PCR	(Petropoulos et al. 2010)
	Human retinal pigment epithelial (RPE) D407 cells	Western blot and RT-PCR	(Zhang et al. 2012)
	Cytotrophoblasts isolated from normal human full-term placentas	RT-PCR	(Manceau et al. 2012)
	CD-1 mice (brain capillaries)	Western blot	(Chan et al. 2013b)
Diclofenac	Human intestinal epithelial Caco-2 cells (colorectal adenocarcinoma)	RT-PCR	(Takara et al. 2009)
Digoxin	Human intestinal epithelial Caco-2 cells (colorectal adenocarcinoma) and Human intestinal epithelial LS 180 cells (Dukes' type B, colorectal adenocarcinoma)	RT-PCR	(Takara et al. 2003a; Takara et al. 2002)
	Human intestinal epithelial T84 cells (colorectal adenocarcinoma)	Western blot, Immunocytochemistry and RT-PCR	(Haslam et al. 2008b)
	Human intestinal epithelial HT29 cells (colorectal adenocarcinoma)	Western blot and RT-PCR	(Riganti et al. 2009a)
	Human intestinal epithelial T84 cells (colorectal adenocarcinoma) and human intestinal epithelial Caco-2 cells (colorectal adenocarcinoma)	RT-PCR	(Naruhashi et al. 2011)
1α,25-Dihydroxyvitamin D3	Human epithelial renal HK2 cells	Western blot and RT-PCR	(Romiti et al. 2002)
	[e]fxr(−/−) and wild-type fxr(+/+) mice (kidney and brain)	Western blot and RT-PCR	(Chow et al. 2011)
	Human brain microvessel endothelial hCMEC/D3 cells, rat brain microvessel endothelial RBE4 cells and isolated rat brain capillaries	Western blot and RT-PCR	(Durk et al. 2012)
Diltiazem	Human intestinal epithelial LS 180 cells and its drug-resistant sublines, LS 180-Ad50 and LS 180-Vb2 cells (Dukes' type B, colorectal adenocarcinoma)	Western blot and Northern blot	(Herzog et al. 1993)
Dimethylformamide	Human intestinal epithelial SW620 cells (Dukes' type C, colorectal adenocarcinoma)	RNase protection assay	(Mickley et al. 1989)

Table 7. (cont.) Known P-gp inducers

Inducer	Experimental Model	Experimental Method	Literature Reference
6,16α-dimethylpregnenolone	Human intestinal epithelial LS 174T cells (Dukes' type B, colorectal adenocarcinoma)	Northern blot	(Geick et al. 2001)
Dimethylsulfoxide	Human intestinal epithelial SW620 cells (Dukes' type C, colorectal adenocarcinoma)	RNase protection assay	(Mickley et al. 1989)
Docetaxel	Human intestinal epithelial LS180 cells (Dukes' type B, colorectal adenocarcinoma)	Western blot	(Harmsen et al. 2009)
Doxorubicin	Rat PC12 cells (pheochromocytoma), rat L6 cells (skeletal muscle myocyte), rat NRK-52E cells (normal kidney), rat IEC-18 cells (ileum), rat H4IIEC cells (liver) and mouse NIH 3T3 cells (fibroblast)	Slot blot and Northern blot	(Chin et al. 1990a)
	Human leukaemia cell lines: K562 (bone marrow lymphoblast; chronic myelogenous leukaemia) and H9 cells (cutaneous T lymphocyte;lymphoma)	cDNA-PCR	(Chaudhary and Roninson 1993)
	Human carcinoma cell lines: KB-3-1 (cervix carcinoma)	cDNA-PCR	(Chaudhary and Roninson 1993)
	Human CEM/A7R cells (a variant of CCRF-CEM cells -human peripheral blood T lymphoblasts derived from acute lymphoblastic leukaemia)	Flow cytometry and Northern blot	(Hu et al. 1995)
	Rat liver epithelial cells and primary rat hepatocytes	Western blot and Northern blot	(Fardel et al. 1997)
	Solid human tumours (sarcoma pulmonary metastases)	RT-PCR	(Abolhoda et al. 1999)
	Human T lymphoblasts MOLT-4 cells (acute lymphoblastic leukaemia)	Flow cytometry and RT-PCR	(Liu et al. 2002b)
	Mouse skin lymphoblast (lymphocytic leukaemia)	Western blot	(Boháčová et al. 2006)
	Human intestinal epithelial Caco-2 cells (colorectal adenocarcinoma)	Flow cytometry	(Wongwanakul et al. 2013)
Doxycycline	Human breast carcinoma epithelial MCF-7 cells	Western blot and Northern blot	(Mealey et al. 2002)
Efavirenz	Human brain microvessel endothelial hCMEC/D3 cells	Western blot	(Chan et al. 2013a)
Emetine[d]	Primary rat hepatocytes, Human Hep G2 cells (hepatocellular carcinoma), Mouse Hepa 1 cells (mouse hepatoma cells) and Rat RC3 cells (a single cell clone of the rat H4-II-E hepatoma cell line)	Northern blot	(Gant et al. 1992)
Epigallocatechin-3-gallate (EGCG)	Human intestinal epithelial Caco-2 cells (colorectal adenocarcinoma)	Western blot and RT-PCR	(Lohner et al. 2007)
Epirubicin	Human CEM/A7R cells (a variant of CCRF-CEM cells -human peripheral blood T lymphoblasts derived from acute lymphoblastic leukaemia)	Flow cytometry and Northern blot	(Hu et al. 1999; Hu et al. 1995)
Eriodictyol	Human intestinal epithelial Caco-2 cells (colorectal adenocarcinoma)	Western blot	(Lohner et al. 2007)
Erythromycin	Rhesus monkeys (liver)	Western blot and Northern blot	(Gant et al. 1995)

Table 7. (cont.) Known P-gp inducers

Inducer	Experimental Model	Experimental Method	Literature Reference
Erythromycin (cont.)	Human intestinal epithelial LS180 cells (Dukes' type B, colorectal adenocarcinoma)	Western blot	(Schuetz et al. 1996a)
β-Estradiol	Ovariectomized Swiss-Webster mice (uterine endometrial secretory epithelium)[f]	*In situ* hybridization and Immunocytochemistry	(Arceci et al. 1990)
	Human intestinal epithelial LS180 cells (Dukes' type B, colorectal adenocarcinoma)	Western blot and RT-PCR	(Abuznait et al. 2011a)
Etoposide	Human leukaemia K562 cells (bone marrow lymphoblast; chronic myelogenous leukaemia	cDNA-PCR	(Chaudhary and Roninson 1993)
	Human KB epidermoid carcinoma Kst-6 cells	[a]CAT activity assay (*MDR1* promoter activity)	(Ohga et al. 1998)
	Human epithelial HeLa cells (cervix adenocarcinoma)	Luciferase activity assay (*MDR1* promoter activity)	(Vilaboa et al. 2000)
	ddY mice (mucosal membrane of the ileal tissues)	Western blot	(Kobori et al. 2013b)
Fenbufen	Human intestinal epithelial Caco-2 cells (colorectal adenocarcinoma)	RT-PCR	(Takara et al. 2009)
Flavone	Human intestinal epithelial Caco-2 cells (colorectal adenocarcinoma)	Western blot, Flow cytometry and RT-PCR	(Lohner et al. 2007)
	C57BL/6 mice (jejunum, duodenum and ileum)	Western blot	(Lohner et al. 2007)
Fluorouracil	Human leukaemia K562 cells (bone marrow lymphoblast; chronic myelogenous leukaemia	cDNA-PCR	(Chaudhary and Roninson 1993)
Flutamide	Human intestinal epithelial LS180 cells (Dukes' type B, colorectal adenocarcinoma)	Western blot	(Harmsen et al. 2009)
Fluticasone	Human intestinal epithelial Caco-2 cells (colorectal adenocarcinoma) , sub-clone CLEFF 9	Western blot	(Crowe and Tan 2012)
Genistein	Human intestinal epithelial Caco-2 cells (colorectal adenocarcinoma)	Western blot, Flow cytometry and RT-PCR	(Lohner et al. 2007)
Ginkgolides A and B	Human intestinal epithelial LS180 cells (Dukes' type B, colorectal adenocarcinoma)	Western blot and RT-PCR	(Satsu et al. 2008)
Hydroxyurea	Human leukaemia K562 cells (bone marrow lymphoblast; chronic myelogenous leukaemia	cDNA-PCR	(Chaudhary and Roninson 1993)
Hyperforin	Human intestinal epithelial LS180 cells (Dukes' type B, colorectal adenocarcinoma)	Western blot and RT-PCR	(Abuznait et al. 2011a; Tian et al. 2005)

Table 7. (cont.) Known P-gp inducers

Inducer	Experimental Model	Experimental Method	Literature Reference
Hyperforin (cont.)	Isolated brain capillaries from CB6F1 hPXR transgenic mice[g]	Western blot and immunocytochemistry	(Bauer et al. 2006)
Hypericin	Human intestinal epithelial LS180V cells (MDR sub-line selected from the parental LS180 cell line with 4 ng ml^{-1} vinblastine (Dukes' type B, colorectal adenocarcinoma)	Western blot	(Perloff et al. 2001b)
Hypericum perforatum extracts	Human intestinal epithelial LS180V cells (MDR sub-line selected from the parental LS180 cell line with 4 ng ml^{-1} vinblastine (Dukes' type B, colorectal adenocarcinoma)	Western blot	(Perloff et al. 2001b)
	Human intestinal epithelial LS180 cells (Dukes' type B, colorectal adenocarcinoma)	Western blot	(Tian et al. 2005)
Idarubicin	Human CEM/A7R cells (a variant of CCRF-CEM cells -human peripheral blood T lymphoblasts derived from acute lymphoblastic leukaemia)	Flow cytometry and Northern blot	(Hu et al. 1999)
Ifosfamide	Human intestinal epithelial LS180 cells (Dukes' type B, colorectal adenocarcinoma)	Western blot	(Harmsen et al. 2009)
Indinavir	Human intestinal epithelial LS180V cells (LS180 cells selected for elevated P-gp levels with increasing concentrations of vinblastine) (Dukes' type B, colorectal adenocarcinoma)	Western blot	(Perloff et al. 2000)
Indomethacin	Human intestinal epithelial Caco-2 cells (colorectal adenocarcinoma)	RT-PCR	(Takara et al. 2009)
Insulin	Rat hepatoma H-4-II-E cells	RNase Protection Assay	(Zhou and Kuo 1997)
	Sprague–Dawley rats (cerebral cortex and primarily cultured rat brain microvessel endothelial cells)	Western blot and RT-PCR	(Liu et al. 2008)
	Primarily cultured rat brain microvessel endothelial cells	Western blot	(Liu et al. 2009)
Isosafrole	Fischer rats (Liver)	Northern blot	(Burt and Thorgeirsson 1988)
	Human intestinal epithelial LS 180 cells (Dukes' type B, colorectal adenocarcinoma)	Western blot	(Schuetz et al. 1996a)
Isoxanthohumol	Human intestinal epithelial Caco-2 cells (colorectal adenocarcinoma)	Western blot, Flow cytometry and RT-PCR	(Lohner et al. 2007)
Ivermectin	JWZ murine hepatic cells	RT-PCR	(Ménez et al. 2012)
Lopinavir	Human brain microvessel endothelial hCMEC/D3 cells	Western blot	(Chan et al. 2013a)
LY191401	Human intestinal LS1 80/AD5O cells (adriamycin-resistant subline) (Dukes' type B, colorectal adenocarcinoma)	Western blot and Northern blot	(Bhat et al. 1995)

Table 7. (cont.) Known P-gp inducers

Inducer	Experimental Model	Experimental Method	Literature Reference
Mangiferin (polyphenol from *Mangifera indica*)	Human epithelial renal HK2 cells	Western blot and RT-PCR	(Chieli et al. 2010)
Methotrexate	Human leukaemia cell lines: K562 (bone marrow lymphoblast; chronic myelogenous leukaemia) and H9 cells (cutaneous T lymphocyte;lymphoma)	cDNA-PCR	(Chaudhary and Roninson 1993)
	Mouse fibroblast 3T6-C26 cells	Flow cytometry	(de Graaf et al. 1996)
Methylprednisolone	Human intestinal epithelial Caco-2 cells (colorectal adenocarcinoma) , sub-clone CLEFF 9	Western blot	(Crowe and Tan 2012)
	Human alveolar type II-like epithelial A549 cells (lung carcinoma)	Western blot and RT-PCR	(Zerin et al. 2012)
Midalozam	Human intestinal epithelial LS 180 cells and the adriamycin-resistant subline, LS1 80/AD5O cells (Dukes' type B, colorectal adenocarcinoma)	Western blot	(Schuetz et al. 1996a)
Mifepristone (RU486)	Human intestinal epithelial LS 174T cells (Dukes' type B, colorectal adenocarcinoma)	Northern blot	(Geick et al. 2001)
Mitoxantrone	Wistar rats (liver, intestine, kidney) and primary cultured rat and mouse hepatocytes	Western blot and Northern blot	(Schrenk et al. 1996)
	Rat PC12 cells (pheochromocytoma), rat L6 cells (skeletal muscle myocyte), rat NRK-52E cells (normal kidney), rat IEC-18 cells (ileum), rat H4IIEC cells (liver) and mouse NIH 3T3 cells (fibroblast)	Slot blot and Northern blot	(Chin et al. 1990a)
Morphine	Sprague–Dawley rats (brain)	Western blot	(Aquilante et al. 2000)
	Sprague–Dawley rats (brain vessels)	Western blot and RT-PCR	(Yousif et al. 2012)
MX2	Human CEM/A7R cells (a variant of CCRF-CEM cells -human peripheral blood T lymphoblasts derived from acute lymphoblastic leukaemia)	Flow cytometry and Northern blot	(Hu et al. 1999)
Myricetin	Human intestinal epithelial Caco-2 cells (colorectal adenocarcinoma)	Western blot, Flow cytometry and RT-PCR	(Lohner et al. 2007)
Naringenin	Human intestinal epithelial Caco-2 cells (colorectal adenocarcinoma)	Western blot	(Lohner et al. 2007)
Nefazodone	Human intestinal epithelial LS180V cells (LS180 cells selected for elevated P-gp levels with increasing concentrations of vinblastine) (Dukes' type B, colorectal adenocarcinoma)	Western blot	(Störmer et al. 2001)
Nelfinavir	Human intestinal epithelial LS180V cells (LS180 cells selected for elevated P-gp levels with increasing concentrations of vinblastine) (Dukes' type B, colorectal adenocarcinoma)	Western blot	(Perloff et al. 2000)
Nevirapine	Human brain microvessel endothelial hCMEC/D3 cells	Western blot	(Chan et al. 2013a)

Table 7. (cont.) Known P-gp inducers

Inducer	Experimental Model	Experimental Method	Literature Reference
Nicardipine	Human intestinal epithelial LS 180 cells and its drug-resistant sublines, LS 180-Ad50 and LS 180-Vb2 cells (Dukes' type B, colorectal adenocarcinoma)	Western blot and Northern blot	(Herzog et al. 1993)
Nifedipine	Human intestinal epithelial LS 180 cells and its drug-resistant sublines, LS 180-Ad50 and LS 180-Vb2 cells (Dukes' type B, colorectal adenocarcinoma)	Western blot and Northern blot	(Herzog et al. 1993; Schuetz et al. 1996a)
	Human intestinal epithelial LS 174T cells (Dukes' type B, colorectal adenocarcinoma)	Northern blot	(Geick et al. 2001)
Nimesulide	Human intestinal epithelial Caco-2 cells (colorectal adenocarcinoma)	RT-PCR	(Takara et al. 2009)
Norathyriol (polyphenol from *Mangifera indica*)	Human epithelial renal HK2 cells	Western blot and RT-PCR	(Chieli et al. 2010)
Oleocanthal	Human intestinal epithelial LS180 cells (Dukes' type B, colorectal adenocarcinoma)	Western blot and Immunocytochemistry	(Abuznait et al. 2011b)
Ouabain	Human intestinal epithelial HT29 cells (colorectal adenocarcinoma)	Western blot and RT-PCR	(Riganti et al. 2009a)
Oxycodone	Sprague Dawley rats (intestine, liver, kidney and brain)	Western blot and	(Hassan et al. 2007)
Paclitaxel	Human intestinal epithelial LS180 cells (Dukes' type B, colorectal adenocarcinoma)	Western blot	(Harmsen et al. 2009)
Parthenolide	Human intestinal epithelial HT29 cells (colorectal adenocarcinoma)	Western blot and RT-PCR	(Riganti et al. 2009b)
Pentylenetetrazole	Human intestinal epithelial LS180 cells (Dukes' type B, colorectal adenocarcinoma)	Western blot and RT-PCR	(Abuznait et al. 2011a)
Phenobarbital	Human intestinal epithelial LS 180 cells and the adriamycin-resistant subline, LS1 80/AD5O cells (Dukes' type B, colorectal adenocarcinoma)	Western blot	(Schuetz et al. 1996a)
	Sprague–Dawley rats (capillary endothelial vessels, brain cortex and hippocampus)	Western blot and Immunohistochemistry	(Wen et al. 2008)
Phenothiazine	Fischer rats (Liver)	Northern blot	(Burt and Thorgeirsson 1988)
	Wistar rats (isolated bile canalicular membrane vesicles)	Western blot	(Watanabe et al. 1995)
	Sprague-Dawley rats (Liver)	Western blot	(Tateishi et al. 1999)
Phenytoin	Human intestinal epithelial LS 180 cells and the adriamycin-resistant subline, LS1 80/AD5O cells (Dukes' type B, colorectal adenocarcinoma)	Western blot	(Schuetz et al. 1996a)
	Sprague–Dawley rats (capillary endothelial vessels, brain cortex and hippocampus)	Western blot and Immunohistochemistry	(Wen et al. 2008)
Phorbol 12-myristate 13-acetate (PMA)	Human promonocytic U937 cells	Flow cytometry	(Combates et al. 1997)

Table 7. (cont.) Known P-gp inducers

Inducer	Experimental Model	Experimental Method	Literature Reference
Piperine	Wistar rats (ileum) and Human intestinal epithelial Caco-2 cells (colorectal adenocarcinoma)	Western blot and RT-PCR	(Han et al. 2008)
Platelet-activating factor	Human epithelial renal HK2 cells	Western blot and RT-PCR	(Romiti et al. 2002)
Prednisolone	Dogs (lamina propria lymphocytes of duodenal biopsy samples)	Immunohistochemistry	(Allenspach et al. 2006)
5β-Pregnane-3,20-dione	Human intestinal epithelial LS 174T cells (Dukes' type B, colorectal adenocarcinoma)	Northern blot	(Geick et al. 2001)
Pregnenolone-16α-carbonitrile	Human intestinal epithelial LS 174T cells (Dukes' type B, colorectal adenocarcinoma)	Northern blot	(Geick et al. 2001)
	Isolated brain capillaries from Isolated brain capillaries from CB6F1 wild type mice	Western blot and immunocytochemistry	(Bauer et al. 2006)
Probenecid	Rhesus monkeys (liver)	Northern blot	(Gant et al. 1995)
Quercetin	Human intestinal epithelial Caco-2 cells (colorectal adenocarcinoma)	Western blot, Flow cytometry and RT-PCR	(Lohner et al. 2007)
Quinidine	Human intestinal epithelial T84 cells (colorectal adenocarcinoma)	RT-PCR	(Haslam et al. 2008a)
Rapamycin or Sirolimus	Human intestinal epithelial LS 180 cells (Dukes' type B, colorectal adenocarcinoma)	Western blot	(Schuetz et al. 1996a)
Reduced rifampicin derivative (RedRif)	Rat brain microvessel endothelial RBE4 cells	Western blot	(Vilas-Boas et al. 2013b)
Rescinnamine	Human intestinal LS1 80/AD5O cells (adriamycin-resistant subline) (Dukes' type B, colorectal adenocarcinoma)	Western blot and Northern blot	(Bhat et al. 1995)
Reserpine	Human intestinal LS1 80/AD5O cells (adriamycin-resistant subline) (Dukes' type B, colorectal adenocarcinoma)	Western blot and Northern blot	(Bhat et al. 1995)
	Human intestinal epithelial LS 180 cells (Dukes' type B, colorectal adenocarcinoma)	Western blot and Northern blot	(Schuetz et al. 1996a)
	Human intestinal epithelial LS 174T cells (Dukes' type B, colorectal adenocarcinoma)	Northern blot	(Geick et al. 2001)
Retinoic acid	Human neuroblastoma cell lines: SK-N-SH cells, SH-SY5Y cells, SK-N-BE(2) cells and LA1-15n cells	Western blot, Northern blot and RNase protection assay	(Bates et al. 1989)
	Rat brain microvessel endothelial RBE4 cells	Flow cytometry	(El Hafny et al. 1997b)

Table 7. (cont.) Known P-gp inducers

Inducer	Experimental Model	Experimental Method	Literature Reference
Rifampicin	Rhesus monkeys (liver)	Western blot and Northern blot	(Gant et al. 1995)
	Human intestinal epithelial LS 180 cells and the adriamycin-resistant subline, LS1 80/AD5O cells (Dukes' type B, colorectal adenocarcinoma)	Western blot and Northern blot	(Schuetz et al. 1996a)
	Sprague-Dawley rats (liver)	Western blot and RNase protection assay	(Salphati and Benet 1998)
	Human healthy volunteers (duodenal biopsy specimens)	Western blot and immunohistochemistry	(Greiner et al. 1999)
	Human healthy volunteers (duodenal biopsy specimens)	Western blot, immunohistochemistry and RT-PCR	(Westphal et al. 2000)
	Human intestinal epithelial LS 174T cells (Dukes' type B, colorectal adenocarcinoma)	Northern blot	(Geick et al. 2001)
	Human intestinal epithelial LS180 cells (Dukes' type B, colorectal adenocarcinoma)	Western blot and RT-PCR	(Abuznait et al. 2011a; Abuznait et al. 2011b; Maier et al. 2007; Tian et al. 2005; Weiss and Haefeli 2013; Weiss et al. 2013)
	Isolated brain capillaries from CB6F1 hPXR transgenic mice[g]	Western blot and immunocytochemistry	(Bauer et al. 2006)
	Healthy humans (lymphocytes)	Western blot and RT-PCR	(Owen et al. 2006)
	Wistar rats (Liver and intestine)	Western blot	(Kageyama et al. 2006)
	Human intestinal epithelial Caco-2 cells (colorectal adenocarcinoma)	RT-PCR	(Ehret et al. 2007)
	Human intestinal epithelial T84 cells (colorectal adenocarcinoma)	Western blot, Immunocytochemistry and RT-PCR	(Haslam et al. 2008b)
	Human brain microvessel endothelial hCMEC/D3 cells	Western blot and Immunocytochemistry	(Zastre et al. 2009)
	Human brain microvascular endothelial cells (HBMEC)	Western blot	(Bachmeier et al. 2011)
	Human intestinal epithelial T84 cells (colorectal adenocarcinoma)	RT-PCR	(Naruhashi et al. 2011)
	Human brain microvessel endothelial hCMEC/D3 cells	Western blot	(Chan et al. 2013a)
	Rat brain microvessel endothelial RBE4 cells	Western blot	(Vilas-Boas et al. 2013b)
Rilpivirine	Human intestinal epithelial LS180 cells (Dukes' type B, colorectal adenocarcinoma)	RT-PCR	(Weiss and Haefeli 2013)
Rhinacanthin-C	Human intestinal epithelial Caco-2 cells (colorectal adenocarcinoma)	Flow cytometry	(Wongwanakul et al. 2013)

Table 7. (cont.) Known P-gp inducers

Inducer	Experimental Model	Experimental Method	Literature Reference
Ritonavir	Human intestinal epithelial LS180V cells (LS180 cells selected for elevated P-gp levels with increasing concentrations of vinblastine) (Dukes' type B, colorectal adenocarcinoma)	Western blot	(Perloff et al. 2000; Perloff et al. 2001a; Perloff et al. 2001b; Störmer et al. 2001)
	CD-1 rats (intestinal microsomes and brain microvessel endothelial cells)	Western blot	(Perloff et al. 2004)
	Primary bovine brain microvessel endothelial cells (BMEC)	Western blot	(Perloff et al. 2007)
	Human brain microvessel endothelial hCMEC/D3 cells	Western blot and Immunocytochemistry	(Zastre et al. 2009)
Saquinavir	Human intestinal epithelial LS180V cells (LS180 cells selected for elevated P-gp levels with increasing concentrations of vinblastine) (Dukes' type B, colorectal adenocarcinoma)	Western blot	(Perloff et al. 2000)
Small molecule tyrosine kinase inhibitors: erlotinib, gefitinib, nilotinib, sorafenib, vandetanib	Human intestinal epithelial LS180 cells (Dukes' type B, colorectal adenocarcinoma)	Western blot	(Harmsen et al. 2013)
Sodium arsenite	Human kidney epithelial HTB-46 cells (clear cell carcinoma)	Northern blot	(Chin et al. 1990b)
	Human hepatic HepG2 cells (hepatocellular carcinoma), Human epithelial cervix HeLa cells (adenocarcinoma) and monkey CV-I cells	Slot blot hybridization and RNase protection assay	(Kioka et al. 1992b)
	Mouse FM3A/M and P388/M cells (MDR sub-lines isolated from parental P388 mouse leukaemia cell line and FM3A mouse mammary carcinoma cell line, respectively)	[a]CAT activity assay (*MDR1* promoter activity)	(Kim et al. 1998)
	Human epithelial HeLa cells (cervix adenocarcinoma)	Luciferase activity assay (*MDR1* promoter activity)	(Vilaboa et al. 2000)
	Chronic arsenic-exposed (CAsE) cells (rat liver epithelial TRL1215 cells submitted to a long-term exposure (18 or more weeks) to 125-500 nM sodium arsenite	Western blot	(Liu et al. 2001)
Sodium butyrate	Human neuroblastoma cell lines: SK-N-BE(2) cells and LA1-15n cells	RNase protection assay	(Bates et al. 1989)
	Human intestinal epithelial cell lines: SW620 cells (Dukes' type C, colorectal adenocarcinoma), HCT-15 (Dukes' type C, colorectal adenocarcinoma), LS180 cells (Dukes' type B, colorectal adenocarcinoma) DLD-1 cells (Dukes' type C, colorectal adenocarcinoma).	Western blot, Northern blot, RNase protection assay, Flow cytometry and cDNA-PCR	(Frommel et al. 1993; Mickley et al. 1989)
	Human intestinal epithelial SW620 cells and a MDR sub-line selected with doxorubicin (Ad1000) SW620 cells (Dukes' type C, colorectal adenocarcinoma)	RNase protection assay and luciferase activity assay (*MDR1* promoter activity)	(Jin and Scotto 1998; Morrow et al. 1994)

Table 7. (cont.) Known P-gp inducers

Inducer	Experimental Model	Experimental Method	Literature Reference
Sodium butyrate (cont.)	Human epithelial HeLa cells (cervix adenocarcinoma)	Luciferase activity assay (*MDR1* promoter activity)	(Vilaboa et al. 2000)
Spironolactone	Wistar rats (Brush-border membranes from enterocytes of the small intestine) Human hepatic HepG2 cells (hepatocellular carcinoma)	Western Blot and Immunohistochemistry Western blot and RT-PCR	(Ghanem et al. 2006) (Rigalli et al. 2011)
SR12813	Human brain microvessel endothelial hCMEC/D3 cells	Western blot and Immunocytochemistry	(Chan et al. 2013a; Zastre et al. 2009)
Tacrolimus (FK-506)	Human intestinal epithelial LS180 cells (Dukes' type B, colorectal adenocarcinoma)	Western blot	(Schuetz et al. 1996a)
Taldalafil	Human intestinal epithelial LS180 cells (Dukes' type B, colorectal adenocarcinoma)	Western blot and RT-PCR	(Weiss et al. 2013)
Tamoxifen	Rhesus monkeys (liver) Lewis rats (liver)	Western blot and Northern blot RT-PCR	(Gant et al. 1995) (Riley et al. 2000)
Tangeretin	Human intestinal epithelial LS180 cells (Dukes' type B, colorectal adenocarcinoma)	Western blot and RT-PCR	(Satsu et al. 2008)
Taurocholate	Human intestinal epithelial T84 cells (colorectal adenocarcinoma) and Human intestinal epithelial Caco-2 cells (colorectal adenocarcinoma)	RT-PCR	(Naruhashi et al. 2011)
Taxifolin	Human intestinal epithelial Caco-2 cells (colorectal adenocarcinoma)	Western blot, Flow cytometry and RT-PCR	(Lohner et al. 2007)
γ-Tocotrienol	Human intestinal epithelial LS180 cells (Dukes' type B, colorectal adenocarcinoma)	Western blot and Immunocytochemistry	(Abuznait et al. 2011b)
Topotecan	Human intestinal epithelial T84 cells (colorectal adenocarcinoma)	RT-PCR	(Haslam et al. 2008a)
Trazodone	Human intestinal epithelial LS180V cells (LS180 cells selected for elevated P-gp levels with increasing concentrations of vinblastine) (Dukes' type B, colorectal adenocarcinoma)	Western blot	(Störmer et al. 2001)
Triactyloleandomycin	Human intestinal epithelial LS 180 cells (Dukes' type B, colorectal adenocarcinoma)	Western blot	(Schuetz et al. 1996a)
Trichostatin A	Human intestinal epithelial SW620 cells (Dukes' type C, colorectal adenocarcinoma)	RNase protection assay and luciferase activity assay(*MDR1* promoter activity)	(Jin and Scotto 1998)
Trimethoxybenzoylyohimbine	Human intestinal LS1 80/AD5O cells (adriamycin-resistant subline) (Dukes' type B, colorectal adenocarcinoma)	Western blot and Northern blot	(Bhat et al. 1995)

Table 7. (cont.) Known P-gp inducers

Inducer	Experimental Model	Experimental Method	Literature Reference
Venlafaxine	Human intestinal epithelial Caco-2 cells (colorectal adenocarcinoma)	RT-PCR	(Ehret et al. 2007)
	Human brain endothelial cells (HBMEC)	Western blot	(Bachmeier et al. 2011)
	Friend Virus B-Type (FVB) mice (intestine)	ELISA	(Bachmeier et al. 2013)
Verapamil	Human intestinal epithelial LS 180 cells and its drug-resistant sublines, LS 180-AD50 and LS 180-Vb2 cells (Dukes' type B, colorectal adenocarcinoma)	Western blot, Northern blot and RT-PCR	(Abuznait et al. 2011a; Herzog et al. 1993; Schuetz et al. 1996a)
	Human intestinal epithelial Caco-2 cells (colorectal adenocarcinoma)	Flow cytometry	(Anderle et al. 1998)
	Human intestinal epithelial LS180V cells (LS180 cells selected for elevated P-gp levels with increasing concentrations of vinblastine) (Dukes' type B, colorectal adenocarcinoma)	Western blot	(Perloff et al. 2000; Perloff et al. 2001a)
	Human monocyte-derived dendritic cells	Flow cytometry	(Ishri et al. 2006)
Vinblastine	Human leukaemia cell lines: K562 (bone marrow lymphoblast; chronic myelogenous leukaemia) and H9 cells (cutaneous T lymphocyte;lymphoma)	cDNA-PCR	(Chaudhary and Roninson 1993)
	Mouse fibroblast 3T6-C26 cells	Flow cytometry	(de Graaf et al. 1996)
	Human peripheral blood promyeloblasts, HL-60 cells (acute promyelocytic leukaemia)	Flow cytometry	(Decleves et al. 1998)
	Human intestinal epithelial Caco-2 cells (colorectal adenocarcinoma)	Flow cytometry, Western blot and RT-PCR	(Anderle et al. 1998; Shirasaka et al. 2006)
	Human T lymphoblasts MOLT-4 cells (acute lymphoblastic leukaemia)	Flow cytometry and RT-PCR	(Liu et al. 2002b)
	Human intestinal epithelial LS180 cells (Dukes' type B, colorectal adenocarcinoma)	Western blot	(Harmsen et al. 2009)
Vincristine	Mouse skin lymphoblast (lymphocytic leukaemia)	Western blot	(Boháčová et al. 2006)
	Human intestinal epithelial LS180 cells (Dukes' type B, colorectal adenocarcinoma)	Western blot	(Harmsen et al. 2009)

[a] CAT - chloramphenicol acetyl-transferase; [b] Stereoselective regulation of MDR1 expression in Caco-2 cells by cetirizine enantiomers, since S-cetirizine decreased P-gp levels; [c]Kst-6 cells - human KB carcinoma cell line that has a stably integrated CAT reporter gene under the control of the human mdr-1 promoter; [d] The effects observed were not due to the compounds *per se*, but rather to their ability to inhibit the protein synthesis of a trans-acting transcriptional repressor (involved in the regulation of mouse and rat *mdr1a* and *mdr*1b and human *MDR1* gene expression);[e] FXR, secondary farnesoid X receptor; [f] In combination with progesterone; [g] hPXR, human pregnane X receptor. RT-PCR - Real-Time Polymerase Chain Reaction.

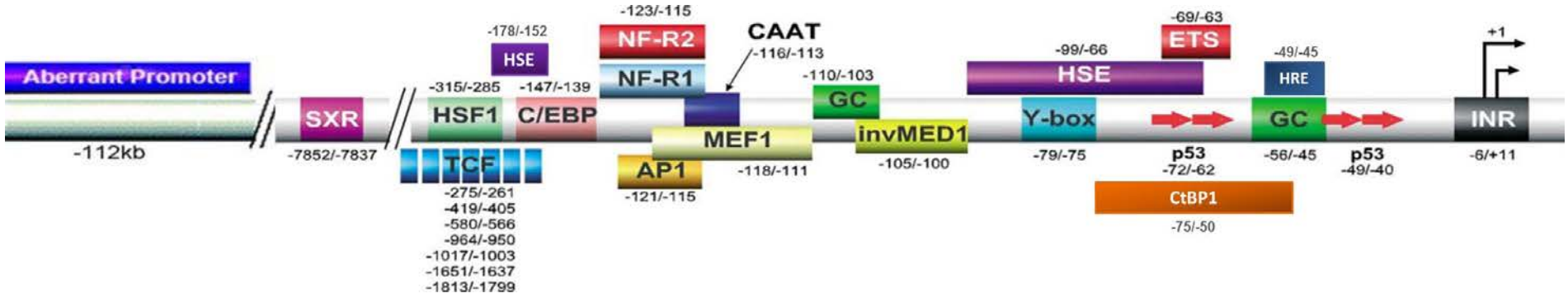

Figure 12. Schematic representation of the untranslated 5' regulatory region of the h*MDR1* gene showing promoter elements and their relative start sites.

The numbers under each promoter element indicate their position with respect to the +1 start site. Two arrows over the initiator window indicate the major and secondary start sites reported in the literature. Note that some binding sites overlap, and it is likely that different factors interact with these sites under different conditions. With the exception of PCAF, which is recruited to the *MDR1* promoter through interaction with NF-Y and Sp proteins, all other factors shown interact directly with DNA. TCF/LEF binds to several sites within the *MDR1* promoter, ranging from -1813 to -261. **INR**: initiator element - sequences between -6 and +11, which are sufficient for proper initiation of transcription; **GC-Box**: GC-rich region - binding site for nuclear transcription factor Sp1 (specificity protein 1); **Y-Box**: inverted CCAAT element - binding site for nuclear factor Y (NF-Y) and Y-box binding protein 1 (YB-1); **p53:** proposed binding sites for p53 tumor suppressor protein; **AP-1**: activator protein 1 - binding site for c-*jun* and c-*fos* transcription factors; **CAAT**: CAAT element binds a complex of nuclear factor κB/p65 and c-*fos* proteins; **C/EBP:** binding site for CCAAT-box/enhancer binding proteins (C/EBP); **HSE:** heat shock elements - binding sites for heat-shock transcription factors (HSF); **TCF:** T cell factor elements - involved in over-expression of P-gp in tumor cells; **invMED1:** inverted mediator-1 element *cis*-activates h*MDR1*; **MEF-1:** *MDR1* promotor-enhancing factor 1 up-regulates h*MDR1*; **NF-R1/2:** binding site for recently discovered transcription regulatory proteins, NF-R1/2; **ETS:** binding site for *ets* ('E twenty-six') proteins; **SXR:** steroid xenobiotic receptor - binding site for pregnane xenobiotic/retinoid xenobiotic receptor α (PXR/RXRα) heterodimer; **HRE**: hypoxia responsive element; **CtBP1:** binding site for C-terminal-binding protein 1. Adapted from (Labialle et al. 2002b).

The h*MDR1* gene greatly differs from its murine homologues, since its promoter lacks a TATA-box, as previously mentioned, and it contains an initiator element (INR), which is necessary to direct basal transcription at the major initiation start point (Figure 12) (Labialle et al. 2002b; Smale and Baltimore 1989). Moreover, transient transfection studies performed in HeLa cells demonstrated that sequences between -6 and +11(INR) were sufficient for proper transcriptional initiation, whereas deletion of sequences downstream of +11 resulted in a strong reduction of properly initiated transcripts (van Groenigen et al. 1993). Additionally, for the h*MDR1* gene, several promoter elements have already been found, including a GC-box, a Y-box, a p53 element, an inverted mediator-1 element (invMED1), an activator protein 1 (AP-1) element, an heat shock element (HSE) and a steroid xenobiotic receptor (SXR) element, among others (Figure 12) (Labialle et al. 2002b). Also, the regulation of the transcriptional activity of the h*MDR1* gene depends on several *trans*-acting proteins (transcription factors) that bind these consensus *cis*-elements, and does not occur via direct drug binding to P-gp (Figure 12) (Labialle et al. 2002b). In the up-regulation of the *MDR1* gene transcription, several transcription factors are involved, including heat-shock transcription factor 1 (HSF-1), specificity protein 1 (Sp1), activator protein 1 (AP-1), CCAAT/enhancer-binding protein beta (C/EBPβ or NF-IL-6, nuclear factor for IL-6 expression), nuclear factor Y (NF-Y), early growth response protein 1 (EGR-1), and Y-box binding protein 1 (YB-1) (Combates et al. 1994; Daschner et al. 1999; Hu et al. 2000; McCoy et al. 1995; Ogretmen and Safa 1999a; Ohga et al. 1998; Vilaboa et al. 2000). On the other hand, cross-coupling of nuclear factor-κB/p65 (NF-κB/p65) and c-fos inhibits its transcription (Ogretmen and Safa 1999b). In the following sections a detailed overview will be made on the constitutive and induced transcription of the h*MDR1* gene, highlighting the promoter elements and related transcription factors involved. Also, some studies on the transcription regulation of mouse *mdr1* genes will be focused. The elements involved in the constitutive P-gp overexpression in drug-resistant cells [MEF-1 (MDR1 promoter-enhancing factor 1) element, InvMED-1 (inverted mediator-1) element and aberrant promoter] (Figure 12) will not be discussed in the present dissertation.

I.6.2.2.1. Constitutive transcription of the h*MDR1 gene - constitutive regulators*

The ‘GC’ elements and the ‘CCAAT’ boxes (Figure 12) referred above are among the most ubiquitous Pol II promoter elements and are found in the majority of TATA-less promoters (Scotto 2003). Each element can interact with different families of proteins through sequence-specific DNA recognition and, since mutation or removal of these

elements often leads to a complete transcription loss, the proteins that interact with these elements were initially referred to as constitutive or 'basal' transcription factors (Scotto 2003). However, this label can be misleading, since more recent studies have demonstrated the role of these factors in mediating activation by exogenous agents, particularly those that regulate chromatin structure (Scotto 2003). Moreover, transfection analyses of promoter constructs mutated in one or both of these elements confirmed the requirement for each element in the constitutive (i.e. operative under normal growth conditions) expression of *MDR1* in some cell lines (Scotto 2003). Therefore, the following elements will be discussed with respect to both constitutive and inducible expression.

I.6.2.2.1.1. GC-BOX

In the h*MDR1* promoter, two GC-rich regions (GC-box) were identified from -110 to -103 and -56 to -45 bases upstream of the major +1 start site in the h*MDR1* promoter (Figure 12), and mutations in these regions were reported to modulate the promoter activity (Cornwell and Smith 1993b).

Located -56 to -45 bases upstream of major +1 start site is a GC-rich region called -50 GC-Box (Figure 12), that interacts with members of the Sp (specificity protein) family of transcription factors (Cornwell and Smith 1993a; Cornwell and Smith 1993b; Scotto 2003; Sundseth et al. 1997). In fact, it was demonstrated that this region is where specificity protein 1 (Sp1), a 105 kDa constitutive and ubiquous nuclear transcription factor, was found to bind (Cornwell and Smith 1993b). Sp1 was the first acetylene-type zinc finger-containing transcription factor to be isolated and cloned from mammalian cells and it regulates many proteins, particularly those involved in the regulation of nucleic acid biosynthesis and metabolism (including thymidylate synthase, adenine deaminase and DNA polymerase), and in the regulation of the cell cycle or proliferation (such as cyclin D, E2F, c-fos, transforming growth factor α [TGF-α]) (Safe and Abdelrahim 2005). Moreover, previous studies have demonstrated the Sp1 transcriptional stimulatory activity in the *MDR1* gene, since a mutation in the GC-box resulted in a 5-fold reduction in the promoter activity (Cornwell and Smith 1993b). Additionally, it was also demonstrated that this region contains overlapping sites that allows the specific binding of Sp1 but also of early growth response protein 1 (EGR-1), a zinc finger 80 kDa protein already implicated in the h*MDR1* gene activation (Cornwell and Smith 1993b). In fact, during aberrant P-gp expression in hematopoietic cancers, 12-*O*-tetradecanoylphorbol-13-acetate (TPA) was reported to activate the h*MDR1* gene promoter through binding of EGR-1, thus increasing h*MDR1* gene transcription (McCoy et al. 1995). Moreover, in the same studies, Wilms' tumor (WT) suppressor 1 (WT-1), another member of the EGR family, inhibited the response of the *MDR1* promoter to TPA in K562 cells, down-regulating h*MDR1* gene transcription through

direct binding of WT-1 to the same CG element (McCoy et al. 1999). Therefore, these results suggest that the h*MDR1* gene is antagonistically regulated by EGR-1 and WT-1, which compete for the same binding region of the h*MDR1* gene promoter, during normal and aberrant hematopoiesis.

Located -110 to -103 bases upstream of major +1 start site in the h*MDR1* promoter is another GC-rich region, called -110 GC-Box (Figure 12) that is incapable of interacting with Sp1, and which demonstrated to act as a binding site for a transcriptional repressor (Cornwell and Smith 1993b). In fact, mutation of the -110 G-box (-110 to -103) resulted in a 6-fold increase in the promoter activity and inhibited the formation of a specific nuclear protein complex, suggesting that this region functions as a transcriptional "repressor" binding site in cycling cells (in log-phase KB-8-5 cells) (Cornwell and Smith 1993b). Moreover, no binding to purified Sp1 or EGR-1 was observed at this GC-region (Cornwell and Smith 1993b). However, the cellular conditions under which the -110 GC-box modulates the h*MDR1* promoter activity, as well as the identity of the -110 G-box-binding protein remain unclear. It was proposed that this GC-region may interact with another member of the Sp family or the highly related Kruppel factor family of transcription factors (Bieker 2001).

A very recent study, which aimed to identify cell-specific controls on the *MDR1* transcription in human brain endothelium, using reporter assays, identified a region of 500 bp around the transcription start site that was optimally active in brain endothelium (Gromnicova et al. 2012). Chromatin immunoprecipitation identified specificity protein 3 (Sp3) and transcription factor II D (TFIID) associated with this region. Moreover, electrophoretic mobility shift assays (EMSA) confirmed that Sp3 binds preferentially to a Sp-target site (GC-box) on the *MDR1* promoter in brain endothelium (Gromnicova et al. 2012). Therefore, these results contrast with findings in other cell types in which Sp1 preferentially associates with the *MDR1* promoter (Scotto 2003). Moreover, in this same study, using Caco-2 cells, it was demonstrated that Sp1 binds to the *MDR1* GC-rich box, thus agreeing with those previous findings implying Sp1 as the preferential binding protein, but also indicating that *MDR1* is then differently controlled in brain endothelium (Gromnicova et al. 2012). Furthermore, the differences in *MDR1* transcriptional control between brain endothelium and Caco-2 cells could not be explained by the relative abundance of Sp1:Sp3 nor by the ratio of Sp3 variants, because activating variants of Sp3 were present in both cell types (Gromnicova et al. 2012).

I.6.2.2.1.2. Y-BOX (inverted CCAAT element)

Y-box is a CCAAT element that is found in the sense orientation or in the inverse complement ATTGG, present in one-third of all known promoters (Labialle et al. 2002b). In the h*MDR1* gene, it is present at the -79 to -75 sequence position (Figure 12), and its involvement in the h*MDR1* gene induction by various anticancer drugs and by UV radiation was already demonstrated (Ohga et al. 1998). The Y-box demonstrated to be crucial for the basal and inducible expression of the h*MDR1* gene, as shown by mutational analysis of the *MDR1* promoter (Goldsmith et al. 1993; Sundseth et al. 1997).

Nuclear factor Y (NF-Y), a trimeric transcription factor, was pointed out as the most likely protein to bind to this element and, thus, activate the h*MDR1* gene in tumor cell lines (Figure 13) (Hu et al. 2000; Jin and Scotto 1998; Sundseth et al. 1997). In fact, this CCAAT box-binding protein was reported to mediate *MDR1* activation by the histone deacetylase (HDAC) inhibitors, trichostatin A and sodium butyrate, through the recruitment to the promoter of a p300/CREB binding protein-associated factor (P/CAF), a transcriptional co-activator with intrinsic histone acetyltransferase (HAT) activity (Jin and Scotto 1998). Histone-modifying enzymes, HAT and HDAC, were reported to be involved in gene transcriptional activation and repression, respectively. HATs specifically catalyse the acetylation of the amino group of lysine residues at the N-terminal domain of histones, weakening histone-DNA interactions and leading to a destabilization of nucleosome structure (open chromatin), while HDACs remove the acetyl group, leading to a more closed chromatin configuration (Jin and Scotto 1998). It has been proposed that this restructuring of chromatin regulates accessibility of transcription factors to their DNA targets, whereby open chromatin allows for factor binding and closed chromatin does not (Jin and Scotto 1998). Incubation of human colon carcinoma SW620 cells with trichostatin A, a specific HDAC inhibitor, increased 20-fold the steady-state level of *MDR1* mRNA, and trichostatin A treatment of cells transfected with a wild-type *MDR1* promoter/luciferase construct resulted in a 10- to 15-fold induction of the promoter activity. Moreover, deletion and point mutation analysis determined that an inverted CCAAT box was essential for this activation, and that overexpression of P/CAF activated the wild-type *MDR1* promoter, but not a promoter containing a mutation in the CCAAT box. Moreover, deletion of the P/CAF HAT domain abolished the activation. Additionally, gel shift and super-shift analyses identified NF-Y as the CCAAT-box binding protein in these cells, and co-transfection of a dominant negative NF-Y expression vector decreased the activation of the *MDR1* promoter by trichostatin A. That was the first report of a natural promoter that is modulated by HAT and HDAC activities, in which NF-Y was identified as the transcription factor mediating this regulation (Figure 13) (Jin and Scotto 1998).

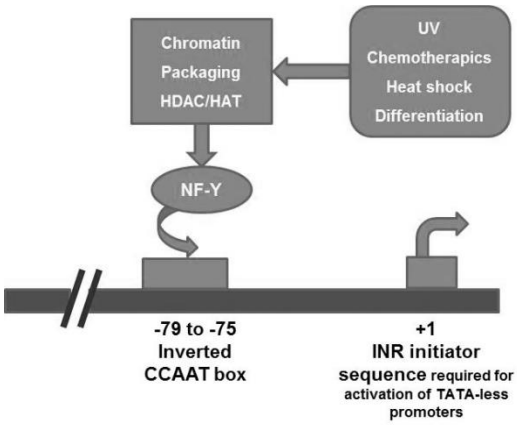

Figure 13. NF-Y mediated activation of the h*MDR1* gene.
Adapted from (Sukhai and Piquette-Miller 2000).

Other studies have reported that Y-box binding protein 1 (YB-1), a gene regulatory protein that preferentially interacts with RNA and single-stranded DNA, specifically interacts with the *MDR1* Y-Box to mediate transcription (Ohga et al. 1998). In fact, *in vitro* studies demonstrated that UV irradiation significantly increased 2-3-fold the nuclear YB-1 level in Kst6 cells, but it was unchanged in cells transfected with the antisense plasmid (Ohga et al. 1998). Moreover, gel mobility assays with nuclear extracts indicated that UV irradiation induced the activation of an inverted CCAAT box (Y-box) binding protein in those cells, being that enhancement of DNA binding activity to the Y-box abolished when cells were transfected with antisense YB-1 plasmids (Ohga et al. 1998). Thus, UV-induced activation of a Y-box DNA binding protein appeared to be correlated with the nuclear amount of YB-1 protein (Ohga et al. 1998).

In an effort to determine whether NF-Y, YB-1, or both transcription factors are required for *MDR1* induction by UV irradiation, it was demonstrated that the activation of the *MDR1* promoter by UV irradiation is dependent on the CCAAT box (-82 to -73), as well as on a proximal GC element (-56 to -42) (Hu et al. 2000). Moreover, gel shift and super-shift analyses with nuclear extracts prepared from human KB-3-1 cells identified NF-Y as the transcription factor interacting with the CCAAT box, while Sp1 was the predominant factor binding to the GC element. Additionally, mutations that abrogated binding of either of these factors reduced or abolished *MDR1* activation by UV irradiation, and co-expression of a dominant-negative NF-Y protein reduced the UV-activated transcription. Interestingly, it was demonstrated that YB-1 was unable to interact with double-stranded oligonucleotides containing the *MDR1* CCAAT box in nuclear extracts, while it interacted only with a single-stranded oligonucleotide containing this element (Hu et al. 2000). Mutations within the *MDR1* CCAAT box that abolished transcription and NF-Y binding, thus abolishing the *MDR1* activation by UV-irradiation, had no effect on the interaction of YB-1 with the single-stranded oligonucleotide. Also, co-transfection of a YB-1 expression plasmid had a repressive effect on UV-inducible transcription (Hu et al. 2000). These

results strongly suggested that NF-Y, but not YB-1, is the factor regulating *MDR1* transcription through the CCAAT element. Therefore, Hu et al. pointed the role of both NF-Y and Sp1 in the transcriptional activation of the *MDR1* gene by genotoxic stress, and indicated that YB-1, if involved, is not sufficient to mediate this activation (Hu et al. 2000).

Nevertheless, a number of studies have linked the YB-1 expression or its nuclear localization with an increase in *MDR1* gene expression (Bargou et al. 1997b; Oda et al. 2003; Ohga et al. 1998; Saji et al. 2003). For example, it was demonstrated that the acquisition of MDR in B-lymphoblasts (Daudi cells) upon exposure to doxorubicin is associated with enhanced YB-1 nuclear translocation and mitogen-activated protein kinase (MAPK)/extracellular signal-regulated kinase (ERK) activity (Shen et al. 2011). An electrophoretic mobility shift assay revealed that doxorubicin increased binding of YB-1 to the Y-box of *MDR1* promoter and luciferase reporter assays demonstrated that the Y-box region is essential for YB-1 regulation of *MDR1* expression (Shen et al. 2011). Silencing of YB-1 gene resulted in decreased expression levels of the *MDR1* gene and P-gp protein induced by doxorubicin. Also, when Daudi cells were pre-treated with a MAPK inhibitor, the phosphorylation of ERK was effectively inhibited as well as the nuclear translocation of YB-1 and the expression of *MDR1* gene. Therefore, doxorubicin can increase P-gp expression through activating MAPK/ERK transduction pathway, that in turns increases the expression of YB-1, inducing YB-1 nuclear translocation, and enhancing DNA-binding activity of YB-1 (Shen et al. 2011).

The h*MDR1* gene transcriptional regulation at Y-box seems to be more complex and mutational analyses have demonstrated that the Y-box and the closely located GC-box (-50 GC-Box) seem to act cooperatively in the regulation of h*MDR1* gene expression (Sundseth et al. 1997). In fact, these two elements (Y-box and GC elements) were, as mentioned above, reported as essential for the *hMDR1* gene transcriptional activation after UV irradiation (Hu et al. 2000), suggesting a cooperative interaction between the GC- and the Y-boxes. Additionally, it was demonstrated that a mutation of the proximal Y-box in other promoters can lead to the disruption of binding to the adjacent GC-box (Linhoff et al. 1997). Therefore, these results raised the suspicion that NF-Y could play an essential role in both the architectural and functional organization of TATA-less promoters, possibly by connecting upstream regulators to the general transcriptional machinery (Mantovani 1998). In conclusion, NF-Y plays a pivotal role in the regulation of *MDR1* gene expression under genotoxic stress conditions, and it is thought to be a good molecular target to overcome the MDR phenotype (Hu et al. 2000).

To evaluate the stress-induced activation of the *MDR1* gene, in a study reported by Shareef et al. (2008), the activity of the *MDR1* promoter in response to different doses of ionizing radiation was investigated (Shareef et al. 2008). In this study, two squamous cell

carcinoma oral cavity cell lines, T-167 and T-409 cells, were exposed to either a standard clinical dose of 2 gray (Gy, international unit of absorbed dose) or low-dose fractionated radiation therapy (LDFRT), delivered as 0.5 Gy in four fractions. *MDR1* gene expression and degree of cell death were assessed and clinically relevant 2-Gy dose of radiation resulted in increased *MDR1* expression, as evaluated by RT-PCR and luciferase reporter assays in both cell lines (T-167 and T-409), whereas LDFRT did not. Moreover, LDFRT caused enhanced apoptosis when compared with the 2-Gy dose in these cells, as assessed by terminal nucleotidyl transferase-mediated nick end labelling (TUNEL) assay. Interestingly, 2 Gy robustly induced both NF-Y and nuclear factor-κB (NF-κB) in both cell lines, but no induction was observed when exposed to LDFRT (Figure 14). Silencing the expression of the DNA binding subunit of NF-κB, p50, by small interfering RNA vector resulted in a decrease of *MDR1* function in T167 cells exposed to 2 Gy, as evaluated by the rhodamine 123 efflux assay (Shareef et al. 2008). These results provide evidence for NF-Y and NF-κB involvement in *MDR1* expression, and suggest an important role for LDFRT in combinatorial cancer therapy by preventing P-gp induction and possibly acting as an adjuvant for chemotherapy.

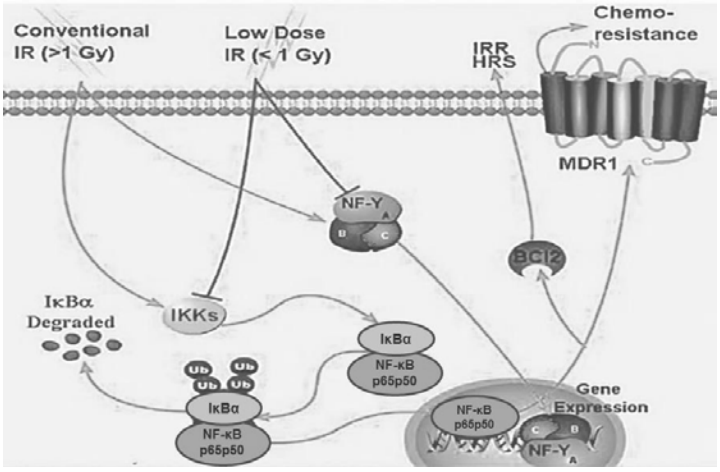

Figure 14. Schematic representation of the molecular mechanisms involved in the modulation of MDR1 gene by radiation.
The primary event in the molecular response is either the activation or inhibition of NF-κB and NF-Y in conventional dose irradiation and LDFRT, respectively. The activation of these factors triggers the induction of pro-survival factor Bcl-2, which causes induced radiation resistance (IRR) potentially through MDR1 expression, which induces chemoresistance. When there is absence or limited activation of these factors, i.e., NF-κB and NF-Y, in LDFRT, there is no induction of either Bcl-2 or *MDR1* gene expression, thereby giving rise to hyper-radiosensitivity (HRS) among the cells. Cells are thus more chemosensitive due to the loss of *MDR1* induction. Adapted from (Shareef et al. 2008).

I.6.2.2.1.3. p53 Element

High levels of expression of multidrug transporters are often observed in drug-naïve tumours, even when the tissue of origin exhibits little or no expression of the corresponding gene. Hence, constitutive *MDR1* gene expression is likely regulated in some cells by components that are involved in malignant transformation (Scotto 2003). It has been well established that tumours can develop as a result of both uncontrolled proliferation and an intrinsic ability to escape cell death, mediated by the altered expression of various oncogenes and tumor suppressor proteins. It has become apparent

that altered expression of several growth and death-controlling proteins can adversely affect drug therapy in two ways: (1) by altering the cell's ability to respond to death signals and (2) by influencing the transcription and, thus, the expression of drug-resistant genes (Scotto 2003). Therefore, knowing that several tumours that have never been in contact with anticancer drugs express the P-gp-dependent MDR phenotype, and since cellular oncogenes and tumor suppressor genes are often reported to be altered in the cancer progression, it is likely that the resulting altered proteins may be involved in the regulation of P-gp expression (Labialle et al. 2002b). The first evidence that a tumor suppressor protein could influence the expression of a drug-resistance gene came from the observation that wild-type p53 repressed transcription of the *MDR1* gene (Chin et al. 1992; Thottassery et al. 1997; Zastawny et al. 1993). Since then, several studies focused on the effects of the p53 suppressor gene and protein on the MDR phenotype.

Tumor suppressor protein p53 can either positively or negatively regulate the *MDR1* transcription (Li et al. 1997; Thottassery et al. 1997). In fact, it was reported an inhibitory role for wild type p53 on the h*MDR1* gene promoter, whereas mutant versions of p53 act as activators (Nguyen et al. 1994), probably through the loss of their inhibitor effect (Chin et al. 1992; Johnson et al. 2001b). Although several mechanisms had been proposed to explain the wild-type p53 repression, it was shown that this effect is mediated by a direct interaction of p53 with a novel binding element within the proximal *MDR1* promoter (-72 to -40) (Figure 12), making *MDR1* the prototype for a new class of p53-repressed promoters (Johnson et al. 2001b). Moreover, binding of p53 to this element, termed the HT (head-to-tail) site, appears to induce a novel tetrameric conformation of p53 that converts p53 from an activator to a repressor, perhaps through the differential recruitment of co-factors (Johnson et al. 2001b). This repression mediated by wild-type p53 has also been reported for the mouse and hamster *mdr1* homologues (Bush and Li 2002; Zastawny et al. 1993), while other studies suggest an activating role of p53 on the murine *mdr1* promoter in response to DNA damage and stress (Mathieu et al. 2001).

Paradoxically, as already mentioned, several common mutant p53 proteins demonstrated to activate, rather than repress, the *MDR1* promoter (Chin et al. 1992; Dittmer et al. 1993; Johnson et al. 2001b). At least one of these mutants activates *MDR1* through a cooperative, and apparently mutant-specific, interaction with the proto-oncogenic ETS-1 transcription factor (E twenty-six' protein 1) at a binding site within the proximal promoter region (located from -69 to -63 bases of the h*MDR1* promoter) (Figure 12) (Sampath et al. 2001).

The role of p53 in the regulation of drug resistance genes is still controversial, with opposite effects observed in different cells or under different conditions (Bahr et al. 2001). In fact, in some cases, wild-type p53 demonstrated to activate the gene h*MDR1* (Bahr et

al. 2001; Goldsmith et al. 1995), an apparent contradiction probably due to relevant differences in experimental conditions. The p53-mediated regulation of the h*MDR1* gene seems to involve the minimal promoter region from -39 to +53, and the consensus p53 biding site consists of two half-sites, each comprising two repeats of five nucleotides arranged head-to-head (May and May 1999). It was later proposed a new model to explain the action of p53 on the h*MDR1*promoter, in which, as previously referred, a binding region has been proposed in the h*MDR1* gene in which the two half-sites are arranged in a head-to-tail configuration leading to p53 repression (Johnson et al. 2001b).

Together with all the debates concerning the direct binding of p53 on the h*MDR1* promoter, it is also difficult to predict a modulating effect resulting from p53 interaction with other factors such as Sp1, NF-Y, C/EBPβ (CCAAT/enhancer-binding protein beta), or AP-1 (activator protein 1), all binding the h*MDR1* promoter (Labialle et al. 2002b) (Figure 12). Therefore, the complexity of these systems should not be underestimated, and it is important to keep in mind that the intricate architecture of the individual promoters, the complement of endogenous p53 (mutant or wild-type), the presence or absence of other p53 family members, as well as variations in cell- and tissue-specific co-effectors of p53 activity are all likely to influence the ultimate transcriptional readout in a given cell, tissue or tumor type (Scotto 2003).

I.6.2.2.1.4. NF-κB, TNF-α and PI3K signalling pathway

Apart from its involvement in the modulation of the *MDR1* gene by radiation (see I.6.2.2.1.2), the involvement of NF-κB in the *MDR1* expression was also demonstrated in other studies. NF-κB is a family of ubiquitous transcription factors. In most cells, the NF-kB dimers (consisting mainly of the proteins p65 and p50) are retained by an inhibitor (IkB) in the cytoplasm of non-stimulated cells (Figure 15). Following different stimuli, such as cytokines or DNA-damaging agents, including chemotherapeutic drugs, IκB is phosphorylated by the IκB kinase (IKK) complex, polyubiquitinated and degraded (Karin 1999). Then, the NF-κB nuclear localization signal (NLS) is released allowing the nuclear translocation of the transcription factor and the induction of its target genes. These target genes code for pro-inflammatory molecules, as well as for pro- or anti-apoptotic proteins (Pahl 1999). NF-κB has also been shown to play an anti-apoptotic role in cancer cells. In B lymphocytes, Hodgkin disease and some breast cancer cells, NF-κB activity is constitutive and protects against apoptosis (Bargou et al. 1997a; Sovak et al. 1997; Wu et al. 1996). Indeed, NF-κB inhibition in these cells often induces cell death. Numerous apoptotic signals, such as tumor necrosis factor alpha (TNF-α), ionizing radiations and chemotherapeutic drugs, have been shown to induce NF-κB (Pahl 1999). In what concerns to *MDR1* expression, it has been reported that an insulin-induced *mdr1*

expression is mediated by NF-κB in rat hepatoma cells (Zhou and Kuo 1997) and that NF-κB can protect kidney proximal tubule cells from cadmium and oxidative stress by increasing P-gp expression (Thevenod et al. 2000). Also, NF-κB was reported to be involved in TNF-α-induced *mdr1* expression in rat hepatocytes (Ros et al. 2001), in 2-acetylaminofluorene-induced *MDR1* expression in human liver cells (Kuo et al. 2002) and in constitutive *MDR1* expression in human drug-resistant cells (Um et al. 2001). Moreover, NF-κB induced a significant decrease in the cytotoxicity of chemotherapeutic drugs, which was found to be linked to the up-regulation of P-gp expression (Bentires-Alj et al. 2003; Thevenod et al. 2000).

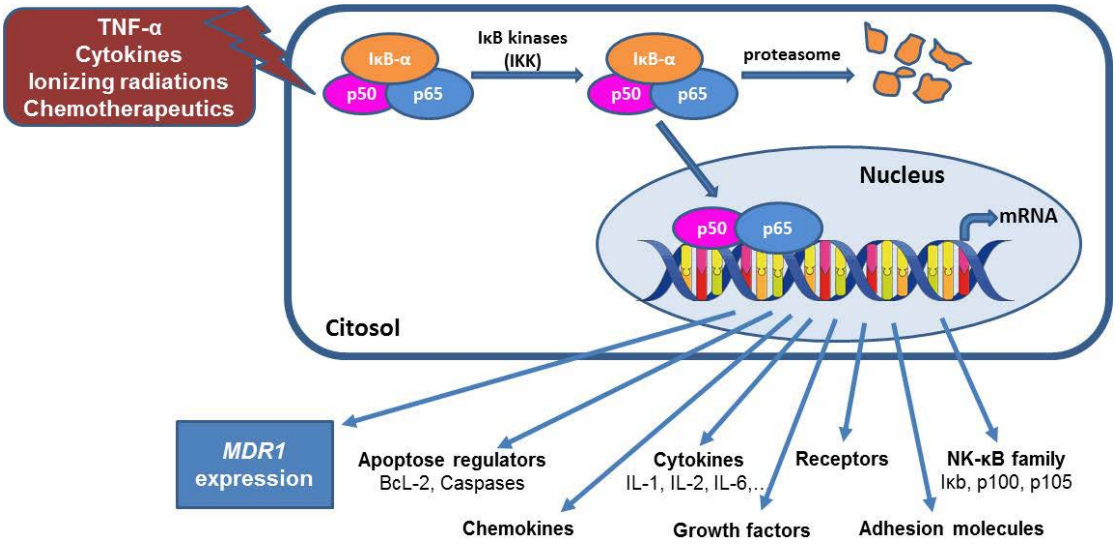

Figure 15. Classical activation of NF-κB pathway.

Additionally, NF-κB is activated in tumour cells by mutations in genes encoding NF-κB and in genes that control NF-κB activity, such as the inhibitor of κB (IkB) gene (Melisi and Chiao 2007). Chromosomal alterations of NF-κB family genes have frequently been found in MDR human cancers, indicating that this transcription factor also plays a crucial role in the MDR phenomenon (Hien et al. 2010). Because the *MDR1* gene expression appears to be NF-κB dependent, inhibitors of this transcription factor used in cancer chemotherapy may have the additional desirable effect of helping to prevent or overcome MDR. However, the role of NF-κB in *MDR1* regulation appears to be more complex, since NF-κB has been also shown to repress *MDR1* transcription (Ogretmen and Safa 1999b) (see below).

Interestingly, a CAAT element, located at the -116 to -113 sequence position in the h*MDR1* gene (Figure 12) (Labialle et al. 2002b), has been already implicated as the binding site for a protein complex consisting of NF-kB/p65 and c-*Fos* transcription factors (Ogretmen and Safa 1999b). These proteins have demonstrated a negative regulatory

effect on sensitive MCF-7 human breast cancer cells, but not on their resistant variant, the MCF-7/Adr cells (Ogretmen and Safa 1999b). Moreover, incubating MCF-7 nuclear extracts with antibodies specific for NF-κB/p65 or c-Fos almost completely inhibited the binding of the complex to the *MDR1* promoter, suggesting a cooperative interaction of NF-κB/p65 and c-Fos with the *MDR1* promoter (Ogretmen and Safa 1999b). Furthermore, the undetectable levels of NF-κB/p65-c-Fos interacting with the CAAT region of the *MDR1* promoter in MCF-7/Adr cells may explain the increased *MDR1* promoter activity in these cells (Ogretmen and Safa 1999b).Therefore, these results provided evidence that the molecular interplay (cross-coupling) between the NF-κB /p65 and c-Fos transcription factors exhibits a negative regulatory function on *MDR1* promoter by interacting with the CAAT region in MCF-7 cells, but not in MCF-7/Adr cells. As a consequence, these results highlight a new regulatory mechanism in which two unrelated factors interact to exert a negative transcriptional regulation. NF-κB thus appears to play a dual role in the regulation of *MDR1*, as an intermediate for rapid activation in response to stress, and as a transcriptional repressor in cells that have been chronically exposed to chemotherapeutic agents.

Additionally, it was also demonstrated the sensitization to radiation of a head and neck cancer cell line, UM-SCC-9 cells, using a mutant IκB (Kato et al. 2000). Also, the inhibition of NF-κB activity sensitizes resistant colon cancer cells (HCT15) through a decreased *MDR1* expression, being this effect cell- and signal-specific and dependent on the level of NF-κB inhibition. Indeed, NF-κB or P-gp inhibition in the HCT15 colon cancer cells led to increased apoptotic cell death in response to daunomycin treatment. Interestingly, NF-κB inhibition through transfection of a plasmid coding for a mutated IkB increased daunomycin cell uptake. Moreover, the inhibition of NF-κB reduced *MDR1* mRNA and P-gp expression in these cells. A consensus NF-kB binding site was identified in the first intron of the h*MDR1* gene and it was demonstrated that NF-κB complexes could bind to this intronic site. Also, NF-kB transactivated an *MDR1* promoter luciferase construct (Bentires-Alj et al. 2003). Therefore, these results demonstrated a role for NF-κB and its heterodimeric components in the resistance to chemotherapy through the regulation of the *MDR1* gene expression in cancer cells, which may be cell type specific (Bentires-Alj et al. 2003).

Another signalling pathway, which is frequently implicated in apoptosis, tumorigenesis and chemotherapeutic resistance, is the phosphoinositide-3-kinase (PI3K)/Akt cascade (Figure 21). The PI3Ks are a family of lipid kinases that propagate intracellular signalling cascades regulating a wide range of cellular processes, being this signalling pathway known to influence drug resistance (Wong et al. 2010). The serine/threonine kinase Akt (also known as protein kinase B or PKB) is a downstream

target of PI3K and has become a major focus of attention because of its critical regulatory role in diverse cellular processes, including cancer progression and insulin metabolism. It was demonstrated that the PI3K/Akt pathway is also linked to P-gp-mediated chemoresistance in the L1210 leukemia cell model (Barancik et al. 2006). Also, hyaluronan oligosaccharides have been shown to sensitize P-gp positive vincristine-resistant lymphoma cells through the modulation of P-gp activity and PI3K/Akt pathway (Cordo Russo et al. 2008). Several other studies have demonstrated that inhibitors of the PI3K/Akt pathway modulate MDR by impairing the function of P-gp, which allows drugs to accumulate in the cells, induce apoptosis and ultimately prevent the growth of drug-resistant cancer cells (Barancik et al. 2006; Chiarini et al. 2008; Garcia et al. 2009). Inhibition of Akt kinase also enhances susceptibility to TRAIL (TNF-related apoptosis-inducing ligand) by up-regulating death receptors and down-regulating P-gp expression in multidrug-resistant human T-acute leukemia cells (Seo et al. 2010). PI3K and Akt are upstream signals in the activation of Rac (Figure 21), a small (~21 kDa) signalling G protein, which is also associated with the induction of *MDR1* expression and may contribute to the development of drug resistance in liver cancer cells (Kuo et al. 2002).

In what concerns to TNF-α, promising results have indicated its potential as an anticancer therapeutic agent acting by affecting immunity and cellular remodelling, and influencing apoptosis and cell survival (Szlosarek and Balkwill 2003). Evidence from numerous studies indicates that expression and activity of P-gp can be controlled by the activity of TNF-α. For example, it was found that cells resistant to vincristine and doxorubicin are regulated by a TNF-α mediated NF-κB signalling pathway (Figure 21), and inhibition of TNF-α or NF-κB may be a useful treatment for MDR leukaemias (Garcia et al. 2005). Many different pathways of signal transduction are involved in the regulation of TNF-α, and recent advances in the understanding of upstream and downstream events may allow MDR to be overcome.

Finally, PTEN, a 403 amino acid protein present on the plasma membrane and in the nucleus, which has dual lipid and protein phosphatase function, have demonstrated to have a role in MDR and in the regulation of the PI3K/Akt cascade (Lee et al. 2004) (Figure 21). The PTEN network encompasses signals from cell surface growth factor receptors to nuclear transcription factors and includes connections to other tumour suppressor and oncogenic signalling pathways (Keniry and Parsons 2008). PTEN keeps cellular phosphatidylinositol 3,4,5-triphosphate (PIP_3) at a low level *in vivo*, removing the 3′-phosphate from PI3K generated PIP_3 and converting it to phosphatidylinositol 4,5-diphosphate (PIP_2) (Figure 21)(Maehama and Dixon 1998). The protein phosphatase activity of PTEN is suppressive with a dual role in tumorigenesis. Reduction of PTEN in the human adenocarcinoma cell line OVCAR-3 resulted in the development of MDR (Lee

et al. 2005). These alterations conferred cisplatin resistance via PTEN-mediated activation of the PI3K/Akt signalling pathway in a blockade of apoptosis (Lee et al. 2005). PTEN is able to alter cell sensitivity to drugs, depending on the mechanism of action of the drug, and lead to other specific signalling environments (mitogen-activated protein kinase [MAPK], p53, B-cell lymphoma 2 protein [Bcl-2], etc.) that could induce P-gp-mediated MDR in various cancers (Ji et al. 2007).

I.6.2.2.1.5. AP-1 Element

Many studies have proposed that activator protein-1 (AP-1) mediated signals may be important regulators of h*MDR1* (Labialle et al. 2002b). AP-1 is the general term for transcription factor complexes composed of members of the Fos and Jun oncogene families (Shaulian and Karin 2001), containing either the leucine zipper proteins, *Fos-Jun*, or *Jun-Jun* complexes, which bind to target elements and promote transcription (Callaghan et al. 2008). AP-1 is constitutively expressed in many cell types, and the complex binding to DNA is induced by serum stimulation, phorbol esters, a variety of growth factors, as well as by various stress stimuli (Scotto 2003). In fact, AP-1 activity is regulated by the cellular redox state, which is thought to be a consequence of specific cysteine residues located at the interface between the 2 c-Jun subunits (Janssen et al. 1995). The stressors invoke a signal cascade that begins with the activation of mitogen-activated protein kinases (MAPKs) and ends with the activation of AP-1 (Callaghan et al. 2008).

There is some evidence, albeit indirect, that the AP-1 complex may be involved in the transcription of several drug transporters. One argument that supports the involvement of AP-1 in the regulation of h*MDR1* is the fact that MDR cells often contain a higher level of c-*fos* and c-*jun* proteins relative to their sensitive parental cells (Daschner et al. 1999; Kim and Beck 1994). Additionally, inhibition of protein kinase A (PKA), an inducer of the AP-1 complex, by H-87, a PKA inhibitor, inhibited the activity of the *MDR1* promoter in a dose-dependent manner, and decreased the expression of h*MDR1* in the P388/M leukemia cell line (Kim et al. 1993). However, since PKA has also been implicated in the regulation by Sp1 (Rohlff and Glazer 1998), the interpretation of this data is complex.

The roles of cAMP-dependent PKA and its activator cAMP in the development of the P-gp-induced MDR phenotype have been extensively studied (Figure 21). cAMP is synthesized from ATP by adenylyl cyclase and is rapidly broken down via hydrolysis to adenosine 5′-monophosphate (5′-AMP) by cAMP phosphodiesterases (Merkle and Hoffmann 2011). Numerous extracellular signals exist, which lead to cAMP-dependent activation of PKA-related proteins that could result in activation of the multispecific *MDR1* gene (Rohlff and Glazer 1995). A cAMP-dependent PKA pathway for *mdr1* activation was

shown in primary rat hepatocytes, supporting that cAMP/PKA phosphatase activity modulates P-gp expression (Ziemann et al. 2006). MAPK (Misra and Pizzo 2009) and PI3K/Akt (Leone et al. 2007) signalling pathways are also known to affect cAMP and PKA. It is likely that the MDR phenotype involves interaction among all these signalling pathways (see I.6.2.2.4) (Figure 21).

Studies of the c-Jun NH_2-terminal protein kinase (JNK) (Figure 21), which also activates AP-1, also contributed to the evidence of AP-1 involvement in the h*MDR1* transcription. The proposed role for JNK in the regulation of the *MDR1* gene has been controversially discussed with evidence supporting both an activation effect and a repressive effect on the h*MDR1* transcription. JNK is a member of the MAPK family, which binds to and phosphorylates the NH_2-terminal activation domain of the transcription factor c-Jun (Weston and Davis 2002), and that is activated in response to many stressful stimuli including heat shock, UV irradiation, protein synthesis inhibitors, and inflammatory cytokines (Osborn and Chambers 1996). Moreover, evidence suggests that JNK modulates the development of the MDR phenotype (Bark and Choi 2010; Lagadinou et al. 2008; Sui et al. 2011; Zhang et al. 2009). In human KB-3 carcinoma cells, treatment with doxorubicin resulted in a time- and dose-dependent activation of JNK up to 40-fold, and treatment with vinblastine or etoposide also activated JNK, with maximum increases of 6.5- and 4.3-fold, respectively. Consistent with these findings, increased c-jun phosphorylation was observed after these drug treatments. Additionally, two multidrug-resistant variants of KB-3 cells, KB-A1 and KBV1, selected for resistance to doxorubicin and vinblastine, respectively, showed increased basal levels of JNK activity, when compared to the KB-3 parental cell line, with no change in JNK protein expression, indicating that JNK is present in a highly activated form in the MDR cell lines. Moreover, under conditions optimal for JNK activation, doxorubicin, vinblastine, and etoposide induced *MDR1* mRNA expression in KB-3 cells, suggesting that JNK activation is an important component of the cellular response to structurally and functionally distinct anticancer drugs, and may also play a role in the MDR phenotype (Osborn and Chambers 1996). The overexpression of the MAP3K1 gene (also known as MEKK 1) in the human cell line HeLa selectively activated JNK, leading to an increase in the levels of MDR1 mRNA and P-gp protein (Figure 21) (Comerford et al. 2004).

Several putative nonconsensus AP-1 binding sites have been reported the *hMDR1* promoter, as well as on rodent P-gp promoters. (Labialle et al. 2002b; Scotto 2003). While the AP-1 site in the murine homologue mediates the repression of this gene (Ikeguchi et al. 1991), the AP-1-binding elements in the promoters of the hamster (-55 to -49) (Teeter et al. 1991a; Teeter et al. 1991b) and human genes (Daschner et al. 1999) are involved in transcriptional activation. Located -121 to -115 bases upstream of the major +1 start site

in the h*MDR1* promoter (Figure 12) is an AP-1 promoter element, being this a binding site for important regulators of the h*MDR1* gene, such as the c-*jun* dimer (Daschner et al. 1999). In this study, it was observed an increase in the amount of both c-jun and c-fos mRNA in cells with 12-, 65-, or 200-fold higher resistance to doxorubicin (MDR MCF-7 cells) when compared to drug-sensitive MCF-7 wild-type cells. Moreover, an increase in the DNA binding activity of an AP-1 complex in nuclear extracts from MDR MCF-7 cells was shown, when compared to extracts from wild-type cells. Also, it was reported a proportional increase in luciferase expression from a reporter vector containing consensus AP-1 binding sites in transiently transfected MDR cells, when compared to wild-type MCF-7 cells, indicating that AP-1 mediated gene expression is increased in drug-resistant MCF-7 cells. Nuclear extracts from resistant MCF-7 cells also displayed an increased level of DNA binding of jun/jun dimers to an oligonucleotide probe that contained the relevant *MDR1* promoter sequences (-123 to -108), indicating that AP-1 was capable of binding to this promoter site (Daschner et al. 1999). Additionally, co-transfection of wild-type cells with a c-jun expression vector and AP-1 luciferase constructs demonstrated that c-jun could activate gene expression from both the consensus and the *MDR1* AP-1 sites in a dose dependent manner. Noteworthy, RT-PCR and western blot analysis also showed that levels of *MDR1* mRNA and P-gp were increased in c-jun transfected wild-type cells. Therefore, these data indicate that increased AP-1 activity may be an important mediator of MDR by regulating the expression of *MDR1* gene (Daschner et al. 1999).

Additionally, a very recent study performed with vinblastine resistant Caco-2 cells (Caco-2 vbl) provided evidence that AP-1 and NF-κB are involved in the P-gp induction in these resistant cells (Chen et al. 2013). Since vinblastine induces both AP-1 and NF-κB, the role of these transcription factors in the regulation of the *MDR1* gene expression was investigated using reporter gene assays. The results indicated that the AP-1 and NF-κB luciferase activity was higher in Caco-2 vbl cells than in Caco-2 cells. Also, the mRNA expression of AP-1 subunit c-Jun and NF-κB was increased, and the c-Jun inhibitor, SP600125, and NF-κB inhibitor, pyrrolidine dithiocarbamate (PDTC), suppressed the expression of *MDR1* mRNA in these Caco-2 vbl cells (Chen et al. 2013).

However, contradictory results were also reported suggesting that c-Jun and JNK activation can inhibit the expression of *MDR1* in human MDR cells. MDR FM3A/M cells overexpressing P-gp demonstrated to have significantly lower basal and drug-stimulated JNK activity than parental FM3A/M cells, and were resistant to anticancer drugs. After JNK gene transfection, MDR FM3A/M cells recover the basal and drug-stimulated activities of JNK and the susceptibility to anticancer drugs (Kang et al. 2000). Other studies indicated that reactive oxygen species (ROS) down-regulated P-gp expression and activated JNK in multicellular prostate tumor spheroids (Wartenberg et al. 2001b).

Also, TNF-α can suppress *MDR1* expression in MDR cells (Stein et al. 1996) and promote c-jun expression (Chen and Goeddel 2002). In mouse hepatoma cell lines, a canonical AP-1 binding sequence in the promoter of mdr3/mdr-1a negatively regulated gene expression (Ikeguchi et al. 1991). Moreover, in a study performed by Miao et al. it was demonstrated that c-Jun activation down-regulates *MDR1* gene expression in the human K562/A02 MDR cell line (Miao and Ding 2003). Indeed, it was shown that salvicine, a topoisomerase II inhibitor, suppressed *MDR1* expression in MDR cells and promoted c-jun expression in both MDR and parental K562 cells. Moreover, the levels of c-jun expression were enhanced by salvicine in K562/A02 cells before the reduction of *MDR1* mRNA and P-gp protein levels. Furthermore, c-jun antisense oligodeoxynucleotides prevented salvicine-stimulated enhancement of c-Jun protein and reduction of *MDR1* gene expression, but did not affect the increase in c-jun mRNA levels, confirming that c-Jun activation is a prerequisite for reduction of *MDR1* mRNA and P-gp protein levels. Salvicine also enhanced the levels of the active forms of JNK (promoting its phosphorylation) and c-Jun, in both MDR K562/A02 and parental K562 cells, and raised the DNA-binding activity of AP-1. Additionally, c-jun antisense oligodeoxynucleotides also inhibited salvicine-induced apoptosis and cytotoxicity in MDR and parental K562 cells. Therefore, the authors proposed a possible pathway for the down-regulation of *MDR1* expression by salvicine, through the stimulation of JNK phosphorylation and activation, resulting in c-Jun phosphorylation and activation. Activated c-Jun promotes expression of c-jun itself, represses *MDR1* transcription, and triggers pro-apoptotic signals, resulting in low *MDR1* expression and cell death. These findings suggested that c-jun might be a potential drug target for circumventing tumor MDR (Miao and Ding 2003). In accordance, it was later demonstrated that the adenovirus-mediated enhancement of JNK reduced the level of P-gp in a dose- and time-dependent manner, being this decrease independent of the protein stability, and primarily occurring at the mRNA level (Zhou et al. 2006). It was shown that P-gp down-regulation required the catalytic activity of JNK and was mediated by c-Jun, as both pharmacologic inhibition of JNK activity and dominant-negative suppression of c-Jun remarkably abolished the ability of JNK to down-regulate P-gp. Also, the observed decrease in P-gp was associated with a significant increase in intracellular drug accumulation and dramatically enhanced the sensitivity of MDR cancer cells to chemotherapeutic agents (Zhou et al. 2006). Therefore, this study provided direct evidence that enhancement of the JNK pathway down-regulates P-gp and reverses P-gp-mediated MDR in cancer cells. In a more recent study, using photodynamic therapy with pheophorbide, it was also found that JNK pathway activation down-regulated P-gp, which enhanced intracellular doxorubicin accumulation in MDR human liver tumor cells (Tang et al. 2009).

It was recently reported a possible interplay between the JNK/c-Jun/AP-1 and NF-κB-mediated pathways. In fact, it was demonstrated that PSC833, a well-known non-immunosuppressant cyclosporine analogue that functionally inhibits P-gp, not only sensitizes SK-MES-1/DX1000 cells to doxorubicin by enhancing drug accumulation, but also down-regulates *MDR1* mRNA and P-gp expression in a time- and concentration-dependent manner, by activating JNK/c-Jun/AP-1 and suppressing NF-κB (Bark and Choi 2010). In general, NF-κB and JNK are known to be simultaneously activated under a variety of stress conditions. Since, activation of NF-κB inhibits JNK activation, inhibition of NF-κB sensitizes stress responses through enhanced or prolonged JNK activation (Zhang and Chen 2004). Although the JNK pathway activates *MDR1* expression in hypoxia, which is dependent on hypoxia-inducible factor 1 rather than AP-1 (Liu et al. 2007), contradictory results were also reported, as previously referred, in which the JNK pathway and the transcription factor c-Jun play an important role in the down-regulation of *MDR1* expression (Miao and Ding 2003; Zhou et al. 2006). On the other hand, activation of NF-κB was shown to induce *MDR1* expression (Bentires-Alj et al. 2003) (see I.6.2.2.1.4). Moreover, it is known that NF-κB and JNK signalling pathways are functionally interconnected. In fact, the anti-apoptotic function of NF-κB is mediated in part through its ability to down-regulate JNK activation (Nakano 2005). Thus, it is not surprising that JNK and NF-κB are involved as rivals in the PSC833-induced down-regulation of *MDR1* expression (Bark and Choi 2010).

I.6.2.2.1.6. Ras/Raf and WT-1 signalling pathways

The *MDR1* gene seems to be also a target of the ras/raf signalling pathway (Figure 21) (Kim et al. 1997; Miltenberger et al. 1995). The serine/threonine kinase Raf-1, is a component of intracellular signalling pathways that control responses to extracellular stimuli (Miltenberger et al. 1995). Raf becomes activated by membrane-associated signals once receptor tyrosine kinase-activated Ras recruits cytosolic Raf to the plasma membrane (Leevers et al. 1994). Raf then initiates a protein kinase cascade that results in activation of the MAPKs [also known as ERKs, for extracellular signal- regulated kinases (Howe et al. 1992)] (Figure 21), being this pathway known as Ras/MAPK pathway. The MAPKs are a family of serine/threonine kinases that directly regulate cytosolic and cell surface enzymes, as well as a number of transcription factors (Davis 1993). Although there are alternative signalling pathways that act independently of Ras and Raf, genetic evidence indicates that the majority of receptor tyrosine kinase- and/or Ras-dependent signalling events are mediated by Raf to the downstream MAPKs (Miltenberger et al. 1995). Specific inhibitors of the MAPK pathway significantly reduced the survival of MDR1-mediated MDR cancer cells, suggesting that the activation of such pathways leads

to P-gp overexpression is an intrinsic MDR phenotype (Duraj et al. 2005; Kisucka et al. 2001). Also, novel derivatives of tetrandrine and 3-(5′hydroxymethyl-2′-furyl)-1-benzylindazole were shown to effectively reverse P-gp-mediated MDR by inhibiting the MAPK signalling pathway (Sui et al. 2012).

Several transcription factors have been implicated as downstream targets in Raf-mediated pathways. For example, MAPK-related proteins directly phosphorylate the Ets related factor Elk-1(Ets, E-twenty six family of transcription factors) (Janknecht et al. 1993) and the proto-oncogene c-*jun* (Smeal et al. 1991). Phosphorylation of Elk-1 stimulates transactivation by the serum response factor (SRF) at the serum response element (SRE) to mediate the immediate-early serum response of genes such as c-*fos* (Gille et al. 1992). Complexes of c-*Jun* and c-*Fos* bind to AP-1 sites, as previously described, and regulate transcription of genes such as collagenase and interleukin 2 in response to growth-promoting phorbol esters (Angel et al. 1987; Angel and Karin 1991). In support of a link between Raf and MAPK, studies have shown that the constitutively active kinase, v-Raf, can increase transcription mediated by the SRE or AP-1 sites (Miltenberger et al. 1993). Furthermore, Raf inhibition by a dominant-negative mutant that prevents Ras-Raf association (Zhang et al. 1993) specifically blocks transcription from overlapping AP-1/Ets binding sites (Bruder et al. 1992), indicating that Raf is an obligate upstream regulator of AP-1 and Ets factors.

Moreover, PI3K activation may be necessary for Ras induced MDR, although preliminary studies suggest that inhibition of PI3K signalling alone may not be the only way to effectively overcome P-gp-mediated MDR *in vitro* (McCubrey et al. 2006). Indeed, activation of multiple signal transduction pathways, including the PI3K/Akt pathway and MAPK cascade, induced MDR in cancer cells (Wang et al. 2011). These studies suggest that established cancers with Ras mediated pathways may not be sensitive to single-agent PI3K pathway inhibitors.

As previously referred, EGR-1, a ubiquitous immediate early factor, and WT-1, the Wilms' tumor suppressor protein 1, also interact with GC sequences through their zinc-finger domains. Interestingly, both EGR-1 and WT-1 recognize a site within the *MDR1* GC element that overlaps the Sp1/Sp3-binding sequence, being the activation of *MDR1* by TPA mediated by EGR-1 (McCoy et al. 1995) and suppressed by WT-1 (McCoy et al. 1999) (see I.6.2.2.1.1). Therefore, it appears that the regulation of *MDR1* expression by ras/raf and WT-1 involves a complex interplay of transcription factors within a very discrete promoter region (Scotto 2003).

Additionally, the p38-MAPK pathway, another MAPK cascade, also seems to play an important role in modulating P-gp-mediated drug resistance. Constitutive overexpression of the *MDR1* gene in drug-resistant human gastric cancer SGC7901/VCR

cells was shown to be dependent on p38-MAPK phosphorylation (Guo et al. 2008). Inhibition of the p38-MAPK pathway restored the sensitivity of these cells not only to P-gp substrates but also to non-P-gp-substrates (Guo et al. 2008). Previous reports had shown that the MDR phenotype was clearly associated with increased levels and activity of p38 MAPK in the murine leukaemia cell line L1210/VCR, and SB203580 (an inhibitor of the p38 MAPK pathway) significantly reduced the degree of vincristine resistance by inducing tumour cell apoptosis (Barancik et al. 2001). Moreover, the p38-MAPK pathway inhibition reversed the P-gp-mediated MDR without affecting P-gp expression (Barancik et al. 2001). This inhibitor did not influence P-gp expression in human colorectal cancer cells HCT-15 and SW620-14 (Katayama et al. 2007). Therefore, p38-MAPK appears to modulate P-gp transport activity rather than P-gp transcription. The MAPK cascades (ERK, p38-MAPK, and JNK) are, thus, important signal transduction pathways that are activated by many different stimuli (Breier et al. 2013) and have an important role in P-gp modulation.

I.6.2.2.1.7. NF-R1 and NF-R2 elements

The sequence between -123 to -115 at the *MDR1* promoter has demonstrated to bind two different proteins, NF-R1 and NF-R2, resulting in antagonistic effects on the *MDR1* transcription (Ogura et al. 1992; Takatori et al. 1993) (Figure 12). In fact, Ogura et al. identified and purified NF-R1, a 110-kDa protein, and found that it specifically binds to two unrelated motifs, the ATTCAGTCA motif (sequence between –123 and –115) and the GC-box motif (between -56 and -45; the Sp1/EGR-1 site), on the MDR1 proximal promoter (Ogura et al. 1992) (Figure 12). Moreover, methylation interference analysis revealed that the nucleotides were in close contact with the purified NF-R1 on the ATTCAGTCA and GC-box motifs, and by competition gel mobility shift assay using point mutated oligonucleotides it was demonstrated that the nucleotides were required for the NF-R1 binding. Additionally, a chloramphenicol acetyltransferase (CAT) expression assay was performed, using the corresponding point-mutated *MDR1* promoter fused to a CAT gene (2 bp scanning mutations within either the upstream or the downstream GC-box), and showed the inhibition of NF-R1 binding to the promoter, which resulted in a 2- to 3-fold increase of CAT activity, as compared to the intact promoter in doxorubicin-resistant K562 cells, suggesting the presence of a repressor binding site. Thus, NF-R1 exerts a negative regulation of the *MDR1* gene transcription (Ogura et al. 1992). While a repressor site had already been described in the promoter region of -110 (Cornwell and Smith 1993b), the presence of a repressor in the downstream site appears to be in conflict with the aforementioned study in which Sp1 and EGR-1 functioned as activators at the

downstream GC-box. However, different mutations and different cell lines were analysed in these conflicting studies, preventing direct comparison of the results.

On the other hand, NF-R2, another DNA-binding protein, was also reported to interact with the *MDR1* gene proximal promoter sequence, binding within the -119 and -111 region, which contains the previously mentioned ATTCAGTCA motif (Takatori et al. 1993) (Figure 12). This protein was purified from the nuclear extract of K562/ADM cells and run as a single protein of 75 kDa on SDS-PAGE. CAT expression assay and gel mobility shift competition assay with mutated promoters revealed that the ATTCAGTCA motif is a positive regulatory element of *MDR1* gene and that the motif is important for NF-R2 binding, thus suggesting that NF-R2 may be involved in the positive regulation of the *MDR1* gene transcription (Takatori et al. 1993). Because this overlaps the binding site for NF-R1, and mutations in the site reduced the binding of both complexes, the relative role of NF-R1 and NF-R2 in *MDR1* regulation through the upstream GC-box is not yet clear. In fact, the role of these two proteins still remains unclear as no further data have been reported.

I.6.2.2.1.8. TCF Elements

Among the T-cell factor (TCF) family, some members have already been reported as tumor inducers and as being involved in the cancer proliferation and progression (Roose and Clevers 1999; Soler et al. 1999). These factors are transcriptionally inactive but are activated upon interaction with β-catenin, a dual function protein regulating the coordination of cell-cell adhesion and gene transcription (Brembeck et al. 2006; Gumbiner 2005), and in turn over-activate their target genes as a result of increased levels of β-catenin in many cancer types, including colorectal adenomas and to skin and liver tumours (Labialle et al. 2002b). The elevated levels of β-catenin result from a mutation in the *adenomatous polyposis coli* (APC) gene, a tumor suppressor gene, or from a mutation in the β-catenin gene, that stabilize the protein (Labialle et al. 2002b). In fact, mutations in the tumor suppressor APC gene have been documented in greater than 80% of all sporadic hereditary colon cancers (Bright-Thomas and Hargest 2003). Loss of APC function leads to the nuclear accumulation of β -catenin, that co-activates the transcription complex TCF/LEF (T-cell factor/lymphoid enhancer factor) (Scotto 2003). Specifically, a TCF4/β-Catenin complex, binding to seven elements spanning the -1813 to -261 sequence of the *h*MDR1 gene (Figure 12), has been reported as an h*MDR1* transcriptional activator, which may promote early abnormal expression of this gene in colorectal carcinogenesis (Yamada et al. 2000), providing one possible explanation for the overexpression of *MDR1*, and 'intrinsic' drug resistance in many colorectal cancers. Using a large-scale comparison of 7000 genes by two-color fluorescence hybridization of cDNA

microarray, *MDR1* was found to be transcriptionally down-regulated after the inactivation of TCF4. Additionally, aberrant expression of *MDR1*, concomitant with the accumulation of β-catenin, occurs even in small pre-cancerous lesions of familial adenomatous polyposis patients. Therefore, it was proposed that the *MDR1* gene promoter contains multiple TCF4-binding sequences, and is a direct target gene of the TCF4/β-catenin transcriptional complex (Yamada et al. 2000).

Recently, Corrêa et al. demonstrated that the Wnt/β-catenin pathway (also known as the canonical Wnt pathway) regulates *MDR1* in chronic myeloid leukemia (CML)(Correa et al. 2012). In fact, the advanced phases of CML are known to be more resistant to therapy, being this resistance associated with the overexpression of *MDR1*. Also, CML progression has been associated, among others, with the canonical pathway of Wnt signalling. Activation of this pathway leads to nuclear accumulation of β-catenin, which activates the TCF/LEF1 family of transcriptional factors (Figure 16). Therefore, given the existence of seven TCF/LEF1 consensus binding sites on the basal promoter of this gene (Figure 12) (Labialle et al. 2002b) it was hypothesized the possibility of *MDR1* regulation by the canonical Wnt pathway. Using MDR (overexpressing *MDR1*) and non-MDR cell lines (Lucena and K562, respectively) as models of CML, it was demonstrated that β-catenin was present in the protein complex on the basal promoter of *MDR1* in both cell lines, *in vitro*, but its binding was more pronounced in the resistant cell line, as evaluated by a ChIP assay, which allows analysis of nuclear protein-DNA interactions. Lucena cells exhibited higher β-catenin levels compared to its parental cell line. Also, it was demonstrated that β-catenin binds to the TCF/LEF consensus binding site at the *MDR1* promoter. *MDR1* positive regulation by the canonical pathway of Wnt signalling was clearly demonstrated with Wnt1 and β-catenin depletion, and overexpression of nuclear β-catenin, together with TCF binding sites activation (Correa et al. 2012).

The Wnt/β-catenin pathway was also involved in neuroblastoma (NB) (Flahaut et al. 2009) and breast cancer (Bourguignon et al. 2009) chemoresistance. In fact, Flahaut *et* al. investigated the mechanisms underlying the chemoresistant phenotype in NB by gene expression profiling of a doxorubicin (DoxR)-resistant and a sensitive parental cell line (Flahaut et al. 2009). Not surprisingly, the *MDR1* gene was included in the identified up-regulated genes, although the highest overexpressed transcript in both cell lines was the frizzled-1 Wnt receptor (FZD1) gene, an essential component of the Wnt/β-catenin pathway (Figure 16). FZD1 up-regulation in resistant variants was shown to mediate sustained activation of the Wnt/β-catenin pathway, as revealed by the nuclear β-catenin translocation and target genes transactivation (Figure 16). Interestingly, specific micro-adapted short hairpin RNA (shRNAmir)-mediated FZD1 silencing induced a parallel strong decrease in the expression of *MDR1*, restoring drug sensitivity, thus revealing a complex

role for FZD1 in Wnt/β-catenin-mediated chemoresistance. Moreover, RNA samples from 21 patient tumours (at diagnosis and post-chemotherapy), showed a highly significant FZD1 and/or *MDR1* overexpression after treatment (Flahaut et al. 2009). These data implicated the Wnt/β-catenin pathway in NB chemoresistance and identified potential new targets to treat aggressive and resistant NB.

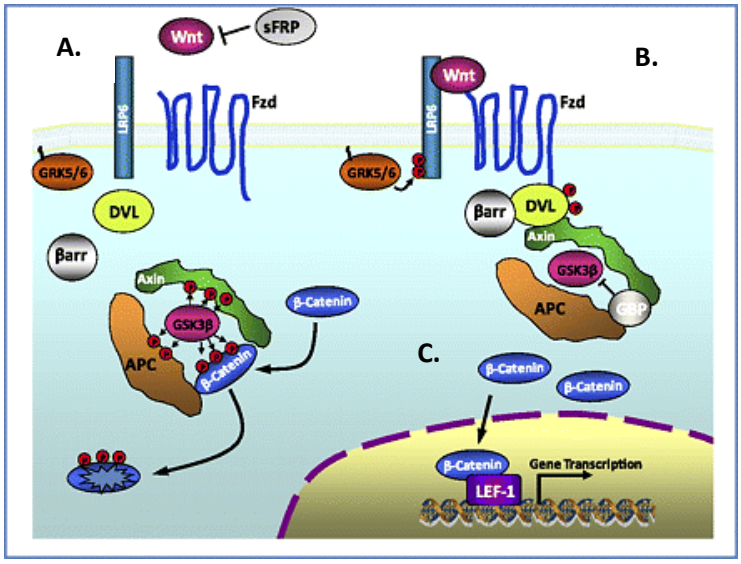

Figure 16. Wnt signaling pathway. **A.** In the absence of a Wnt ligand, cytosolic β-catenin is phosphorylated by GSK3β. Adenomatous polyposis coli (APC) and axin complex with GSK3β and β-catenin to enhance this destruction process. Phosphorylated β-catenin is recognized by the ubiquitin ligase βTrCP, ubiquinated, and degraded by the proteasome machinery. Hence the Wnt signaling is in an "off" state and there is no transcription of Wnt target genes (left). **B.** Wnts bind both Frizzled and LRP5/6 receptors to initiate GRK5/6-mediated LRP phosphorylation as well as dishevelled/β-arrestin-mediated Frizzled internalization. Dishevelled membrane translocation and phosphorylation lead to dissociation of the axin/APC/GSK3β destruction complex. **C.** Hence β-catenin phosphorylation is inhibited and it accumulates in the cytosol. The accumulated cytosolic β-catenin translocates into the nucleus to bind to LEF/TCFs co-transcription factors, which results in the Wnt-responsive gene transcription (right). Fzd, Frizzled; GBP, GSK3β binding proteins; DVL, Dishevelled; βarr, β-arrestin; GRK, G protein-coupled receptor kinase. Taken from (Chen et al. 2010b).

Additionally, Bourguignon et al. investigated hyaluronan (HA)-mediated CD44 (an HA receptor) interactions with p300 (a histone acetyltransferase) and SIRT1 (a histone deacetylase) in human breast tumor cells (MCF-7 cells) (Bourguignon et al. 2009). The obtained results demonstrated that HA binding to CD44 up-regulates p300 expression and its acetyltransferase activity that, in turn, promotes acetylation of β-catenin and NF-kB-p65, leading to activation of β-catenin-associated TCF/LEF transcriptional co-activation and NF-kB-specific transcriptional up-regulation, respectively. As a consequence, these changes increased the expression of the *MDR1* gene and of the anti-apoptotic gene Bcl-x(L), resulting in chemoresistance in MCF-7 cells. In accordance, the down-regulation of p300, β-catenin, or NF-kB-p65 in MCF-7 cells (by transfecting cells with p300-, β-catenin-, or NF-kB-p65-specific small interfering RNAs) inhibited the HA/CD44-mediated β-catenin/NF-kB-p65 acetylation and abrogated the aforementioned transcriptional activities, with a significant decrease in both *MDR1* and Bcl-x(L) gene expression and an enhancement in caspase-3 activity and chemosensitivity in these breast tumor cells. Further analyses indicated that activation of SIRT1 (deacetylase) by resveratrol (a natural antioxidant) induced SIRT1-p300 association and acetyltransferase inactivation, leading to

deacetylation of β-catenin and NF-kB-p65, inhibition of β-catenin-TCF/LEF and NF-kB-specific transcriptional activation, and the impairment of *MDR1* and Bcl-x(L) gene expression. All these multiple effects lead to an activation of caspase-3 and a reduction of chemoresistance. Together, these findings suggest that the interactions between HA/CD44-stimulated p300 (acetyltransferase) and resveratrol-activated SIRT1 (deacetylase) play pivotal roles in regulating the balance between cell survival versus apoptosis, and multidrug resistance versus sensitivity in breast tumor cells (Bourguignon et al. 2009).

I.6.2.2.2. Stress induction of the hMDR1 gene – inducible regulators

From the earliest studies of P-gp function and regulation, it has been suggested that P-gp is a 'stress response gene' since its activity can be modulated by environmental adversity, being highly responsive to these stress signals (Scotto and Egan 1998). *MDR1* is, thus, well equipped for the task of cellular defence, and its promiscuity means that it is a highly reliable protective mechanism. Therefore, rapid up-regulation of the multidrug transporter by extracellular and intracellular stress protects the cell against a multitude of adverse insults, including heat shock, the surgical insult of partial hepatectomy, inflammation, exposure to carcinogens, and UV- and X-irradiation (Scotto 2003).

Additionally, in what concerns to cancer cells, it is recognised that these cells in solid tumours encounter a harsh local environment and are exposed to both endogenous stresses, such as glucose deprivation, anaerobic metabolism, hypoxia, free radical formation, and acidosis, as well as exogenous stress in the form of chemotherapy and radiotherapy (Callaghan et al. 2008), causing a breakdown in the oxidant-antioxidant balance (Brown and Bicknell 2001). Such adverse conditions force tumour cells to adapt. As tumour blood supply is often inadequate and irregular, cells are deprived of oxygen and nutrients, leading to a cascade of events responsible for the development of an independent tumor vasculature (Bernards and Weinberg 2002).

Accumulating evidence suggests that ROS are involved in the regulation of signal transduction pathways and gene expression, therefore acting as indicators of the level of cellular stress that, upon activation of nonspecific stress response pathways, enable the cells to adapt to a potentially harmful change in environment (Figure 17) (Callaghan et al. 2008).

It was consequently hypothesised that increased ROs levels could increase *MDR1* expression and multiple pathways seem to be involved (Dalton et al. 1999; Klaunig and Kamendulis 2004; Nwaozuzu et al. 2003; Ziemann et al. 1999). In a study where several signalling pathways were investigated to link H_2O_2–mediated elevation of ROS with *MDR1*

expression, positive regulation was observed for the PI3K (phosphoinositide 3-kinase), ERKs (extracellular signal-regulated kinases; or mitogen-activated protein kinases, MAPKs), JNK (c-Jun NH2-terminal protein kinase), and PKC (protein kinase C) pathways and a negative regulation for NF-κB (Nwaozuzu et al. 2003). Exposure to H_2O_2 increased the input from the positively regulating pathways but reduced NF-κB-mediated suppression of *MDR1*. Therefore, it was demonstrated that the control of *MDR1* expression is multifactorial involving communication between several pathways and can be influenced by changing ROS level by H_2O_2 treatment (Nwaozuzu et al. 2003). Further evidence for ROS-mediated *MDR1* transcriptional activation was reported for the stress-inducing compounds 2-acetylaminofluorene (2-AAF) (Kuo et al. 2002) and cadmium (Thevenod et al. 2000), both of which activate the NF-κB pathway, thus showing that NF-κB can act either as positive or negative regulator of *MDR1* transcription. In addition, AP-1 has also been shown to directly respond to ROS (Abate et al. 1990).

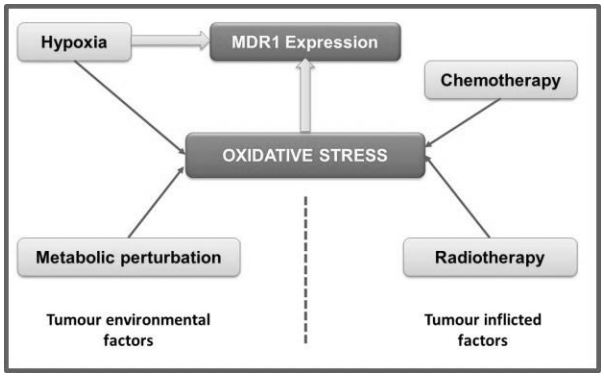

Figure 17. Induction of MDR1 expression due to oxidative stress caused by micro-environmental factors.
Adapted from (Callaghan et al. 2008).

The following section will focus on how cellular stress induces the expression of the multidrug transporter MDR1. Particular attention will be given on how the tumour microenvironment itself elicits oxidative stress and how this stress activates downstream stress response pathways, and their consequences on the *MDR1* expression. As can be seen in Figure 17, there is a convergence of various stress factors on the oxidative balance of a cell. A primary causative factor for many of these stresses is, as previously mentioned, the harsh microenvironment (i.e., the inadequate tumor blood supply), which leads to glucose deprivation, hypoxia, reversion to anaerobic respiration, accumulation of lactate and pyruvate, and variability in tumor pH (Callaghan et al. 2008).

I.6.2.2.2.1. Heat Shock

In response to heat shock, an increase in both h*MDR1* mRNA levels (Chin et al. 1990b) and h*MDR1* gene transcription (Kioka et al. 1992b) can be observed. Moreover, several putative heat shock element (HSE) sequences have been identified in the h*MDR1*

promoter, suggesting that it may be considered a stress gene (Labialle et al. 2002b). In the *MDR1* promoter Chin et al. (1990) reported three HSEs upstream from the major transcriptional initiation start sites, while the remaining HSEs were located downstream between the start sites and the first AUG codon (Chin et al. 1990b). One of these HSEs sequences is located at the -99 to -66 sequence position in the h*MDR1* promoter (Figure 12) and has been proposed as a requirement for the heat shock response (Miyazaki et al. 1992). Also, gel shift assays showed that the heat-shock transcription factor (HSF) could bind to a HSE motif located at the -178 to -152 sequence position in the *MDR1* promoter (Miyazaki et al. 1992) (Figure 12).

In accordance, it has been shown that both heat shock and sodium arsenite increase the activity of h*MDR1* promoter via HSEs, and that the Raf-dependent signalling pathway controls the transcription of h*MDR1* gene via a mechanism involving the modulation of HSF activity (Kim et al. 1996; Kioka et al. 1992b; Miyazaki et al. 1992). In a study performed by Kioka et al. it was demonstrated that the expression of the h*MDR1* gene in the HepG2 hepatocarcinoma cell line was significantly increased by exposure to sodium arsenite. In fact, it was shown that sodium arsenite activated the *MDR1* promoter and that this response was dependent on a promoter region containing a tandem repeat of HSEs. Noteworthy, deletion analysis of the *MDR1* promoter indicated that this transcriptional activation depended on a 60-bp region (-193 to -133) containing two HSEs (-174 to -161 and -161 to -148) (Kioka et al. 1992b).

Additionally, it was demonstrated that the *MDR1* promoter is responsive to the activated Raf that, as mentioned before, functions as a component of the MAPK signal transduction pathway, and that the Raf over-expression was associated with acquired MDR phenotype in monkey kidney fibroblasts CV-1 cells (Kim et al. 1993). Moreover, the activated Raf-mediated stimulation of the *MDR1* promoter was associated with the activation of HSF (Kim et al. 1996). Indeed, phosphorylation of HSFs, which occurs at multiple serine and threonine residues, may be important for attaining maximal transcriptional activity (Nieto-Sotelo et al. 1990) and the activation of the protein kinase cascade, including Raf-1, induces gene expression through phosphorylation of transcription factors, including HSF (Hunter and Karin 1992). The stimulation of Raf-dependent signal transduction increased the activity of the *MDR1* promoter with maximum activation occurring at a sequence containing an upstream HSE motif without other regulatory elements. On the other hand, the constructs containing the downstream HSE motif showed a relatively weaker activation by Raf (Kim et al. 1996). Since previous studies showed that HSF could bind to the upstream HSE motif (-178 to -152) in the *MDR1* promoter (Miyazaki et al. 1992) (Figure 12), these results suggested the possibility of a strong correlation between the effect of the activated Raf pathway on the induction of

the *MDR1* gene and the activity of HSF/HSE (HSF might trans-activate the expression of *MDR1* gene in response to the activated Raf) (Kim et al. 1996). Moreover, given the observed induction of the promoter activity (CAT activity) by sodium arsenite (which stimulates binding of HSF to HSE) and the activated Raf-induced potentiation of CAT activity by sodium arsenite or heat shock, it was suggested the possibility that the activated Raf pathway may be associated with phosphorylation of HSF (Kim et al. 1996).

In addition, there are some evidences that a down-regulation of *MDR1* expression occurs by inhibition of protein kinase A (PKA) (Abraham et al. 1990; Kim et al. 1996; Kim et al. 1993) that binds and activates heat-shock transcription factor 1 (HSF-1) (Murshid et al. 2010), thus reinforcing the role of this transcription factor on the regulation of P-gp expression. In fact, H-87, a specific PKA inhibitor, decreased the drug resistance and *MDR1* gene expression in c-raf-1 transfected CV-1 cells (Kim et al. 1993). In another study, it was also demonstrated that H-87 inhibited *MDR1* promoter activity in both Gxb-I and Gha-I cells, and blocked the stimulation of the *MDR1* promoter by the activated Raf in GHE-L cells (Kim et al. 1996). Moreover, *MDR1* promoter deletion analysis suggested that H-87 probably inhibits the phosphorylation of HSF and/or the cAMP responsive element (CRE) binding protein, showing an important role for PKA in the regulation of the *MDR1* gene (Figure 21) (Kim et al. 1996). Consequently, the authors proposed that both Raf- and PKA-dependent pathways control the transcription of the *MDR1* gene via a mechanism involving the modulation of HSF activity (Kim et al. 1996).

Accordingly to the previous studies, it has also been reported that MDR cells, such as FM3A/M and P388/M cells, show a constitutively activated HSF (constitutive HSF DNA-binding activity), and consequently express, in the absence of stress, heat shock proteins 70 and 90 (Hsp70 and Hsp90) and P-gp at higher levels than their parental cells, suggesting that HSF could be an useful target for reversing MDR (Kim et al. 1997). Quercetin, one of the most widely distributed flavonoids in nature, dose-dependently inhibits the constitutive HSF DNA-binding activity and the sodium arsenite-induced HSF DNA-binding activity in MDR cells and, consequently, suppresses the *mdr1* gene expression, thereby overcoming the MDR phenotype of FM3A/M cells (Kim et al. 1998). Quercetin was also shown to inhibit Hsp synthesis after heat shock in a human colon carcinoma cell line and in Hela cells (Hosokawa et al. 1992), and also to interfere with the formation of the complex between the HSE and HSF, and to down-regulate the level of HSF-1 (Nagai et al. 1995a). The accumulation of *MDR1* mRNA after exposure to arsenite was also inhibited by quercetin in HepG2 cells(Kioka et al. 1992a), and these data also supported the involvement of HSEs in the induction of the *MDR1* gene expression, since quercetin interacts with HSF to inhibit the induction of the heat shock response (Nagai et al. 1995b).

Another HSE (HSF1) region located at the -315 to -285 sequence position in the h*MDR1* promoter (Figure 12) was also reported to regulate the h*MDR1* expression through a mechanism mediated by the HSF-1 (Vilaboa et al. 2000). In fact, infection of HeLa cells with adenovirus-carrying HSF-1^{+} cDNA, which encodes a mutated form of HSF-1 with constitutive transactivation capacity, increased *MDR1* mRNA level and P-gp cell surface content, decreased rhodamine 123 accumulation and stimulated vinblastine efflux activity. Moreover, HSF-1 up-regulation of P-gp expression occurred at the transcriptional level since HSF-1^{+} bound the heat-shock consensus elements in the *MDR1* gene promoter and also activated the expression of a *MDR1* promoter driven reporter plasmid [pMDR1(21202)] (Vilaboa et al. 2000). Also, heat-shock increased the *pMDR1*(21202) promoter activity and this effect was totally inhibited by co-transfection with an expression plasmid carrying HSF-1^{-}, a dominant negative mutant of HSF-1, reinforcing the direct regulation of the *hMDR1* gene expression by HSF-1(Vilaboa et al. 2000).

A recent study has implicated HSF-1 in the regulation of mdr1b expression by a distinct mechanism (Krishnamurthy et al. 2012). In fact, HSF-1 ablation [HSF-1(-/-) mice] induced the *mdr1b* in the heart and increased expression of its product. This increase enhanced the extrusion of doxorubicin, thus reducing doxorubicin-induced heart failure and mortality in mice. NF-κB expression in the heart was also increased. Moreover, DNA-binding activity of NF-κB was higher in HSF-1(-/-) mice, and IκB, the NF-κB inhibitor, was depleted due to enhanced IκB kinase-α activity. According to the obtained results, a unique mechanism was proposed in which HSF-1 represses NF-κB activation of the *mdr1* gene in the heart and, consequently, ablation of HSF-1 enhances NF-κB, which in turn induces the *mdr1b* (Krishnamurthy et al. 2012). Moreover, *mdr1* promoter activity was higher in HSF-1(-/-) cardiomyocytes, whereas a mutant *mdr1* promoter with a HSE mutation showed increased activity only in HSF-1(+/+) cardiomyocytes. However, deletion of HSE and NF-κB binding sites diminished luminescence in both HSF-1(+/+) and HSF-1(-/-) cardiomyocytes, suggesting that HSF-1 inhibits *mdr1* promoter activity in the heart (Krishnamurthy et al. 2012).

In conclusion, HSFs that regulate the expression of *HSP* genes through the binding to specific HSEs sequences present in the promoter of these genes, also enhance *MDR1* gene expression with several proofs of evidence, namely: (a) HSEs have been identified in the *MDR1* gene promoter (Chin et al. 1990b; Kioka et al. 1992b); (b) typical stress inducers, such as heat-shock and arsenite, which induce HSP gene expression, also induced *MDR1* gene expression in some cell types (Chin et al. 1990b; Kioka et al. 1992b); (c) some MDR cell lines exhibit constitutively high HSF-DNA binding activity (Kim et al.

1997), (d) quercetin, which inhibits HSF-HSE binding, also inhibits HSF-DNA binding and P-gp expression in MDR cells, reverting this phenotype (Kim et al. 1998) and (e) detection of HSF-1 bound to HSEs in the *MDR1* gene promoter denotes regulation at the transcriptional level (Vilaboa et al. 2000).

I.6.2.2.2.2. Inflammation -C/EBP and GR

The 'acute-phase response' is a general term for the complex changes that take place in mammals in response to inflammatory stimuli such as bacterial infection or burn injury. This response is often experimentally simulated *in vivo* by the administration of bacterial lipopolysaccharide (LPS). In response to LPS, macrophages secrete inflammatory cytokines such as interleukin (IL)-1, IL-6 and TNF-α, which in turn act on the liver to induce a change in the gene expression program, resulting in the synthesis of a range of acute-phase proteins (Akira and Kishimoto 1992).

Most of the studies on the expression of drug transporters during inflammation have relied on the rodent model system, and data have been obtained primarily for the transcription of the rodent homologues (Scotto 2003). Although not necessarily applicable to the human genes, the high degree of promoter conservation among family members, together with the similar response of the human and rodent genes to inflammatory agents, suggests that similar transcription pathways exist (Scotto 2003).

Under acute-phase conditions, P-gp genes were reported to be induced in the liver (Nakatsukasa et al. 1993). Furthermore, several studies have shown that the IL-6-induced CAAT enhancer-binding protein (C/EBPβ, also called NF-IL-6) can activate the mouse and human *MDR1* genes in transfection assays (Figure 18) (Combates et al. 1997; Combates et al. 1994; Yu et al. 1995). The CCAAT-enhancer-binding proteins (C/EBP) are a family of transcription factors involved in the basal and tissue-specific expression of a number of genes (Labialle et al. 2002b; Ramji and Foka 2002) having, therefore, an important role in a number of processes, including differentiation, inflammatory response, liver regeneration and metabolism (Ramji and Foka 2002).

C/EBPβ is usually expressed at low levels in most tissues (Labialle et al. 2002b). However, in response to inflammatory cytokines (IL-1, IL-6 and TNF-α), lipopolysaccharides, and retinoic acid, its expression may be rapidly induced (Labialle et al. 2002b; Ramji and Foka 2002) (Figure 18). At the h*MDR1* gene, the putative binding sequence for this transcription factor is located between positions -147 to -139 (Figure 12 and Figure 18) (Labialle et al. 2002b). It was also shown that the homologous region in the hamster p-gp1 promoter also contains a C/EBPβ binding site and that activation through this site can be modulated by the binding of the glucocorticoid receptor (GR) (Scotto 2003). These results suggest that this element may be important as a site for

crosstalk between the inflammatory signals (mediated by cytokines through C/EBPβ), and the anti-inflammatory signals (mediated by glucocorticoids through their receptor).

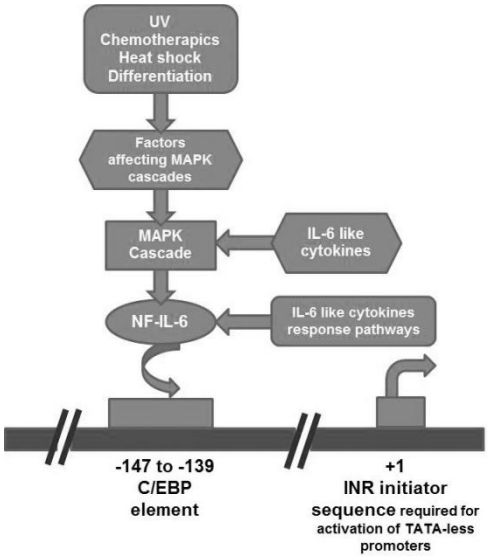

Figure 18. Activation of h*MDR1* gene by NF-IL-6 in response to several stress stimuli.

A number of studies have also suggested a role for glucocorticoids in the regulation of *MDR1* gene transcription, but the responses are cell-type and gene-class dependent (Scotto 2003; Scotto and Egan 1998). Using the mouse hepatoma cell lines, Hepa 1–6 and hepa1c1c, it was demonstrated that the synthetic glucocorticoid, dexamethasone, elicited an increase in the expression of the two murine *MDR1* homologues, *mdr1a* and *mdr1b*, but not in *mdr2* expression (Zhao et al. 1993). This increase occurred at least in part at the transcriptional level, and the induction apparently required new protein synthesis since no increases in *mdr1a* and *mdr1b* transcripts were found when cultured cells were simultaneously treated with dexamethasone and cycloheximide, an inhibitor of protein synthesis. Therefore, the observed induction abrogation under protein synthesis inhibition suggested that GR was influencing this promoter through an indirect mechanism (Zhao et al. 1993). A similar increase in h*MDR1* mRNA levels was observed in the HepG2 human hepatoma cell line (Zhao et al. 1993). In rat primary hepatocytes, however, dexamethasone treatment led to a decrease in *mdr1b* expression, and no increase was seen in the non-hepatoma mouse LMtk- and NIH3T3 cell lines, or in the human HeLa cell line upon dexamethasone treatment, suggesting that the effect is cell line-specific (Zhao et al. 1993).

A glucocorticoid response element (GRE) was identified in the promoter of the hamster *mdr1* homologue, p-gp1 (Scotto 2003; Scotto and Egan 1998). This site, between -96 and -83, mediated the repression of p-gp1 transcription by GR in both DC-3F Chinese hamster lung cells and in a human osteosarcoma cell line, U2-OS. The GRE overlaps a

binding site for C/EBPβ and it appears that GR represses p-gp1 transcription by interfering with the actions of C/EBPβ, as both sites are required for repression to occur. Interestingly, these elements are conserved in the h*MDR1* gene and *MDR1* transcription can also be repressed by GR in some cell types, suggesting that a similar mechanism may be involved (Scotto 2003; Scotto and Egan 1998).

Finally, NF-κB is another factor involved in the inflammatory response and can also, as previously referred, regulate P-gp expression (Zhou and Kuo 1997) (see I.6.2.2.1.4).

I.6.2.2.2.3. Alteration of Bioenergetic Metabolism

A major consequence of the poor tumor blood supply is the reduction of oxygen availability, which severely compromises aerobic respiration, forcing tumor cells to revert to glycolytic metabolism, resulting in elevated acidic metabolites, such as lactate, (Callaghan et al. 2008), that accumulate since the reduced blood flow prevents their removal. As a consequence, tumor tissue is intrinsically more acidic than normal tissue, sometimes having a pH ≤ 6 (Helmlinger et al. 1997). It has also been shown that acidosis activates the transcription factors NF-κB and AP-1 (Sies 1997), both having been demonstrated to regulate *MDR1* expression as previously discussed. Additionally, a study performed by Thews *et* al., using prostate carcinoma cells exposed to an acidic extracellular environment (pH 6.6) for up to 24 hours, showed that reduced extracellular pH had no effect on *MDR1* expression but doubled the activity of the protein after 3 to 6 hours (Thews et al. 2006), indicating that the increased transport rate is the result of functional modulation. In fact, the data indicated that P-gp activity was increased by low extracellular pH presumably as a result of lowered intracellular calcium levels and inhibition of protein kinase C (PKC). Moreover, the cytotoxicity of daunorubicin showed pronounced reduction at low pH, an effect that was reversible upon co-incubation with a P-gp inhibitor (Thews et al. 2006). Therefore, these findings may explain the reduced cytotoxicity of chemotherapeutic agents in hypoxic/acidic tumours. Unfortunately, the link between the regulation of signalling pathways, acidosis, and the expression of *MDR1* is relatively unstudied, and therefore its contribution to MDR remains unclear.

Moreover, in what concerns to PKC, an isoenzyme with serine/threonine kinase function that has been shown to play a key role in the signal transduction pathway elicited by a variety of extracellular stimuli, such as growth factors, hormones and neurotransmitters, early observations led to the conclusion that PKC acts as a downstream effector of the Ras system (Rimler et al. 2006). In addition, phorbol ester activation of PKC induced a transient MDR phenotype in wild-type human breast cancer cells, which was associated with decreased intracellular drug accumulation and increased drug resistance (Fine et al. 1988). Fine et al. reported that cellular PKC activity was

elevated in doxorubicin-selected MCF7-MDR cells compared with the parental cells (Fine et al. 1988). This was subsequently attributed to a 30-fold increase in PKCα and a decrease in other PKC isozymes in the drug-selected cells (Blobe et al. 1993). This finding was supported by other studies that showed that phorbol ester PKC activation induces resistance to chemotherapeutic drugs and causes a corresponding reduction in intracellular drug accumulation (Bergman et al. 1997; Brugger et al. 2002; Gekeler et al. 1995).

I.6.2.2.2.4. Glucose Deprivation

Reduced blood supply to tumor cells can also result in glucose deprivation. Studies involving chemically induced glucose deprivation in MCF-7 breast carcinoma cells have shown rapid induction of cellular oxidative stress, thought to be due to depletion of intracellular pyruvate (Lee et al. 1998; Spitz et al. 2000). Moreover, MAPK was activated within 3 min after culture in glucose-free medium and remained activated for 3 h (Lee et al. 1998). Also, the observed glucose deprivation-induced cytotoxicity and alterations in MAPK signal transduction are mediated by oxidative stress in MCF-7/ADR cells. In fact, these effects were suggested to prevent the breakdown of endogenous oxygen radicals; thereby disrupting the oxidant-antioxidant balance (Lee et al. 1998; Spitz et al. 2000). Subsequent studies have demonstrated that glucose deprivation of liver cancer cells (rat hepatoma cell line, Fao cells) generated resistance to doxorubicin via increased *mdr1* expression (Ledoux et al. 2003). Indeed, incubation of Fao cells with a glucose-free medium enhanced *mdr1* mRNA and protein expression in a time-dependent manner, up to 400% at 40 h, an effect that was also associated with a stimulation of [^{3}H]vinblastine efflux by P-gp. This effect was reproduced by inducers of endoplasmic reticulum stress response, such as 2-deoxyglucose (DG), tunicamycin, and thapsigargin (Ledoux et al. 2003). Moreover, P-gp mRNA induction by DG was preceded by an increase in activator protein binding activity, c-Jun expression, and phosphorylation. In contrast, NF-kB binding activity was unaffected by DG. Furthermore, the antioxidant N-acetylcysteine partially reversed the increase in P-gp mRNA and protein levels induced by DG, as well as decreased the enhancement of c-Jun phosphorylation and activator protein binding activity. Finally, transient transfection of the cells with a deleted mutant of c-Jun abolished the DG-induced P-gp mRNA expression and *mdr1b* promoter activation. In conclusion, glucose deprivation enhanced P-gp expression and transport function in liver cancer cells and this effect was mediated by endoplasmic reticulum stress response and involved MDR transcriptional induction through c-Jun activation. These results emphasize the importance of glucose metabolism in chemoresistance (Ledoux et al. 2003). Noteworthy, the observed partial reversion of DG-induced increases in mdr1 mRNA and protein levels

by N-acetyl-cysteine suggest a key role for ROS in mediating the effect (Ziemann et al. 1999).

ROS generation is also involved in *mdr1* overexpression induced by a number of factors including, UV irradiation, epidermal growth factor (EGF), TNF-α, and doxorubicin (Ziemann et al. 1999). In a study performed by Ziemann et al., primary rat hepatocyte cultures, which exhibit time-dependent overexpression of the *mdr1b* gene, were used as a model system to investigate whether ROS might participate in the regulation of intrinsic *mdr1b* overexpression (Ziemann et al. 1999). Addition of H_2O_2 to the culture medium resulted in a significant increase in *mdr1b* mRNA and P-gp after 3 days of culture, with maximal (~2-fold) induction being observed with 0.5 - 1 mM H_2O_2. Furthermore, H_2O_2 led to activation of poly(ADP-ribose) polymerase, a nuclear enzyme activated by DNA strand breaks, indicating that ROS reached the nuclear compartment (Ziemann et al. 1999). Moreover, the use of antioxidants, such as ascorbate, markedly suppressed intrinsic *mdr1b* mRNA and P-gp overexpression. Also, using rhodamine 123 as substrate it was observed that mdr1-dependent efflux was increased in hepatocytes pre-treated with H_2O_2 and decreased in antioxidant-treated cells. Therefore, the induction of *mdr1b* mRNA and of functionally active P-gp by elevation in intracellular ROS levels, and the repression of intrinsic *mdr1b* mRNA and P-gp overexpression by antioxidant compounds, support the conclusion that the expression of the mdr1b P-gp is regulated in a redox-sensitive manner (Ziemann et al. 1999).

On the other hand, in what concerns to the regulation of glucose homeostasis, insulin was reported to up-regulate the *MDR1* gene (Liu et al. 2008; Liu et al. 2009; Zhou and Kuo 1997). Insulin is a key hormone regulating glucose homeostasis and has many cellular effects on metabolism, growth, and differentiation (Liu et al. 2009). It was reported that insulin-induced signal transduction occurs via PI3K, MAPK and PKC signalling pathways (Angelova et al. 2004; Brand et al. 2006; Cao et al. 2007). Both PKC and PI3K were, as previously stated, reported to be associated with the P-gp regulation (Barancik et al. 2006; Fine et al. 1996). PKC is activated by insulin, and receptor tyrosine kinase regulates insulin-induced activation of PKC (Brand et al. 2006). It was reported that the activation of the PKC pathway was linked to up-regulated expression of P-gp (Fine et al. 1996), and several experimental evidence suggested that phosphorylation of P-gp by PKC might play a role in regulating MDR (Germann et al. 1995; Grunicke et al. 1994). Consequently, P-gp phosphorylation was found to be determinant for P-gp expression. Therefore, tyrosine protein kinase and PKC were considered as promising targets for inducing P-gp. NF-κB is also a downstream signalling molecule of the insulin signal transduction and can be, as mentioned before, a potent activator in modulating gene transcription (Vivanco and Sawyers 2002). Moreover, it was shown that NF-κB mediated

the induction of *mdr1b* expression by insulin in rat hepatoma cells (Zhou and Kuo 1997), so NF-κB might also be a promising target for inducing P-gp.

PKB/Akt is another major downstream target of receptor tyrosine kinases in response to stimuli such as insulin or insulin growth factors, and it is activated by PI3K (Vara et al. 2004). Moreover, it was reported that PI3K/Akt kinase pathway was possibly involved in modulation of P-gp in a direct way, in addition to the NF-κB-mediated pathway described before (Barancik et al. 2006). More recently, a study aimed to investigate whether the PKC/NF-κB pathway or the PI3K/Akt pathway were involved in insulin-mediated P-gp function and expression in the blood-brain barrier, using rat brain microvessel endothelial cells as an *in vitro* model (Liu et al. 2009). Previous work performed by the same authors, showed that, both *in vivo* and *in vitro*, treatment of rats with insulin increased the function and expression of P-gp in the BBB (Liu et al. 2008). Moreover, *in vitro*, the insulin-induced function and expression of P-gp occurred in concentration-dependent manner (Liu et al. 2008). Additionally, insulin restored impaired function and expression of P-gp in diabetic BBB (Liu et al. 2008). However, the exact mechanism by which insulin regulated P-gp expression was not well understood. Therefore, they latter evaluated the intracellular pathways involved in insulin-mediated regulation of P-gp and it was found that, after incubation with 50 mU/l insulin, P-gp function and expression in rat brain microvessel endothelial cells were significantly increased (Liu et al. 2009). This induction effect was blocked by an insulin receptor antibody, an insulin receptor tyrosine kinase inhibitor (I-OMe-AG538), a PKC selective inhibitor (chelerythrine) and a NF-κB inhibitor (pyrrolidine dithiocarbamate ammonium; PDTC). However, the effect was not inhibited by the selective inhibitor of the PI3K/Akt pathway (LY294002). Moreover, insulin receptor, receptor tyrosine kinase, PKC inhibitor, and NF-κB inhibitor had no effect on rhodamine 123 uptake in rat brain microvessel endothelial cells in the absence of insulin, showing that baseline insulin did not affect P-gp function, and excluded the possibility that the five inhibitors decreased the P-gp function in a non-specific way (Liu et al. 2009). Therefore, these results indicated that the regulatory effect of insulin on P-gp function and expression occurs through signal transduction pathways involving the activation of PKC/NF-κB, but not the PI3K/Akt pathway (Liu et al. 2009). Although previously demonstrated that the PI3K/Akt kinase pathway was possibly involved in the modulation of P-gp-mediated MDR (Barancik et al. 2006), another study also showed that LY294002 did not block insulin-induced P-gp function (Vlahos et al. 1994), thus reinforcing that the PI3K/Akt pathway might not be involved in insulin-mediated regulation of P-gp in rat brain microvessel endothelial cells.

I.6.2.2.2.5. Hypoxia -HIF-1α

In addition to deprivation of nutrients, another hallmark of inadequate vascularization is oxygen insufficiency. In fact, the microenvironment of many large and rapidly growing tumours lacks a sufficient vascular supply, resulting in oxygen deprivation or hypoxia (Callaghan et al. 2008; Scotto 2003; Scotto and Egan 1998). Prolonged hypoxia has been linked to metastasis, since it increases genomic instability, genomic heterogeneity, and may act as a selective pressure for tumor cell variants (Subarsky and Hill 2003). This hypoxic environment results in the induction of many stress-response genes, including glycolytic enzymes, proangiogenic factors and pro-inflammatory genes (Semenza 1998). Accordingly, it has been demonstrated that P-gp expression is increased in hypoxic cells, and that this increase is mediated by the hypoxia-inducible factor-1α (HIF-1α), a transcription factor that normally resides in the cytoplasm of normoxic cells and is believed to be shuttled to the nucleus upon hypoxic stress (Scotto 2003). In fact, HIF-1α mediates essential homeostatic responses to reduced O_2 availability in mammals and recent studies provided insights into the O_2-dependent regulation of HIF-1α expression, target genes regulated by HIF-1α, and the effects of HIF-1α deficiency on cellular physiology and embryonic development (Semenza 1998; Semenza 2002). This transcription factor plays, thus, a central role in cellular response to hypoxia by up-regulating the expression of numerous hypoxia inducible genes (Semenza 1998; Semenza 2002).

The majority of studies under hypoxic conditions support a positive correlation between the HIF-1α activity and *MDR1* expression (Wartenberg et al. 2003). Indeed, Wartenberg et al. argued that the altered oxygen tension in 3D tumor spheroid models is directly correlated with P-gp expression (Wartenberg et al. 2003; Wartenberg et al. 2001a), while Comerford *et* al. have demonstrated that JNK pathway activation is required for hypoxia-induced HIF-1α activity (Comerford et al. 2004; Comerford et al. 2002). In addition, the JNK inhibitor, SP600125, inhibits hypoxia-induced *MDR1* promoter activity (Comerford et al. 2004). Therefore, these results suggest that under hypoxia, the *MDR1* gene expression is dependent on HIF-1α activation and that this activation is partially dependent on signalling through JNK activation (see below).

Given the apparent presence of an HIF-1α binding site in the *MDR1* promoter (Hypoxia Responsive Element, HRE, located between positions -49 to -45) (Figure 12) (Ueda et al. 1987) two questions may arise: is there proof of a direct link between HIF-1α and *MDR1* expression? Or is there an indirect effect of altered oxygen tension on *MDR1* expression through oxidative stress? Comerford et al. suggested the former hypothesis, in a study where the response of epithelia cell lines to reduced oxygen tension was evaluated by quantitative RNA analysis, and a moderate (2-fold) increase in *MDR1* transcripts subsequent to a 6-hour hypoxia, and a 7-fold increase after an 18-hour

exposure, were observed (Comerford et al. 2002). Moreover, the P-gp increases at the cell surface were not detectable until 24 to 48 hours of hypoxia, a time course that correlated with increasing doxorubicin resistance of a multicellular spheroid model of tumor growth (Comerford et al. 2002). Importantly, the introduction of antisense oligonucleotides to HIF-1α blocked both HIF-1α expression and the hypoxia-induced increase in *MDR1* transcription, causing a nearly complete loss of basal *MDR1* expression. Furthermore, fusions of regions of the *MDR1* promoter region to a reporter gene (luciferase) demonstrated the presence of a HIF-1α binding site upstream of the transcription start site that was both necessary and sufficient for hypoxia induced activation of the reporter gene (Comerford et al. 2002). These studies using luciferase promoter constructs revealed a significant increase in promoter activity in cells subjected to hypoxia, and such hypoxia inducibility was lost in truncated constructs lacking the HIF-1α site and in HIF-1α binding site mutants (Comerford et al. 2002). Moreover, this P-gp induction may increase tumour cell capacity to actively extrude chemotherapeutic agents and, thus, may contribute to tumour drug resistance (Comerford et al. 2002). In a later study, the same authors investigated, as previously referred, the role of JNK in the signalling mechanisms underlying these events (Comerford et al. 2004). Overexpression of MEKK-1 (a protein kinase of the STE11 family), which preferentially activates JNK (Figure 21), mimicked the hypoxia-induced activity of the *MDR1* promoter and expression of *MDR1* mRNA and P-gp. Furthermore, the JNK inhibitor SP600125 selectively and specifically inhibited both hypoxia- and MEKK-1-induced *MDR1* promoter activity in a dose-dependent manner. JNK inhibition also reversed hypoxia- and MEKK-1-induced activity of an HIF-1α-dependent reporter gene. MEKK-1-induced *MDR1* expression depended on a functional HIF-1α binding site (the hypoxia-responsive element). Also, hypoxia-dependent HIF-1α-DNA binding and transcriptional activation were inhibited by SP600125, indicating that hypoxia-induced signalling to HIF-1α depends on JNK activation. Moreover, since ROS are increased in hypoxia and related to JNK activation, their role in this signalling was also investigated. Whereas exogenous addition of H_2O_2 was sufficient to activate JNK, ROS scavengers were without effect on hypoxia-induced JNK or HIF-1α activation, indicating that these events are independent of the generation of reactive oxygen intermediates, and that JNK may represent a therapeutic target in the prevention of tumour resistance to chemotherapeutic treatment (Comerford et al. 2004). Moreover, HIF-1α activates the *MDR1* promoter through a consensus binding sequence (5`GCGTG3`; -49 to -45) (Figure 12) that overlaps the GC element, which is, as previously referred, involved in both constitutive and inducible *MDR1* expression (Comerford et al. 2002). Indeed, preliminary evidence suggests that the GC-binding protein Sp1 may also be involved in the hypoxic response (Comerford et al. 2002). All these previously

discussed results may in part explain the reason for hypoxic tumour cells being more refractory to anticancer agents (Brown and Giaccia 1998).

However, an alternative view was presented by Song et al. In fact, it was demonstrated that hypoxia-induced chemoresistance to cisplatin and doxorubicin in human non-small cell lung cancer cells (NSCLC) occurred through the HIF pathway in these cells (Song et al. 2006). However, no significant increase in P-gp expression was induced by hypoxia, suggesting that *MDR1* regulation may be at least partially unrelated to hypoxia-induced chemoresistance (Song et al. 2006). In accordance, in a more recent study, the expression of three genes (*MDR1*, *HIF*-1α and *MRP1*) were investigated and associated with resistance to chemotherapy and radiotherapy in chordoma and in a chordoma cell line, CM-319 cells. Expression of HIF-1α and MRP1 was observed in most chordoma specimens and in CM-319 cells, and the expression of HIF-1α was correlated with MRP1. On the other hand, expression of MDR1 was not correlated with the expression of HIF-1α or MRP1. In fact, MDR1 was not expressed in CM-319 cells, and only very weakly expressed or not at all in more than 50% of the chordoma samples studied. Therefore, the authors concluded that both HIF-1α and MRP1 may play a role in the multidrug resistance of chordoma to chemotherapy. (Ji et al. 2010).

Different results were reported in a very recent study, which aimed to evaluate the expression of HIF-1α and P-gp in human laryngeal squamous cell carcinoma (LSCC) tissues and also to investigate the regulation of the *MDR1* gene expression by HIF-1α in Hep-2 cells under hypoxic conditions. Under hypoxia, HIF-1α expression was inhibited by RNA interference. HIF-1α and P-gp expression was high in the LSCC tissues and was associated with the clinical stage and lymph node metastasis. HIF-1α expression was positively correlated with P-gp expression. In the Hep-2 cells, HIF-1α and P-gp expression significantly increased in response to hypoxia. The inhibition of HIF-1α expression synergistically downregulated the expression of the *MDR1* gene in hypoxic Hep-2 cells. Therefore, the positive correlation between HIF-1α expression and P-gp expression found in LSCC indicates that the two proteins may serve as potential biomarkers for predicting the malignant progression and metastasis of LSCC. Moreover, HIF-1α may be critical for the upregulation of *MDR1* gene expression induced by hypoxia in Hep-2 cells (Xie et al. 2013).

Hypoxia does, however, induce oxidative stress, through a number of distinct mechanisms. For example, necrosis and DNA degradation caused by hypoxia results in the up-regulation of the enzyme thymidine phosphorylase, which breaks down thymidine to thymine and 2-deoxy-D-ribose-1-phosphate (Brown et al. 2000). The latter compound is a very powerful reducing sugar that glycates proteins, which can result in oxidative stress given the high level of oxidants within carcinoma cells. Furthermore, this enzyme has

been shown to cause oxidative stress *in vitro*, as well as being up-regulated in human breast carcinomas (Brown et al. 2000). Interestingly, the removal of vasculature leading to hypoxia can increase vascular endothelial growth factor (VEGF) production, promoting angiogenesis and leading to restoration of oxygen supply. However, reoxygenation or reperfusion is known to drive ROS formation, therefore causing oxidative stress. The culminating activation of stress pathways from both hypoxic and oxidative stress could in turn result in substantially increased *MDR1* expression (Callaghan et al. 2008). Whether this is directly correlated with drug resistance in cancer cells has yet to be determined.

In conclusion, several studies have clearly demonstrated that the loss of a vascular network or, to a lesser extent, macrophage infiltration, leads to a variety of stresses, be it oxidative, hypoxic, or acidic upon tumor cells. In order to overcome these adverse conditions, the cells adapt and activate nonspecific stress-response pathways, activating general stress responses. One of these responses involves the up-regulation and expression of *MDR1*. It appears likely that hypoxia and glucose deprivation play a role in *MDR1* regulation with oxidative stress being a common feature for both in signal transduction activation.

I.6.2.2.2.6. Chemotherapeutic drugs

In the previous sections, the *MDR1* expression was faced in the context of stress induced due to the inherent properties of a tumor. However, *MDR1* expression is also known to be up-regulated *in vivo* by the cellular damage caused by the treatment designed to destroy the tumor, namely chemotherapy and radiotherapy. Indeed, considerable evidence have indicated that the expression of drug transporter genes can be transiently induced in response to chemotherapeutics (Asakuno et al. 1994; Brugger et al. 2002; Chin et al. 1990a; Gekeler et al. 1988; Hu et al. 1995; Ichihashi and Kitajima 2001; Kohno et al. 1989; Liu et al. 2002b; Ohga et al. 1996; Schuetz et al. 1996a). This effect was first reported in CCRF-CEM/ActD cells that exhibited an increased steady-state level of *MDR1* RNA following short-term exposure to actinomycin D, being this increase mediated, at least in part, at the transcriptional level. (Gekeler et al. 1988). Moreover, early studies indicated that the *MDR1* promoter region from -136 to -76 was involved in activation by actinomycin D (Ohga et al. 1996), and the interaction of this site with a transcription factor believed to be YB-1 (although not directly shown) was increased in the presence of actinomycin D (Asakuno et al. 1994; Ohga et al. 1996). This region was later characterized as the *MDR1* enhancesome (Hu et al. 2000; Jin and Scotto 1998; Jin et al. 2007; Scotto 2003) (see I.6.2.2.2.8).

Although it was initially assumed that only those drugs associated with the MDR phenotype would induce the expression of P-gp genes, further studies in a variety of cell

lines derived from tumor types indicated that *MDR1* transcription could also be induced by non-MDR-inducing drugs, such as antifolates, cisplatin and hydoxyurea (Chaudhary and Roninson 1993). *MDR1* induction was associated with morphological indications of cell damage, suggesting that increased *MDR1*transcription could be part of a general cellular response to damaging agents (Chaudhary and Roninson 1993).

The finding that *MDR1* gene expression can be induced by transient exposure to chemotherapeutics has since then gained potential clinical significance. In fact, *in vivo* experiments in human patients have shown that transient exposure to doxorubicin leads to a rapid (20–50 min) induction of MDR1 expression in lung metastases (Abolhoda et al. 1999). This observation may explain why a correlation between outcome and P-gp expression has been difficult to establish in solid tumours, since this transient overexpression of P-gp induced by the MDR drug itself would not be detected in tumours subsequent to treatment.

Interestingly, some drugs, such as mitomycin C and other DNA cross-linking agents, can suppress mRNA expression of the *MDR1* gene, leading to a subsequent suppression of P-gp protein levels and a concomitant decrease in drug efflux, although the mechanism by which this occurs has not yet been fully determined (Ihnat et al. 1997). Moreover, pre-treatment with mitomycin C led to a 5- to 10-fold decrease in the EC_{50} for cell killing by a second agent, such as the P-gp substrate doxorubicin, but did not affect the lethality of the non-P-gp substrate, cisplatin. Accordingly, using stably transfected Madin-Darby canine kidney C7 epithelial cells expressing a human P-gp tagged with green fluorescent protein under the proximal human *MDR1* gene promoter, it was demonstrated that mitomycin C and doxorubicin have differential effects on P-gp expression and function (Maitra et al. 2001). Doxorubicin caused a progressive increase in the cell-surface expression of P-gp and function and, in contrast, mitomycin C initially increased plasma membrane expression and function at a time when total cellular P-gp was constant and P-gp mRNA expression had been suppressed. This was followed by a rapid and sustained decrease in cell-surface expression at later times, presumably as a consequence of the initial decrease in mRNA expression (Maitra et al. 2001). These studies imply that there are at least two independent chemosensitive steps that can alter P-gp biogenesis: one at the level of mRNA transcription and the other at the level of P-gp trafficking. Understanding the combined consequences of these two mechanisms might lead to novel chemotherapeutic approaches to overcome drug resistance in human cancers by altering either P-gp mRNA expression or trafficking to the membrane.

Damage exerted by chemotherapeutics may also induce ROS generation causing a dramatic elevation of oxidants that exceeds the compensatory changes in the levels of enzymatic and nonenzymatic antioxidants (Corna et al. 2004; Schweyer et al. 2004).

Moreover, as noted earlier, the oxidative stress induced by chemotherapy activates signalling pathways such as NF-κB, MAPK and PKC (Chaudhary and Roninson 1993; Wang et al. 1998b), and the prolonged activation of these pathways ultimately leads to apoptosis. However, transient activation is suggested to cause the transcriptional activation of genes, such as *MDR1* (Chaudhary and Roninson 1993; Davis et al. 2001). Therefore, the induction of *MDR1* expression may be mediated through a common ROS-induced pathway independent of the cytotoxic stimulus. Moreover, if a ROS-inducing compound such as 2-AAF (a NF-κB pathway activator) (Deng et al. 2001) is capable of inducing *MDR1*, such an effect would seem inherently applicable to chemotherapeutics. This proposal is supported by the fact that anthracyclines, etoposides, and platinum complexes, all demonstrated to generate ROS (Yokomizo et al. 1995). Anthracyclines, such as daunorubicin, activate neutral sphingomyelinase enzyme and induce elevated levels of the potent signalling lipid ceramide. This induction of ceramide contributes to ROS generation, as evidenced by the effects of cell-permeant ceramides on U937 human monoblastic leukemia cells. The increased ROS produces JNK activation and apoptosis. Moreover, the cell permeant ceramides are inhibited by the antioxidants N-acetylcysteine and pyrrolidine dithiocarbamate (Mansat-de Mas et al. 1999).

Moreover, other signalling pathways may also be involved in the chemotherapy-induced P-gp expression. It was demonstrated that repeated oral administration of etoposide (ETP), an anticancer drug, which is a P-gp substrate (Allen et al. 2003), attenuates oral morphine analgesia with a decrease in its serum and brain levels possibly attributed to the up-regulation of intestinal P-gp (Fujita-Hamabe et al. 2012). It was also reported that the up-regulation of intestinal P-gp was caused by activating the Ras homolog gene family member A (RhoA) (Kobori et al. 2012) and RhoA-associated coiled-coil containing kinase (ROCK) (Kobori et al. 2013a), one of the effectors of RhoA (Figure 21). The ezrin/radixin/moesin (ERM) protein family (Kobori et al. 2013a) has also been shown to regulate the localization of several drug efflux transporters to the plasma membrane (Kikuchi et al. 2002; Luciani et al. 2002; Yang et al. 2007). Oral treatment with ETP dramatically increased the association of ERM with the plasma membrane (Kobori et al. 2013a). This action results in the activation of ERM (Hirao et al. 1996) or in the production of phosphorylated ERM (p-ERM), which leads to prolongation of the activated state of ERM (Matsui et al. 1998). Interestingly, activation or phosphorylation of ERM has been shown to be dependent upon RhoA or ROCK, respectively (Kobori et al. 2013a), which is consistent with other reports (Hirao et al. 1996; Matsui et al. 1998). Therefore, it was postulated that repeated oral treatment with ETP increased P-gp expression at the ileal membrane by a mechanism possibly mediated by increased expression of ERM/p-ERM via activation of RhoA/ROCK, resulting in decreases in the analgesia of oral

morphine (a substrate for P-gp) (Kobori et al. 2013a; Kobori et al. 2012). However, reports indicating the temporal changes in either ERM, RhoA or ROCK, after initiation and cessation of repeated treatment with the P-gp substrate drugs, including ETP, were lacking.

Patients usually receive cancer chemotherapy on several consecutive days (e.g., 5–21 days) followed by discontinuation of therapy for 1 week or a few weeks (Stadler et al. 2006; Walker et al. 2011). Moreover, repeated treatment with P-gp substrate drugs for several consecutive days results in an increase in P-gp expression, whereas P-gp expression declines to values similar to control levels after cessation of treatment (Fujita-Hamabe et al. 2012; Jette et al. 1996; Lin 2003). Several reports have focused on the involvement of various factors, including tumor necrosis factor-alpha (TNF-α) and endothelin-1 (ET-1) (Bauer et al. 2007, Hartz, 2008 #1845), JNK/c-Jun/AP-1 (Hartz et al. 2008), and RhoA/ROCK signalling (Figure 21) (Doublier et al. 2008; Riganti et al. 2006; Zhong et al. 2010), in the alteration of the expression or functional activity of intestinal P-gp. However, reports examining the details of the relationships between temporal changes in the expressions of P-gp and those of RhoA, ROCK, ERM, and p-ERM, after initiation and/or cessation of repeated treatment with substrate drugs for P-gp were lacking. In a very recent study, the same authors aimed to investigate the time-dependent changes in P-gp expression, in addition to changes in the expression of RhoA, ROCK, ERM, and p-ERM in the ileum, after initiation or cessation of repeated oral treatment with ETP (Kobori et al. 2013b). According to the obtained results, RhoA at the ileal membrane was increased 3 days after initiating ETP treatment. Moreover, on treatment days 5 or 7, the expression of ROCK, ERM, and p-ERM was increased along with increments in P-gp expression, leading to decreases in oral morphine analgesia. All these changes returned towards normal levels 3 days after cessation of ETP. These data suggest that regulating the active state of the above-mentioned proteins during cancer chemotherapy, or creating a timeframe of discontinuation a few days after cessation of chemotherapy, may enable effective palliative care using oral opioids (Kobori et al. 2013b).

It should also be noted that overexpression of *MDR1* gene in response to chemotherapeutics was shown to be a result of changes in mRNA stabilization and translational initiation in several leukemia cell lines, with no apparent transcriptional component (Yague et al. 2003). Thus, it is likely that multiple mechanisms exist in different cell types that either cooperatively or exclusively regulate *MDR1* gene output.

I.6.2.2.2.7. Ionizing radiation

Numerous research studies have demonstrated the effect of ionizing radiation on *MDR1* levels (see I.6.2.2.1.2 and Figure 14). Most of these studies (employing cell lines

rather than more complex tumor models) are consistent with the surviving cell population showing greater expression of the MDR1 protein, with concomitant increase in the future drug resistance of the radiation-selected cells (Callaghan et al. 2008; Hill et al. 1994; McClean et al. 1993; Nielsen et al. 1998). Noteworthy, transcriptional activation of the *MDR1* gene by ionizing radiation is not a common feature of these studies. Instead, it was proposed that radiation may select for, or stabilize, a chromosomal alteration which leads to greater *MDR1* expression in the surviving cells (McClean et al. 1993). Since ionizing radiation itself is known to cause almost instantaneous increases in ROS (Spitz et al. 2004), it was suggested that therapeutic doses of radiation may cause transcriptional activation of *MDR1* via ROS mediated stress response pathways.

In contrast, other forms of irradiation such as UV (where the proportion of surviving cells is greater *in vitro*) have been shown to cause increases in the transcription of the *MDR1* gene via a Y-box element in the promoter region (Ohga et al. 1998) (see I.6.2.2.1.2). Indeed, initial studies demonstrated that UV-irradiation activates a human *MDR1*-CAT reporter construct approximately by 20-fold following transfection into human KB cells, and two elements, one extending from -136 to -76 and the second extending from +1 to +121, were required for this activation (Uchiumi et al. 1993). More recently, it was shown that the induction of *MDR1* transcription is mediated by the inverted CCAAT box, and that down-regulation of the CCAAT box binding protein, YB-1, decreases promoter response to UV (Ohga et al. 1998).

I.6.2.2.2.8. MDR1 enhancesome

According to the previous sections, it has been well established that the *MDR1* gene expression can be activated by UV radiation, differentiation agents such as sodium butyrate, HDAC inhibitors, phorbol esters and certain chemotherapeutics. Additionally, several studies have indicated that the signals from all these divergent stimuli converge on a region of the *MDR1* promoter later referred to as the ‘MDR1 enhancesome’ (Figure 19) (Hu et al. 2000; Jin and Scotto 1998; Jin et al. 2007; Scotto 2003). This region includes binding sites for the trimeric transcription factor NF-Y and the Sp family of GC-binding transcription factors (Hu et al. 2000; Jin and Scotto 1998; Jin et al. 2007; Scotto 2003) (see I.6.2.2.1.1 and I.6.2.2.1.2). Together, these DNA-binding proteins cooperate to recruit the histone acetyltransferase P/CAF to the *MDR1* promoter, resulting in the acetylation of promoter-proximal histones and subsequent transcriptional activation that is likely mediated by further chromatin remodelling (Scotto 2003). Also, chromatin immunoprecipitation studies have identified a ‘switch’ in DNA-binding Sp family members following induction (Scotto 2003). Further studies are required to determine whether this change in binding factors results in recruitment of new coactivators/corepressors to the

MDR1 promoter, and whether other factors that have been shown to bind to the *MDR1* GC element are also involved in stress response through the enhancesome complex (Scotto 2003). Although the mechanism by which each agent transduces the signal that results in promoter activation has yet to be determined, the role of the *MDR1* enhancesome in the regulation of transcription by a variety of stimuli makes it an attractive target for therapeutic intervention.

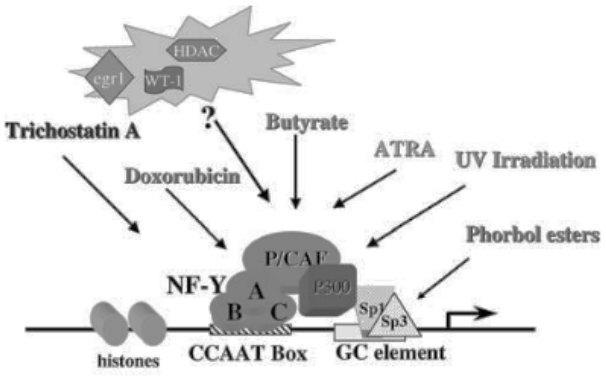

Figure 19. The *MDR1* 'enhancesome'
A variety of environmental signals, including those induced by hormones (all-*trans* retinoic acid, ATRA), radiation, HDAC inhibitors (trichostatin A, butyrate), some chemotherapeutics, phorbol esters and others converge on the MDR1 enhancesome, which includes the DNA binding proteins Sp1, Sp3 and NF-Y, the histone acetylases P/CAF and P/300. Depending on the conditions, the transcription factors egr1, WT-1 and the corepressor HDAC1 may also be found at the promoter. Taken from (Scotto 2003).

More recently, it was demonstrated that C-terminal-binding protein 1 (CtBP1), a transcriptional co-regulator, was increased (~4-fold) in human MDR cancer cell lines, NCI/ADR-RES and A2780/DX, as compared to their sensitive counterparts (Jin et al. 2007). CtBP1 has long been known as a transcriptional co-repressor. Although the exact mechanism of its repressive effect on gene transcription has not yet been fully defined, it is generally accepted that through association with transcription factors that contain Pro-X-Asp-Leu-Ser (PXDLS) motifs, CtBP1 can be recruited to DNA, thereby repressing gene transcription through epigenetic events, such as chromatin remodelling (Jin et al. 2007). However, in the previously mentioned study, the effect of CtBP1 on *MDR1* gene transcription was stimulatory rather than repressive, since silencing of CtBP1 expression decreased the *MDR1* mRNA and P-gp, enhanced the sensitivity of MDR cells to chemotherapeutic drugs that are transported by P-gp, and increased intracellular drug accumulation. Moreover, it was show that CtBP1 directly binds to the *MDR1* promoter, and enhances the promoter activity of this gene. Indeed, in a reporter gene assay, co-transfection of *MDR1* promoter constructs with a CtBP1 expression vector resulted in a ~2-4-fold induction of *MDR1* promoter activity. These results revealed the role for CtBP1 as an ‘‘activator’’ of *MDR1* transcription. In chromatin immunoprecipitation and electromobility shift assays, CtBP1 appeared to contribute to the activation of *MDR1* transcription through directly interacting with the *MDR1* promoter, as evidenced by its physical binding to the promoter region of the *MDR1* gene. Using *MDR1* promoter deletion constructs, the sequence between -75 and -4 was identified as the CtBP1 responsive

region. This conclusion was further supported by the results of chromatin immunoprecipitation and electromobility shift assays, which, respectively, showed that CtBP1 binds to the MDR1 promoter sequence and that the binding occurs between -75 and -50 within the promoter (Jin et al. 2007) (Figure 12). Since these sequences contain the *MDR1* enhancesome, a promoter region that, as previously referred, includes binding sites for some transcription factors such as NF-Y and Sp1 and responds to a variety of stressful stimuli, it is likely that CtBP1 acts on the *MDR1* enhancesome. These results suggest that, in addition to acting as a transcription co-repressor, CtBP1 can also activate gene transcription through its direct effect on the promoter region of genes. The function of CtBP as a transcriptional activator has also been reported for Wnt target genes. It was demonstrated that CtBP directly activates Wnt transcriptional targets through its interaction with the Wnt-regulated enhancer of the genes (Fang et al. 2006).

Additionally, the role for CtBP1 in the activation of MDR1 expression was also demonstrated not only in MDR cancer cell lines whose expression of P-gp is induced by drug treatments, but also in the cancer cells that intrinsically express P-gp (Jin et al. 2007). These results revealed a novel role for CtBP1 as an activator of *MDR1* gene transcription, and suggest that CtBP1 might be one of the key transcription factors involved in the induction of the *MDR1* gene. Therefore, also CtBP1 may represent a potential new target for inhibiting drug resistance mediated by overexpression of the *MDR1* gene.

I.6.2.2.2.9. Nuclear Receptors

Nuclear receptors (NRs) are important components of mammalian intercellular signalling mechanisms and the mammalian NR superfamily comprises more than 70 distinct members that are divided into two general subclasses, based on their ligand binding requirement (Chen et al. 2012b). The first subclass is comprised of ligand-dependent NRs that are regulated by a diverse group of exogenous compounds and endogenous substrates. These receptors include the glucocorticoid receptor (GR), estrogen receptor, androgen receptor (AR), and the retinoic acid receptor (RAR). The second subclass of nuclear receptors includes the so-called orphan receptors. These receptors share sequence identity with NRs but their regulatory ligands have yet to be fully identified (Chen et al. 2012b). Orphan receptors actually account for approximately 60% of the known NRs. Several key orphan receptors, including peroxisome proliferator activated receptors (PPARs), liver X receptors (LXRs), aryl hydrocarbon receptor (AhR), constitutive androstane receptor (CAR) and pregnane X receptor (PXR; also termed steroid xenobiotic receptor, SXR), are known to play crucial roles in development, homeostasis, and disease, therefore justifying the reason for the intense academic and

industrial research efforts concerning these targets for the development of novel therapeutic agents (Chen et al. 2012b).

Multi-drug resistance is, as previously referred, a clinical phenomenon characterized by decreased intracellular drug retention and changed tumor response, being, therefore, one of the primary factors that limit effective cancer therapy (Leonessa and Clarke 2003). Great attention has been directed towards the mechanism(s) underlying drug resistance and many efforts have been put into identifying therapeutic approaches that mitigate drug resistance. However, these clinical applications have shown limited success, partially because MDR is a complex process and no single drug metabolizing enzyme (DME) (Garcia-Martin et al. 2006) or ABC transporter (Haber et al. 2006) can induce MDR alone. Therefore, novel multi-targeted strategies are needed to overcome the induction of MDR. Several NRs families that regulate drug metabolism and disposition are increasingly recognized for their significance in this process, and treatments targeting them are promising new opportunities to attenuate, or even prevent, MDR. Among these NRs, PXR and CAR exhibit great flexibility in recognizing structurally diverse compounds, share significant similarities in ligand binding, and cross communicate during the transcriptional activation of their target gene promoters, which include cytochrome P450s (CYP 450, e.g. CYP2B6, CYP3A4 and CYP2C9) (Gerbal-Chaloin et al. 2002; Sueyoshi and Negishi 2001) and MDR-associated ABC transporters (e.g. P-gp) (Maglich et al. 2002) (Figure 20). PXR and CAR have been speculated to play important roles in cancer MDR, because of their elevated expressions in breast, prostate, intestinal, colon and endometrial cancers, and because of their roles as master transcription regulators of a broad spectrum of genes that encode phase I DMEs, phase II DMEs and efflux transporters (Chen et al. 2012b)(I.6.2.2.3).

Nuclear receptors are transcription factors that function as heterodimers to regulate target promoters (Chen et al. 2012b). Retinoid xenobiotic receptor (RXR) is present in all heterodimers and the second partner determines the substrate ligand and the target promoters that will be activated (Freedman 1999). Apart from CAR and PXR, other NRs have also been shown to be involved in transcription of drug transporters, including RAR and farnesoid receptor (FXR). The RXR-containing heterodimers regulate a broad range of hepatic metabolic functions, including bile acid synthesis, fatty acid and oxysterol metabolism, and cytochrome oxidase drug metabolism (Scotto 2003).

RARα in complex with RXRα has been shown to regulate transcription of the rat *mrp2* promoter (Denson et al. 2000). However, although the *MDR1* promoter is activated in neuroblastoma cell lines by all-*trans* retinoic acid, this activation appears to be independent of RAR/RXR binding, and is instead mediated by the differential binding of Sp family members to the GC element within the *MDR1* enhancesome (Scotto 2003).

In what concerns to PXR, numerous studies have characterized endogenous and exogenous PXR agonists. Indeed, this nuclear receptor was reported to bind to a wide range of structurally distinct chemicals, including anticancer drugs, plant extracts, cholesterol-lowering statins and SR12813, the anti-tuberculosis antibiotic rifampicin, HIV protease inhibitors, vitamins, carotenoids, endocrine disruptors, pesticides, plasticizers and PPAR and other nuclear receptor antagonists (Chen et al. 2012b). In response to the aforementioned xenobiotics, PXR activates the transcription of a series of biologically crucial phase I and II DMEs, as well as drug transporters (Figure 20) (Maglich et al. 2002; Rosenfeld et al. 2003). Among the drug transporters, PXR activation has been reported to regulate important efflux transporters such as multidrug resistance-associated proteins (MRPs), breast cancer resistance protein (BCRP), and P-gp (Dussault et al. 2001; Geick et al. 2001; Kast et al. 2002; Rosenfeld et al. 2003; Synold et al. 2001; Watkins et al. 2003).

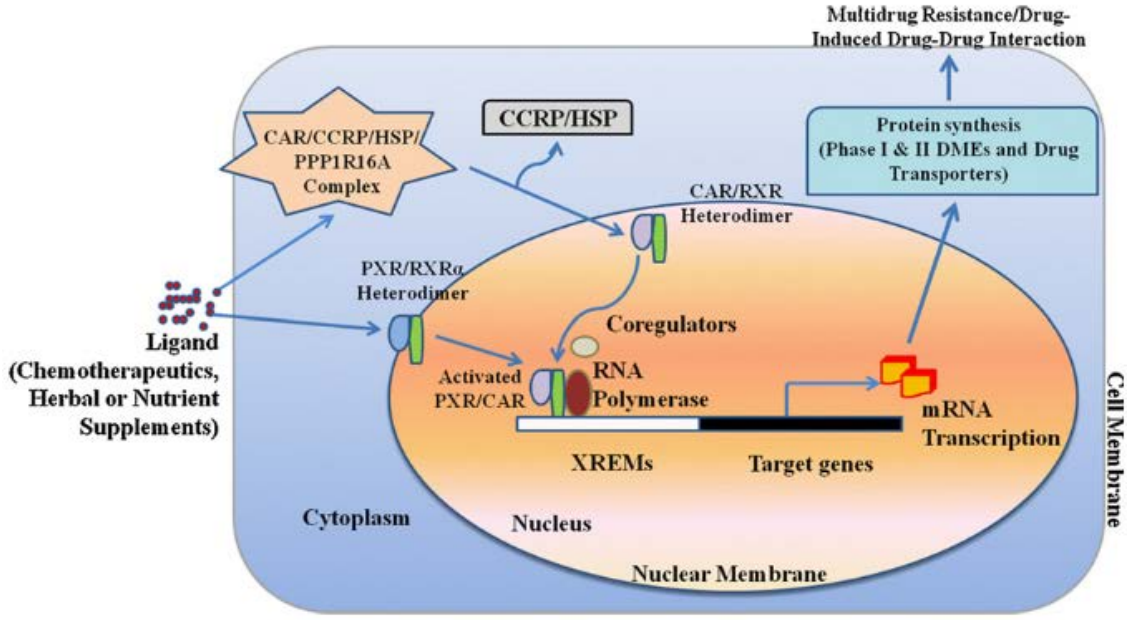

Figure 20. Regulation of phase I and II DMEs and drug transporter genes by nuclear receptors PXR and CAR.

After ligand binding, cytoplasmic fractions of PXR translocates to the nucleus while CAR dissociates from its complex, comprised of tetratricopeptide repeat (TTR), cytoplasmic CAR retention protein (CCRP), 90-kDa heat shock protein (hsp90) and PPP1R16A, and translocates from the cytoplasm to the nucleus. Subsequently, both PXR and CAR form heterodimers with RXR and bind to their respective response elements to stimulate transcription of phase I and II DMEs and drug transporters. Taken from (Chen et al. 2012b).

A direct PXR binding site (DR-4 motif) has been identified in the upstream enhancer of the *MDR1* gene (Geick et al. 2001; Synold et al. 2001). Indeed, attributed to the -7852 to -7837 sequence in the h*MDR1* promoter (SXR, Figure 12) is this upstream enhancer containing a motif related to broad specificity xenobiotic sensitivity, and thus called steroid

xenobiotic receptor (SXR) element. This sequence was reported to bind a pregnane xenobiotic/retinoid xenobiotic receptor α (PXR/RXRα) heterodimer that activates *MDR1* transcription in response to several PXR ligands, including R-12813, rifampicin, clotrimazole, nifedipine, and mifepristone, potently promoting P-gp expression in human primary hepatocytes and colon cancer cell lines (Geick et al. 2001; Synold et al. 2001). Moreover, it was also reported that LS180 cells that constitutively express active PXR also express P-gp in the absence of ligands (Synold et al. 2001). Additionally, Haslam *et* al. reported that, in T84 cells, rifampicin increased *MDR1* expression accompanied by increased PXR expression, whereas digoxin increased *MDR1* expression without changes in PXR expression, thus suggesting another type of regulation such as *via* CAR (Haslam et al. 2008b).

Initially isolated as an orphan nuclear receptor and named MB67, CAR is predominantly expressed in the liver and maintains only a limited presence in certain extrahepatic tissues in humans (Baes et al. 1994). Wild-type CAR does not require ligand binding to become activated. Instead, it readily forms heterodimers with RXR and targets retinoic acid response elements in target gene promoters (Chen et al. 2012b). Much like PXR, CAR functions as a chemical sensor and regulates a broad range of hepatic and intestinal phase I DMEs (CYP3A4, CYP2Bs and CYP2Cs), phase II DMEs (UGTs and GSTs), and drug transporters (MDR1, MRPs and OATP2) (Figure 20) (Chen et al. 2012b). Indeed, CAR was shown to regulate *MDR1* expression through DR-4 motifs (Burk et al. 2005). CAR also appears to cross-talk with PXR during xenobiotic response and these NRs recognize similar response elements and share a significant number of target genes (Xie et al. 2000). Nevertheless, because CAR can induce gene expression independently of ligand binding, it regulates xenobiotic metabolism in a way that is distinct from that of PXR (Chen et al. 2012b).

NRs such as CAR and PXR are also expressed in cancer cells (Chen et al. 2012b). Although PXR is mainly expressed in liver and intestinal tissues, its expression has been also detected in breast, prostate, and gastrointestinal cancers, and its expression in tumor cells is functional, underscoring its clinical relevance in oncology (Chen et al. 2012b). PXR activation in breast and prostate cancer cells was reported to stimulate the expression of CYP3A4 and MDR1, thus increasing cancer cell resistance towards chemotherapeutics (Chen et al. 2009; Chen et al. 2007) (see I.6.2.2.3). Interestingly, an *in silico* analysis of the correlation between PXR/CAR expression and mRNA levels of selective DMEs and transporters in prostate tumor tissues was recently performed (Chen et al. 2012b). According to the obtained results, *CYP3A4* mRNA expression is strongly correlated with the expression of PXR and CAR, and *MDR1* mRNA expression is significantly correlated with PXR expression in prostate tumor tissues (Chen et al. 2012b).

Furthermore, commonly used chemotherapeutic agents can activate human PXR, highlighting its relevance in cancer therapy (Huang et al. 2006; Jacobs et al. 2005; Mani et al. 2005; Masuyama et al. 2005; Synold et al. 2001). For example, among the chemotherapeutics, both hydroxylated and nonhydroxylated tamoxifen activate PXR (Jacobs et al. 2005) and the anti-mitotic agent paclitaxel activates PXR and enhances P-gp mediated drug clearance (Synold et al. 2001). Nevertheless, not all chemotherapeutics are subjected to PXR mediated drug metabolism. The semi-synthetic paclitaxel analog, docetaxel, is not a potent PXR activator and exhibits significantly longer plasma and intercellular half-lives (Mani et al. 2005).

The expression of functional PXR in cancer cells and activation of PXR by chemotherapeutics or other compounds can significantly impact tumor response to chemotherapy (Chen et al. 2009; Chen et al. 2007). Enhanced expression of drug transporters, resulting from PXR activation, increases the severity of drug resistance exhibited by tumor cells. Therapeutic agents that activate PXR may achieve lower clinical effectiveness in patients with high tumor PXR expression, since PXR may alter local concentrations of these antineoplastic agents. Therefore, untoward activation of PXR in tumor cells can lead to altered metabolism and disposition of chemotherapeutics within tumor tissues. Decreased concentrations of chemotherapeutics at the tumor site, in turn, substantially impact the intended efficacy of chemotherapy, especially *in vivo,* when the bioavailability of active chemotherapeutics is often a limiting factor (Chen et al. 2012b).

Finally, another implication of untoward PXR activation is the potential drug-drug interactions involved in cancer therapeutics, given its role in the regulation of DMEs and drug transporters (see I.6.2.2.3). Cancer patients often take other drugs, such as pain relievers, anti-depressants, anti-emetics, or alternative medicines including herbal supplements, in addition to the drugs that target the cancer. In many of these cases, PXR activation by drugs like rifampicin or the St. John’s Wort component hyperforin leads to up-regulation of DMEs (Chen et al. 2012b) and, thus, to unexpected pharmacokinetic interactions. Additionally, in order to reverse MDR, calcium channel blockers (such as verapamil, nifedipine), steroids, immunosuppresive agents (cyclosporine A) and calmodulin antagonists (such as phenothiazine) are used and many of these compounds are generally metabolized by CYP3A (Bertz and Granneman 1997; Wacher et al. 1995), therefore decreasing their concentrations at the target cells.

Although PXR is most often described as being involved in P-gp transcriptional control (Kliewer et al. 2002), two other NRs were considered to be modulators of *mdr1* gene transcription: i) the vitamin D receptor (VDR) and ii) the thyroid hormone receptor (TR) (Saeki et al. 2011). Taken together, these results suggest that activation of drug

transporters through multiple NRs can alter the efflux, and therefore the pharmacokinetics and bioavailability of a variety of compounds, including chemotherapeutic agents.

In what concerns to down-regulation of P-gp transcription, another type of ligand-activated NRs - peroxisome proliferator activated receptors (PPARs) - may be involved. Activation of PPARγ by its ligand troglitazone reversed P-gp-mediated MDR in SGC7901/ VCR cells by down-regulating P-gp at both the mRNA and protein levels (Chen et al. 2010a). Down-regulation of P-gp expression and activity was also demonstrated in P-gp-positive L1210 cells after activation of NRs for retinoic acid (RAR) with all-trans retinoic acid (Sulova et al. 2008). Like the NRs known to induce P-gp transcription (e.g., PXR, CAR, TR and VDR) (Saeki et al. 2011), both PPAR and RAR receptor types are also known to be effective after dimerization with RXR (Brtko and Thalhamer 2003; IJpenberg et al. 2004). Therefore, PPAR and RAR ligands may provide an advantage by promoting their interaction with RXR, thus being a challenge in MDR reversal. RAR and PPAR, which are fully activated by their ligands, may consequently crowd out from effective dimerization the NRs that actively induce P-gp transcription. Indeed, for RAR receptors and all-trans retinoic acid this possibility was already suggested (Breier et al. 2013).

I.6.2.2.3. Co-regulation of P-gp and CYP3A expression

As previously mentioned, P-gp is expressed in many normal tissues, particularly in epithelial cells in tissues with secretory or excretory functions, and in endothelial cells of capillaries at blood-tissue barriers. The *MDR1* expression in normal hepatic and “barrier” tissues fostered examination of its role in drug pharmacokinetics. P-gp increases the excretion of drugs from the liver and kidney, in addition to reducing drug penetration into sensitive tissues such as the brain and testes (see I.5). Moreover, this role in modifying drug disposition is not limited to chemotherapeutic agents since P-gp is also able to interact with numerous endobiotics (Suzuki and Sugiyama 2000). The metabolism and elimination of xenobiotics also involves enzymatic reactions catalysed by phase I (mainly cytochromes P450, CYPs) and by phase II enzymes (Xu et al. 2005). It is generally assumed that through these metabolic pathways, a hydrophobic compound is converted into a more polar product, which can be readily eliminated, although some notorious exceptions exist. CYPs are inducible hemoproteins that belong to a multi-gene family and, in the pharmacology field, the CYP3A subfamily is the most important (Nelson et al. 1996). It has been described that CYP3A is involved in the oxidative metabolism of more than 50% of drugs commonly used in humans, including anticancer drugs such as taxol, taxotere, vinca alkaloids, and epipodophyllotoxins (Bertz and Granneman 1997; Zhou-Pan et al. 1993).

A substantial proportion of known P-gp substrates (Table 4) are also subject to metabolic transformation by the CYP3A isoform (Kim et al. 1999; Lan et al. 2000; Schuetz et al. 1996a; Schuetz et al. 1996b), and this substantial overlap in substrate specificity (Kim et al. 1999) also extends to complementary expression patterns (Wacher et al. 1995). Of particular importance is the co-expression in hepatocytes and in the gut wall. This combination of metabolic biotransformation by CYP3A and active efflux via P-gp results in the reduced oral availability of numerous pharmacologic agents (Benet and Cummins 2001; Kim et al. 1999), and increases the potential for unwanted drug-drug interactions (Hennessy et al. 2002; Lan et al. 2000).

For compounds capable of inducing the expression of both P-gp and CYP3A (Callaghan et al. 2008), a co-induction mechanism has been proposed. In fact, it was reported that, in human HepG2 cells, both *MDR1* and *CYP3A4* genes were co-induced by dexamethasone, as well as the *mdr1b* and *Cyp3a* genes in the liver of NMRI mice (Sérée et al. 1998). However, the study of mRNA levels of *CYP3A4* and *MDR1* genes from a human liver bank revealed a large inter-individual variability in the expression of these two genes and no correlation between MDR1 and CYP3A4 expression was observed. Therefore, these results appear to indicate that *CYP3A4* and *MDR1* genes are not co-regulated in human liver, although the possibility of co-induction cannot be ruled out (Sérée et al. 1998). Indeed, the human *CYP3A4* and *MDR1* genes may not be co-regulated in human liver but could be co-induced by drugs such as dexamethasone, as demonstrated in HepG2 cells.

The members of the entire CYP450 family are subject to induction in an isoform specific manner, thus enabling to a tissue to rapidly respond to the presence of high substrate concentrations in order to prevent the unwanted build-up of exogenous molecules or endogenously derived cellular metabolites. The induction of CYP-isoforms occurs also through transcriptional activation and involves a large number of liver enriched transcription factors (eg, hepatocyte nuclear factor 1 α [HNF1α], CCAAT/enhancer-binding proteins [C/EBP]) and, in particular, several members of the nuclear receptor family (Akiyama and Gonzalez 2003). In recent years, the induction of *MDR1* in normal tissues, particularly in the “barrier tissues”, has been shown to be closely related to the mechanisms involved in *CYP* induction (Callaghan et al. 2008).

The proposal that NRs coordinate the expression of CYP3A4 and MDR1 was supported by the paclitaxel-mediated induction of both proteins in hepatocytes, being the induction of *MDR1* directly attributed to the specific interaction of paclitaxel with PXR (Synold et al. 2001). Further proof of the general mechanism was provided by the observation that PXR also induced expression of CYP3A4 and MDR1 in other tissues, namely the blood-brain barrier (Bauer et al. 2004; Bauer et al. 2006) and intestinal cell

lines (Geick et al. 2001; Greiner et al. 1999). Therefore, these results suggested a coordinated expression mechanism for a metabolizing enzyme and a nonspecific transporter to ensure drug detoxification and elimination, respectively. However, further studies are required to elucidate if there is differentially increased expression of CYP3A4 and MDR1 in response to PXR activation. For example, it is important to understand if at certain concentrations, a given compound may activate expression of CYP3A4 but not MDR1, thus altering the balance between drug detoxification and drug export. Moreover, it is important to note that MDR1 and CYP3A4 are not the sole proteins involved in drug detoxification and induced by PXR activators. The enzymes UDP-glucuronosyltransferase (UDPGT), sulphotransferases (SULTS), and glutathione-S-transferases (GST), which mediate the conjugation reaction of phase II metabolism, of xeno- and endobiotics, are induced by known ligands of the NRs, such as PXR and CAR (Callaghan et al. 2008). Also, other members of the ABC superfamily are induced through mechanisms involving NRs. Moreover, in contrast to *MDR1* whose expression is only induced specifically by the PXR-RXR heterodimer, the *MRP1*, *MRP2* and *MRP3* isoforms display multiple and isoform-dependent transcriptional regulation by NRs. For example, *MRP1* is induced by PXR, *MRP2* is induced by CAR, PXR, and FXR, while the expression of *MRP3* is affected by PXR and CAR (Callaghan et al. 2008).

In conclusion, the mechanism underlying a co-regulation between *CYP3A* and *MDR1* genes remains to be fully clarified in humans, but the study of such an interaction is interesting since: 1) CYP3A and P-gp have common substrates including drugs often used to reverse MDR, 2) the two genes are often expressed in the same human tissues such as liver, lung, colon, and 3) following analysis of the genomic sequence of these two genes, it would appear that common *cis*-regulating elements are present in their promoters (Sérée et al. 1998). Therefore, this overlap suggests that CYP3A and MDR1 may work together to limit or modify the bioavailability of a large number of drugs and xenobiotics, and the development of dual inducers may constitute a new antidotal pathway against toxic P-gp substrates that are also detoxified through CYP3A metabolization.

I.6.2.2.4. Crosstalk between signalling pathways

The preceding sections have demonstrated that regardless the source of extra- or intracellular stress, there is a commonly induced imbalance in oxidants and antioxidants through which signal transduction may be activated and *MDR1* up-regulated. However, a great deal remains to be understood about how particular stresses induce ROS generation and how this is translated into increased *MDR1* expression. In addition, greater

clarity is required to understand how ROS preferentially activate certain signalling pathways, under what conditions this takes place, and why particular cell types appear to increase *MDR1* expression by signalling through one pathway and not another in response to stress. Furthermore, the studies suggest a complex regulation pattern of the h*MDR1* promoter, probably extending beyond the simple house-keeping TATA-less gene concept. Despite the abundance of studies attempting to determine how P-gp expression is regulated, little emphasis is placed upon the interconnection and communication between the signalling pathways (Figure 21). Perhaps an obvious starting point to look for an interconnection is that between the NF-κB and the PKC pathways, as both are known to be activated early in response to stress and control anti-apoptotic responses (Hill and Treisman 1995). *MDR1* expression has been demonstrated to be driven via both pathways using a common agonist, namely, the phorbol ester 12-O-tetradecanoyl-13-acetate (TPA) (Gill et al. 2001; Vertegaal et al. 2000; Yang et al. 2001). Moreover, there is direct evidence for TPA-mediated induction of the *MDR1* gene in cancer cell lines (Gill et al. 2001; Vertegaal et al. 2000). The link between NF-κB and PKC pathways was also supported in a study, in which specific PKC inhibitors blocked the drug (eg, calphostin C) induced activation of NF-κB (Das and White 1997). Crosstalk has also been demonstrated between PI3K pathway and NF-κB. For example, 2-AAF, that activates NF-κB by causing IκB degradation, also activates the PI3K pathway, and its downstream effectors Akt, Rac1, and NAD(P)H oxidase (Kuo et al. 2002). It was therefore suggested that 2-AAF up-regulates *MDR1* expression through a mechanism mediated by the effectors of the PI3K pathway, such as NF-κB (Kuo et al. 2002).

Moreover, the previous sections highlighted the overlap of several of the binding sites for transcription factors in the h*MDR1* promoter (Figure 12 and Figure 19), suggesting that they may act through competitive or cooperative interactions. However, in most cases, it is not yet known whether multiple factors can simultaneously occupy their promoter site at the same time, or whether their interaction with the promoter is mutually exclusive. Nevertheless, is now clear that overlapping binding elements play functional roles in the regulation of gene transcription through competition between several factors for DNA binding (Ackerman et al. 1991). However, such competition depends on both tissue and cell co-expression of transcription factors and on changes in their relative amounts according with physiological and environmental conditions (Ackerman et al. 1991). Under these circumstances, the -123 to -75 at the h*MDR1* promoter (Figure 12), which contains, among others, the *MDR1* enhancesome, represents an important region for the regulation of this gene.

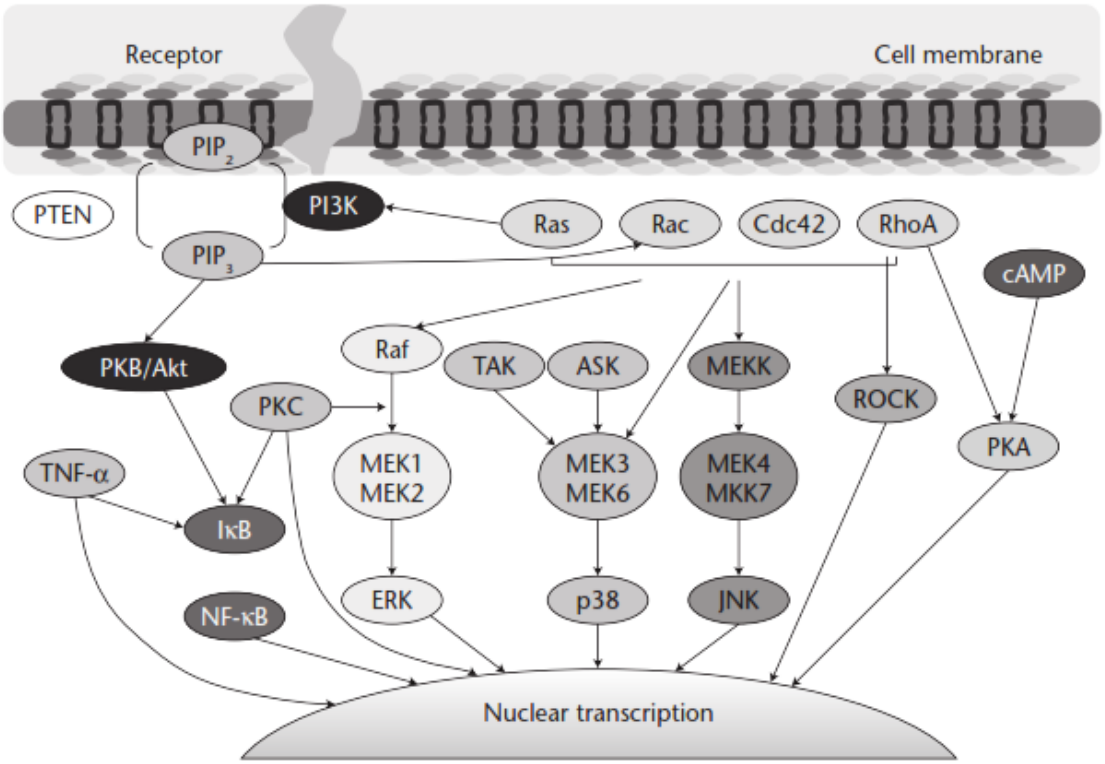

Figure 21. Signal transduction pathways and transcription factors that mediate the acquisition of P-gp-mediated multiple drug resistance in human MDR cancer cells.

PTEN, phosphatase and tensin homologue; PIP2/3, phosphatidylinositol 4,5-biphosphate/ phosphatidylinositol 3,4,5-triphosphate; PI3K, phosphatidylinositol 3-kinase; Cdc42, cell division control protein 42 homologue; RhoA, Ras homologue gene family, member A; cAMP: cyclic adenosine monophosphate; PKB/Akt, protein kinase B; PKC, protein kinase C; TAK, transforming growth factor β activated kinase; ASK, apoptosis signal regulating kinase; MEKK, mitogen-activated protein kinase kinase; ROCK, rho-associated, coiled-coil containing protein kinase; PKA: protein kinase A; TNF-α, tumor necrosis factor-α; IκB, inhibitor of NF-κB; MEK1/2/3/4/6, mitogen-activated protein kinase 1/2/3/4/6; MKK7, mitogen-activated protein kinase kinase 7; NF-κB, nuclear factor κB; ERK, extracellular signal-regulated kinase; JNK, c-Jun NH_2 terminal kinase. Taken from (Sui et al. 2012).

Also, it is important to keep in mind that most of the studies performed to identify the factors that regulate the *MDR1* transcription were performed in tissue cultured cells, and the relevance of these findings to the *in vivo* situation, particularly in the clinical setting, remains to be determined.

Additionally, apart from this protein interplay, the accessibility of promoter elements to their binding factors is regulated at the level of chromatin assembly. Levels of both histone acetylation and DNA methylation are known to regulate gene expression and the *MDR1* gene is no exception (El-Osta et al. 2002; Kusaba et al. 1999).

In conclusion, despite the intense research in this area, the relationship between signal transduction pathways and P-gp expression is far from being established. It is clearly a complex process involving more than a single pathway triggered by a specific extracellular stimulus, although it is not yet apparent how the different pathways are interconnected. Indeed, the situation may be more complex, combining translational with transcriptional effects mediated by signal transduction pathways. Such interconnections

reflect the redundancy of signalling pathways for *MDR1,* and underscore the ubiquity of multidrug resistance-induction through expression of this transporter

I.6.3. P-gp Activation – a new class of compounds that interact with P-gp

A new class of compounds that interact with P-gp has recently been identified, and designated as P-gp activators. This class represents compounds with the ability to immediately increase P-gp activity without increasing its expression (Sterz et al. 2009; Vilas-Boas et al. 2013b). While a P-gp inducer acts by increasing the protein expression from which an associated increase in its activity is expected, a P-gp activator is a compound that binds to P-gp and induces a conformational change that stimulates the transport of a substrate bound on another binding site (Sterz et al. 2009; Vilas-Boas et al. 2013b). Therefore, this activation mechanism promotes P-gp transport function without interfering with the protein expression levels, making it a more rapid process than P-gp induction (Vilas-Boas et al. 2013b). Moreover, this approach is in line with the functional P-gp model, which suggests that the efflux pump contains, at least, two distinct sites for drug binding and transport, and that these sites interact in a positively cooperative manner (Shapiro and Ling 1997c).

Although this class of compounds has been recently defined, it has long been known that there are compounds that bind to P-gp and stimulate the transport of a substrate on another binding site (Shapiro et al. 1999; Shapiro and Ling 1997c; Shapiro and Ling 1998a). For example, Hoechst-33342 and rhodamine 123 act by this cooperative mode of action, as evidenced by the kinetics of transport of both substrates in isolated P-gp-rich plasma membrane vesicles from Chinese hamster ovary CH'B30 cells, that demonstrated that each substrate stimulated P-gp-mediated transport of the other (Shapiro and Ling 1997c; Shapiro and Ling 1998a). Also, colchicine and quercetin stimulated rhodamine 123 transport and inhibited Hoechst 33342 transport. In contrast, anthracyclines such as daunorubicin and doxorubicin stimulated Hoechst 33342 transport and inhibited rhodamine 123 transport. Vinblastine, actinomycin D, and etoposide inhibited transport of both dyes. These results are consistent with a functional P-gp model containing at least two positively cooperative sites (H site and R site, for Hoechst-33342 and rhodamine 123, respectively) for drug binding and transport (see I.3.1) (Shapiro and Ling 1997c). Therefore, one site (R) preferentially recognizes rhodamine 123, doxorubicin and daunorubicin and the other site (H) preferentially recognizes Hoechst 33342 and colchicine. Vinblastine, actinomycin D, and etoposide interact equally with both sites. Binding of drug at the R site stimulates transport of Hoechst 33342 by the H site and binding of drug at the H site stimulates transport of Rhodamine 123 by the R site (Shapiro and Ling 1997c; Shapiro and Ling 1998a). Moreover, this model is consistent with earlier

observations of competitive and non-competitive effects of P-gp substrates and chemosensitizers (Shapiro and Ling 1997c). This two-site hypothesis is one of the most convenient working models for explaining the mutual stimulation of P-gp-mediated transport by several substrates (Sterz et al. 2009).

Shapiro et al. (1999) later demonstrated that P-gp possesses at least three positively cooperating drug binding sites (Shapiro et al. 1999), an H site selective for Hoechst 33342 and colchicine, an R site selective for rhodamine 123 and anthracyclines, in accordance with its preliminary results (Shapiro and Ling 1997c; Shapiro and Ling 1998a), and a third binding site for progesterone (a allosteric binding site exhibiting a regulatory function) (Shapiro et al. 1999). According to the obtained results, it was again demonstrated that drug binding to one site stimulates transport at the other binding site. In fact, prazosin and progesterone stimulated the transport of both Hoechst 33342 and rhodamine 123. Moreover, rhodamine 123 and prazosin (or progesterone), in combination, stimulated Hoechst 33342 transport in an additive manner. In contrast, Hoechst 33342 and either prazosin or progesterone interfere with each other, so that the stimulatory effect of the combination on rhodamine 123 transport is less than that of each individually. Non-P-gp-specific effects of prazosin on membrane fluidity and permeability were excluded and the obtained results indicated the existence of a third drug-binding site on P-gp with a positive allosteric effect on drug transport by the H and R sites (Shapiro et al. 1999), highlighting the existence of a cooperative mechanism of action also for prazosin and progesterone. Moreover, this allosteric site appears to be one of the sites of photoaffinity labelling of P-gp by [125I]iodoarylazidoprazosin (Safa et al. 1994) and does not seem to be involved in drug transport (Shapiro et al. 1999).

A four-P-gp-binding-sites model was also proposed, which supports the presence of three transport sites, at which translocation of drug across the membrane can occur, and one regulatory site, which modifies P-gp function. This last site allosterically alters the conformation of the transport binding sites for substrates from low to high affinity, thus increasing the rate of translocation (Martin et al. 2000). In this study, radioligand-binding techniques were used to directly characterize drug interaction sites on P-gp and how these multiple sites interact. The drugs used were classified as either 1) substrates, which are known to be transported by P-gp (e.g., vinblastine) or 2) modulators, which alter P-gp function but are not themselves transported by the protein (e.g., XR9576). Drug interactions with P-gp were either competitive, binding at a common site, or non-competitive, when binding at distinct sites. Intriguingly, some modulators interacted with P-gp at a transport site rather than a regulatory site. The pharmacological data also demonstrated that both transport and regulatory sites were able to switch between high- and low-affinity conformations. The multiple sites on P-gp displayed complex allosteric

interactions through which interaction of drug at one site switches other sites between high- or low-affinity conformations (Martin et al. 2000). In line with this, it has long been suggested that the adaption and survival mechanisms of living beings has allowed the binding of several xenobiotics at the same time to P-gp (Safa 1993; Safa 1998), increasing the transport of each other, not competing but activating the transport cycle (Safa 2004).

Moreover, current models of P-gp drug binding suggest a large, flexible drug-binding region, confirmed by the high-resolution crystal structure (Aller et al. 2009), rather than one or a few discrete drug-binding sites (see I.3.1). This region is thought to contain multiple hydrophilic electron donor/acceptor groups, charged groups, and aromatic amino acids, to create a number of sub-sites where drugs can bind. The flexibility of the binding pocket would allow induced fit of multiple drugs via hydrophobic interactions, hydrogen bonding, and electrostatic interactions with residues lining the binding pocket. The number and strength of these interactions would dictate the affinity of drug binding to the protein. In fact, the drug binding pocket of P-gp contains, as previously mentioned, primarily hydrophobic and aromatic residues. The substrate-binding cavity contains 73 solvent-accessible residues, of which 15 are polar and only two are potentially charged. More polar and charged residues are located near the bottom of the drug-binding pocket than in the upper portion, and it is thought that drug substrates carrying a charge will bind such that their charged portions interact with the polar/charged residues in the lower region (Aller et al. 2009).

In a very interesting study, several small molecules, first designed as inhibitors of the p53 protein, demonstrated different effects on the cellular accumulation of distinct P-gp substrates (Kondratov et al. 2001). By screening a chemical library for the compounds protecting cells from doxorubicin, a series of small molecules was isolated, which interfered with the doxorubicin accumulation in mouse fibroblasts by enhancing efflux of the drug. Isolated compounds also stimulated rhodamine 123 efflux. Moreover, stimulation of drug efflux was detectable in the cells expressing P-gp, but not in their P-gp-negative variants, and was completely reversible by the P-gp inhibitors. A dramatic stimulation of P-gp-mediated efflux of doxorubicin and rhodamine 123 by the identified compounds was accompanied by suppression of P-gp-mediated efflux of other substrates, such as paclitaxel or Hoechst 33342, indicating that they act as modulators of P-gp substrate specificity. Consistently, these P-gp modulators dramatically altered the pattern of cross-resistance of P-gp-expressing cells to different P-gp substrates: an increase in resistance to doxorubicin, daunorubicin, and etoposide was accompanied by cell sensitization to Vinca alkaloids, gramicidin D, and paclitaxel, with no effect on cell sensitivity to colchicine, actinomycin D, puromycin, and colcemid, as well as to several non-P-gp substrates.

Moreover, the most potent compounds were QB102 and QB11, which stimulated the transport of anthracyclines and rhodamine 123, whereas efflux of Vinca alkaloids and Hoechst 33342 was inhibited (Kondratov et al. 2001). A particularly interesting aspect of that work (Kondratov et al. 2001) was that the effect of these modulators seems to depend at least partially on the substrate binding site postulated by Shapiro and Ling (Shapiro and Ling 1997c). Moreover, the relative effect of P-gp modulators against different substrates varied among the isolated compounds that can be used as fine tools for analysing mechanisms of P-gp drug selectivity. These results raised the possibility of a rational control over cell sensitivity to drugs and toxins through modulation of P-gp activity by small molecules (Kondratov et al. 2001).

More recently, the P-gp modulating properties of 27 different imidazobenzothiazoles and imidazobenzimidazoles compounds structurally related to the previously reported P-gp activators, QB102 and QB11, were investigated (Sterz et al. 2009). Most of the tested compounds were able to stimulate P-gp-mediated efflux of daunorubicin and rhodamine 123 in a concentration-dependent manner, although some of the compounds also displayed weak inhibitory effects. Additionally, P-gp-mediated efflux of vinblastine and colchicine was inhibited by several of the tested compounds. Therefore, according to the obtained results, these novel compounds seem to bind to the P-gp H site and activate the efflux of specific substrates of the R site in a positive cooperative manner, whereas binding of H-type substrates is competitively inhibited. This hypothesis was further confirmed by the observation that these modulators do not influence hydrolysis of ATP or its affinity towards P-gp (Sterz et al. 2009).

It was also recently demonstrated that a synthetic derivative of rifampicin (a reduced derivative, RedRif) that modulated P-gp expression and activity could increase P-gp activity even at time points at which no increase in protein content occurred, thus acting as a P-gp activator, in a model of the rat blood-brain barrier (RBE4 cells). Interaction of RedRif with P-gp drug-binding pocket *in silico* was consistent with an activation mechanism of action, which was confirmed by docking studies (Vilas-Boas et al. 2013b).

Therefore, P-gp activators that exert various effects on the intracellular accumulation of distinct P-gp substrates are useful tools for investigating the interactions between multiple drug binding sites of this transport protein (Sterz et al. 2009).

I.7. Polymorphisms of the MDR1 gene: implications in drug therapy and disease

The *MDR1* gene is located on the long arm of chromosome 7 and consists of a core promoter region and 29 exons with a total length of 209 kb (Zhou 2008). *MDR1* is polymorphic and numerous mutations have been documented in various ethnic

populations. Indeed, more than 50 polymorphisms, including single nucleotide polymorphisms (SNPs) and insertions/deletions, are known in the *MDR1* gene (Choudhuri and Klaassen 2006; Sharom 2008; Sharom 2011). Some of these polymorphisms appear to change the mRNA expression, protein expression and P-gp function (Sharom 2008; Sharom 2011). Knowing that changes in P-gp expression and function would be expected to alter the absorption, plasma concentration, tissue distribution and excretion of its substrates, P-gp polymorphisms may be thus responsible for the variation in drug responses observed between different individuals and populations and, consequently may influence the outcome of drug treatment (Sharom 2008; Sharom 2011). Therefore, in recent years, there has been considerable interest in these polymorphisms. However, there have been many conflicting reports in this field, and no clear associations between genotype and altered response to drug treatment have emerged so far (Sharom 2008).

A point mutation that occurs in at least 1% of the population is considered to be an SNP (Sharom 2008). Some SNPs result in a change in the amino acid coding sequence of the protein (nonsynonymous), whereas others do not (synonymous; silent) (Sharom 2008). The first polymorphism to be reported in the *hMDR1* gene was the G2677T variant, which is a non-synonymous SNP resulting in a change in the amino acid sequence, Ala893Ser (Ser893 polymorphism). Since then, about 30 SNPs have been discovered by sequencing the *MDR1* gene in large numbers of individuals of different ethnic origin (Fromm 2002; Marzolini et al. 2004; Schwab et al. 2003a). The most common variants have probably been identified, although it is possible that some rare polymorphisms still remain to be detected. Moreover, considerable differences exist in the frequency of these variant alleles in different populations of Caucasian, African and Asian origin (Chelule et al. 2003).

P-gp SNPs have been reported to potentially alter both the expression and the function of the transporter. For example, the synonymous C3435T polymorphism (exon 26, C>T at 3435 position) was reported to be associated with reduced P-gp mRNA expression in a few studies, but this was later contradicted by other groups (Leschziner et al. 2007). Indeed, a twofold reduction in the duodenal P-gp levels in C3435T individuals was initially reported, which was associated with an increased oral absorption and higher plasmatic levels of digoxin (Hoffmeyer et al. 2000). However, a meta-analysis has later suggested that the C3435T SNP has no effect on the expression of *MDR1* mRNA or in the pharmacokinetics of digoxin (Chowbay et al. 2005). Furthermore, subsequent studies on other P-gp substrates, such as tacrolimus, fexofenadine and cyclosporine A, failed to confirm this association (Leschziner et al. 2007), and the overall consensus is that such an association is not significant. Several other SNPs have also failed to demonstrate an association with the levels of P-gp expression (Leschziner et al. 2007), leading thus to

inconclusive results. Another study has demonstrated that the C3435T polymorphism results in the expression of a P-gp that has a slightly different tertiary structure and altered interaction with drugs and modulators, despite having the same amino acid sequence (Kimchi-Sarfaty et al. 2007). These functional differences were reported to arise from altered folding kinetics during protein biosynthesis as a result of rare codon usage. Furthermore, it was demonstrated that reduced fexofenadine uptake might be associated with the non-synonymous SNP G2677T, suggesting that this variant has increased activity *in vivo (Kim et al. 2001)*. Also, a more-well documented link has been reported between the C3455T polymorphism and the epilepsy that is refractory to treatment with multiple drugs (Siddiqui et al. 2003). Moreover, since conflicting data have been reported on the effects of other alleles using various drug substrates, the controversy seems likely to continue.

More recent works have been focused on the association of protein expression levels with haplotypes (a set of SNPs). Distinct haplotypes exist, with considerable heterogeneity found within a single ethnic group, although all ethnic groups appear to possess the three most common haplotypes, which were found in >70% of the total population (Leschziner et al. 2006). One common haplotype includes the SNPs C1236T (exon 12, synonymous), G2677T (exon 21, non-synonymous), and C3435T (exon 26, synonymous), and is found in European Americans, whereas C1236T- G2677T- C3435C haplotype is common in African Americans (Kim et al. 2001). *MDR1* haplotypes, rather than individual SNPs, are more likely to affect the pharmacokinetics of MDR1 substrates (Sharom 2007). Two common P-gp polymorphisms (G2677T/A and C3435T) may play a role in the differential response to the cholesterol-lowering statin drugs (Kajinami et al. 2004). The C3455T variant was associated with lower response to atorvastatin in female patients, and haplotype analyses identified a subgroup of individuals with a remarkable response to treatment that was not linked to a single polymorphism (Kajinami et al. 2004). Response to treatment with fluvastatin was associated with a haplotype containing the G2677T/A allele (Bercovich et al. 2006). However, the association between haplotype and P-gp mRNA expression need to be further explored, not forgetting that factors such as medications, diet, interindividual differences in drug metabolism and the presence of an underlying disease may complicate the interpretation of the obtained results.

Noteworthy, using mammalian cell lines expressing P-gps carrying SNPs identified in human populations, it was demonstrated that many of this variants have little or no effect on either P-gp surface expression or transport function (Kimchi-Sarfaty et al. 2007) (Morita et al. 2003; Sakurai et al. 2007). Moreover, several non-synonymous polymorphisms in mammalian cells displayed modest changes in substrate specificity and drug-ATPase activity (Sakurai et al. 2007). However, the non-synonymous mutations of

G2677T/A/C, which result in the amino acid changes Ala893Ser, Ala893Thr and Ala893Pro, caused changes in both substrate specificity and ATPase kinetic properties, as evaluated with 41 different compounds (Sakurai et al. 2007). Also, the extent of those functional changes depended on the particular drug tested. Thus, the polymorphisms at the amino acid 893, which is located within the second intra-cellular loop in the C-terminal half of P-gp, appear to potentially influence the disposition and therapeutic efficacy of drugs administered clinically.

However, the effect of P-gp polymorphisms on the outcome of anticancer drug treatment has also been described for several different tumor types and treatment regimens (Leschziner et al. 2007) and, although some positive associations have been reported, no clear pattern exist.

Additionally, given the P-gp role in protecting tissues and organs from toxicants, it would not be surprising to find that polymorphisms play a role in the susceptibility of individuals to various disease states. In fact, *MDR1* polymorphisms have been reported to alter the susceptibility of certain individuals to various disease states, including colon cancer, renal cancer, inflammatory bowel disease and Parkinson's disease (Sharom 2008). For example, *mdr1* knockout mice demonstrated to spontaneously develop a form of colitis that can be prevented by antibiotic treatment (Maggio-Price et al. 2005), suggesting that P-gp functions as a defence against bacteria or toxins in the intestine. Confirming this idea, inflammatory bowel diseases (Crohn's disease and ulcerative colitis) are linked to the missense variant Ala893Ser/Thr (Brant et al. 2003), and patients with ulcerative colitis (but not Crohn's disease) have a higher frequency of the C3435T genotype, which results in lowered P-gp expression in the intestine (Schwab et al. 2003b). Additionally, genotyping of 249 ulcerative colitis and 179 Crohn's disease patients and 260 healthy controls was conducted and a highly significant association between the common haplotypes and ulcerative colitis, but not Crohn's disease, was observed (Ho et al. 2006). Additionally, human patients with the C3435T polymorphism, which is associated with lower intestinal expression of P-gp, are over-represented among patients with ulcerative colitis (Ho et al. 2006). Therefore, these reports provide compelling evidence to support the contribution of the *MDR1* gene in determining risk to ulcerative colitis but not to Crohn's disease.

Furthermore, variant P-gp alleles were reported to also affect cancer susceptibility. For example, although the genotypic frequency of the C3435T SNP was not altered in colorectal tumor cells from a total patient population as compared to controls (Humeny et al. 2003), when an under-50 years old patient population was examined, carriers of the 3435TT genotype or 3435T allele were at substantially higher risk of developing the disease (Kurzawski et al. 2005). Also, there is evidence suggesting that P-gp

polymorphisms influence the risk of developing renal epithelial tumours, again with the C3435T and C3435TT carriers presenting a higher risk (Siegsmund et al. 2002).

Since P-gp in the BBB protects the brain by eliminating toxins, the mutation-induced P-gp malfunction could contribute to the development of some neurological diseases. Indeed, Parkinson's disease susceptibility has been linked to P-gp polymorphisms in Chinese populations, where a *MDR1* haplotype containing the SNPs 2677T and 3435T was found to protect against the disease (Tan et al. 2005). Also, in another study, the 3435 TT genotype was highest in the early-onset Parkinson's disease group, second highest in the late-onset group, and lowest in controls (Drozdzik et al. 2003). Another report also noted that the C3435T allele occurred with higher frequency when compared with wild-type patients with early-onset Parkinson's disease (Furuno et al. 2002). Since the C3435T allele is associated with lower P-gp expression and Parkinson's disease is thought to possibly result, in part, from the gradual accumulation of environmental toxins in the brain, it is possible that the *MDR1* polymorphism genotype exposes the neurones to higher concentration of toxic P-gp substrates due to reduced efflux capability (Furuno et al. 2002).

In conclusion, *MDR1* polymorphisms are associated with increased susceptibility to ulcerative colitis, cancer, Parkinson's disease, and possibly other human diseases. This knowledge can help health professionals to make early and appropriate interventions to reduce the likelihood of a particular illnesses, keeping in mind that other factors, such as diet, life style, race, and environment, have also a major impact on the disease susceptibility and progress. Therefore, this is a rapidly developing field that will require substantial further investigation before firm conclusions can be reached.

II. OBJECTIVES

P-glycoprotein is the most extensively studied ATP-binding cassette transporter due to its role in modulating drug pharmacokinetics and in the development of the multidrug resistance (MDR) phenomenon. In fact, since its discovery in 1976, many scientific efforts led to the development of P-gp inhibitors, including structure- and ligand-based design methods. Therefore, this efflux pump has been viewed for decades as an important target for inhibition to overcome the well-known problems of MDR. However, P-gp was later found to be also present in normal tissues, including the brain, liver, kidney, placenta, testis and intestine. Given its cellular polarized expression in many excretory and barrier tissues, its broad substrate specificity, and its efflux capacity, this important pump constitutes a crucial cellular defence mechanism against its potentially toxic substrates, contributing towards the reduction of their intracellular accumulation.

Therefore, taking into consideration the important physiological role of P-gp in the elimination of harmful compounds and in affording protection to susceptible organs, the main aim of the present work was **the screening and development of specific and potent P-gp inducers and/or activators, which could act as potential antidotes in toxic P-gp substrates intoxications.** For that purpose, the following specific objectives were set to accomplish with the main aim of the present work:

- **To validate Caco-2 cells as a suitable model for the screening of new P-gp inducers/activators.** Doxorubicin was initially used as a model of a known P-gp inducer to evaluate the effect on both the expression and activity of P-gp.
- **To evaluate the P-gp induction/activation ability of commercially available and newly synthesised compounds**, including, colchicine, hypericin and newly synthetized xanthonic and thioxanthonic derivatives.
- **To evaluate whether the potential effects of the tested compounds on both P-gp expression and activity could afford an effective protection against toxic P-gp substrates.** For that purpose, paraquat (PQ) was used as a model of a known toxic P-gp substrate, and the protective effects against its cytotoxicity were correlated with the corresponding ability of the tested compounds for P-gp induction/activation. Moreover, by using different experimental designs of incubation with the tested inducers/activators, several issues could be addressed including, mechanistic insight (when the inducer was incubated with the cells prior to the toxic insult), effectiveness of protection if the potential antidote was present in the ingested toxic formulation (when the inducer and the harmful substrate were

simultaneously incubated), and effectiveness as antidote following intoxication (by incubating the inducer/activator after the toxic insult).

- **To elucidate the transport mechanisms involved in PQ intestinal uptake**. Although PQ is responsible for thousands of deaths due to accidental or intentional ingestion, only limited information is available on its gastrointestinal absorption. Therefore, knowing that the most effective way to reduce PQ blood concentrations, and, consequently, limit its accumulation in the lung is to inhibit its gastrointestinal absorption, we also sought to elucidate the transport mechanisms involved in the PQ uptake in Caco-2 cells. For that purpose, substrates and inhibitors for choline, amino acids and polyamines transporters were used to clarify their involvement in the herbicide's uptake and, consequently, in its toxicity.
- **Development of in *silico* strategies for P-gp inducers and activators.** Since the implication of P-gp in the development of MDR in cancer cells, many *in silico* studies have been conducted to predict P-gp substrates and inhibitors, and included structure- and ligand-based design methods. However, the search for P-gp inducers or activators has been mainly performed by random screening. Therefore, based on the *in vitro* activation/induction results, we aimed to develop a pharmacophore model for P-gp activation and P-gp induction, which could be used in the future for predicting new P-gp ligands through the rapid screening for new P-gp inducers and activators, respectively. Furthermore, since the xanthonic derivatives are positional isomers, we also sought to create a 2D QSAR model to elucidate the descriptor implicated in the P-gp activation ability of these compounds.

PART II

III. EXPERIMENTAL SECTION

III.1. Brief considerations on the experimental *in vitro* model and in the model of a toxic P-gp substrate (paraquat) used in the studies, and in the protocol used for evaluation of P-gp activity

III.1.1. Caco-2 Cells - a model of the human intestinal epithelium

Knowing that many intoxications by P-gp substrates result from accidental or intentional ingestion, the P-gp mediated defence mechanism is particularly relevant at the intestinal level, by significantly reducing their intestinal absorption and, consequently, their access to the target organs. Therefore, human intestinal epithelial Caco-2 cells were used in the present studies as an *in vitro* model of the human intestinal epithelium. Caco-2 cells, derived from human colorectal adenocarcinoma, are a widely accepted and reliable *in vitro* model for predicting drug intestinal absorption and excretion in humans (Barta et al. 2008; Huynh-Delerme et al. 2005; Watanabe et al. 2005; Yamashita et al. 2000; Yamashita et al. 2002a; Yamashita et al. 2002b). These cells closely mimic the enterocytes of the small intestine (Barta et al. 2008) and exhibit spontaneous morphological and biochemical enterocytic differentiation after confluence in culture (Huynh-Delerme et al. 2005). Caco-2 cells express P-gp (Hidalgo and Jibin 1996 ; Hunter et al. 1993; Shen et al. 2007; Watanabe et al. 2005), as well as other transporters involved in drug absorption and excretion (Hirohashi et al. 2000; Taipalensuu et al. 2001). Moreover, the P-gp expression levels in these cells are in good agreement with those of the normal human jejunum (Taipalensuu et al. 2001) and this efflux protein was already characterized as having an apical membrane localization in this intestinal cell line (Hunter et al., 1993).

Previous studies have reported the influence of cell- and culture-related factors on Caco-2 cells functional characteristics (Sambuy et al. 2005). Among the cell-related factors, the number of passages in culture is one of the major factors reported to influence different functions and activities of this cell line (Sambuy et al. 2005). To avoid the impact of this factor on the obtained results, the cells used in all the experiments were always taken between the 58^{th} and 65^{th} passages. Among the culture-related factors, it has long been known that the time of culture and seeding cell densities can influence the evolution of a cell culture in what concerns to cell replication, senescence and differentiation (Sambuy et al. 2005). Moreover, with respect to P-gp, an age-dependent expression of this pump in Caco-2 cell monolayers was already demonstrated (Hosoya et al. 1996). Therefore, these culture-related factors were strictly standardized in order to obtain a

reproducible experimental model, making possible to establish comparisons between the different compounds tested. For that purpose, the cells were always seeded at a density of 60,000 cells/cm^2 and used always with the same culture age, 4 days after seeding, when confluence was reached.

III.1.2. Paraquat – a model of a toxic P-gp substrate

Paraquat (PQ, 1,1′-dimethyl-4,4′-bipyridinium dichloride) is an extremely toxic herbicide, which was already reported to be a P-gp substrate (Dinis-Oliveira et al. 2006c; Vilas-Boas et al. 2013a; Vilas-Boas et al. 2013b). Moreover, previous *in vivo* studies have demonstrated that the *de novo* synthesis of P-gp in the lungs of PQ-intoxicated rats, induced by a single dose of dexamethasone (100 mg/kg i.p) 2 h after PQ intoxication (25 mg/kg i.p.), resulted in a remarkable decrease in PQ accumulation in the lung (by 40%, when compared to the group exposed to only PQ), with a significant increase in its fecal excretion (Dinis-Oliveira et al. 2006c). Additionally, there was an evident decrease in lung damage, with lower lipid peroxidation and carbonyl groups content, and a normalization of myeloperoxidase activity, as well as a significant enhancement in survival (Dinis-Oliveira et al. 2006a).

Considering these previously reported results and the exhaustive know-how acquired by our research group on PQ toxicity, this herbicide was used in the present studies as a model of a toxic P-gp substrate and we aimed to correlate the effects of the tested compounds on both P-gp expression and activity with a possible reduction in PQ intracellular accumulation and, consequently, with a potential reduction in its toxicity. For that purpose, PQ cytotoxicity was evaluated in Caco-2 cells (by the MTT reduction or by the neutral red uptake assays), with or without exposure to the tested inducers. Therefore, three different experimental designs of incubation were used:

- Pre-incubation with the tested inducer for 24, 48 or 72 h, followed by PQ incubation for 24 h. This experimental design aimed to directly correlate the observed effect on PQ-induced toxicity with a possible effect on P-gp expression and activity caused by the pre-exposure to the inducer. In fact, since the cells have no simultaneous contact with both PQ and inducer, the possible effects, other than P-gp induction, caused by the inducer are, therefore, minimized.
- Incubation with the inducer 6 h after the beginning of PQ exposure (total PQ incubation time of 24 h), reflecting a real-life intoxication scenario. In fact, in many cases, an effective antidote exerts its protective effects well after the intoxicant contacts with the target tissues. Moreover, this schedule for inducer incubation (6

h after PQ exposure) was chosen taking into account the estimated average arrival time of the patient to hospital, after PQ intoxication.

- Simultaneous incubation with the tested inducer and with PQ for 24 h, to mimic the presence of the potential antidote in the PQ formulation. This experimental design was chosen to evaluate if the inducer could be used as an effective antidote against PQ intoxications, acting as the first therapeutic measure employed to limit the herbicide absorption.

In all cases, PQ cytotoxicity was evaluated 24 h after exposure of Caco-2 cells to the herbicide.

The PQ concentrations used in the present studies are within those that could be expected to be attained *in vivo* in a real human intoxication scenario. The reported cases of PQ intoxications in humans available in the literature show wide variation in the *post-mortem* blood, urine and tissue concentrations of the herbicide (Dinis-Oliveira et al. 2009; Moreira et al. 2012). In most of these cases 25-50 mL of the PQ formulation are typically ingested (Dinis-Oliveira et al. 2009). Most of the commercially available formulations contain 20 g/100 mL of the herbicide that would translate into an orally ingested dose of approximately 5-10 g, which is absorbed up to a maximum of 5% (Roberts 2011). Under such intoxication scenarios blood concentrations up to 0.1 g/L (0.4 mM) could be easily achieved. Additionally, PQ concentrates in the target organs, such as the lung, reaching concentrations up to 10 times higher than those found in the blood (Dinis-Oliveira et al. 2008). Moreover, in the intestine, high concentrations may also be expected, since almost all of the ingested dose comes into contact with the enterocytes. Furthermore, the concentrations found at autopsy are probably lower than the peak concentrations that are expected to occur after intake, especially in the cases where the victims are submitted to emergency-care treatments to control the intoxications, such as hemodialysis and charcoal hemoperfusion.

III.2. MANUSCRIPT I

In vitro study of P-glycoprotein induction as an antidotal pathway to prevent cytotoxicity in Caco-2 cells

Reprinted from **Archives of Toxicology**,

volume 85, issue 4, pages 315 to 326

Arch Toxicol (2011) 85:315–326
DOI 10.1007/s00204-010-0587-8

MOLECULAR TOXICOLOGY

In vitro study of P-glycoprotein induction as an antidotal pathway to prevent cytotoxicity in Caco-2 cells

Renata Silva · Helena Carmo · Ricardo Dinis-Oliveira · Anabela Cordeiro-da-Silva · Sofia Costa Lima · Félix Carvalho · Maria de Lourdes Bastos · Fernando Remião

Received: 21 May 2010 / Accepted: 1 September 2010 / Published online: 21 September 2010

Abstract The Caco-2 cell line is a reliable in vitro model for predicting drug intestinal absorption and P-glycoprotein (P-gp)-mediated excretion in humans. Recent in vivo studies suggested the induction of P-gp as a cellular protection tool against paraquat poisoning, through the increase in its pulmonary and intestinal excretion. Thus, the aim of the present work was to evaluate P-gp expression and activity in Caco-2 cells exposed to doxorubicin (a known P-gp inducer) and to correlate these changes with paraquat toxic effects. Cytotoxicity of doxorubicin (0–100 μM) and paraquat (0–1,000 μM) was evaluated for a maximum period of 96 h. In doxorubicin-exposed cells, P-gp expression and transport activity were evaluated by flow cytometry, using a fluorescein isothiocyanate–conjugated antibody and the P-gp fluorescent subtract rhodamine 123, respectively. A significant increase in P-gp expression was observed as soon as 6 h after exposure to 5 μM doxorubicin. P-gp activity also increased after 6 h, but only at higher doxorubicin concentrations (over 50 μM). Paraquat (0–5,000 μM) cytotoxicity was then evaluated with or without previous exposure of the cells to doxorubicin (5–100 μM, a concentration range causing both an increase in P-gp expression and activity). Under P-gp induction, a significant reduction in paraquat cytotoxicity was observed. Furthermore, when these cells were incubated with a specific P-gp inhibitor (UIC2 antibody) the doxorubicin protective effects were blocked, confirming the involvement of P-gp in the reduction in paraquat cytotoxicity. In conclusion, the human Caco-2 cell line model can be used

R. Silva (✉) · H. Carmo · R. Dinis-Oliveira · F. Carvalho · M. de Lourdes Bastos · F. Remião (✉)
REQUIMTE, Toxicology Department, Faculty of Pharmacy, University of Porto, Rua Aníbal Cunha, 164, 4099-030 Porto, Portugal
e-mail: rsilva@ff.up.pt

F. Remião
e-mail: remiao@ff.up.pt

H. Carmo
e-mail: helenacarmo@ff.up.pt

F. Carvalho
e-mail: felixdc@ff.up.pt

M. de Lourdes Bastos
e-mail: mlbastos@ff.up.pt

R. Dinis-Oliveira
Faculty of Medicine, University of Porto, Al. Prof. Hernâni Monteiro, 4200-319 Porto, Portugal
e-mail: ricardinis@ff.up.pt

R. Dinis-Oliveira
Department of Clinical Analysis and Public Health, Center of Research in Health Technologies (CITS)-IPSN-CESPU, CRL, Vila Nova de Famalicão, Rua José António Vidal, 81, 4760-409 Vila Nova de Famalicão, Portugal

A. Cordeiro-da-Silva
Laboratory of Biochemistry, Faculty of Pharmacy, University of Porto, Rua Aníbal Cunha, 164, 4099-030 Porto, Portugal
e-mail: cordeiro@ibmc.up.pt

A. Cordeiro-da-Silva · S. C. Lima
IBMC—Institute of Molecular and Cellular Biology, University of Porto, Rua do Campo Alegre, 823, 4150-180 Porto, Portugal

S. C. Lima
e-mail: slima@ibmc.up.pt

for the study of P-gp induction as an antidotal pathway against substrates of this transporter system.

Keywords P-glycoprotein induction · P-glycoprotein transport activity · Paraquat toxicity · Caco-2 cells

Abbreviations

BCRP	Breast cancer–resistant protein
DMEM	Dulbecco's modified Eagle's medium
DOX	Doxorubicin
EDTA	Ethylenediamine tetraacetic acid
FBS	Fetal bovine serum
FITC	Fluorescein isothiocyanate
MTT	(4,5-dimethylthiazol-2-yl)-2,5-diphenyl tetrazolium bromide
NEAA	Nonessential aminoacids
NSAIDs	Nonsteroidal anti-inflammatory drugs
PBS	Phosphate-buffered saline solution
P-gp	P-glycoprotein
PQ	Paraquat
RHO 123	Rhodamine 123

Introduction

P-glycoprotein (P-gp; ABCB1) is an ATP-dependent efflux pump encoded by the MDR1 gene in humans (Ambudkar et al. 1999; Chang 2003; Gottesman et al. 2002; Shirasaka et al. 2008; Silverman 1999). It belongs to the ATP-binding cassette (ABC) superfamily of transporters (Ambudkar et al. 1999; Chang 2003; Gottesman et al. 2002; Shirasaka et al. 2008; Silverman 1999), which also includes the multidrug resistance–associated proteins (MRP1, MRP2, MRP3, MRP4 and MRP5), and the breast cancer–resistant protein (BCRP/ABCG2), an ABC half-transporter (Chang 2003).

This efflux protein is highly expressed in neoplastic cells from several cancer types, conferring a multidrug resistance phenotype to those cells, which become resistant to chemotherapy with anticancer drugs such as vinblastine, actinomycin D and daunorubicin (Chang 2003; Gottesman et al. 2002; Shirasaka et al. 2008; Silverman 1999).

In addition to the expression in tumor cells, P-gp is widely distributed in the apical surfaces of normal human epithelial tissues including the gastrointestinal tract, kidney, placenta, testes and the blood–brain barrier (Thiebaut et al. 1987). In these tissues, this 170-kDa protein plays an important role in the excretion of a variety of structurally and pharmacologically unrelated hydrophobic compounds including vinca alkaloids, colchicine, antibiotics, anthracyclines, cardiac glycosides, organic cations and pesticides (Cordon-Cardo et al. 1990; Gottesman et al. 2002). Given its cellular polarized expression, broad substrate specificity and efflux capacity, this protein may be suggested as an intracellular protection mechanism against xenobiotics (Hunter et al. 1993b; Huynh-Delerme et al. 2005; Watanabe et al. 2005).

P-gp is inducible by many drugs including dexamethasone, rifampicin, the herbal antidepressant St John's wort (hyperforin and hypericin) and chemotherapeutic agents namely, doxorubicin, daunorubicin and vinblastine (Zhou 2008). P-gp is induced not only by a number of chemical compounds but also by physical stress, such as X-irradiation, UV-irradiation and heat shock (Zhou 2008).

Caco-2 cells closely mimic the enterocytes of the small intestine (Barta et al. 2008). This well-established human carcinoma cell line, derived from human colorectal adenocarcinoma, exhibits spontaneous morphological and biochemical enterocytic differentiation after confluence in culture (Huynh-Delerme et al. 2005). These cells have been widely accepted as a reliable in vitro model for predicting drug intestinal absorption and excretion in humans (Barta et al. 2008; Huynh-Delerme et al. 2005; Watanabe et al. 2005; Yamashita et al. 2000; Yamashita et al. 2002a; Yamashita et al. 2002b). Caco-2 cells express P-gp (Hidalgo and Jibin 1996; Hunter et al. 1993b; Shen et al. 2007; Watanabe et al. 2005) as well as other transporters (Hirohashi et al. 2000; Taipalensuu et al. 2001) and, except for BCRP, the expression levels in these cells are in good agreement with those of the normal human jejunum (Taipalensuu et al. 2001). Moreover, the apical membrane localization of P-gp in Caco-2 cells was confirmed, demonstrating its polarized expression in this intestinal cell line (Hunter et al. 1993b).

Paraquat dichloride (methyl viologen; PQ), a known P-gp substrate, is a widely used herbicide that is highly toxic upon ingestion as a result of its pneumocyte accumulation through active transport. Previous studies developed by our group confirmed that P-gp induction was an effective antidotal pathway against paraquat-induced lung toxicity in rats exposed to high doses of the herbicide (Dinis-Oliveira et al. 2006a; Dinis-Oliveira et al. 2006b). The dexamethasone-induced de novo synthesis of P-gp in intestine and lungs resulted in a remarkable decrease in paraquat accumulation in the lung, with an increase in its fecal excretion (Dinis-Oliveira et al. 2006b). Additionally, there was an evident decrease in lung damage, with lower lipid peroxidation and carbonyl groups content, and a normalization of myeloperoxidase activity, as well as a significant enhancement in survival time (Dinis-Oliveira et al. 2006a).

These results prompted the development of an in vitro model for the screening and selection of potent and safe P-gp inducers using the Caco-2 cell line. Although several chemicals and clinically used drugs induce P-gp, no specific P-gp inducer has yet been described. For this purpose, we evaluated P-gp expression and transport activity in the presence of doxorubicin, a known P-gp inducer.

Additionally, we tested this model by effectively reducing the toxic effect of a xenobiotic (paraquat) through P-gp induction and correlated the changes in P-gp expression and activity with the observed paraquat cytotoxic effects.

Materials and methods

Materials

Caco-2 cells were kindly provided by Rosário Monteiro from the Biochemistry Department, Faculty of Medicine, University of Porto, Portugal. Dulbecco's modified Eagle's medium (DMEM) with 4.5 g/L glucose and GlutMAX™, nonessential amino acids (NEAA), fetal bovine serum (FBS), 0.25% trypsin/1 mM EDTA, antibiotic (10,000 U/mL penicillin, 10,000 μg/mL streptomycin), fungizone (250 μg/mL amphotericin B) and human transferrin (4 mg/mL) were purchased from Gibco Laboratories (Lenexa, KS). AccuGENE® (1 × PBS buffer) was purchased from Lonza Laboratories (Verviers, Belgium). Doxorubicin (DOX), rhodamine 123 (RHO 123), paraquat (PQ), cyclosporine, verapamil and (4,5-dimethylthiazol-2-yl)-2,5-diphenyl tetrazolium bromide (MTT) were obtained from Sigma (St. Louis, MO, USA). P-glycoprotein monoclonal antibody (clone UIC2) conjugated with fluorescein isothiocyanate (FITC) was purchased from Abcam (Cambridge, United Kingdom). Monoclonal anti-human P-glycoprotein antibody (IOTest® CD243) used in the P-gp inhibition studies was purchased from Beckman Coulter, Inc. (Fullerton, USA). Flow cytometry reagents (BD FacsFlow™ and Facs Clean™) were purchased from Becton, Dickinson and Company (San Jose, CA). Mouse IgG2a-FITC (negative moAb control to UIC2) was purchased from ImmunoTools GmbH, (Friesoythe, Germany).

All the reagents used were of analytical grade or of the highest grade available.

Caco-2 cell culture

Caco-2 cells were routinely cultured in 75-cm^2 flasks using DMEM medium supplemented with 10% FBS, 1% NEAA, 1% antibiotic, 1% fungizone and 6 μg/mL transferrin. Cells were maintained in a 5% CO_2–95% air atmosphere at 37°C, and the medium was changed every 2 days. Cultures were passaged weekly by trypsinization (0.25% trypsin/1 mM EDTA). The cells used for all the experiments were taken between the 58 and 63th passages.

Doxorubicin cytotoxicity assays

For the in vitro evaluation of DOX cytotoxicity, the MTT assay that measures mitochondrial activity was performed. The cells were seeded onto 48-well plates at a density of 60,000 cells/cm^2 to obtain confluent monolayers at the day of the experiment. On the day of the experiment, the cells were washed twice with PBS buffer (pH 7.4) and exposed to DOX (0–100 μM) in fresh cell culture medium for 6, 12, 24, 48, 72 and 96 h.

For the MTT assay, at each selected time point, the cell culture medium was removed, and the cells were washed twice with PBS (pH 7.4), followed by the addition of fresh cell culture medium containing 0.5 mg/L MTT and incubation at 37°C in a humidified, 5% CO_2–95% air atmosphere for 1 h. After this incubation period, the cell culture medium was removed, and the formed formazan crystals dissolved in 100% DMSO. The absorbance was measured at 550 nm in a multi-well plate reader (BioTek Instruments, Vermont, US). The percent cell viability relative to that of the control cells was used as the cytotoxicity measure.

P-glycoprotein expression and activity

For the in vitro evaluation of P-gp expression and activity, the cells were seeded onto 24-well plates at a density of 60,000 cells/cm^2 to obtain confluent monolayers at the day of the experiment. On the day of the experiment, the cells were washed twice with PBS buffer (pH 7.4) and exposed to DOX (0–100 μM) in fresh cell culture medium for 6, 12, 24, 48, 72 and 96 h. After the incubation period, the cells were washed twice with PBS and trypsinized with 0.25% trypsin /1 mM EDTA to obtain a cell suspension. The cells were then divided into two aliquots of approximately 250,000 cells, for the evaluation of P-gp activity and expression, respectively. Given the cytotoxicity data obtained, for the 50 and 100 μM DOX concentrations, P-gp expression and transport activity were only evaluated up to 24 h after exposure.

For the evaluation of P-gp expression, the cells were centrifuged (300*g* /10 min) and suspended in PBS buffer (pH 7.4) containing 10% FBS and P-gp antibody [UIC2] conjugated with FITC. The antibody dilution in this experiment was applied according to the manufacturer's instructions for flow cytometry. Mouse IgG2a_FITC was used as an isotype-matched negative control to estimate nonspecific binding of the FITC-labeled anti-P-glycoprotein antibody [UIC2]. The cells were then incubated for 30 min at 37°C in the dark. After this incubation period, the cells were washed twice with PBS buffer (pH 7.4) containing 10% FBS, suspended in ice-cold PBS and kept on ice until analysis. Fluorescence measurements of isolated cells were taken with a flow cytometer (FACSCalibur, Becton-Dickinson Biosciences). The green fluorescence of FITC-UIC2 antibody was measured by a 530 ± 15 nm band-pass filter (FL1). Acquisition of data for 10,000 cells was gated to include viable cells based on their forward and side light scatters and the propidium iodide (4 μg/mL) incorporation

(propidium iodide interlaces with a nucleic acid helix with a resultant increase in fluorescence intensity emission at 615 nm). Logarithmic fluorescence was recorded and displayed as a single parameter histogram. The geometric mean of fluorescence intensity for 10,000 cells was the parameter used for comparison (calculated as percentage of control). Nonlabeled cells (with or without doxorubicin) were analyzed in each experiment by a 530 ± 15 nm band-pass filter (FL1) in order to detect a possible contribution from cells autofluorescence to the analyzed fluorescence signals.

The P-gp transport activity was also evaluated by flow cytometry using 1 μM RHO 123 as a P-gp fluorescent substrate and 10 μM cyclosporine as a P-gp inhibitor. Rhodamine 123 and cyclosporine cytotoxicity (evaluated after a 30-min incubation period, the time necessary for RHO 123 accumulation) was previously determined by the propidium iodide incorporation assay. The P-gp transport activity assay consisted of two phases: (i) an accumulation phase, in which P-gp activity was blocked with 10 mM NaN_3 (to inhibit energy production) and 10 μM cyclosporine (a known P-gp inhibitor) in order to accumulate the substrate inside the cells and (ii) an efflux phase where the energy-dependent P-gp function was re-established due to removal of the P-gp inhibitor (cyclosporine) and the addition of an energy source (DMEM with 4.5 g/mol glucose). When P-gp activity increases, the amount of RHO 123 effluxed from the cells is higher and accompanied by a decrease in the fluorescence intensity due to the corresponding decrease in intracellular RHO 123. For the accumulation phase, the cells were centrifuged (300*g*/ 10 min), suspended in PBS buffer (pH 7.4) containing 10 mM NaN_3, 10 μM cyclosporine and 1 μM RHO123 and incubated at 37°C for 30 min. After the accumulation of the fluorescent substrate, the cells were washed twice with ice-cold PBS with 10% FBS and centrifuged (300*g*/10 min) at 4°C. For the efflux phase, the obtained cell pellet was then suspended in DMEM medium containing 4.5 g/L glucose and incubated for 30 min at 37°C. After this efflux period, the cells were washed twice with ice-cold PBS with 10% FBS, suspended in ice-cold PBS and immediately analyzed as described above for the P-gp expression assay using the FACSCalibur. The green intracellular fluorescence of Rho123 was measured by a 530 ± 15 nm band-pass filter (FL1).

Paraquat cytotoxicity assays

Paraquat (PQ) cytotoxicity was evaluated in Caco-2 cells by the MTT assay. Briefly, the cells were seeded onto 48-well plates, at a density of 60,000 cells/cm^2 and incubated, after confluence, with PQ (0–1,000 μM) for 6, 12, 24, 48, 72 and 96 h. At each time point, cytotoxicity was evaluated as described above for the DOX cytotoxicity assay.

Based on the obtained results, PQ cytotoxicity was then evaluated with or without previous exposure of the cells to doxorubicin after a 24-h incubation period and at a larger concentration range (0–5,000 μM). The cells were seeded onto 48-well plates to obtain confluent monolayers at the day of the experiment. On the day of the experiment, the cells were washed twice with PBS buffer (pH 7.4) and exposed to doxorubicin (0, 5, 10, 50 and 100 μM) in fresh cell culture medium for 24 h. After this incubation period, the cells were washed twice with PBS buffer (pH 7.4) and exposed to PQ (0–5,000 μM) in fresh cell culture medium for another 24 h. Cytotoxicity was evaluated by the MTT assay, as described before. To confirm the involvement of P-gp in the DOX protective effects, these incubations were repeated in the presence of a P-gp specific inhibitor (20 μL of the UIC2 antibody stock solution for 500,000 cells, according to the manufacturer instructions). In this assay, the protocol was similar to that described above but with previous P-gp inhibitor incubation for 30 min before PQ exposure. A schematic representation of this protocol is illustrated in Fig. 1.

The nonspecific inhibitors verapamil (50 and 100 μM) and cyclosporine (5 and 10 μM) were also tested for P-gp inhibition. With these inhibitors, and in the absence of doxorubicin exposure, the cytotoxicity of PQ decreased. This occurs probably due to an inhibiting effect on PQ transporter, blocking the PQ entrance into the cells. The inhibiting effect of both cyclosporine and verapamil on the carrier-mediated transport system for choline was already reported (Crowe et al. 2002) and therefore, these inhibitors were not further tested.

Statistical analysis

For each assay, all experiments were performed in triplicate and SD values were always < 10%.

Data obtained in the DOX cytotoxicity assays and P-gp expression and transport activity assay are expressed as mean ± SEM (standard error of the mean) from 4 independent experiments. All statistical calculations were performed with the GraphPad Prism version 5.00 for Windows (GraphPad Software, San Diego California, USA). Normality of the data distribution was assessed by three tests (KS normality test, D'Agostino and Pearson omnibus

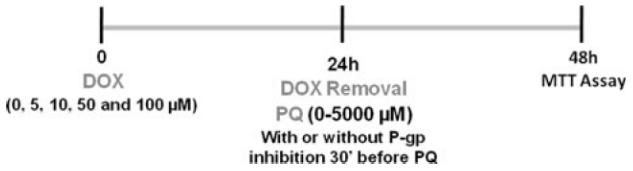

Fig. 1 Schematic representation of the experimental protocol for the evaluation of doxorubicin (DOX) protective effects against paraquat (PQ) cytotoxicity

normality test and Shapiro–Wilk normality test). Statistical comparison between groups was estimated using the non-parametric method of Kruskal–Wallis [one-way analysis of variance (ANOVA) on ranks] followed by Dunn's post hoc test. In all cases, *P* values lower than 0.05 were considered statistically significant.

Data obtained with the PQ cytotoxicity assays are expressed as mean ± SEM from 3 independent experiments. Statistical comparison between groups was estimated using the parametric method of one-way ANOVA on ranks followed by the Bonferroni's post hoc test. In all cases, *P* values lower than 0.05 were considered statistically significant.

For the PQ cytotoxicity assay performed with or without previous exposure to DOX and in the presence or absence of the P-gp inhibitor (UIC2 antibody), 3 independent experiments were performed. Concentration–response curves were fitted using least squares as the fitting method, and the comparisons between curves (bottom, top and LOG EC50) were made using the extra sum-of-squares *F* test. In all cases, *P* values lower than 0.05 were considered statistically significant.

Results

Doxorubicin cytotoxicity assays

Previous to the evaluation of the effect of doxorubicin on P-gp expression and activity, the cytotoxicity of this inducer was determined at different concentrations and time points. The conversion of MTT to formazan crystals by mitochondrial dehydrogenases was used as an index of mitochondrial viability and was evaluated up to a maximum period of 96 h. Figure 2 presents the cytotoxic effects of 0–100 μM DOX in Caco-2 cells. Doxorubicin exposure resulted in a concentration- and time-dependent cytotoxic effect that was more pronounced after 48 h of incubation. The obtained results show that up to a period of 6 h incubation, no significant effect on mitochondrial viability occurred at any of the tested DOX concentrations. For DOX concentrations up to 1 μM, no significant cytotoxic effect was observed over 72 h of incubation. For the 5–100 μM concentration range, after 12 and 24 h, a small but significant decrease in mitochondrial viability was observed (values between 85 and 91% compared to control), although at the highest 100 μM DOX concentration and after 24 h of incubation, a higher cytotoxicity occurred (80% cell viability compared to control). For exposure times higher than 48 h, there was a significant and more pronounced reduction in mitochondrial activity, mainly at the 5–100 μM DOX concentration range. At the end of the experiment (96 h), mitochondrial viability decreased to values of 56–49% when compared to the control cells within this concentration range.

P-glycoprotein expression and activity

The effect of DOX on P-gp expression in Caco-2 cells was evaluated by flow cytometry, using a P-gp monoclonal antibody [UIC2] conjugated with FITC. Nonspecific binding of the FITC-labeled–anti-P-glycoprotein antibody [UIC2] was not observed as estimated by the fluorescence obtained with the isotype-matched negative control. The results presented in Fig. 3 show that DOX significantly increased P-gp expression in a time- and concentration-dependent manner. At 5, 10, 50 and 100 μM DOX, a significant increase in P-gp expression as soon as 6 h was observed (147, 186, 312 and 365% when compared to control, respectively), whereas for 1 μM DOX similar results were obtained only after 48 h (204% when compared to control). At the 0.1 and 0.5 μM DOX concentrations, no significant increase was observed during the time course of the experiment.

The P-gp transport activity was also studied by flow cytometry using 1 μM rhodamine 123 (RHO 123) as a P-gp fluorescent substrate and 10 μM cyclosporine as a P-gp inhibitor. No cytotoxic effects were observed for RHO 123 and cyclosporine at these concentrations after 30 min of incubation (data not shown). Figure 4 represents the results obtained for the evaluation of P-gp transport activity in Caco-2 cells when exposed to 0–100 μM DOX at different time points (6, 12, 24, 48, 72 and 96 h). A time- and concentration-dependent significant increase in P-gp transport activity was observed as soon as 6 h after DOX exposure. For the 50 and 100 μM concentrations, after 6 h of incubation, P-gp transport activity significantly increased to values of 126 and 132% when compared to control, respectively. Moreover, for the 0.5–10 μM DOX concentration range, P-gp activity significantly increased after 48 h (128–136% when compared to control). When Caco-2 cells were exposed to the lower 0.1 μM DOX concentration, no significant effect in P-gp transport activity was observed during the time course of the experiment.

Paraquat cytotoxicity assays

Paraquat cytotoxicity (0–1,000 μM) was evaluated by the MTT assay over a time period of 96 h. Figure 5 represents the results expressed as percent viability compared to control. Cell death occurred in a concentration- and time-dependent manner. For the 0–10 μM PQ concentration range, no significant effect was observed in cell viability during the time course of the experiment. For the higher tested PQ concentrations (500 and 1,000 μM), a small but significant decrease in cell viability was observed as soon as 6 h (down to 94 and 90% when compared to control values, respectively). At the end of the experiment, for

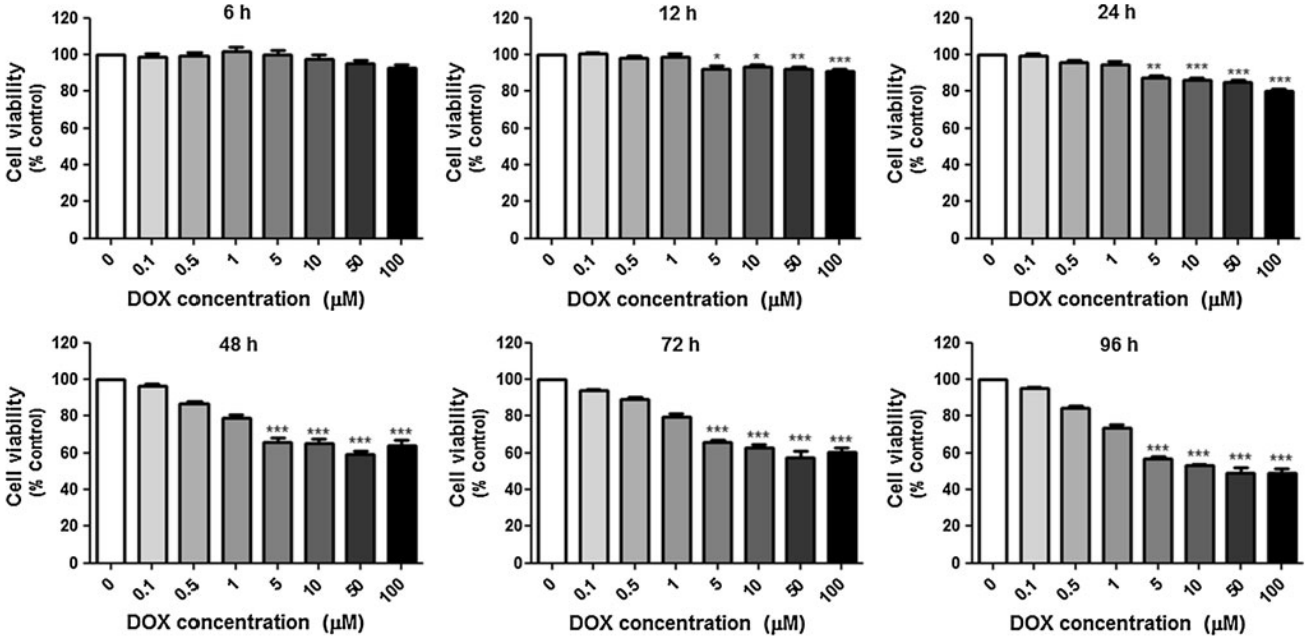

Fig. 2 Doxorubicin (DOX) cytotoxicity in Caco-2 cells at different time points. Results are presented as mean ± SEM from 4 independent experiments (triplicates were performed in each experiment). Statistical comparisons were made using the Kruskal Wallis test followed by the Dunn's multiple comparison post hoc test (*$p < 0.05$; **$p < 0.01$; ***$p < 0.001$ vs control)

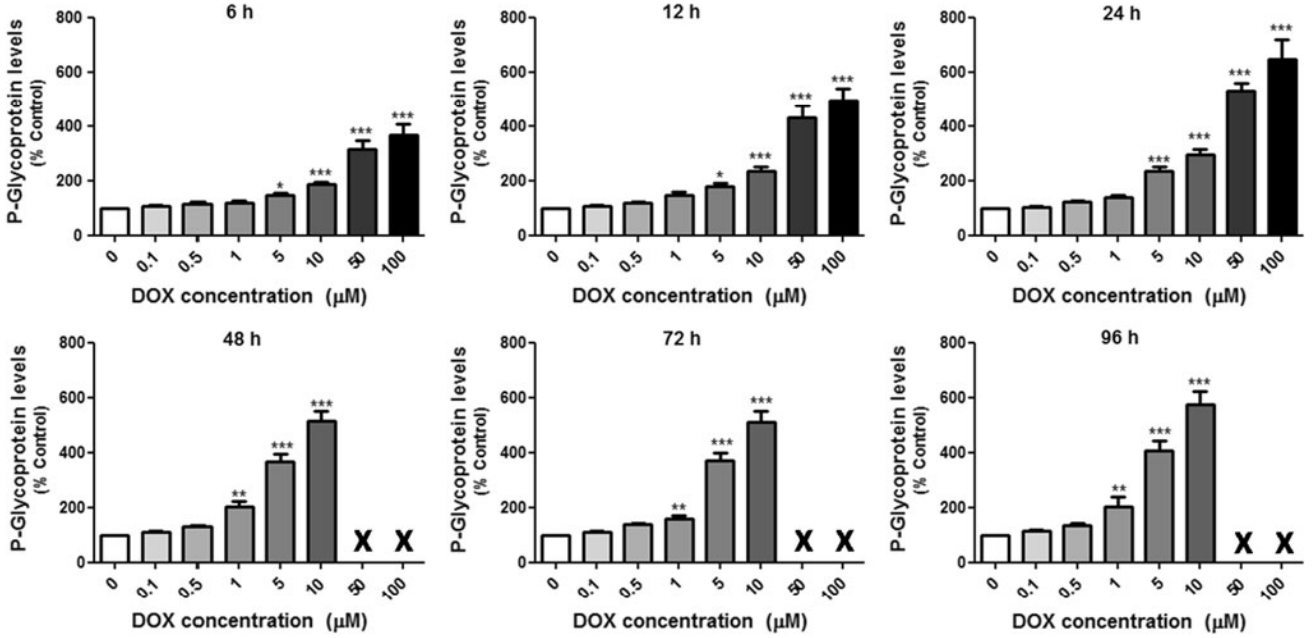

Fig. 3 P-glycoprotein expression levels in Caco-2 cells exposed to doxorubicin (DOX) (0 100 μM) at different time points (6, 12, 24, 48, 72 and 96 h). X means that these concentrations were not tested. Results are presented as mean ± SEM from 4 independent experiments (triplicates were performed in each experiment). Statistical comparisons were made using the Kruskal Wallis test followed by the Dunn's multiple comparison post hoc test (*$p < 0.05$; **$p < 0.01$; ***$p < 0.001$ vs control)

these two concentrations, a significant cytotoxic effect could be observed (down to 27 and 9% cell viability when compared to the control, respectively). For the 50 and 100 μM concentrations, a significant decrease in cell viability was observed after 24 h of exposure (down to 89 and 80% when compared to control, respectively), which was more pronounced after 96 h of incubation (87 and 73% when compared to control, respectively).

To study the protective effects of the increase in P-gp expression and activity, the cytotoxicity of PQ (0–5,000 μM)

Arch Toxicol (2011) 85:315 326

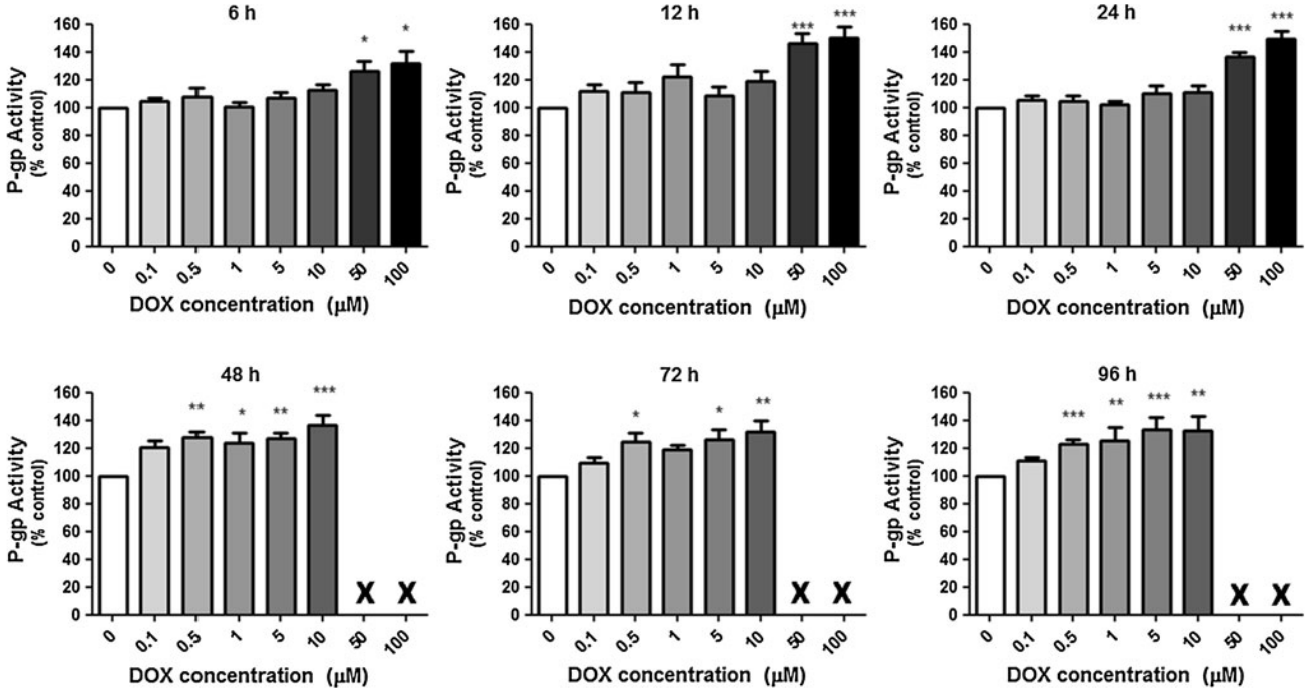

Fig. 4 P-glycoprotein transport activity in Caco-2 cells exposed to doxorubicin (DOX) (0 100 μM) at different time points (6, 12, 24, 48, 72 and 96 h). X means that these concentrations were not tested. Results are presented as mean ± SEM from 4 independent experiments (triplicates were performed in each experiment). Statistical comparisons were made using the Kruskal Wallis test followed by the Dunn's multiple comparison post hoc test ($*p < 0.05$; $**p < 0.01$; $***p < 0.001$ vs control)

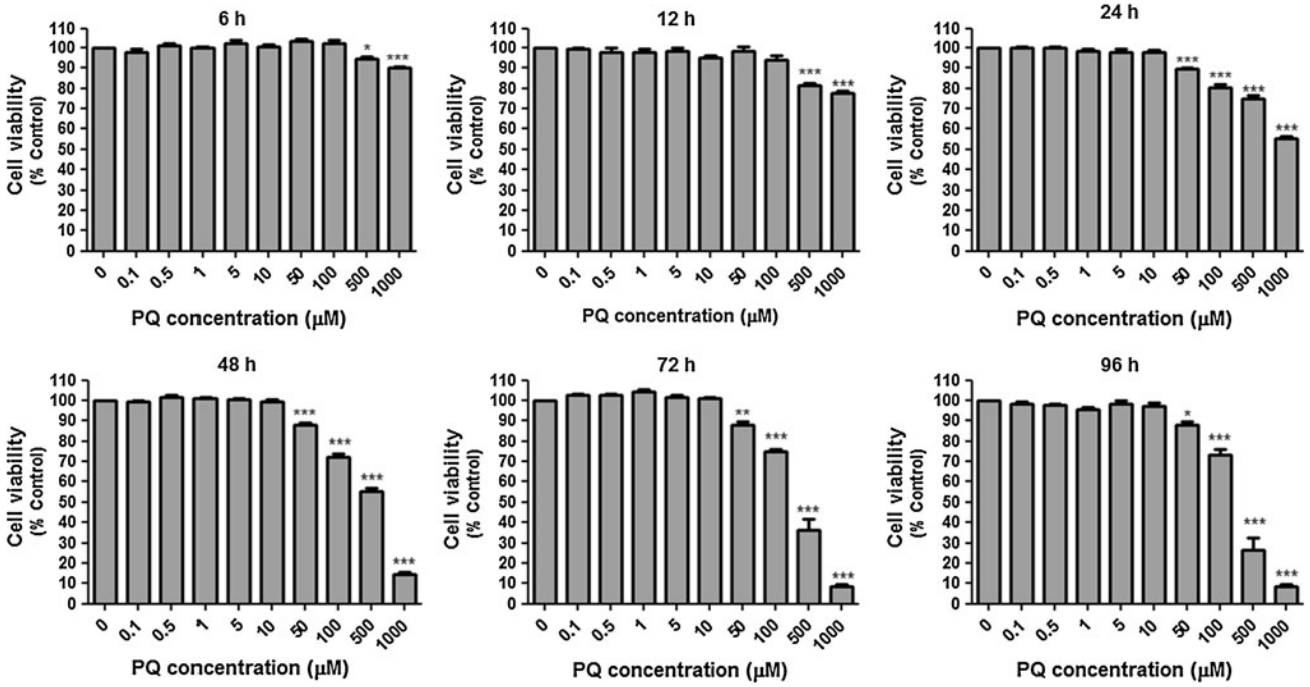

Fig. 5 Paraquat (PQ) cytotoxicity in Caco-2 cells at different time points. Results are presented as mean ± SEM from 3 independent experiments (triplicates were performed in each experiment). Statistical comparisons were made using one-way analysis of variance followed by the Bonferroni's multiple comparison post hoc test ($*p < 0.05$; $**p < 0.01$; $***p < 0.001$ vs control)

was further evaluated with or without DOX pre-incubation. Doxorubicin concentration range (5–100 μM) and pre-incubation time (24 h) were selected due to the previously noted absence of relevant cytotoxicity and significant increase in P-gp induction (protein expression and transport activity) under these conditions.

Cytotoxicity was evaluated by the MTT assay 24 h after PQ exposure. Figure 6 shows the concentration–response curves obtained with only paraquat (PQ) and with DOX pre-incubation (PQ + DOX). Maximal cell death occurred at the 5,000 μM PQ concentration both with and without DOX pre-incubation (70% cell death when compared to control values). However, significant differences were observed for the EC50 values of both curves (representing the half-maximum-effect concentrations from the fitted curves) at all DOX tested concentrations. Significant rightward shifts of the PQ concentration–response curves (Fig. 6), accompanied by significant increases in the EC50 values, were observed for all the tested DOX concentrations (Table 1). The observed increases in the EC50 values were not concentration dependent, with similar EC50 values being found for all the tested DOX concentrations.

To correlate the observed EC50 increases with P-gp expression and activity, this study was repeated in the presence of a specific P-gp inhibitor (PQ + UIC2 and PQ + UIC2 + DOX curves, Fig. 7). Under P-gp inhibition with the UIC2 antibody, an increase in the maximum cytotoxic PQ effect was observed for all curves (Fig. 7) when compared to the cytotoxicity curves obtained in the absence of this specific P-gp inhibition (Fig. 6). A leftwards shift in the PQ + UIC2 + DOX concentration–response curves was observed with significant decreases in the respective EC50 values (Table 2). The observed decreases in the EC50 values were not concentration dependent, with similar EC50 values being found for all the tested DOX concentrations.

Discussion

P-glycoprotein (P-gp) has been viewed as a therapeutic target for specific inhibition to overcome the well-known problems of drug resistance in anticancer therapy. On the other hand, its polarized expression is consistent with the

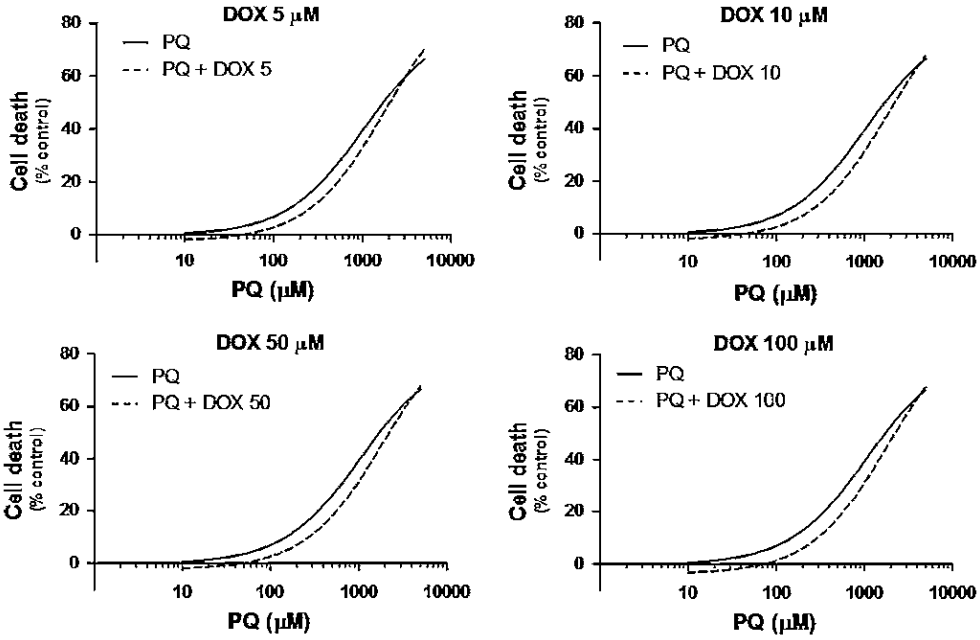

Fig. 6 Paraquat concentration–response (cell death) curves with (PQ + DOX) or without (PQ) previous exposure to doxorubicin (5, 10, 50 and 100 μM). Three independent experiments were performed (triplicates were performed in each experiment). Concentration–response curves were fitted using least squares as the fitting method, and the comparisons between PQ + DOX and control (PQ) curves (bottom, top and LOG EC50) were made using the extra sum-of-squares *F* test. In all cases, *P* values < 0.05 were considered statistically significant

Table 1 EC50 values (half-maximum-effect concentrations) of the paraquat concentration–response fitted curves, with (PQ + DOX) or without (PQ) previous exposure of Caco-2 cells to doxorubicin

Doxorubicin concentration (μM)	0 (PQ)	5 (PQ + DOX5)	10 (PQ + DOX10)	50 (PQ + DOX50)	100 (PQ + DOX100)
EC50 (μM)	1,047	1,825	1,899	1,853	1,806
EC50 *P* value (comparison between EC50 values)	–	0.0016	0.0007	0.0025	0.0207
Curve *P* value (comparison between the fitted curves)	–	<0.0001	<0.0001	<0.0001	<0.0001

Concentration–response curves were fitted using least squares as the fitting method, and the comparisons between PQ + DOX and control (PQ) curves were made using extra sum-of-squares *F* test. In all cases, *P* values < 0.05 were considered statistically significant

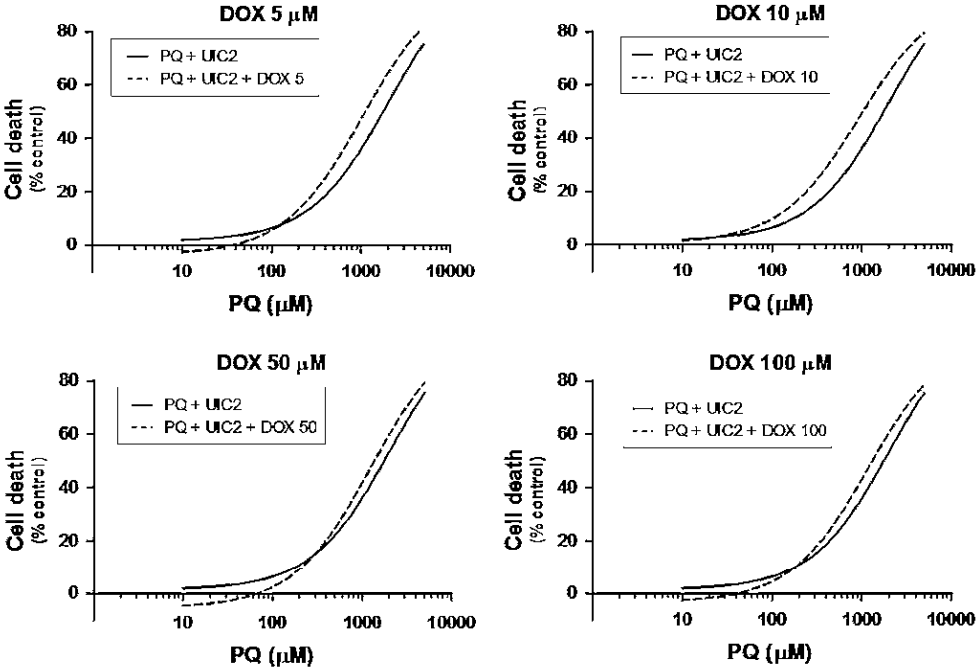

Fig. 7 Paraquat concentration–response (cell death) curves in the presence of a specific p-glycoprotein inhibitor (UIC2 antibody) with (PQ + UIC2 + DOX) or without (PQ + UIC2) previous exposure to doxorubicin (5, 10, 50 and 100 μM). Three independent experiments were performed (triplicates were performed in each experiment). Concentration–response curves were fitted using least squares as the fitting method, and the comparisons between PQ + UIC2 + DOX and control (PQ + UIC2) curves (bottom, top and LOG EC50) were made using the extra sum-of-squares *F* test. In all cases, *P* values < 0.05 were considered statistically significant

Table 2 EC50 values (half-maximum-effect concentrations) of the paraquat concentration–response fitted curves, in the presence of a specific p-glycoprotein inhibitor (UIC2 antibody) with (PQ + UIC2 + DOX) or without (PQ + UIC2) previous exposure to doxorubicin (5, 10, 50 and 100 μM)

Doxorubicin concentration (μM)	0 (PQ + UIC2)	5 (PQ + UIC2 + DOX5)	10 (PQ + UIC2 + DOX10)	50 (PQ + UIC2 + DOX50)	100 (PQ + UIC2 + DOX100)
EC50 (μM)	1,933	1,034	927.7	1,246	1,187
EC50 *P* value (comparison between EC50 values)	–	<0.0001	<0.0001	0.0024	0.0111
Curve *P* value (comparison between the fitted curves)	–	<0.0001	<0.0001	<0.0001	0.0012

Concentration–response curves were fitted using least squares as the fitting method, and the comparisons between PQ + UIC2 + DOX and control (PQ + UIC2) curves were made using extra sum-of-squares *F* test. In all cases, *P* values < 0.05 were considered statistically significant

proposed role of P-gp as a secretory protective system, contributing to the gastrointestinal epithelial barrier in limiting the bioavailability of its substrates (Hunter et al. 1993b). Thus, by using its efflux properties, a possible antidotal pathway against the damage induced by xenobiotics that are substrates of this transporter could be proposed. By increasing the expression and activity of this important transport protein, a consequent increase in the cellular efflux of such xenobiotics and a corresponding decrease in their accumulation could therefore culminate in an overall decrease in cytotoxicity.

Caco-2 cells have been reported to express P-gp (Hidalgo and Jibin 1996; Hunter et al. 1993b; Shen et al. 2007; Watanabe et al. 2005), and the expression levels are in good agreement with those of normal human jejunum (Taipalensuu et al. 2001). Therefore, this in vitro model could be used and validated for the screening and selection of potent and safe P-gp inducers and also for the study of the induction mechanism underlying their potential protective effects.

Several compounds were already reported to increase P-gp expression in Caco-2 cells such as vinblastine (Shirasaka et al. 2006b), venlafaxine (Ehret et al. 2007), R-cetirizine (Shen et al. 2007), cadmium (Huynh-Delerme et al. 2005) and benzo(e)pyrene (Sugihara et al. 2007). Flavonoids, a subclass of dietary polyphenolic compounds present in fruits, vegetables, and herbal plants, that are thought to promote human health through their antioxidant, antiviral and anticarcinogenic properties also induced P-gp expression in Caco-2 cells (Lohner et al. 2007).

To validate the Caco-2 cells as a suitable in vitro model to study and select safe, potent and specific P-gp inducers

as a tool for cell protection against xenobiotics, doxorubicin, a known P-gp inducer (Zhou 2008), was used to investigate changes in P-gp expression and activity and to correlate this induction with cellular protection against paraquat cytotoxicity.

Our results clearly indicated that doxorubicin is effective in increasing P-gp expression and activity. In fact, when in the presence of this known P-gp inducer, P-gp expression and transport activity increased in a concentration- and time-dependent manner, with significant results observed as soon as 6 h after incubation (Figs. 3 and 4). This rapid increase in P-gp expression was also reported by Ehret et al. (2007), who showed that venlafaxine increases the expression of MDR1 and MRP genes in Caco-2 cells during an acute (1.5, 3 and 6 h) treatment period. Similar results were observed for another known P-gp inducer, rifampicine (Ehret et al. 2007), and for several nonsteroidal anti-inflammatory drugs (NSAIDs) including diclofenac, fenbufen, indomethacin and nimesulide (Takara et al. 2009).

The observed remarkable increases in P-gp expression levels induced by doxorubicin were not accompanied by proportional increases in P-gp transport activity. For example, the exposure of Caco-2 cells to 50 μM DOX for 24 h increased P-gp expression levels to approximately 530% of control values, although P-gp transport activity increased only by 137%. This suggests that although P-gp is being highly expressed and incorporated into the cell membrane (since the monoclonal antibody recognizes an external P-gp epitope), this transport efflux pump is not yet fully functional. Noteworthy, our data suggest that, for the screening of P-gp inducers, both P-gp expression and activity should be investigated, since an increase in the first may not be reflected in an increase in the second parameter. Similarly, Takara et al. (2009) noted that P-gp transport function remained unchanged in Caco-2 cells exposed to several NSAIDs in spite of the observed increase in MDR1 mRNA (Takara et al. 2009).

One possible explanation for the differences noted between P-gp expression and activity levels in these cells is that Caco-2 full differentiation into enterocytes could be needed to obtain fully functional P-gp. In fact, in a study performed by Hosoya et al. (1996), based on the directionality of cyclosporine and verapamil transport, it was observed that in spite of the observed early P-gp expression, the protein was only fully functional after the 17th day in culture (Hosoya et al. 1996). Moreover, in that study the rank order of P-gp expression levels was 4 weeks $\approx$ 1 week $>$ 3 weeks $>$ 2 weeks at equal loading of cell proteins. These authors also observed, at the late stage of culture ($\sim$27 days), an enhanced cyclosporine transport in the basal-to-apical direction, which was due not only to an increased level of P-gp expression in the apical cell membrane but also to the full development of cell polarity, which may be the most important factor in effecting efflux pump function (Hosoya et al. 1996).

Paraquat dichloride (PQ) is an effective and widely used herbicide as desiccant and defoliant in a variety of crops. PQ is the third most extensively used herbicide in the world, causing thousands of deaths due to accidental or intentional ingestion (Dinis-Oliveira et al. 2006a,2006b, 2008). Studies performed by Nagao et al. 1993 suggested that PQ is absorbed through a specialized mechanism associated with the carrier-mediated transport system for choline on the brush-border membrane (Nagao et al. 1993). This carrier-mediated transport system for choline is present in Caco-2 cells (Kamath et al. 2003), allowing PQ to accumulate inside these cells. Noteworthy, a new therapeutic approach for PQ poisonings, involving its intestinal excretion, was already proposed by induction of de novo synthesis of P-gp (Dinis-Oliveira et al. 2006b). Taking these findings into account, PQ was used in the present study as a model for a xenobiotic that is able to enter into the Caco-2 cells and that is a known P-gp substrate.

The protective effects mediated by P-gp were studied through the evaluation of PQ cytotoxic effects with or without previous exposure to the P-gp inducer. We observed that pre-exposure of these cells to DOX resulted in a significant decrease in PQ cytotoxicity as shown by the PQ + DOX concentration–response curves shift to the right (Fig. 6) and by the corresponding significant increases in EC50 values (Table 1). However, the protective effects mediated by DOX were not concentration dependent for the DOX tested concentrations since the EC50 values obtained with the different DOX concentrations were very similar. In fact, the EC50 values increased from 1,047 μM in the absence of DOX to 1,825, 1,899, 1,853 and 1,806 μM when the cells were pre-exposed to 5, 10, 50 and 100 μM DOX, respectively (Table 1). This can be explained because in spite of the significant differences between P-gp expression levels for these DOX concentrations, smaller differences in P-gp transport activity were noted. In fact, P-gp expression levels were increased by 237, 294, 529 and 646% after 24 h incubation with 5, 10, 50 and 100 μM DOX, respectively (Fig. 3). However, the corresponding increases in P-gp activity were only of 110, 111, 136 and 150% (Fig. 4). These data indicate that although the P-gp expression levels increased in a concentration-dependent manner upon exposure to the tested inducer, the magnitude of the expected protective effect against a xenobiotic such as PQ did not increase in a similar trend. Several monoclonal antibodies recognizing discontinuous extracellular epitopes of P-gp have been developed. UIC2, in particular, seems to inhibit P-gp-mediated drug export in vitro (Chaudhary et al. 1992; Mechetner 2007; Mechetner and Roninson 1992). Thus,

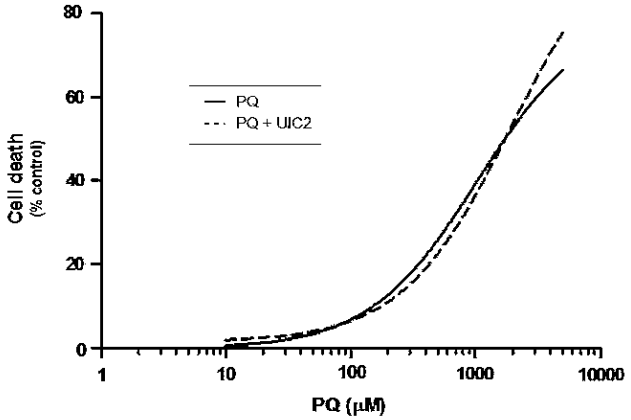

Fig. 8 Paraquat concentration–response (cell death) curves in the presence (PQ + UIC2) and in the absence (PQ) of a specific p-glycoprotein inhibitor (UIC2 antibody). Three independent experiments were performed (triplicates were performed in each experiment). Concentration–response curves were fitted using least squares as the fitting method

this inhibitor was chosen to investigate whether there is a link between P-gp induction and the reduction in PQ-induced cytotoxicity. Under P-gp inhibition, the maximum cytotoxic effect was increased for PQ (PQ + UIC2) when compared with PQ alone (Fig. 8). Similarly, for all PQ + UIC2 + DOX curves it was also observed an increase in the maximum cytotoxic effect when compared with the PQ + DOX curves (Figs. 6 and 7). This can be explained by the higher intracellular PQ accumulation that is expected when P-gp is inhibited. Given these differences in the observed maximum cytotoxic effect, the EC50 values (defined as the concentration of PQ that causes 50% of the observed maximum effect) can only be compared among the same experimental group (either in the presence or in the absence of the UIC2 antibody).

The analysis of concentration–response curves in the presence of the UIC2 antibody revealed that DOX protective effect was completely abolished in the presence of this P-gp specific inhibitor, with the PQ + UIC2 + DOX curves leftwards shift and with the corresponding decrease in the EC50 values (Table 2). In fact, when the cells were pre-exposed to doxorubicin and afterward co-exposed to PQ + UIC2, the EC50 values decreased significantly from 1,933 μM in the absence of DOX to 1,034, 927.7, 1,246 and 1,187 μM when the cells were pre-exposed to 5, 10, 50 and 100 μM DOX, respectively (Table 2).

These results suggest that P-gp induction by DOX protected the cells from PQ cytotoxicity. Moreover, this mechanistic study proved that P-gp induction can be an extremely important cellular protection tool against xenobiotics toxicity and an important antidotal pathway to be explored.

In conclusion, effective antidotal pathways can be achieved by promoting the cellular efflux of deleterious xenobiotics. As such, appropriate in vitro models addressing P-gp induction are needed. Our results showed that P-gp induction with doxorubicin was effective in increasing P-gp expression and activity, indicating that the present in vitro model could be useful for the screening of potential P-gp inducers. However, it should be noted that for the quantitative estimation of the P-gp-mediated drug transport, higher differentiation of the Caco-2 cells for maximal enterocytic differentiation may be required. Moreover, it was possible to prove the involvement of P-gp in the decrease in paraquat cytotoxicity.

Acknowledgments This work was supported by the Fundação para a Ciência e Tecnologia (FCT) - project [PTDC/SAU-OSM/101437/2008] - QREN initiative with EU/FEDER financing through COMPETE - Operational Programme for Competitiveness Factors. Renata Silva acknowledges FCT for her PhD grant [SFRH/BD/29,559/2006]. Ricardo Dinis-Oliveira acknowledges FCT for his pos-Doc grant [SFRH/BPD/36,865/2007].

Caco-2 cells were kindly provided by Rosário Monteiro from the Biochemistry Department, Faculty of Medicine, University of Porto, Portugal.

Conflict of interest The authors declare that there are no conflicts of interest.

References

Ambudkar SV, Dey S, Hrycyna CA, Ramachandra M, Pastan I, Gottesman MM (1999) Biochemical, cellular, and pharmacological aspects of the multidrug transporter. Annu Rev Pharmacol Toxicol 39:361–398

Barta CA, Sachs-Barrable K, Feng F, Wasan KM (2008) Effects of monoglycerides on p-glycoprotein: modulation of the activity and expression in caco-2 cell monolayers. Mol Pharm 5:863–875

Chang G (2003) Multidrug resistance ABC transporters. FEBS Lett 555:102–105

Chaudhary PM, Mechetner EB, Roninson IB (1992) Expression and activity of the multidrug resistance P-glycoprotein in human peripheral blood lymphocytes. Blood 80:2735–2739

Cordon-Cardo C, O'Brien JP, Boccia J, Casals D, Bertino JR, Melamed MR (1990) Expression of the multidrug resistance gene product (P-glycoprotein) in human normal and tumor tissues. J Histochem Cytochem 38:1277–1287

Crowe AP, Lockman PR, Abbruscato TJ, Allen DD (2002) Novel choline transport characteristics in Caco-2 cells. Drug Dev Ind Pharm 28:773–781

Dinis-Oliveira RJ, Duarte JA, Remiao F, Sanchez-Navarro A, Bastos ML, Carvalho F (2006a) Single high dose dexamethasone treatment decreases the pathological score and increases the survival rate of paraquat-intoxicated rats. Toxicology 227:73–85

Dinis-Oliveira RJ, Remiao F, Duarte JA, Ferreira R, Sanchez Navarro A, Bastos ML, Carvalho F (2006b) P-glycoprotein induction: an antidotal pathway for paraquat-induced lung toxicity. Free Radic Biol Med 41:1213–1224

Dinis-Oliveira RJ, Duarte JA, Sanchez-Navarro A, Remiao F, Bastos ML, Carvalho F (2008) Paraquat poisonings: mechanisms of

lung toxicity, clinical features, and treatment. Crit Rev Toxicol 38:13–71

Ehret MJ, Levin GM, Narasimhan M, Rathinavelu A (2007) Venlafaxine induces P-glycoprotein in human Caco-2 cells. Hum Psychopharmacol 22:49–53

Gottesman MM, Fojo T, Bates SE (2002) Multidrug resistance in cancer: role of ATP-dependent transporters. Nat Rev Cancer 2:48–58

Hidalgo IJ, Jibin L (1996) Carrier-mediated transport and efflux mechanisms in Caco-2 cells. Adv Drug Deliv Rev 22:53–66

Hirohashi T, Suzuki H, Chu X-Y, Tamai I, Tsuji A, Sugiyama Y (2000) Function and expression of multidrug resistance-associated protein family in human colon Adenocarcinoma Cells (Caco-2). J Pharmacol Exp Ther 292:265–270

Hosoya KI, Kim KJ, Lee VH (1996) Age-dependent expression of P-glycoprotein gp170 in Caco-2 cell monolayers. Pharm Res 13:885–890

Hunter J, Jepson MA, Tsuruo T, Simmons NL, Hirst BH (1993) Functional expression of P-glycoprotein in apical membranes of human intestinal Caco-2 cells. Kinetics of vinblastine secretion and interaction with modulators. J Biol Chem 268:14991–14997

IIuynh-Delerme C, IIuet II, Noel L, Frigieri A, Kolf-Clauw M (2005) Increased functional expression of P-glycoprotein in Caco-2 TC7 cells exposed long-term to cadmium. Toxicol In Vitro 19:439–447

Kamath AV, Darling IM, Morris ME (2003) Choline uptake in human intestinal Caco-2 cells is carrier-mediated. J Nutr 133:2607–2611

Lohner K, Schnabele K, Daniel H, Oesterle D, Rechkemmer G, Gottlicher M, Wenzel U (2007) Flavonoids alter P-gp expression in intestinal epithelial cells in vitro and in vivo. Mol Nutr Food Res 51:293–300

Mechetner E (2007) Detection of the MDR1 P-glycoprotein expression and function. Methods Mol Biol 378:175–193

Mechetner EB, Roninson IB (1992) Efficient inhibition of P-glycoprotein-mediated multidrug resistance with a monoclonal antibody. Proc Natl Acad Sci U S A 89:5824–5828

Nagao M, Saitoh H, Zhang WD, Iseki K, Yamada Y, Takatori T, Miyazaki K (1993) Transport characteristics of paraquat across rat intestinal brush-border membrane. Arch Toxicol 67:262–267

Shen S, He Y, Zeng S (2007) Stereoselective regulation of MDR1 expression in Caco-2 cells by cetirizine enantiomers. Chirality 19:485–490

Shirasaka Y, Kawasaki M, Sakane T, Omatsu H, Moriya Y, Nakamura T, Sakaeda T, Okumura K, Langguth P, Yamashita S (2006) Induction of human P-glycoprotein in Caco-2 cells: development of a highly sensitive assay system for P-glycoprotein-mediated drug transport. Drug Metab Pharmacokinet 21:414–423

Shirasaka Y, Sakane T, Yamashita S (2008) Effect of P-glycoprotein expression levels on the concentration-dependent permeability of drugs to the cell membrane. J Pharm Sci 97:553–565

Silverman JA (1999) Multidrug-resistance transporters. Pharm Biotechnol 12:353–386

Sugihara N, Toyama K, Okamoto T, Kadowaki M, Terao K, Furuno K (2007) Effects of benzo(e)pyrene and benzo(a)pyrene on P-glycoprotein-mediated transport in Caco-2 cell monolayer: a comparative approach. Toxicol In Vitro 21:827–834

Taipalensuu J, Tornblom H, Lindberg G, Einarsson C, Sjoqvist F, Melhus H, Garberg P, Sjostrom B, Lundgren B, Artursson P (2001) Correlation of gene expression of ten drug efflux proteins of the ATP-binding cassette transporter family in normal human jejunum and in human intestinal epithelial Caco-2 cell monolayers. J Pharmacol Exp Ther 299:164–170

Takara K, Hayashi R, Kokufu M, Yamamoto K, Kitada N, Ohnishi N, Yokoyama T (2009) Effects of nonsteroidal anti-inflammatory drugs on the expression and function of P-glycoprotein/MDR1 in Caco-2 cells. Drug Chem Toxicol 32:332–337

Thiebaut F, Tsuruo T, Hamada H, Gottesman MM, Pastan I, Willingham MC (1987) Cellular localization of the multidrug-resistance gene product P-glycoprotein in normal human tissues. Proc Natl Acad Sci U S A 84:7735–7738

Watanabe T, Onuki R, Yamashita S, Taira K, Sugiyama Y (2005) Construction of a functional transporter analysis system using MDR1 knockdown Caco-2 cells. Pharm Res 22:1287–1293

Yamashita S, Furubayashi T, Kataoka M, Sakane T, Sezaki H, Tokuda H (2000) Optimized conditions for prediction of intestinal drug permeability using Caco-2 cells. Eur J Pharm Sci 10:195–204

Yamashita S, Hattori E, Shimada A, Endoh Y, Yamazaki Y, Kataoka M, Sakane T, Sezaki H (2002a) New methods to evaluate intestinal drug absorption mediated by oligopeptide transporter from in vitro study using Caco-2 cells. Drug Metab Pharmacokinet 17:408–415

Yamashita S, Konishi K, Yamazaki Y, Taki Y, Sakane T, Sezaki H, Furuyama Y (2002b) New and better protocols for a short-term Caco-2 cell culture system. J Pharm Sci 91:669–679

Zhou SF (2008) Structure, function and regulation of P-glycoprotein and its clinical relevance in drug disposition. Xenobiotica 38:802–832

III.3. MANUSCRIPT II

Doxorubicin decreases Paraquat accumulation and toxicity in Caco-2 cells

Reprinted from **Toxicology Letters**,

volume 217, issue 1, pages 34 to 41

Toxicology Letters 217 (2013) 34–41

Contents lists available at SciVerse ScienceDirect

Toxicology Letters

journal homepage: www.elsevier.com/locate/toxlet

Doxorubicin decreases paraquat accumulation and toxicity in Caco-2 cells

Renata Silva[a,*], Helena Carmo[a], Vânia Vilas-Boas[a], Paula Guedes de Pinho[a], Ricardo Jorge Dinis-Oliveira[a,b,c,d], Félix Carvalho[a], Isabel Silva[e], Paulo Correia-de-Sá[e], Maria de Lourdes Bastos[a], Fernando Remião[a,*]

[a] REQUIMTE – Laboratory of Toxicology, Department of Biological Sciences, Faculty of Pharmacy, University of Porto, Rua de Jorge Viterbo Ferreira, 228, 4050-313 Porto, Portugal
[b] Department of Forensic Sciences, Faculty of Medicine, University of Porto, Jardim Carrilho Videira, 4050-167 Porto, Portugal
[c] Department of Sciences, Advanced Institute of Health Sciences – North, CESPU, CRL, R. Central de Gandra, 1317, 4585-116 Gandra, Portugal
[d] Department of Diagnostic and Therapeutic Technologies, Polytechnic Health Institute – North, CESPU, CRL, Vila Nova de Famalicão. Rua José António Vidal, 81. 4760-409 Vila Nova de Famalicão, Portugal
[e] Laboratory of Pharmacology and Neurobiology/UMIB, Instituto de Ciências Biomédicas de Abel Salazar (ICBAS) – University of Porto (UP), Rua de Jorge Viterbo Ferreira, 228, 4050-313 Porto, Portugal

HIGHLIGHTS

- No effective antidote exists against paraquat (PQ) poisonings.
- Doxorubicin protects against PQ cytotoxicity inducing P-gp.
- Doxorubicin protects against PQ cytotoxicity inhibiting choline uptake system.
- Compounds that both promote PQ efflux and limit PQ uptake can be used as antidotes.

ARTICLE INFO

Article history:
Received 19 October 2012
Received in revised form
27 November 2012
Accepted 29 November 2012
Available online 7 December 2012

Keywords:
P-glycoprotein induction
P-glycoprotein transport activity
Paraquat toxicity
Caco-2 cells
Choline transport system

ABSTRACT

P-glycoprotein (P-gp) is an efflux pump belonging to the ATP-binding cassette transporter superfamily expressed in several organs. Considering its potential protective effects, the induction of de novo synthesis of P-gp could be used therapeutically in the treatment of intoxications by its substrates. The herbicide paraquat (PQ) is a P-gp substrate responsible for thousands of fatal intoxications worldwide that still lacks an effective antidote.

The aim of the present work was to evaluate the effectiveness of such an antidote by testing whether doxorubicin (DOX), a known P-gp inducer, could efficiently protect Caco-2 cells against PQ cytotoxicity, 6 h after the incubation with the herbicide, reflecting a real-life intoxication scenario. Cytotoxicity was evaluated by the MTT assay and PQ intracellular concentrations were measured by gas chromatography–ion trap-mass spectrometry (GC–IT-MS). Also, the DOX modulatory effect on choline uptake transport system was assessed by measuring the uptake of [^{3}H]-choline.

The results show that DOX exerts protective effects against PQ cytotoxicity, preventing the intracellular accumulation of the herbicide. These protective effects were not completely prevented by the incubation with the UIC2 antibody, a specific P-gp inhibitor, suggesting the involvement of alternative protection mechanisms. In fact, DOX also efficiently inhibited the choline transport system that influences PQ cellular uptake.

In conclusion, in this cellular model, DOX effectively protects against PQ toxicity by inducing P-gp and through the interaction with the choline transporter, suggesting that compounds presenting this double feature of promoting the efflux and limiting the uptake of PQ could be used as effective antidotes to treat intoxications.

Abbreviations: ABCB1, ATP-binding cassette sub-family B member 1; BSA, bovine serum albumin; DMEM, Dulbecco's Modified Eagle's Medium; DOX, doxorubicin; EDTA, ethylenediamine tetraacetic acid; EPQ, ethylparaquat; FBS, fetal bovine serum; GC–IT-MS, gas chromatography–ion trap-mass spectrometry; HC-3, hemicholinium-3; HEPQ, hydrogenated ethylparaquat; HPQ, hydrogenated paraquat; MDR, multi-drug resistance phenomenon; MDR1, multi-drug resistance 1 gene; MTT, (4,5-dimethylthiazol-2-yl)-2,5-diphenyl tetrazolium bromide; NEAA, non-essential amino acids; PBS, phosphate buffered saline solution; P-gp, P-glycoprotein; PQ, paraquat; SPE, solid-phase extraction.

* Corresponding authors. Tel.: +351 220428596; fax: +351 226093390.
E-mail addresses: rsilva@ff.up.pt (R. Silva), helenacarmo@ff.up.pt (H. Carmo), v_vilasboas@yahoo.com (V. Vilas-Boas), pguedes@ff.up.pt (P.G.d. Pinho), ricardinis@med.up.pt (R.J. Dinis-Oliveira), felixdc@ff.up.pt (F. Carvalho), isabelsds@gmail.com (I. Silva), farmacol@icbas.up.pt (P. Correia-de-Sá), mlbastos@ff.up.pt (M.d.L. Bastos), remiao@ff.up.pt (F. Remião).

0378-4274/$ – see front matter © 2012 Elsevier Ireland Ltd. All rights reserved.
http://dx.doi.org/10.1016/j.toxlet.2012.11.028

1. Introduction

P-glycoprotein (P-gp; ABCB1) is an ATP-dependent efflux pump with broad substrate specificity. This protein belongs to the ATP-binding cassette (ABC) superfamily of transporters (Ambudkar et al., 1999; Chang, 2003; Gottesman et al., 2002; Silverman, 1999). Apart from its high expression in neoplasic cells, it is widely distributed in the apical surfaces of normal human epithelial tissues including the gastrointestinal tract, kidney, placenta, testes, and the blood–brain barrier, limiting the bioavailability of xenobiotics, including drugs, in these tissues (Ambudkar et al., 1999; Thiebaut et al., 1987). This important protein is recognized as a crucial defence mechanism, which is due to its cellular polarized expression, broad substrate specificity, and efflux capacity, resulting in decreased intracellular accumulation of xenobiotics (Dinis-Oliveira et al., 2006a; Hunter et al., 1993; Huynh-Delerme et al., 2005; Silva et al., 2011; Watanabe et al., 2005).

Caco-2 cells, derived from human colorectal adenocarcinoma, are a widely accepted and reliable in vitro model for predicting drug intestinal absorption and excretion in humans (Barta et al., 2008; Huynh-Delerme et al., 2005; Watanabe et al., 2005; Yamashita et al., 2000). These cells closely mimic the enterocytes of the small intestine (Barta et al., 2008) and express several transporters involved in drug absorption and excretion, including P-gp (Hidalgo and Jibin, 1996; Hunter et al., 1993; Shen et al., 2007; Watanabe et al., 2005). P-gp expression levels in Caco-2 cells are in good agreement with those of the normal human jejunum (Taipalensuu et al., 2001) and this efflux protein was already characterized as having an apical membrane localization in this intestinal cell line (Hunter et al., 1993). We have previously demonstrated that the P-gp substrate doxorubicin (DOX) strongly induced P-gp in the Caco-2 cell model, in a time- and concentration-dependent manner (Silva et al., 2011).

Paraquat (PQ) is involved in thousands of intoxications worldwide. No effective antidote has yet been found for this extremely toxic herbicide. Since PQ is known P-gp substrate, P-gp induction would be expected to protect the cells against the cytotoxic effects of this herbicide. In a real-life PQ intoxication scenario, for any P-gp inducer to be used as an effective antidote, it must exert its protective effects after PQ contact with the target tissues. Thus, the aim of the present study was to evaluate whether DOX could protect Caco-2 cells against PQ cytotoxicity 6 h after the cells had been exposed to PQ.

2. Materials and methods

2.1. Materials

Caco-2 cells were kindly provided by Rosário Monteiro from the Biochemistry Department, Faculty of Medicine, University of Porto, Portugal. Dulbecco's Modified Eagle's Medium (DMEM) with 4.5 g/L glucose and GlutMAX™, nonessential amino acids (NEAA), fetal bovine serum (FBS), 0.25% trypsin/1 mM EDTA, antibiotic (10,000 U/mL penicillin, 10,000 μg/mL streptomycin), fungizone (250 μg/mL amphotericin B) and human transferrin (4 mg/mL) were purchased from Gibco Laboratories (Lenexa, KS). AccuGENE® (1× PBS buffer) was purchased from Lonza Laboratories (Verviers, Belgium). Doxorubicin (DOX), paraquat (PQ), ethylparaquat (EPQ), sodium borohydride ($NaBH_4$), bovine serum albumin (BSA), hemicholinium-3 (HC-3), choline chloride and (4,5-dimethylthiazol-2-yl)-2,5-diphenyl tetrazolium bromide (MTT) were obtained from Sigma (St. Louis, MO, USA). Monoclonal anti-human P-glycoprotein UIC2 antibody (IOTest® CD243) used in the P-gp inhibition studies was purchased from Beckman Coulter, Inc. (Fullerton, USA). Bio-Rad DC protein assay kit was purchased from Bio-Rad (Hercules, CA). C18 cartridges (Bond Elut® C18) were purchased from Agilent (California, USA). Nitrogen (99.99% purity) and helium (99.99% purity) were obtained from Gasin (Portugal).

Radiolabeled [methyl-^{3}H] choline chloride (ethanol solution, 80.6 Ci mmol^{-1}) and scintillation cocktail (Insta-gel Plus) were obtained from Perkin Elmer (Boston, USA).

All the reagents used were of analytical grade or of the highest grade available.

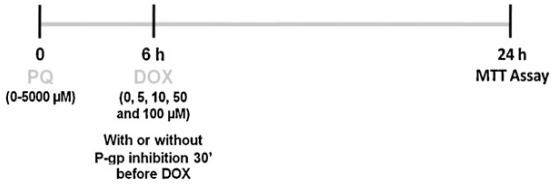

Fig. 1. Schematic representation of the experimental protocol developed for the evaluation of the protective effects against paraquat (PQ) cytotoxicity resulting from exposure of Caco-2 cells to doxorubicin (DOX) 6 h after the beginning of exposure to PQ.

2.2. Caco-2 cell culture

Caco-2 cells were routinely cultured in 75 cm^2 flasks using DMEM supplemented with 10% FBS, 1% NEAA, 1% antibiotic, 1% fungizone and 6 μg/mL transferrin. Cells were maintained in a 5% CO_2-95% air atmosphere at 37 °C and the medium was changed every 2 days. Cultures were passaged weekly by trypsinization (0.25% trypsin/1 mM EDTA). The cells used for all the experiments were taken between the 58th and 64th passages. In all experiments, the cells were seeded at a density of 60,000 cells/cm^2 and used 4 days after seeding when confluence was reached.

2.3. Paraquat cytotoxicity assays

Paraquat cytotoxicity was evaluated in Caco-2 cells by the MTT assay, with and without incubation with DOX, 6 h after PQ. Briefly, the cells were seeded onto 48-well plates to obtain confluent monolayers at the day of the experiment. After reaching confluence, the cells were exposed to five different PQ concentrations (100–5000 μM) in fresh cell culture medium. Six hours after the beginning of PQ exposure, DOX was added to obtain the final concentrations of 0, 10, 50 and 100 μM. This DOX concentration range was selected due to the previously noted absence of relevant cytotoxicity and significant P-gp induction (protein expression and transport activity) under these experimental conditions (Silva et al., 2011). Cytotoxicity was evaluated 24 h after PQ exposure (corresponding to an 18 h-incubation period with DOX). To confirm the involvement of P-gp in the DOX protective effects these incubations were repeated in the presence of a P-gp specific inhibitor (20 μL of the UIC2 antibody stock solution for 500,000 cells, according to the manufacturer instructions). In this assay, the protocol was similar to that described above but with previous P-gp inhibitor incubation for 30 min before DOX exposure. A schematic representation of this protocol is illustrated in Fig. 1.

For the MTT assay, the cell culture medium was removed and the cells were washed twice with PBS (pH 7.4), followed by the addition of fresh cell culture medium containing 0.5 mg/mL MTT and incubation at 37 °C in a humidified, 5% CO_2-95% air atmosphere for 1 h. After this incubation period, the cell culture medium was removed and the formed formazan crystals dissolved in 100% DMSO. The absorbance was measured at 550 nm in a multi-well plate reader (BioTek Instruments, Vermont, USA). The percent cell viability relative to that of the control cells (incubated without PQ) was used as the cytotoxicity measure.

2.4. Quantification of paraquat intracellular levels

2.4.1. Preparation of standard solutions

A PQ stock solution was prepared by dissolving an appropriate amount of compound in PBS in order to achieve a concentration of 5 mM. Working paraquat standard solutions were prepared through serial dilution of the stock standard solution with PBS in order to obtain a 0–500 μM calibration curve. A stock solution of the internal standard (ethylparaquat, EPQ) was prepared by dissolving an appropriate amount of the compound in PBS in order to achieve a concentration of 1 mg/mL. All stock solutions were stored at −80 °C.

2.4.2. Sample preparation

Caco-2 cells were seeded onto 48-well plates, at a density of 60,000 cells/cm^2 and incubated, after reaching confluence, with PQ (0–5000 μM) in cell culture medium. Incubation with 50 μM DOX was performed 6 h after PQ exposure, in the presence and absence of a P-gp specific inhibitor (UIC2 antibody), as previously described (Fig. 1). Twenty-four hours after PQ exposure (corresponding to an 18 h-incubation period with DOX), the cell culture medium was removed and the cells washed three times with PBS buffer (pH 7.4). The cells were then killed by freezing the cell monolayer at −80 °C with 500 μL distilled water. After homogenization, the cell lysates were centrifuged at 3000 × *g* 10 min 4 °C and the supernatant used for PQ extraction and quantification. The cell pellet was dissolved in NaOH 0.3 M and used for protein quantification.

2.4.3. Paraquat extraction

PQ extraction from samples was performed according to a previously validated method with slight modifications (Dinis-Oliveira et al., 2009; Moreira et al., 2012). Briefly, an aliquot of 450 μL of sample or standards, 1.5 mL of PBS (pH 7.4) and 20 μL of EPQ solution (100 μg/mL) were pipetted into a 15 mL glass tube with screw cap.

Table 1
EC50 (half-maximum-effect concentrations) and TOP (maximal effect) values of the paraquat concentration–response fitted curves, with (PQ + DOX) and without (PQ) exposure of Caco-2 cells to doxorubicin 6 h after PQ.

Doxorubicin concentration (μM)	0 (PQ)	5 (PQ + DOX5)	10 (PQ + DOX10)	50 (PQ + DOX50)	100 (PQ + DOX100)
EC50 (μM)	1244	1425	1307	458.6	368.8
TOP (maximal cell death, % control)	93.7	88.1	81.5	48.4	38.9
TOP *p* value (comparison between TOP values)	–	0.3363	**0.0428**	**<0.0001**	**<0.0001**
Curve *p* value (comparison between the fitted curves)	–	**<0.0001**	**<0.0001**	**<0.0001**	**<0.0001**

Concentration–response curves were fitted using least squares as the fitting method and the comparisons between PQ + DOX and control (PQ) curves were made using extra sum-of-squares *F* test. In all cases, *p* values <0.05 were considered statistically significant.

Ten milligrams of sodium borohydride ($NaBH_4$) were added to the solution in order to reduce PQ and the EPQ to their hydrogenated derivatives, respectively HPQ and HEPQ. This reduction reaction mixture was kept at 60 °C for 10 min. For solid-phase extraction (SPE), the C18 cartridge was preconditioned with 2 mL of methanol and 2 mL of phosphate buffer (pH 8.0). The sample solution was transferred to the C18 cartridge that was further washed with 2 mL of deionized water. The PQ and EPQ elution was then performed with 2 mL of methanol and the eluate was evaporated at room temperature under a gentle nitrogen stream. The residue was reconstituted in 100 μL of methanol and 1 μL was injected into the gas chromatography–ion trap mass spectrometry (GC–IT-MS) apparatus.

2.4.4. Instrumentation

GC–IT-MS analyses of PQ and EPQ were performed using a Varian CP-3800 gas chromatographer (USA) equipped with a VARIAN Saturn 4000 mass selective detector (USA) and a Saturn GC/MS workstation software version 6.8. A chromatographic column, VF-5 ms (30 m × 0.25 mm i.d. × 0.25 μm film thickness) from VARIAN, was used. The injector port was heated to 250 °C and was operated in splitless mode. The carrier gas was helium at a constant flow rate of 1.0 mL/min. The oven temperature was 80 °C (for 1 min), then increased 2 °C/min until 270 °C and held for 20 min. All mass spectra were acquired by electron impact (EI, 70 eV) in full scan mode. Ionization was maintained off during the first 2 min, to avoid solvent overloading. The ion-trap detector was set as follows: the transfer line, manifold and trap temperatures were 280, 50 and 180 °C, respectively. The mass range was 50–600 *m/z*, with a scan rate of 6 scan/s. The emission current was 50 μA, and the electron multiplier was set in relative mode to autotune procedure. The maximum ionization time was 25,000 μs, with an ionization storage level of 35 *m/z*. Chromatographic peak areas of PQ and EPQ were determined by the re-constructed FullScan chromatogram (FSC) using specific ions for each compound. A selected ion monitoring chromatogram (SIMC) was obtained. The ions selected for quantification were: *m/z* 96, 148, 192 for reduced—PQ and *m/z* 110, 162, 220 for reduced—EPQ.

2.5. Choline uptake study—inhibition by doxorubicin

Caco-2 cells were seeded onto 6-well plates at a density of 60,000 cells/cm^2. After reaching confluence, the cells were washed twice with uptake buffer (137 mmol/L NaCl, 5.4 mmol/L KCl, 2.8 mmol/L $CaCl_2$, 1.2 mmol/L $MgCl_2$, 10 mmol/L HEPES, pH 7.4) and incubated, at 37 °C for 20 min, with 0.5 μmol/L choline (0.005 μmol/L [^{3}H]-choline + 0.495 μmol/L unlabeled choline dissolved in uptake buffer) in the presence and absence of DOX (5, 10, 50 and 100 μM). The effect of hemicholinium-3 (HC-3), a known inhibitor of choline uptake, was also tested by incubating the cells at 37 °C for 20 min, with 0.5 μmol/L choline (0.005 μmol/L [^{3}H]-choline + 0.495 μmol/L unlabeled choline dissolved in uptake buffer) in the presence of 100 μM HC-3 and in the presence and absence of DOX (10 and 100 μM). The choline uptake was stopped by aspiration of the incubation buffer and washing the cells three times with ice-cold stop solution (137 mmol/L NaCl, 14 mmol/L Tris, pH 7.4). The cells were then lysed on ice for 20 min by adding 500 μL of 0.5% Triton-X-100 to each well, followed by centrifugation at 300 × *g*, 4 °C, for 15 min. Radioactivity was determined by adding 3.5 mL of scintillation cocktail to 300 μL of the supernatant and tritium outflow was evaluated by liquid scintillation spectrometry (TriCarb2900TR Perkin Elmer, Boston, USA). The cell pellet was dissolved in NaOH 0.3 M and used for protein quantification. The effects of doxorubicin and hemicholinium-3 in the choline uptake were expressed as percentage over control, after normalized to the protein content.

2.6. Protein quantification

The protein concentration was determined using the Bio-Rad DC protein assay kit, according to the manufacturer's instructions. Bovine serum albumin was used as protein standard.

2.7. Statistical analysis

All statistical calculations were performed with the GraphPad Prism version 5.00 for Windows (GraphPad Software, San Diego California, USA).

For the PQ cytotoxicity assay performed with and without DOX incubation 6 h after PQ and in the presence and absence of the P-gp inhibitor (UIC2 antibody), 4 independent experiments were performed. Concentration–response curves were fitted using least squares as the fitting method and the comparisons between curves (BOTTOM, TOP and LOG EC50) were made using the extra sum-of-squares *F* test. In all cases, *p* values lower than 0.05 were considered statistically significant.

For the intracellular PQ quantification assay, 3 independent experiments were performed and data obtained are expressed as mean ± SEM. Statistical comparison between groups was estimated using the parametric method of Two-way ANOVA on ranks followed by the Bonferroni's post hoc test. In all cases, *p* values lower than 0.05 were considered statistically significant.

Data obtained in the choline uptake assay are expressed as mean ± SD from 4 independent experiments. Normality of the data distribution was assessed by three different tests (KS normality test, D'Agostino & Pearson omnibus normality test and Shapiro–Wilk normality test). Statistical comparison between groups was estimated using the parametric method of One-way ANOVA on ranks followed by the Bonferroni's post hoc test. In all cases, *p* values lower than 0.05 were considered statistically significant.

3. Results

3.1. Doxorubicin protective effects against paraquat cytotoxicity

The concentration–response curves obtained with only paraquat (PQ) and with DOX incubation 6 h after PQ (PQ + DOX) show that significant differences exist between PQ and PQ + DOX curves in what concerns to the maximal cell death (Fig. 2). Since these curves present different maximal effects, the EC50 (i.e. the half-maximum-effect concentrations) could not be used to compare the curves. For this reason, the TOP values (maximal cell death effect) were used instead for the comparison between the different fitted curves.

As observed in Table 1, the overall comparison between the fitted curves (TOP, BOTTOM and EC50 values) revealed that the PQ cell death curve is significantly different from all the PQ + DOX curves ($p < 0.0001$). Additionally, significant differences were observed in the TOP values (representing the maximal effect of the fitted curves) of both PQ and PQ + DOX curves for 10, 50 and 100 μM DOX (Table 1). Moreover, besides the significant decreases in the TOP values, rightward shifts of the PQ concentration–response curves were observed for all the tested DOX concentrations (Fig. 2; Table 1). The observed decreases in the TOP values of the fitted curves were concentration-dependent, down to 88.1, 81.5, 48.4 and 38.9% maximal cell death, for PQ + DOX 5, PQ + DOX 10, PQ + DOX 50 and PQ + DOX 100 curves, respectively (Table 1).

To evaluate if the observed rightward shifts and TOP values decreases were due to increased P-gp expression and activity, the cells were incubated with a specific P-gp inhibitor (UIC2 antibody) 30 min before DOX (Fig. 1). Under P-gp inhibition the maximal cytotoxic effect increased for PQ (PQ + UIC2) when compared with PQ alone (Fig. 3), with significant differences in the fitted curves ($p < 0.0001$) and in the TOP values ($p = 0.0318$) (Table 2), confirming the involvement of P-gp in PQ efflux and cytotoxicity. Similarly, for all DOX concentrations tested, the increases in the TOP values of the fitted curves were also observed in the presence of the UIC2 antibody (PQ + DOX + UIC2) when compared to the curves obtained in the absence of the inhibitor (PQ + DOX) (Fig. 3). Additionally, it was possible to observe a leftward shift in the PQ + DOX + UIC2

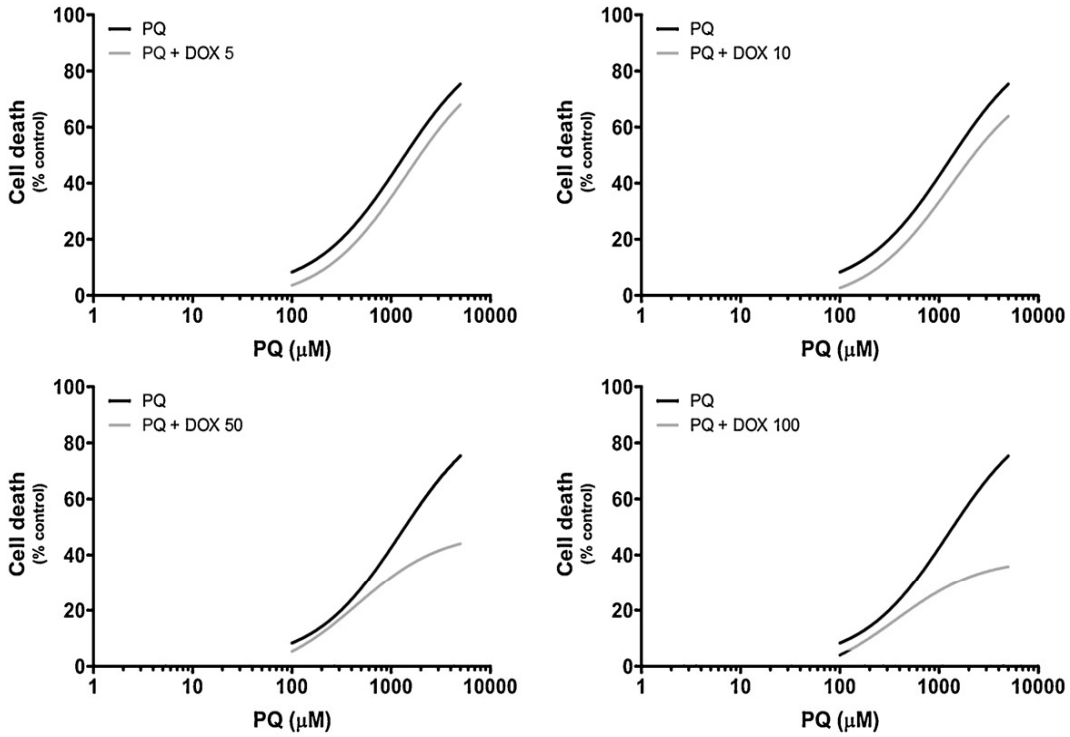

Fig. 2. Paraquat concentration–response (cell death) curves in the absence (PQ) or in the presence of 5, 10, 50 and 100 μM DOX (PQ + DOX) 6 h after the beginning of PQ exposure. Four independent experiments were performed (run in triplicates). Concentration–response curves were fitted using least squares as the fitting method and the comparisons between PQ + DOX and PQ curves (BOTTOM, TOP and LOG EC50) were made using the extra sum-of-squares *F* test. In all cases, *p* values <0.05 were considered statistically significant.

concentration–response curves when compared to the PQ + DOX curves (Fig. 3).

However, the comparison between the PQ + UIC2 and the PQ + DOX + UIC2 curves reveals that the DOX protective effects were not completely reverted in the presence of the P-gp specific inhibitor given the rightward shift observed for all the PQ + DOX + UIC2 curves (Fig. 3) and the concentration-dependent decrease in the TOP value (Table 3) for the two highest DOX concentrations tested (50 and 100 μM). In fact, in the absence of DOX (PQ + UIC2) it was observed a TOP value of ~100% whereas in the

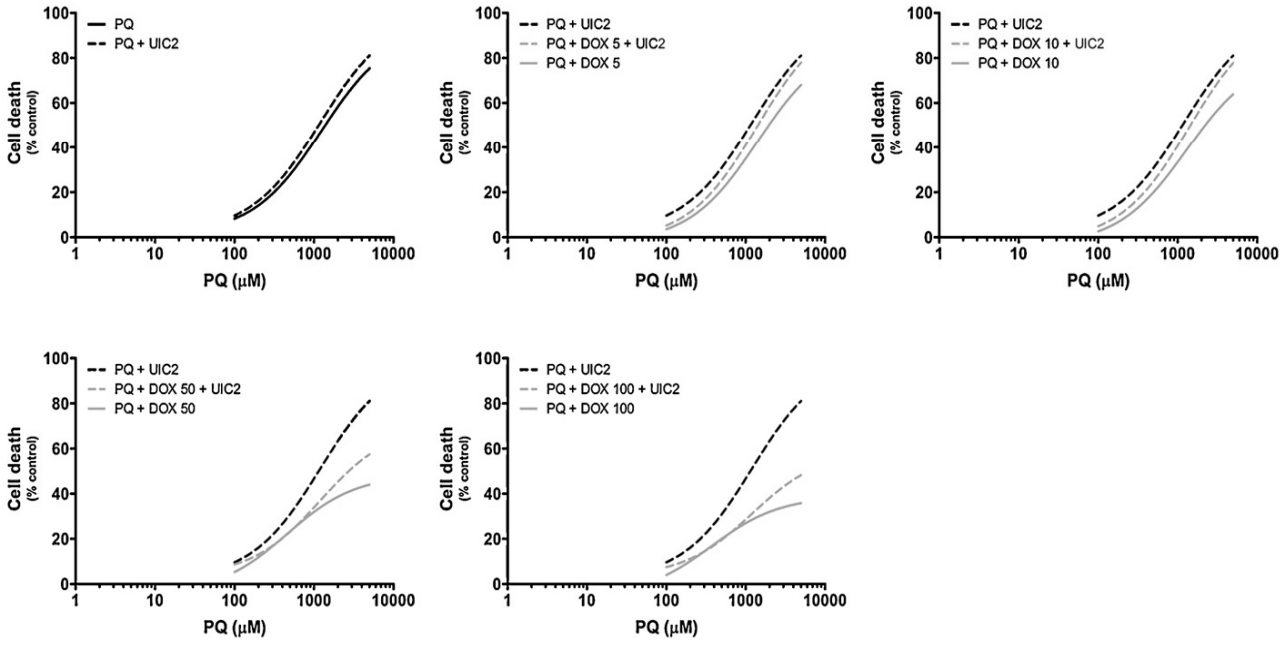

Fig. 3. Paraquat concentration–response (cell death) curves in the presence of a specific p-glycoprotein inhibitor (UIC2 antibody) with (PQ + DOX + UIC2) or without (PQ + UIC2) exposure to doxorubicin (5, 10, 50 and 100 μM) 6 h after the beginning of PQ exposure. The PQ and PQ + DOX cell death curves were included for comparison. Four independent experiments were performed (run in triplicates). Concentration–response curves were fitted using least squares as the fitting method and the comparisons between PQ + DOX + UIC2 and control (PQ + UIC2) curves (BOTTOM, TOP and LOG EC50) were made using the extra sum-of-squares *F* test. In all cases, *p* values <0.05 were considered statistically significant.

Table 2
EC50 (half-maximum-effect concentrations) and TOP (maximal effect) values of the paraquat concentration–response fitted curves, in the absence (PQ) and presence (PQ + UIC2) of a specific *p*-glycoprotein inhibitor (UIC2 antibody).

	PQ	PQ + UIC2
EC50 (μM)	1244	1199
TOP (maximal cell death, % control)	88.1	~100
TOP *p* value (comparison between TOP values)	–	**0.0318**
Curve *p* value (comparison between the fitted curves)	–	**<0.0001**

Concentration–response curves were fitted using least squares as the fitting method and the comparisons between PQ and PQ + UIC2 curves were made using extra sum-of-squares *F* test. In all cases, *p* values <0.05 were considered statistically significant.

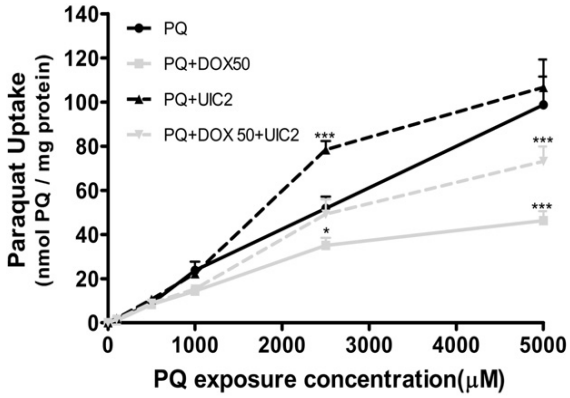

Fig. 4. Paraquat intracellular levels in Caco-2 cells in the presence (PQ + DOX) and in the absence (PQ) of 50 μM DOX 6 h after continuous exposure to PQ, and in the presence (PQ + UIC2 and PQ + DOX + UIC2) and in the absence (PQ and PQ + DOX) of a specific p-glycoprotein inhibitor (UIC2 antibody). Results are presented as mean ± SEM from 3 independent experiments (triplicates were performed in each experiment). Statistical comparisons were made using Two-way analysis of variance followed by the Bonferroni's Multiple Comparison post hoc test (*$p < 0.05$, **$p < 0.01$, ***$p < 0.0001$ vs. control).

presence of 50 and 100 μM DOX (PQ + DOX 50 + UIC2 and PQ + DOX 100 + UIC2) the TOP value decreased to 70.4 and 59.1%, respectively (Table 3).

3.2. Intracellular paraquat accumulation

To corroborate the hypothesis that the significant decreases in PQ toxicity observed in the presence of DOX were due to decreased cellular accumulation of the herbicide, the intracellular levels of PQ were quantified by GC–IT-MS. For that purpose, Caco-2 cells were exposed to 0, 100, 500, 1000, 2500 and 5000 μM PQ, followed by 50 μM DOX 6 h after PQ, in the presence and absence of the P-gp specific inhibitor (Fig. 1). As shown in Fig. 4, significant differences in the accumulation of PQ were obtained, especially for the two highest PQ concentrations (2500 and 5000 μM). In fact, at both these PQ concentrations and in the presence of 50 μM DOX, significant decreases in the intracellular levels of PQ were observed (35.03 and 46.25 nmol PQ/mg protein for PQ + DOX 50 versus 51.81 and 97.71 nmol PQ/mg protein for PQ only, respectively). The P-gp inhibitor, UIC2 antibody, partially attenuated the protective effect of 50 μM DOX on intracellular PQ accumulation, i.e. the UIC2 antibody increased PQ accumulation in cells treated with DOX from 49.19 to 73.13 nmol PQ/mg protein. The accumulation of PQ inside the cells when DOX was added together with the UIC2 antibody was still smaller than that observed with the UIC2 antibody alone (78.41 and 106.59 nmol PQ/mg protein for PQ exposure concentration of 2500 and 5000 μM, respectively). These findings could only partially explain why we observed an incomplete reversion of DOX protective effects on PQ cytotoxicity with the P-gp specific inhibitor (Fig. 3) and raised questions on whether DOX could also interfere with other mechanisms responsible for PQ cellular uptake.

3.3. Choline uptake

To determine whether DOX could also inhibit the uptake of choline in Caco-2 cells, we measured the uptake of 0.5 mol/L choline using a mixture containing 0.005 mol/L [^{3}H]-choline plus 0.495 mol/L unlabeled choline, which was incubated in the absence and in the presence of 0–100 μM DOX. The effect of 100 μM hemicholinium-3 (HC-3), a known competitive inhibitor of both sodium-dependent and sodium-independent choline transport, was also tested to compare the magnitude of its inhibitory effect with that produced by DOX. A 20-min time point was selected based on previous studies suggesting that it is within the linear range of choline uptake in this cell line (Kamath et al., 2003). The results represented in Fig. 5 show that DOX significantly inhibits choline uptake in a concentration-dependent manner. In fact, incubation with 5, 10, 50 and 100 μM DOX, significantly reduced intracellular ^{3}H-choline to 42.9, 31.3, 19.9 and 16.9% of the control value, respectively. On the other hand, HC-3 (100 μM) significantly reduced ^{3}H-choline uptake by the cells to 24.0% of the control value. Interestingly, DOX (50 and 100 μM) was more effective than HC-3 (100 μM) in inhibiting choline uptake in Caco-2 cells (Fig. 5). Moreover, incubation with DOX (50 and 100 μM) together with HC-3 (100 μM) further enhanced the inhibitory effect of HC-3 on ^{3}H-choline uptake to 17.4 and 12.0%, of the control value, respectively (Fig. 5).

4. Discussion

The present data demonstrate that DOX is protective against PQ cytotoxicity when the drug is applied 6 h after PQ exposure of Caco-2 cells, meaning that it could function as an effective antidote against PQ intoxications by restraining the intestinal absorption of the herbicide and by favoring its efflux. Since DOX is a potent inducer of de novo synthesis of P-gp (Silva et al., 2011), we hypothesized that this transport system could be involved in the protective effect of DOX against PQ poisoning. P-glycoprotein was the first ATP-dependent system implicated in multi-drug resistance (MDR) phenomena (Juliano and Ling, 1976) and has been extensively characterized ever since (Ambudkar et al., 1999; Chang, 2003; Gottesman et al., 2002; Hoffmann and Kroemer, 2004; Silverman,

Table 3
EC50 (half-maximum-effect concentrations) and TOP (maximal effect) values of the paraquat concentration–response fitted curves, in the presence of a specific p-glycoprotein inhibitor (UIC2 antibody) with (PQ + DOX + UIC2) and without (PQ + UIC2) exposure to doxorubicin (5, 10, 50 and 100 μM) 6 h after PQ.

Doxorubicin concentration (μM)	0 (PQ + UIC2)	5 (PQ + DOX5 + UIC2)	10 (PQ + DOX10 + UIC2)	50 (PQ + DOX50 + UIC2)	100 (PQ + DOX100 + UIC2)
EC50 (μM)	1199	1383	1396	1203	1207
TOP (maximal cell death, % control)	~100	~100	~100	70.4	59.1
TOP *p* value (comparison between TOP values)	–	0.9997	0.9927	**0.0043**	**0.0018**
Curve *p* value (comparison between the fitted curves)	–	**0.0496**	**0.0214**	**<0.0001**	**<0.0001**

Concentration–response curves were fitted using least squares as the fitting method and the comparisons between PQ + DOX + UIC2 and control (PQ + UIC2) curves were made using extra sum-of-squares *F* test. In all cases, *p* values <0.05 were considered statistically significant.

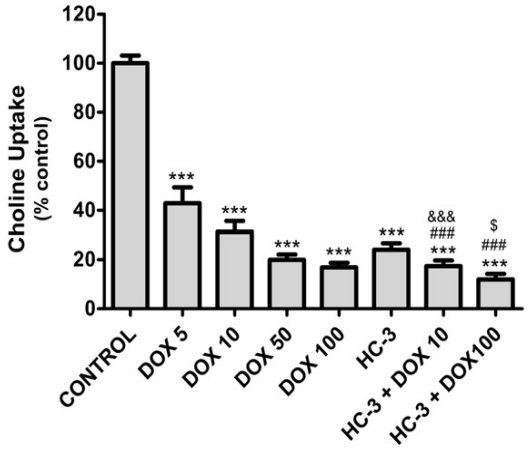

Fig. 5. Effect of doxorubicin and hemicholinium-3 on choline uptake in Caco-2 cells. Uptake of [^{3}H]-choline (0.5 mol/L) was measured at 20 min in the absence (control) and presence of doxorubicin (DOX 5, 10. 50 and 100 μM), hemicholinium (HC-3 100 μM) or both compounds (HC-3 + DOX 10 and HC-3 + DOX 100). Results are presented as mean ± SD from 4 independent experiments (triplicates were performed in each experiment). Statistical comparisons were made using One-way analysis of variance followed by the Bonferroni's Multiple Comparison post hoc test ($^{*}p < 0.05$, $^{**}p < 0.01$, $^{***}p < 0.0001$ vs. control; $^{\#}p < 0.05$, $^{\#\#}p < 0.01$, $^{\#\#\#}p < 0.0001$ vs. HC-3; $^{\&}p < 0.05$, $^{\&\&}p < 0.01$, $^{\&\&\&}p < 0.0001$ vs. DOX 10; $^{\$}p < 0.05$, $^{\$\$}p < 0.01$ $^{\$\$\$}p < 0.0001$ vs. DOX 100).

1999). P-gp plays an important role in normal absorption, distribution, and excretion of many commonly used pharmacological agents and xenobiotics, regulating the cellular and tissue levels of these agents (Ambudkar et al., 1999).

We have previously shown that doxorubicin, a known P-gp inducer, was effective in increasing both P-gp expression and activity in Caco-2 cells in a concentration and time-dependent manner (Silva et al., 2011). In fact we have previously reported that as soon as 6 h after 5–100 μM doxorubicin incubation, P-gp levels increased in Caco-2 cells by 147–365% of the control levels. After 24 h these observed P-gp increases ranged from 237 to 645% for this doxorubicin concentration range (Silva et al., 2011). Those remarkable increases in P-gp expression and transport activity resulted in a significant protection against PQ toxicity, which was completely reverted in the presence of a P-gp specific inhibitor, proving that P-gp induction may be an extremely important cellular protection tool against toxicity of xenobiotics (Silva et al., 2011). PQ was used in this study as a model of a xenobiotic that is able to penetrate Caco-2 cells, which is also a well-known P-gp substrate (Silva et al., 2011). Noteworthy, the rationale for this novel therapeutic approach for PQ poisonings, involving prevention of intestinal absorption of the toxic has been already pursuit concerning the induction of de novo synthesis of P-gp in vivo with dexamethasone (Dinis-Oliveira et al., 2006a, 2006b).

Surprisingly, it was observed that exposure of Caco-2 cells to DOX, 6 h after PQ, resulted in a more pronounced protection against PQ cytotoxicity when compared to the results obtained with the protocol using pre-exposure to DOX before PQ incubation, resulting in huge decreases in the observed maximal cell death (Fig. 2). In the previous study it was possible to observe significant decreases in PQ cytotoxicity with DOX pre-incubation, resulting in rightward shifts of PQ + DOX concentration–response curves and, consequently, to significant increases in EC50 values. However, the protective effects mediated by DOX were not concentration-dependent and no significant differences were observed in the maximal cell death values (Silva et al., 2011). In the present study, significant rightward shifts of the PQ + DOX concentration–response curves were also observed but, most importantly, these changes were accompanied by remarkable decreases in maximal cell death values for all DOX concentrations tested (Fig. 2; Table 1). Moreover, this study provided information indicating that the preventive effect of DOX against PQ cytotoxicity is concentration-dependent (Table 1). Concentrations of DOX above 50 μM reduced maximal cell death by more than 50% of control values in the absence of the drug. Involvement of P-gp in the toxicity induced by PQ was confirmed by the leftward shift of the PQ concentration–response curve in the presence of the P-gp inhibitor, the UIC2 antibody (Fig. 3).

In contrast to the results obtained by pre-incubating the Caco-2 cells with DOX before PQ exposure, the protective effects of DOX applied 6 h after the PQ insult, were not completely prevented by the UIC2 antibody (Fig. 3). Comparison between the PQ + DOX and PQ + DOX + UIC2 curves reveals that the reversion of PQ cytotoxicity was partially due to P-gp inhibition, since PQ toxicity increased in the presence of UIC2 (leftward shift and increased maximal cell death of the PQ + DOX + UIC2 curves). However, the comparison of the PQ + UIC2 and the PQ + DOX + UIC2 curves reveals that, even in the presence of the P-gp inhibitor, DOX is still able to protect the Caco-2 cells from PQ toxicity, as can be seen by the rightward shifts of the PQ + DOX + UIC2 curves and by the lower values of maximal cell death (Fig. 3). Quantification of PQ intracellular levels corroborated these results demonstrating that DOX (50 μM) reduced intracellular PQ accumulation. The inhibitory effect of DOX was more obvious upon increasing the concentrations of PQ above 2500 μM, and was observed regardless of the presence of the P-gp specific inhibitor (Fig. 4). Thus, these results suggest that mechanisms other than P-gp induction seem to be involved in DOX protection against PQ cytotoxicity.

In spite of being responsible for thousands of deaths due to accidental or intentional ingestion of PQ, there is still little information on the gastrointestinal absorption of the herbicide in the small intestine (Nagao et al., 1993). The mechanism of PQ intestinal absorption was studied by Nagao et al. (1993) who suggested that this quaternary ammonium compound is absorbed through a specialized mechanism associated with the carrier-mediated transport system for choline on the brush-border membrane (Nagao et al., 1993). In that study, rat intestinal loops and brush-border membrane vesicles were used as the study model. The results indicated that PQ absorption was greater than expected and could not be explained by simple diffusion based on the pH-partition hypothesis, suggesting the involvement of a specialized transport mechanism (Nagao et al., 1993). Additionally, early stage-PQ uptake was saturable and significantly inhibited by structurally related quaternary ammonium compounds, including choline and tetramethylammonium. Thus, according to the authors, PQ is partly absorbed via this carrier-mediated transport system for choline and inhibitors of this transport system could ameliorate PQ poisonings after oral ingestion of the herbicide (Nagao et al., 1993).

Moreover, this carrier-mediated transport system for choline was already characterized in Caco-2 cells (Crowe et al., 2002; Kamath et al., 2003). Data indicate that this transport system is active in Caco-2 cells, is both pH- and Ca^{2+}-dependent, and has unique characteristics when compared to traditional choline transport models (Crowe et al., 2002). For instance, accumulation of choline in Caco-2 cells is independent of the inwardly directed Na^+ gradient and is temperature-dependent, saturable, and substrate-specific (Kamath et al., 2003). Choline uptake in Caco-2 cells was significantly inhibited by excess of choline and by HC-3, a structural analog of choline which is a known competitive inhibitor of both Na^+-dependent and Na^+-independent choline transporters in many tissues (Kamath et al., 2003). Moreover, two typical P-gp substrates, 100 μM daunomycin and 100 μM verapamil, both inhibited choline transport by significantly decreasing choline accumulation inside cells by 85 and 51%, respectively (Kamath et al., 2003). Taking these findings into consideration it was hypothesized that DOX, a typical

P-gp substrate structurally similar to daunomycin, could protect against PQ toxicity through the inhibition of the carrier-mediated transport system for choline in addition to significantly increasing PQ efflux through P-gp induction (Silva et al., 2011). In fact, it was observed that DOX significantly inhibited choline transport in Caco-2 cells in a concentration-dependent manner (Fig. 5). Noteworthy, concentrations of DOX above 50 μM were more potent than HC-3 regarding choline uptake inhibition (Fig. 5).

Our data clearly indicate that the protective effects of DOX against PQ cytotoxicity result from a concerted action of the drug via two distinct mechanisms, namely choline transport inhibition and increased P-gp expression/activity in Caco-2 cells, which might result in decreased intracellular PQ accumulation and, thereby reduced toxicity (Fig. 4).

To the best of our knowledge there is currently no in vivo evidence of such a protective effect for DOX against PQ. However, previous in vivo experiments have already demonstrated that dexamethasone, another P-gp inducer, significantly increased the survival rate of the exposed animals by reducing the pulmonary toxicity of the herbicide and by increasing its fecal excretion (Dinis-Oliveira et al., 2006b). A similar effect would be expected to occur with DOX since the present in vitro data clearly demonstrates that the protective effects of DOX are partially explained through the P-gp induction caused by the drug.

An important feature of the present findings is the effectiveness of the DOX protective effects 6 h after PQ contact with the cells. This experimental setting would reflect a real-life intoxication scenario. In fact, an effective antidote must exert its protective effects in many cases well after the intoxicant contacts with the target tissues. Therefore, this schedule for DOX incubation (6 h after PQ exposure) was chosen taking into account the estimated average arrival time of the patient to hospital, after PQ intoxication. Also, the peak plasma concentrations of PQ are expected to occur 1–6 h after oral ingestion (Dinis-Oliveira et al., 2008).

The concentrations of PQ used in the present study are within those that could be expected to be attained in vivo in an intoxication scenario. The reported cases of PQ intoxications in humans available in the literature show wide variation in the post-mortem blood, urine and tissue concentrations of the herbicide (Dinis-Oliveira et al., 2009; Moreira et al., 2012). In most of these cases 25–50 mL of the PQ formulation is typically ingested (Dinis-Oliveira et al., 2009). Most of the commercially available formulations contain 20 g/100 mL of the herbicide which would translate into an orally ingested dose of approximately 5–10 g that is absorbed up to a maximum of 5% of the ingested dose (Roberts, 2011). Under such intoxication scenarios blood concentrations up to 0.1 g/L (0.4 mM) could be easily achieved. Also, the extensive corrosive injury to the gastrointestinal tract may increase the amount absorbed (Dinis-Oliveira et al., 2008). Additionally, PQ concentrates in the target organs such as the lung, reaching concentrations up to 10 times higher than the blood (Dinis-Oliveira et al., 2008). Moreover, these concentrations found at autopsy are probably lower than the peak concentrations that are expected to occur after intake, especially in the cases where the victims are submitted to emergency-care treatments to control the intoxications.

In conclusion, effective antidotal pathways can be achieved by reducing intestinal absorption and by promoting the cellular efflux of deleterious xenobiotics. The study and development of compounds that have the ability of both inhibiting the xenobiotics entrance and increasing their excretion are promising new sources of antidotal pathways to be explored. According to our data, doxorubicin demonstrated this double and unique feature in what concerns PQ poisonings. P-gp substrates may efficiently inhibit choline uptake through specific or nonspecific interactions with the choline transporter but the mechanism underlying this interaction is presently unknown (Kamath et al., 2003). Thus, the study of these mechanisms is of enormous importance and should be considered as an important tool against PQ toxicity.

Conflict of interest statement

The authors declare that there are no conflicts of interest.

Acknowledgments

This work was supported by the Fundação para a Ciência e Tecnologia (FCT)-project PTDC/SAU-OSM/101437/2008 – QREN initiative with EU/FEDER funded through COMPETE – Operational Programme for Competitiveness Factors.

This work was supported by the Portuguese Foundation for Science and Technology (FCT) through grant PEst-C/EQB/LA0006/2011.

Renata Silva acknowledges FCT for her PhD grant [SFRH/BD/29559/2006]. Ricardo Dinis-Oliveira acknowledges FCT for his pos-Doc grant [SFRH/BPD/36865/2007].

The work performed at ICBAS-UP was supported by FCT within the framework of Strategic Projects for Scientific Research Units of R&D (project PEst-OE/SAU/UI0215/2011).

Caco-2 cells were kindly provided by Rosário Monteiro from the Biochemistry Department, Faculty of Medicine, University of Porto, Portugal.

References

Ambudkar, S.V., Dey, S., Hrycyna, C.A., Ramachandra, M., Pastan, I., Gottesman, M.M., 1999. Biochemical, cellular, and pharmacological aspects of the multidrug transporter. Annual Review of Pharmacology and Toxicology 39, 361–398.

Barta, C.A., Sachs-Barrable, K., Feng, F., Wasan, K.M., 2008. Effects of monoglycerides on p-glycoprotein: modulation of the activity and expression in caco-2 cell monolayers. Molecular Pharmacology 5, 863–875.

Chang, G., 2003. Multidrug resistance ABC transporters. FEBS Letters 555, 102–105.

Crowe, A.P., Lockman, P.R., Abbruscato, T.J., Allen, D.D., 2002. Novel choline transport characteristics in Caco-2 cells. Drug Development and Industrial Pharmacy 28, 773–781.

Dinis-Oliveira, R.J., de Pinho, P.G., Santos, L., Teixeira, H., Magalhaes, T., Santos, A., de Lourdes Bastos, M., Remiao, F., Duarte, J.A., Carvalho, F., 2009. Postmortem analyses unveil the poor efficacy of decontamination, anti-inflammatory and immunosuppressive therapies in paraquat human intoxications. PLoS ONE 4, e7149.

Dinis-Oliveira, R.J., Duarte, J.A., Remiao, F., Sanchez-Navarro, A., Bastos, M.L., Carvalho, F., 2006a. Single high dose dexamethasone treatment decreases the pathological score and increases the survival rate of paraquat-intoxicated rats. Toxicology 227, 73–85.

Dinis-Oliveira, R.J., Duarte, J.A., Sanchez-Navarro, A., Remiao, F., Bastos, M.L., Carvalho, F., 2008. Paraquat poisonings: mechanisms of lung toxicity, clinical features, and treatment. Critical Reviews in Toxicology 38, 13–71.

Dinis-Oliveira, R.J., Remiao, F., Duarte, J.A., Ferreira, R., Sanchez Navarro, A., Bastos, M.L., Carvalho, F., 2006b. P-glycoprotein induction: an antidotal pathway for paraquat-induced lung toxicity. Free Radical Biology and Medicine 41, 1213–1224.

Gottesman, M.M., Fojo, T., Bates, S.E., 2002. Multidrug resistance in cancer: role of ATP-dependent transporters. Nature Reviews Cancer 2, 48–58.

Hidalgo, I.J., Jibin, L., 1996. Carrier-mediated transport and efflux mechanisms in Caco-2 cells. Advanced Drug Delivery Reviews 22, 53–66.

Hoffmann, U., Kroemer, H.K., 2004. The ABC transporters MDR1 and MRP2: multiple functions in disposition of xenobiotics and drug resistance. Drug Metabolism Reviews 36, 669–701.

Hunter, J., Jepson, M.A., Tsuruo, T., Simmons, N.L., Hirst, B.H., 1993. Functional expression of P-glycoprotein in apical membranes of human intestinal Caco-2 cells. Kinetics of vinblastine secretion and interaction with modulators. The Journal of Biological Chemistry 268, 14991–14997.

Huynh-Delerme, C., Huet, H., Noel, L., Frigieri, A., Kolf-Clauw, M., 2005. Increased functional expression of P-glycoprotein in Caco-2 TC7 cells exposed long-term to cadmium. Toxicology in Vitro 19, 439–447.

Juliano, R.L., Ling, V., 1976. A surface glycoprotein modulating drug permeability in Chinese hamster ovary cell mutants. Biochimica et Biophysica Acta 455, 152–162.

Kamath, A.V., Darling, I.M., Morris, M.E., 2003. Choline uptake in human intestinal Caco-2 cells is carrier-mediated. Journal of Nutrition 133, 2607–2611.

Moreira, P.N., de Pinho, P.G., Baltazar, M.T., Bastos, M.L., Carvalho, F., Dinis-Oliveira, R.J., 2012. Quantification of paraquat in postmortem samples by gas chromatography–ion trap mass spectrometry and review of the literature. Biomedical Chromatography 26, 338–349.

Nagao, M., Saitoh, H., Zhang, W.D., Iseki, K., Yamada, Y., Takatori, T., Miyazaki, K., 1993. Transport characteristics of paraquat across rat intestinal brush-border membrane. Archives of Toxicology 67, 262–267.

Roberts, D.M., 2011. Herbicides. In: Nelson, L.S., Lewin, N.A., Howland, M.A., Hoffman, R.S., Goldfrank, L.R., Flomenbaum, N.E. (Eds.), Goldfrank's Toxicologic Emergencies. , ninth ed. McGraw-Hill Companies, Inc., New York, pp. 1494–1515.

Shen, S., He, Y., Zeng, S., 2007. Stereoselective regulation of MDR1 expression in Caco-2 cells by cetirizine enantiomers. Chirality 19, 485–490.

Silva, R., Carmo, H., Dinis-Oliveira, R., Cordeiro-da-Silva, A., Lima, S.C., Carvalho, F., de Lourdes Bastos, M., Remiao, F., 2011. In vitro study of P-glycoprotein induction as an antidotal pathway to prevent cytotoxicity in Caco-2 cells. Archives of Toxicology 85, 315–326.

Silverman, J.A., 1999. Multidrug-resistance transporters. Pharmaceutical Biotechnology 12, 353–386.

Taipalensuu, J., Tornblom, H., Lindberg, G., Einarsson, C., Sjoqvist, F., Melhus, H., Garberg, P., Sjostrom, B., Lundgren, B., Artursson, P., 2001. Correlation of gene expression of ten drug efflux proteins of the ATP-binding cassette transporter family in normal human jejunum and in human intestinal epithelial Caco-2 cell monolayers. Journal of Pharmacology and Experimental Therapeutics 299, 164–170.

Thiebaut, F., Tsuruo, T., Hamada, H., Gottesman, M.M., Pastan, I., Willingham, M.C., 1987. Cellular localization of the multidrug-resistance gene product P-glycoprotein in normal human tissues. Proceedings of the National Academy of Sciences of the United States of America 84, 7735–7738.

Watanabe, T., Onuki, R., Yamashita, S., Taira, K., Sugiyama, Y., 2005. Construction of a functional transporter analysis system using MDR1 knockdown Caco-2 cells. Pharmaceutical Research 22, 1287–1293.

Yamashita, S., Furubayashi, T., Kataoka, M., Sakane, T., Sezaki, H., Tokuda, H., 2000. Optimized conditions for prediction of intestinal drug permeability using Caco-2 cells. European Journal of Pharmaceutical Sciences 10, 195–204.

III.4. MANUSCRIPT III

Colchicine effect on P-glycoprotein expression and activity: in silico and in vitro studies

Submitted for publication

TITLE

Colchicine effect on P-glycoprotein expression and activity: *in silico* and *in vitro* studies

AUTHORS

Renata Silva[a*], Helena Carmo[a], Vânia Vilas-Boas[a], Daniel José Barbosa[a], Andreia Palmeira[b], Emília Sousa[b], Félix Carvalho[a], Maria de Lourdes Bastos[a] and Fernando Remião[a*]

AFFILIATIONS

[a]REQUI*M*TE, Laboratório de Toxicologia, Departamento de Ciências Biológicas, Faculdade de Farmácia, Universidade do Porto, Rua de Jorge Viterbo Ferreira, 228, 4050-313, Porto, Portugal.

[b]Centro de Química Medicinal (CEQUIMED-UP), Laboratório de Química Orgânica e Farmacêutica, Departamento de Ciências Químicas, Faculdade de Farmácia, Universidade do Porto, Rua Jorge Viterbo Ferreira 228, 4050-313, Porto, Portugal

*CORRESPONDING AUTHORS

Renata Silva (e-mail: rsilva@ff.up.pt) and Fernando Remião (e-mail: remiao@ff.up.pt)
REQUI*M*TE, Laboratório de Toxicologia, Departamento de Ciências Biológicas, Faculdade de Farmácia, Universidade do Porto, Rua de Jorge Viterbo Ferreira, 228, 4050-313, Porto, Portugal.
Phone: 00351220428596
Fax: 00351226093390

RUNNING TITLE

Colchicine effect on P-glycoprotein expression and activity

ABSTRACT

Colchicine is a P-glycoprotein (P-gp) substrate that induces its expression, thus increasing the risk for unexpected pharmacokinetic interactions with this drug. Because increased P-gp expression does not always correlate with increased activity of this efflux pump, we evaluated the changes in both P-gp expression and activity induced by colchicine using an *in vitro* model. Caco-2 cells were incubated with 0.1–100 μM colchicine up to 96h. Cytotoxicity was evaluated by the MTT and LDH leakage assays, P-gp expression and activity were evaluated by flow cytometry and P-gp ATPase activity was measured in MDR1-Sf9 membrane vesicles. Furthermore, colchicine fitting in P-gp induction and competitive inhibition pharmacophore hypothesis, and docking studies evaluating the interaction between colchicine and P-gp drug binding pocket were tested *in silico*.

Significant cytotoxicity was noted after 48h. At 24h a significant increase in P-gp expression was observed, which was not accompanied by an increase in transport activity. Moreover, colchicine significantly increased P-gp ATPase activity, demonstrating to be actively transported by the pump. New pharmacophores were constructed to predict P-gp modulatory activity. Colchicine fitted both the P-gp induction and competitive inhibition models. *In silico*, colchicine was predicted to bind to the P-gp drug-binding pocket suggesting a competitive mechanism of transport.

These results show that colchicine induced P-gp expression in Caco-2 cells but the activity of the protein remained unchanged, highlighting the need to simultaneously evaluate P-gp expression and activity. With the newly constructed pharmacophores, new drugs can be initially screened *in silico* to predict such potential pharmacokinetic interactions.

KEYWORDS

P-glycoprotein induction; P-glycoprotein transport activity; colchicine; Caco-2 cells; *In silico*; ATPase activity.

GRAPHICAL ABSTRACT

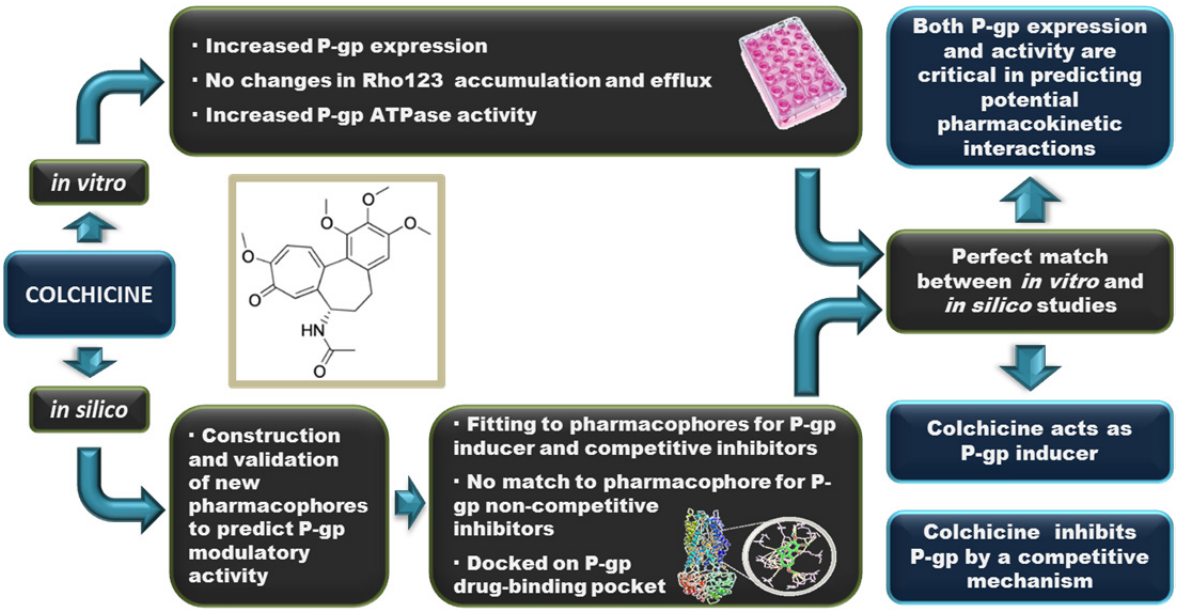

ABBREVIATIONS

COL – Colchicine
DMEM – Dulbecco's modified Eagle's medium
EDTA – Ethylenediamine tetraacetic acid
FBS – Fetal bovine serum
FITC – Fluorescein isothiocyanate
GeoMean – Geometric mean of fluorescence intensity
Hb – Hydrogen bond
IA – Inhibited rhodamine 123 Accumulation
IAE – Inhibited rhodamine 123 accumulation followed by efflux in the absence of P-gp inhibitor
IAEI – Inhibited rhodamine 123 accumulation followed by efflux in the presence of P-gp inhibitor
i.p. – Intraperitoneal
MTT – (4,5-Dimethylthiazol-2-yl)-2,5-diphenyl tetrazolium bromide
MDR – Multidrug resistance
NA – Normal rhodamine 123 accumulation
NEAA – Non-essential amino acids
NSAIDs – Nonsteroidal anti-inflammatory drugs
PBS – Phosphate buffered saline solution
P-gp – P-glycoprotein
RHO 123 – Rhodamine 123
RMS – Root-mean-square

1. INTRODUCTION

Colchicine is an alkaloid derived from the plant of the family *Colchicum autumnale* and plant extracts containing colchicine have been used to treat gout for more than 2000 years, and pseudogout and familial Mediterranean fever for several decades (Ben-Chetrit and Levy 1991; Famaey 1988; Niel and Scherrmann 2006). However, it has a narrow therapeutic index, with no clear-cut distinction between nontoxic, toxic, and lethal doses (Finkelstein et al. 2010). Moreover, colchicine's toxicity stems from its mechanism of action as this alkaloid binds to the intracellular protein tubulin causing a disruption of the microtubular network resulting in impaired protein assembly in the Golgi apparatus, decreased endocytosis and exocytosis, altered cell shape, depressed cellular motility, and arrest of mitosis (Finkelstein et al. 2010).

Colchicine is also a known P-glycoprotein (P-gp) substrate (Ambudkar et al. 1999; Decleves et al. 1998; El Hafny et al. 1997; Niel and Scherrmann 2006). P-gp is an efflux pump encoded by the human MDR1 gene being the most extensively studied ATP-binding cassette transporter due to its role in modulating drug pharmacokinetics. This important efflux pump was initially implicated in the multidrug resistance (MDR) phenomenon observed in hamster ovary cultured cells (Juliano and Ling 1976), and was later found to be also present in normal tissues including the brain, liver, kidney, placenta, testis and intestine (Thiebaut et al. 1987). In fact, in these tissues, it is involved in the absorption, distribution and excretion of drugs and other xenobiotics (Lin and Yamazaki 2003a; Lin and Yamazaki 2003b) and, consequently, was already implicated in pharmacokinetic drug-drug interactions. Therefore, when other P-gp modulators are prescribed in combination with colchicine, the changes in P-gp activity may lead to either intracellular accumulation of colchicine, and thereby to increased pharmacological or toxic effects, or to a reduction in colchicine intracellular levels and decreased effects (Niel and Scherrmann 2006). Thus, the interaction due to concomitant use of P-gp inhibitors and colchicine was already described and therefore, the concurrent use of these compounds with colchicine is contraindicated in patients with hepatic or renal impairment (Finkelstein et al. 2010).

Moreover, colchicine was reported to have P-gp inducing properties, both *in vitro* and *in vivo* (Decleves et al. 1998; Licht et al. 2000; Vollrath et al. 1994). In fact, colchicine was shown to increase the *mdr* mRNA levels in rat liver *in vivo,* as early as 3 h after a single injection (2 mg per kg, i.p.), peaking after 24 h (Vollrath et al. 1994). Additionally, Declèves *et. al* (1998) also demonstrated that colchicine (25 nM) was able to significantly increase P-gp expression in the promyelocytic HL-60 cell line after 24 of exposure (Decleves et al. 1998). Therefore, colchicine mediated increase in P-gp expression may

result in an increased excretion of the alkaloid, as well as increased excretion of other P-gp substrates prescribed in combination, resulting in a decreased therapeutic efficacy. However, the ability of colchicine in modulating the activity of this important efflux transporter was not evaluated in these previous studies. For an optimized evaluation of possible pharmacokinetic interactions mediated by P-gp inducers, both P-gp expression and activity should be simultaneously evaluated, as P-gp activity may not be necessarily correlated with the protein content. In fact, we have previously shown that doxorubicin, a potent P-gp inducer, causes remarkable increases in P-gp expression levels that are not accompanied by proportional increases in P-gp transport activity (Silva et al. 2011). Similarly, using the same experimental model, Takara *et. al* showed that NSAIDs greatly increased P-gp expression without concomitant increase in pump activity (Takara et al. 2009).

Thus, the aim of the present work was to evaluate if colchicine is able to simultaneously invoke changes in P-gp expression and activity, since protein expression may be greatly increased without a corresponding increase in its transport activity (Silva et al. 2011; Takara et al. 2009).

In this study, *in vitro* studies were performed using the caco-2 cell line. The Caco-2 cells, derived from human colorectal adenocarcinoma, are widely accepted as an *in vitro* model for predicting drug intestinal absorption and excretion in humans (Balimane et al. 2006; Barta et al. 2008; Biganzoli et al. 1999; Huynh-Delerme et al. 2005; Watanabe et al. 2005; Yamashita et al. 2000). These cells express P-gp at levels that are in good agreement with those of the normal human jejunum (Taipalensuu et al. 2001) and are suitable for the screening of specific P-gp inducers (Silva et al. 2011; Silva et al. 2013). To better understand colchicine mode of action and its possible interaction with P-gp, *in silico* studies were also performed. For that purpose, pharmacophore models for P-gp induction and inhibition were constructed based on known inducers and inhibitors, and they were used as a query for colchicine mapping, and docking studies were performed in order to further investigate the potential mechanism of action of this alkaloid.

2. EXPERIMENTAL SECTION

2.1. Materials

Colchicine, rhodamine 123 (RHO 123), cyclosporine, (4,5-dimethylthiazol-2-yl)-2,5-diphenyl tetrazolium bromide (MTT), triton X-100, β-nicotinamide adenine dinucleotide reduced form (β-NADH), pyruvic acid, adenosine-5′-triphosphate (ATP), d-luciferin sodium salt and luciferase were obtained from Sigma (St. Louis, MO, USA). Reagents used in cell culture, including Dulbecco's modified Eagle's medium (DMEM) with 4.5 g/L glucose and GlutaMAX™, nonessential amino acids (NEAA), heat inactivated fetal bovine serum (FBS), 0.25% trypsin/1 mM EDTA, antibiotic (10000 U/mL penicillin, 10000 µg/mL streptomycin), fungizone (250 µg/mL amphotericin B) and human transferrin (4 mg/mL) were purchased from Gibco Laboratories (Lenexa, KS, USA). AccuGENE® (1x PBS buffer) was purchased from Lonza Laboratories (Verviers, Belgium). P-glycoprotein monoclonal antibody (clone UIC2) conjugated with fluorescein isothiocyanate (FITC) was purchased from Abcam (Cambridge, United Kingdom). IgG2a (negative mAb control to UIC2) conjugated with FITC was obtained from ImmunoTools GmbH (Friesoythe, Germany). Flow cytometry reagents (BD FacsFlow™ and Facs Clean™) were purchased from Becton, Dickinson and Company (San Jose, CA, USA). MDR1 Predeasy ATPase assay kit was purchased from Solvo Biotechnology (Szeged, Hungary). All the reagents used were of analytical grade or of the highest grade available.

2.2. Caco-2 cell culture

Caco-2 cells were routinely cultured in 75 cm^2 flasks using DMEM medium supplemented with 10% FBS, 1% NEAA, 1% antibiotic, 1% fungizone and 6 µg/mL transferrin. Cells were maintained in a 5% CO_2–95% air atmosphere at 37ºC and the medium was changed every 2 days. Cultures were passaged weekly by trypsinization (0.25% trypsin/1 mM EDTA). The cells used for all the experiments were taken between the 58^{th} and 62^{th} passages.

2.3. Colchicine cytotoxicity assays

Colchicine (0 – 100 µM) cytotoxicity was evaluated at different time points (6, 24, 48, 72 and 96 h) by the 4,5-dimethylthiazol-2-yl)-2,5-diphenyl tetrazolium bromide (MTT) reduction assay and by the lactate dehydrogenase (LDH) leakage assay.

2.3.1. MTT reduction assay

Colchicine cytotoxicity was evaluated by the MTT reduction assay, in which mitochondrial activity is used to estimate cell viability. For that purpose, the cells were

seeded onto 96-well plates, at a density of 60,000 cells/cm^2, to obtain confluent monolayers at the experimental day. The cells were then exposed to colchicine (0 – 100 μM) in fresh cell culture medium for 6, 24, 48, 72 and 96 h. At each selected time point, the cell culture medium was removed, and new fresh cell culture medium containing 0.5 mg/mL MTT was added, followed by incubation at 37°C in a humidified, 5% CO_2-95% air atmosphere for 1 h. After this incubation period, the cell culture medium was removed and the formed formazan crystals dissolved in 100% DMSO. The absorbance was measured at 550 nm in a multi-well plate reader (PowerWave X, Bio-Tek Instruments, Vermont, USA). The percentage cell viability relative to that of the control cells was used as the cytotoxicity measure.

2.3.2. LDH leakage assay

This assay is based on the measurement of LDH activity in the extracellular medium and was performed as previously described (Pontes et al. 2008). The loss of intracellular LDH and its release into the cell culture medium is an indicator of irreversible cell death due to cell membrane damage. The cells were seeded onto 48-well plates, at a density of 60,000 cells/cm^2. After reaching confluence, the cells were exposed to colchicine (0 – 100 μM) in fresh cell culture medium for 6, 24 and 48 h. At each time-point, 50 μL of cell culture medium was removed for the extracellular LDH measurement. The LDH activity was determined by following the rate of oxidation of NADH, measured at 340 nm and results are expressed as percentage of control values.

2.4. Evaluation of P-glycoprotein expression

For the *in vitro* evaluation of P-gp expression, the cells were seeded onto 24-well plates, at a density of 60,000 cells/cm^2, to obtain confluent monolayers at experimental day. On the day of the experiment, the cells were exposed to colchicine (0 – 100 μM) in fresh cell culture medium for 24 h (given the cytotoxicity data obtained, P-gp expression and transport activity was only evaluated after 24 h of exposure). After the incubation period, the cells were washed twice with PBS and harvested by trypsinization (0.25% trypsin/1mM EDTA) to obtain a cell suspension. The cells were then centrifuged (300 *g* for 10 min) and resuspended in PBS buffer (pH 7.4) containing 10% FBS and P-gp antibody [UIC2] conjugated with FITC. The antibody dilution used in this experiment was applied according to the manufacturer's instructions for flow cytometry. Mouse IgG2a_FITC was used as an isotype-matched negative control to estimate non-specific binding of the FITC-labelled anti-P-glycoprotein antibody [UIC2]. The conformational epitope that is recognized by UIC2 corresponds to a transient conformational state present during

catalytic cycle for substrate transport (Mechetner et al. 1997). Depending on the cell type, some P-gp substrates have been shown to increase UIC2 reactivity. However, in several cell lines, colchicine (tested at concentrations up to 1.25 mM) failed to produce such an interaction (Druley et al. 2001; Mechetner et al. 1997). Moreover, the incubation with the UIC2 antibody occurs always in the absence of colchicine since the media is removed, and the cells are washed twice prior to the trypsinization. Therefore, increases in fluorescence intensity should only reflect increased cell surface P-gp expression. The cells were incubated with either IgG2a_FITC or UIC2 antibodies for 30 min at 37°C in the dark. After this incubation period, the cells were washed twice with PBS buffer (pH 7.4) containing 10% FBS, centrifuged (300 *g* for 10 min), resuspended in ice-cold PBS and kept on ice until flow cytometry analysis. Fluorescence measurements of isolated cells were performed with a flow cytometer (FACSCalibur, Becton-Dickinson Biosciences). The green fluorescence of FITC-UIC2 antibody was measured by a 530 ± 15 nm band-pass filter (FL1). Acquisition of data for 10,000 cells was gated to include viable cells on the basis of their forward and side light scatters and the propidium iodide (4 µg/mL) incorporation (propidium iodide interlaces with a nucleic acid helix with a resultant increase in fluorescence intensity emission at 615 nm). Logarithmic fluorescence intensity was recorded and displayed as a single parameter histogram. The geometric mean of fluorescence intensity (GeoMean) for 10,000 cells was the parameter used for comparison (calculated as percentage of control). Non labelled cells (with or without colchicine) were analysed in each experiment by a 530 ± 15 nm band-pass filter (FL1) in order to detect a possible contribution from cells autofluorescence to the analysed fluorescence signals.

2.5. Evaluation of P-glycoprotein transport activity

The P-gp transport activity was evaluated by flow cytometry using 1 µM RHO 123 as a P-gp fluorescent substrate. P-gp transport activity was evaluated through the analysis of RHO 123 accumulation and RHO 123 efflux.

2.5.1. RHO 123 accumulation assay

Caco-2 cells were seeded onto 12-well plates, at a density of 60,000 cells/cm^2, to obtain confluent monolayers at the experimental day. After reaching confluence, the cells were exposed to colchicine (0 – 100 µM) in fresh cell culture medium for 24 h. After the incubation period, the cells were washed twice with PBS and harvested by trypsinization (0.25% trypsin /1mM EDTA) to obtain a cellular suspension. The cells were then submitted to a RHO 123 accumulation assay as previously described with minor

modifications (Vilas-Boas et al. 2013). Briefly, the cell suspension was divided into 2 aliquots to be submitted to the following procedures:

a) Normal rhodamine accumulation (NA): the cells were centrifuged (300 *g* for 10 min), resuspended in PBS buffer (pH 7.4) containing 1 μM RHO123, and incubated at 37ºC for 30 min in the absence of the P-gp inhibitor (cyclosporine A). After the incubation period the cells were washed twice with ice-cold PBS with 10% FBS, centrifuged (300 *g* for 10 min) at 4°C and kept on ice until flow cytometry analysis;

b) Inhibited rhodamine accumulation (IA): the cells were centrifuged (300 *g* for 10 min), suspended in PBS buffer (pH 7.4) containing 1 μM RHO 123 and the P-gp inhibitor cyclosporine A (10 μM), and incubated at 37ºC for 30 min. After the accumulation of the fluorescent substrate, the cells were washed twice with ice-cold PBS with 10% FBS, centrifuged (300 *g* for 10 min) at 4°C and kept on ice until flow cytometry analysis.

No cytotoxic effects were observed for RHO 123 and cyclosporine at these concentrations after 30 min of incubation. Fluorescence measurements of isolated cells were performed as described in section 2.4 (Evaluation of P-gp expression). The green intracellular fluorescence of RHO 123 was measured by a 530 ± 15 nm band-pass filter (FL1). The results were calculated according to the ratio defined in Equation 1 and expressed as percentage of control values. A higher ratio results from a smaller GeoMean NA which is a consequence of a higher P-gp activity as the dye is being pumped out of the cells during the accumulation phase.

$$RHO\ 123\ accumulation = \frac{GeoMean\ inhibited\ rhodamine\ accumulation\ (IA)}{GeoMean\ \ normal\ rhodamine\ accumulation\ (NA)}$$

Equation 1: Rhodamine 123 accumulation.

Positive control for P-gp inhibition was performed in each independent experiment using 10 μM cyclosporine A (Figure S2A, supporting information).

2.5.2. RHO 123 efflux assay

Caco-2 cells were seeded onto 12-well plates, at a density of 60,000 cells/cm^2, to obtain confluent monolayers at the experimental day. The cells were then exposed to colchicine (0 – 100 μM) in fresh cell culture medium for 24 h. After the incubation period, the cells were washed twice with PBS and harvested by trypsinization (0.25% trypsin /1mM EDTA) to obtain a cell suspension. In this assay, the evaluation of P-gp transport activity consisted of two phases, (i) an inhibited accumulation phase, in which P-gp activity

was inhibited with 10 μM cyclosporine A, in order to accumulate the substrate inside the cells (performed as described in section 2.5.1 - RHO 123 accumulation assay), and (ii) an efflux phase where the energy-dependent P-gp function was re-established by removing the P-gp inhibitor (cyclosporine) and adding an energy source (DMEM supplemented with 4.5 g/mol glucose). For that purpose, after the inhibited accumulation phase, the cells were washed twice with ice-cold PBS with 10% FBS, centrifuged (300 *g* for 10 min) at 4°C, and divided into two aliquots. The first aliquot was kept on ice until analysis by flow cytometry and corresponds to the cells submitted only to an IA phase. The second aliquot was submitted to an efflux phase performed under normal conditions (inhibited rhodamine accumulation followed by rhodamine efflux in the absence of P-gp inhibitor –IAE). For the efflux phase the cells were suspended in DMEM medium containing 4.5 g/L glucose and incubated for 45 min at 37°C. After this efflux period, the cells were washed twice with ice-cold PBS with 10% FBS and suspended in ice-cold PBS immediately before analysis. The fluorescence measurements of isolated cells were performed as described in section 2.4 (Evaluation of P-gp expression). The green intracellular fluorescence of RHO 123 was measured by a 530 ± 15 nm band-pass filter (FL1). The percentage of RHO 123 that was pumped out of the cells during the efflux phase was calculated according to Equation 2 and the results expressed as percentage of control values. When P-gp activity increases, the amount of RHO 123 effluxed from the cells will be higher and accompanied by a decrease in the fluorescence intensity due to the corresponding decrease in intracellular RHO 123 (decrease in GeoMean IAE).

$$\%\ pumped\ RHO\ 123 = \frac{GeoMean\ accumulated\ RHO\ 123(IA) - GeoMean\ remaining\ RHO\ 123\ (IAE)}{GeoMean\ accumulated\ RHO\ 123\ (IA)}\ X\ 100$$

Equation 2: Percentage of RHO 123 pumped during the efflux phase.

Positive control for P-gp inhibition was performed in each independent experiment using 10 μM cyclosporine A (Figure S2B, supporting information).

2.6. Evaluation of P-glycoprotein ATPase activity

P-gp pumps its substrates out of the cell using ATP hydrolysis as an energy source. ATP hydrolysis yields inorganic phosphate (Pi), which may be detected by a simple colorimetric reaction. P-gp ATPase activity was evaluated using the MDR1 Predeasy ATPase assay kit according to the manufacturer's instructions. Briefly, MDR1-Sf9 membrane vesicles (4 μg/well) were incubated in 50 μL ATPase assay buffer with 2 mM ATP and colchicine (1, 10 and 100 μM) for 10 min at 37 °C using two distinct protocols:

a) Activation study: incubation of colchicine (1, 10 and 100 μM) with or without 1.2 mM sodium orthovanadate (Na_3VO_4)
b) Inhibition study: incubation of colchicine (1, 10 and 100 μM) simultaneously with 40 μM verapamil (a known P-gp substrate used in this assay as the reference P-gp activator) and with or without 1.2 mM Na_3VO_4 incubation.

Controls without colchicine and with a control P-gp inhibitor (40 μM cyclosporine A) were also performed. The reaction was stopped by adding 100 μL of developer solution to each well, followed by 100 μL of blocker solution and an additional 30 min incubation at 37 ºC. The absorbance was measured at 630 nm, in a multi-well plate reader (PowerWave X, Bio-Tek Instruments), reflecting the amount of inorganic phosphate (Pi) liberated by the transporter which is proportional to its ATPase activity.

The MDR1-Sf9 membrane vesicles contain other ATPases besides P-gp. As P-gp is effectively inhibited by Na_3VO_4, P-gp ATPase activity was measured as the vanadate sensitive portion of the total ATPase activity. Thus, ATPase activities were always determined as the difference of Pi liberation measured with and without incubation with 1.2 mM Na_3VO_4 (i.e., vanadate-sensitive ATPase activity) and expressed as nmol Pi liberated/mg protein/min. Results are presented as mean ± SD from three independent experiments.

In the activation test, vanadate-sensitive ATPase activity in the absence of colchicine is referred to as the basal vanadate-sensitive ATPase activity. In the inhibition test, membrane vesicles exposed only to verapamil are referred to as fully activated membranes and the corresponding activity as the maximal vanadate-sensitive ATPase activity (ATPase activity of fully activated membranes). Cyclosporine A (40 μM) was used in the present test as the positive control for the inhibition studies and the corresponding activity referred to as inhibited ATPase activity.

2.7. Statistical analysis

All statistical calculations were performed with the GraphPad Prism version 5.00 for Windows (GraphPad Software, San Diego California, USA). Normality of the data distribution was assessed by three different tests (KS normality test, D'Agostino & Pearson omnibus normality test and Shapiro-Wilk normality test). Statistical comparison between groups was estimated using the nonparametric method of Kruskal–Wallis [one-way analysis of variance (ANOVA) on ranks] followed by Dunn's post hoc test. In all cases, *p* values lower than 0.05 were considered significant. Data obtained from the colchicine cytotoxicity and P-gp expression assays are expressed as mean ± SD from 4 independent experiments (each experiment was performed in triplicate). The results

obtained in the P-gp transport activity assays and in the P-gp ATPase assay are expressed as mean ± SD from 3 independent experiments (each experiment was performed in triplicate).

2.8. Pharmacophores for P-gp modulation

2.8.1. Pharmacophore for P-gp inducers

Thirty-four known P-gp inducers were collected from the literature (Table S1, supporting information). These molecules were drawn and subject to energy minimization using HyperChem version 8.0. The semi-empirical AM1 (Austin Model 1) method with the Polak-Ribière algorithm was employed for molecular minimization. As those compounds have distinct and non-overlapping scaffolds, prior to building a pharmacophore for P-gp induction, a ligand clustering analysis was performed on the thirty-four known P-gp inducers (Scheme 1A). Clustering was based on the root-mean-square (RMS) deviation of descriptor properties and Tanimoto distance for fingerprints (Accelrys 2.1, San diego, CA, USA). The output clusters composed of more than 2 molecules were used on the following pharmacophore construction. Common feature pharmacophore models were created from a set of 4 to 8 known P-gp inducers (Table S1, supporting information) used as training set. HipHop module of Catalyst (Accelrys 2.1, San Diego, CA, USA) was employed to generate common feature pharmacophores among a set of active known P-gp inducers. A maximum of 250 conformers were saved, within an energy window of 20 kcal/mol above the global minimum, using the “best” quality generation type. Concerning the hypothesis generation methodology, hydrogen bond (Hb)-acceptors and donors, hydrophobic groups, positive ionizable groups, and aromatic rings were used. The “maximum features” value was set to 10 and the “minimum features” value was set to 1. The “minimum interfeature distance” was set to 2.97Å. The “maximum omitted features” value was set to 0, and default settings were used for the other options. Validation of the pharmacophores was performed by alignment of that pharmacophore with a test set of 4 known inducers: amprenavir (Huang et al. 2001), nelfinavir (Huang et al. 2001), puromycin (Male 2009), and yohimbine (Bhat et al. 1995). Catalyst identified the compounds that map to the pharmacophore, and optionally aligns the ligands to the query. “All conformations” parameter was set, and the “best” quality generation type was used.

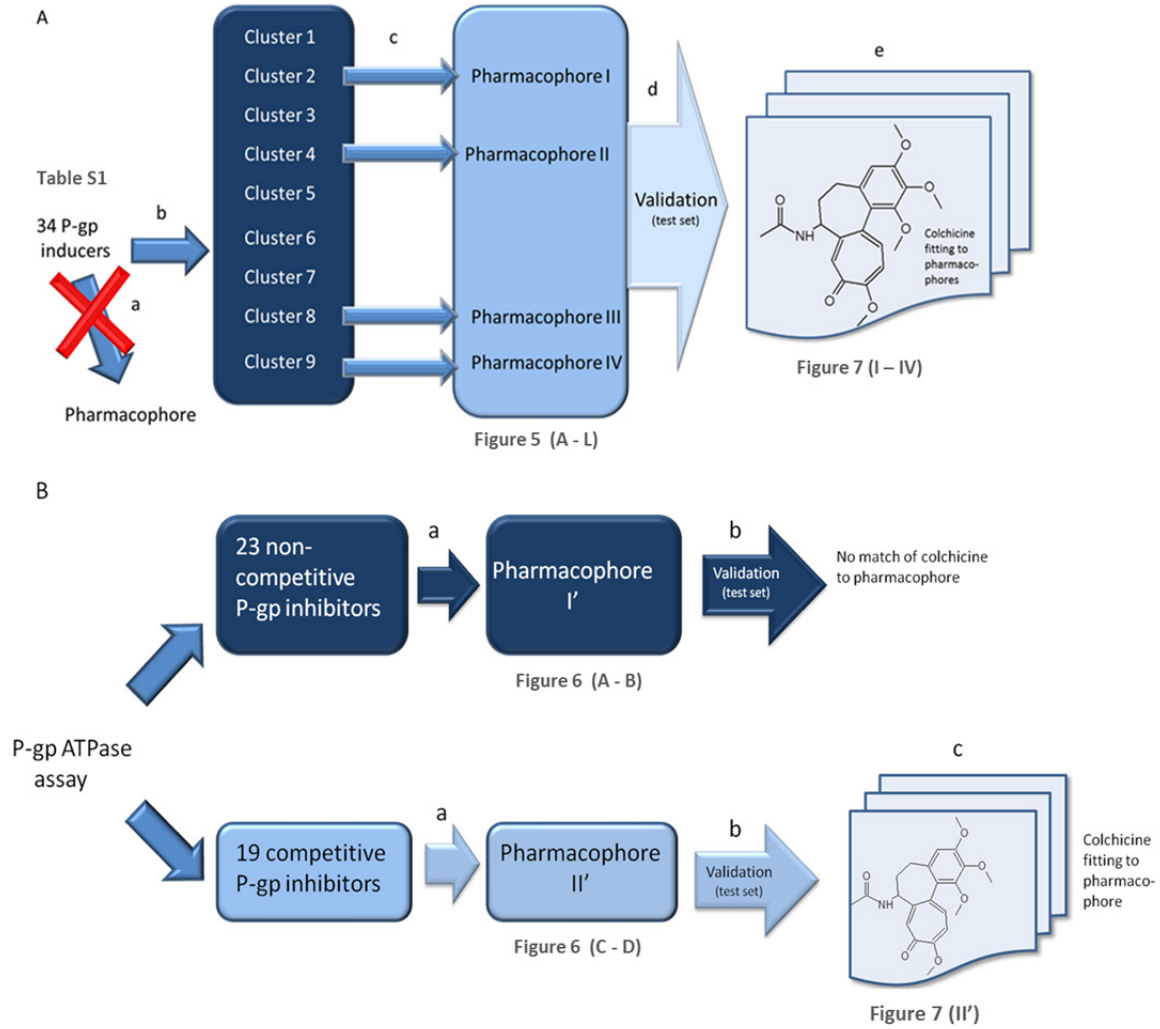

Scheme 1. (A) P-gp inducers ligand-based study. A common feature pharmacophore using 34 already described P-gp inducers (a) was not feasible due to structural diversity. A clustering analysis was performed (b) and clusters containing more than 2 molecules (c) were selected for pharmacophore construction by superimposition and alignment of ligands. A validation was performed using a test set of known inducers (d). Colchicine, that induced P-gp expression in the biochemical screening, was fit to the pharmacophores (e).
(B) P-gp inhibitors ligand-based study. A pharmacophore for P-gp competitive and noncompetitive inhibition was developed based on *in vitro* data previously published by our group (a), followed by adequate validation using test sets of known P-gp inhibitors (b). Colchicine was fit only to pharmacophore for competitive P-gp inhibitors (c).

2.8.2. Pharmacophore for competitive and noncompetitive P-gp inhibitors

Two 3D-pharmacophore models were created using HypoGen module of Catalyst program (Kurogi and Guner 2001; Patel et al. 2002) according to the results obtained in the ATPase assay for twenty three noncompetitive and for nineteen competitive inhibitors, both newly synthetized thioxanthonic derivatives and commercial drugs previously described by our group (Scheme 1B) (Palmeira et al. 2011; Palmeira et al. 2012c). For each molecule, the number of conformers generated using the 'best' functionality for each

inhibitor was limited to a maximum number of 255 (with an energy range of 20 kJ/mol). Ten hypotheses were generated using these conformers for the twenty three or nineteen inhibitors and the % values of luminescence related to ATPase activity. The feature groups selected were Hb-donor and -acceptor, hydrophobic, positive and negative ionizable, and remaining default parameters. After assessing all ten hypotheses generated, the lowest energy-cost hypothesis was considered the best, because it possessed features representative of all the hypotheses. The generated HypoGen models were evaluated in terms of cost functions and statistical parameters, which were calculated by HypoGen module during hypothesis generation. Validation of the best pharmacophore for each activity was performed using test set composed of eleven known P-gp inhibitors and analyzing the capacity of those compounds to fit the pharmacophores.

2.8.3. Mapping of pharmacophore onto colchicine

The mapping of pharmacophores onto colchicine was performed using the “Best Fit” method in catalyst. During the flexible fitting process, conformations on colchicine were calculated within the 20 kcal/mol energy threshold. Fitting was evaluated by the analysis of the fit score.

2.9. Docking of colchicine onto P-gp

Docking simulations between drug binding pocket formed by the transmembrane domain interfaces of a P-gp model previously described (Palmeira et al. 2012c) and colchicine were performed in AutoDock Vina (Scripps Research Institute, USA). AutoDock Vina considered the target conformation as a rigid unit while colchicine was allowed to be flexible and adaptable to the target. Vina searched for the lowest binding affinity conformations and returned nine different conformations for colchicine. AutoDock Vina was run using an exhaustiveness of 8 and a grid box with the dimensions 37.0, 30.0, 40.0, engulfing the channel formed by the transmembrane domains. Conformations and interactions were visualized using PyMOL version 1.3.

3. RESULTS

3.1. Colchicine cytotoxicity assays

Colchicine cytotoxicity was evaluated to establish the concentration range and time of exposure that would not cause significant cell death. Figure S1 (Supporting information) illustrates the cytotoxic effects of 0-100 μM colchicine in Caco-2 cells at different time points (6, 24, 48, 72 and 96 h) as evaluated by the MTT reduction assay. Colchicine exposure resulted in a concentration-dependent cytotoxicity that was significant after 48 h of incubation and increased over time. Up to a period of 24 h of incubation no significant effect on mitochondrial function occurred at any of the tested colchicine concentrations. The LDH leakage assay, which assesses cell membrane integrity, was also performed and provided similar results (data not shown). Therefore, colchicine effect on P-gp expression and activity was evaluated 24 h after exposure.

3.2. P-glycoprotein expression

The effect of colchicine on P-gp expression in Caco-2 cells was evaluated by flow cytometry as previously described, using a P-gp monoclonal antibody [UIC2] conjugated with FITC (Silva et al. 2011). Non-specific binding of the FITC-labelled anti-P-glycoprotein antibody [UIC2] was not observed, as estimated by the isotype-matched negative control. The obtained results are represented in Figure 1 and it is possible to observe that colchicine significantly increased P-gp expression in a concentration-dependent manner. In fact, at 0.5, 1, 5, 10, 50 and 100 μM colchicine, P-gp expression significantly increased by 129, 135, 145, 150, 154 and 183%, respectively. At 0.1 μM colchicine, no significant increase was observed in P-gp expression.

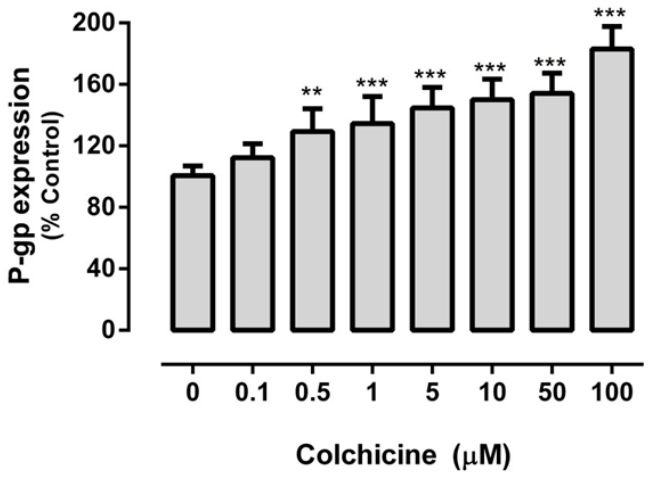

Figure 1. P-glycoprotein expression levels in Caco-2 cells exposed to colchicine (COL) (0 – 100 μM) for 24 h. Results are presented as mean ± SD from 4 independent experiments performed in triplicate. Statistical comparisons were made using the Kruskal-Wallis test followed by the Dunn's Multiple Comparison post hoc test [**p<0.01; ***p<0.001 concentration *vs*. control (0 μM)].

3.3. P-glycoprotein transport activity

The evaluation of P-gp transport activity was also determined by flow cytometry using 1 μM RHO 123 as a P-gp fluorescent substrate. For that purpose, both RHO 123 accumulation and efflux were quantified. In the RHO 123 accumulation assay, the obtained results, calculated using Equation 1, are represented in Figure 2. As observed, colchicine did not significantly increase P-gp activity at any of the tested concentrations.

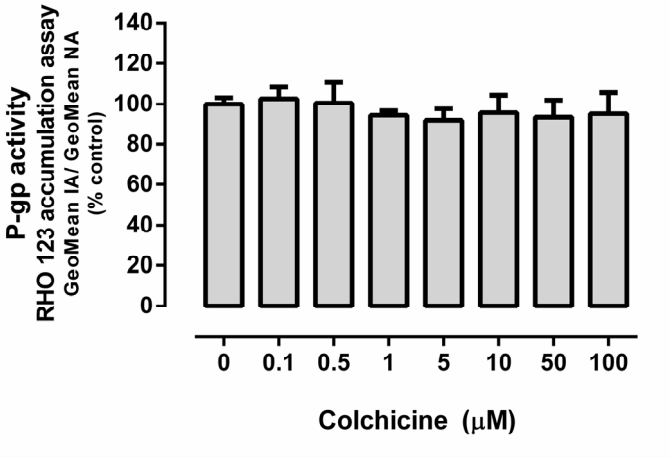

Figure 2. P-glycoprotein activity evaluated by the RHO 123 accumulation assay in Caco-2 cells exposed to colchicine (COL) (0 – 100 μM) for 24 h. Results are presented as mean ± SD from 3 independent experiments performed in triplicate. Statistical comparisons were made using the Kruskal-Wallis test followed by the Dunn's Multiple Comparison post hoc test.

Rhodamine 123 efflux was also tested to evaluate P-gp transport activity. The results are represented in Figure 3, in which the percentage of RHO-123 effluxed from the cells was calculated using Equation 2 and expressed as percentage over control. The obtained results corroborated the results obtained in the RHO 123 accumulation assay, since no significant differences were obtained for all the tested colchicine concentrations.

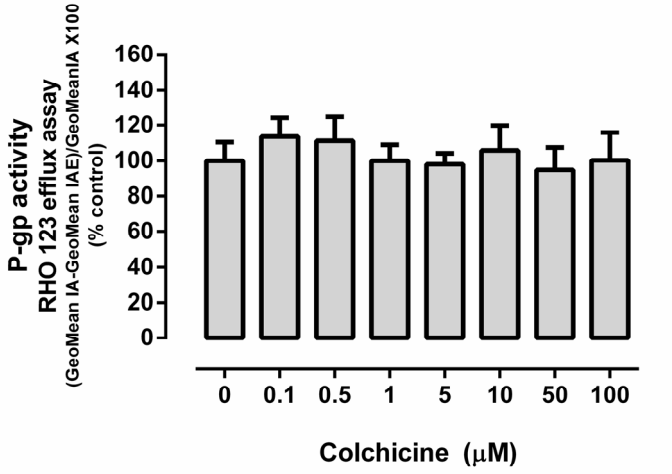

Figure 3. P-glycoprotein activity evaluated by the RHO 123 efflux assay in Caco-2 cells exposed to colchicine (COL) (0 – 100 μM) for 24 h. Results are presented as mean ± SD from 3 independent experiments performed in triplicate. Statistical comparisons were made using the Kruskal-Wallis test followed by the Dunn's Multiple Comparison post hoc test.

3.4. P-glycoprotein ATPase activity

The P-gp ATPase assay consisted of two different tests, an activation and an inhibition test. In the activation test, P-gp substrates may cause the stimulation of baseline vanadate sensitive ATPase activity. As observed in Figure 4 - activation study, colchicine, at the highest tested concentration (100 μM), significantly increased the amount of Pi liberated by the transporter resulting in a stimulation of the baseline vanadate sensitive ATPase activity (23 nmol Pi liberated/mg protein/min for 100 μM colchicine, when compared to 15 nmol Pi liberated/mg protein/min for basal P-gp vanadate sensitive ATPase activity, $p<0.001$).

The inhibition test was performed in the presence of verapamil (40 μM), a known P-gp activator. P-gp inhibitors or slowly transported compounds may inhibit the maximal vanadate sensitive ATPase activity. As observed in Figure 4 - inhibition study, no significant differences were observed in the vanadate sensitive ATPase activity for all the tested colchicine concentrations, when compared to fully activated membrane vesicles.

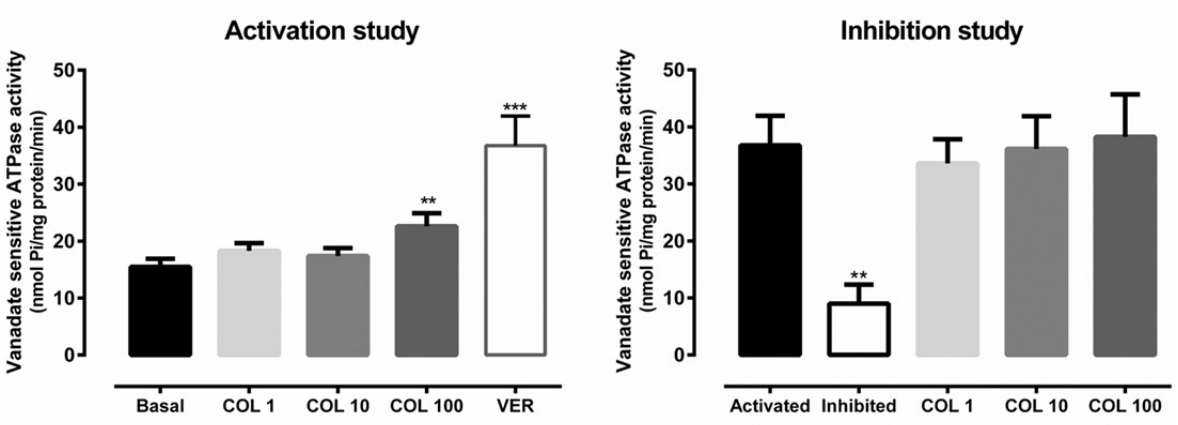

Figure 4. Vanadate sensitive ATPase activity (nmol Pi/mg protein/min) in MDR1-Sf9 membrane vesicles (4 μg/well) exposed to 1, 10, and 100 μM colchicine (COL). In the inhibition study, membrane vesicles exposed only to verapamil (40 μM) are referred to as fully activated membranes. Cyclosporine A (40 μM) was used as the positive control for the inhibition studies and the corresponding membrane vesicles are referred to as inhibited membranes. Results are presented as mean ± SD from 3 independent experiments (performed in triplicate). Statistical comparisons were made using the Kruskal-Wallis test followed by the Dunn's Multiple Comparison post hoc test (**p<0.01; ***p<0.001 concentration vs. basal or fully activated membranes).

3.5. Mapping of colchicine onto P-gp induction and inhibition pharmacophores

Four pharmacophores for P-gp induction were built based on 34 published P-gp inducers (Scheme 1A, Figure 5 A-L). Pharmacophore I had a score of 52.9 and was composed of six features: 3 hydrophobic features, and 3 hydrogen bond (Hb)-acceptor groups (Figure 5 A-C). This was the pharmacophore with the highest number of features found. Pharmacophore II has a score of 64.3 and was composed of 3 features: 2 Hb donor groups, and 1 Hb acceptor group (Figure 5 D-F). Pharmacophore III has a score of

61.4 and was composed of 5 features: 3 Hb acceptor groups and 2 hydrophobic groups (Figure 5 G-I). Pharmacophore IV has a score of 40.9 and was composed of 3 features: 1 Hb donor group and 2 hydrophobic groups (Figure 5 J-L). In order to validate the P-gp induction pharmacophores, a test set formed of 4 know P-gp inducers, amprenavir (Huang et al. 2001), nelfinavir (Huang et al. 2001), puromycin (Male 2009), and yohimbine (Bhat et al. 1995), was used (Figure 5, right column). Those compounds were detected as P-gp inducers when using pharmacophores I-IV as query (validation of pharmacophores on supporting information - Table S2).

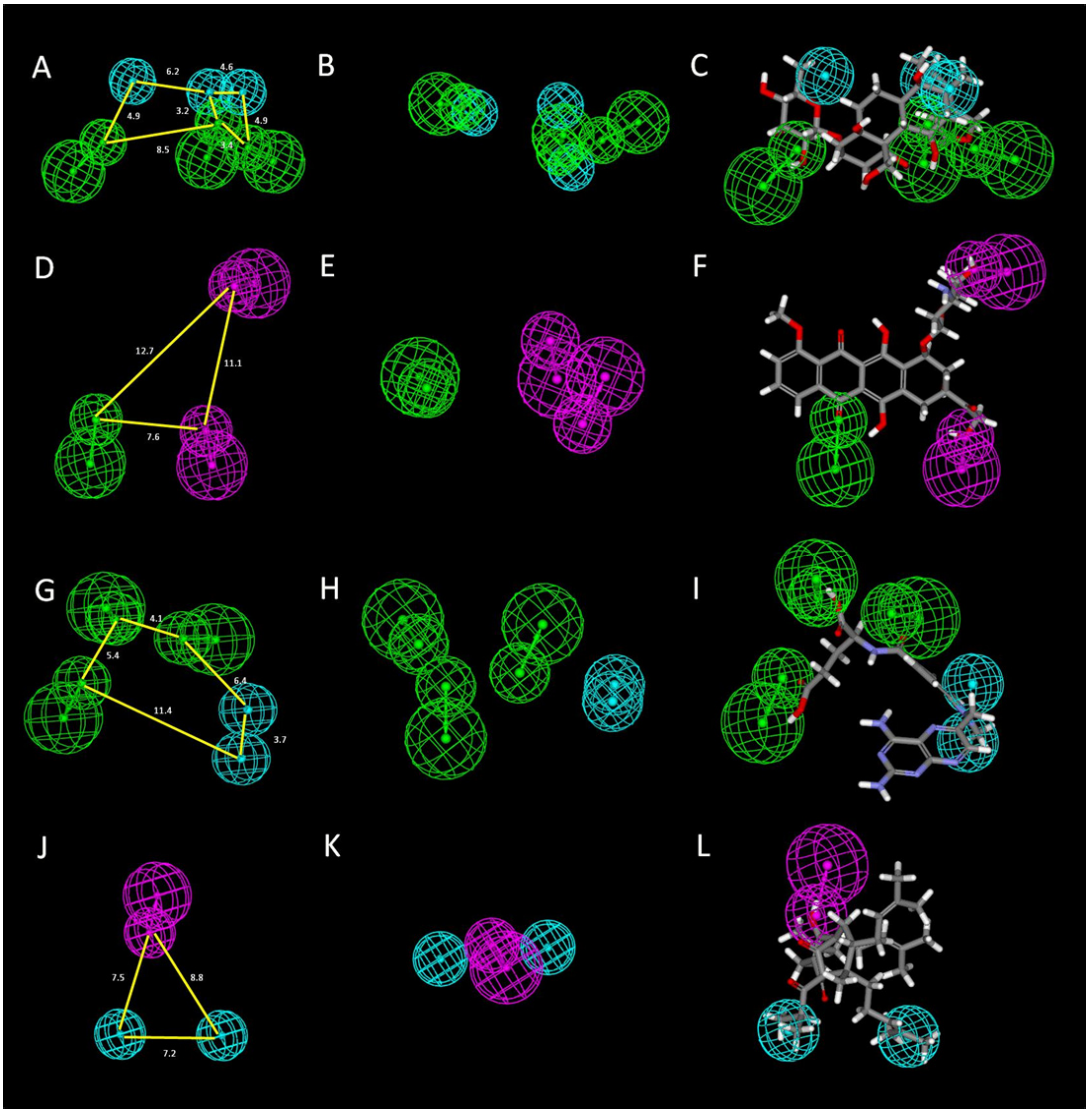

Figure 5. The top-ranked chemical feature-based pharmacophore models for P-gp inducers developed using the HipHop module in Catalyst. Pharmacophore I, obtained from cluster 2 (A, B), and pharmacophore I superimposed with oubain (C). Pharmacophore II, obtained from cluster 4 (D, E), and pharmacophore II superimposed with doxorubicin (F). Pharmacophore III, obtained from cluster 8 (G, H), and pharmacophore III superimposed with methotrexate (I). Pharmacophore IV, obtained from cluster 9 (J, K), and pharmacophore IV superimposed with hyperforin (L). Yellow lines represent interfeature distances (distances are given in Angstrom). Blue= hydrophobic, green= hydrogen bond acceptor, magenta= hydrogen bond donor.

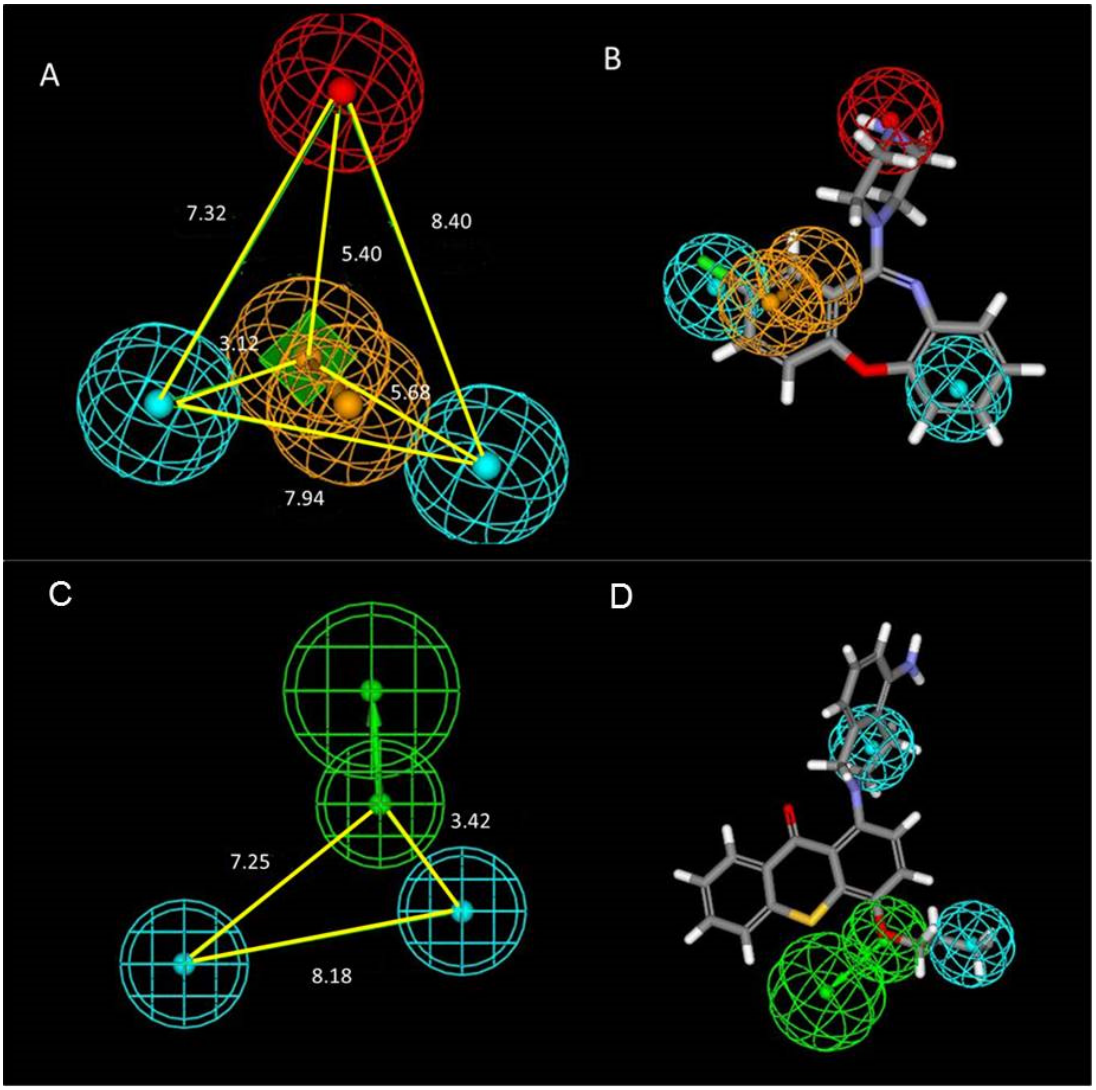

Figure 6. (A) The pharmacophore model I' for P-gp noncompetitive inhibitors generated by Hypogen in which the red sphere represents a positive ion interaction site, the blue spheres represent hydrophobic interaction sites and the orange sphere represent an aromatic ring. (B) Amoxapine fit to pharmacophore (Palmeira et al. 2011). (C) The pharmacophore model II' for P-gp competitive inhibitors generated by Hypogen in which the blue spheres represent hydrophobic interaction sites and the green sphere represent a hydrogen acceptor site. (D) Thioxanthonic derivative fit to pharmacophore (Palmeira et al. 2012c).

A pharmacophore for P-gp competitive inhibition (three features, Figure 6 C-D) and a pharmacophore for P-gp noncompetitive inhibition (four features, Figure 6 A-B) were identified based on 42 previously described inhibitors (Scheme 1B) (Palmeira et al. 2011; Palmeira et al. 2012c). The chosen pharmacophore for P-gp noncompetitive inhibition (pharmacophore I', Figure 6A) is characterized by the lowest total cost value (88.12), the lowest root-mean-square (RMS) deviation (0.551), and the best correlation coefficient (0.686), contains four features, namely, two hydrophobic regions, one aromatic ring and one positive ionizable group, which were intercalated with each other. The fixed cost and null cost are 75.65 and 116.85 bits, respectively (validation of pharmacophore on

supporting information - Table S3). Amoxapine, a previously described P-gp noncompetitive inhibitor (Palmeira et al. 2011), was able to superimpose the four-feature pharmacophore model (Figure 6B).

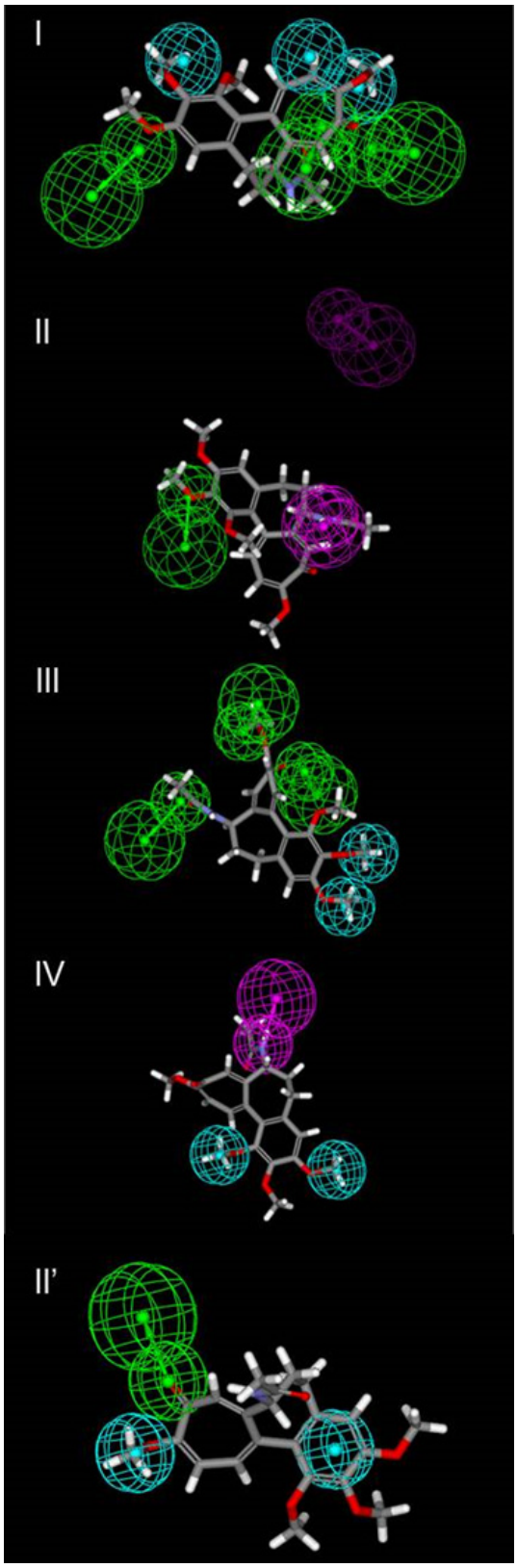

Figure 7. Colchicine alignment to pharmacophore I to IV (inducers) and II' (competitive inhibitors). Blue= hydrophobic, green= hydrogen bond acceptor, magenta= hydrogen bond donor.

The chosen pharmacophore for P-gp competitive inhibition (pharmacophore II', Figure 6C) is characterized by the lowest total cost value (77.19), the lowest RMS deviation (0.604), and the best correlation coefficient (0.742), contains three features, namely, two hydrophobic regions and one Hb acceptor group which is intercalated with the other two features. The fixed cost and null cost are 69.74 and 112.93 bits, respectively. A thioxanthonic P-gp competitive inhibitor 1-(5-amino-3,4-dihydroisoquinolin-2(1*H*)-yl)-4-propoxy-9H-thioxanthen-9-one (Palmeira et al. 2012c), is fit on the pharmacophore as example (Figure 6D). In order to better understand the difference between both pharmacophores, an alignment was performed (Figure S3, supporting information).

Colchicine fits the P-gp induction (Figure 7 I-V) and P-gp competitive inhibition pharmacophore hypothesis (Figure 7 II').

Furthermore, docking studies were performed onto the drug binding pocket formed by the transmembrane domain using a P-gp model (Figure 8) and the predicted binding affinity of the most stable colchicine-P-gp complex was -7.7 kJ/mol.

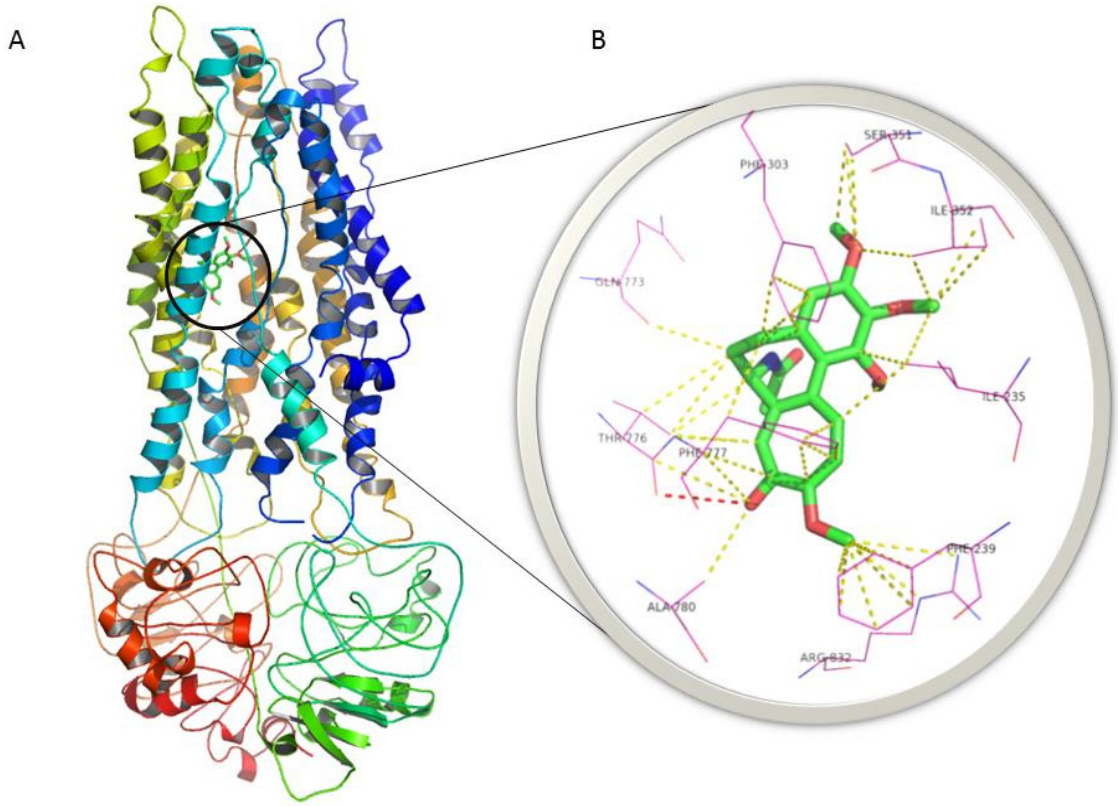

Figure 8. (A)Three dimensional structure of a P-gp model (Palmeira et al. 2012c) represented as ribbon, and the lowest conformation of colchicine (represented as sticks) docked on P-gp drug-binding pocket. (B) Residues predicted as being involved in the interaction between P-gp and colchicine. Hydrogen interactions are represented as red dashes; other interactions are represented as yellow dashes.

4. DISCUSSION AND CONCLUSIONS

Our data show that colchicine, a known P-gp substrate (Ambudkar et al. 1999; Decleves et al. 1998; Decleves et al. 2006; El Hafny et al. 1997; Niel and Scherrmann 2006), increased P-gp expression in Caco-2 cells without a concomitant increase in the activity of the protein. In fact, the observed results revealed that this P-gp substrate is able to significantly induce P-gp expression in a concentration dependent manner, up to 183% for the highest colchicine concentration tested (100 μM). Other studies also reported the ability of colchicine to modulate P-gp expression, both *in vitro* and *in vivo* (Decleves et al. 1998; Licht et al. 2000; Vollrath et al. 1994). For instance, Declèves et. al (1998) demonstrated that colchicine (25 nM) was able to significantly increase P-gp expression in the promyelocytic HL-60 cells after 24 h of exposure, reaching maximal values after 72 h of incubation (Decleves et al. 1998). The effect of colchicine on P-gp expression was also reported *in vivo* where it was demonstrated an increase in *mdr* mRNA levels in rat liver as early as 3 h (2 mg per kg, i.p.), peaking after 24 h (Vollrath et al. 1994). However, in these reports the ability of colchicine to modulate the activity of this important efflux transporter was not evaluated. In the present study, the evaluation of P-gp transport activity was performed through the evaluation of both RHO 123 accumulation and RHO 123 efflux. It was demonstrated that, in spite of the significant increase in P-gp expression, no significant effect was observed in the activity of this efflux pump, at any of the tested colchicine concentrations. Therefore, these results suggest that although P-gp is being expressed at higher levels and incorporated in the cell membrane (since the monoclonal antibody recognizes an external P-gp epitope), this transport efflux pump may not be yet fully functional. Importantly, these results emphasize that P-gp activity is not necessarily correlated with the corresponding protein content. Other reports agree with our findings, suggesting that an increase in P-gp expression may not be reflected in an increase in its activity. In fact, Takara and co-workers (2009) noted that P-gp transport function remained unchanged in Caco-2 cells exposed to several NSAIDs in spite of the observed increase in *MDR1* mRNA (Takara et al. 2009). Moreover, Vilas-Boas and co-workers (2011) also found that P-gp activity in human lymphocytes did not follow the significant increase in its expression during aging (Vilas-Boas et al. 2011).

To efficiently predict P-gp modulatory activity *in silico* studies were performed and new pharmacophores were developed. Although computational studies for predicting substrates or inhibitors of P-glycoprotein are emerging (Chen et al. 2012; Palmeira et al. 2012b), these do not address P-gp inducers. P-gp inducers have several potential mechanisms of action. Multiple pathways may explain the diversity of scaffolds of P-gp inducers (Table S1, supporting information). Due to the diversity of targets of P-gp

inducers, a pharmacophore study using known P-gp inducers is the best option when the structure of the target is not known (Scheme 1). The structural diversity of the described P-gp inducers did not allow a superimposition of those molecules. Hence, no common feature pharmacophore could be obtained by common feature alignment. A solution to this problem was a ligand clustering analysis. This procedure clusters the input molecules into subsets (cluster) of molecules so that each molecule in the same cluster has similar property or fingerprints.

Ten clusters were obtained (Table S1, 3rd column; Scheme 1), but clusters 1, 3, and 7 are not real clusters as they are composed by only 1 molecule. Phenothiazine (cluster 1) and cisplatin (cluster 3) are small and low molecular weight molecules with a S-heterocycle tryciclic system or an inorganic compound, respectively; 1α,25-dihydroxyvitamin D3 (cluster 7), in spite of being a long molecule, formed by long hydrophobic carbonated chain, and by three hydroxyl groups, that may be hydrogen bond donors and acceptors, had no similarity with the remaining studied molecules. Therefore, these three molecules were excluded from the analysis. Clusters 5 and 6 are formed by only 2 molecules; the limited number of molecules in these clusters triggered their withdrawal from the following computational studies. Therefore, only clusters 2, 4, 8, and 9 (Table S1, supporting information) better represent the structural diversity of P-gp inducers and, hence, were used to build P-gp induction pharmacophores by common feature alignment.

Catalyst HipHop (Hecker et al. 2002; Kurogi and Guner 2001) generates common feature pharmacophore models from a set of active molecules. Four pharmacophoric analyses were run and the pharmacophore, with the best ranking score and with higher number of features, was selected on each run. Pharmacophores are diverse in terms of type and number of pharmacophoric features, and interfeature distances, reflecting structural diversity of compounds that increase P-gp expression (Figure 5 A-L). It is interesting to notice that pharmacophores I and II allow the alignment with linear molecules, composed by aromatic or non-aromatic ring systems with different substituents and diverse locations (hydrophobic or polar groups). On the other hand, pharmacophores III and IV fit with angular molecules, with alkyl and/or aryl chains, and carbonyl and amine groups are frequent. These pharmacophores represent the diversity of scaffolds and substituents in P-gp inducers.

Finally, Catalyst was used to identify if colchicine maps onto pharmacophores I-IV, aligning that molecule to the query. The fit value is a measure of how well the small molecule fits the pharmacophore. The higher the fit score, the better the match. Figure 7 I-IV shows colchicine alignment against pharmacophores I to IV. This alignment represents a good match of features present in the ligand to the pharmacophore model III (Fit score =

4.039/5) and mainly to pharmacophore model IV (Fit score = 2.963/3). The alignment of colchicine with pharmacophore model I is possible but with low fitting score (Fit score = 0.912/6) and to pharmacophore model II missing one of the features (Fit score = 1.978/3) (Figure 5). Pharmacophore IV was the colchicine's best fitting pharmacophore; it has three features, and hence, the maximum fit value of any ligand alignment with this model would be 3.0 (the fit score obtained is 2.963). The hydrogen bound to nitrogen on the amide group align with the Hb donor vector feature, and methoxyl groups fit the nondirectional hydrophobic pharmacophoric features (Figure 7 IV). Alignment of pharmacophore IV with training set compounds was performed and found to give fit scores ranging from 2.685 to 2.999 (data not shown). Fitting score of colchicine is within this interval of values, and, therefore, it is probable that colchicine is in fact a P-gp inducer by a mechanism similar to that of compounds represented in cluster 9.

In spite of all the pharmacophore models for P-gp inhibition described in the literature (Chen et al. 2012; Palmeira et al. 2012a; Palmeira et al. 2012b), a characterization of pharmacophoric groups important for competitive and noncompetitive P-gp inhibition has not been done yet. In this work, using *in vitro* ATPase results obtained for thioxanthonic derivatives (Palmeira et al. 2012c) and several commercially available drugs (Palmeira et al. 2011) obtained using the same protocol and the same conditions, a distinction between pharmacophores for competitive and noncompetitive P-gp inhibitors has been achieved. The best pharmacophore models for each activity are represented on Figure 6. These pharmacophores are consistent with others described in the literature that proposed a general pharmacophore model with hydrophobic, Hb acceptor and positive ionizable features (Li et al. 2007; Pajeva and Wiese 2002). Other groups defined pharmacophores with hydrophobic and Hb acceptor features (Cianchetta et al. 2005; Pajeva and Wiese 2002). However, a clear distinction between pharmacophores for competitive and noncompetitive inhibitors has never been accomplished before, being described here for the first time.

Colchicine was mapped onto both pharmacophores I' and II'. However, colchicine was not able to align to pharmacophore I' (noncompetitive P-gp inhibitors), but it was fit to pharmacophore II', as shown in Figure 7 II'. Benzene ring and methoxyl group fit in the hydrophobic features while carbonyl from the amide group acts as Hb acceptor (Figure 7 II').

These data suggests that colchicine is not only a P-gp inducer (demonstrated by computational and biochemical results) but it may also be transported by P-gp, acting as a competitive P-gp inhibitor. This activity may not be adequately detected experimentally due to the simultaneous increase in P-gp expression. Docking studies of colchicine onto P-gp drug-binding pocket further emphasized the possibility of that drug being a P-gp

competitive inhibitor (Figure 8). In fact, a favourable energy for the most stable colchicine-P-gp complex (7.7 kJ/mol) was predicted when compared to the scores obtained for known substrates or competitive P-gp inhibitors (-4.5 kJ/mol) (Palmeira et al. 2012c). Further testing, namely the P-gp ATPase assay, was performed to further clarify colchicine's mechanism of action and it was possible to observe that colchicine, at the highest tested concentration (100 μM), significantly increased the basal vanadate sensitive ATPase activity of membrane vesicles enriched in human P-gp (Figure 4). Thus, according to the present data, colchicine stimulated P-gp ATPase activity, which is compatible to the previous computational studies that demonstrated that it may be actively transported by P-gp. Therefore, although colchicine causes a remarkable and significant increase in P-gp expression in Caco-2 cells, it can inhibit other P-gp substrates efflux by interfering with their transport in a competitive mode, at least partially explaining why P-gp activity is not proportionally increased. Shapiro and Ling (1997) have proposed a model suggesting two different P-gp functional binding sites (H site and R site) that interact in a positive cooperative manner and demonstrated that colchicine belongs to the H-type of P-gp substrates (Shapiro and Ling 1997). Additionally, binding of compounds to the H site of P-gp can activate the efflux of specific substrates of the R site in a positive cooperative manner, whereas binding of H-type substrates is competitively inhibited (Sterz et al. 2009).

Although COL plasmatic concentrations in humans under typical therapeutic dosing regimens are usually below 10 ng/mL (approximately 25 nM) (Berkun et al. 2012; Wason et al. 2012), higher concentrations were used in the present study. In fact, knowing that the approved dosing regimen for acute gout attacks requires a single dose of 1.2 mg to be taken immediately on the first signs of an acute flare, followed by a 0.6-mg dose 1 h later (Wason et al. 2012), higher concentrations are thus expected at the gut wall. After oral administration, COL is absorbed in the jejunum and ileum following a single zero-order rate process, with 44% bioavailability (Rochdi et al. 1994). Therefore, in the intestine, higher concentrations may be expected since almost all of the ingested dose comes into contact with the enterocytes. In accordance, the COL concentrations used in this *in vitro* mechanistic study intended to mimic the higher concentrations expected to be attained at the intestinal barrier.

In conclusion, our data shows a perfect match between computational and *in vitro* studies. These results indicate that the use of such *in silico* strategies can help predict the P-gp modulatory effects of new drugs that can be initially screened through these newly developed pharmacophores. Moreover, it was shown that colchicine induced P-gp expression in Caco-2 cells without a concomitant increase in the protein activity. Therefore, we suggest that although colchicine is a P-gp inducer it also acts as a P-gp

competitive inhibitor. Both our computational and biological data emphasize the importance of the simultaneous evaluation of P-gp expression and activity in the screening of P-gp inducers, since an increase in the first may not be reflected in an increase in the second. Therefore, for the screening of possible pharmacokinetic drug-drug interactions mediated by a P-gp inducer it is of utmost importance to evaluate if the inducer is able not only to increase P-gp protein expression, but also if it is able to promote the cellular efflux of drugs actively transported by the pump, which will eventually lead to decreased therapeutic efficacy.

5. ACKNOWLEDGMENTS

This work was supported by the Fundação para a Ciência e Tecnologia (FCT)-project PTDC/SAU-OSM/101437/2008 - QREN initiative with EU/FEDER funded through COMPETE - Operational Programme for Competitiveness Factors.

The work was also supported by FCT within the framework of Strategic Projects for Scientific Research Units of R&D (projects PEst-C/EQB/LA0006/2011 and Pest-OE/SAU/UI4040/2011).

Renata Silva and Daniel José Barbosa acknowledge FCT for their PhD grants [SFRH/BD/29559/2006] and [SFRH/BD/64939/2009], respectively.

6. CONFLICT OF INTEREST STATEMENT

The authors declare that there are no conflicts of interest.

7. REFERENCES

Allenspach K, Bergman PJ, Sauter S, Grone A, Doherr MG, Gaschen F (2006) P-glycoprotein expression in lamina propria lymphocytes of duodenal biopsy samples in dogs with chronic idiopathic enteropathies. J Comp Pathol 134:1-7.

Ambudkar SV, Dey S, Hrycyna CA, Ramachandra M, Pastan I, Gottesman MM (1999) Biochemical, cellular, and pharmacological aspects of the multidrug transporter. Annu Rev Pharmacol Toxicol 39:361-398.

Angelini A, Centurione L, Sancilio S, et al. (2011) The effect of the plasticizer diethylhexyl phthalate on transport activity and expression of P-glycoprotein in parental and doxo-resistant human sarcoma cell lines. J Biol Regul Homeost Agents 25:203-211.

Balimane PV, Han YH, Chong S (2006) Current industrial practices of assessing permeability and P-glycoprotein interaction. AAPS J 8:1-13.

Barta CA, Sachs-Barrable K, Feng F, Wasan KM (2008) Effects of monoglycerides on p-glycoprotein: modulation of the activity and expression in caco-2 cell monolayers. Mol Pharm 5:863-875.

Ben-Chetrit E, Levy M (1991) Colchicine prophylaxis in familial Mediterranean fever: reappraisal after 15 years. Semin Arthritis Rheum 20:241-246.

Berkun Y, Wason S, Brik R, et al. (2012) Pharmacokinetics of colchicine in pediatric and adult patients with familial Mediterranean fever. Int J Immunopathol Pharmacol 25:1121-1130.

Bhat UG, Winter MA, Pearce HL, Beck WT (1995) A structure-function relationship among reserpine and yohimbine analogues in their ability to increase expression of mdr1 and P-glycoprotein in a human colon carcinoma cell line. Mol Pharmacol 48:682-689.

Biganzoli E, Cavenaghi LA, Rossi R, Brunati MC, Nolli ML (1999) Use of a Caco-2 cell culture model for the characterization of intestinal absorption of antibiotics. Farmaco 54:594-599.

Cermanova J, Fuksa L, Brcakova E, et al. (2009) Up-regulation of renal Mdr1 and Mrp2 transporters during amiodarone pretreatment in rats. Pharmacol Res 61:129-135.

Chen L, Li Y, Yu H, Zhang L, Hou T (2012) Computational models for predicting substrates or inhibitors of P-glycoprotein. Drug Discov Today 17:343-351.

Chow EC, Durk MR, Cummins CL, Pang KS (2011) 1Alpha,25-dihydroxyvitamin D3 up-regulates P-glycoprotein via the vitamin D receptor and not farnesoid X receptor in both fxr(-/-) and fxr(+/+) mice and increased renal and brain efflux of digoxin in mice in vivo. J Pharmacol Exp Ther 337:846-859.

Cianchetta G, Singleton RW, Zhang M, et al. (2005) A pharmacophore hypothesis for P-glycoprotein substrate recognition using GRIND-based 3D-QSAR. J Med Chem 48:2927-2935.

de Graaf D, Sharma RC, Mechetner EB, Schimke RT, Roninson IB (1996) P-glycoprotein confers methotrexate resistance in 3T6 cells with deficient carrier-mediated methotrexate uptake. Proc Natl Acad Sci U S A 93:1238-1242.

Decleves X, Chappey O, Boval B, Niel E, Scherrmann JM (1998) P-glycoprotein is more efficient at limiting uptake than inducing efflux of colchicine and vinblastine in HL-60 cells. Pharm Res 15:712-718.

Decleves X, Niel E, Debray M, Scherrmann JM (2006) Is P-glycoprotein (ABCB1) a phase 0 or a phase 3 colchicine transporter depending on colchicine exposure conditions? Toxicol Appl Pharmacol 217:153-60.

Demeule M, Brossard M, Beliveau R (1999) Cisplatin induces renal expression of P-glycoprotein and canalicular multispecific organic anion transporter. Am J Physiol 277:832-840.

Druley TE, Stein WD, Ruth A, Roninson IB (2001) P-glycoprotein-mediated colchicine resistance in different cell lines correlates with the effects of colchicine on P-glycoprotein conformation. Biochemistry 40:4323-4331.

Ehret MJ, Levin GM, Narasimhan M, Rathinavelu A (2007) Venlafaxine induces P-glycoprotein in human Caco-2 cells. Hum Psychopharmacol 22:49-53.

El Hafny B, Cano N, Piciotti M, Regina A, Scherrmann JM, Roux F (1997) Role of P-glycoprotein in colchicine and vinblastine cellular kinetics in an immortalized rat brain microvessel endothelial cell line. Biochem Pharmacol 53:1735-1742.

Famaey JP (1988) Colchicine in therapy. State of the art and new perspectives for an old drug. Clin Exp Rheumatol 6:305-317.

Fardel O, Lecureur V, Daval S, Corlu A, Guillouzo A (1997) Up-regulation of P-glycoprotein expression in rat liver cells by acute doxorubicin treatment. Eur J Biochem 246:186-192.

Finkelstein Y, Aks SE, Hutson JR, et al. (2010) Colchicine poisoning: the dark side of an ancient drug. Clin Toxicol (Phila) 48:407-414.

Furuya KN, Thottassery JV, Schuetz EG, Sharif M, Schuetz JD (1997) Bromocriptine transcriptionally activates the multidrug resistance gene (pgp2/mdr1b) by a novel pathway. J Biol Chem 272:11518-11525.

Giessmann T, May K, Modess C, et al. (2004) Carbamazepine regulates intestinal P-glycoprotein and multidrug resistance protein MRP2 and influences disposition of talinolol in humans. Clin Pharmacol Ther 76:192-200.

Harmsen S, Meijerman I, Febus CL, Maas-Bakker RF, Beijnen JH, Schellens JH (2009) PXR-mediated induction of P-glycoprotein by anticancer drugs in a human colon adenocarcinoma-derived cell line. Cancer Chemother Pharmacol 66:765-771.

Haslam IS, Jones K, Coleman T, Simmons NL (2008) Induction of P-glycoprotein expression and function in human intestinal epithelial cells (T84). Biochem Pharmacol 76:850-861.

Hecker EA, Duraiswami C, Andrea TA, Diller DJ (2002) Use of catalyst pharmacophore models for screening of large combinatorial libraries. J Chem Inf Comput Sci 42:1204-1211.

Huang L, Wring SA, Woolley JL, Brouwer KR, Serabjit-Singh C, Polli JW (2001) Induction of P-glycoprotein and cytochrome P450 3A by HIV protease inhibitors. Drug Metab Dispos 29:754-760.

Huynh-Delerme C, Huet H, Noel L, Frigieri A, Kolf-Clauw M (2005) Increased functional expression of P-glycoprotein in Caco-2 TC7 cells exposed long-term to cadmium. Toxicol In Vitro 19:439-447.

Juliano RL, Ling V (1976) A surface glycoprotein modulating drug permeability in Chinese hamster ovary cell mutants. Biochim Biophys Acta 455:152-162.

Kageyama M, Fukushima K, Togawa T, et al. (2006) Relationship between excretion clearance of rhodamine 123 and P-glycoprotein (Pgp) expression induced by representative Pgp inducers. Biol Pharm Bull 29:779-784.

Kageyama M, Namiki H, Fukushima H, et al. (2005) Effect of chronic administration of ritonavir on function of cytochrome P450 3A and P-glycoprotein in rats. Biol Pharm Bull 28:130-137.

Kim KA, Park PW, Liu KH, et al. (2008) Effect of rifampin, an inducer of CYP3A and P-glycoprotein, on the pharmacokinetics of risperidone. J Clin Pharmacol 48:66-72.

Kurogi Y, Guner OF (2001) Pharmacophore modeling and three-dimensional database searching for drug design using catalyst. Curr Med Chem 8:1035-1055.

Lemaire S, Van Bambeke F, Mingeot-Leclercq MP, Tulkens PM (2007) Modulation of the cellular accumulation and intracellular activity of daptomycin towards phagocytized Staphylococcus aureus by the P-glycoprotein (MDR1) efflux transporter in human THP-1 macrophages and madin-darby canine kidney cells. Antimicrob Agents Chemother 51:2748-2757.

Li X, Li JP, Yuan HY, et al. (2007) Recent advances in P-glycoprotein-mediated multidrug resistance reversal mechanisms. Methods Find Exp Clin Pharmacol 29:607-617.

Licht T, Goldenberg SK, Vieira WD, Gottesman MM, Pastan I (2000) Drug selection of MDR1-transduced hematopoietic cells ex vivo increases transgene expression and chemoresistance in reconstituted bone marrow in mice. Gene therapy 7:348-358.

Lin JH, Yamazaki M (2003a) Clinical relevance of P-glycoprotein in drug therapy. Drug Metab Rev 35:417-454.

Lin JH, Yamazaki M (2003b) Role of P-glycoprotein in pharmacokinetics: clinical implications. Clin Pharmacokinet 42:59-98.

Liu H, Yang H, Wang D, et al. (2009) Insulin regulates P-glycoprotein in rat brain microvessel endothelial cells via an insulin receptor-mediated PKC/NF-kappaB pathway but not a PI3K/Akt pathway. Eur J Pharmacol 602:277-282.

Male DK (2009) Expression and induction of p-glycoprotein-1 on cultured human brain endothelium. J Cereb Blood Flow Metab 29:1760-1763.

Mealey KL, Barhoumi R, Burghardt RC, Safe S, Kochevar DT (2002) Doxycycline induces expression of P glycoprotein in MCF-7 breast carcinoma cells. Antimicrob Agents Chemother 46:755-761.

Mechetner EB, Schott B, Morse BS, et al. (1997) P-glycoprotein function involves conformational transitions detectable by differential immunoreactivity. Proc Natl Acad Sci U S A 94:12908-12913.

Niel E, Scherrmann JM (2006) Colchicine today. Joint Bone Spine 73:672-678.

Nielsen D, Eriksen J, Maare C, Jakobsen A, Skovsgaard T (1998) P-glycoprotein expression in Ehrlich ascites tumour cells after in vitro and in vivo selection with daunorubicin. Br J Cancer 78:1175-1180.

Pajeva IK, Wiese M (2002) Pharmacophore model of drugs involved in P-glycoprotein multidrug resistance: explanation of structural variety (hypothesis). J Med Chem 45:5671-5686.

Palmeira A, Rodrigues F, Sousa E, Pinto M, Vasconcelos MH, Fernandes MX (2011) New uses for old drugs: pharmacophore-based screening for the discovery of P-glycoprotein inhibitors. Chem Biol Drug Des 78:57-72.

Palmeira A, Sousa E, Vasconcelos MH, Pinto MM (2012a) Three decades of P-gp inhibitors: Skimming through several generations and scaffolds. Curr Med Chem 19:1946-2025.

Palmeira A, Sousa E, Vasconcelos MH, Pinto MM, Fernandes MX (2012b) Structure and ligand-based design of P-glycoprotein inhibitors: a historical perspective. Curr Pharm Design 18:4197-4214.

Palmeira A, Vasconcelos MH, Paiva A, Fernandes MX, Pinto M, Sousa E (2012c) Dual inhibitors of P-glycoprotein and tumor cell growth: (re)discovering thioxanthones. Biochem Pharmacol 83:57-68.

Patel Y, Gillet VJ, Bravi G, Leach AR (2002) A comparison of the pharmacophore identification programs: Catalyst, DISCO and GASP. J Comput Aided Mol Des 16:653-681.

Pontes H, Sousa C, Silva R, et al. (2008) Synergistic toxicity of ethanol and MDMA towards primary cultured rat hepatocytes. Toxicology 254:42-50.

Prenkert M, Uggla B, Tina E, Tidefelt U, Strid H (2009) Rapid induction of P-glycoprotein mRNA and protein expression by cytarabine in HL-60 cells. Anticancer Res 29:4071-4076.

Rigalli JP, Ruiz ML, Perdomo VG, Villanueva SS, Mottino AD, Catania VA (2011) Pregnane X receptor mediates the induction of P-glycoprotein by spironolactone in HepG2 cells. Toxicology 285:18-24.

Riganti C, Doublier S, Viarisio D, et al. (2009) Artemisinin induces doxorubicin resistance in human colon cancer cells via calcium-dependent activation of HIF-1α and P-glycoprotein overexpression. Br J Pharmacol 156:1054-1066.

Rochdi M, Sabouraud A, Girre C, Venet R, Scherrmann JM (1994) Pharmacokinetics and absolute bioavailability of colchicine after i.v. and oral administration in healthy human volunteers and elderly subjects. Eur J Clin Pharmacol 46:351-354.

Shapiro AB, Ling V (1997) Positively cooperative sites for drug transport by P-glycoprotein with distinct drug specificities. Eur J Biochem 250:130-137.

Silva R, Carmo H, Dinis-Oliveira R, et al. (2011) In vitro study of P-glycoprotein induction as an antidotal pathway to prevent cytotoxicity in Caco-2 cells. Arch Toxicol 85:315-326.

Silva R, Carmo H, Vilas-Boas V, et al. (2013) Doxorubicin decreases paraquat accumulation and toxicity in Caco-2 cells. Toxicol Lett 217:34-41.

Sterz K, Mollmann L, Jacobs A, Baumert D, Wiese M (2009) Activators of P-glycoprotein: Structure-activity relationships and investigation of their mode of action. ChemMedChem 4:1897-1911.

Taipalensuu J, Tornblom H, Lindberg G, et al. (2001) Correlation of gene expression of ten drug efflux proteins of the ATP-binding cassette transporter family in normal human jejunum and in human intestinal epithelial Caco-2 cell monolayers. J Pharmacol Exp Ther 299:164-170.

Takara K, Hayashi R, Kokufu M, et al. (2009) Effects of nonsteroidal anti-inflammatory drugs on the expression and function of P-glycoprotein/MDR1 in Caco-2 cells. Drug Chem Toxicol 32:332-337.

Tateishi T, Nakura H, Asoh M, et al. (1999) Multiple cytochrome P-450 subfamilies are co-induced with P-glycoprotein by both phenothiazine and 2-acetylaminofluorene in rats. Cancer Lett 138:73-79.

Thiebaut F, Tsuruo T, Hamada H, Gottesman MM, Pastan I, Willingham MC (1987) Cellular localization of the multidrug-resistance gene product P-glycoprotein in normal human tissues. Proc Natl Acad Sci U S A 84:7735-7738.

Tian R, Koyabu N, Morimoto S, Shoyama Y, Ohtani H, Sawada Y (2005) Functional induction and de-induction of P-glycoprotein by St. John's wort and its ingredients in a human colon adenocarcinoma cell line. Drug Metab Dispos 33:547-554.

Vilaboa NE, Galan A, Troyano A, de Blas E, Aller P (2000) Regulation of multidrug resistance 1 (MDR1)/P-glycoprotein gene expression and activity by heat-shock transcription factor 1 (HSF1). J Biol Chem 275:24970-24976.

Vilas-Boas V, Silva R, Gaio AR, et al. (2011) P-glycoprotein activity in human Caucasian male lymphocytes does not follow its increased expression during aging. Cytometry A 79:912-919.

Vilas-Boas V, Silva R, Palmeira A, et al. (2013) Development of novel rifampicin-derived P-glycoprotein activators/inducers. Synthesis, in silico analysis and application in the RBE4 cell model, using paraquat as substrate. PLoS One 8:e74425.

Vollrath V, Wielandt AM, Acuna C, Duarte I, Andrade L, Chianale J (1994) Effect of colchicine and heat shock on multidrug resistance gene and P-glycoprotein expression in rat liver. J Hepatol 21:754-763.

Wason S, DiGiacinto JL, Davis MW (2012) Effects of grapefruit and seville orange juices on the pharmacokinetic properties of colchicine in healthy ubjects. Clin Ther 34:2161-2173.

Watanabe T, Onuki R, Yamashita S, Taira K, Sugiyama Y (2005) Construction of a functional transporter analysis system using MDR1 knockdown Caco-2 cells. Pharm Res 22:1287-1293.

Yamada S, Yasui-Furukori N, Akamine Y, Kaneko S, Uno T (2009) Effects of the P-glycoprotein inducer carbamazepine on fexofenadine pharmacokinetics. Ther Drug Monit 31:764-768.

Yamashita S, Furubayashi T, Kataoka M, Sakane T, Sezaki H, Tokuda H (2000) Optimized conditions for prediction of intestinal drug permeability using Caco-2 cells. Eur J Pharm Sci 10:195-204.

SUPPORTING INFORMATION

Supporting information table of contents

S1. Colchicine cytotoxicity

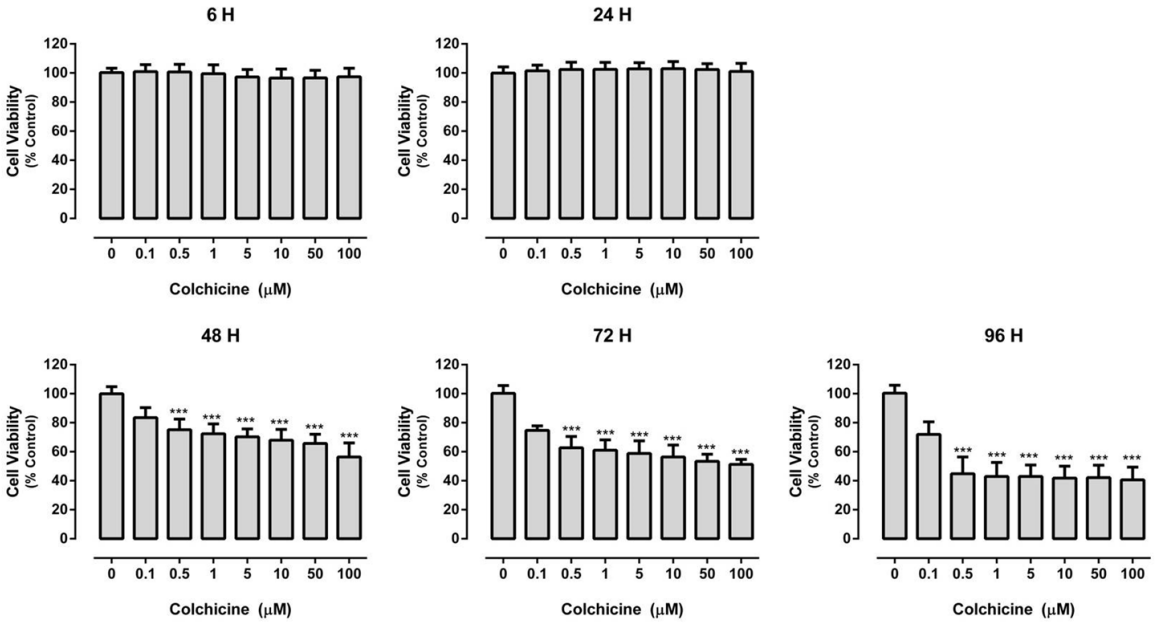

Figure S1. Colchicine (COL) (0 – 100 μM) cytotoxicity in Caco-2 cells at different time-points. Results are presented as mean ± SD from 4 independent experiments performed in triplicate. Statistical comparisons were made using the Kruskal-Wallis test followed by the Dunn's Multiple Comparison post hoc test [***p<0.001 concentration *vs*. control (0 μM)].

S2. Positive control for P-gp inhibition in the RHO 123 accumulation and RHO 123 efflux assays

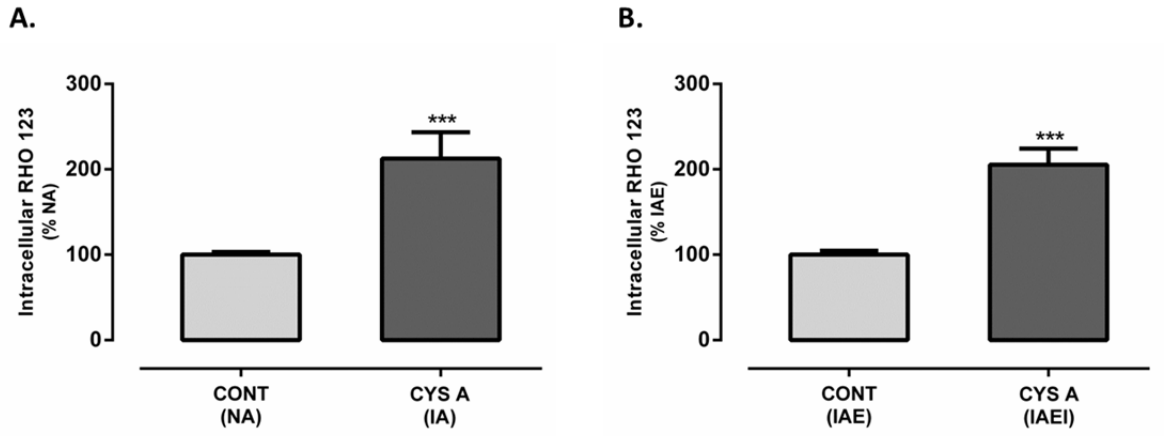

Figure S2. Effect of 10 μM cyclosporine A in RHO 123 intracellular content (positive control for P-gp inhibition). **A.** Rhodamine 123 accumulation assay in the absence (NA, normal accumulation) and in the presence (IA, inhibited accumulation) of 10 μM cyclosporine A. Results are presented as mean ± SD from 3 independent experiments performed in triplicate. Statistical comparisons were made using the Unpaired Student *t* test (***p<0.001 *vs*. NA). In the presence of cyclosporine A, intracellular RHO 123 increased to 212.72 %, when compared to NA. **B.** Rhodamine 123 efflux assay in the absence (IAE, inhibited accumulation followed by normal efflux) and in the presence (IAEI, inhibited accumulation followed by inhibited efflux) of 10 μM cyclosporine A. To allow maximal RHO 123 intracellular accumulation, in both cases RHO 123 accumulation was performed under P-gp inhibition. Results are presented as mean ± SD from 3 independent experiments performed in triplicate. Statistical comparisons were made using the Unpaired Student *t* test (***p<0.001 *vs*. IAE). In the presence of cyclosporine A, intracellular RHO 123 increased to 205.41 %, when compared to IAE. CYS A – cyclosporine A.

S3. Table with the known inducers used to build a pharmacophore for P-gp induction

Table S1. Known P-gp inducers and cluster analysis.

Inducer	Cluster	Reference
Phenothiazine	**1**	(Tateishi et al. 1999)
Dexamethasone	**2**	(Kageyama et al. 2006)
Ouabain	**2**	(Lemaire et al. 2007)
Prednisolone	**2**	(Allenspach et al. 2006)
Spironolactone	**2**	(Rigalli et al. 2011)
Cisplatin	**3**	(Demeule et al. 1999)
Atorvastatin	**4**	(Haslam et al. 2008)
Cytarabine	**4**	(Prenkert et al. 2009)
Daunorubicin	**4**	(Nielsen et al. 1998)
Doxorubicin	**4**	(Fardel et al. 1997; Silva et al. 2011)
Etoposide	**4**	(Vilaboa et al. 2000)
Rifampicin	**4**	(Kim et al. 2008)
Ritonavir	**4**	(Kageyama et al. 2005)
Venlafaxine	**4**	(Ehret et al. 2007)
Cyclophosphamide	**5**	(Harmsen et al. 2009)
Ifosfamide	**5**	(Harmsen et al. 2009)
2-Acetylaminofluorene	**6**	(Tateishi et al. 1999)
Flutamide	**6**	(Harmsen et al. 2009)
1α,25-Dihydroxyvitamin D3	**7**	(Chow et al. 2011)
Amiodarone	**8**	(Cermanova et al. 2009)
Bromocriptine	**8**	(Furuya et al. 1997)
Irinotecan	**8**	(Haslam et al. 2008)
Methotrexate	**8**	(de Graaf et al. 1996)
Topotecan	**8**	(Haslam et al. 2008)
Carbamazepine	**9**	(Giessmann et al. 2004; Yamada et al. 2009)
Docetaxel	**9**	(Harmsen et al. 2009)
Doxycycline	**9**	(Mealey et al. 2002)
Hyperforin	**9**	(Tian et al. 2005)
Insulin	**9**	(Liu et al. 2009)
Paclitaxel	**9**	(Harmsen et al. 2009)
Vincristine	**9**	(Harmsen et al. 2009)
Vinblastine	**9**	(Harmsen et al. 2009)
Artemisinine	**10**	(Riganti et al. 2009)
Diethylhexyl phthalate	**10**	(Angelini et al. 2011)

S4. Validation of pharmacophores for P-gp induction using a test set of known P-gp inducers

Table S2. Pharmacophore validation using test set of known P-gp inducers (Bhat et al. 1995; Huang et al. 2001; Male 2009).

	Fit Value			
Compounds	**Pharmacophore I**	**Pharmacophore II**	**Pharmacophore III**	**Pharmacophore IV**
Amprenavir	3.367	2.444	2.945	2.994
Nelfedipin	3.492	2.546	4.000	3.000
Puromycin	2.728	2.173	4.534	2.997
Yohimbine	No match	1.986	1.081	2.685

Molecules from the test set were able to fit all the pharmacophores with different fit values, with the exception of yohimbine that was only able to align to pharmacophores II to IV. The higher the fit value, the better is the mapping of the molecule to the pharmacophore.

S5. Validation of pharmacophores for P-gp inhibition using a test set of known P-gp inhibitors

Table S3. Pharmacophores validation using test sets of known P-gp inhibitors.

	Fit Value		Fit Value
Compounds (Palmeira et al. 2012c)	**Noncompetitive inhibitors pharmacophore (I')**	**Compounds** (Palmeira et al. 2012a)	**Competitive inhibitors pharmacophore (II')**
8-Geranyldehydrosilybin	3.537	**Cyclosporin A**	2.728
6-Prenyldehydrosilybin	3.504	**Valspodar**	2.723
Sylibin	3.500	**Biricodar**	2.722
8-Prenyldehydrosilybin	3.498	**Dexniguldipine**	2.71
6-Geranyldehydrosilybin	3.496	**Erytromycin**	2.708
Dehydrosilybin	3.495	**Laniquidar**	2.70
Chrysin	3.156	**S9788**	2.648
2',4',6'-Trihydroxy-4-dexyloxychalcone	3.071	**SR33667**	2.555

Flavonoids, described as acting as noncompetitive P-gp inhibitors by directly binding to P-gp ATP-binding site, were used as test set to validate P-gp pharmacophore I' for noncompetitive inhibitors. Competitive inhibitors belonging to several generations of P-gp inhibitors were used as test set to validate P-gp pharmacophore II' for competitive inhibitors. Molecules from the test sets were able to fit the respective pharmacophores. The higher the fit value, the better is the mapping of the molecule to the pharmacophore.

S6. Alignment of pharmacophore for P-gp inhibition

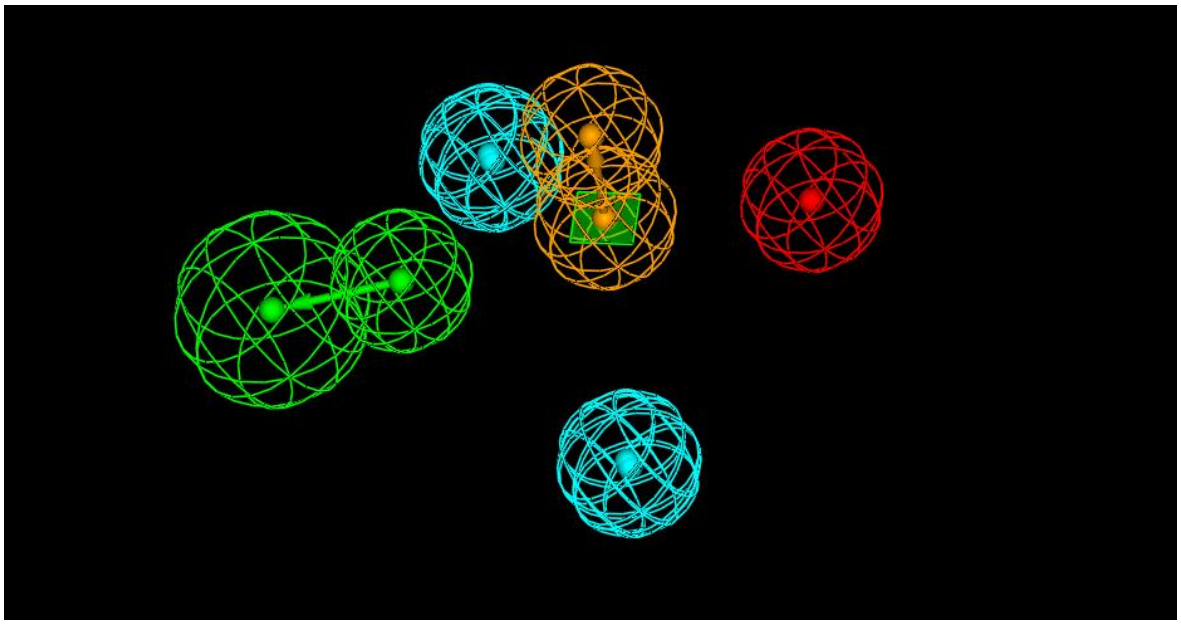

Figure S3. Pharmacophores alignment. There is an almost perfect superimposition between the H1 and H2 from the pharmacophore I, and H'1 and H'2 from the pharmacophore II. The major discrepancy occurred in the remaining features, PI and AR from pharmacophore I and HAc from pharmacophore II that cannot be aligned. These results suggest that the presence of a positive ionizable group, such as an amine, for the establishment of ionic interactions, and the presence of an aromatic ring, for π-π or hydrophobic interactions, may be important for molecules to bind tightly to ATP-binding site or an allosteric region, causing a noncompetitive inhibition of P-gp. In contrast, the presence of a hydrogen bond acceptor (e.g. ether group, amine) may be important for the drug to bind the substrate site of P-gp, and, therefore, causing competitive inhibition. It is interesting to notice that an amine group can be an ionizable group (included on pharmacophore I) or a hydrogen bond acceptor (included on pharmacophore II), and can be present in both competitive and noncompetitive inhibitors of P-gp. Notwithstanding, the distance between this group and the hydrophobic regions is different for competitive and noncompetitive inhibitors.

III.5. MANUSCRIPT IV

Hypericin protects Caco-2 cells against Paraquat toxicity through P-glycoprotein induction

Unsubmitted manuscript

TITLE

Hypericin protects Caco-2 cells against Paraquat toxicity through P-glycoprotein induction

AUTHORS

Renata Silva[a*], Helena Carmo[a], Vânia Vilas-Boas[a], Daniel José Barbosa[a]; Maria de Lourdes Bastos[a] and Fernando Remião[a*]

AFFILIATIONS

[a]REQUI*MT*E, Laboratório de Toxicologia, Departamento de Ciências Biológicas, Faculdade de Farmácia, Universidade do Porto, Rua de Jorge Viterbo Ferreira, 228, 4050-313 Porto, Portugal.

***CORRESPONDING AUTHORS**

Renata Silva (e-mail: rsilva@ff.up.pt) and Fernando Remião (e-mail: remiao@ff.up.pt)
REQUIMTE - Laboratory of Toxicology, Department of Biological Sciences, Faculty of Pharmacy, University of Porto, Rua de Jorge Viterbo Ferreira, 228, 4050-313 Porto, Portugal.
Phone: 00351220428596
Fax: 00351226093390

RUNNING TITLE

Hypericin protection against paraquat toxicity

ABSTRACT

P-glycoprotein (P-gp) is a membrane-bound glycoprotein widely expressed in several organs, where it plays a crucial role in limiting the absorption of xenobiotics. Hypericin (HYP) is one of the major constituents of the St. John's wort flower extract and its P-gp inducing properties remain controversial. Thus, the aim of the present work was to evaluate the P-gp induction profile of HYP (expression and activity) in Caco-2 cells, and to correlate it with a possible protective effect against paraquat (PQ)-induced toxicity.

Hypericin cytotoxicity was evaluated by the NR uptake and LDH leakage assays up to 96 h of incubation, and P-gp expression and activity were evaluated by flow cytometry up to 72 h of incubation. P-gp ATPase activity was measured using recombinant human P-gp-enriched membranes and Caco-2 cells ATP intracellular levels were evaluated through a luciferase-based bioluminescent technique. Paraquat cytotoxicity was evaluated by the NR uptake assay, with or without exposure to HYP, using different experimental designs of HYP incubation: (1) pre-incubation for 24, 48 or 72 h, followed by PQ incubation for 24 h; (2) incubation 6 h after PQ exposure; and (3) simultaneous incubation with PQ for 24 h. The nuclear expression of the YB-1 transcription factor, a gene regulatory protein that can stimulate the transcription of the *MDR1* gene, was evaluated by Western blotting.

Exposure of Caco-2 cells to HYP resulted in a significant increase in both P-gp expression and activity, according to the concentration and time of exposure tested. The observed P-gp induction resulted in a significant protection against PQ-induced cytotoxicity, which was completely abolished in the presence of the UIC2 antibody, a specific P-gp inhibitor. Noteworthy, HYP afforded protection against PQ-induced cytotoxicity even when incubated 6 h after PQ exposure, thus mimicking a real-life intoxication scenario. Furthermore, HYP demonstrated to be a P-gp substrate, as observed by the significant increase in P-gp ATPase activity. Although HYP significantly increased both P-gp transport and ATPase activity, no significant differences were observed in the Caco-2 cells ATP intracellular levels. YB-1 nuclear expression was significantly reduced upon exposure to HYP for 72 h.

In conclusion, our data shows that HYP significantly increases both P-gp protein expression and activity in this cell model of the human intestinal epithelium, and highlight P-gp induction as an intracellular detoxification mechanism against the cytotoxicity of harmful xenobiotics, such as PQ.

KEYWORDS

P-glycoprotein induction; P-glycoprotein transport activity; Paraquat toxicity; Caco-2 cells; Hypericin; YB-1.

ABBREVIATIONS

ATP - Adenosine-5′-triphosphate
BSA - Bovine serum albumin
BOTTOM – Baseline of the fitted concentration-response curve
CYP3A - Cytochrome P450 3A
DMEM - Dulbecco's Modified Eagle's Medium
EC_{50} - Half-maximum-effect concentration
EDTA - Ethylenediamine tetraacetic acid
FBS - Fetal bovine serum
FITC - Fluorescein isothiocyanate
GeoMean - Geometric mean of fluorescence intensity
HYP - Hypericin
IA - Inhibited rhodamine 123 Accumulation
IAE - Inhibited rhodamine 123 accumulation followed by efflux in the absence of P-gp inhibitor
LDH - Lactate dehydrogenase
MDR - Multi drug resistance
MDR1 - Multi-Drug Resistance 1 gene
MWM - Molecular weight marker
NADH - Nicotinamide adenine dinucleotide reduced form
NAD^+ - Nicotinamide adenine dinucleotide oxidized form
NEAA - Non essential amino acids
NF-κB - Nuclear factor kappa-B
NR - Neutral red
NT - Untreated samples
PBS - Phosphate buffered saline solution
P-gp - P-glycoprotein
PQ - Paraquat
RHO 123 - Rhodamine 123
RLU - Relative light units
ROS - Reactive oxygen species
SDS-PAGE - Sodium dodecyl sulfate
SDS-PAGE - Sodium dodecyl sulfate-*polyacrylamide gel electrophoresis*
SJW - St. John's wort
TBS - Tris-buffered saline solution
TBS-T - Tris-buffered saline solution with 0.05% Tween 20 (v/v)
TC - Test compound-treated samples
TOP - Maximal cell death
YB-1 - Nuclease-sensitive element-binding protein 1

1. INTRODUCTION

P-glycoprotein (P-gp) is an ATP-dependent efflux pump encoded by the *MDR1* gene in humans and was first detected over-expressed in Chinese hamster ovary cultured cells selected for multidrug resistance (MDR), where it mediated resistance to many amphipathic drugs (Juliano and Ling 1976). However, P-gp was later found constitutively expressed in normal human epithelial tissues, including the gastrointestinal tract, kidney, placenta, testes, and the blood-brain barrier (Thiebaut et al. 1987). This expression profile shifted the main attention on this efflux pump towards its impact on the intracellular concentrations of drugs and xenobiotics. In fact, P-gp substrates comprise a variety of structurally and pharmacologically unrelated hydrophobic compounds, including vinca alkaloids, colchicine, antibiotics, anthracyclines, HIV protease inhibitors, cardiac glycosides, organic cations, and pesticides (Ambudkar et al. 1999; Cordon-Cardo et al. 1990; Gottesman et al. 2002). Thus, this broad substrate specificity together with its efflux capacity and its cellular polarized expression suggested a role in the intracellular protection against xenobiotics-induced toxicity (Dinis-Oliveira et al. 2006; Silva et al. 2011; Silva et al. 2013b).

Hypericin (HYP) is one of the major constituents of St. John's wort (SJW), one of the most commonly used herbal products, which is responsible for severe drug-herbal interactions (Pal and Mitra 2006). The reported SJW-drug interactions, characterized by lower bioavailability of orally dosed drugs, have been attributed to cytochrome P450 3A (CYP3A) and/or P-gp induction (Perloff et al. 2001). SJW contains more than two dozen bioactive constituents and, in most of the reported works, the ability of SJW to modulate P-gp has been mainly attributed to hyperforin, another major constituent of the herbal extract (Tian et al. 2005). Therefore, the present work aimed to elucidate the capacity of HYP to induce both P-gp expression and activity in Caco-2 cells, and to correlate those effects with a potential protective effect against the toxicity of a known toxic P-gp substrate, the herbicide paraquat (PQ). For that purpose, different experimental designs of incubation with both xenobiotic and potential inducer were tested, including (1) pre-incubation with HYP for 24, 48 or 72 h, followed by PQ incubation for 24 h; (2) HYP incubation 6 h after the beginning of PQ exposure (total PQ incubation time of 24 h); and (3) simultaneous incubation to HYP and PQ for 24 h. With the first experimental design we aimed to directly correlate the observed increases in P-gp expression and activity with a potential protective effect against PQ-induced toxicity. Using the second experimental design we aimed to mimic a real-life intoxication scenario, where the antidote contacts with the target cells well after the intoxicant insult. Finally, using the third experimental design, and by simultaneously incubating PQ with the tested inducer, we sought to

investigate the usefulness of the presence of the potential antidote in the toxic PQ formulation. Such strategy of adding the potential antidote to the toxic PQ formulation was already reported in several *in vivo* studies (Baltazar et al. 2013; Wilks et al. 2008).

Furthermore, studies with Caco-2 cells nuclear proteins separated by a liquid chromatography/SDS-PAGE electrophoresis approach and identified by MALDI-TOF/TOF analysis, demonstrated that nuclease-sensitive element-binding protein 1 (YB -1) was differently expressed after exposure to 10 μM HYP for 72 h relative to control cells (*unpublished data*). YB-1 is gene regulatory protein and a number of studies have linked its expression or its nuclear localization with an increase in *MDR1* gene expression (Bargou et al. 1997; Oda et al. 2003; Ohga et al. 1998; Saji et al. 2003). Therefore, we finally sough to evaluate changes in YB-1 nuclear expression using western blot analysis, and to correlate HYP-induced P-gp expression with the YB-1 nuclear contents.

2. MATERIALS AND METHODS

2.1. Materials

All reagents used in this study were of analytical grade or of the highest grade available. Reagents used in cell culture, including Dulbecco's Modified Eagle's Medium (DMEM) with 4.5 g/L glucose and GlutaMAX™, non-essential amino acids (NEAA), heat inactivated fetal bovine serum (FBS), 0.25% trypsin/1 mM EDTA, antibiotic (10000 U/mL penicillin, 10000 µg/mL streptomycin), fungizone (250 µg/mL amphotericin B), human transferrin (4 mg/mL) and phosphate-buffered saline solution (PBS) were purchased from Gibco Laboratories (Lenexa, KS, USA). Paraquat (PQ), bovine serum albumin (BSA), neutral red (NR) solution, ethyl alcohol absolute, acetic acid, cyclosporine A, rhodamine 123 (RHO 123), Triton X-100, β-nicotinamide adenine dinucleotide reduced form (β-NADH), pyruvic acid, adenosine-5′-triphosphate (ATP), d-luciferin sodium salt, luciferase, glycine, Tris-HCl, Tris-base, SDS, glycerol and NP-40 were obtained from Sigma Aldrich (St. Louis, MO, USA). Ethylenediamine tetraacetic acid (EDTA), KH_2PO4, $K_2HPO_4.3H_2O$, $HClO_4$, NaOH and $KHCO_3$ were obtained from Merck (Darmstadt, Germany). P-glycoprotein monoclonal antibody (clone UIC2) conjugated with fluorescein isothiocyanate (FITC) and rabbit monoclonal anti-YB-1 antibody were purchased from Abcam (Cambridge, United Kingdom). IgG2a (negative mAb control to UIC2) conjugated with FITC was obtained from ImmunoTools GmbH, (Friesoythe, Germany). Monoclonal anti-human P-glycoprotein UIC2 antibody (IOTest® CD243) used in the P-gp inhibition studies was purchased from Beckman Coulter, Inc. (Fullerton, USA). Flow cytometry reagents (BD FacsFlow™ and Facs Clean™) were purchased from Becton, Dickinson and Company (San Jose, CA). Bio-Rad DC protein assay kit was purchased from Bio-Rad (Hercules, CA). Hypericin was purchased from Cymit Química (Barcelona, Spain). P-gp-Glo™ Assay Kit was purchased from Promega (Germany). Nitrocellulose membranes (Hybond ECL), anti-rabbit IgG-peroxidase polyclonal antibody, high-range rainbow molecular weight marker and ECL Plus chemiluminescence reagents were purchased from Amersham Pharmacia Biotech (Buckinghamshire, United Kingdom). All other chemicals were purchased from Sigma-Aldrich.

Caco-2 cells, derived from human colorectal adenocarcinoma, were obtained from the American Type Culture Collection (ATCC; Manassas, VA, USA).

2.2. Caco-2 cell culture

Caco-2 cells were routinely cultured in 75 cm^2 flasks using DMEM with 4,5 g/L glucose and GlutaMAX™, supplemented with 10% heat inactivated FBS, 100 µM NEAA, 100 U/mL penicillin, 100 µg/mL streptomycin, 2.5 µg/ml amphotericin B and 6 µg/mL

transferrin. Cells were maintained in a 5% CO_2–95% air atmosphere, at 37 ºC, and the medium was changed every 2 days. Cultures were passaged weekly by trypsinization (0.25% trypsin/1 mM EDTA). The cells used in all the experiments were taken between the 58th and 63th passages. In all experiments, the cells were seeded at the density of 60,000 cells/cm^2, and used 4 days after seeding, when confluence was reached.

2.3. Hypericin cytotoxicity assays

Hypericin (0 - 100 μM) cytotoxicity was evaluated at different time points (6, 24, 48, 72 and 96 h) by the neutral red (NR) uptake assay and by the lactate dehydrogenase (LDH) leakage assay.

2.3.1. Neutral red uptake assay

The NR uptake assay is based on the ability of viable cells to incorporate and bind the supravital dye neutral red in the lysosomes. The assay was performed as previously described with minor modifications (Vilas-Boas et al. 2013b). Briefly, the cells were seeded onto 96-well plates at a density of 60,000 cells/cm^2, and exposed, after reaching confluence, to HYP (0 - 100 μM) in fresh cell culture medium, for 6, 24, 48, 72 and 96 h. At the selected time-points the cells were incubated with NR (50 μg/mL in cell culture medium) at 37 °C, in a humidified, 5% CO_2-95% air atmosphere, for 90 min. After this incubation period, the cell culture medium was removed, the dye absorbed only by viable cells extracted (using ethyl alcohol /distilled water (1:1) with 5% acetic acid), and the absorbance measured at 540 nm in a multi-well plate reader (PowerWave X, Bio-Tek Instruments, Vermont, USA). The percentage of NR uptake relative to that of the control cells (0 μM HYP) was used as the cytotoxicity measure. Results are presented as mean ± SEM from 6 independent experiments (performed in triplicate).

2.3.2. LDH leakage assay

LDH leakage assay is based on the measurement of the cellular leakage of the cytosolic enzyme LDH. The intracellular LDH release into the cell culture medium is an indicator of irreversible cell death due to cell membrane damage. LDH activity was determined as previously described (Barbosa et al. 2013; Pontes et al. 2008), with minor modifications. Briefly, the cells were seeded onto 96-well plates, at a density of 60,000 cells/cm^2 and exposed, after reaching confluence, to HYP (0 - 100 μM) in fresh cell culture medium, for 6, 24, 48, 72 and 96 h. At each time-point, 50 μL of cell culture medium from each well were transferred to a new 96-well plate (to measure extracellular LDH), in duplicate, after which triton X-100 5% (v/v) (final concentration of 0.5%) was added to the

cells (to lyse all cells) and the plates were incubated again for 30 min, at 37 ºC, in a humidified 5% CO_2-95% air atmosphere. After this incubation period, 25 µL of medium from each well were transferred again to a new 96-well plate (to measure the LDH after the full kill), also in duplicate. LDH activity was determined spectrophotometrically by following the rate of oxidation of NADH to nicotinamide adenine dinucleotide oxidized form (NAD^+), at 340 nm. Thus, in the 96-well plates, the collected medium fractions were mixed with 200 µL of reagent solution containing 0.21 mM NADH, dissolved in LDH buffer (33.3 mM KH_2PO_4 and 66.7 mM $K_2HPO_4.3H_2O$, pH 7.4). The reaction was started with 25 µL sodium pyruvate (22.7 mM, prepared in LDH buffer) and the kinetic formation of NAD^+ from NADH was followed for 5 min, at 340 nm, in a 96-well plate reader (PowerWave X, Bio-Tek Instruments). To measure LDH after the full kill, 25 µL of LDH buffer were added to each well before sodium pyruvate addition to complete the 275 µL final volume of reaction. Extracellular LDH, from 6 independent experiments (each experiment performed in triplicate), is expressed as percentage of total LDH (Mean ± SEM), considering total LDH = extracellular LDH + LDH released from full kill.

2.4. P-glycoprotein expression

The *in vitro* evaluation of P-gp expression was performed as previously described (Silva et al. 2011; Silva et al. 2013a; Silva et al. 2013c). Briefly, the cells were seeded onto 24-well plates, at a density of 60,000 cells/cm^2. After reaching confluence, the cells were exposed to HYP (0 - 10 µM), in fresh cell culture medium, for 24, 48, and 72 h. After each incubation period, the cells were washed twice with PBS and harvested by trypsinization (0.25% trypsin/1mM EDTA) to obtain a cell suspension. The cells were then centrifuged (300 *g*, for 10 min, at 4ºC) and resuspended in PBS buffer (pH 7.4) containing 10% heat inactivated FBS and P-gp antibody [UIC2] conjugated with FITC. The antibody dilution used in this experiment was applied according to the manufacturer's instructions for flow cytometry. Mouse IgG2a_FITC was used as an isotype-matched negative control to estimate non-specific binding of the FITC-labelled anti-P-glycoprotein antibody [UIC2]. The cells were then incubated for 30 min, at 37 °C, in the dark. After this incubation period, the cells were washed twice with PBS buffer (pH 7.4) containing 10% heat inactivated FBS, centrifuged (300 *g*, for 10 min, at 4ºC), resuspended in ice-cold PBS and kept on ice until flow cytometry analysis. Fluorescence measurements of isolated cells were performed with a flow cytometer (FACSCalibur, Becton-Dickinson Biosciences). The green fluorescence of FITC-UIC2 antibody was measured by a 530 ± 15 nm band-pass filter (FL1). Acquisition of data for 15,000 cells was gated to include viable cells on the basis of their forward and side light scatters and the propidium iodide (4 µg/mL)

incorporation (propidium iodide interlaces with a nucleic acid helix with a resultant increase in fluorescence intensity emission at 615 nm). Logarithmic fluorescence intensity was recorded and displayed as a single parameter histogram. The geometric mean of fluorescence intensity (GeoMean) for 15,000 cells was the parameter used for comparison (calculated as percentage of control). Non labelled cells (with or without hypericin) were analysed in each experiment by a 530 ± 15 nm band-pass filter (FL1) in order to detect a possible contribution from cells autofluorescence to the analysed fluorescence signals. Results are expressed as mean ± SEM from 4 independent experiments (performed in triplicate).

2.5. P-glycoprotein transport activity – RHO 123 efflux assay

The P-gp transport activity was evaluated by flow cytometry using 1 μM RHO 123 as a P-gp fluorescent substrate, as previously described (Silva et al. 2013a). In this assay, the evaluation of P-gp transport activity consisted of two phases: (i) an inhibited accumulation phase (IA), in which P-gp activity was inhibited with 10 μM cyclosporine A, in order to accumulate the fluorescent substrate inside the cells; and (ii) an efflux phase, where the energy-dependent P-gp function was re-established by removing the P-gp inhibitor (cyclosporine A) and adding an energy source (DMEM supplemented with 4.5 g/mol glucose). Briefly, Caco-2 cells were seeded onto 12-well plates, at a density of 60,000 cells/cm^2. After reaching confluence, the cells were exposed to HYP (0 - 10 μM), in fresh cell culture medium, for 24, 48 and 72 h. At each time point, the cells were washed twice with PBS and harvested by trypsinization (0.25% trypsin /1mM EDTA) to obtain a cell suspension. The cells were then centrifuged (300 *g*, for 10 min, at 4ºC), suspended in PBS buffer (pH 7.4) containing 10 μM cyclosporine A and 1μM RHO 123, and incubated at 37 ºC, for 30 min. After the accumulation of the fluorescent substrate (IA phase), the cells were washed twice with ice-cold PBS with 10% heat inactivated FBS, and divided into two aliquots. The first aliquot was centrifuged (300 *g*, for 10 min, at 4ºC) and kept on ice until analysis by flow cytometry, and corresponds to the cells submitted only to an IA phase. The second aliquot was submitted to an efflux phase performed under normal conditions (inhibited RHO 123 accumulation followed by RHO 123 efflux in the absence of P-gp inhibitor - IAE). For the efflux phase the cells were centrifuged (300 *g*, for 10 min, at 4ºC), resuspended in DMEM medium containing 4.5 g/L glucose and incubated, for 45 min, at 37°C. After this efflux period, the cells were washed twice with ice-cold PBS with 10% FBS and suspended in ice-cold PBS immediately before analysis. The fluorescence measurements of isolated cells were performed as described in section 2.4 (Evaluation of P-gp expression). The green intracellular fluorescence of RHO 123 was measured by a

530 ± 15 nm band-pass filter (FL1). The percentage of RHO 123 that was pumped out of the cells during the efflux phase was calculated according to Equation 1, and the results expressed as percentage of control values (Mean ± SEM). When P-gp activity increases, the amount of RHO 123 effluxed from the cells will be higher and accompanied by a decrease in the fluorescence intensity due to the corresponding decrease in intracellular RHO 123 (decrease in GeoMean IAE). Five independent experiments were performed (run in triplicate).

$$\%\ pumped\ RHO\ 123 = \frac{GeoMean\ accumulated\ RHO\ 123(IA) - GeoMean\ remaining\ RHO\ 123\ (IAE)}{GeoMean\ accumulated\ RHO\ 123\ (IA)}\ X\ 100$$

Equation 1: Percentage of RHO 123 pumped during the efflux phase.

2.6. Evaluation of P-glycoprotein ATPase activity

P-gp ATPase activity was evaluated using the luminescent ATP detection kit (P-gp-Glo™ Assay Kit, Promega, Germany) according to the manufacturers' instructions. Briefly, HYP (1, 5 and 10 µM), 100 µM sodium vanadate (Na_3VO_4, selective P-gp inhibitor used as positive control for P-gp ATPase activity inhibition) or 200 µM verapamil (P-gp substrate that stimulates P-gp ATPase activity used as positive control for stimulation of P-gp ATPase activity) in buffer solution were incubated with 25 µg of human P-gp-enriched membranes and 5 mM MgATP, at 37 ºC, for exactly 40 min. Untreated control reactions (NT) were also performed in the absence of drug. The remaining ATP was detected, as a luciferase-generated luminescent signal, 20 minutes after resting at room temperature to allow luminescent signal to develop. Accordingly, P-gp-dependent decreases in luminescence reflect ATP consumption by the pump, meaning that the greater the decrease in signal, the higher is the P-gp ATPase activity. The difference between the average relative light units (RLU) from Na_3VO_4-treated samples (RLU Na_3VO_4) and untreated (NT) samples (RLU NT) were calculated to determine ΔRLU basal, which reflects basal P-gp ATPase activity. The difference between the average luminescent signals from Na_3VO_4-treated samples (RLU Na_3VO_4) and test compound-treated samples (RLU TC) were also calculated to determine ΔRLU that reflects P-gp ATPase activity in the presence of the tested compounds (HYP and verapamil). Results are presented as mean ± SEM from three independent experiments. By comparing basal P-gp ATPase activity to the test compound-treated ATPase activities, the compounds can be ranked as stimulating, inhibiting or having no effect on basal P-gp ATPase activity. Accordingly, compounds that act as P-gp substrates typically stimulate its ATPase activity (Ambudkar et al. 1999).

2.7. ATP quantification assay

ATP intracellular levels were determined at two different time-points: immediately after exposure to HYP and after submitting the cells to an IAE protocol. Briefly, the cells were seeded onto 48-well plates, at a density of 60,000 cells/cm^2 and exposed, after reaching confluence, to HYP (1, 5 and 10 μM) for 24, 48 and 72 h. At each time-point, the cells were washed twice with PBS and harvested by trypsinization (0.25% trypsin /1mM EDTA) to obtain a cell suspension. The cells were then divided into two aliquots. The cells in the first aliquot were centrifuged (300 *g* for 10 min, at 4ºC), resuspended in $HClO_4$ 5% and frozen at -80 ºC until ATP determination. The cells in the second aliquot were also centrifuged (300 g for 10 min, at 4ºC), the cell culture medium was removed, and the cells were then submitted to an IAE protocol, as described in section 2.5. After the efflux phase, the cells were washed with PBS, centrifuged (300 *g* for 10 min, at 4ºC), resuspended in $HClO_4$ 5% and frozen at -80 ºC until ATP determination. Cellular ATP levels were evaluated through a luciferase-based bioluminescent technique, as previously described (Pontes et al. 2008; Vilas-Boas et al. 2013a). Briefly, samples in 5% $HClO_4$ were centrifuged (16,000 g for 10 min, at 4 ºC), the supernatant was collected and the cell pellet was dissolved in NaOH 0.3 M and used for protein quantification. The supernatant was then neutralized with equal volume of $KHCO_3$ 0.76 M. After centrifugation (16,000g for 2 min, at 4 °C), 100 μL of the neutralized supernatants were transferred to a 96-well plate, in duplicate, and 100 μL of luciferin–luciferase assay solution [0.15 mM luciferin, 300,000 light units of luciferase from *Photinus pyralis* (American firefly), 50 mM glycine, 10 mM $MgSO_4$, 1 mM Tris, 0.55 mM EDTA, 1% BSA (pH 7.6)] were added. ATP calibration curves were routinely performed (ATP standard stocks in 5% $HClO_4$ were kept at −80 °C until the assay). Sample ATP levels are proportional to the intensity of the light emitted by luciferine, in a reaction catalyzed by luciferase, which was measured using a 96-well Microplate Luminometer (BioTek Instruments, Vermont, USA). ATP intracellular levels were normalized to the total protein content and the final results, from 4 independent experiments (each experiment was performed in triplicate), are expressed as percentage of control (Mean ± SEM).

2.8. Paraquat cytotoxicity assays

Paraquat cytotoxicity was evaluated in Caco-2 cells by the NR uptake assay, with or without incubation with HYP (1, 5 and 10 μM). For that purpose, and as previously mentioned, three different experimental designs of HYP incubation were performed: (1) pre-incubation with HYP for 24, 48 or 72 h, followed by PQ incubation for 24 h; (2) HYP

incubation 6 h after the beginning of PQ exposure (total PQ incubation time of 24 h); and (3) simultaneous incubation to HYP and PQ for 24 h.

2.8.1. Pre-exposure to HYP

The cells were seeded onto 96-well plates and exposed, after reaching confluence, to HYP (1, 5 and 10 μM) for 24, 48 and 72 h. This pre-incubation protocol minimizes the contribution of effects other than P-gp induction in the observed cytotoxicity, since the inducer is removed before PQ incubation. After this incubation period, the cells were washed twice with PBS buffer (pH 7.4) and exposed to PQ (0 - 5,000 μM) in fresh cell culture medium for 24 h. Cytotoxicity was evaluated by the NR uptake assay, as previously described (section 2.3.1). Results are presented as mean ± SEM from at least 4 independent experiments (performed in triplicate).

To confirm the involvement of P-gp on the HYP protective effects, for the highest pre-incubation period (72 h), these assays were repeated in the presence of a specific P-gp inhibitor (20 μL of the UIC2 antibody stock solution for 500,000 cells, according to the manufacturer instructions, added 30 min before PQ). Results are presented as mean ± SEM from at least 3 independent experiments (performed in triplicate).

2.8.2. Exposure to HYP 6 h after PQ

The cells were seeded onto 96-well plates and exposed, after reaching confluence, to PQ (0 - 5,000 μM) in fresh cell culture medium. Six hours after the beginning of PQ incubation [based on the estimated mean time of arrival at the emergency department of intoxicated patients, and on the absorption rate of PQ in humans (Dinis-Oliveira et al. 2008)], HYP was added to obtain the final concentrations of 0, 1, 5 and 10 μM. Cytotoxicity was evaluated 24 h after PQ exposure (corresponding to an 18 h incubation period with HYP, and a total 24h incubation period for PQ) by the NR uptake assay, as previously described in section 2.3.1. For the highest tested HYP concentration (10 μM), these incubations were also repeated in the presence of a specific P-gp inhibitor (UIC2 antibody), to evaluate P-gp involvement in the HYP protective effects (20 μL of the UIC2 antibody stock solution for 500,000 cells, according to the manufacturer instructions, added 30 min before HYP). Results are presented as mean ± SEM [from 5 independent experiments (performed in triplicate) in the studies without the P-gp inhibitor, and from 4 independent experiments (performed in duplicate) in the studies performed with the UIC2 antibody].

2.8.3. Simultaneous exposure to HYP and PQ

The cells were seeded onto 96-well plates and exposed, after reaching confluence, to PQ (0 - 5,000 μM), in fresh cell culture medium, with or without simultaneous exposure to HYP (1, 5 and 10 μM). This exposure protocol mimics the presence of a potential antidote in the toxic formulation. In such cases, it is anticipated that the enterocytes will come into contact with both the inducer and PQ simultaneously. Cytotoxicity was evaluated 24 h after exposure by the NR uptake assay, as previously described in section 2.3.1. As previously, for 10 μM HYP, these incubations were repeated in the presence of a specific P-gp inhibitor, the UIC2 antibody (added 30 min before PQ + HYP exposure). Results are presented as mean ± SEM [from 3 independent experiments (performed in triplicate) in the studies without the P-gp inhibitor, and from 4 independent experiments (performed in duplicate) in the studies performed with the UIC2 antibody].

2.9. Western blotting analysis of YB-1

To evaluate the nuclear expression of the YB-1 protein, western blot analysis was performed in nuclear extracts of Caco-2, with or without previous exposure to 10 μM HYP. Briefly, Caco-2 cells were seeded onto 75 cm^2 flasks, at a density of 60,000 cells/cm^2, and exposed, after reaching confluence, to HYP (0 and 10 μM) in fresh cell culture medium for 72 h. At the end of the experiment, the cells were washed twice with PBS buffer (pH 7.4), harvested by trypsinization (0.25% trypsin /1mM EDTA) to obtain a cell suspension and then the nuclear proteins were extracted.

For nuclear proteins extraction, Caco-2 cells were washed twice with PBS and centrifuged (300 g for 10 min, at 4 °C). The cell pellet was resuspended in NP-40 buffer (0.01 M Tris-HCl, 0.01 M NaCl, 0.003 M $MgCl_2$, 0.03 M sucrose and 0.5% NP-40, pH 7.0) and again centrifuged (1500 g for 10 min, at 4ºC). The supernatant was removed and the pellet resuspended again in NP-40 buffer. After centrifugation (1500 g for 10 min, at 4 ºC), the supernatant was removed and the pellet resuspended in $CaCl_2$ buffer (0.01 M Tris-HCl, 0.01 M NaCl, 0.003 M $MgCl_2$, 0.03 M sucrose and 0.1 mM $CaCl_2$, pH 7.0). After centrifugation (1500 g for 10 min, at 4 ºC) this last step was repeated. Finally, a last centrifugation step (1500 g for 10 min, at 4 ºC) was performed, the supernatant removed and the pellet containing the nuclear proteins was used for western blot analysis.

The pellets containing the nuclear proteins were resuspended in $CaCl_2$ buffer and the protein concentration determined using the Bio-Rad DC protein assay kit. Samples were then diluted to equal protein concentration, and 50 μL were added with 25 μL sodium dodecyl sulfate (SDS)-PAGE reducing buffer [4 % SDS (w/v), 87.5 mM Tris base (pH 6.8), 22.5 % glycerol (v/v), 1 % bromophenol blue (w/v) and 20 % β-mercaptoethanol

(v/v)]. Sixty micrograms of protein were loaded and separated on 12.5 % SDS/polyacrylamide gels, at a constant voltage of 150 mV, using a running buffer [25 mM Tris Base, 192 mM glycine and 0.1 % SDS (w/v), pH 8.6]. Gels were allowed to equilibrate in transfer buffer [20 % methanol (v/v) in 25 mM Tris Base and 192 mM glycine, pH 8.3], and then transferred to nitrocellulose membranes (Hybond ECL, Amersham Pharmacia Biotech), at a constant current of 200 mA, for 2.5 h, in a Bio-Rad semidry transfer apparatus (Bio-Rad Laboratories), according to the manufacturer's protocol. Then, the membranes were rinsed in Tris-buffered saline solution (TBS: 20 mM Tris base and 300 mM NaCl, pH 8.0). To verify an equal amount of sample loading, membranes containing the transferred proteins were reversibly stained with Ponceau S. After rinsing the membranes with TBS to the complete removal of Ponceau S, non-specific sites were blocked, overnight, in blocking buffer [5% nonfat powdered skim milk (w/v) in Tris-buffered saline solution with 0.05% Tween 20 (v/v) (TBS-T)], at 4 ºC. Membranes were then incubated with primary antibody, rabbit monoclonal anti-YB-1 antibody (1:500), overnight, at 4 ºC. After incubation with the primary antibody, membranes were washed 3 times (10 min each wash) with TBS-T and incubated with the secondary antibody [anti-rabbit IgG-peroxidase polyclonal antibody (1:2,000)], for 2 h, at room temperature. All antibodies were diluted in blocking buffer. Following 3 washes in TBS-T (10 min each wash), the immunoblots were incubated with ECL Plus chemiluminescence reagents (Amersham Pharmacia Biotech), according to the supplier`s instructions, and exposed between 10 and 120 s on a Molecular Imager ChemiDoc^{TM} XRS^{+} System (Bio-Rad Laboratories). ECL images were taken using the Chemi Hi resolution application of the software Image Lab^{TM} (Bio-Rad Laboratories) and the YB-1 bands quantified. Final results, from 4 independent experiments, are expressed as fold change over control (0 µM HYP) (Mean ± SEM).

2.10. Protein quantification

The protein concentration in the samples used for ATP quantification and for YB-1 analysis was determined using the Bio-Rad DC protein assay kit, according to the manufacturer's instructions. Bovine serum albumin (BSA) was used as protein standard.

2.11. Statistical analysis

All statistical analyses were performed with the GraphPad Prism version 6.00 for Windows (GraphPad Software, San Diego, California, USA). Normality of the data distribution was assessed by three different tests: Kolmogorov–Smirnov normality test, D'Agostino & Pearson omnibus normality test and Shapiro-Wilk normality test. For data with a parametric distribution, statistical comparisons were made using the parametric

method of One-way ANOVA, followed by the Bonferroni's multiple comparisons *post hoc* test. For data with a nonparametric distribution, statistical comparisons were estimated using the nonparametric method of Kruskal–Wallis (one-way ANOVA on ranks), followed by Dunn's *post hoc* test. In experiments with two variables, statistical comparisons between groups were estimated using Two-way ANOVA, followed by the Sidak's multiple comparisons *post hoc* test. In the PQ cytotoxicity assays, the PQ concentration-response curves were fitted using the least squares as the fitting method and the comparisons between the curves (LOG EC_{50}, TOP, BOTTOM and Hill slope) were made using the extra sum-of-squares F test. Optical densities of YB-1 bands were exported from Image Lab™ to GraphPad Prism™, expressed as fold change over control and the statistical comparison was estimated using the Unpaired Student *t* test. Details of the performed statistical analysis are described in each figure legend. In all cases, *p* values lower than 0.05 were considered significant.

3. RESULTS

3.1. Hypericin cytotoxicity assays

Prior to the evaluation of the HYP effect on P-gp expression and activity, its cytotoxicity was determined, at different concentrations (0-100 μM) and times of exposure (6 - 96 h), by the NR uptake and LDH leakage assays, to establish the concentration range and time of exposure that would not cause significant cell death.

As shown in Figure S1A (supplementary data), no significant toxicity was observed up to 72 h of incubation, for all the tested concentrations. However, 96 h after exposure a slight but significant effect on NR uptake was observed for the highest concentrations tested (81.1 and 79.9 % for 50 and 100 μM HYP, respectively) As shown in Figure S1B (supplementary data), no significant increases in the extracellular LDH were observed up to 96 h of incubation. Thus, according to the obtained results, HYP, at the tested concentration range (0 - 100 μM), is innocuous to Caco-2 cells up to 72 h of incubation.

3.2. P-glycoprotein Expression

HYP (0 - 10 μM) effect on P-gp expression was evaluated, by flow cytometry, 24, 48 and 72 h after exposure, using a P-gp monoclonal antibody [UIC2] conjugated with FITC. Nonspecific binding of the FITC-labeled-anti-P-glycoprotein antibody [UIC2] was not observed, as estimated by the fluorescence obtained with the isotype-matched negative control (data not shown).

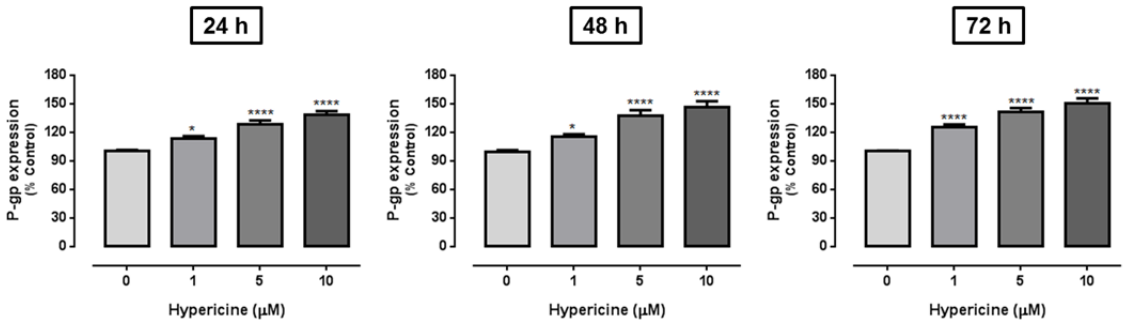

Figure 1. P-glycoprotein expression levels in Caco-2 cells exposed to hypericin (HYP) (0 - 10 μM) for 24, 48 and 72 h. Results are presented as mean ± SEM from 4 independent experiments (performed in triplicate). Statistical comparisons were made using one-way ANOVA, followed by the Bonferroni's multiple comparisons *post hoc test* [*p<0.05; ****p<0.0001 concentration *vs*. control (0 μM)].

As shown in Figure 1, HYP significantly increased P-gp expression according with the concentration and time of exposure tested. In fact, 24 h after exposure to 1, 5 and 10 μM HYP, the protein expression significantly increased to 113.8, 128.3 and 138.3 %, respectively, when compared to control (0 μM). Increasing the exposure time to 48 h, the observed significant increases in P-gp expression were more accentuated (115.7, 137.9

and 146.9 % for 1, 5 and 10 μM HYP, respectively). Finally, for the highest incubation time tested (72 h), the highest increase in the protein expression was observed for all the tested concentrations (125.4, 142.0 and 151.0 % for 1, 5 and 10 μM HYP, respectively).

3.3. P-glycoprotein Activity

P-gp transport activity was studied by flow cytometry, using 1 μM RHO 123 as a P-gp fluorescent substrate and 10 μM cyclosporine A as a P-gp inhibitor. No cytotoxic effects were observed for RHO 123 and cyclosporine A at these concentrations, after 30 min of incubation (data not shown). As shown in Figure 2, and similar to what occurred with P-gp expression, HYP also significantly increased the pump activity according with the concentration and time of exposure tested. After 24 h of exposure, P-gp-mediated RHO 123 efflux significantly increased to 116.5, 117.9 and 128.6 % for 1, 5 and 10 μM HYP, respectively. Increasing HYP exposure time to 48 h, the pump function significantly increased to 119.6, 121.8 and 142.3 %, for 1, 5 and 10 μM HYP, respectively. The highest increase in the pump activity was observed for the highest exposure time tested (119.0, 129.4 and 150.5 % after 72 h of exposure to 1, 5 and 10 μM HYP, respectively).

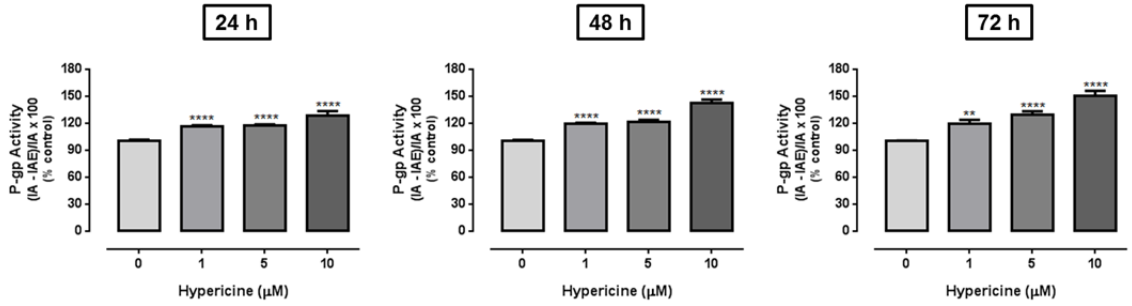

Figure 2. P-glycoprotein activity in Caco-2 cells exposed to hypericin (HYP) (0 - 10 μM) for 24, 48 and 72 h, evaluated through the RHO 123 efflux assay. Results are presented as mean ± SEM from 5 independent experiments (performed in triplicate). Statistical comparisons were made using one-way ANOVA, followed by the Bonferroni's multiple comparisons *post hoc test* [**p<0.01; ****p<0.0001 concentration *vs*. control (0 μM)].

3.4. P-glycoprotein ATPase Activity

Using the Pgp-Glo™ assay kit it was observed that HYP significantly increased the pump ATPase activity (Figure 3), according to the tested concentration. In fact, the difference in luminescent signal between Na_3VO_4-treated samples and samples treated with 5 and 10 μM HYP significantly increased to $2.75x10^5$ and $3.27x10^5$ ΔRLU, respectively, when compared to $1.95x10^5$ ΔRLU for basal P-gp ATPase activity. Moreover, verapamil (used as positive control for P-gp activation) yielded the highest increase in P-gp ATPase activity (change in luminescence of $5.45x10^5$ ΔRLU). According to the obtained results, HYP is actively transported by the pump, resulting in an increased ATP

consumption. However, the ability of HYP to stimulate the P-gp ATPase activity is significantly smaller, when compared to verapamil-induced stimulation.

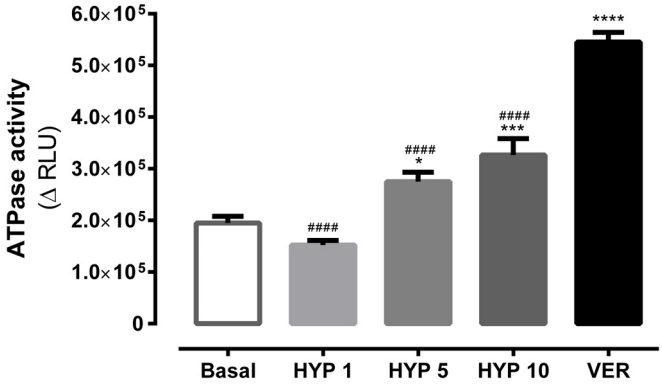

Figure 3. P-gp ATPase activity in recombinant human P-gp enriched membrane vesicles (25 µg/well) exposed to 1, 5, and 10 µM hypericin (HYP). Results are expressed as change in relative light units (ΔRLU ± SEM) between 100 µM sodium orthovanadate (Na_3VO_4)-treated membranes and membranes treated with HYP. Basal P-gp ATPase activity was defined as the ΔRLU between untreated samples (NT) and Na_3VO_4-treated samples. Verapamil (200 µM) was used as a positive control substrate (positive control for drug stimulation of P-gp ATPase activity). Three independent experiments were performed in duplicate. Statistical comparisons were made using one-way ANOVA, followed by the Bonferroni's multiple comparisons *post hoc test* (*p<0.05; ***p<0.001; ****p<0.0001 *vs*. basal ATPase activity; $^{\#\#\#\#}p$<0.0001 *vs.* verapamil).

3.5. ATP intracellular levels

In the present assay, ATP intracellular levels were quantified 24, 48 and 72 h after exposure to 1, 5 and 10 µM HYP, to evaluate if the compound could cause any change in the ATP content that could compromise the pump activity. In accordance with the cytotoxicity assays (Figure S1A and S1B, supplementary data), no significant differences were observed in the ATP intracellular levels, for all the tested concentrations and times of exposure (Figure S2A, supplementary data). Moreover, ATP intracellular content was also evaluated in cells exposed to 1, 5 and 10 µM HYP for 24, 48 and 72 h, which, after exposure, were submitted to a RHO 123 efflux assay. In spite of the previously observed significant increase in RHO 123 efflux (Figure 2), no significant energy depletion was detected, given the lack of significant differences in the intracellular ATP levels, at any of the tested concentrations and times of exposure (Figure S2B, supplementary data). Therefore, the ATP consumed in RHO 123 efflux was not sufficient to significantly reduce the ATP intracellular contents (Figure S2B, supplementary data).

3.6. Paraquat cytotoxicity assays

We evaluated the effect of HYP on PQ-induced cytotoxicity and correlated those effects with the observed increases in both P-gp expression and activity.

As shown in Figure 4, pre-exposure of Caco-2 cells to all the tested HYP concentrations (1, 5 or 10 µM) for 24 h, caused a significant protective effect against the PQ-induced cytotoxicity, as demonstrated by the significant rightwards shift of all the PQ + HYP curves relative to the PQ curve, resulting in significant differences in the cell death observed for

the higher PQ concentrations (1000 - 5000 µM). For 5 and 10 µM HYP, since the TOP values (maximal cell death) of the PQ + HYP curves were significantly different from the TOP value of the PQ curve (Table 1), this was the parameter used for comparison between the fitted curves. Pre-exposure to 5 and 10 µM HYP resulted in a significant decrease in the TOP value to 67.49 and 63.80 %, respectively, when compared to the TOP value of the PQ curve (92.46 %; Table 1). For 1 µM HYP, although the fitted curve is significantly different from the PQ curve, no significant differences were observed for the TOP and EC_{50} values (Table 1).

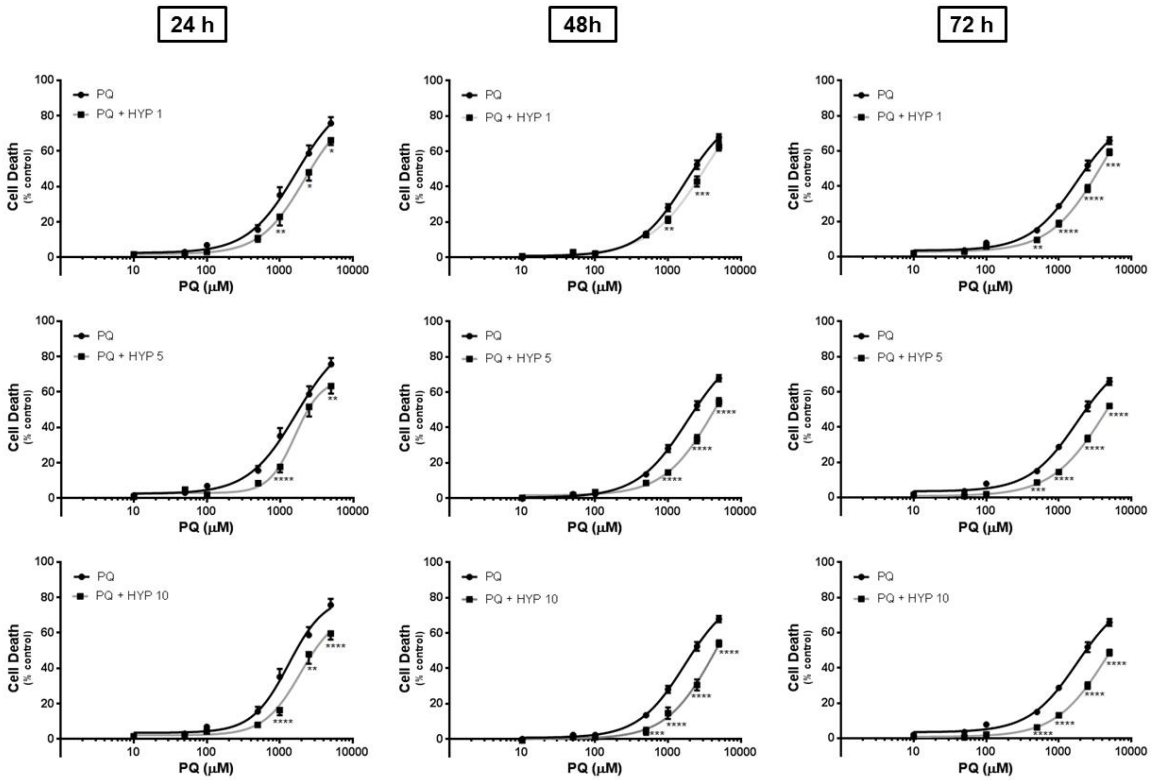

Figure 4. Paraquat concentration–response (cell death) curves with (PQ + HYP) or without (PQ) pre-exposure of Caco-2 cells to hypericin (HYP 1, 5 or 10 µM) for 24 h, 48 h and 72 h. Results are presented as mean ± SEM from 4 independent experiments (performed in triplicate). Concentration-response curves were fitted using least squares as the fitting method and the comparisons between the fitted curves (LOG EC_{50}, TOP, BOTTOM and Hill slope) were made using the extra sum-of-squares F test. Statistical comparisons were made using Two-way ANOVA, followed by the Sidak's multiple comparisons *post hoc* test (*p<0.05; **p<0.01; ***p<0.001; ****p<0.0001 *vs.* PQ alone). In all cases, p values lower than 0.05 were considered significant.

Increasing HYP pre-exposure time to 48 or 72 h, a similar protective effect against PQ toxicity was also observed for all the tested HYP concentrations (1, 5 or 10 µM). In fact, a significant rightwards shift of the PQ + HYP curves was observed, as a result of a significant decrease in the cell death observed for the higher PQ concentrations (500 - 5000 µM) (Figure 4). For these HYP pre-exposure times no significant differences were observed neither in the maximal cell death (TOP), nor in baseline (BOTTOM) of the fitted PQ + HYP curves, when compared to the PQ curve (Table 2 and Table 3). Therefore, the

EC_{50} value, which represents the half-maximum-effect concentration of the fitted curve, was used for comparison. As shown in Table 2, after 48 h, the observed rightwards shifts of the PQ + HYP concentration-response curves were accompanied by significant increases in the EC_{50} values, when compared to the EC_{50} of the PQ curve (3243, 4490 and 4493 μM for 1, 5 and 10 μM HYP, respectively, *vs.* 1692 μM for the PQ curve). Increasing HYP pre-exposure time to 72 h, a significant increase in the EC_{50} value of all the PQ + HYP curves was also observed, when compared to the EC_{50} of the PQ curve (3843, 4518 and 4609 μM for 1, 5 and 10 μM HYP, respectively, *vs.* 1783 μM for the PQ curve) (Table 3).

Table 1. EC_{50} (half-maximum-effect concentrations), TOP (maximal effect), BOTTOM (baseline) and Hill slope values of the PQ concentration-response curves, with (PQ + HYP) or without (PQ) pre-exposure to HYP (1, 5 or 10 μM) for 24 h.

	PQ	PQ + HYP 1	PQ + HYP 5	PQ + HYP 10
EC_{50} (μM)	**1656**	**2161**	**1599**	**1642**
TOP	92.46	85.62	67.49	63.80
BOTTOM	2.523	1.790	2.943	3,048
Hill slope	1.316	1.425	2.404	2.388
LOG EC_{50} *p* value (comparison between LOG EC_{50} values)	-	0.5585	0.9132	0.9791
TOP *p* value (comparison between TOP values)	-	0.7613	**0.0417**	**0.0255**
BOTTOM *p* value (comparison between BOTTOM values)	-	0.7762	0.8667	0.8309
Hill slope *p* value (comparison between Hill slope values)	-	0.8147	0.0552	0.0634
Curve *p* value (Comparison between the Fitted Curves)	-	**0.0002**	**< 0.0001**	**< 0.0001**

Concentration-response curves were fitted using least squares as the fitting method and the comparisons between PQ and PQ + HYP curves were made using extra sum-of-squares F test. In all cases, *p* values lower than 0.05 were considered significant.

Table 2. EC_{50} (half-maximum-effect concentrations), TOP (maximal effect), BOTTOM (baseline) and Hill slope values of the PQ concentration-response curves, with (PQ + HYP) or without (PQ) pre-exposure to HYP (1, 5 or 10 μM) for 48 h.

	PQ	PQ + HYP 1	PQ + HYP 5	PQ + HYP 10
EC_{50} (μM)	**1692**	**3243**	**4490**	**4493**
TOP	83.14	~ 100.0	~ 100.0	~ 100.0
BOTTOM	0.6605	1.007	1.365	0.004269
Hill slope	1.360	1.131	1.219	1.287
LOG EC_{50} *p* value (comparison between LOG EC_{50} values)	-	0.0482	**0.0042**	**0.0081**
TOP *p* value (comparison between TOP values)	-	0.2364	0.2839	0.3373
BOTTOM *p* value (comparison between BOTTOM values)	-	0.8145	0.6034	0.6926
Hill slope *p* value (comparison between Hill slope values)	-	0.2822	0.4711	0.7611
Curve *p* value (Comparison between the Fitted Curves)	-	**< 0.0001**	**< 0.0001**	**< 0.0001**

Concentration-response curves were fitted using least squares as the fitting method and the comparisons between PQ and PQ + HYP curves were made using extra sum-of-squares F test. In all cases, *p* values lower than 0.05 were considered significant.

Table 3. EC_{50} (half-maximum-effect concentrations), TOP (maximal effect), BOTTOM (baseline) and Hill slope values of the PQ concentration-response curves, with (PQ + HYP) or without (PQ) pre-exposure to HYP (1, 5 or 10 μM) for 72 h.

	PQ	PQ + HYP 1	PQ + HYP 5	PQ + HYP 10
EC_{50} (μM)	**1783**	**3843**	**4518**	**4609**
TOP	82.05	~ 100.0	97.60	91.87
BOTTOM	3.431	2.727	0.7430	0.7944
Hill slope	1.317	1.226	1.159	1.226
LOG EC_{50} *p* value (comparison between LOG EC_{50} values)	-	**0.0490**	**0.0398**	**0.0348**
TOP *p* value (comparison between TOP values)	-	0.3211	0.5589	0.7363
BOTTOM *p* value (comparison between BOTTOM values)	-	0.6048	0.0607	0.0630
Hill slope *p* value (comparison between Hill slope values)	-	0.6822	0.5904	0.7728
Curve *p* value (Comparison between the Fitted Curves)	-	**< 0.0001**	**< 0.0001**	**< 0.0001**

Concentration-response curves were fitted using least squares as the fitting method and the comparisons between PQ and PQ + HYP curves were made using extra sum-of-squares F test. In all cases, *p* values lower than 0.05 were considered significant.

To evaluate if the rightwards shifts and EC_{50} values increases observed for all HYP tested concentrations were due to the previously observed increase in P-gp expression and activity, the cells pre-exposed to HYP for 72 h were incubated with PQ in the presence of a specific P-gp inhibitor (UIC2 antibody). As shown in Figure 5A, a significant increase in the cell death was observed in the presence of the UIC2 antibody, resulting in a significant leftwards shift of the PQ + UIC2 curve, when compared to the PQ curve, thus confirming the involvement of P-gp on PQ-induced toxicity. Moreover, under P-gp inhibition, HYP protective effects were completely abolished, as observed by the lack of significant differences in the cell death observed for all the tested PQ concentrations (Figure 5B). Consequently, no significant differences were obtained neither in the overall comparison of the fitted curves, nor in the comparison of the individual curve parameters (LOG EC_{50}, TOP, BOTTOM and Hill slope) (Table 4).

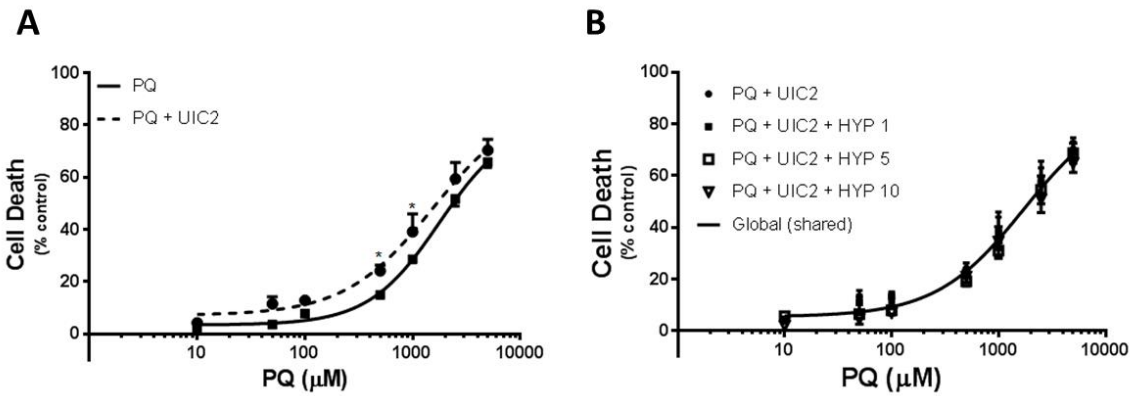

Figure 5. (A) Paraquat concentration–response (cell death) curves in the presence (PQ + UIC2) or in the absence (PQ) of a specific p-glycoprotein inhibitor (UIC2 antibody). **(B)** Paraquat concentration–response (cell death) curves, in the presence of a specific p-glycoprotein inhibitor (UIC2 antibody), with (PQ + UIC2 + HYP) or without (PQ + UIC2) pre-exposure of Caco-2 cells to hypericin (HYP 1, 5 or 10 μM) for 72 h. Results are presented as mean ± SEM from at least 3 independent experiments (performed in triplicate). Concentration–response curves were fitted using least squares as the fitting method and the comparisons between the fitted curves (LOG EC_{50}, TOP, BOTTOM and Hill slope) were made using the extra sum-of-squares F test. Statistical comparisons were made using Two-way ANOVA, followed by the Sidak's multiple comparisons *post hoc* test (**p*<0.05 *vs.* PQ alone). In all cases, *p* values lower than 0.05 were considered significant.

Additionally, the comparison between all the PQ + HYP curves highlighted significant differences in the observed protective effects according to the HYP concentration and time of pre-exposure tested (Figure S3, Figure S4, Table S1 and Table S2, supplementary data), which is correlated with the observed effect of HYP on both P-gp expression and activity.

Table 4. EC_{50} (half-maximum-effect concentrations), TOP (maximal effect), BOTTOM (baseline) and Hill slope values of the PQ concentration-response curves, in the presence of a specific P-gp inhibitor (UIC2 antibody), with (PQ + HYP) or without (PQ) pre-exposure to HYP (1, 5 or 10 μM) for 72 h.

	PQ + UIC2	PQ+ UIC2 + HYP 1	PQ+ UIC2 + HYP 5	PQ+ UIC2 + HYP 10
EC_{50} (μM)	**1529**	**1984**	**1780**	**1936**
TOP	88.78	96.59	85.58	91.66
BOTTOM	7.097	6.266	5.800	1.146
Hill slope	1.072	0.9474	1.282	0.8993
LOG EC_{50} *p* value (comparison between LOG EC_{50} values)	-	0.8355	0.8587	0.8391
TOP *p* value (comparison between TOP values)	-	0.8791	0.9209	0.9500
BOTTOM *p* value (comparison between BOTTOM values)	-	0.9033	0.8051	0.3447
Hill slope *p* value (comparison between Hill slope values)	-	0.8763	0.7642	0.8040
Curve *p* value (Comparison between the Fitted Curves)	-	0.9923	0.2846	0.1462

Concentration-response curves were fitted using least squares as the fitting method and the comparisons between PQ + UIC2 and PQ+ UIC2 + HYP curves were made using extra sum-of-squares F test. In all cases, *p* values lower than 0.05 were considered significant.

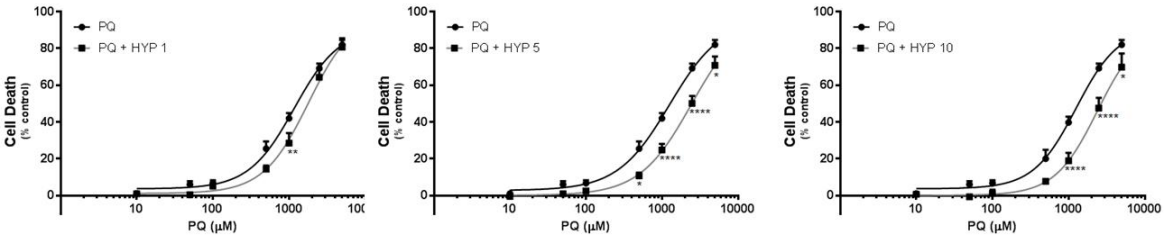

Figure 6. Paraquat concentration–response (cell death) curves with (PQ + HYP) or without (PQ) incubation of Caco-2 cells with hypericin (HYP 1, 5 or 10 μM) 6 h after the beginning of PQ exposure. Results are presented as mean ± SEM from 5 independent experiments (performed in triplicate). Concentration–response curves were fitted using least squares as the fitting method and the comparisons between the fitted curves (LOG EC_{50}, TOP, BOTTOM and Hill slope) were made using the extra sum-of-squares F test. Statistical comparisons were made using Two-way ANOVA, followed by the Sidak's multiple comparisons *post hoc* test (**p*<0.05; ***p*<0.01; *****p*<0.0001 *vs.* PQ alone).

Additionally, HYP effect on PQ-induced toxicity was also evaluated with HYP incubation 6 h after the beginning of PQ insult. As shown in Figure 6, a significant rightwards shift of the PQ + HYP curves was observed for all the HYP concentrations tested (1, 5 and 10 μM), when compared to the PQ curve (Figure 6), thus indicating a significant protection against PQ-induced toxicity. Additionally, this protective effect was significant for the higher PQ concentrations (500 - 5000 μM), as observed by the

significant decreases in the cell death observed (Figure 6). Moreover, for 5 and 10 μM HYP, it was observed a significant increase in the EC_{50} value of the fitted curves, when compared to the PQ curve (2408 and 2437 μM, respectively, *vs.* 1268 μM for the PQ curve) (Table 5).

To confirm the involvement of P-gp in the observed HYP protective effects, for the highest HYP concentration (10 μM), PQ cytotoxicity was further evaluated in the presence of the UIC2 antibody. As shown in Figure 7, a complete abolishment of HYP protective effect was observed in the presence of the P-gp inhibitor, since no significant differences were detected in the cell death observed for all the PQ concentrations tested. Moreover, no significant differences were obtained neither in the overall comparison of the fitted curves, nor in the comparison of the individual parameters (LOG EC_{50}, TOP, BOTTOM and Hill slope) (Table 6), confirming that the HYP protective effect against PQ-induced toxicity is P-gp-mediated.

Table 5. EC_{50} (half-maximum-effect concentrations), TOP (maximal effect), BOTTOM (baseline) and Hill slope values of the PQ concentration-response curves, with (PQ + HYP) or without (PQ) exposure to HYP (1, 5 or 10 μM) 6 h after the beginning of PQ exposure.

	PQ	PQ + HYP 1	PQ + HYP 5	PQ + HYP 10
EC_{50} (μM)	**1268**	**1622**	**2408**	**2437**
TOP	96.46	93.11	98.29	92.50
BOTTOM	2.721	1.678	0.1322	0.4915
Hill slope	1.259	1.788	1.285	1.549
LOG EC_{50} *p* value (comparison between LOG EC_{50} values)	-	0.3024	**0.0303**	**0.0158**
TOP *p* value (comparison between TOP values)	-	0.8291	0.9417	0.8803
BOTTOM *p* value (comparison between BOTTOM values)	-	0.7904	0.4446	0.5405
Hill slope *p* value (comparison between Hill slope values)	-	0.3842	0.9516	0.5741
Curve *p* value (Comparison between the Fitted Curves)	-	**0.0027**	**< 0.0001**	**< 0.0001**

Concentration-response curves were fitted using least squares as the fitting method and the comparisons between PQ and PQ + HYP curves were made using extra sum-of-squares F test. In all cases, *p* values lower than 0.05 were considered significant.

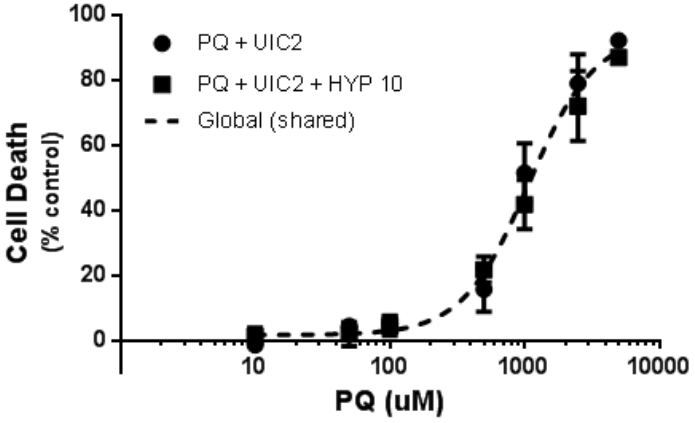

Figure 7. Paraquat concentration-response (cell death) curves, in the presence of a specific p-glycoprotein inhibitor (UIC2 antibody), with (PQ + UIC2 + HYP 10) or without (PQ + UIC2) incubation of Caco-2 cells with hypericin (HYP 10 μM) 6 h after the beginning of PQ exposure. Results are presented as mean ± SEM from 4 independent experiments (performed in duplicate). Concentration–response curves were fitted using least squares as the fitting method and the comparisons between the fitted curves (LOG EC_{50}, TOP, BOTTOM and Hill slope) were made using the extra sum-of-squares F test. Statistical comparisons were made using Two-way ANOVA, followed by the Sidak's multiple comparisons *post hoc* test.

Table 6. EC_{50} (half-maximum-effect concentrations), TOP (maximal effect), BOTTOM (baseline) and Hill slope values of the PQ concentration-response curves, with (PQ + UIC2 + HYP) or without (PQ + UIC2) incubation with HYP (10 μM) 6 h after the beginning of PQ exposure, and in the presence of a specific P-gp inhibitor (UIC2 antibody).

	PQ + UIC2	PQ + UIC2 + HYP 10
EC_{50} (μM)	**953.4**	**1288**
TOP	91.85	99.67
BOTTOM	1.885	1.243
Hill slope	2.322	1.407
LOG EC_{50} *p* value (comparison between LOG EC_{50} values)	-	0.3625
TOP *p* value (comparison between TOP values)	-	0.6644
BOTTOM *p* value (comparison between BOTTOM values)	-	0.9245
Hill slope *p* value (comparison between Hill slope values)	-	0.3484
Curve *p* value (Comparison between the Fitted Curves)	-	0.5915

Concentration-response curves were fitted using least squares as the fitting method and the comparisons between PQ + UIC2 and PQ + UIC2 + HYP 10 curves were made using extra sum-of-squares F test. In all cases, *p* values lower than 0.05 were considered significant.

To further support the potential use of HYP as an effective antidote against PQ intoxications, PQ cytotoxicity was also evaluated after simultaneous exposure to HYP (1, 5 and 10 μM). As shown in Figure 8, and for all the tested HYP concentrations, a significant reduction in the cell death was again observed for the higher PQ concentrations (500 - 5000 μM), resulting also in a significant rightwards shift of all the PQ + HYP curves, when compared to the PQ curve. Moreover, for 5 and 10 μM HYP, a significant increase in the EC_{50} values of the fitted curves was observed (2400 and 2469 μM, for 5 and 10 μM HYP, respectively, *vs.* 1240 μM for the PQ curve) (Table 7).

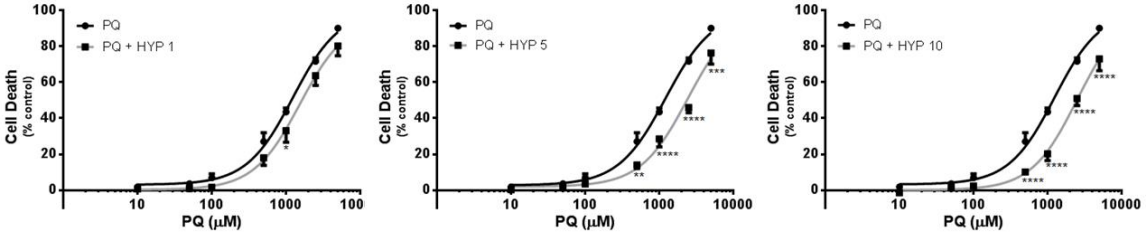

Figure 8. Paraquat concentration–response (cell death) curves with (PQ + HYP) or without (PQ) simultaneous exposure of Caco-2 cells to hypericin (HYP 1, 5 or 10 μM). Results are presented as mean ± SEM from 3 independent experiments (performed in triplicate). Concentration–response curves were fitted using least squares as the fitting method and the comparisons between the fitted curves (LOG EC_{50}, TOP, BOTTOM and Hill slope) were made using the extra sum-of-squares F test. Statistical comparisons were made using Two-way ANOVA, followed by the Sidak's multiple comparisons *post hoc* test (**p*<0.05; ***p*<0.01; ****p*<0.001; *****p*<0.0001 *vs.* PQ alone).

Table 7. EC_{50} (half-maximum-effect concentrations), TOP (maximal effect), BOTTOM (baseline) and Hill slope values of the PQ concentration-response curves, with (PQ + HYP) or without (PQ) simultaneous exposure to HYP (1, 5 or 10 μM).

	PQ	PQ + HYP 1	PQ + HYP 5	PQ + HYP 10
EC_{50} (μM)	**1240**	**1594**	**2400**	**2469**
TOP	~ 100.0	97.60	~ 100.0	99.48
BOTTOM	3.032	0.02581	1.128	0.2062
Hill slope	1.395	1.346	1.261	1.442
LOG EC_{50} *p* value (comparison between LOG EC_{50} values)	-	0.2799	**0.0003**	**0.0005**
TOP *p* value (comparison between TOP values)	-	0.8773	0.9991	0.9808
BOTTOM *p* value (comparison between BOTTOM values)	-	0.3060	0.4737	0.2626
Hill slope *p* value (comparison between Hill slope values)	-	0.8816	0.4033	0.8057
Curve *p* value (Comparison between the Fitted Curves)	-	**0.0003**	**< 0.0001**	**< 0.0001**

Concentration-response curves were fitted using least squares as the fitting method and the comparisons between PQ and PQ + HYP curves were made using extra sum-of-squares F test. In all cases, *p* values lower than 0.05 were considered significant.

Furthermore, the simultaneous incubation of PQ and 10 μM HYP in the presence of the UIC2 antibody resulted in the complete disappearance of HYP protective effect against PQ-induced toxicity, since no significant differences were detected neither in the cell death observed for all the PQ tested concentrations (Figure 9), nor in the overall comparison of the fitted curves (LOG EC_{50}, TOP, BOTTOM and Hill slope) (Table 8). Moreover, as observed in the pre-exposure assays, HYP incubation both simultaneously or 6 h after PQ exposure also demonstrated to differ according to the HYP concentration

tested, as evaluated by the significant differences in the cell death observed (Figure S5A, Figure S5B, Table S3 and Table S4, supplementary data). However, no significant differences exist between these two different experimental designs of HYP incubation, since no significant differences were observed in the fitted curves for all tested HYP concentrations (Figure S6, supplementary data). The slow PQ absorption rate reported in humans, which occurs over 1-6 h (Dinis-Oliveira et al. 2008), may explain the similar HYP protective effect observed under simultaneous exposure or 6 h after the beginning of PQ exposure.

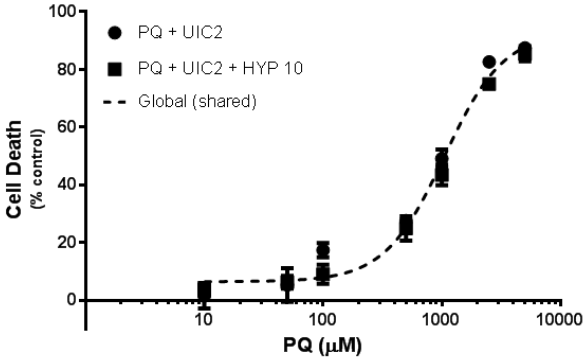

Figure 9. Paraquat concentration–response (cell death) curves, in the presence of a specific p-glycoprotein inhibitor (UIC2 antibody), with (PQ + UIC2 + HYP 10) or without (PQ + UIC2) simultaneous exposure of Caco-2 cells to hypericin (10 μM). Results are presented as mean ± SEM from 4 independent experiments (performed in duplicate). Concentration–response curves were fitted using least squares as the fitting method and the comparisons between the fitted curves (LOG EC_{50}, TOP, BOTTOM and Hill slope) were made using the extra sum-of-squares F test. Statistical comparisons were made using Two-way ANOVA, followed by the Sidak's multiple comparisons *post hoc* test.

Table 8. EC_{50} (half-maximum-effect concentrations), TOP (maximal effect), BOTTOM (baseline) and Hill slope values of the PQ concentration-response curves, with (PQ + UIC2 + HYP) or without (PQ + UIC2) simultaneous exposure to HYP (10 μM), and in the presence of a specific P-gp inhibitor (UIC2 antibody).

	PQ + UIC2	PQ + UIC2 + HYP 10
EC_{50} (μM)	**975.5**	**1168**
TOP	92.77	94.58
BOTTOM	7.640	5.568
Hill slope	1.873	1.555
LOG EC_{50} *p* value (comparison between LOG EC_{50} values)	-	0.2479
TOP *p* value (comparison between TOP values)	-	0.8202
BOTTOM *p* value (comparison between BOTTOM values)	-	0.5386
Hill slope *p* value (comparison between Hill slope values)	-	0.4731
Curve *p* value (Comparison between the Fitted Curves)	-	0.1254

Concentration-response curves were fitted using least squares as the fitting method and the comparisons between PQ + UIC2 and PQ+ UIC2 + HYP 10 curves were made using extra sum-of-squares F test. In all cases, *p* values lower than 0.05 were considered significant.

3.7. YB-1 nuclear levels

Nuclear levels of YB-1 were evaluated after exposure of Caco-2 cells to 10 μM HYP to evaluate the possible involvement of this transcription factor in HYP-mediated P-gp induction. Although the molecular mass calculated by the YB-1 amino acid sequence is about 35.9 kDa, during SDS gel electrophoresis YB-1 migrates as a protein with a mass of about 50 kDa (Eliseeva et al. 2011). As observed in Figure 10, a dramatic decrease in YB-1 nuclear levels was observed upon exposure to the tested compound for 72 h. In fact, after exposure to 10 μM HYP the nuclear levels of YB-1 were approximately 0.29 fold of control (0 μM HYP).

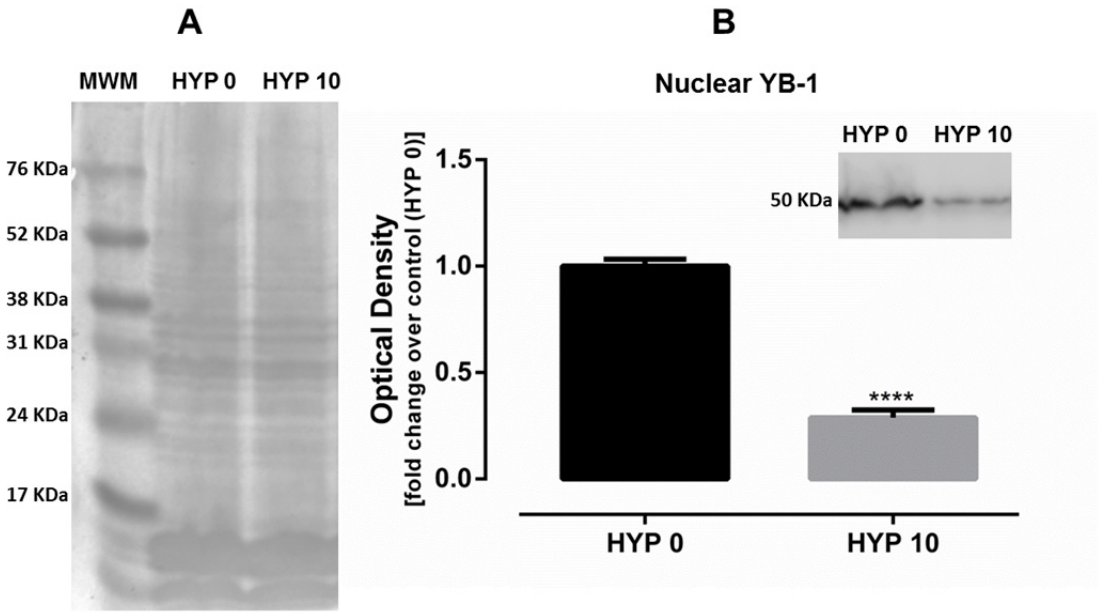

Figure 10. Hypericin effect on the nuclear YB-1 content. Caco-2 cells were exposed to 10 μM hypericin for 72 h and YB-1 nuclear expression was evaluated by western blot. **A:** Ponceau S staining of nuclear proteins showing equal protein loading. **B:** Representative Western blot from the YB-1 band and graphic representation of the effect of hypericin on the nuclear amount of YB-1. Results are presented as mean ± SEM from 4 independent experiments. Statistical comparisons were made using Unpaired Student *t* test ($^{****}p<0.0001$ HYP 0 *vs.* HYP 10). MWM - Molecular weight marker.

4. DISCUSSION

Our data clearly demonstrate that HYP is a P-gp inducer, which is able to significantly increase, in Caco-2 cells, both P-gp protein expression and activity according to the concentration and time of exposure tested. Caco-2 cells are a well characterized *in vitro* model that closely mimics the enterocytes of the small intestine (Barta et al. 2008; Biganzoli et al. 1999). Derived from human colorectal adenocarcinoma, this cell line is widely accepted as an *in vitro* model for predicting drug intestinal absorption and excretion in humans (Balimane et al. 2006; Barta et al. 2008; Biganzoli et al. 1999; Watanabe et al. 2005; Yamashita et al. 2000; Yamashita et al. 2002). Indeed, these cells express several transporters involved in drug transport, including P-gp (Hidalgo and Jibin 1996 ; Hochman et al. 2000; Hochman et al. 2001; Hunter et al. 1993; Shen et al. 2007; Shirasaka et al. 2006; Watanabe et al. 2005; Wu et al. 2000), and the expression levels of this efflux transporter are in good agreement with those of the normal human jejunum (Taipalensuu et al. 2001). Additionally, our own previous studies have already validated the use of Caco-2 cells as a suitable *in vitro* model for the study and selection of safe, potent, and specific P-gp inducers (Silva et al. 2011; Silva et al. 2013b).

Furthermore, accordingly to the obtained data, HYP elicited similar increases in P-gp expression and activity. In fact, it has long been known that increases in protein expression may not be necessarily correlated with proportional increases in the pump activity (Silva et al. 2011; Silva et al. 2013a; Takara et al. 2009; Vilas-Boas et al. 2011). Indeed, we have previously shown, using the same *in vitro model,* that doxorubicin, a potent P-gp inducer, caused remarkable increases in P-gp expression levels, which were not accompanied by proportional increases in P-gp transport activity (Silva et al. 2011). Additionally, colchicine was also able to significantly increase P-gp expression in Caco-2 cells, without increasing the pump activity (Silva et al. 2013a). Noteworthy, the observed HYP-mediated increases in P-gp expression reveal a higher level of expression and incorporation in the cell membrane, since the monoclonal UIC2 antibody recognizes an external P-gp epitope.

Hypericin is one of the major components of SJW, a flower extract from *Hypericum perforatum*, used for centuries in holistic medicine to accelerate wound healing and treat nerve pain (Perloff et al. 2001). This flower extract is responsible for severe drug-herbal interactions (Pal and Mitra 2006) attributed, among other factors, to P-gp induction (Perloff et al. 2001). Even though P-gp induction by SJW is mainly associated with hyperforin (Tian et al. 2005), our data clearly demonstrates that HYP is also able to induce the pump protein expression and activity in Caco-2 cells. Furthermore, although the HYP ability to induce P-gp remains controversial, in accordance with our data, other studies have also

reported the ability of this compound to act as a P-gp inducer (Perloff et al. 2001). Indeed, using another human colon adenocarcinoma cell line, the LS-180 cells, it was demonstrated that P-gp expression was strongly induced by HYP (700% at 3 μM), as well as by SJW (400% increase at 300 μg/ml), in a dose-dependent manner (Perloff et al. 2001), as evaluated by western blot 72 h after exposure. Furthermore, an increase in the P-gp transport activity was also observed, since cells chronically treated with SJW decreased RHO 123 accumulation, which was reversed with verapamil, a P-gp inhibitor. Indeed, SJW treatment caused concentration-dependent decreases in RHO 123 cell accumulation which correlated with the observed increases in P-gp immunoreactive protein. Moreover, these findings were validated by fluorescence microscopy in intact cells (Perloff et al. 2001).

As noted above, conflicting data was also reported showing that SJW (75 μg/ml) and hyperforin (1 μM), but not HYP (0.1 μM), increased the P-gp protein expression in LS 180 cells, in a time- and dose-dependent manner, and the removal of SJW resulted in a restoration of P-gp levels within 48 h. Moreover, the hyperforin content in SJW extract was high enough to induce P-gp, suggesting that the induction of P-gp by SJW can be almost exclusively attributed to hyperforin (Tian et al. 2005). Furthermore, LS 180 cells chronically exposed to SJW or hyperforin (for 24 and 48 h) exhibited increased P-gp function, as assessed by the evaluation of the digoxin efflux, and the P-gp activities were well correlated with P-gp protein level. In accordance with the lack of P-gp induction, no increased efflux of digoxin was observed in HYP-treated cells. However, using the same *in vitro* model, it was later reported that *MDR1* mRNA expression was induced by both HYP and hyperforin, single constituents of SJW, at a concentration of 10 μM (Gutmann et al. 2006). To note that, in that case, higher HYP concentrations were tested, and the induction was evaluated at the *MDR1* mRNA level, whereas in the first study it was assessed at the protein level. Therefore, although an increased transcription was observed upon HYP exposure, it may not be reflected in increased protein content.

P-gp ATPase activity assays have been long used to evaluate possible interactions with P-gp function, and compounds that act as P-gp substrates typically stimulate its ATPase activity (Ambudkar et al., 1999). Accordingly, our results showed an increased ATP consumption in P-gp-enriched membranes, which occurs as a result of P-gp-mediated HYP transport. Therefore, this compound is a P-gp substrate actively transported by the pump.

Since P-gp transport function requires ATP as the energy source, the ATP intracellular levers were determined. According to the present data, no ATP depletion, which could compromise the pump activity, was observed neither immediately after exposure to HYP for 24, 48 and 72 h, nor after submitting the cells to a RHO 123 efflux

assay. Therefore, in spite of the significant increase in P-gp-mediated RHO 123 efflux and the significant increase in P-gp ATPase activity, no significant decrease in the intracellular ATP content was observed.

Considering the observed effects of HYP on P-gp expression and activity, we further sought to evaluate the impact of those effects on the cytotoxicity induced by a toxic P-gp substrate, the herbicide paraquat. Indeed, the suitability of this study model using PQ as the P-gp toxic substrate was already demonstrated in previous *in vitro* studies with the P-gp inducer doxorubicin, in Caco-2 cells (Silva et al. 2011; Silva et al. 2013b), and with a reduced rifampicin derivative (RedRif), in RBE4 cells (Vilas-Boas et al. 2013b).

According to our data, mimicking the presence of the P-gp inducer in the PQ formulation, it was possible to observe, *in vitro*, a significant reduction in PQ-induced cytotoxicity towards Caco-2 cells, being this effective protection also observed for the other tested experimental designs of HYP incubation. Furthermore, as the protection afforded by HYP was completely abolished in the presence of the P-gp inhibitor, the UIC2 antibody, it is possible to confirm that HYP protects Caco-2 cells from the herbicide's cytotoxicity exclusively through a P-gp-mediated mechanism. Additionally, the PQ concentrations used in the present study are within what is expected to be observed *in vivo,* in a real intoxication scenario. In fact, in most of the reported cases of human PQ intoxication, 25–50 mL of a 20 g/100 mL PQ formulation are typically ingested (Dinis-Oliveira et al. 2009), which corresponds to an orally ingested dose of approximately 5-10 g, absorbed up to a maximum of 5 % (Roberts 2011). Therefore, blood concentrations up to 0.1 g/L (0.4 mM) could be easily achieved and, in the intestine, high concentrations may be expected since almost all the ingested dose comes into contact with the enterocytes.

The YB-1 protein performs its functions both in the cytoplasm and in the cell nucleus, and by passing from the cytoplasm to the cell nucleus, this transcription factor can influence the transcription of many genes, including genes involved in cell division, apoptosis, immune response, multidrug resistance, stress response, and tumor growth (Eliseeva et al. 2011). Furthermore, YB-1 regulates transcription through its direct interaction with the specific Y-box-containing regions in gene promoters (Eliseeva et al. 2011). In fact, in what concerns to the *MDR1* gene, it was demonstrated that YB-1 can stimulate its transcription and it was suggested that this occurs as a result of YB-1 binding to the Y-box sequence in the promoter of this gene (Ohga et al. 1996; Ohga et al. 1998; Sengupta et al. 2011; Stein et al. 2001). However, in other studies, YB-1 was not identified within DNA/protein complexes assembled in nuclear lysates on double-stranded oligonucleotides corresponding to the *MDR1* gene promoter regions (Hu et al. 2000; Sundseth et al. 1997). This challenge can be explained by different experimental

conditions or by different ways of detecting YB-1 within these complexes (the knockdown of YB-1 in the first case and the use of antibodies in the second). It has been assumed that YB-1 is involved in the activation of *MDR1* transcription only under strictly specific conditions and interacts with the gene promoter only when in complex with other proteins (Eliseeva et al. 2011).

According to our results, the significant increase in cell surface P-gp expression was followed by a significant decrease in the YB-1 nuclear levels, 72 h after exposure to 10 μM HYP. As a rule, the major part of YB-1 is within the cytoplasm in association with mRNA and, in response to intra- and extracellular signals, a significant portion of YB-1 can move to the cell nucleus (Eliseeva et al. 2011). In the cell nucleus, Y-Box binding proteins can be located on chromatin both as a result of their interaction with DNA in gene promoters and in damaged regions under reparation, or due to their association with newly synthesized mRNA (Eliseeva et al. 2011). Furthermore, it was previously suggested that YB-1 can move from the nucleus to the cytoplasm complexed with the newly synthesized mRNA (Ranjan et al. 1993). Additionally, one of the major functions of this transcription factor in the cytoplasm is in the translation regulation (Eliseeva et al. 2011; Soop et al. 2003). Therefore, since the HYP-induced increase in P-gp expression was detected as soon as 24 h after exposure, and the YB-1 nuclear content was evaluated only 72 h exposure, the significant decrease upon exposure to HYP may be explained by its migration to the cytoplasm along with the newly synthesized mRNA.

In conclusion, HYP demonstrated to be an effective P-gp inducer, which was able to significantly increase both cell surface P-gp expression and activity, resulting in a significant protection against PQ-induced cytotoxicity, even when it contacts with the affected cells well after the harmful xenobiotic. Furthermore, as the observed protection was mediated exclusively through its effects on P-gp, this compound represents an excellent candidate for drug design of new potent and specific P-gp inducers.

5. ACKNOWLEDGMENTS

This work was supported by the Fundação para a Ciência e Tecnologia (FCT)-project PTDC/SAU-OSM/101437/2008 - QREN initiative with EU/FEDER funded through COMPETE - Operational Programme for Competitiveness Factors.

The work was also supported by FCT within the framework of Strategic Projects for Scientific Research Units of R&D (projects PEst-C/EQB/LA0006/2011 and Pest-OE/SAU/UI4040/2011).

Renata Silva and Daniel José Barbosa acknowledge FCT for their PhD grants [SFRH/BD/29559/2006] and [SFRH/BD/64939/2009], respectively.

6. CONFLICT OF INTEREST STATEMENT

The authors declare that there are no conflicts of interest.

7. REFERENCES

Ambudkar SV, Dey S, Hrycyna CA, Ramachandra M, Pastan I, Gottesman MM (1999) Biochemical, cellular, and pharmacological aspects of the multidrug transporter. Annu Rev Pharmacol Toxicol 39:361-398.

Balimane PV, Han YH, Chong S (2006) Current industrial practices of assessing permeability and P-glycoprotein interaction. AAPS J 8:1-13.

Baltazar MT, Dinis-Oliveira RJ, Guilhermino L, de Lourdes Bastos M, Duarte JA, Carvalho F (2013) New formulation of paraquat with lysine acetylsalicylate with low mammalian toxicity and effective herbicidal activity. Pest Manag Sci 69:553-558.

Barbosa DJ, Capela JP, Silva R, et al. (2013) The mixture of "ecstasy" and its metabolites is toxic to human SH-SY5Y differentiated cells at in vivo relevant concentrations. Arch Toxicol.

Bargou RC, Jurchott K, Wagener C, et al. (1997) Nuclear localization and increased levels of transcription factor YB-1 in primary human breast cancers are associated with intrinsic MDR1 gene expression. Nat Med 3:447-450.

Barta CA, Sachs-Barrable K, Feng F, Wasan KM (2008) Effects of monoglycerides on p-glycoprotein: modulation of the activity and expression in caco-2 cell monolayers. Mol Pharm 5:863-875.

Biganzoli E, Cavenaghi LA, Rossi R, Brunati MC, Nolli ML (1999) Use of a Caco-2 cell culture model for the characterization of intestinal absorption of antibiotics. Farmaco 54:594-599.

Cordon-Cardo C, O'Brien JP, Boccia J, Casals D, Bertino JR, Melamed MR (1990) Expression of the multidrug resistance gene product (P-glycoprotein) in human normal and tumor tissues. J Histochem Cytochem 38:1277-1287.

Dinis-Oliveira RJ, de Pinho PG, Santos L, et al. (2009) Postmortem analyses unveil the poor efficacy of decontamination, anti-inflammatory and immunosuppressive therapies in paraquat human intoxications. PLoS One 4:e7149.

Dinis-Oliveira RJ, Duarte JA, Remiao F, Sanchez-Navarro A, Bastos ML, Carvalho F (2006) Single high dose dexamethasone treatment decreases the pathological score and increases the survival rate of paraquat-intoxicated rats. Toxicology 227:73-85.

Dinis-Oliveira RJ, Duarte JA, Sanchez-Navarro A, Remiao F, Bastos ML, Carvalho F (2008) Paraquat poisonings: mechanisms of lung toxicity, clinical features, and treatment. Crit Rev Toxicol 38:13-71.

Eliseeva IA, Kim ER, Guryanov SG, Ovchinnikov LP, Lyabin DN (2011) Y-box-binding protein 1 (YB-1) and its functions. Biochemistry (Mosc) 76:1402-1433.

Gottesman MM, Fojo T, Bates SE (2002) Multidrug resistance in cancer: role of ATP-dependent transporters. Nat Rev Cancer 2:48-58.

Gutmann H, Poller B, Buter KB, Pfrunder A, Schaffner W, Drewe J (2006) Hypericum perforatum: which constituents may induce intestinal MDR1 and CYP3A4 mRNA expression? Planta Med 72:685-690.

Hidalgo IJ, Jibin L (1996) Carrier-mediated transport and efflux mechanisms in Caco-2 cells. Adv Drug Deliv Rev 22:53-66.

Hochman JH, Chiba M, Nishime J, Yamazaki M, Lin JH (2000) Influence of P-glycoprotein on the transport and metabolism of indinavir in Caco-2 cells expressing cytochrome P-450 3A4. J Pharmacol Exp Ther 292:310-318.

Hochman JH, Chiba M, Yamazaki M, Tang C, Lin JH (2001) P-glycoprotein-mediated efflux of indinavir metabolites in Caco-2 cells expressing cytochrome P450 3A4. J Pharmacol Exp Ther 298:323-330.

Hu Z, Jin S, Scotto KW (2000) Transcriptional activation of the MDR1 gene by UV irradiation: Role of NF-Y and Sp1. J Biol Chem 275:2979-2985.

Hunter J, Hirst BH, Simmons NL (1993) Drug absorption limited by P-glycoprotein-mediated secretory drug transport in human intestinal epithelial Caco-2 cell layers. Pharm Res 10:743-749.

Juliano RL, Ling V (1976) A surface glycoprotein modulating drug permeability in Chinese hamster ovary cell mutants. Biochim Biophys Acta 455:152-162.

Oda Y, Ohishi Y, Saito T, et al. (2003) Nuclear expression of Y-box-binding protein-1 correlates with P-glycoprotein and topoisomerase II alpha expression, and with poor prognosis in synovial sarcoma. J Pathol 199:251-258.

Ohga T, Koike K, Ono M, et al. (1996) Role of the human Y box-binding protein YB-1 in cellular sensitivity to the DNA-damaging agents cisplatin, mitomycin C, and ultraviolet light. Cancer Res 56:4224-4228.

Ohga T, Uchiumi T, Makino Y, et al. (1998) Direct involvement of the Y-box binding protein YB-1 in genotoxic stress-induced activation of the human multidrug resistance 1 gene. J Biol Chem 273:5997-6000.

Pal D, Mitra AK (2006) MDR- and CYP3A4-mediated drug-drug interactions. J Neuroimmune Pharmacol 1:323-339.

Perloff MD, von Moltke LL, Stormer E, Shader RI, Greenblatt DJ (2001) Saint John's wort: an in vitro analysis of P-glycoprotein induction due to extended exposure. Br J Pharmacol 134:1601-1608.

Pontes H, Sousa C, Silva R, et al. (2008) Synergistic toxicity of ethanol and MDMA towards primary cultured rat hepatocytes. Toxicology 254:42-50.

Ranjan M, Tafuri SR, Wolffe AP (1993) Masking mRNA from translation in somatic cells. Genes Dev 7:1725-1736.

Roberts DM (2011) Herbicides. In: Nelson LS, Lewin NA, Howland MA, Hoffman RS, Goldfrank LR, Flomenbaum NE (eds) Goldfrank's Toxicologic Emergencies, Ninth Edition McGraw-Hill Companies, Inc., p 1494-1515.

Saji H, Toi M, Saji S, Koike M, Kohno K, Kuwano M (2003) Nuclear expression of YB-1 protein correlates with P-glycoprotein expression in human breast carcinoma. Cancer Lett 190:191-197.

Sengupta S, Mantha AK, Mitra S, Bhakat KK (2011) Human AP endonuclease (APE1/Ref-1) and its acetylation regulate YB-1-p300 recruitment and RNA polymerase II loading in the drug-induced activation of multidrug resistance gene MDR1. Oncogene 30:482-493.

Shen S, He Y, Zeng S (2007) Stereoselective regulation of MDR1 expression in Caco-2 cells by cetirizine enantiomers. Chirality 19:485-490.

Shirasaka Y, Kawasaki M, Sakane T, et al. (2006) Induction of human P-glycoprotein in Caco-2 cells: development of a highly sensitive assay system for P-glycoprotein-mediated drug transport. Drug Metab Pharmacokinet 21:414-423.

Silva R, Carmo H, Dinis-Oliveira R, et al. (2011) In vitro study of P-glycoprotein induction as an antidotal pathway to prevent cytotoxicity in Caco-2 cells. Arch Toxicol 85:315-326.

Silva R, Carmo H, Vilas-Boas V, et al. (2013a) Colchicine effect on P-glycoprotein expression and activity: in silico and in vitro studies. Submitted for publication.

Silva R, Carmo H, Vilas-Boas V, et al. (2013b) Doxorubicin decreases paraquat accumulation and toxicity in Caco-2 cells. Toxicol Lett 217:34-41.

Silva R, Palmeira A, Carmo H, et al. (2013c) P-glycoprotein induction in Caco-2 cells by newly synthetized thioxanthones prevents Paraquat cytotoxicity. Submitted for publication.

Soop T, Nashchekin D, Zhao J, et al. (2003) A p50-like Y-box protein with a putative translational role becomes associated with pre-mRNA concomitant with transcription. J Cell Sci 116:1493-1503.

Stein U, Jurchott K, Walther W, Bergmann S, Schlag PM, Royer HD (2001) Hyperthermia-induced nuclear translocation of transcription factor YB-1 leads to enhanced expression of multidrug resistance-related ABC transporters. J Biol Chem 276:28562-28569.

Sundseth R, Macdonald G, Ting J, King AC (1997) DNA elements recognizing NF-Y and Sp1 regulate the human multidrug-resistance gene promoter. Mol Pharmacol 51:963-971.

Taipalensuu J, Tornblom H, Lindberg G, et al. (2001) Correlation of gene expression of ten drug efflux proteins of the ATP-binding cassette transporter family in normal human jejunum and in human intestinal epithelial Caco-2 cell monolayers. J Pharmacol Exp Ther 299:164-170.

Takara K, Hayashi R, Kokufu M, et al. (2009) Effects of nonsteroidal anti-inflammatory drugs on the expression and function of P-glycoprotein/MDR1 in Caco-2 cells. Drug Chem Toxicol 32:332-337.

Thiebaut F, Tsuruo T, Hamada H, Gottesman MM, Pastan I, Willingham MC (1987) Cellular localization of the multidrug-resistance gene product P-glycoprotein in normal human tissues. Proc Natl Acad Sci U S A 84:7735-7738.

Tian R, Koyabu N, Morimoto S, Shoyama Y, Ohtani H, Sawada Y (2005) Functional induction and de-induction of P-glycoprotein by St. John's wort and its ingredients in a human colon adenocarcinoma cell line. Drug Metab Dispos 33:547-554.

Vilas-Boas V, Silva R, Gaio AR, et al. (2011) P-glycoprotein activity in human Caucasian male lymphocytes does not follow its increased expression during aging. Cytometry A 79:912-919.

Vilas-Boas V, Silva R, Nunes C, et al. (2013a) Mechanisms of P-gp inhibition and effects on membrane fluidity of a new rifampicin derivative, 1,8-dibenzoyl-rifampicin. Toxicol Lett 220:259-266.

Vilas-Boas V, Silva R, Palmeira A, et al. (2013b) Development of novel rifampicin-derived P-glycoprotein activators/inducers. Synthesis, in silico analysis and application in the RBE4 cell model, using paraquat as substrate. PLoS One 8:e74425.

Watanabe T, Onuki R, Yamashita S, Taira K, Sugiyama Y (2005) Construction of a functional transporter analysis system using MDR1 knockdown Caco-2 cells. Pharm Res 22:1287-1293.

Wilks MF, Fernando R, Ariyananda PL, et al. (2008) Improvement in survival after paraquat ingestion following introduction of a new formulation in Sri Lanka. PLoS Med 5:e49.

Wu X, Whitfield LR, Stewart BH (2000) Atorvastatin transport in the Caco-2 cell model: contributions of P-glycoprotein and the proton-monocarboxylic acid co-transporter. Pharm Res 17:209-215.

Yamashita S, Furubayashi T, Kataoka M, Sakane T, Sezaki H, Tokuda H (2000) Optimized conditions for prediction of intestinal drug permeability using Caco-2 cells. Eur J Pharm Sci 10:195-204.

Yamashita S, Hattori E, Shimada A, et al. (2002) New methods to evaluate intestinal drug absorption mediated by oligopeptide transporter from in vitro study using Caco-2 cells. Drug Metab Pharmacokinet 17:408-415.

SUPPLEMENTARY DATA

Supplementary Figures

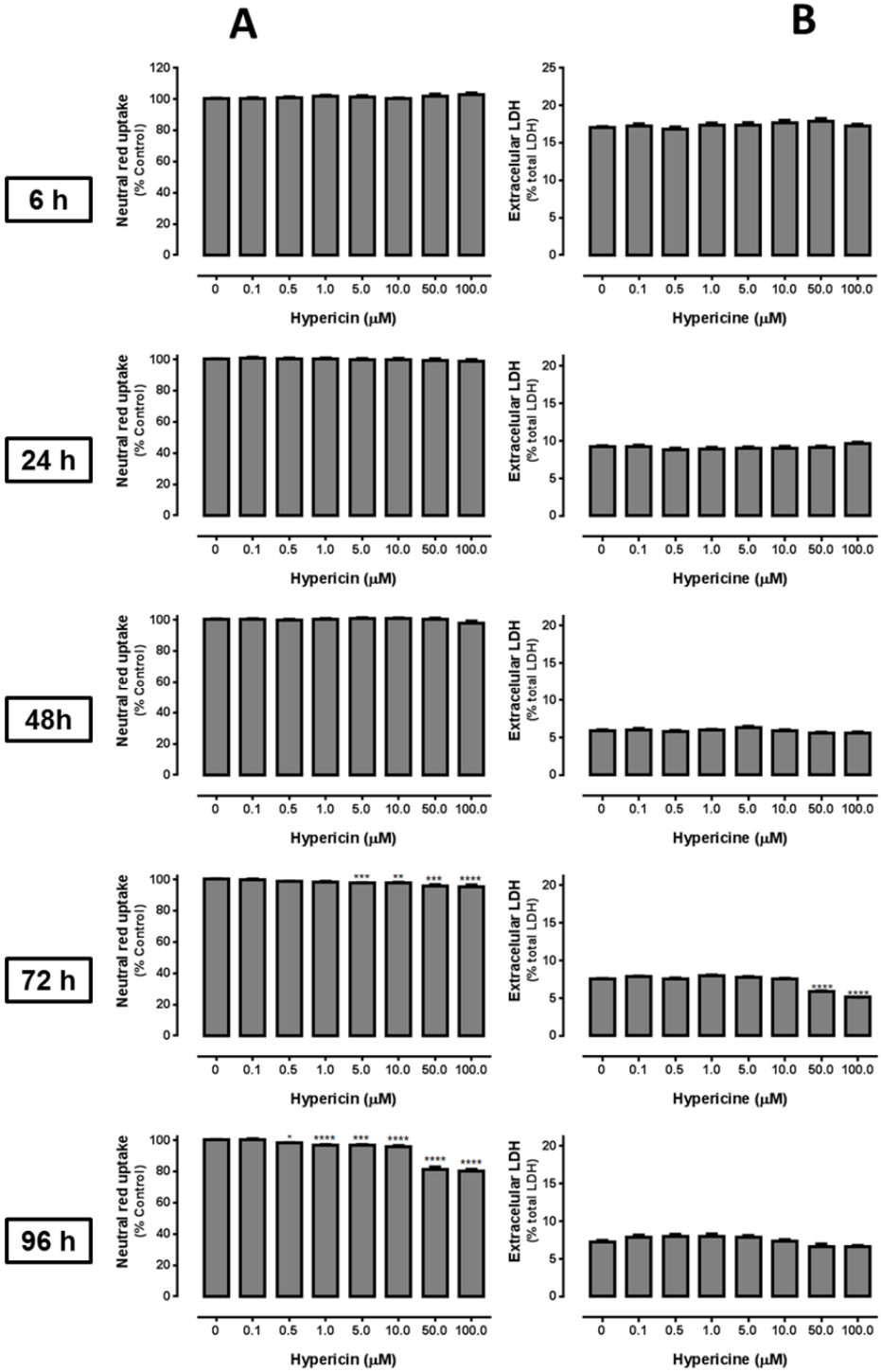

Figure S1. **(A)** Hypericin (HYP) cytotoxicity in Caco-2 cells, evaluated by the NR uptake assay at different time points (6, 24, 48, 72 and 96 h). Results are presented as mean ± SEM from 6 independent experiments (performed in triplicate). Statistical comparisons were made using the nonparametric method of Kruskal–Wallis (one-way ANOVA on ranks), followed by Dunn's *post hoc* test (*p<0.05; **p<0.01; ***p<0.001; ****p <0.0001 *vs*. Control). **(B)** Hypericin (HYP) cytotoxicity in Caco-2 cells, evaluated by the LDH leakage assay at different time points (6, 24, 48, 72 and 96 h). Extracellular LDH activity was expressed as a percentage of total LDH activity. Results are presented as mean ± SEM from 6 independent experiments (performed in triplicate). Statistical comparisons were made using the nonparametric method of Kruskal–Wallis (one-way ANOVA on ranks), followed by Dunn's *post hoc* test (****p <0.0001 *vs*. Control).

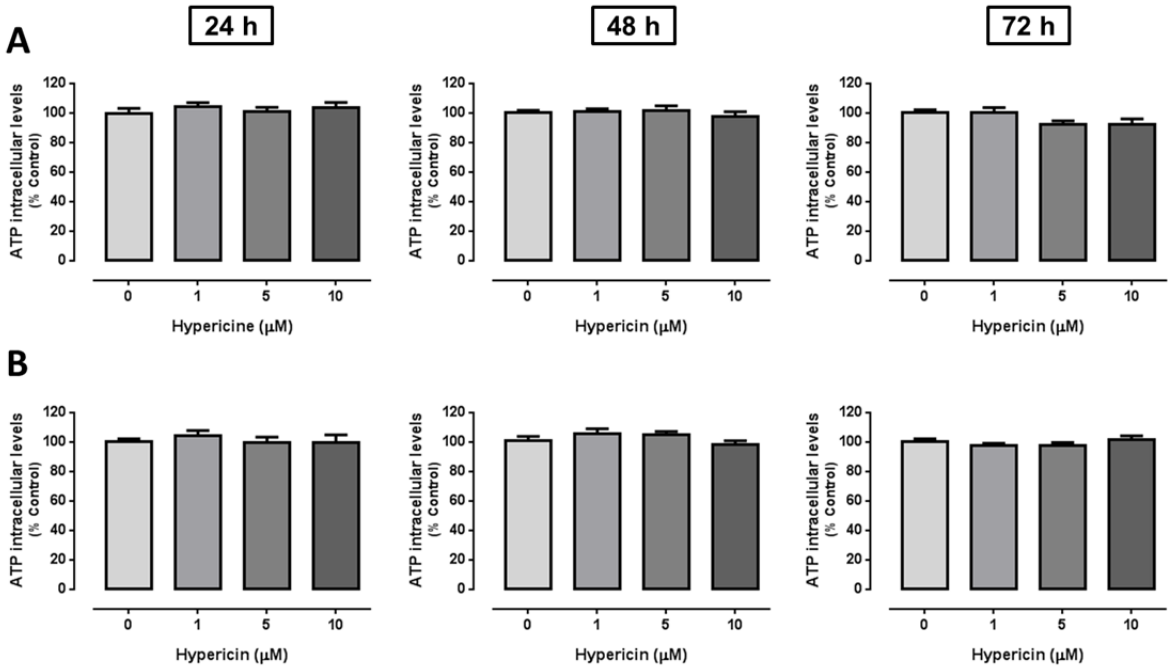

Figure S2 (A) ATP intracellular levels in Caco-2 cells exposed to hypericin (HYP 0, 1, 5and 10 µM) for 24, 48 or 72 h. **(B)** ATP intracellular levels in Caco-2 cells exposed to hypericin (HYP 0, 1, 5 and 10µM) for 24, 48 or 72 h, and then submitted to a RHO 123 IAE procedure. ATP intracellular content was normalized to the total protein content and the final results, from 4 independent experiments (performed in triplicate), are expressed as percentage of control (Mean ± SEM). Statistical comparison between groups was estimated using the nonparametric method of Kruskal–Wallis (one-way ANOVA on ranks) followed by Dunn's *post hoc* test.

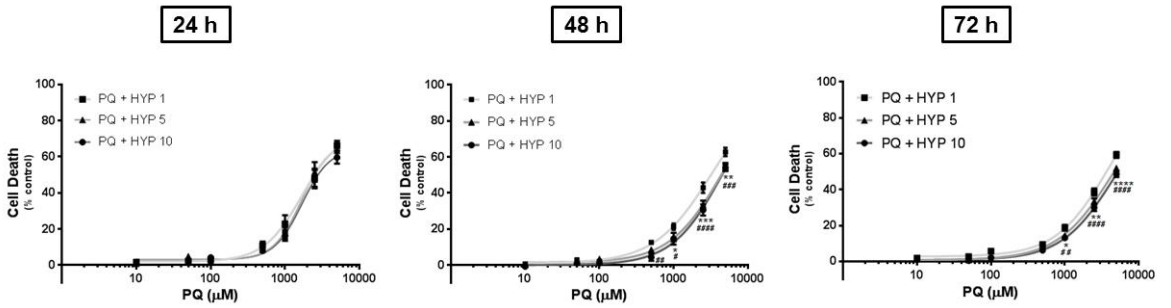

Figure S3. Paraquat concentration–response (cell death) curves with pre-exposure of Caco-2 cells to hypericin (HYP 1, 5 or 10 µM) for 24 h, 48 h and 72 h. Results are presented as mean ± SEM from at least 4 independent experiments (performed in triplicate). Concentration–response curves were fitted using least squares as the fitting method and the comparisons between the fitted curves (LOG EC_{50}, TOP, BOTTOM and Hill slope) were made using the extra sum-of-squares F test. Statistical comparisons were made using Two-way ANOVA, followed by the Sidak's multiple comparisons *post hoc* test (**p*<0.05; ***p*<0.01; ****p*<0.001; *****p*<0.0001 PQ + HYP 1 *vs.* PQ + HYP 5; $^{\#}p$<0.05; $^{\#\#}p$<0.01; $^{\#\#\#}p$<0.001; $^{\#\#\#\#}p$<0.0001 PQ + HYP 1 *vs.* PQ + HYP 10).

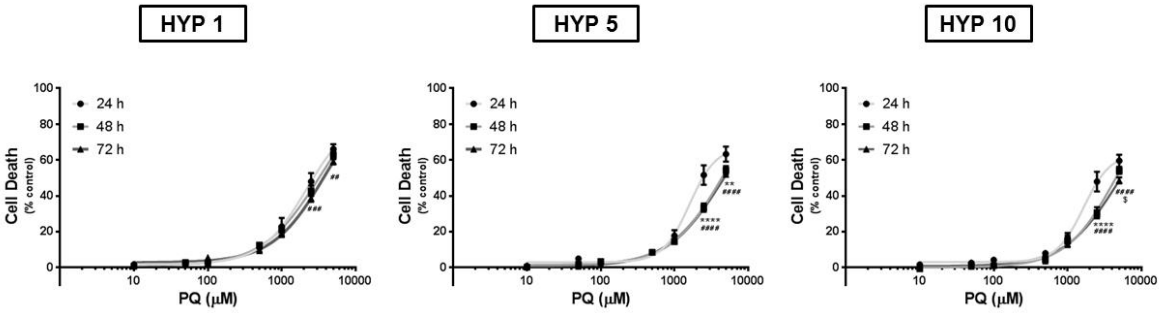

Figure S4. Paraquat concentration–response (cell death) curves with pre-exposure of Caco-2 cells to 1, 5 or 10 µM hypericin for 24 h, 48 h and 72 h. Results are presented as mean ± SEM from at least 4 independent experiments (performed in triplicate). Concentration–response curves were fitted using least squares as the fitting method and the comparisons between the fitted curves (LOG EC_{50}, TOP, BOTTOM and Hill slope) were made using the extra sum-of-squares F test. Statistical comparisons were made using Two-way ANOVA, followed by the Sidak's multiple comparisons *post hoc* test (**p<0.01; ****p<0.0001 24 h *vs.* 48 h; $^{\#\#}p$<0.01; $^{\#\#\#}p$<0.001; $^{\#\#\#\#}p$<0.0001 24 h *vs.* 72 h; $^{\$}p$<0.05 48 h *vs.* 72 h).

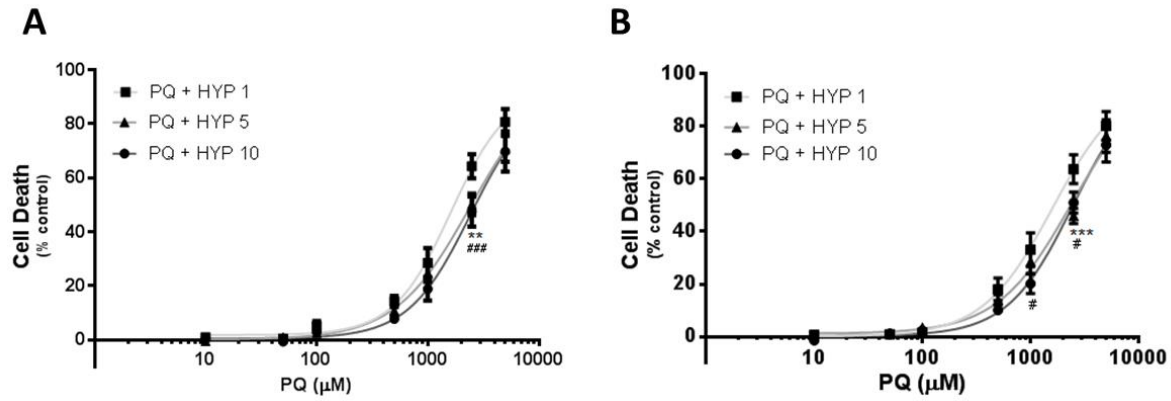

Figure S5. (A) Paraquat concentration–response (cell death) curves with incubation of Caco-2 cells with hypericin (HYP 1, 5 or 10 µM) 6 h after the beginning of PQ exposure. Results are presented as mean ± SEM from 5 independent experiments (performed in triplicate). **(B)** Paraquat concentration–response (cell death) curves with simultaneous exposure of Caco-2 cells to hypericin (HYP 1, 5 or 10 µM). Results are presented as mean ± SEM from 3 independent experiments (performed in triplicate).Concentration–response curves were fitted using least squares as the fitting method and the comparisons between the fitted curves (LOG EC_{50}, TOP, BOTTOM and Hill slope) were made using the extra sum-of-squares F test. Statistical comparisons were made using Two-way ANOVA, followed by the Sidak's multiple comparisons *post hoc* test (**p<0.01; ***p<0.001 PQ + HYP 1 *vs.* PQ + HYP 5; $^{\#}p$<0.05; $^{\#\#\#}p$<0.001 PQ + HYP 1 *vs.* PQ + HYP 10).

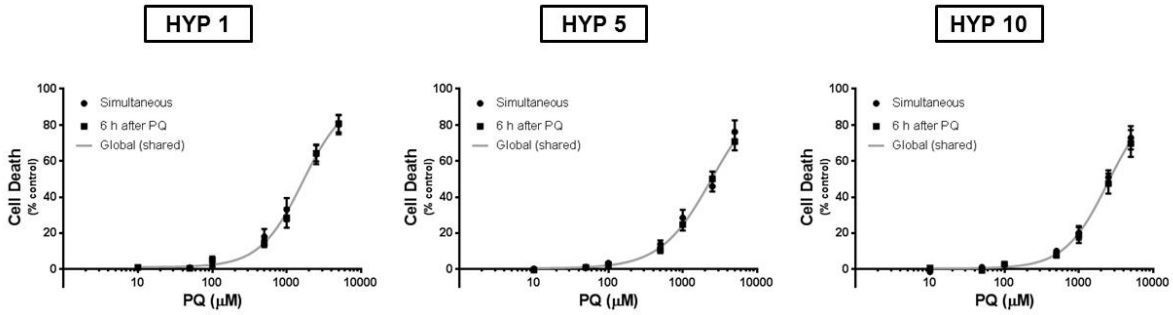

Figure S6. Paraquat concentration–response (cell death) curves in the presence of HYP (1, 5 or 10 μM), both simultaneously and 6 h after PQ incubation. Results are presented as mean ± SEM from at least 3 independent experiments (performed in triplicate). Concentration–response curves were fitted using least squares as the fitting method and the comparisons between the fitted curves (LOG EC_{50}, TOP, BOTTOM and Hill slope) were made using the extra sum-of-squares F test. Statistical comparisons were made using Two-way ANOVA, followed by the Sidak's multiple comparisons *post hoc* test.

Supplementary Tables

Table S1. EC_{50} (half-maximum-effect concentrations), TOP (maximal effect), BOTTOM (baseline) and Hill slope values of the PQ concentration-response curves, with pre-exposure to HYP (1, 5 or 10 µM) for 24, 48 or 72 h.

	24 h			48 h			72 h		
	PQ + HYP 1	**PQ + HYP 5**	**PQ + HYP 10**	**PQ + HYP 1**	**PQ + HYP 5**	**PQ + HYP 10**	**PQ + HYP 1**	**PQ + HYP 5**	**PQ + HYP 10**
EC_{50} (µM)	**2161**	**1599**	**1642**	**3243**	**4490**	**4493**	**3843**	**4518**	**4609**
TOP	85.62	67.49	63.80	~ 100.0	~ 100.0	~ 100.0	~ 100.0	97.60	91.87
BOTTOM	1.790	2.943	3,048	1.007	1.365	0.004269	2.727	0.7430	0.7944
Hill slope	1.425	2.404	2.388	1.131	1.219	1.287	1.226	1.159	1.226
Curve *p* value	-	0.5369*	0.2026* 0.7625#	-	**< 0.0001***	**< 0.0001*** 0.5381#	-	**< 0.0001***	**< 0.0001*** **0.0449#**

Concentration-response curves were fitted using least squares as the fitting method and the comparisons between the PQ + HYP curves were made using extra sum-of-squares F test. In all cases, *p* values lower than 0.05 were considered significant. * Comparison *vs*. PQ + HYP 1; # Comparison *vs*. PQ + HYP 5, at each time-point.

Table S2. EC_{50} (half-maximum-effect concentrations), TOP (maximal effect), BOTTOM (baseline) and Hill slope values of the PQ concentration-response curves, with pre-exposure to HYP (1, 5 or 10 µM) for 24, 48 or 72 h.

	PQ + HYP 1			PQ + HYP 55			PQ + HYP 10		
	24 h	**48 h**	**72 h**	**24 h**	**48 h**	**72 h**	**24 h**	**48 h**	**72 h**
EC_{50} (µM)	**2161**	**3243**	**3843**	**1599**	**4490**	**4518**	**1642**	**4493**	**4609**
TOP	85.62	~ 100.0	~ 100.0	67.49	~ 100.0	97.60	63.80	~ 100.0	91.87
BOTTOM	1.790	1.007	2.727	2.943	1.365	0.7430	3,048	0.004269	0.7944
Hill slope	1.425	1.131	1.226	2.404	1.219	1.159	2.388	1.287	1.226
EC50 p value	-	0.3477*	0.1961* 0.4980#	-	**0.0016***	**0.0010*** 0.9896#	-	**0.0037***	**0.0014*** 0.9640#
Curve *p* value	-	0.3433*	**0.0002*** **0.0324#**	-	**< 0.0001***	**< 0.0001*** 0.8931#	-	**< 0.0001***	**< 0.0001*** 0.1879#

Concentration-response curves were fitted using least squares as the fitting method and the comparisons between the PQ + HYP curves were made using extra sum-of-squares F test. In all cases, *p* values lower than 0.05 were considered significant. * Comparison *vs*. 24 h; # Comparison *vs*. 48 h, at each HYP concentration.

Table S3. EC_{50} (half-maximum-effect concentrations), TOP (maximal effect), BOTTOM (baseline) and Hill slope values of the PQ concentration-response curves, with exposure to HYP (1, 5 or 10 μM) 6 h after the beginning of PQ exposure.

	PQ + HYP 1	PQ + HYP 5	PQ + HYP 10
EC_{50} (μM)	**1622**	**2408**	**2437**
TOP	93.11	98.29	92.50
BOTTOM	1.678	0.1322	0.4915
Hill slope	1.788	1.285	1.549
Curve *p* value (Comparison between the Fitted Curves)	-	**0.0036***	**0.0008*** 0.6804#

Concentration-response curves were fitted using least squares as the fitting method and the comparisons between the PQ + HYP curves were made using extra sum-of-squares F test. In all cases, *p* values lower than 0.05 were considered significant. * Comparison *vs*. PQ + HYP 1; # Comparison *vs*. PQ + HYP 5.

Table S4. EC50 (half-maximum-effect concentrations), TOP (maximal effect), BOTTOM (baseline) and Hill slope values of the paraquat concentration-response curves, with simultaneous exposure to hypericin (1, 5 or 10 μM).

	PQ + HYP 1	PQ + HYP 5	PQ + HYP 10
EC_{50} (μM)	**1594**	**2400**	**2469**
TOP	97.60	~ 100.0	99.48
BOTTOM	0.02581	1.128	0.2062
Hill slope	1.346	1.261	1.442
Curve *p* value (Comparison between the Fitted Curves)	-	**0.0398***	**0.0024*** 0.7149#

Concentration-response curves were fitted using least squares as the fitting method and the comparisons between the PQ + HYP curves were made using extra sum-of-squares F test. In all cases, *p* values lower than 0.05 were considered significant. * Comparison *vs*. PQ + HYP 1; # Comparison *vs*. PQ + HYP 5.

III.6. MANUSCRIPT V

Several transport systems contribute to the intestinal uptake of Paraquat, modulating its cytotoxic effects

Submitted for publication

TITLE

Several transport systems contribute to the intestinal uptake of Paraquat, modulating its cytotoxic effects

AUTHORS

Renata Silva[a*], Helena Carmo[a], Vânia Vilas-Boas[a]; Daniel José Barbosa[a], Márcia Monteiro[a], Paula Guedes de Pinho[a], Maria de Lourdes Bastos[a] and Fernando Remião[a*]

AFFILIATIONS

[a]REQUI*M*TE, Laboratório de Toxicologia, Departamento de Ciências Biológicas, Faculdade de Farmácia da Universidade do Porto, Rua de Jorge Viterbo Ferreira, 228, 4050-313 Porto, Portugal.

*CORRESPONDING AUTHORS

Renata Silva (e-mail: rsilva@ff.up.pt) and Fernando Remião (e-mail: remiao@ff.up.pt)
REQUI*M*TE - Laboratório de Toxicologia, Departamento de Ciências Biológicas, Faculdade de Farmácia da Universidade do Porto, Rua de Jorge Viterbo Ferreira, 228, 4050-313 Porto, Portugal.
Tel: 00351220428596
Fax: 00351226093390

RUNNING TITLE

Paraquat uptake into Caco-2 cells

ABSTRACT

Nearly all poisonings with the extremely toxic herbicide paraquat (1,1'-dimethyl-4,4'-bipyridylium, PQ) result from accidental or intentional ingestion. Therefore, treatment has relied primarily upon limiting intestinal absorption. However, the mechanisms involved in its intestinal uptake remain largely unknown. In this study we sought to elucidate these transport mechanisms using Caco-2 cells as a model of the human intestinal epithelium. With this purpose, the cells were incubated with a range of PQ concentrations (0-5000 μM) for 24 h with or without simultaneous exposure to choline or hemicolinium-3 (for choline carrier-mediated transport system inhibition) and putrescine, trifluoperazine, valine, lysine, arginine or N-ethylmalemide (for basic amino acids transport systems inhibition). PQ cytotoxicity with or without competitive transport inhibition was evaluated by the MTT reduction assay and correlated with PQ intracellular levels quantified by gas chromatography-ion trap-mass spectrometry (GC-IT/MS).

Our results showed a significant reduction in PQ intracellular accumulation and, consequently, in PQ cytotoxicity, in the presence of both choline (substrate) and hemicolinium-3 (inhibitor) demonstrating that the choline carrier-mediated transport system is partially involved in PQ intestinal uptake. Likewise, PQ cytotoxicity and intracellular accumulation were significantly attenuated by simultaneous exposure to putrescine, trifluoperazine, valine, lysine, arginine and N-ethylmalemide. In fact, the obtained results pointed to the involvement of more than one of the basic amino acids transport systems, including the y^+, $b^{0,+}$ or y^+L systems.

In conclusion, this study demonstrated that several transport systems mediate PQ intestinal absorption and, therefore, their modulation may provide alternative efficient pathways for limiting PQ toxicity in intoxication scenarios.

KEYWORDS

Paraquat intestinal uptake; Arginine; Lysine; Putrescine; Choline; y^+ transport system.

ABBREVIATIONS

ARG - L-Arginine
BBB - Blood Brain Barrier
BSA - Bovine Serum Albumin
Ca^{2+}/CaM - Calcium/Calmodulin
CHO - Choline
DMEM - Dulbecco's Modified Eagle's Medium
EDTA - Ethylenediamine Tetraacetic Acid
EPQ – Ethylparaquat
FBS - Fetal Bovine Serum
GC–IT/MS - Gas Chromatography-Ion Trap-Mass Spectrometry
HBSS - Hank′s Balanced Salt Solution
HC-3 - Hemicholinium-3
HEPQ – Hydrogenated Ethylparaquat
HPQ - Hydrogenated Paraquat
LYS - L-Lysine
MTT - (4,5-dimethylthiazol-2-yl)-2,5-diphenyl Tetrazolium bromide
MSTFA - N-methyl-N-(trimethylsilyl)trifluoroacetamide
NEAA - Non-Essential Amino Acids
NEM - N-ethylmalemide
NOR - Norvaline
PBS - Phosphate Buffered Saline Solution
PQ - Paraquat
PUT - Putrescine
SPE - Solid-Phase Extraction
TFP - Trifluoperazine
VAL - L-Valine

1. INTRODUCTION

Paraquat (1,1'-dimethyl-4,4'-bipyridylium, PQ) is the third most extensively used herbicide in the world, as a result of its highly effectiveness as desiccant and defoliant in a variety of crops. However, it is responsible for thousands of deaths due to accidental or intentional ingestion (Dinis-Oliveira et al. 2006a; Dinis-Oliveira et al. 2008; Dinis-Oliveira et al. 2006c; Dinis-Oliveira et al. 2007; Heylings et al. 2007) and no effective antidote has yet been found for this extremely toxic herbicide. Paraquat intoxication, both in man and in animals, results in severe lung damage and renal failure (Dinis-Oliveira et al. 2008; Heylings et al. 2007), with these organs showing the highest PQ concentrations, regardless of the route of administration (Dinis-Oliveira et al. 2008). In fact, in the lung, PQ concentrations can be 6 to 10 times higher than those found in plasma, with a long-lasting sustained accumulation after blood levels start to decrease (Dinis-Oliveira et al. 2008).

Early works have demonstrated, in the lung, that PQ uptake against a concentration gradient is an ATP-driven process (Rose et al. 1974), competitively inhibited by a number of naturally occurring amines, such as putrescine, cadaverine, spermidine and spermine (Smith 1982; Wyatt et al. 1988). It was hypothesized that PQ accumulation in the alveolar type I and II cells and in the Clara cells occurs through this active pulmonary polyamine uptake system, probably due to the structural similarity with these endogenous polyamines substrates (Smith 1982).

Although most of the experimental studies on PQ poisonings are focused on the toxic damage to peripheral tissues, such as the lung, kidney and liver, toxic effects were also observed in the brain of patients who died from PQ poisoning (Grant et al. 1980; Shimizu et al. 2001). In the brain, numerous clinical and experimental studies demonstrated that PQ can induce neural damage, probably due to its structural similarity with the known dopaminergic neurotoxin, N-methyl-4-phenylpyridinium cation (MPP^+), that cannot penetrate into the central nervous system (Shimizu et al. 2001), thus raising concern of a possible involvement of PQ in the development of Parkinson's disease (Dinis-Oliveira et al. 2006b). However, contrary to MPP^+, PQ is known to penetrate the blood-brain barrier (BBB) in a dose-dependent manner (Shimizu et al. 2001). Because polyamine transporters are not expressed in the BBB (Shin et al. 1985), it was hypothesized that the amino acid transporters, which are highly expressed in the BBB, could be involved in the PQ BBB penetration (Shimizu et al. 2001). In fact, it was shown that the neutral amino acid transport system was implicated in the PQ brain uptake (Shimizu et al. 2001).

Only limited information is available on the PQ gastrointestinal absorption. Absorption occurs mainly in the small intestine (and very poorly in the stomach), over an

1–6 h period, and estimated to be approximately 1–5% of the ingested dose in humans (Dinis-Oliveira et al. 2008). It has been suggested that PQ may be absorbed to a low extent through a specialized mechanism associated with the carrier-mediated transport system for choline on the brush-border membrane (Nagao et al. 1993). Additionally, studies with the rat small intestine crypt IEC-6 cell line, showed that putrescine competitively inhibited PQ uptake and that W-7, a putative calmodulin antagonist, reduced PQ uptake in a dose-dependent manner, thus suggesting the involvement of the polyamine transport system (Grabie et al. 1993). Moreover, given the similarity in the characteristics of polyamines and the y+ basic amino acid transport systems, the existence of a common transport site for polyamines and the basic amino acids in rat intestinal epithelial cells was already proposed (Sharpe and Seidel 2005).

Taking these findings in consideration and since the most effective way to reduce PQ blood concentrations, and consequently limit its accumulation in the lung, is to inhibit its gastrointestinal absorption (Heylings et al. 2007), we sought to further elucidate the transport mechanisms involved in its intestinal uptake. For that purpose, substrates and inhibitors for choline, amino acids and polyamines transporters were used to clarify their involvement in the herbicide uptake and, consequently, in its toxicity. Caco-2 cells, which are derived from human colorectal adenocarcinoma, were used, since they are a reliable and validated *in vitro* model widely used for predicting drug intestinal absorption in humans (Barta et al. 2008; Huynh-Delerme et al. 2005; Watanabe et al. 2005; Yamashita et al. 2000).

2. MATERIALS AND METHODS

2.1. Materials

Paraquat (PQ), ethyl paraquat (EPQ), sodium borohydride ($NaBH_4$), bovine serum albumin (BSA), choline (CHO) chloride, hemicolinium-3 (HC-3), L-arginine (ARG), L-lysine (LYS), L-valine (VAL), putrescine (PUT), norvaline (NOR), N-ethylmalemide (NEM), trifluoperazine (TFP), N-methyl-N-(trimethylsilyl)trifluoroacetamide (MSTFA) and (4,5-dimethylthiazol-2-yl)-2,5-diphenyl tetrazolium (MTT) bromide were obtained from Sigma (St. Louis, MO, USA). Reagents used in cell culture, including Dulbecco's Modified Eagle's Medium (DMEM) with 4.5 g/L glucose and GlutaMAX™, non-essential amino acids (NEAA), heat inactivated fetal bovine serum (FBS), 0.25% trypsin/1 mM EDTA, antibiotic (10000 U/mL penicillin, 10000 µg/mL streptomycin), fungizone (250 µg/mL amphotericin B), human transferrin (4 mg/mL), phosphate-buffered saline solution (PBS) and Hanks' balanced salt solution with Ca^{2+} and Mg^{2+} [HBSS (+/+)] were purchased from Gibco Laboratories (Lenexa, KS, USA). Bio-Rad DC protein assay kit was purchased from Bio-Rad (Hercules, CA, USA). C18 cartridges (Bond Elut® C18) were purchased from Agilent (California, USA). All other reagents used were of analytical grade or of the highest grade available.

2.2. Caco-2 cell culture

Caco-2 cells were routinely cultured in 75 cm^2 flasks using DMEM with 4.5 g/L glucose and GlutaMAX™, supplemented with 10% heat inactivated FBS, 1% NEAA, 1% antibiotic, 1% fungizone and 6 µg/mL transferrin. Cells were maintained in a 5% CO_2–95% air atmosphere, at 37 ºC, and the medium was changed every 2 days. Cultures were passaged weekly/ by trypsinization (0.25% trypsin/1 mM EDTA). The cells used in all the experiments were taken between the 58th and 64th passages. In all experiments, the cells were seeded at the density of 60,000 cells/cm^2, and used 4 days after seeding, when confluence was reached.

2.3. Cytotoxicity assay

The cytotoxicity of all compounds used in this study was initially evaluated at 24 h by the MTT reduction assay, in which mitochondrial activity is used to estimate cell viability. Briefly, the cells were seeded onto 96-well plates and, after reaching confluence, the cell culture medium was removed and replaced by fresh cell culture medium supplemented with CHO (0 - 500 µM), HC-3 (0 - 500 µM), ARG (500 µM), LYS (500 µM), VAL (500 µM), PUT (0 - 250 µM), NEM (0 - 5 µM) and TFP (0 - 20 µM). Twenty-four hours after exposure, the cell culture medium was removed, and fresh cell culture medium containing

0.5 mg/mL MTT was added, followed by incubation at 37 °C, in a humidified, 5% CO_2-95% air atmosphere, for 1 h. After this incubation period, the cell culture medium was removed and the formed formazan crystals dissolved in 100% DMSO. The absorbance was measured at 550 nm in a multi-well plate reader (PowerWave X, Bio-Tek Instruments, Vermont, USA). The percentage of MTT reduction relative to that of the control cells was used as the cytotoxicity measure. Results are presented as mean ± SEM from 8 independent experiments (performed in triplicate).

2.4. Paraquat cytotoxicity - effect of choline and hemicolinium-3

Paraquat cytotoxicity was evaluated by the MTT reduction assay, with or without incubation with CHO or HC-3, following two distinct protocols. Briefly, the cells were seeded onto 96-well plates, to obtain confluent monolayers at the day of the experiment. In the first protocol the cells were exposed to PQ (0 - 5000 μM) with or without simultaneous exposure to 100, 250 or 500 μM CHO or HC-3. In the second protocol, the cells were exposed to PQ (0 - 5000 μM) and six hours after CHO or HC-3 (100 μM) were added. In both protocols, cytotoxicity was evaluated 24 h after PQ exposure by the MTT reduction assay (as described in section 2.3). Results are presented as mean ± SEM from at least 4 independent experiments (performed in triplicate).

2.5. Paraquat cytotoxicity - effect of putrescine

Paraquat cytotoxicity was evaluated in Caco-2 cells by the MTT reduction assay, with or without simultaneous incubation with putrescine (PUT), a potent inhibitor of PQ uptake into lung tissue (Shimizu et al. 2001). Briefly, the cells were seeded onto 96-well plates to obtain confluent monolayers at the day of the experiment. After reaching confluence, the cells were exposed to PQ (0 - 5000 μM) in fresh cell culture medium with or without simultaneous exposure to 50, 100 or 250 μM PUT. Cytotoxicity was then evaluated 24 h after PQ exposure by the MTT reduction assay (as described in section 2.3).

Polyamines transport was reported to be calcium/calmodulin (Ca^{2+}/CaM) sensitive (Sharpe and Seidel 2005). Therefore, PQ cytotoxicity was also evaluated with or without simultaneous exposure to 5, 10 or 20 μM trifluoperazine (TFP), a potent competitive inhibitor of the Ca^{2+}/CaM complex (Alexander et al. 1988). Results are presented as mean ± SEM from 6 independent experiments (performed in triplicate).

2.6. Paraquat cytotoxicity - effect of amino acids

Paraquat cytotoxicity was evaluated in Caco-2 cells by the MTT assay, with or without simultaneous incubation with different amino acids. Briefly, the cells were seeded onto 96-well plates to obtain confluent monolayers at the day of the experiment. After reaching confluence, the cells were exposed to PQ (0 - 5000 μM) in fresh cell culture medium with or without simultaneous exposure to 500 μM ARG, LYS or VAL. PQ cytotoxicity was then evaluated 24 h after exposure by the MTT reduction assay (as described in section 2.3). Paraquat (0 - 5000 μM) cytotoxicity was further evaluated in the presence or absence of NEM (0.5, 1 and 5 μM), an inhibitor of the y^+ lysine transport system (Sharpe and Seidel 2005). Results are presented as mean ± SEM from 6 independent experiments (performed in triplicate).

2.7. Quantification of paraquat intracellular levels

PQ intracellular levels were measured in Caco-2 cells with or without simultaneous exposure to the tested compounds, to correlate the observed cytotoxicity with putative effects on PQ uptake.

2.7.1. Preparation of standard solutions

A PQ stock solution (5 mM) was prepared in PBS. Working PQ standard solutions were prepared through serial dilution of the stock standard solution with PBS (pH 7.4) to obtain a 0-100 μM calibration curve. A stock solution of the internal standard (ethylparaquat, EPQ) (1 mg/mL) was prepared in PBS. All stock solutions were stored at -20 °C.

2.7.2. Sample preparation

Caco-2 cells were seeded onto 48-well plates, at a density of 60,000 cells/cm^2 and incubated, after reaching confluence, with PQ (0, 500, 1000, 2500 or 5000 μM) in fresh cell culture medium, with or without simultaneous exposure to the tested compounds: 500 μM CHO, 500 μM HC-3, 500 μM ARG, 500 μM LYS, 500 μM VAL, 250 μM PUT, 5 μM NEM and 20 μM TFP. Twenty-four hours after PQ exposure, the cell culture medium was removed and the cells washed three times with PBS (pH 7.4). The cells were then killed by freezing at -80 ºC with 1000 μL distilled water. After homogenization, the cell lysates were centrifuged at 3,000 g, for 10 min, at 4 ºC, and the supernatant used for PQ extraction and quantification. The cell pellet was dissolved in 0.3 M NaOH and protein content was quantified.

2.7.3. Paraquat extraction

PQ extraction was performed as previously described with slight modifications (Silva et al. 2013). Briefly, samples or standards were pipetted into a 5 mL glass tube containing 1.5 mL of PBS (pH 7.4) and 20 µL of EPQ solution (100 µg/mL). Ten milligrams of sodium borohydride ($NaBH_4$) were added to the solution, followed by heating at 60 °C for 10 min, to reduce PQ and EPQ to their hydrogenated derivatives, HPQ and HEPQ, respectively. The analytes were then extracted by using solid-phase extraction (SPE) C18 cartridges, which were previously preconditioned with 2 mL methanol followed by 2 mL PBS (pH 7.4). The samples or standards were transferred to the C18 cartridges that were further washed with 2 mL of distilled water. HPQ and HEPQ elution was then performed with 2 mL methanol and the eluate was evaporated at room temperature under a gentle nitrogen stream. The residue was dissolved in 100 µL methanol.

2.7.4. Gas chromatography-ion trap-mass spectrometry (GC-IT/MS) analysis

GC-IT/MS analyses of HPQ and HEPQ were performed using a Varian CP-3800 gas chromatograph (USA) equipped with a VARIAN Saturn 4000 mass selective detector (USA) and a Saturn GC/MS workstation software version 6.8. A chromatographic column, VF-5 ms (30 m×0.25 mm i.d. ×0.25 µm film thickness) from VARIAN, was used. Two microliters of each sample or standard were injected using a Combi PAL automatic autosampler (Varian, Palo Alto, CA). The injector port was heated to 250 °C and was operated in splitless mode. The carrier gas, helium, was delivered at a constant flow rate of 1.0 mL/min. The oven temperature was 80 °C (for 1 min), then increased 2 °C/min until 270 °C and held for 20 min. All mass spectra were acquired by electron impact (EI, 70 eV) in full scan mode. Ionization was maintained off during the first 2 min to avoid solvent overloading. The ion-trap detector was set as follows: the transfer line, manifold and trap temperatures were 280, 50 and 180 °C, respectively. The mass range was 50 to 600 *m/z*, with a scan rate of 6 scan/seconds. The emission current was 50 µA, and the electron multiplier was set in relative mode to autotune procedure. The maximum ionization time was 25,000 µseconds, with an ionization storage level of 35 *m/z*. Chromatographic peak areas of HPQ and HEPQ were determined by the reconstructed FullScan chromatogram (FSC) using specific ions for each compound. The ions selected for quantification were: *m/z* 96, 148, and 192 for HPQ, and *m/z* 110, 162, and 220 for HEPQ. Results are presented as mean ± SEM from 4 independent experiments (performed in duplicate).

2.8. Quantification of Lysine intracellular levels

2.8.1. Preparation of standard solutions

A stock solution of norvaline (NOR, 0.3 mg/ml), used as internal standard, was prepared in absolute ethanol and a stock solution of LYS (10 mM) was prepared in PBS (pH 7.4). Working LYS standard solutions were prepared through serial dilution of the stock standard solution in absolute ethanol added with 0.3 µg/mL NOR to obtain a 0-400 µM calibration curve. All stock solutions were stored at -20 °C.

2.8.2. Sample preparation

Caco-2 cells were seeded onto 6-well plates, at a density of 60,000 cells/cm^2, and incubated, after reaching confluence, with 3000 µM LYS in HBSS (+/+) in the presence or absence of 3000 µM ARG, 3000 µM VAL, PUT (3000 µM or 5000 µM), 5 µM NEM or 20 µM TFP, at 37 ºC, for 30 min. Control cells, incubated only with HBSS (+/+), were also performed. The LYS uptake was stopped by aspiration of the incubation mixture, and the cells were washed three times with HBSS (+/+). After addition of 1000 µL absolute ethanol (containing 0.3 µg/mL NOR), cells were incubated for 20 min, at 40 ºC, to allow complete LYS extraction. After homogenization, the cell lysates were centrifuged at 3,000 g, for 10 min, at 4 ºC, and the supernatant used for LYS derivatization and quantification. The cell pellet was dissolved in 0.3 M NaOH and protein content was quantified.

2.8.3. Derivatization

The samples supernatants and standards were evaporated to dryness at room temperature, under a gentle nitrogen stream. Fifty microliters of the derivatizing agent, MSTFA, were added to the residue, the vial was capped and vortexed, and heated at 40 ºC, for 20 min. Finally, 50 µL of ethyl acetate were added to the derivatized samples/standards.

2.8.4. Gas chromatography-ion trap-mass spectrometry analysis

GC–IT/MS analysis was performed as previously described (Pereira et al. 2012) in a Varian CP-3800 gas chromatograph, coupled to a Varian Saturn 4000 mass selective ion trap detector (USA) and a Saturn GC/MS workstation software version 6.8. A VF-5 ms (30 m x 0.25 mm x 0.25 µm) column from Varian was used in the analysis. The chromatographic conditions are described below. Two microliters of each sample or standard were injected using a CombiPAL automatic autosampler (Varian, Palo Alto, CA). The injector port was heated to 250 ºC. Injections were performed in split mode, with a

ratio of 1/40. The carrier gas was helium C-60 (Gasin, Portugal), at a constant flow of 1 mL/min. The oven temperature was set at 100 ºC for 1 min then increasing 20 ºC min^{-1} to 250ºC, held for 2 min, 10 ºC/min to 300 ºC and held for 10 min. All mass spectra were acquired in electron impact (EI) mode. Ionization was maintained off during the first 4 min to avoid solvent overloading. The ion trap detector was set as follows: transfer line, manifold and trap temperatures were 280, 50, and 180 ºC, respectively. The mass ranged from 50 to 600 m/z, with a scan rate of 6 scan/s. The electron multiplier was set in relative mode to auto tune procedure emission, with a current of 50 µA. The maximum ionization time was 25,000 µs, with an ionisation storage level of 35 m/z. The analysis was performed in full scan mode. Chromatographic peak areas of LYS and NOR were determined by the reconstructed FullScan chromatogram (FSC) using specific ions (m/z) for each compound. The ions selected for quantification were: *m/z* 84, 156, and 362 for LYS, and *m/z* 73, 144, and 218 for NOR. The LYS amount present in the cells extracts was calculated from the calibration curve of the respective standard. Results are presented as mean ± SEM from 4 independent experiments (performed in triplicate).

2.9. Protein quantification

The protein concentration was determined using the Bio-Rad DC protein assay kit, according to the manufacturer's instructions. Bovine serum albumin was used as protein standard.

2.10. Statistical analysis

All statistical analyses were performed with the GraphPad Prism version 6.00 for Windows (GraphPad Software, San Diego, California, USA). Normality of the data distribution was assessed by three different tests: KS normality test, D'Agostino & Pearson omnibus normality test and Shapiro-Wilk normality test.

For the MTT reduction assay, statistical comparisons between groups were made using the nonparametric method of Kruskal–Wallis (one-way ANOVA on ranks), followed by the Dunn's *post hoc* test.

All concentration-response curves were fitted using least squares as the fitting method and the comparisons between curves (LOG EC_{50}, TOP, BOTTOM and Hill slope) were made using the extra sum-of-squares F test. Statistical comparisons between groups were made using Two-way ANOVA, followed by the Sidak's multiple comparisons *post hoc* test. In all cases, *p* values lower than 0.05 were considered significant.

For the quantification of PQ intracellular levels, statistical comparisons were made using Two-way ANOVA, followed by the Bonferroni's multiple comparison *post-hoc* test.

For the quantification of LYS intracellular levels, statistical comparisons were made using One-way ANOVA, followed by the Bonferroni's multiple comparisons *post hoc* test.

Details of the statistical analysis are described in each figure legend. In all cases, *p* values lower than 0.05 were considered significant.

3. RESULTS

3.1. Test compounds cytotoxicity

Prior to the evaluation of the possible effect of the selected test compounds on PQ cytotoxicity their own cytotoxicity was evaluated by the MTT reduction assay, 24 h after exposure, to select non-cytotoxic working concentrations. Overall, for all tested concentrations (0 - 500 µM choline and hemicolinium-3; 500 µM arginine, lysine and valine; 0 - 250 µM putrescine; 0 - 20.0 µM trifluoperazine; and 0 - 5.0 µM N-ethylmaleimide) no significant mitochondrial dysfunction was observed in Caco-2 cells (Figure S1, Supplementary data).

3.2. Paraquat cytotoxicity

3.2.1. Effect of choline and hemicolinium-3

Previous studies have implicated the carrier-mediated transport system for CHO on PQ absorption in the rat brush-border membrane (Nagao et al. 1993). Moreover, other studies have demonstrated that doxorubicin significantly decreased PQ accumulation and, consequently, its cytotoxicity in Caco-2 cells, partially due to the inhibition of the choline transporter (Silva et al. 2013). Thus, to assess the relative contribution of the carrier-mediated transport system for CHO on PQ uptake, and consequently on its toxicity, we evaluated the effect of its natural substrate, CHO (100, 250 or 500 µM), on PQ cytotoxicity.

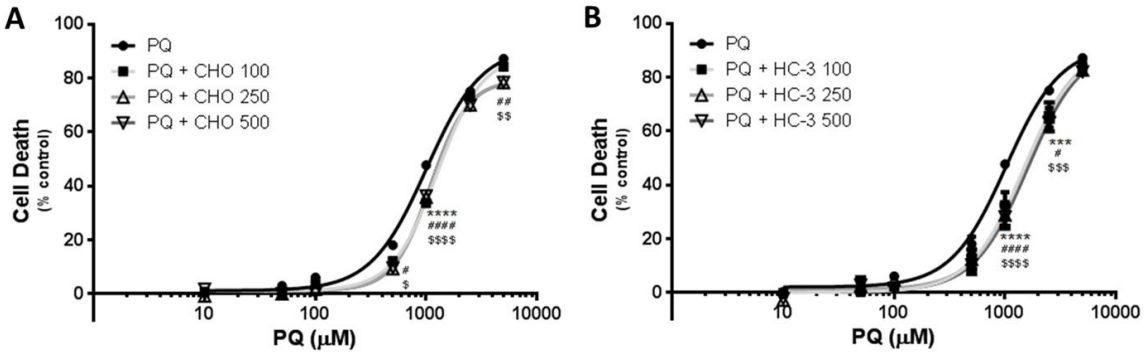

Figure 1. (A) Paraquat concentration–response (cell death) curves with (PQ + CHO) or without (PQ) simultaneous exposure to choline (100, 250 or 500 µM). **(B)** Paraquat concentration-response (cell death) curves with (PQ + HC-3) or without (PQ) simultaneous exposure to hemicolinium-3 (100, 250 or 500 µM).Results are presented as mean ± SEM from 4 independent experiments (performed in triplicate). Concentration–response curves were fitted using least squares as the fitting method and the comparisons between PQ and PQ + CHO or PQ + HC-3 curves (LOG EC_{50}, TOP, BOTTOM and Hill slope) were made using the extra sum-of-squares F test. Statistical comparisons were made using Two-way ANOVA, followed by the Sidak's multiple comparisons *post hoc* test. **(A)** $^{****}p < 0.0001$ PQ + CHO 100 *vs.* PQ alone; $^{\#}p < 0.05$, $^{\#\#}p < 0.01$, $^{\#\#\#\#}p < 0.0001$ PQ + CHO 250 *vs.* PQ alone; $^{\$}p < 0.05$, $^{\$\$}p < 0.01$, $^{\$\$\$\$}p < 0.0001$ PQ + CHO 500 *vs.* PQ alone. **(B)** $^{***}p < 0.001$, $^{****}p < 0.0001$ PQ + HC-3 100 *vs.* PQ alone; $^{\#}p < 0.05$, $^{\#\#\#\#}p < 0.0001$ PQ + HC-3 250 *vs.* PQ alone; $^{\$\$\$}p < 0.001$, $^{\$\$\$\$}p < 0.0001$ PQ + HC-3 500 *vs.* PQ alone.

Table 1. EC_{50} (half-maximum-effect concentration), TOP (maximal effect), BOTTOM (baseline) and Hill slope values of the paraquat concentration-response curves, with (PQ + CHO) or without (PQ) simultaneous exposure to choline (100, 250 and 500 μM).

	PQ	PQ + CHO 100	PQ + CHO 250	PQ + CHO 500
EC_{50} (half-maximum-effect concentration, μM)	**1012**	**1262**	**1098**	**1091**
TOP (maximal cell death, % control)	91.05	88.86	79.75	79.49
BOTTOM (baseline, % control)	2.179	1.170	0.09262	0.6233
Hill slope	1.801	2.144	2.482	2.516
LOG EC_{50} *p* value (comparison between LOG EC_{50} values)	-	**0.0157***	0.3027* 0.2095$	0.3405* 0.1797$ 0.9405#
TOP *p* value (comparison between TOP values)	-	0.6671*	**0.0128*** 0.0919$	**0.0112*** 0.0770$ 0.9514#
BOTTOM *p* value (comparison between BOTTOM values)	-	0.5722*	0.2229* 0.5999$	0.3625* 0.7860$ 0.7783#
Hill slope *p* value (comparison between Hill slope values)	-	0.2956*	0.0621* 0.4820$	0.0560* 0.4413$ 0.9490#
Curve *p* value (Comparison between the Fitted Curves)	-	**< 0.0001***	**< 0.0001*** 0.3678$	**< 0.0001*** 0.3787$ 0.9984#

Concentration-response curves were fitted using least squares as the fitting method and the comparisons between the fitted curves were made using extra sum-of-squares F test. In all cases, *p* values lower than 0.05 were considered significant. * Comparison *vs*. PQ; $ Comparison *vs*. PQ + CHO 100; # Comparison *vs*. PQ + CHO 250.

As observed in Figure 1A, CHO, at all tested concentrations, caused a significant rightwards shift of the PQ concentration-response curves, resulting in significant differences in the overall comparison of the fitted curves (PQ + CHO) when compared to the PQ curve (Table 1). For 100 μM CHO, no significant differences were observed, neither in the maximal cell death (TOP), nor in baseline (BOTTOM) of the fitted PQ + CHO 100 curve, when compared to the PQ curve (Table 1). Therefore, the EC_{50} value, which represents the half-maximum-effect concentration of the fitted curve, was used for comparison. As shown in Table 1, for 100 μM CHO, the observed rightwards shift of the PQ concentration-response curve was accompanied by a significant increase in the EC_{50} value, when compared to the EC_{50} of the PQ curve (1262 μM vs. 1012 μM for PQ curve). For 250 and 500 μM CHO, significant differences were observed in the maximal cell death (TOP) of the fitted curves (Table 1). For this reason, the TOP values were used instead for the comparison between the different fitted curves. As observed in Table 1, for the higher CHO concentrations tested (250 and 500 μM), a significant decrease was observed

in the TOP values of the fitted curves (79.75 and 79.49 %, respectively). However, the observed protective effect of CHO on PQ cytotoxicity was not concentration-dependent as no significant differences exist in the overall comparison of all the PQ + CHO curves (Table 1).

Table 2. EC_{50} (half-maximum-effect concentration), TOP (maximal effect), BOTTOM (baseline) and Hill slope values of the paraquat concentration-response curves, with (PQ + HC-3) or without (PQ) simultaneous exposure to hemicolinium-3 (100, 250 and 500 μM).

	PQ	PQ + HC-3 100	PQ + HC-3 250	PQ + HC-3 500
EC_{50} (half-maximum-effect concentration, μM)	**1012**	**1527**	**1519**	**1654**
TOP (maximal cell death, % control)	91.05	94.08	92.07	94.08
BOTTOM (baseline, % control)	2.179	0.06233	1.248	0.3201
Hill slope	1.801	1.722	1.852	1.733
LOG EC_{50} *p* value (comparison between LOG EC_{50} values)	-	**0.0005***	**0.0002*** 0.9773$^{\$}$	**< 0.0001*** 0.7052$^{\$}$ 0.8935$^{\#}$
TOP *p* value (comparison between TOP values)	-	0.6751*	0.8825* 0.8496$^{\$}$	0.7017* 0.9996$^{\$}$ 0.9772$^{\#}$
BOTTOM *p* value (comparison between BOTTOM values)	-	0.2577*	0.6116* 0.6148$^{\$}$	0.3159* 0.9140$^{\$}$ 0.8695$^{\#}$
Hill slope *p* value (comparison between Hill slope values)	-	0.7949*	0.8790* 0.7542$^{\$}$	0.8299* 0.9773$^{\$}$ 0.9441$^{\#}$
Curve *p* value (Comparison between the Fitted Curves)	-	**< 0.0001***	**< 0.0001*** 0.9906$^{\$}$	**< 0.0001*** 0.8902$^{\$}$ 0.9895$^{\#}$

Concentration-response curves were fitted using least squares as the fitting method and the comparisons between the fitted curves were made using extra sum-of-squares F test. In all cases, *p* values lower than 0.05 were considered significant. * Comparison *vs*. PQ; $^{\$}$ Comparison *vs*. PQ + HC-3 100; $^{\#}$ Comparison *vs*. PQ + HC-3 250.

Hemicolinium-3 is a structural analogue of choline and a known competitive inhibitor of both Na^+-dependent and Na^+-independent choline transporters in many tissues (Kamath et al. 2003). For this reason, to further clarify the possible involvement of the choline transporter, PQ cytotoxicity was evaluated with or without simultaneous exposure to HC-3 (100, 250 or 500 μM) for 24 h. As observed in Figure 1B, the simultaneous exposure to HC-3, at all the tested concentrations, resulted in a significant rightwards shift of the PQ concentration-response curves (PQ + HC-3), which was accompanied by significant increases in the EC_{50} values (Table 2). In fact, the observed increases in the EC_{50} values for all PQ + HC-3 curves result from the notorious reduction in the cell death,

which was significant for the 1000 and 2500 µM PQ concentrations (Figure 1B). However, as observed for CHO, the HC-3 observed protective effect was concentration-independent with no significant differences neither in the overall comparison of the fitted curves, nor in the comparison of the individual parameters (LOG EC_{50}, TOP, BOTTOM and Hill slope) (Table 2).

PQ absorption in humans is estimated to be 1–5% over 1–6 h (Dinis-Oliveira et al. 2008). Therefore, the protective effect of both CHO (100 µM) and HC-3 (100 µM) was also evaluated when adding the compounds 6 h after the beginning of PQ exposure. As no significant differences were obtained for the TOP and BOTTOM values of the fitted curves (Table 3), the EC_{50} values were used as comparative measure. As observed in Figure 2, both CHO (100 µM) and HC-3 (100 µM) significantly protected against PQ toxicity, as observed by the significant rightwards shifts of the PQ + CHO 100 and PQ + HC-3 100 curves, and confirmed by significant increases in the EC_{50} values of the fitted curves (Table 3). In fact, the simultaneous exposure to 100 µM CHO or 100 µM HC-3 resulted in a significant increase in the EC_{50} value to 1335 and 1511 µM, respectively, when compared to the EC_{50} of the PQ curve (1011 µM) (Table 3). Additionally, for both compounds, the observed rightwards shifts of the fitted curves result from the significant reduction in cell death, with significant effect for the 500 - 2500 µM PQ concentration range (Figure 2). Interestingly, no significant differences exist between the two different experimental designs, since no differences were observed between the fitted curves when PQ and CHO or HC-3 were incubated simultaneously and when CHO and HC-3 were added 6 h after the beginning of PQ exposure (Table S1, Supplementary data).

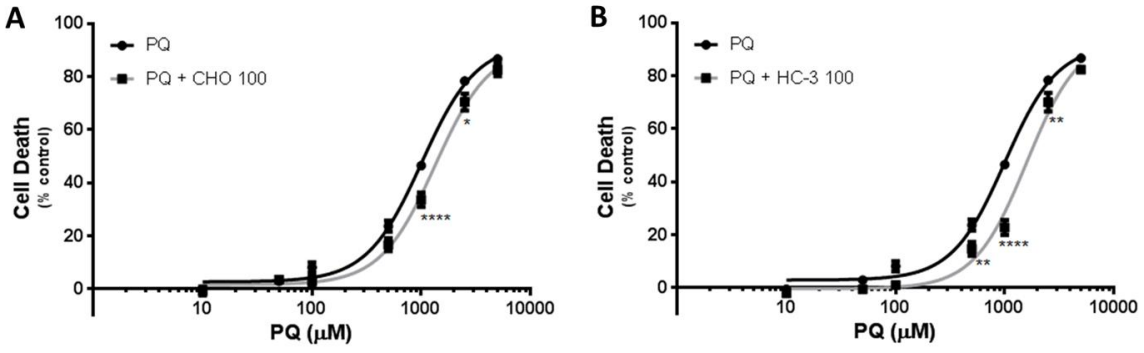

Figure 2. (A) Paraquat concentration–response (cell death) curves with (PQ + CHO) or without (PQ) exposure to choline (100 µM) 6 h after PQ. **(B)** Paraquat concentration–response (cell death) curves with (PQ + HC-3) or without (PQ) exposure to hemicolinium-3 (100 µM) 6 h after PQ. Results are presented as mean ± SEM from 5 independent experiments (performed in triplicate). Concentration–response curves were fitted using least squares as the fitting method and the comparisons between PQ and PQ + CHO or PQ + HC-3 curves (LOG EC_{50}, TOP, BOTTOM and Hill slope) were made using the extra sum-of-squares F test. Statistical comparisons between groups were made using Two-way ANOVA, followed by the Sidak's multiple comparisons *post hoc* test (*p<0.05; **p<0.01; ****p<0.0001 *vs.* PQ alone).

Table 3. EC_{50} (half-maximum-effect concentration), TOP (maximal effect), BOTTOM (baseline) and Hill slope values of the paraquat concentration-response curves, with (PQ + CHO and PQ + HC-3) or without (PQ) exposure to choline or hemicolinium-3 (100 μM) 6 h after the beginning of PQ exposure.

	PQ	PQ + CHO 100	PQ + HC-3 100
EC_{50} (half-maximum-effect concentration, μM)	**1011**	**1335**	**1511**
TOP (maximal cell death, % control)	92.74	91.46	91.10
BOTTOM (baseline, % control)	2.698	1.627	0.2614
Hill slope	1.727	1.744	2.033
LOG EC_{50} *p* value (comparison between LOG EC_{50} values)	-	**0.0076**	**< 0.0001**
TOP *p* value (comparison between TOP values)	-	0.8432	0.7798
BOTTOM *p* value (comparison between BOTTOM values)	-	0.5605	0.1912
Hill slope *p* value (comparison between Hill slope values)	-	0.9561	0.3479
Curve *p* value (Comparison between the Fitted Curves)	-	**< 0.0001**	**< 0.0001**

Concentration-response curves were fitted using least squares as the fitting method and the comparisons between PQ and PQ + CHO or PQ + HC-3 curves were made using extra sum-of-squares F test. In all cases, *p* values lower than 0.05 were considered significant.

3.2.2. Effect of putrescine and trifluoperazine

PQ lung uptake was described to occur through the polyamine uptake system (Rose et al. 1976; Rose et al. 1974; Smith 1982). In addition, it appears to be competitively inhibited by a number of naturally occurring amines, such as putrescine, cadaverine, spermidine and spermine (Smith 1982; Wyatt et al. 1988). Thus, in the present study, the effect of putrescine (50, 100 or 250 μM) on PQ cytotoxicity was evaluated in Caco-2 cells. As shown in Figure 3A, PUT, at all the tested concentrations, caused a significant protective effect against the PQ cytotoxicity, as demonstrated by the rightwards shift of all the PQ + PUT curves, resulting in significant differences in the cell death observed mainly for the higher PQ concentrations (500 - 5000 μM). For 50 μM PUT, no significant differences were observed in both TOP and BOTTOM values of the fitted curves, when compared to the PQ curve (Table 4). Therefore, the EC_{50} value was used as comparative measure.

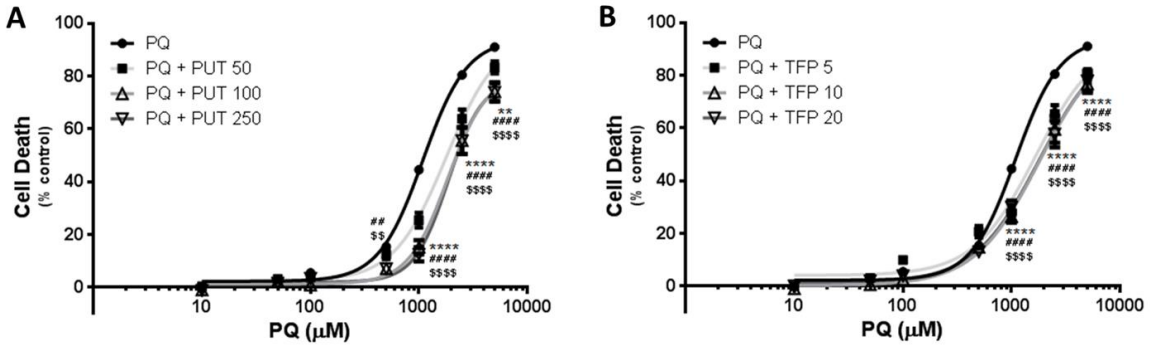

Figure 3. (A) Paraquat concentration–response (cell death) curves with (PQ + PUT) or without (PQ) simultaneous exposure to putrescine (50, 100 or 250 μM). **(B**) Paraquat concentration–response (cell death) curves with (PQ + TFP) or without (PQ) simultaneous exposure to trifluoperazine (5, 10 or 20 μM). Results are presented as mean ± SEM from 6 independent experiments (performed in triplicate). Concentration–response curves were fitted using least squares as the fitting method and the comparisons between the fitted curves (LOG EC_{50}, TOP, BOTTOM and Hill slope) were made using the extra sum-of-squares F test. Statistical comparisons between groups were made using Two-way ANOVA, followed by the Sidak's multiple comparisons *post hoc* test. **(A)** $^{**}p < 0.01$, $^{****}p < 0.0001$ PQ + PUT 50 *vs.* PQ alone; $^{\#\#}p < 0.01$, $^{\#\#\#\#}p < 0.0001$ PQ + PUT 100 *vs.* PQ alone; $^{\$\$}p < 0.01$, $^{\$\$\$\$}p < 0.0001$ PQ + PUT 250 *vs.* PQ alone. **(B)** $^{****}p < 0.0001$ PQ + TFP 5 *vs.* PQ alone; $^{\#\#\#\#}p < 0.0001$ PQ + TFP 10 *vs.* PQ alone; $^{\$\$\$\$}p < 0.0001$ PQ + TFP 20 *vs.* PQ alone.

Simultaneous exposure to 50 μM PUT significantly increased the EC_{50} value of PQ cytotoxicity (1786 μM vs. 1088 μM for PQ curve). For 100 and 250 μM PUT, although significant differences were observed in the EC_{50} values (Table 4), since the TOP values of the PQ + PUT curves were significantly different from the TOP value of the PQ curve, the maximal cell death was the parameter used for comparison between the fitted curves. Simultaneous exposure to 100 and 250 μM PUT resulted in a significant decrease in the TOP value to 81.13 and 78.69 %, respectively (Table 4). In addition, the PQ + PUT 100 and PQ + PUT 250 curves were significantly different from the PQ + PUT 50 curve, with a significant reduction in PQ-induced toxicity for the 1000-5000 μM PQ concentration range (Table 4 and Figure S2A, supplementary data). Although no significant effects were observed in the EC_{50} values of the PQ + PUT curves (Table 4), it was observed a significant decrease in the TOP value of the PQ + PUT 250 curve, when compared to the PQ + PUT 50 curve.

Previous studies have demonstrated that the polyamine transport, in cultured gastrointestinal epithelial cells, is Ca^{2+}/CaM sensitive (Groblewski et al. 1992; Scemama et al. 1993; Sharpe and Seidel 2005). Therefore, PQ cytotoxicity was further evaluated with or without simultaneous exposure to trifluoperazine (TFP - 5, 10 or 20 μM), a potent competitive inhibitor of the Ca^{2+}/CaM complex. As observed in Figure 3B, simultaneous exposure to TFP significantly decreased PQ cytotoxicity (rightwards shift of all the PQ + TFP curves, when compared to the PQ curve), shown also by the significant decrease in the cell death observed for the higher PQ concentrations (1000 - 5000 μM). Additionally,

as shown in Table 5, a significant increase in the EC_{50} value was observed for all TFP concentrations (1827, 1871 and 1964 μM for PQ + TFP 5, 10 and 20 μM, respectively, *vs.* 1088 μM for the PQ curve). Furthermore, no significant differences were observed neither in the overall comparison of all the PQ + TFP curves, nor in the EC_{50} and TOP values (Table 5).

Table 4. EC_{50} (half-maximum-effect concentration), TOP (maximal effect), BOTTOM (baseline) and Hill slope values of the paraquat concentration-response curves, with (PQ + PUT) or without (PQ) simultaneous exposure to putrescine (50, 100 and 250 μM).

	PQ	PQ + PUT 50	PQ + PUT 100	PQ + PUT 250
EC_{50} (half-maximum-effect concentration, μM)	**1088**	**1786**	**1840**	**1863**
TOP (maximal cell death, % control)	94.16	96.25	81.13	78.69
BOTTOM (baseline, % control)	2.301	2.389	1.258	2.024
Hill slope	2.137	1.799	2.382	2.764
LOG EC_{50} *p* value (comparison between LOG EC_{50} values)	-	**< 0.0001***	**< 0.0001*** 0.8529$^{\$}$	**< 0.0001*** 0.7836$^{\$}$ 0.9264$^{\#}$
TOP *p* value (comparison between TOP values)	-	0.7486*	**0.0488*** 0.1106$^{\$}$	**0.0093*** **0.0384**$^{\$}$ 0.7507$^{\#}$
BOTTOM *p* value (comparison between BOTTOM values)	-	0.9505*	0.4487* 0.5827$^{\$}$	0.8372* 0.8557$^{\$}$ 0.7200$^{\#}$
Hill slope *p* value (comparison between Hill slope values)	-	0.1947*	0.4617* 0.2010$^{\$}$	0.0915* 0.0514$^{\$}$ 0.5479$^{\#}$
Curve *p* value (Comparison between the Fitted Curves)	-	**< 0.0001***	**< 0.0001*** **0.0001**$^{\$}$	**< 0.0001*** **< 0.0001**$^{\$}$ 0.9653$^{\#}$

Concentration-response curves were fitted using least squares as the fitting method and the comparisons between the fitted curves were made using extra sum-of-squares F test. In all cases, *p* values lower than 0.05 were considered significant. * Comparison *vs*. PQ; $^{\$}$ Comparison *vs*. PQ + PUT 50; $^{\#}$ Comparison *vs*. PQ + PUT 100.

Table 5. EC_{50} (half-maximum-effect concentration), TOP (maximal effect), BOTTOM (baseline) and Hill slope values of the paraquat concentration-response curves, with (PQ + TFP) or without (PQ) simultaneous exposure to trifluoperazine (5, 10 and 20 μM).

	PQ	PQ + TFP 5	PQ + TFP 10	PQ + TFP 20
EC_{50} (half-maximum-effect concentration, μM)	**1088**	**1827**	**1871**	**1964**
TOP (maximal cell death, % control)	94.16	~100.0	96.62	99.30
BOTTOM (baseline, % control)	2.301	3.671	0.1232	1.037
Hill slope	2.137	1.388	1.404	1.358
LOG EC_{50} *p* value (comparison between LOG EC_{50} values)	-	**< 0.0001***	**< 0.0001*** 0.9176$^{\$}$	**< 0.0001*** 0.7856$^{\$}$ 0.8973$^{\#}$
TOP *p* value (comparison between TOP values)	-	0.4508*	0.8163* 0.8067$^{\$}$	0.6634* 0.9637$^{\$}$ 0.8950$^{\#}$
BOTTOM *p* value (comparison between BOTTOM values)	-	0.3620*	0.1681* 0.1231$^{\$}$	0.4210* 0.2470$^{\$}$ 0.7083$^{\#}$
Hill slope *p* value (comparison between Hill slope values)	-	**0.0081***	**0.0074*** 0.9559$^{\$}$	**0.0051*** 0.9190$^{\$}$ 0.9071$^{\#}$
Curve *p* value (Comparison between the Fitted Curves)	-	**< 0.0001***	**< 0.0001*** 0.0689$^{\$}$	**< 0.0001*** 0.2271$^{\$}$ 0.9844$^{\#}$

Concentration-response curves were fitted using least squares as the fitting method and the comparisons between the fitted curves were made using extra sum-of-squares F test. In all cases, *p* values lower than 0.05 were considered significant. * Comparison *vs*. PQ; $^{\$}$ Comparison *vs*. PQ + TFP 5; $^{\#}$ Comparison *vs*. PQ + TFP 10.

3.2.3. Effect of amino acids and N-ethylmalemide

Previous studies performed in the IEC-6 small intestinal epithelial cell line, have demonstrated that polyamines and basic amino acids seem to be transported by a common carrier, the y^+ amino acid carrier (Sharpe and Seidel 2005). Thus, the effect of two basic amino acids, arginine and lysine, on PQ cytotoxicity was evaluated. The obtained results show a significant rightwards shift of the PQ + ARG 500 and PQ + LYS 500 curves, when compared to the PQ curve (Figure 4A), thus indicating a significant protection against PQ toxicity. Additionally, this protective effect was clearly significant for the higher PQ concentrations (500 - 5000 μM) (Figure 4A). In the presence of 500 μM ARG, a significant increase in the EC_{50} value of the fitted curve was observed, when compared to the PQ curve (2649 μM *vs.* 1088 μM for the PQ curve), thus confirming the significant protective effect of this amino acid against PQ-induced toxicity (Table 6).

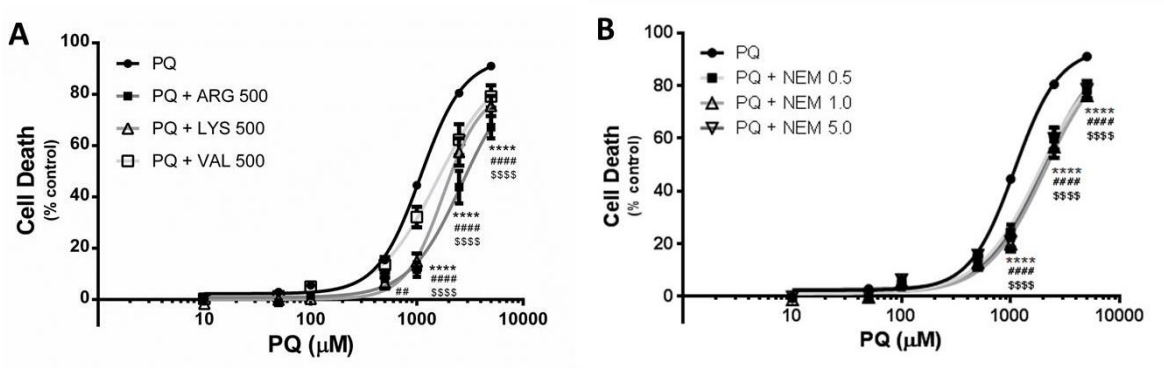

Figure 4. (A) Paraquat concentration–response (cell death) curves with [(PQ + ARG), (PQ + LYS) and (PQ + VAL)] or without (PQ) simultaneous exposure to arginine (500 μM), lysine (500 μM) and valine (500 μM). **(B)** Paraquat concentration–response (cell death) curves with (PQ + NEM) or without (PQ) simultaneous exposure to NEM (0.5, 1.0 or 5.0 μM). Results are presented as mean ± SEM from 6 independent experiments (performed in triplicate). Concentration–response curves were fitted using least squares as the fitting method and the comparisons between the fitted curves (LOG EC_{50}, TOP, BOTTOM and Hill slope) were made using the extra sum-of-squares F test. Statistical comparisons were made using Two-way ANOVA, followed by the Sidak's multiple comparisons *post hoc* test. In all cases, *p* values lower than 0.05 were considered significant. **(A)** $^{****}p < 0.0001$ PQ + ARG 500 *vs.* PQ alone; $^{\#\#}p < 0.01$, $^{\#\#\#\#}p < 0.0001$ PQ + LYS 500 *vs.* PQ alone; $^{\$\$\$\$}p < 0.0001$ PQ + VAL 500 *vs.* PQ alone. **(B)** $^{****}p < 0.0001$ PQ + NEM 0.5 *vs.* PQ alone; $^{\#\#\#\#}p < 0.0001$ PQ + NEM 1.0 *vs.* PQ alone; $^{\$\$\$\$}p < 0.0001$ PQ + NEM 5.0 *vs.* PQ alone.

The simultaneous exposure to LYS (500 μM) resulted in a significant decrease in the TOP value of the PQ + LYS 500 curve, being, therefore, this parameter used for comparison between the fitted curves (Table 6). In the presence of 500 μM LYS the TOP value significantly decreased to 81.87 %, when compared to the PQ curve (94.16 %) (Table 6).

N-ethylmalemide (NEM), a well-known inhibitor of the y^+ transport system, is described to significantly reduce lysine and arginine uptake in IEC-6 cells (Pan et al. 1995; Sharpe and Seidel 2005). Thus, to further clarify the involvement of this transport system, the effect of NEM (0.5, 1.0 and 5.0 μM) on PQ toxicity was evaluated after 24 h of simultaneous exposure to PQ. As observed in Figure 4B, simultaneous exposure to NEM, at all the tested concentrations, significantly protected Caco-2 cells against PQ toxicity, as demonstrated by the significant rightwards shift of all the PQ + NEM curves, when compared to the PQ curve. Moreover, it was observed that the NEM protective effect was clearly significant at the higher PQ concentrations (1000 - 5000 μM). Additionally, the observed differences in the fitted PQ + NEM curves were associated with significant increases in the EC_{50} values (1969, 2076 and 1995 μM for PQ + NEM 0.5, 1.0 and 5.0 μM, respectively, *vs.* 1088 μM for PQ curve) (Table 7). However, no significant differences were observed neither in the overall comparison of all the PQ + NEM curves, nor in the comparison of the individual parameters (LOG EC_{50}, TOP, BOTTOM and Hill slope), thus indicating a NEM concentration independent protective effect on PQ cytotoxicity (Table 7).

Table 6. EC_{50} (half-maximum-effect concentration), TOP (maximal effect), BOTTOM (baseline) and Hill slope values of the paraquat concentration-response curves, with [(PQ + ARG), (PQ + LYS) and (PQ + VAL)] or without (PQ) simultaneous exposure to Arginine, Lysine and Valine (500 μM), respectively.

	PQ	PQ + ARG 500	PQ + LYS 500	PQ + VAL 500
EC_{50} (half-maximum-effect concentration, μM)	**1088**	**2649**	**1782**	**1562**
TOP (maximal cell death, % control)	94.16	89.29	81.87	91.64
BOTTOM (baseline, % control)	2.301	0.7903	0.1060	1.580
Hill slope	2.137	1.754	2.430	1.564
LOG EC_{50} *p* value (comparison between LOG EC_{50} values)	-	**< 0.0001***	**< 0.0001*** 0.1027$^{\$}$	**0.0019*** 0.0931$^{\$}$ 0.1844$^{\#}$
TOP *p* value (comparison between TOP values)	-	0.7783*	**0.0449*** 0.6946$^{\$}$	0.7731* 0.9313$^{\$}$ 0.7161$^{\#}$
BOTTOM *p* value (comparison between BOTTOM values)	-	0.3176*	0.1144* 0.7874$^{\$}$	0.6774* 0.8022$^{\$}$ 0.8786$^{\#}$
Hill slope *p* value (comparison between Hill slope values)	-	0.3648*	0.3719* 0.3420$^{\$}$	0.0502* 0.7806$^{\$}$ 0.3135$^{\#}$
Curve *p* value (Comparison between the Fitted Curves)	-	**< 0.0001***	**< 0.0001*** **0.0067$^{\$}$**	**< 0.0001*** **< 0.0001$^{\$}$** **< 0.0001$^{\#}$**

Concentration-response curves were fitted using least squares as the fitting method and the comparisons between PQ and PQ + ARG, PQ + LYS or PQ + VAL curves were made using extra sum-of-squares F test. In all cases, *p* values lower than 0.05 were considered significant. * Comparison *vs*. PQ; $^{\$}$ Comparison *vs*. PQ + ARG 500; $^{\#}$ Comparison *vs*. PQ + LYS 500.

Previous findings have also demonstrated that PQ-induced brain toxicity was partially dependent on neutral amino acid transporter-mediated PQ uptake (Shimizu et al. 2001). Therefore, to further elucidate the involvement of this carrier-mediated system on PQ intestinal absorption and toxicity, the effect of the neutral amino acid valine on PQ cytotoxicity was evaluated 24 h after simultaneous exposure to PQ. As shown in Figure 4A, a significant rightwards shift of the PQ + VAL 500 curve was observed as a result of significant decrease in cell death obtained for the higher PQ concentrations (1000 - 5000 μM). Moreover, the reduction in the cell death resulted in a significant increase in the EC_{50} value of the PQ + VAL 500 curve (1562 μM *vs.* 1088 μM for PQ curve) (Table 6).

Table 7. EC_{50} (half-maximum-effect concentration), TOP (maximal effect), BOTTOM (baseline) and Hill slope values of the paraquat concentration-response curves, with (PQ + NEM) or without (PQ) simultaneous exposure to NEM (0.5, 1.0 and 5.0 μM).

	PQ	PQ + NEM 0.5	PQ + NEM 1.0	PQ + NEM 5.0
EC_{50} (half-maximum-effect concentration, μM)	**1088**	**1969**	**2076**	**1995**
TOP (maximal cell death, % control)	94.16	98.68	94.94	95.76
BOTTOM (baseline, % control)	2.301	0.8071	1.165	2.595
Hill slope	2.137	1.478	1.621	1.677
LOG EC_{50} *p* value (comparison between LOG EC_{50} values)	-	**< 0.0001***	**< 0.0001*** 0.8570$^{\$}$	**< 0.0001*** 0.9645$^{\$}$ 0.8812$^{\#}$
TOP *p* value (comparison between TOP values)	-	0.6566*	0.9405* 0.8389$^{\$}$	0.8671* 0.8683$^{\$}$ 0.9611$^{\#}$
BOTTOM *p* value (comparison between BOTTOM values)	-	0.3362*	0.4581* 0.8821$^{\$}$	0.8508* 0.4605$^{\$}$ 0.5384$^{\#}$
Hill slope *p* value (comparison between Hill slope values)	-	**0.0184***	0.0928* 0.7416$^{\$}$	0.1517* 0.6556$^{\$}$ 0.9028$^{\#}$
Curve *p* value (Comparison between the Fitted Curves)	-	**< 0.0001***	**< 0.0001*** 0.5896$^{\$}$	**< 0.0001*** 0.9236$^{\$}$ 0.7337$^{\#}$

Concentration-response curves were fitted using least squares as the fitting method and the comparisons between the fitted curves were made using extra sum-of-squares F test. In all cases, *p* values lower than 0.05 were considered significant. * Comparison *vs*. PQ; $^{\$}$ Comparison *vs*. PQ + NEM 0.5; $^{\#}$ Comparison *vs*. PQ + NEM 1.0.

3.3. Paraquat intracellular levels

To evaluate if the observed protective effects against PQ-induced toxicity results from a reduced intracellular PQ accumulation, PQ intracellular levels were quantified with or without simultaneous exposure to the tested compounds. After exposure to 1000, 2500 and 5000 μM PQ alone, the intracellular PQ levels were 56.21, 150.07 and 189.98 nmol PQ/mg protein, respectively. As shown in Figure 5, all compounds caused a marked reduction in PQ intracellular levels, which was significant for the higher PQ concentrations (1000 - 5000 μM). Simultaneous exposure to CHO (500 μM) significantly reduced PQ intracellular levels to 90.89 and 109.32 nmol PQ/mg protein, for 2500 and 5000 μM PQ + CHO, respectively (Figure 5A). For HC-3 (500 μM), the reduction on PQ accumulation was significant even at lower PQ exposure concentrations (25.88, 94.50 and 118.86 nmol PQ/mg protein, for 1000, 2500 and 5000 μM PQ + HC-3, respectively). No significant

differences were observed in the PQ intracellular levels between the simultaneous exposure to CHO or HC-3.

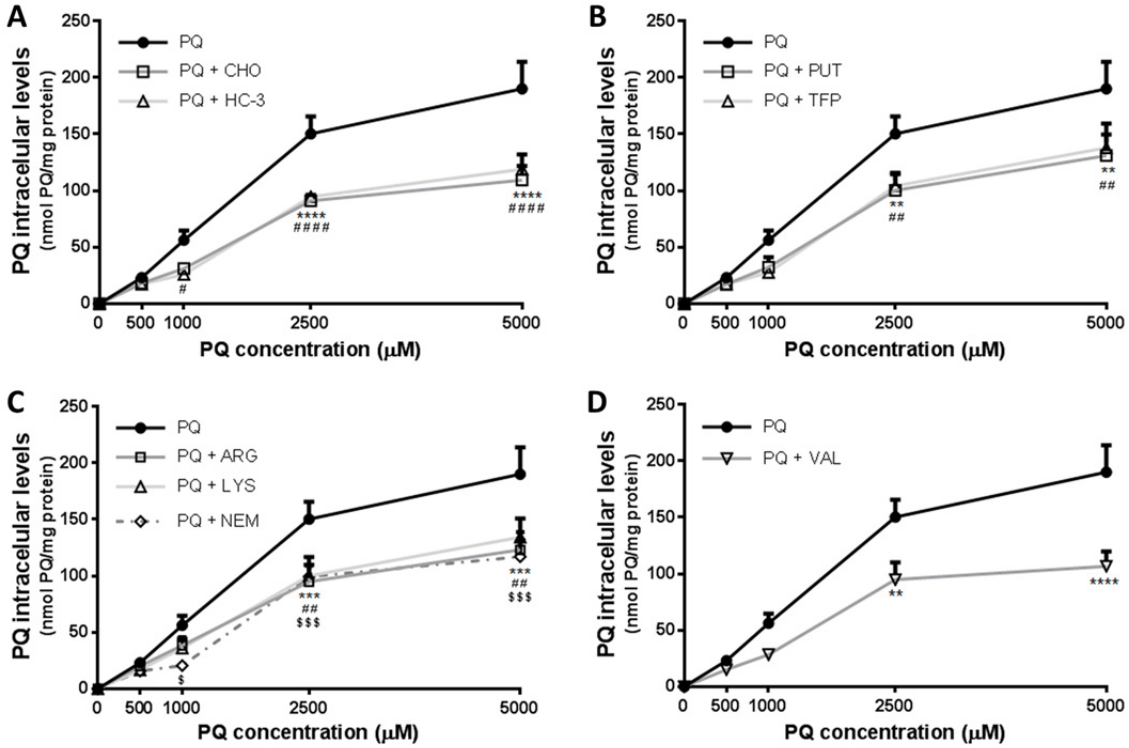

Figure 5. Paraquat intracellular levels, in Caco-2 cells, with or without simultaneous exposure to **(A)** CHO (500 μM) or HC-3 (500 μM), **(B)** PUT (250 μM) or TFP (20 μM), **(C)** ARG (500 μM), LYS (500 μM) or NEM (5 μM) and **(D)** VAL (500 μM), for 24 h. Results are presented as Mean ± SEM from 4 independent experiments (performed in duplicate). Statistical comparisons were made using Two-way analysis of variance followed by the Bonferroni's Multiple Comparison *post hoc* test. **(A)** $^{****}p < 0.0001$ PQ + CHO *vs.* PQ alone; $^{\#}p < 0.05$; $^{\#\#\#\#}p < 0.0001$ PQ + HC-3 *vs.* PQ alone; **(B)** $^{**}p < 0.01$ PQ + PUT *vs.* PQ alone; $^{\#\#}p < 0.01$ PQ + TFP *vs.* PQ alone; **(C)** $^{***}p < 0.001$ PQ + ARG *vs.* PQ alone; $^{\#\#}p < 0.01$ PQ + LYS *vs.* PQ alone; $^{\$}p < 0.05$; $^{\$\$\$}p < 0.001$ PQ + NEM *vs.* PQ alone; **(D)** $^{**}p < 0.01$; $^{****}p < 0.0001$ PQ + VAL *vs.* PQ alone.

Simultaneous exposure to PUT (250 μM) resulted in a significant decrease in PQ intracellular levels to 100.16 and 130.94 nmol PQ/mg protein, for 2500 and 5000 μM PQ + PUT, respectively (Figure 5B). A similar effect was observed in the presence of the well-known competitive inhibitor of the Ca^{2+}/CaM complex, TFP (20 μM) (104.15 and 137.82 nmol PQ/mg protein, for 2500 and 5000 μM PQ + TFP, respectively). Additionally, no significant differences were observed in PQ intracellular levels between the simultaneous exposure to PUT or TFP.

As observed in Figure 5C, PQ intracellular accumulation was also significantly decreased by the simultaneous exposure to the basic amino acids ARG (500 μM) and LYS (500 μM), resulting in a significant decrease in the intracellular PQ content for the two higher PQ concentrations (94.85 and 123.02 nmol PQ/mg protein for 2500 and 5000 μM

PQ + ARG, respectively; 99.95 and 134.18 nmol PQ/mg protein for 2500 and 5000 μM PQ + LYS, respectively).

Additionally, a similar effect was observed for the simultaneous exposure to the inhibitor of the y^+ transport system, NEM (5 μM). However, significant differences were observed at lower PQ exposure concentrations (20.53, 99.29 and 116.94 nmol PQ/mg protein for 1000, 2500 and 5000 μM PQ + NEM, respectively). Nevertheless, no significant differences were observed in PQ intracellular levels among the simultaneous exposure to ARG, LYS or NEM.

Similarly, simultaneous exposure to VAL (500 μM) markedly reduced the intracellular PQ accumulation, with significant differences observed for the 2500 and 5000 μM PQ concentrations (94.80 and 106.55 nmol PQ/mg protein for 2500 and 5000 μM PQ + VAL, respectively) (Figure 5D*).*

3.4. Lysine uptake

Previous studies performed in IEC-6 cells demonstrated that polyamines (PUT) and basic amino acids (ARG and LYS) seem to be actively transported by a common carrier, the y^+ transport system. To further clarify if polyamines and basic amino acids could be sharing a common transport site in Caco-2 cells, LYS intracellular levels were evaluated after 30 min of incubation with LYS (3000 μM), with or without simultaneous incubation with PUT (3000 μM and 5000 μM). Basal LYS intracellular concentrations measured in the control incubations were of 14.67 nmol LYS/mg protein. After incubation with 3000 μM LYS the intracellular levels of the amino acid raised to 82.88 nmol LYS/mg protein. As observed in Figure 6A, PUT significantly inhibited LYS uptake, at both tested concentrations (40.64 and 42.00 nmol LYS/mg protein, for 3000 and 5000 μM PUT + LYS, respectively), thus confirming that, in this cell model, both compounds are transported by a common transport system. Moreover, as the y^+ transport system is Ca^{2+}/CaM sensitive (Sharpe and Seidel 2005), we further tested the effect of TFP (20 μM) on LYS uptake. As shown in Figure 6A, TFP significantly reduced LYS uptake to 31.79 nmol LYS/mg protein.

By using the y^+ transport system inhibitor, NEM (5 μM), similar results were found, as observed by the significant reduction in the intracellular LYS content to 40.41 nmol LYS/mg protein, thus demonstrating that LYS uptake into Caco-2 cells is, at least partially, mediated by this transport system (Figure 6B). Also, the same inhibitory effect on LYS uptake was observed in the presence of ARG (3000 μM), a basic amino acid analogous to LYS, which may be competing for the same transport system, that reduced intracellular LYS to (41.82 nmol LYS/mg protein (Figure 6B).

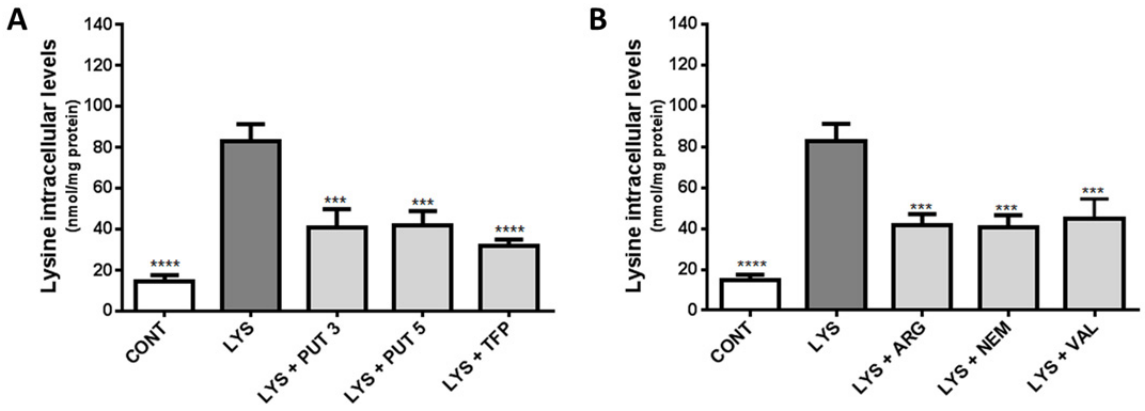

Figure 6. Effect of the tested compounds on lysine uptake in Caco-2 cells. Uptake of lysine (3000 μM) was measured after 30 min of incubation, in the presence or absence of **(A)** PUT(3000 μM or 5000 μM) or TFP (20 μM) or **(B)** ARG (3000 μM), NEM (5 μM) or VAL (3000 μM). Lysine intracellular levels of Caco-2 cells exposed only HBSS were also determined (CONT). Results are presented as mean ± SEM from 4 independent experiments (performed in triplicates). Statistical comparisons were made using One-way analysis of variance followed by the Bonferroni's Multiple Comparison *post hoc* test (***$p < 0.001$, ****$p < 0.0001$ *vs.* LYS).

Additionally, the neutral amino acid, VAL, also significantly reduced LYS intracellular levels to 44.63 nmol LYS/mg protein (Figure 6B). Thus, the obtained results, suggest the presence of an additional LYS transport system in our experimental model, since the y^+ transport system was already reported to present a very weak interaction with neutral amino acids (Deves and Boyd 1998; Pan et al. 1995).

4. DISCUSSION

Our data indicates the existence of more than one transport system contributing for PQ uptake into Caco-2 cells, since a significant reduction in PQ uptake and cytotoxicity in this model of the human intestinal epithelium was elicited by all the compounds involved in the screened transport systems.

PQ is an extremely toxic herbicide responsible for thousands of deaths due to accidental or intentional ingestion. While the lung is the target organ for PQ toxicity, almost 70 % of PQ poisonings result from oral ingestion of the compound. Consequently, the absorption across the gastrointestinal epithelium limits its toxicity (Dinis-Oliveira et al. 2008; Grabie et al. 1993). Although the first step in the treatment of human PQ intoxications should aim primarily the reduction of the herbicide gastrointestinal absorption, little is known about PQ intestinal uptake, namely the transporters specifically involved. PQ absorption seems to occur primarily in the small intestine (and only poorly from the stomach) (Dinis-Oliveira et al. 2008; Heylings 1991), and is estimated to be 1–5% of the ingested dose in humans over 1–6 h (Dinis-Oliveira et al. 2008). In the present study, Caco-2 cells, derived from human colorectal adenocarcinoma, were used to investigate the intestinal absorption of the herbicide, since these cells mimic the enterocytes of the small intestine (Barta et al. 2008) and are widely accepted as a reliable *in vitro* model for predicting drug intestinal absorption in humans (Barta et al. 2008; Huynh-Delerme et al. 2005; Watanabe et al. 2005; Yamashita et al. 2000).

The range of PQ concentrations tested in the present study is within what is expected to be attained *in vivo* in a real human intoxication scenario. In fact, in most of the reported cases of human PQ intoxication, 25–50 mL of the PQ formulations are typically ingested (Dinis-Oliveira et al. 2009). Most of the commercially available formulations contain 20 g/100 mL of PQ, which would translate into an orally ingested dose of approximately 5-10 g that is absorbed up to a maximum of 5% of the ingested dose (Roberts 2011). Thus, under such intoxication scenarios, blood concentrations up to 0.1 g/L (0.4 mM) could be easily achieved. Moreover, PQ concentrations in the target organs, such as the lung, can be 6 to 10 times higher than those in the blood (Dinis-Oliveira et al. 2008), and in the intestine, high concentrations may also be expected since almost all of the ingested dose comes into contact with the enterocytes. Additionally, PQ concentrations found at autopsy are probably lower than the peak concentrations that are expected to occur after intake, as a consequence of the emergency-care treatments used to control the intoxications, such as hemodialysis and charcoal hemoperfusion.

PQ absorption from the gastrointestinal tract was previously associated with the carrier-mediated transport system for choline on the rat brush-border membrane (Nagao

et al. 1993). This transport system is expressed in Caco-2 cells and was already characterized as being saturable, pH-, Ca^{2+}- and temperature-dependent and independent of the inwardly directed Na^{+} gradient (Crowe et al. 2002; Kamath et al. 2003). Additionally, it is significantly inhibited by excess of choline and by HC-3, a structural analog of choline, which is a known competitive inhibitor of both Na^{+}-dependent and Na^{+}-independent choline transporters in many tissues (Kamath et al. 2003). In accordance, our results clearly demonstrated that this transport system is involved on PQ uptake in Caco-2 cells, since the simultaneous exposure to PQ and CHO or HC-3 resulted in a significant reduction on PQ intracellular accumulation and, consequently, in a significant reduction in cell death after PQ exposure. Moreover, the concentration-independent protective effect of CHO and HC-3 on PQ cytotoxicity may be explained by the saturable activity of this transport system (Kamath et al. 2003). Additionally, the similar protective effect observed for CHO and HC-3 both under simultaneous exposure to the herbicide and 6 h after the beginning of PQ exposure may be due to a slow PQ uptake by these cells, given the slow absorption rate of PQ reported in humans (Dinis-Oliveira et al. 2008). In accordance with our results, the choline uptake system was also reported to be involved in PQ uptake in RBE4 cells, an *in vitro model* of the rat's BBB (Vilas-Boas et al. 2013). Indeed, PQ's cytotoxic profile was assessed in the presence of HC-3, and a significant increase in cell viability was observed (significant increase in PQ's EC_{50} value), being this effect accompanied by a significant decrease in PQ intracellular levels observed in the presence of the competitive inhibitor of the choline-uptake system (Vilas-Boas et al. 2013).

The polyamine uptake system was the first transporter implicated in paraquat absorption, being responsible for the high accumulation rate of the herbicide in the lung (Rose et al. 1974; Smith 1982; Wyatt et al. 1988). All mammalian cells are equipped with an efficient polyamine uptake system (Milovic et al. 2001). Furthermore, this system was already implicated in PQ uptake into the IEC-6 rat small intestine epithelial cell line (Grabie et al. 1993). In these cells, the polyamine uptake system was characterized as being energy-dependent, saturable, and modulated by a Ca^{2+}/CaM complex-dependent mechanism (Grabie et al. 1993; Groblewski et al. 1992). Moreover, PQ absorption was greatly inhibited by PUT and the herbicide acted as a competitive inhibitor of PUT uptake (Grabie et al. 1993). However, PQ uptake was slower than that of PUT indicating a lower affinity for the transporter (Grabie et al. 1993). In accordance, our results also demonstrated that PUT and PQ enter into Caco-2 cells through a common transporter, since the simultaneous exposure to the polyamine significantly decreased PQ intracellular levels and therefore, its cytotoxic effects. Additionally our data showed that, in Caco-2 cells, PQ uptake was also regulated by a Ca^{2+}/CaM complex-dependent mechanism, as observed by the significant reduction in the herbicide intracellular content and,

consequently, in its toxicity, after simultaneous exposure to the potent calmodulin antagonist, TFP. However, mechanisms other than polyamine uptake system may also contribute to the marked effect of PUT on PQ uptake into Caco-2 cells. In fact, studies performed in IEC-6 cells have demonstrated that polyamines and basic amino acids, such as LYS and ARG (both are positively charged at neutral pH), are absorbed through a common carrier, the y^+ transport system, given the structural similarity between the compounds (Sharpe and Seidel 2005). Additionally, in that cellular model, PUT inhibited approximately 75 % of LYS transport, thus confirming that a significant fraction of the lysine transport is polyamine sensitive (Sharpe and Seidel 2005). In accordance, our results clearly demonstrated that LYS uptake was also significantly inhibited by PUT, indicating the presence of a common transporter in Caco-2 cells, which seems to be the y^+ transport system, given that it was sensitive to NEM, an accepted inhibitor of the y^+ transport system (Pan et al. 1995; Sharpe and Seidel 2005). Also, and as observed by Sharpe and Seidel (2005) with the IEC-6 cells, LYS uptake into Caco-2 cells was Ca^{2+}/CaM sensitive, resulting in the observed significant reduction in LYS uptake in the presence of TFP. Thus, the protective effect against PQ induced toxicity observed under simultaneous exposure of Caco-2 cells to PUT, ARG, LYS, NEM and TFP is a consequence of a decreased PQ uptake, which seems to be partially mediated by the y^+ transport system.

Amino acid transport systems are usually classified according to the substrate specificity and the sodium dependency of the rate of transport (Deves and Boyd 1998). Four transport systems for cationic amino acids have already been characterized namely, the y^+, $b^{0,+}$, y^+L, and $B^{0,+}$ systems (Deves and Boyd 1998). Among these, the y^+ system is selective for cationic amino acids (interacting weakly with neutral amino acids), whereas the other three systems accept a wider range of substrates, including both cationic and neutral amino acids (Deves and Boyd 1998). However, these systems differ in their interactions with inorganic monovalent ions (Deves and Boyd 1998). According to the sodium dependency, the systems y^+ and $b^{0,+}$ are Na^+-independent, while the system $B^{0,+}$ is Na^+-dependent (Deves and Boyd 1998). On the other hand, the system y^+L exhibits a more complex pattern in its cation interaction, being the transport of basic amino acids, such as LYS, unaffected by Na^+ replacement, whereas its affinity toward neutral amino acids is dramatically decreased if Na^+ in the medium is replaced by K^+ (Deves and Boyd 1998). Our results indicate that uptake systems other than the y^+ transport system seem to be involved in PQ and LYS uptake, since a significant reduction on both PQ and LYS accumulation was observed in the presence VAL, a neutral amino acid.

Previous studies performed in Caco-2 cells have already characterized the transporters involved in the LYS uptake (Ferruzza et al. 1995; Thwaites et al. 1996). In

fact, studies performed by Ferruzza et al. (1995) investigated the transepithelial transport of LYS across monolayers of differentiated Caco-2 cells and showed that the uptake into the cells occurs via one or more sodium-independent carriers, which were able to transport cationic amino acids but also shared by large neutral amino acids (Ferruzza et al. 1995). Moreover, Thwaites et al. (1996) evaluating the fluxes of 10 μM LYS across the apical membrane of Caco-2 cells demonstrated that $b^{o,+}$, y^+ and a nonsaturable component represented 47%, 27%, and 26%, respectively, of the total apical LYS uptake (Thwaites et al. 1996).The uptake of arginine, another basic amino acid, in the apical membranes of Caco-2 cells was also evaluated and equally characterized as mediated predominantly by sodium-independent mechanisms (Pan et al. 1995; Pan et al. 2002). Moreover, the major pathways involved were y^+ (70%) and y^+L or $b^{0,+}$ (30%) systems (Pan et al. 2002). Thus, given the significant reduction in LYS uptake caused by VAL, the significant reduction observed on PQ toxicity in the presence of this neutral amino acid suggests that PQ, LYS (or ARG) and VAL may be sharing a common carrier, namely the y^+L or $b^{0,+}$ systems. Furthermore, significant differences were observed between the curves fitted in the presence of the different amino acids tested (Figure S2B, Supplementary data). From the obtained results, VAL was the compound that afforded a smaller protection. Therefore, the higher protection observed under simultaneous exposure to ARG and LYS may be explained by the involvement of more than one cationic amino acid transport system, whereas VAL protection does not involves, at least, the y^+ transport system, which, as demonstrated by NEM protective effects, has an important role in PQ intestinal uptake.

Contrarily to our results, in the RBE4 cells, PQ demonstrated to unlikely access these cells through the basic amino acid and through the neutral amino acid transport systems, since no significant differences were observed in PQ's cytotoxic profile in the presence of 500 μM ARG and VAL, respectively (Vilas-Boas et al. 2013). Also, and as expected since the polyamine transporters are not expressed in the BBB structure (Shin et al. 1985), the polyamine uptake system was also not involved in PQ uptake, given the lack of significant differences in PQ cytotoxicity observed in the presence of 500 μM PUT (Vilas-Boas et al. 2013).

In conclusion, to the best of our knowledge, this is the first study investigating different mechanisms involved in the PQ absorption through the human intestinal epithelium. PQ uptake into intestinal epithelial cells, namely in Caco-2 cells, seems to be a Ca^{2+}/CaM and NEM sensitive process and more than one transport system appear to be involved. Knowing that limiting PQ intestinal absorption should be the first approach to reduce its toxic effects, the development of specific and potent inhibitors of these transporters may constitute a potential new source of antidotes against PQ intoxications.

5. ACKNOWLEDGMENTS

This work was supported by the Fundação para a Ciência e Tecnologia (FCT)-project PTDC/SAU-OSM/101437/2008 - QREN initiative with EU/FEDER funded through COMPETE - Operational Programme for Competitiveness Factors.

The work was also supported by FCT within the framework of Strategic Projects for Scientific Research Units of R&D (project PEst-C/EQB/LA0006/2011).

Renata Silva, Daniel José Barbosa and Márcia Monteiro acknowledge FCT for their PhD grants [SFRH/BD/29559/2006], [SFRH/BD/64939/2009], and [SFRH/BD/80518/2011], respectively.

6. CONFLICT OF INTEREST STATEMENT

The authors declare that there are no conflicts of interest.

7. REFERENCES

Alexander RW, Saydjari R, MacLellan DG, Townsend CM, Jr., Thompson JC (1988) Calmodulin antagonist trifluoperazine inhibits polyamine biosynthesis and liver regeneration. Br J Surg 75:1160-1162.

Barta CA, Sachs-Barrable K, Feng F, Wasan KM (2008) Effects of monoglycerides on p-glycoprotein: modulation of the activity and expression in caco-2 cell monolayers. Mol Pharm 5:863-875.

Crowe AP, Lockman PR, Abbruscato TJ, Allen DD (2002) Novel choline transport characteristics in Caco-2 cells. Drug Dev Ind Pharm 28:773-781.

Deves R, Boyd CA (1998) Transporters for cationic amino acids in animal cells: discovery, structure, and function. Physiol Rev 78:487-545.

Dinis-Oliveira RJ, de Pinho PG, Santos L, et al. (2009) Postmortem analyses unveil the poor efficacy of decontamination, anti-inflammatory and immunosuppressive therapies in paraquat human intoxications. PLoS One 4:e7149.

Dinis-Oliveira RJ, Duarte JA, Remiao F, Sanchez-Navarro A, Bastos ML, Carvalho F (2006a) Single high dose dexamethasone treatment decreases the pathological score and increases the survival rate of paraquat-intoxicated rats. Toxicology 227:73-85.

Dinis-Oliveira RJ, Duarte JA, Sanchez-Navarro A, Remiao F, Bastos ML, Carvalho F (2008) Paraquat poisonings: mechanisms of lung toxicity, clinical features, and treatment. Crit Rev Toxicol 38:13-71.

Dinis-Oliveira RJ, Remiao F, Carmo H, et al. (2006b) Paraquat exposure as an etiological factor of Parkinson's disease. Neurotoxicology 27:1110-1122.

Dinis-Oliveira RJ, Remiao F, Duarte JA, et al. (2006c) P-glycoprotein induction: an antidotal pathway for paraquat-induced lung toxicity. Free Radic Biol Med 41:1213-1224.

Dinis-Oliveira RJ, Sousa C, Remiao F, et al. (2007) Full survival of paraquat-exposed rats after treatment with sodium salicylate. Free Radic Biol Med 42:1017-1028.

Ferruzza S, Ranaldi G, Di Girolamo M, Sambuy Y (1995) The transport of lysine across monolayers of human cultured intestinal cells (Caco-2) depends on Na(+)-dependent and Na(+)-independent mechanisms on different plasma membrane domains. J Nutr 125:2577-2585.

Grabie V, Scemama JL, Robertson JB, Seidel ER (1993) Paraquat uptake in the cultured gastrointestinal epithelial cell line, IEC-6. Toxicol Appl Pharmacol 122:95-100.

Grant H, Lantos PL, Parkinson C (1980) Cerebral damage in paraquat poisoning. Histopathology 4:185-195.

Groblewski GE, Hargittai PT, Seidel ER (1992) Ca2+/calmodulin regulation of putrescine uptake in cultured gastrointestinal epithelial cells. Am J Physiol 262:1356-1363.

Heylings JR (1991) Gastrointestinal absorption of paraquat in the isolated mucosa of the rat. Toxicol Appl Pharmacol 107:482-493.

Heylings JR, Farnworth MJ, Swain CM, Clapp MJ, Elliott BM (2007) Identification of an alginate-based formulation of paraquat to reduce the exposure of the herbicide following oral ingestion. Toxicology 241:1-10.

Huynh-Delerme C, Huet H, Noel L, Frigieri A, Kolf-Clauw M (2005) Increased functional expression of P-glycoprotein in Caco-2 TC7 cells exposed long-term to cadmium. Toxicol In Vitro 19:439-447.

Kamath AV, Darling IM, Morris ME (2003) Choline uptake in human intestinal Caco-2 cells is carrier-mediated. J Nutr 133:2607-2611.

Milovic V, Turchanowa L, Stein J, Caspary WF (2001) Transepithelial transport of putrescine across monolayers of the human intestinal epithelial cell line, Caco-2. World J Gastroenterol 7:193-197.

Nagao M, Saitoh H, Zhang WD, et al. (1993) Transport characteristics of paraquat across rat intestinal brush-border membrane. Arch Toxicol 67:262-267.

Pan M, Malandro M, Stevens BR (1995) Regulation of system y+ arginine transport capacity in differentiating human intestinal Caco-2 cells. Am J Physiol 268:578-585.

Pan M, Souba WW, Karinch AM, Lin CM, Stevens BR (2002) Specific reversible stimulation of system y(+) L-arginine transport activity in human intestinal cells. J Gastrointest Surg 6:379-386.

Pereira DM, Vinholes J, de Pinho PG, et al. (2012) A gas chromatography-mass spectrometry multi-target method for the simultaneous analysis of three classes of metabolites in marine organisms. Talanta 100:391-400.

Roberts DM (2011) Herbicides. In: Nelson LS, Lewin NA, Howland MA, Hoffman RS, Goldfrank LR, Flomenbaum NE (eds) Goldfrank's Toxicologic Emergencies, Ninth Edition McGraw-Hill Companies, Inc., p 1494-1515.

Rose MS, Lock EA, Smith LL, Wyatt I (1976) Paraquat accumulation: tissue and species specificity. Biochem Pharmacol 25:419-423.

Rose MS, Smith LL, Wyatt I (1974) Evidence for energy-dependent accumulation of paraquat into rat lung. Nature 252:314-315.

Scemama JL, Grabie V, Seidel ER (1993) Characterization of univectorial polyamine transport in duodenal crypt cell line. Am J Physiol 265:851-856.

Sharpe JG, Seidel ER (2005) Polyamines are absorbed through a y+ amino acid carrier in rat intestinal epithelial cells. Amino Acids 29:245-253.

Shimizu K, Ohtaki K, Matsubara K, et al. (2001) Carrier-mediated processes in blood-brain barrier penetration and neural uptake of paraquat. Brain Res 906:135-142.

Shin WW, Fong WF, Pang SF, Wong PC (1985) Limited blood-brain barrier transport of polyamines. J Neurochem 44:1056-1059.

Silva R, Carmo H, Vilas-Boas V, et al. (2013) Doxorubicin decreases paraquat accumulation and toxicity in Caco-2 cells. Toxicol Lett 217:34-41.

Smith LL (1982) Young Scientists Award lecture 1981: The identification of an accumulation system for diamines and polyamines into the lung and its relevance to paraquat toxicity. Arch Toxicol Suppl 5:1-14.

Thwaites DT, Markovich D, Murer H, Simmons NL (1996) Na^+-independent lysine transport in human intestinal Caco-2 cells. J Membr Biol 151:215-224.

Vilas-Boas V, Silva R, Guedes-de-Pinho P, Carvalho F, Bastos ML, Remião F (2013) RBE4 cells are highly resistant to paraquat-induced cytotoxicity: studies on uptake and efflux mechanisms. J Appl Toxicol.

Watanabe T, Onuki R, Yamashita S, Taira K, Sugiyama Y (2005) Construction of a functional transporter analysis system using MDR1 knockdown Caco-2 cells. Pharm Res 22:1287-293.

Wyatt I, Soames AR, Clay MF, Smith LL (1988) The accumulation and localisation of putrescine, spermidine, spermine and paraquat in the rat lung. In vitro and in vivo studies. Biochem Pharmacol 37:1909-1918.

Yamashita S, Furubayashi T, Kataoka M, Sakane T, Sezaki H, Tokuda H (2000) Optimized conditions for prediction of intestinal drug permeability using Caco-2 cells. Eur J Pharm Sci 10:195-204.

SUPPLEMENTARY DATA

Supplementary Figures

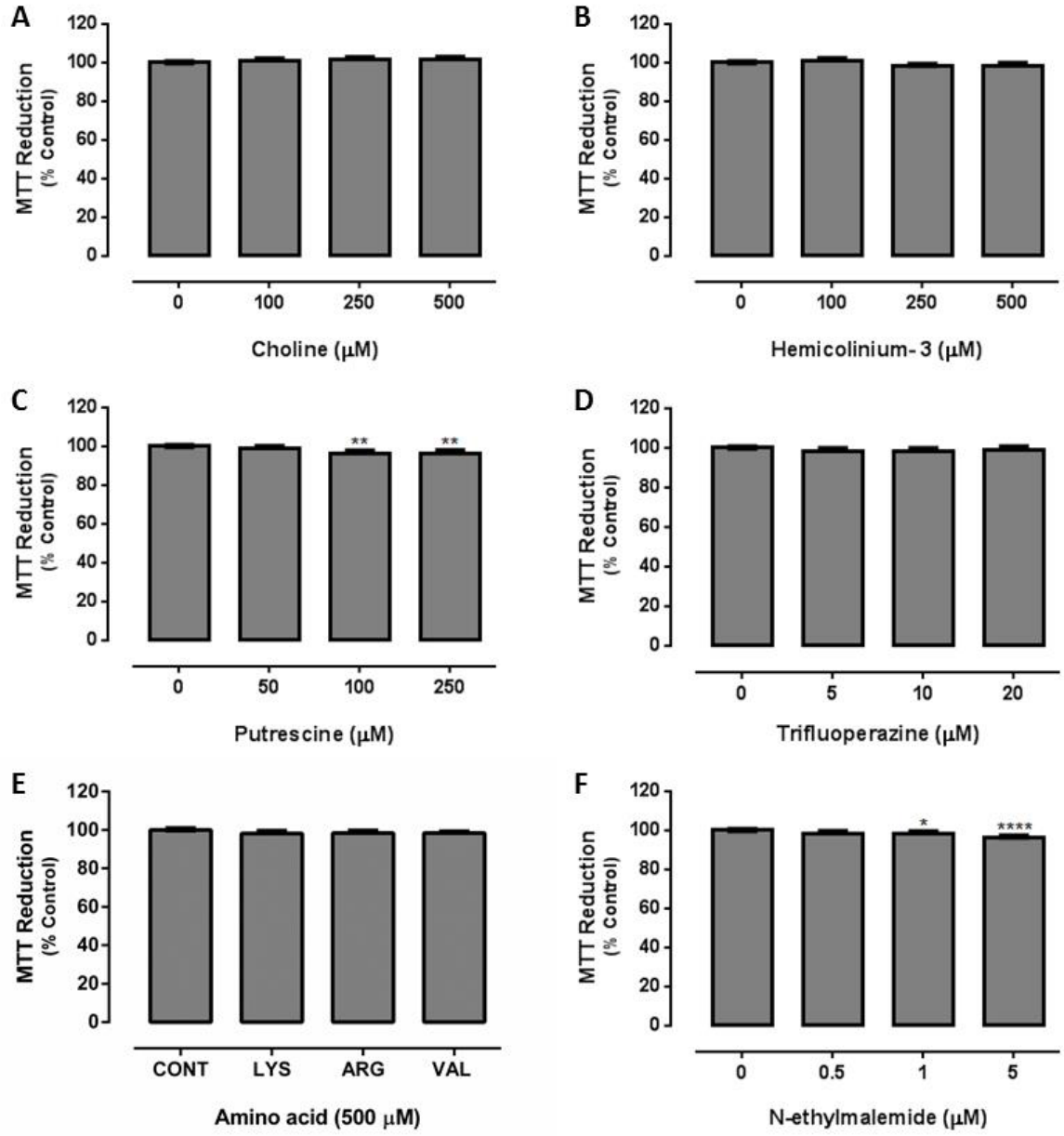

Figure S1. Compounds cytotoxicity in Caco-2 cells 24 h after exposure, evaluated by the MTT reduction assay: **(A)** Choline (0 – 500 μM); **(B)** Hemicolinium-3 (0 – 500 μM); **(C)** Putrescine (0 – 250 μM); **(D)** Trifluoperazine (0 – 20 μM); **(E)** Arginine (500 μM), Lysine (500 μM) and Valine (500 μM) and **(F)** NEM (0 – 5 μM). Results are presented as mean ± SEM from 8 independent experiments (performed in triplicate). Statistical comparisons were made using the nonparametric method of Kruskal–Wallis (one-way ANOVA on ranks), followed by Dunn's *post hoc* test (**p*<0.05; ***p*<0.01; *****p*<0.0001 *vs.* control). For putrescine, a minor, though significant, effect on MTT reduction was observed for the higher concentrations tested (96.5 % and 96.6% for PUT 100 and 250 μM, respectively, as compared to control). Similar results were observed for 1.0 and 5.0 μM NEM (98.1 and 96.1 % of MTT reduction, respectively).

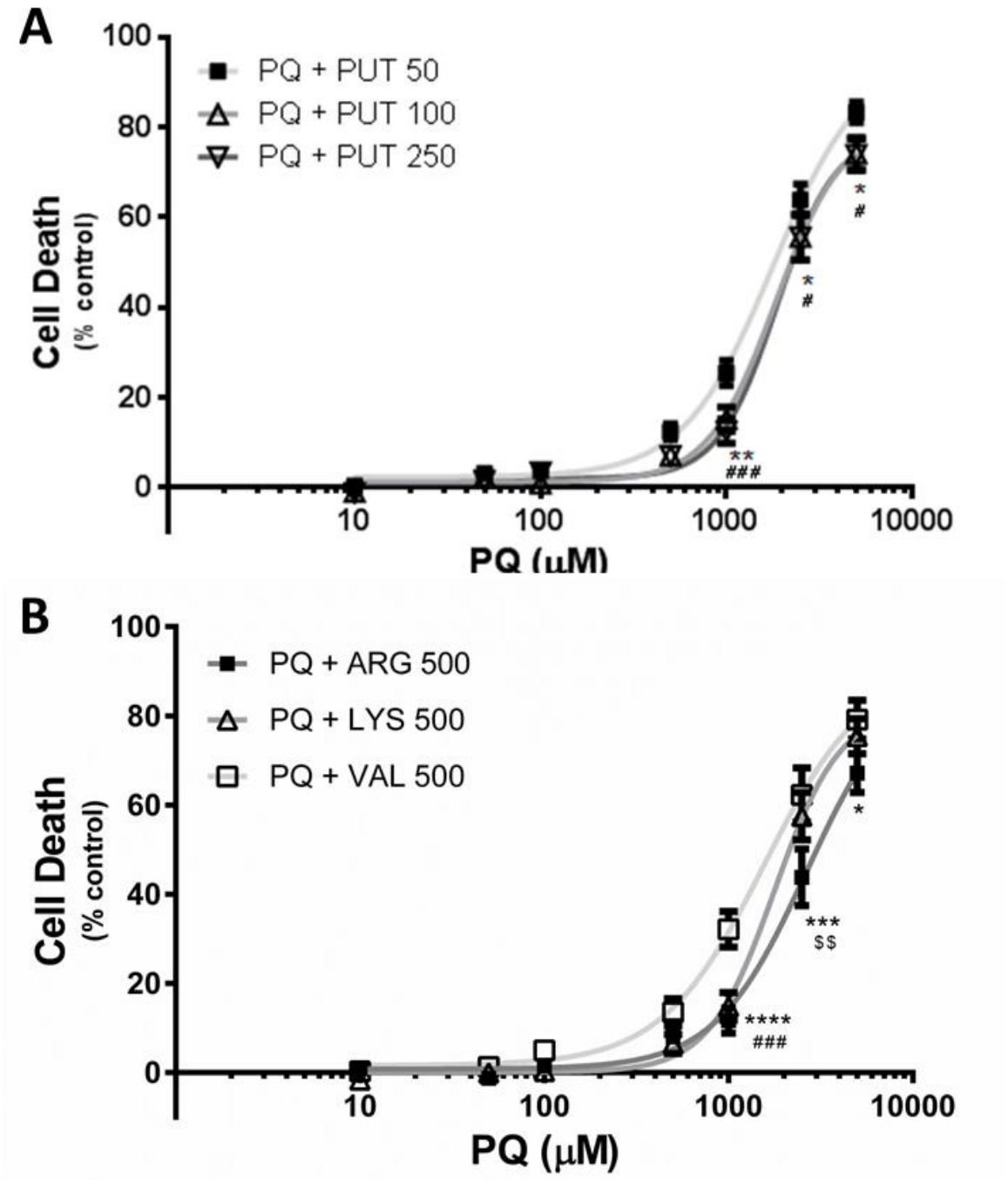

Figure S2. (A) Paraquat concentration–response (cell death) curves with (PQ + PUT) simultaneous exposure to putrescine (50, 100 or 250 µM). **(B)** Paraquat concentration–response (cell death) curves with (PQ + ARG) simultaneous exposure to 500 µM arginine (PQ + ARG 500), 500 µM lysine (PQ + LYS 500) or 500 µM valine (PQ + VAL 500). Results are presented as mean ± SEM from 6 independent experiments (performed in triplicate). Concentration–response curves were fitted using least squares as the fitting method and the comparisons between the fitted curves (LOG EC_{50}, TOP, BOTTOM and Hill slope) were made using the extra sum-of-squares F test. Statistical comparisons between groups were made using Two-way ANOVA, followed by the Sidak's multiple comparisons *post hoc* test. **(A)** **p*<0.05, ***p*<0.01 PQ + PUT 100 *vs.* PQ + PUT 50; $^{\#}p$<0.05; $^{\#\#\#}p$<0.001 PQ + PUT 250 *vs.* PQ + PUT 50**. (B)** **p*<0.05, ****p*<0.001, *****p*<0.0001 PQ + ARG 500 *vs.* PQ + VAL 500; $^{\#\#\#}p$<0.001 PQ + LYS 500 *vs.* PQ + VAL 500; $^{\$\$}p$<0.01 PQ + ARG 500 *vs.* PQ + LYS 500.

Supplementary Tables

Table S1. EC_{50} (half-maximum-effect concentration), TOP (maximal effect), BOTTOM (baseline) and Hill slope values of the paraquat concentration-response curves, in the presence of choline (100 μM) or hemicolinium-3 (100 μM), under simultaneous exposure or 6 h after the beginning of PQ exposure.

	PQ + CHO 100		PQ + HC-3 100	
	simultaneous exposure	**6 h after PQ exposure**	**simultaneous exposure**	**6 h after PQ exposure**
EC_{50} (half-maximum-effect concentration, μM)	**1262**	**1335**	**1527**	**1511**
TOP (maximal cell death, % control)	88.86	91.46	94.08	91.10
BOTTOM (baseline, % control)	1.170	1.627	0.06233	0.2614
Hill slope	2.144	1.744	1.722	2.033
LOG EC_{50} *p* value (comparison between LOG EC_{50} values)	-	0.6808*	-	0.9505#
TOP *p* value (comparison between TOP values)	-	0.7153*	-	0.7430#
BOTTOM *p* value (comparison between BOTTOM values)	-	0.8275*	-	0.9292#
Hill slope *p* value (comparison between Hill slope values)	-	0.3072*	-	0.4374#
Curve *p* value (Comparison between the Fitted Curves)	-	0.6635*	-	0.8507#

Concentration-response curves were fitted using least squares as the fitting method and the comparisons between the fitted curves were made using extra sum-of-squares F test. In all cases, *p* values <0.05 were considered significant (**p* values for the comparison between the PQ + CHO 100 curves; #*p* values for the comparison between the PQ + HC3-3 100 curves).

III.7. MANUSCRIPT VI

P-glycoprotein induction in Caco-2 cells by newly synthetized thioxanthones prevents Paraquat cytotoxicity

Submitted for publication

TITLE

P-glycoprotein induction in Caco-2 cells by newly synthetized thioxanthones prevents Paraquat cytotoxicity

AUTHORS

Renata Silva[a*], Andreia Palmeira[b], Helena Carmo[a], Daniel Barbosa[a], Mariline Gameiro[a], Ana Gomes[a], Ana Mafalda Paiva[b], Emília Sousa[b], Madalena Pinto[b], Maria de Lourdes Bastos[a] and Fernando Remião [a*]

AFFILIATIONS

[a]REQUI*M*TE, Laboratório de Toxicologia, Departamento de Ciências Biológicas, Faculdade de Farmácia, Universidade do Porto, Rua de Jorge Viterbo Ferreira, 228, 4050-313 Porto, Portugal.

[b]Centro de Química Medicinal (CEQUIMED-UP), Laboratório de Química Orgânica e Farmacêutica, Departamento de Ciências Químicas, Faculdade de Farmácia, Universidade do Porto, Rua Jorge Viterbo Ferreira 228, 4050-313, Porto, Portugal.

*CORRESPONDING AUTHORS

Renata Silva (e-mail: rsilva@ff.up.pt) and Fernando Remião (e-mail: remiao@ff.up.pt)
REQUI*M*TE, Laboratório de Toxicologia, Departamento de Ciências Biológicas, Faculdade de Farmácia, Universidade do Porto, Rua de Jorge Viterbo Ferreira, 228, 4050-313 Porto, Portugal.
Phone: 00351220428596
Fax: 00351226093390

RUNNING TITLE

New thioxanthones as P-glycoprotein inducers

ABSTRACT

The induction of P-glycoprotein (P-gp), an ATP-dependent efflux pump, has been proposed as a strategy against the toxicity induced by P-gp substrates such as the herbicide paraquat. The aim of this study was to screen five newly synthetized thioxanthonic derivatives, a group known to interact with P-gp, as potential inducers of the pump´s expression and/or activity, and to evaluate whether they would afford protection against paraquat-induced toxicity in Caco-2 cells.

All five thioxanthones (20 μM) caused a significant increase in both P-gp expression and activity as evaluated by flow cytometry using the UIC2 antibody and rhodamine 123, respectively. Additionally, it was demonstrated that the tested compounds, when present only during the efflux of rhodamine 123, rapidly induced an activation of P-gp. The tested compounds also increased P-gp ATPase activity in MDR1-Sf9 membrane vesicles, indicating that all derivatives acted as P-gp substrates. Paraquat cytotoxicity was significantly reduced in the presence of four thioxanthone derivatives and this protective effect was reversed upon incubation with a specific P-gp inhibitor.

In silico studies showed that all the tested thioxanthones fitted onto a previously described three-feature P-gp induction pharmacophore. Moreover, *in silico* interactions between thioxanthones and P-gp in the presence of paraquat suggested that a co-transport mechanism may be operating. Based on the *in vitro* activation results, a pharmacophore model for P-gp activation was built, which will be of further use in the screening for new P-gp activators.

In conclusion, the study demonstrated the potential of the tested thioxanthonic compounds in protecting against toxic effects induced by P-gp substrates through P-gp induction and activation.

KEYWORDS

P-glycoprotein; Induction; Activation; Thioxanthones; Caco-2 cells.

GRAPHICAL ABSTRACT

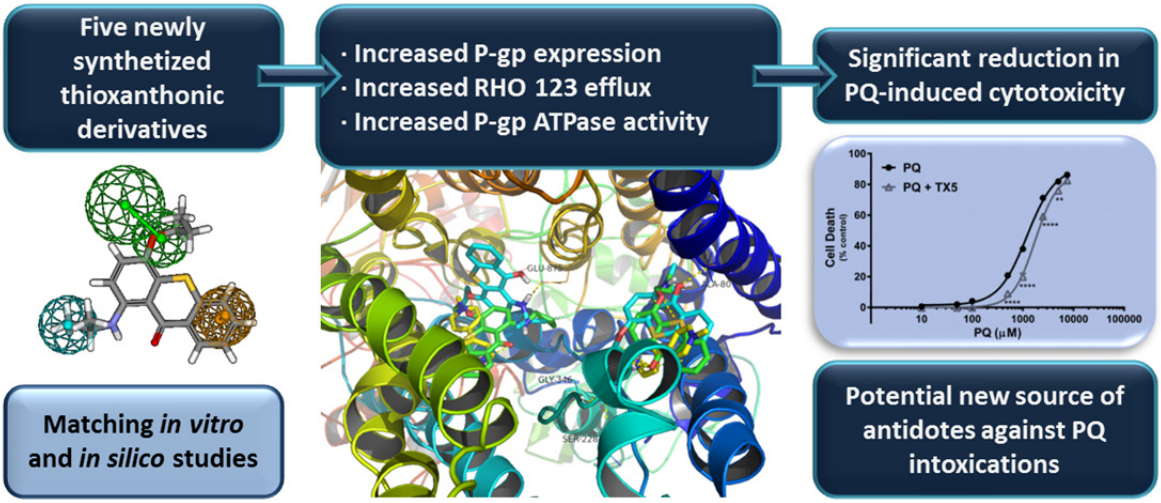

ABBREVIATIONS

DMEM - Dulbecco's modified Eagle's medium
EC_{50} - half-maximum-effect concentration
EDTA - Ethylenediamine tetraacetic acid
FBS - Fetal bovine serum
FITC - Fluorescein isothiocyanate
GeoMean - Geometric mean of fluorescence intensity
Hb - Hydrogen bond
HBSS - Hanks balanced salt solution
IA - Inhibited rhodamine 123 accumulation
IAE - Inhibited rhodamine 123 accumulation followed by efflux in the absence of P-gp inhibitor
IAIE - Inhibited rhodamine 123 accumulation followed by efflux in the presence of P-gp inhibitor
i.p. – Intraperitoneal
MFI - Mean fluorescence intensity
MTT - (4,5-Dimethylthiazol-2-yl)-2,5-diphenyl tetrazolium bromide
MDR - Multi drug resistance
NR - Neutral red
NEAA - Nonessential amino acids
PBS - Phosphate buffered saline solution
P-gp - P-glycoprotein
RHO 123 - Rhodamine 123
TM - transmembrane
TXs - Thioxanthones

1. INTRODUCTION

P-glycoprotein (P-gp), an important member of the ATP-binding cassette superfamily of transporters (Ambudkar et al. 1999; Chang 2003; Gottesman et al. 2002; Silverman 1999), was the first identified efflux protein that was associated with the multi-drug-resistant (MDR) phenomenon in cancer chemotherapy (Juliano and Ling 1976). Although P-pg is highly expressed in MDR tumor cells, it is also present in non-neoplasic cells, with the highest expression levels in excretory and barrier tissues, showing a polarized expression and broad substrate specificity (Thiebaut et al. 1987). In fact, P-gp can export a large number of structurally and pharmacologically unrelated hydrophobic drugs, including anticancer drugs, cardiac glycosides, calcium channel blockers and immunosuppressants (Cordon-Cardo et al. 1990; Gottesman et al. 2002).

Since its discovery in 1976, many scientific approaches have been conducted for the development of P-gp inhibitors and included structure and ligand based design methods (Palmeira et al. 2012a). However, the search for P-gp activators or inducers has been mainly performed by random screening. P-gp is inducible by many drugs, including dexamethasone, rifampicin, the herbal antidepressant St John's wort (hyperforin and hypericin) and several antineoplasic drugs (doxorubicin, daunorubicin and vinblastine) (Zhou 2008). It has been previously hypothesised that an increase in the efflux capacity of P-gp could be used as an effective intracellular protection mechanism to limit the toxicity of its substrates, namely of the widely used paraquat (PQ) herbicide. In fact, *in vitro* studies have demonstrated that doxorubicin, a potent P-gp inducer, was able to strongly increase both P-gp expression and activity in Caco-2 cells, resulting in a significant decrease in the herbicide toxicity as a result of a decreased PQ intracellular accumulation (Silva et al. 2011; Silva et al. 2013b). There is also *in vivo* evidence for such a protective mechanism since the administration of dexamethasone (100 mg/kg i.p.) 2 h after the rats being exposed to a lethal PQ dose (25 mg/kg i.p.), significantly increased the expression of P-gp in the lungs of these animals, increasing their survival rate by 50% (Dinis-Oliveira et al. 2006).

Thioxanthones (TXs), S-heterocycles with a dibenzo-γ-thiopyrone scaffold, constitute an interesting class of molecules with proved biological properties, namely antitumor activity and P-gp modulation (Paiva et al. 2013). In fact, previous studies have already reported the ability of aminated thioxanthones to act as inhibitors of P-gp with improved efficacy in sensitizing a resistant P-gp overexpressing cell line (K562Dox) to doxorubicin (Palmeira et al. 2012b). In those studies, some of the tested thioxanthones caused a significant decrease in the rhodamine 123 (RHO 123) accumulation ratio, an

effect compatible with a possible P-gp activation (Palmeira et al. 2012b), although no further studies were conducted to better clarify their mode of action.

Thus, the aim of the present work was the screening of five newly synthetized thioxanthonic derivatives (Figure 1) as possible inducers of P-gp expression and/or activity. Additionally, we sought to elucidate whether these compounds could protect Caco-2 cells against the toxicity induced by PQ, in an attempt to develop new antidotes using this efficient antidotal pathway. There is currently no specific treatment for PQ intoxications and the mortality rates are extremely high, causing thousands of deaths every year (Dinis-Oliveira et al. 2008).

Computational methods, in particular ligand-protein docking programs, have become essential in any drug discovery program, including in the search for new P-gp modulators (Klepsch et al. 2011; Kothandan et al. 2011; Palmeira et al. 2012b). Estimating binding affinities of ligands within a receptor allows the identification of the energetically most favourable poses, based on its complementarity to the target in terms of shape and properties (Meng et al. 2011; Mohan et al. 2005). Therefore, using a previously published P-gp model (Palmeira et al. 2012b), we aimed to explore the possible binding modes of the thioxanthonic activators *in silico* and to build a common pharmacophore for P-gp activators, which can be used to predict new ligands, as it has been previously performed for P-gp inhibitors and substrates (Cianchetta et al. 2005; Jain et al. 2009; Li et al. 2007; Pajeva and Wiese 2002; Palmeira et al. 2011), but not yet for P-gp activators.

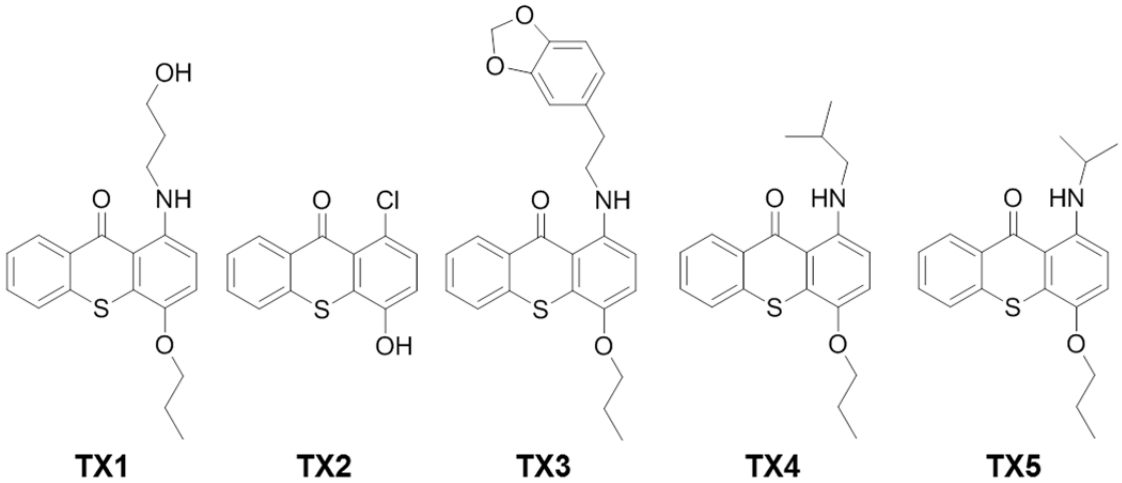

Figure 1. Thioxanthones (TXs **1-5**) investigated in this study: 1-[(3-hydroxypropyl)amino]-4-propoxy-9*H*-thioxanthen-9-one (TX **1**), 1-chloro-4-hydroxy-9*H*-thioxanthen-9-one (TX **2**), 1-{[2-(1,3-benzodioxol-5-yl)ethyl]amino}-4-propoxy-9*H*-thioxanthen-9-one (TX **3**), 1-[(2-methylpropyl)amino]-4-propoxy-9*H*-thioxanthen-9-one (TX **4**), 1-(propan-2-ylamino)-4-propoxy-9*H*-thioxanthen-9-one (TX **5**).

2. MATERIALS AND METHODS

2.1. Materials

Rhodamine 123 (RHO 123), cyclosporine A, (4,5-dimethylthiazol-2-yl)-2,5-diphenyl tetrazolium (MTT) bromide and neutral red (NR) solution were obtained from Sigma (St. Louis, MO, USA). Reagents used in cell culture, including Dulbecco's modified Eagle's medium (DMEM) with 4.5 g/L glucose and GlutaMAX™, nonessential amino acids (NEAA), heat inactivated fetal bovine serum (FBS), 0.25% trypsin/1 mM EDTA, antibiotic (10000 U/mL penicillin, 10000 µg/mL streptomycin), fungizone (250 µg/mL amphotericin B), human transferrin (4 mg/mL), phosphate-buffered saline solution (PBS) and Hank's balanced salt solution (HBSS) were purchased from Gibco Laboratories (Lenexa, KS). P-glycoprotein monoclonal antibody (clone UIC2), conjugated with fluorescein isothiocyanate (FITC), was purchased from Abcam (Cambridge, United Kingdom). IgG2a (negative mAb control to UIC2), conjugated with FITC, was obtained from ImmunoTools GmbH (Friesoythe, Germany). Flow cytometry reagents (BD FacsFlow™ and Facs Clean™) were purchased from Becton, Dickinson and Company (San Jose, CA, USA). MDR1 Predeasy ATPase assay kit was purchased from Solvo Biotechnology (Szeged, Hungary). GF120918 [9,10-dihydro-5-methoxy-9-oxo-N-[4-[2-(1,2,3,4-tetrahydro-6,7-dimethoxy-2-isoquinolinyl)ethyl]phenyl]-4-acridinecarboxamide] was a generous gift from GlaxoSmithKline (Hertfordshire, United Kingdom). All the reagents used were of analytical grade or of the highest grade available.

The synthesis of thioxanthones **1-5** was performed according to the described procedure (Palmeira et al. 2012b).

2.2. Caco-2 cell culture

Caco-2 cells were routinely cultured in 75 cm^2 flasks using DMEM medium supplemented with 10% heat inactivated FBS, 1% NEAA, 1% antibiotic, 1% fungizone and 6 µg/mL transferrin. Cells were maintained in a 5% CO_2-95% air atmosphere, at 37ºC, and the medium was changed every 2 days. Cultures were passaged weekly by trypsinization (0.25% trypsin/1 mM EDTA). The cells used for all the experiments were taken between the 59^{th} and 65^{th} passages. In all experiments, the cells were seeded at a density of 60,000 cells/cm^2, and used 4 days after seeding, when confluence was reached.

2.3. Compounds cytotoxicity assays

Thioxanthones (0 – 100.0 µM) cytotoxicity was evaluated 24 h after exposure by the MTT reduction and by the neutral red (NR) uptake assays.

2.3.1. MTT reduction assay

Thioxanthones cytotoxicity was evaluated by the MTT reduction assay, in which mitochondrial activity is used to estimate cell viability. For that purpose, the cells were seeded onto 96-well plates and exposed, after reaching confluence, to the five tested TXs (0 – 100.0 μM) in fresh cell culture medium for 24 h. At the selected time point, the cell culture medium was removed, followed by the addition of fresh cell culture medium containing 0.5 mg/mL MTT and incubation at 37 °C in a humidified, 5% CO_2-95% air atmosphere for 1 h. After this incubation period, the cell culture medium was removed and the formed formazan crystals dissolved in 100% DMSO. The absorbance was measured at 550 nm in a multi-well plate reader (PowerWave X, Bio-Tek Instruments, Vermont, USA). The percentage of MTT reduction relative to that of the control cells was used as the cytotoxicity measure. Results are presented as mean ± SEM from 5 independent experiments (performed in triplicate).

2.3.2. Neutral red uptake assay

The NR uptake assay is based on the ability of viable cells to incorporate and bind the supravital dye neutral red in the lysosomes, thus providing a quantitative estimation of the number of viable cells in a culture. The cells were seeded onto 96-well plates at a density of 60,000 cells/cm^2, and exposed, after reaching confluence, to the five tested TXs (0 – 100.0 μM) in fresh cell culture medium. Twenty-four hours after exposure, the cells were incubated with neutral red (50 μg/mL in cell culture medium) at 37 °C, in a humidified, 5% CO_2-95% air atmosphere, for 90 min. After this incubation period, the cell culture medium was removed, the dye absorbed only by viable cells extracted (with absolute ethyl alcohol /distilled water (1:1) containing 5% acetic acid), and the absorbance measured at 540 nm in a multi-well plate reader (PowerWave X, Bio-Tek Instruments). The percentage of NR uptake relative to that of the control cells was used as the cytotoxicity measure. Results are presented as mean ± SEM from 5 independent experiments (performed in triplicate).

2.4. Evaluation of P-glycoprotein expression

For the *in vitro* evaluation of P-gp expression, the cells were seeded onto 48-well plates, at a density of 60,000 cells/cm^2 and exposed, four days after seeding, to the five tested TXs (20.0 μM) in fresh cell culture medium for 24 h. After the incubation period, the cells were washed twice with HBSS and harvested by trypsinization (0.25% trypsin /1mM EDTA) to obtain a cellular suspension. The cells were then centrifuged (300 *g*, for 10 min, at 4 ºC) and suspended in PBS buffer (pH 7.4) containing 10% FBS and P-gp antibody

[UIC2] conjugated with FITC. The antibody dilution used in this experiment was applied according to the manufacturer's instructions for flow cytometry. Mouse IgG2a_FITC was used as an isotype-matched negative control to estimate non-specific binding of the FITC-labelled anti-P-glycoprotein antibody [UIC2]. The cells were then incubated for 30 min at 37°C in the dark. After this incubation period, the cells were washed twice with PBS buffer (pH 7.4) containing 10% heat inactivated FBS, centrifuged (300 *g* for 10 min), suspended in ice-cold PBS and kept on ice until analysis. Fluorescence measurements of isolated cells were performed with a flow cytometer (FACSCalibur, Becton-Dickinson Biosciences). The green fluorescence of FITC-UIC2 antibody was measured by a 530 ± 15 nm band-pass filter (FL1). Acquisition of data for 15,000 cells was gated to include viable cells on the basis of their forward and side light scatters and the propidium iodide (4 µg/mL) incorporation (propidium iodide interlaces with a nucleic acid helix with a resultant increase in fluorescence intensity emission at 615 nm). Logarithmic fluorescence was recorded and displayed as a single parameter histogram. The geometric mean of fluorescence intensity (GeoMean) for 15,000 cells was the parameter used for comparison (calculated as percentage of control). Non labelled cells (with or without TXs) were also analysed in each experiment by a 530 ± 15 nm band-pass filter (FL1) in order to detect a possible contribution from cells autofluorescence to the analysed fluorescence signals. Results are presented as mean ± SEM from at least 3 independent experiments (performed in triplicate).

2.5. Evaluation of P-glycoprotein transport activity

The P-gp transport activity was evaluated by flow cytometry using 1 µM RHO 123 as a P-gp fluorescent substrate. For that purpose, two different protocols were used: RHO 123 efflux in the presence of TXs and RHO 123 efflux in cells pre-exposed to TXs for 24 h.

2.6. RHO 123 efflux assay in the presence of thioxanthones

Caco-2 cells were seeded onto 75 cm^2 flasks and, after reaching confluence, washed twice with HBSS and harvested by trypsinization (0.25% trypsin /1mM EDTA) to obtain a cellular suspension. This cell suspension was then divided into aliquots of 500,000 cells/mL. The cells were centrifuged (300 *g*, for 10 min, at 4 ºC), suspended in PBS buffer (pH 7.4) containing 10% heat inactivated FBS, 1 µM RHO 123 and the P-gp inhibitor cyclosporine A (10.0 µM), and incubated at 37 ºC for 30 min to allow maximum RHO 123 accumulation. After the accumulation of the fluorescent substrate, the cells were submitted to an efflux phase, where the energy-dependent P-gp function was re-

established by removing the P-gp inhibitor (cyclosporine A), and by adding an energy source (DMEM supplemented with 4.5 g/L glucose). For that purpose, after the inhibited accumulation (IA) phase, the cells were washed twice with ice-cold PBS with 10% heat inactivated FBS, centrifuged (300 *g* for 10 min, at 4 °C) and resuspended in DMEM medium containing 4.5 g/L glucose, with or without the tested TXs (20.0 μM), and incubated for 45 min at 37 °C. After this efflux period, the cells were washed twice with ice-cold PBS with 10% heat inactivated FBS, and resuspended in ice-cold PBS immediately before analysis. The fluorescence measurements of isolated cells were performed as described in section 2.4. The green intracellular fluorescence of RHO 123 was measured by a 530 ± 15 nm band-pass filter (FL1). When P-gp activity increases, the amount of RHO 123 effluxed from the cells is higher and accompanied by a decrease in the fluorescence intensity due to the corresponding decrease in the intracellular RHO 123 content. As P-gp activity is inversely proportional to the intracellular fluorescence intensity, the inverse of mean fluorescence intensity (1/MFI) was the parameter used for comparison and the results expressed as percentage of control. Results are presented as mean ± SEM from 6 independent experiments (performed in triplicate).

2.6.1. RHO 123 efflux assay in Caco-2 cells pre-expose to thioxanthones for 24 h

Caco-2 cells were seeded onto 24-well plates, at a density of 60,000 cells/cm^2, to obtain confluent monolayers at the day of the experiment. Four days after seeding, the cells were exposed to TXs (20.0 μM), in fresh cell culture medium, for 24 h. After this incubation period the cells were washed twice with HBSS and harvested by trypsinization (0.25% trypsin /1mM EDTA) to obtain a cellular suspension. The cells were then submitted to an inhibited accumulation (IA) phase as described in section 2.5.1. After the IA phase, the cells were washed twice with ice-cold PBS with 10% heat inactivated FBS, centrifuged (300 *g* for 10 min, at 4°C) and divided into two aliquots. The first aliquot was submitted to an efflux phase performed under inhibited conditions (inhibited RHO 123 accumulation followed by inhibited RHO 123 efflux in the presence of the P-gp inhibitor, cyclosporine A– IAIE). The second aliquot was submitted to an efflux phase performed under normal conditions (inhibited RHO 123 accumulation followed by RHO 123 efflux in the absence of P-gp inhibitor – IAE). For the efflux phase the cells were suspended in DMEM medium containing 4.5 g/L glucose, with or without 10.0 μM cyclosporine A, and incubated for 45 min at 37 °C. After this efflux period, the cells were washed twice with ice-cold PBS with 10% heat inactivated FBS, and resuspended in ice-cold PBS immediately before analysis. The fluorescence measurements of isolated cells were

performed as described in section 2.4. The green intracellular fluorescence of RHO 123 was measured by a 530 ± 15 nm band-pass filter (FL1). The ratio between MFI of IAIE and MFI of IAE was the parameter used for comparison, and the results expressed as percentage of control. Results are presented as mean ± SEM from 5 independent experiments (performed in triplicate).

2.7. Evaluation of P-glycoprotein ATPase activity

P-gp ATPase activity was evaluated using the MDR1 Predeasy ATPase assay kit according to the manufacturer's instructions. Briefly, MDR1-Sf9 membrane vesicles (4 µg/well) were incubated in 50 µL ATPase assay buffer with 2 mM ATP and TXs (20.0 µM) for 10 min at 37 °C, with or without simultaneous incubation with 1.2 mM sodium orthovanadate (Na_3VO_4). The reaction was stopped by adding 100 µL of developer solution to each well, followed by 100 µL of blocker solution and an additional 30 min incubation at 37 ºC. The absorbance was measured at 590 nm, in a multi-well plate reader (BioTek Instruments, Vermont, US), reflecting the amount of inorganic phosphate (Pi) liberated by the transporter which is proportional to its activity.

In the present assay, MDR1-Sf9 membrane vesicles were used which, apart from P-gp, contain other ATPases. As P-gp is effectively inhibited by Na_3VO_4, P-gp ATPase activity was measured as the vanadate sensitive portion of the total ATPase activity. Thus, ATPase activities were determined as the difference of Pi liberation measured with and without 1.2 mM sodium orthovanadate (vanadate-sensitive ATPase activity) and expressed as nmol Pi liberated/mg protein/min. Results are presented as mean ± SEM from 4 independent experiments (performed in duplicate). Controls conducted in the absence of TXs were also tested and the corresponding vanadate-sensitive ATPase activity referred to as baseline vanadate-sensitive ATPase activity.

2.8. Paraquat cytotoxicity assays

Paraquat (PQ) cytotoxicity was evaluated in Caco-2 cells by the NR uptake assay, with and without simultaneous incubation with the tested TXs (20.0 µM). Briefly, the cells were seeded onto 96-well plates to obtain confluent monolayers at the day of the experiment. After reaching confluence, the cells were exposed to PQ (0–7500 µM) in fresh cell culture medium in the presence or absence of the studied TXs. Cytotoxicity was evaluated 24 h after exposure by the NR uptake assay as previously described in section 2.3.2. Results are presented as mean ± SEM from 6 independent experiments (performed in triplicate).

To confirm the involvement of P-gp in the TXs protective effects, these incubations were repeated in the presence of a well-known and potent P-gp inhibitor, GF120918 (Dorner et al. 2009; Kanaan et al. 2009), at two noncytotoxic concentrations as evaluated by the NR uptake assay, performed as described above (10.0 μM for TX **1-5** and 20.0 μM for TX **5**). Results are presented as mean ± SEM from at least 4 independent experiments (performed in triplicate).

2.9. Statistical analysis

All statistical calculations were performed with the GraphPad Prism version 6.00 for Windows (GraphPad Software, San Diego California, USA). Normality of the data distribution was assessed by three different tests: KS normality test, D'Agostino & Pearson omnibus normality test and Shapiro-Wilk normality test. For data with parametric distribution, statistical comparisons were made using the parametric method of One-way ANOVA, followed by the Bonferroni's multiple comparisons *post hoc* test. For data with nonparametric distribution, statistical comparisons were estimated using the nonparametric method of Kruskal–Wallis (one-way ANOVA on ranks), followed by the Dunn's *post hoc* test. In experiments with two variables, statistical comparisons between groups were made using Two-way ANOVA, followed by the Sidak's multiple comparisons *post hoc* test.

In the PQ cytotoxicity assays, concentration-response curves were fitted using least squares as the fitting method and the comparisons between curves (LOG EC_{50}, TOP, BOTTOM, and Hill Slope) were made using the extra sum-of-squares F test. Details of the performed statistical analysis are described in each Figure legend. In all cases, *p* values lower than 0.05 were considered significant.

2.10. Docking of thioxanthones on P-gp model

The 3D structures of the small molecules TX **1-5** were drawn using HyperChem 7.5 (Froimowitz 1993), being minimized by the semi-empirical Polak-Ribiere conjugate gradient method (RMS<0.1 kcal.$Å^{-1}$. mol^{-1}) (Zhang et al. 2006).

Docking simulations between the P-gp model built based on Sav1866 [successfully used in the discovery of P-gp modulators in (Palmeira et al. 2012b)] and TXs **1-5**, as well as other known P-gp activators (Palmeira et al. 2011; Palmeira et al. 2012b; Sousa et al. 2013; Sterz et al. 2009) (Table 5), or PQ, and pairs of small molecules (PQ together with a TX) were undertaken in AutoDock Vina (Scripps Research Institute, USA) (Seeliger and de Groot 2010; Trott and Olson 2009). AutoDock Vina considered the target conformation as a rigid unit while the ligands were allowed to be flexible and adaptable to the target.

Vina searched for the lowest binding affinity conformations and returned nine different conformations for each ligand. AutoDock Vina was run using an exhaustiveness of 8 and a grid box with the dimensions 37.0, 30.0, 40.0, engulfing the channel formed by the transmembrane domains. Conformations and interactions were visualized using PyMOL version 1.3 (Lill and Danielson 2010).

2.11. Pharmacophore for P-gp activation

The thioxanthonic derivatives were subjected to energy minimization using HyperChem version 8.0. The semi-empirical AM1 (Austin Model 1) (Froimowitz 1993) method with the Polak-Ribière algorithm was employed for molecular minimization (Zhang et al. 2006). Common feature pharmacophore models (Chen and Foloppe 2008; Guner et al. 2004) were created from a set of 19 known P-gp activators (Table 5) (Palmeira et al. 2011; Palmeira et al. 2012b; Sousa et al. 2013; Sterz et al. 2009). HipHop module of Catalyst (Accelrys 2.1, San diego, CA, USA) (Patel et al. 2002) was employed to generate common feature pharmacophores among a set of active ligands. Minimum features were set to one and maximum features were set to 10. Minimum interfeature distance of 2.97 angstroms was applied. Conformation generation was set to “BEST” and 255 different conformations were generated per molecule and the “Maximum Omitted Features” value was set to 0.

Validation of the pharmacophore was performed by alignment of that pharmacophore with a test set of 8 known P-gp activators with a benzimidazol scaffold (Sterz et al. 2009) (Table 6). Catalyst identified the compounds that mapped to the pharmacophore, and optionally aligned the ligands in the query-selection. “All conformations” parameter was set, and the “best” quality generation type was used.

2.12. Mapping of thioxanthonic derivatives onto pharmacophores for P-gp induction

The mapping of thioxanthonic derivatives onto previously described pharmacophores for P-gp induction (Silva et al. 2013a) was performed using the “Best Fit” method in Catalyst. During the flexible fitting process, conformations of TXs were calculated within the 20 kcal/mol energy threshold. Maximum omitted features were set to zero. Fitting was evaluated by the analysis of the fit score.

3. RESULTS

3.1. Thioxanthones cytotoxicity assays

Thioxanthones cytotoxicity was evaluated by the MTT reduction and the NR uptake assays, in order to select a noncytotoxic working concentration. After 24 h of incubation no cytotoxicity was observed for any of the eight tested concentrations (0 - 100.0 μM) of all five TXs (Figure 2). For the subsequent experiments, the TXs were tested at 20 μM, a noncytotoxic concentration that was already known to interfere with RHO 123 efflux (Palmeira et al. 2012b).

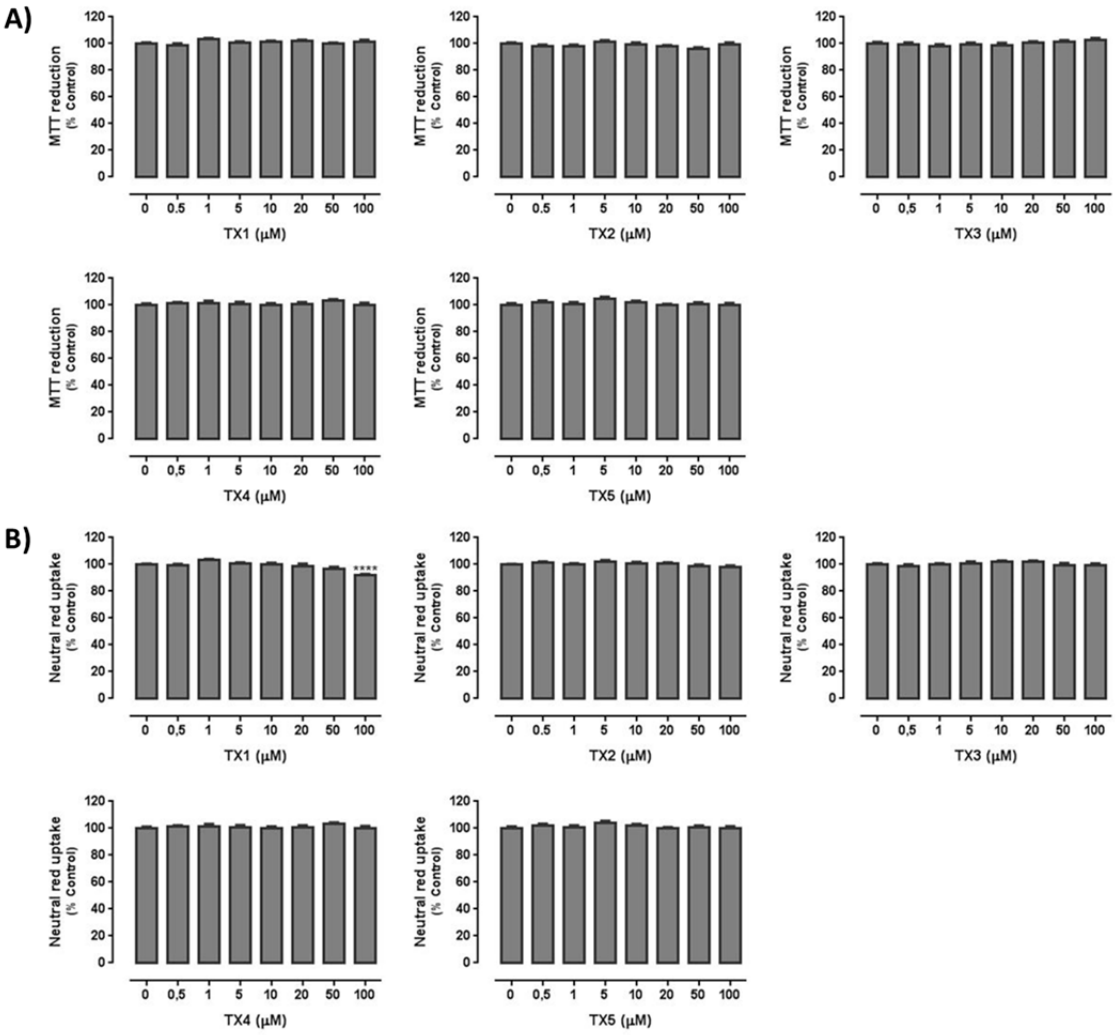

Figure 2. A) TXs **1-5** (0 – 100.0 μM) cytotoxicity in Caco-2 cells 24 h after exposure, evaluated by the MTT reduction assay. Results are presented as mean ± SEM from 5 independent experiments (performed in triplicate). Statistical comparisons were made using the parametric method of One-way ANOVA, followed by the Bonferroni's multiple comparisons *post hoc* test. **B)** TXs **1-5** (0 – 100.0 μM) cytotoxicity in Caco-2 cells 24 h after exposure, evaluated by the NR uptake assay. Results are presented as mean ± SEM from 5 independent experiments (performed in triplicate). Statistical comparisons were made using the parametric method of One-way ANOVA, followed by the Bonferroni's multiple comparisons *post hoc* test [****$p < 0.0001$ *vs.* (0 μM)].

3.2. P-glycoprotein expression

The ability of the tested TXs to induce P-gp expression in Caco-2 cells was evaluated by flow cytometry, using a P-gp monoclonal antibody [UIC2] conjugated with FITC. Nonspecific binding of the UIC2 antibody was not observed as estimated by the fluorescence obtained with the isotype-matched negative control (data not shown). As shown in Figure 3, all the tested TXs (20.0 μM) significantly increased P-gp expression to 155, 133, 125, 120 and 208%, for TX **1**, TX **2**, TX **3**, TX **4,** and TX **5**, respectively. Thus, from the obtained results, TX **5** is the most potent P-gp inducer among the tested compounds.

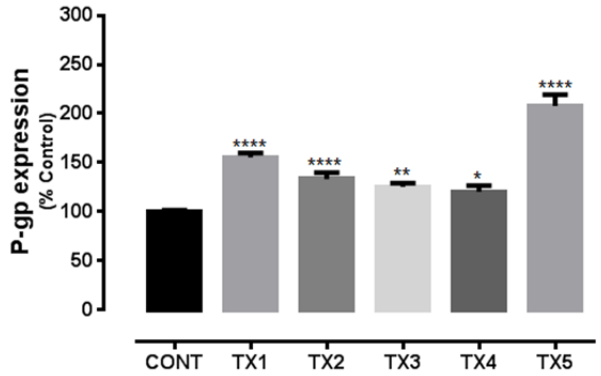

Figure 3. P-glycoprotein expression levels in Caco-2 cells exposed to TX**s 1-5** (20.0 μM) for 24 h. Results are presented as mean ± SEM from at least 3 independent experiments (performed in triplicate). Statistical comparisons were made using the parametric method of One-way ANOVA, followed by the Bonferroni's multiple comparisons *post hoc* test (*$p < 0.05$; **$p < 0.01$; ****$p < 0.0001$ *vs.* control).

3.3. P-glycoprotein transport activity

RHO 123 is a P-gp fluorescent substrate widely used for the evaluation of P-gp activity (Palmeira et al. 2011; Silva et al. 2011; Silva et al. 2013b; Vilas-Boas et al. 2011). In the present study, two different approaches for the evaluation of transport activity were performed. In the first approach, RHO 123 efflux was evaluated in the presence of the tested TXs (20.0 μM) during the efflux phase that lasted 45 min, in order to evaluate immediate effects on P-gp activity as a result of a direct activation of the pump. As observed in Figure 4, all the compounds evoked a significant increase in RHO 123 efflux, when compared to control cells. From the tested TXs, TX **1** and TX **5** were the most efficient P-gp activators, as revealed by the increased RHO 123 efflux (193 and 198%, respectively). The derivatives TX **2**, TX **3**, and TX **4**, although to a lower extent, also increased RHO 123 efflux to 125, 130, and 141%, respectively, thus also indicating P-gp activation.

Using a second approach, RHO 123 efflux was evaluated in Caco-2 cells pre-exposed to the tested TXs (20.0 μM) for 24h. Before the RHO 123 accumulation phase the cell culture media containing the tested TXs was removed prior to trypsinization. With this second protocol it is possible to evaluate whether the increases in P-gp activity are

due to the increased P-gp expression induced by the TXs, given that an increased protein expression does not necessarily translate into an increased transport activity (Silva et al. 2013a; Takara et al. 2009). The obtained results (Figure 5) demonstrated a significant increase in RHO 123 efflux for all the tested compounds. In fact, RHO 123 efflux increased to 121, 112, 126, 122, and 156% for TX **1**, TX **2**, TX **3**, TX **4**, and TX **5**, respectively. It can also be observed that, in the presence of the tested compounds, P-gp expression and activity increased in a similar magnitude, with TX **5** being the compound that induces the highest increase in both protein expression and activity, 24 h after exposure.

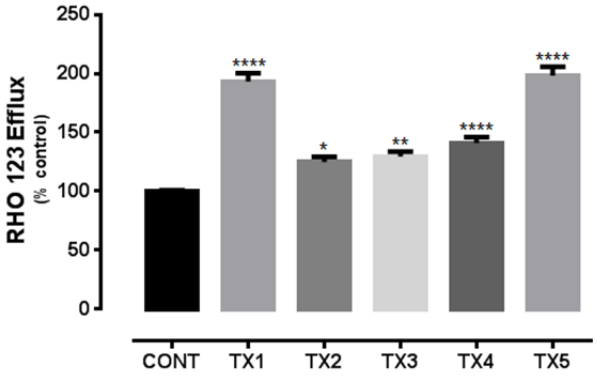

Figure 4. P-glycoprotein activity evaluated through the RHO 123 efflux in the presence of TXs **1-5** (20.0 μM) during the RHO123 efflux phase. Results are presented as mean ± SEM from 6 independent experiments (performed in triplicate). Statistical comparisons were estimated using the nonparametric method of Kruskal–Wallis (one-way ANOVA on ranks), followed by Dunn's *post hoc* test (*p < 0.05; **p < 0.01; ****p < 0.0001 *vs.* control).

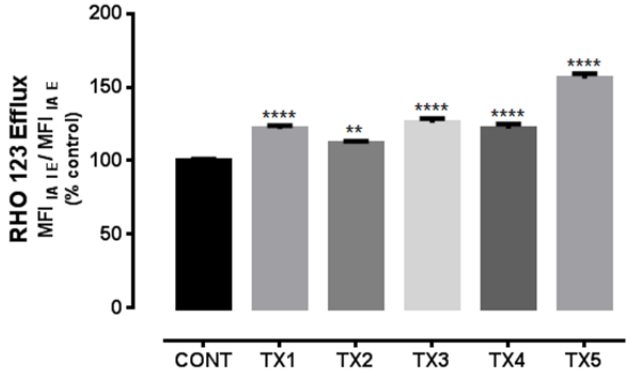

Figure 5. P-glycoprotein activity evaluated through the RHO 123 efflux in Caco-2 cells exposed to TX**s 1-5** (20.0 μM) for 24 h. Results are presented as mean ± SEM from 5 independent experiments (performed in triplicate). Statistical comparisons were made using the parametric method of One-way ANOVA, followed by the Bonferroni's multiple comparisons *post hoc* test (**p < 0.01; ****p < 0.0001 *vs.* control).

3.4. P-glycoprotein ATPase activity

In the P-gp ATPase assay, the stimulation of baseline vanadate sensitive ATPase activity by P-gp substrates is evaluated by the amount of Pi released, as a result of increased ATP consumption and reflecting an increased P-gp activity.

As observed in Figure 6, all the tested TXs (20.0 μM), except TX **3**, significantly increased the amount of Pi released by the transporter. In fact, in comparison to the basal P-gp vanadate sensitive ATPase activity (11.4 nmol Pi liberated/mg protein/min), TX **1**, TX **2**, TX **4**, and TX **5** significantly increased P-gp vanadate sensitive ATPase activity to 22.2,

18.9, 16.7, and 18.7 nmol Pi liberated/mg protein/min, respectively. On the other hand, for TX **3**, though a slight increase in P-gp vanadate sensitive ATPase activity was observed (14.1 nmol Pi liberated/mg protein/min), it did not reach statistical significance. From the obtained data, it was observed that TX **1** was the compound that caused the highest increase in ATP consumption and, consequently, in vanadate sensitive ATPase activity.

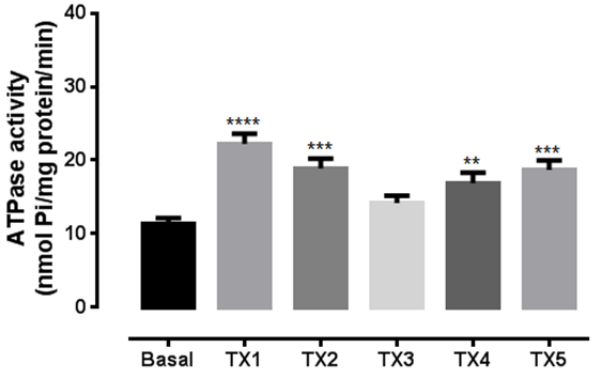

Figure 6. Vanadate sensitive ATPase activity (nmol Pi/mg protein/min) in MDR1-Sf9 membrane vesicles (4 µg/well) exposed to TXs **1-5** (20.0 µM).Results are presented as mean ± SEM from 4 independent experiments (performed in duplicate). Statistical comparisons were made using the parametric method of One-way ANOVA, followed by the Bonferroni's multiple comparisons *post hoc* test (***p* < 0.01; ****p* < 0.001; *****p* < 0.0001 *vs*. basal vanadate sensitive ATPase activity).

3.5. Thioxanthones protective effects against paraquat induced cytotoxicity

To verify if the observed increases in both P-gp expression and activity could result in an effective protection of Caco-2 cells against PQ-induced toxicity, the herbicide cytotoxicity (0–7,500 µM) was evaluated with or without simultaneous exposure to the tested TXs derivatives (20.0 µM). Paraquat cytotoxicity was evaluated by the NR uptake assay, 24 h after exposure. Figure 7 shows the concentration-response curves obtained with only paraquat (PQ) and with simultaneous TXs incubation (PQ + TXs). For all the tested TXs, except for TX **1**, significant differences were observed in the PQ-induced cell death for the 500 – 5000 µM PQ concentration range, resulting in significant rightwards shifts of the PQ concentration-response curves (Figure 7). For all the fitted curves, no significant differences in the maximal cell death (TOP) and in the baseline (BOTTOM) were observed (Table 1). For that reason, the EC_{50} values, which represent the half-maximum-effect concentrations from the fitted curves, were used for statistical comparison. As shown in Table 1, for TX **2**, TX **3**, TX **4**, and TX **5**, significant differences were observed for the EC_{50} values of the fitted curves, when compared to the EC_{50} of the PQ curve. In fact, for TX **2**, TX **3**, TX **4**, and TX **5**, the EC_{50} value significantly increased to 1517, 1359, 1378, and 1749 µM, respectively, when compared to the EC50 of the PQ curve (1204 µM). However, for TX1 no significant differences exist between the PQ and PQ + TX1 curves.

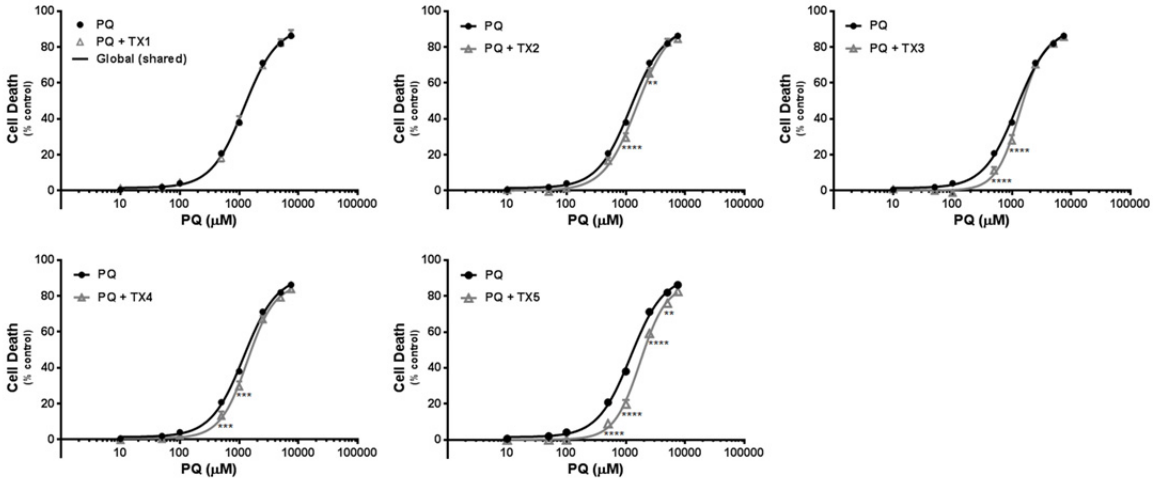

Figure 7. Paraquat concentration–response (cell death) curves in the absence (PQ) or in the presence of 20.0 μM TXs **1-5** (PQ + TXs). Results are presented as mean ± SEM from 6 independent experiments (performed in triplicate). Concentration-response curves were fitted using least squares as the fitting method and the comparisons between PQ and PQ + TXs curves (LOG EC_{50}, TOP, BOTTOM, and Hill Slope) were made using the extra sum-of-squares F test. Statistical comparisons were made using Two-way ANOVA, followed by the Sidak's multiple comparisons *post hoc* test (**p < 0.01; ***p < 0.001; ****p < 0.0001 PQ + TXs *vs.* PQ). In all cases, p values < 0.05 were considered significant.

Table 1. EC_{50} (half-maximum-effect concentration), TOP (maximal effect), BOTTOM (baseline) and Hill Slope values of the PQ concentration-response curves, with (PQ + TXs) or without (PQ) simultaneous exposure to TXs **1-5** (20.0 μM).

	PQ	PQ + TX1	PQ + TX2	PQ + TX3	PQ + TX4	PQ + TX5
EC_{50} (half-maximum-effect concentration, μM)	**1204**	**1262**	**1517**	**1359**	**1378**	**1749**
TOP (maximal cell death, % control)	91.29	91.88	93.63	87.54	86.90	86.85
BOTTOM (baseline, % control)	1.469	2.123	0.006	0.081	0.717	0.029
Hill Slope	1.559	1.609	1.559	2.156	1.878	1.959
LOG EC_{50} *p* value (comparison between LOG EC_{50} values)	-	0.4948	**0.0009**	**0.0321**	**0.0379**	**< 0.0001**
TOP *p* value (comparison between TOP values)	-	0.8437	0.5023	0.1305	0.1520	0.1704
BOTTOM *p* value (comparison between BOTTOM values)	-	0.5467	0.1740	0.2500	0.5435	0.1929
Hill Slope *p* value (comparison between Hill slope values)	-	0.7481	0.9983	**0.0008**	0.0792	**0.0231**
Curve *p* value (Comparison between the Fitted Curves)	-	0.8554	**< 0.0001**	**< 0.0001**	**< 0.0001**	**< 0.0001**

Concentration-response curves were fitted using least squares as the fitting method and the comparisons between PQ and PQ + TXs curves were made using extra sum-of-squares F test. In all cases, p values < 0.05 were considered significant.

To evaluate if these protective effects are related to the observed increases in both P-gp expression and activity, this study was repeated in the presence of a specific and potent P-gp inhibitor, GF120918. The GF120918 inhibitor did not cause toxicity as evaluated by the NR uptake assay, 24 h after exposure at the 10.0 and 20.0 μM tested concentrations (data not shown). The obtained data shows that when PQ is simultaneously incubated with GF120918 (10.0 and 20.0 μM), a leftwards shift of the PQ concentration-response curves occurs, with significant differences observed for the 100-7,500 μM PQ concentrations (Figure 8). Also, the observed leftwards shifts of the fitted curves were accompanied by significant and concentration-dependent decreases in the EC_{50} values, when compared to the PQ curve (Table 2). In the presence of 10.0 and 20.0 μM GF120918, the EC_{50} values of the fitted curves significantly decreased to 985.1 and 764.7 μM, respectively, when compared to the PQ curve (1204 μM). These findings proved that P-gp modulation has an important impact on PQ toxicity and that GF120918 is a suitable inhibitor that can be used to elucidate if the observed TXs protective effects are mediated by P-gp.

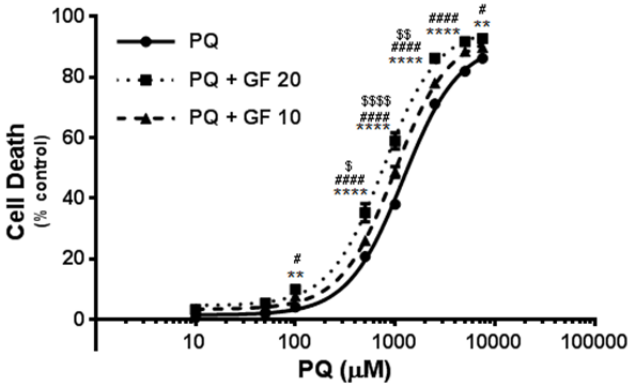

Figure 8. Paraquat concentration–response (cell death) curves in the absence (PQ) or in the presence (PQ + GF 10 and PQ + GF 20) of the potent P-gp inhibitor GF120918, confirming the P-gp involvement in PQ toxicity. Results are presented as mean ± SEM from at least 4 independent experiments (performed in triplicate). Concentration–response curves were fitted using least squares as the fitting method and the comparisons between PQ, PQ + GF 10 and PQ + GF 20 curves (LOG EC_{50}, TOP, BOTTOM, and Hill Slope) were made using the extra sum-of-squares F test. Statistical comparisons were made using Two-way ANOVA, followed by the Sidak's multiple comparisons *post hoc* test (***p* < 0.01, *****p* < 0.0001 PQ + GF 10 *vs.* PQ; $^{\#}p$ < 0.01, $^{\#\#\#\#}p$ < 0.0001 PQ + GF 20 *vs.* PQ; $^{\$\$}p$ < 0.01, $^{\$\$\$}p$ < 0.001, $^{\$\$\$\$}p$ < 0.0001 PQ + GF 10 *vs.* PQ + GF 20). In all cases, *p* values < 0.05 were considered significant.

Under P-gp inhibition with 10 μM GF120918, and for TX **2**, TX **3**, and TX **4**, it was possible to verify a complete abolishment of the previously observed protective effects (Figure 9). In fact, as shown in Table 3, no significant differences exist for the overall comparison of the fitted curves (LOG EC_{50}, TOP, BOTTOM, and Hill Slope). Moreover, for TX **1**, and as observed in the assays performed without P-gp inhibition, no significant differences exist between the PQ + GF 10 and PQ + GF 10 + TX1 curves. However, for TX **5**, in the presence of 10.0 μM GF120918, a small but significant rightwards shift of the PQ + GF 10 + TX5 concentration-response curve can still be observed (Figure 9), showing that in spite of not being able to fully reverse the protective effects, P-gp inhibition can partially reduce the previously observed protection. As shown in Table 3, the

observed rightwards shift was accompanied by a minor, though significant, increase in the corresponding EC_{50} value (1279 μM for PQ + GF 10 + TX5 curve when compared to 985.1 μM for PQ + GF 10 curve).

Table 2. EC_{50} (half-maximum-effect concentration), TOP (maximal effect), BOTTOM (baseline) and Hill Slope values of the PQ concentration-response curves, with (PQ + GF 10 and PQ + GF 20) or without (PQ) simultaneous exposure to 10.0 or 20.0 μM of the P-gp inhibitor, GF120918.

	PQ	PQ + GF 10	PQ + GF 20
EC_{50} (half-maximum-effect concentration, μM)	**1204**	**985.1**	**764.7**
TOP (maximal cell death, % control)	91.29	94.06	96.02
BOTTOM (baseline, % control)	1.469	3.355	4.588
Hill Slope	1.559	1.602	1.615
LOG EC_{50} *p* value (comparison between LOG EC_{50} values)	-	**< 0,0001**	**< 0,0001**
TOP *p* value (comparison between TOP values)	-	0.1167	0.0612
BOTTOM *p* value (comparison between BOTTOM values)	-	0.0226	0.0756
Hill Slope *p* value (comparison between Hill slope values)	-	0.6855	0.7878
Curve *p* value (Comparison between the Fitted Curves)	-	**< 0.0001**	**< 0.0001**

Concentration-response curves were fitted using least squares as the fitting method and the comparisons between PQ and PQ + GF curves were made using extra sum-of-squares F test. In all cases, *p* values < 0.05 were considered significant.

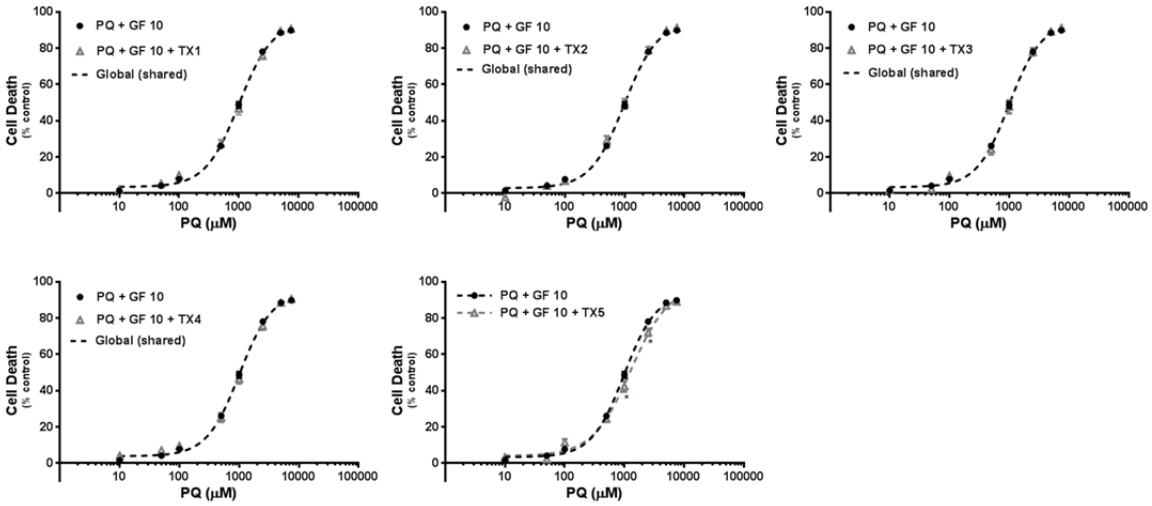

Figure 9. Paraquat concentration–response (cell death) curves in the presence of the potent P-gp inhibitor GF120918 (10 μM) with (PQ + GF10 + TXs) or without (PQ + GF10) simultaneous exposure to TXs **1-5** (20.0 μM). Results are presented as mean ± SEM from 5 independent experiments (performed in triplicate). Concentration–response curves were fitted using least squares as the fitting method and the comparisons between PQ + GF 10 and PQ + GF 10 + TXs curves (LOG EC_{50}, TOP, BOTTOM, and Hill Slope) were made using the extra sum-of-squares F test. Statistical comparisons were made using Two-way ANOVA, followed by the Sidak's multiple comparisons *post hoc* test (*p < 0.05 PQ + GF 10 + TXs *vs.* PQ + GF 10). In all cases, *p* values < 0.05 were considered significant.

As TX **5** was responsible for the highest observed P-gp induction (Figure 3), the incomplete reversion of the protective effect observed for this TX derivative, in the presence of 10 μM GF120918, could be due to an incomplete inhibition of the pump. Therefore, for TX **5**, PQ cytotoxicity was further evaluated by inhibiting P-gp with 20.0 μM GF120918. As shown in Figure 10, similarly to 10.0 μM GF120918 mediated P-gp inhibition, in the presence of 20.0 μM GF120918, a small protective effect of TX **5** could still be noted for the higher PQ concentrations tested (2,500 - 7,500 μM), as observed by the corresponding rightwards shift of the PQ + GF 20 + TX5 curve at those PQ concentrations. Moreover, the small rightwards shift at the top of the PQ + GF 20 + TX5 curve was accompanied by a minor, although significant, increase in the EC50 value (909.4 μM, when compared to 764.7 μM for the PQ + GF 20 curve) (Table 4). However, since the significant and outstanding rightwards shift of the PQ + TX5 curve was almost completely abolished under P-gp inhibition, it was concluded that P-gp is mainly involved on the protective effects mediated by TX **5** in PQ cytotoxicity, as with TX **2**, TX **3**, and TX **4**.

Table 3. EC_{50} (half-maximum-effect concentration), TOP (maximal effect), BOTTOM (baseline) and Hill Slope values of the PQ concentration-response curves, in the presence of the P-gp inhibitor GF120918 (10.0 μM), with (PQ + GF 10 + TXs) or without (PQ + GF 10) simultaneous exposure to TXs **1-5** (20.0 μM).

	PQ + GF 10	PQ + GF 10 + TX1	PQ + GF 10 + TX2	PQ + GF 10 + TX3	PQ + GF 10 + TX4	PQ + GF 10 + TX5
EC_{50} (half-maximum-effect concentration, μM)	**985.1**	**1124**	**968.0**	**1047**	**1126**	**1279**
TOP (maximal cell death, % control)	94.06	98.88	98.73	95.57	95.51	98.37
BOTTOM (baseline, % control)	3.355	4.043	0.5108	3.491	5.949	4.071
Hill Slope	1.602	1.367	1.336	1.611	1.566	1.355
LOG EC_{50} *p* value (comparison between LOG EC_{50} values)	-	0.1152	0.8300	0.3950	0.0745	**0.0035**
TOP *p* value (comparison between TOP values)	-	0.1866	0.1702	0,6280	0.6556	0.3183
BOTTOM *p* value (comparison between BOTTOM values)	-	0.6739	0.0797	0,9282	0.0845	0.6571
Hill Slope *p* value (comparison between Hill slope values)	-	0.2079	0.1437	0.9649	0.8518	0.1958
Curve *p* value (Comparison between the Fitted Curves)	-	0.4491	0.2713	0.8844	0.1916	**0.0024**

Concentration-response curves were fitted using least squares as the fitting method and the comparisons between PQ + GF 10 and PQ + GF 10 + TXs curves were made using extra sum-of-squares F test. In all cases, *p* values < 0.05 were considered significant.

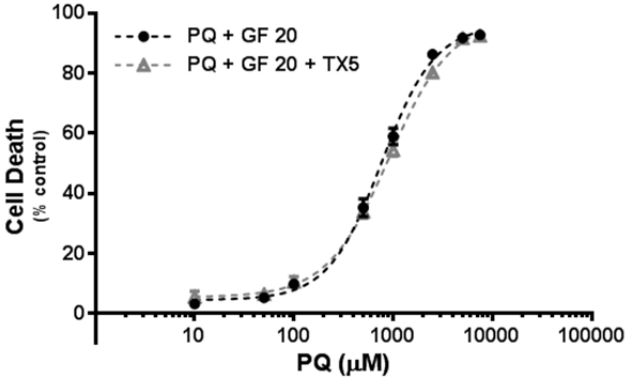

Figure 10. Paraquat concentration–response (cell death) curves in the presence of the potent P-gp inhibitor GF120918 (20.0 μM), with (PQ + GF 20 + TX5) or without (PQ + GF 20) simultaneous exposure to TX **5** (20.0 μM). Results are presented as mean ± SEM from 4 independent experiments (performed in triplicate). Concentration–response curves were fitted using least squares as the fitting method and the comparisons between PQ + GF 20 and PQ + GF 20 + TX5 curves (LOG EC_{50}, TOP, BOTTOM, and Hill Slope) were made using the extra sum-of-squares F test. Statistical comparisons were made using Two-way ANOVA, followed by the Sidak's multiple comparisons *post hoc* test. In all cases, *p* values < 0.05 were considered significant.

Table 4. EC_{50} (half-maximum-effect concentration), TOP (maximal effect), BOTTOM (baseline) and Hill Slope values of the PQ concentration-response curves, in the presence of the P-gp inhibitor GF120918 (20.0 μM), with (PQ + GF 20 + TX5) or without (PQ + GF 20) simultaneous exposure to 20.0 μM TX **5**.

	PQ + GF 20	PQ + GF 20 + TX5
EC_{50} (half-maximum-effect concentration, μM)	**764.7**	**909.4**
TOP (maximal cell death, % control)	96.02	98.26
BOTTOM (baseline, % control)	4.588	5.480
Hill Slope	1.615	1.386
LOG EC_{50} *p* value (comparison between LOG EC_{50} values)	-	**0.0213**
TOP *p* value (comparison between TOP values)	-	0.4712
BOTTOM *p* value (comparison between BOTTOM values)	-	0.6030
Hill Slope *p* value (comparison between Hill slope values)	-	0.2431
Curve *p* value (Comparison between the Fitted Curves)	-	**0.0359**

Concentration-response curves were fitted using least squares as the fitting method and the comparisons between PQ + GF 20 and PQ + GF 20 + TX5 curves were made using extra sum-of-squares F test. In all cases, *p* values < 0.05 were considered significant.

3.6. *In silico* predictions

As P-gp activators showed to stimulate its ATPase activity, TXs **1-5** were hypothesized to bind in the drug-binding pocket formed by the transmembrane (TM) domain interface, and docking simulations were performed in this binding pocket of P-gp. Scores of known P-gp activators are shown in Table 5. As TX **1** and TX **5** were the most active P-gp activators in the *in vitro* studies, a visual inspection of these molecules in the transmembrane domain interface of P-gp was performed (Figure 11). Both TX **1** and TX **5** have two preferential binding sites, engulfed by TM 4, 5, 8-10 and 12, or by TM 1-3, 6, 7, and 11 (Figure 11). TX **5** forms a stable complex with P-gp with a negative energy of -6.7

kJ/mol. TX **5** has shape, size, and stereoelectronic complementarity to P-gp binding pocket, establishing hydrogen interactions with Ala-80, and stacking interactions with Phe-201, described as being part of P-glycoprotein binding pocket (Loo et al. 2009). TX **1** has a docking score of -6.5 kJ/mol, and it established hydrogen interactions with Gly346, known as being evolved in inter-domain communication, causing an helical movement required to ATP hydrolysis and multidrug transport (Storm et al. 2007); and Ser228, also described as being important residue in P-gp drug binding pocket (Loo and Clarke 1999); and stacking interactions with Phe-201.

Table 5. P-gp activators described by the RHO 123 accumulation assay and respective docking scores ($kJ.mol^{-1}$) on transmembrane domains.

Ligand	Binding affinity ($kJ.mol^{-1}$)	Reference
2-(4-Methylphenyl)-5,6,7,8-tetrahydroimidazo[2,1-b][1,3]benzothiazole	-7.2	(Sterz et al. 2009)
2-Phenyl-9-(prop-2-en-1-yl)-5,7,8,9-tetrahydro-6H-imidazo[1,2-a]benzimidazole	-7.6	(Sterz et al. 2009)
Blebbistatin	-8.1	(Palmeira et al. 2011)
Coelenteramide	-7.2	(Palmeira et al. 2011)
Indirubin	-6.5	(Palmeira et al. 2011)
1,2-Dihydroxy-9H-xanthen-9-one	-7	(Sousa et al. 2013)
3,4-Dihydroxy-9H-xanthen-9-one	-6.3	(Sousa et al. 2013)
1-Chloro-9-oxo-9H-thioxanthen-4-yl acetate	-8.4	(Palmeira et al. 2012b)
1-{[4- (Aminomethyl)benzyl]amino}-4-propoxy-9H-thioxanthen-9- one	-7.8	(Palmeira et al. 2012b)
1-{[2- (Phenylamino)ethyl]amino}-4-propoxy-9H-thioxanthen-9-one	-7.5	(Palmeira et al. 2012b)
1-[(3,4- Dimethoxybenzyl)amino]- 4-propoxy-9H-thioxanthen-9-one	-7.4	(Palmeira et al. 2012b)
1-{[(2S)-1- Hydroxy-3- methylbutan-2-yl]amino}-4-propoxy-9H-thioxanthen-9-one	-7.2	(Palmeira et al. 2012b)
4-Hydroxy-9H-thioxanthen-9-one	-7.1	(Palmeira et al. 2012b)
1-[(2S,3R,4S,5R,6R)-2-(4-Aminophenoxy)-6-(hydroxymethyl)tetrahydro-2H-pyran-3,4,5-triol]-4-propoxy-9H-thioxanthen-9-one	-6.2	(Palmeira et al. 2012b)
1-[(3- Hydroxypropyl)amino]-4-propoxy-9H-thioxanthen-9-one (TX **1**)	-6.5	
1-Chloro-4-hydroxy-9H-thioxanthen-9-one (TX **2**)	-6.8	
1-{[2-(1,3- Benzodioxol-5-yl)ethyl]amino}-4-propoxy-9H-thioxanthen-9-one (TX **3**)	-8.1	
1-[(2- Methylpropyl)amino]-4-propoxy-9H-thioxanthen-9-one (TX **4**)	-7.5	
1-(Propan-2-ylamino)-4-propoxy-9H-thioxanthen-9- one (TX **5**)	-6.7	

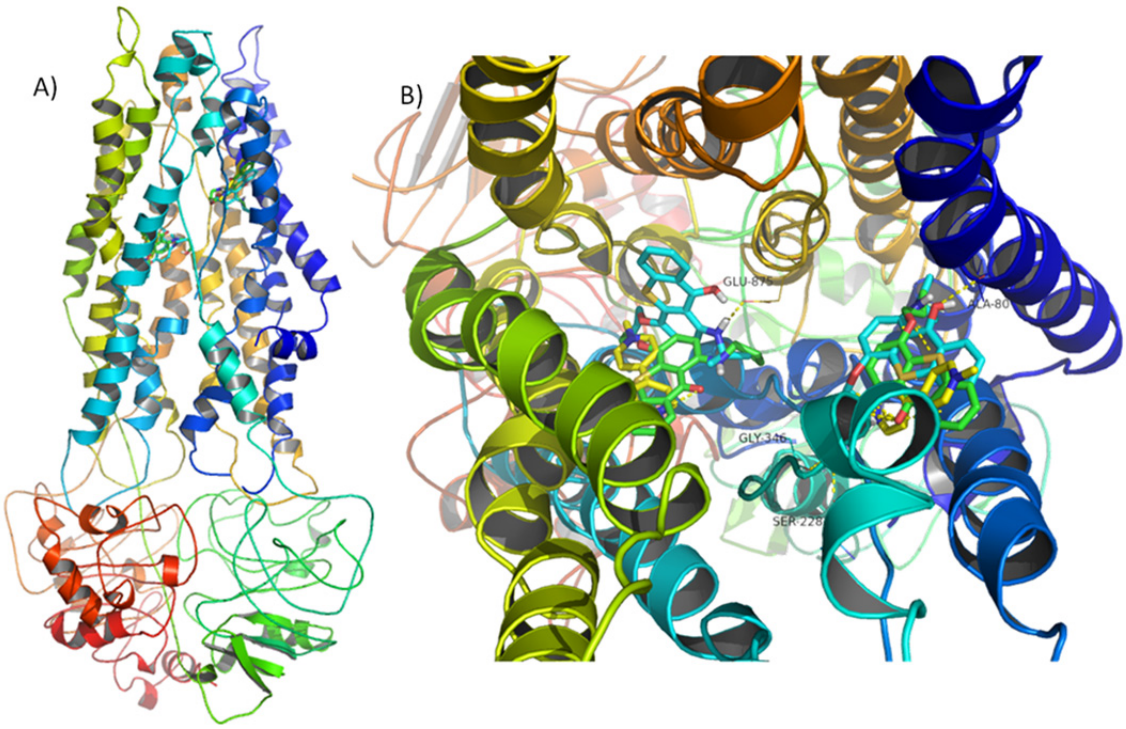

Figure 11. (color) TX **1** (green sticks), TX **5** (blue sticks) and PQ (yellow sticks) docked on two different binding sites in P-gp (only the best scoring poses on each site are represented). Side (A) and top (B) views.

The top rank PQ docking pose presented a score of -5.6 kJ/mol. Paraquat has two preferential binding pockets in P-gp (Figure 11), similarly to the TXs. Therefore, TXs and PQ may bind simultaneously in P-gp in two different binding sites. Moreover, TXs and PQ may establish stacking interactions; this noncovalent complex binds to P-gp with higher affinity than TXs and PQ individually (Figure 12): -10 kJ/mol for both TX **5**:PQ:P-gp, and TX **1**:PQ:P-gp. The two-ligand complex establish polar interactions with P-gp residues, such as Asn839 and Val345, and stacking interactions with P-gp residues, such as Phe201, Phe239, and Phe777 (Figure 12).

A pharmacophore for P-gp activation activity was built based on TXs with *in vitro* activity, as well as other molecules previously described as P-gp activators. The best ranked pharmacophore found (score of 110.3 kcal/mol) is composed of three features: one hydrophobic feature, one aromatic ring, and one hydrogen bond acceptor group (Figure 13).

Our group has previously described four pharmacophores for P-gp induction (Silva et al. 2013a). As the TXs described in the present work demonstrated the ability to increase, *in vitro,* P-gp expression, they were mapped and aligned to the four pharmacophores for P-gp induction. TX **3** was able to fit three of the four pharmacophores. The five screened TXs were able to fit a three-feature P-gp induction

pharmacophore consisting of one hydrogen-bond donor and two hydrophobic groups (previously described as pharmacophore IV).

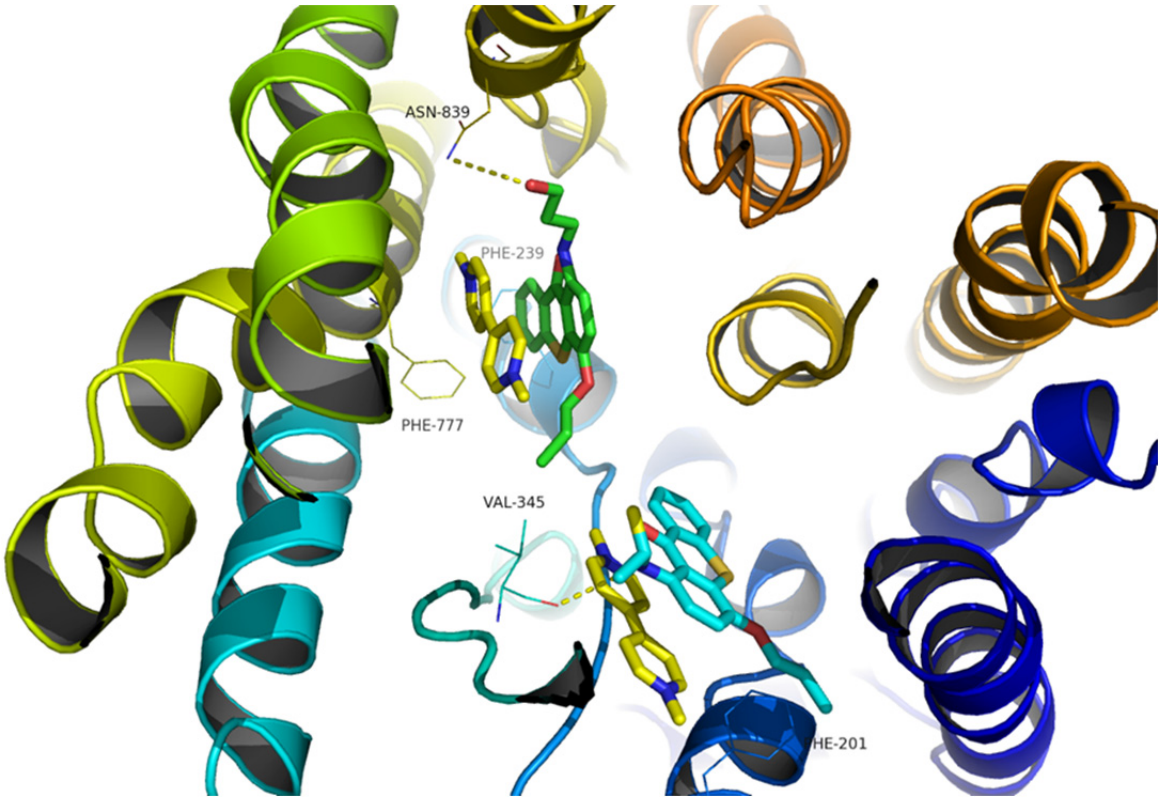

Figure 12. TX **1** (green sticks) and PQ (yellow sticks), and TX **5** (blue sticks) and PQ (yellow) docked simultaneously on P-gp (top view).

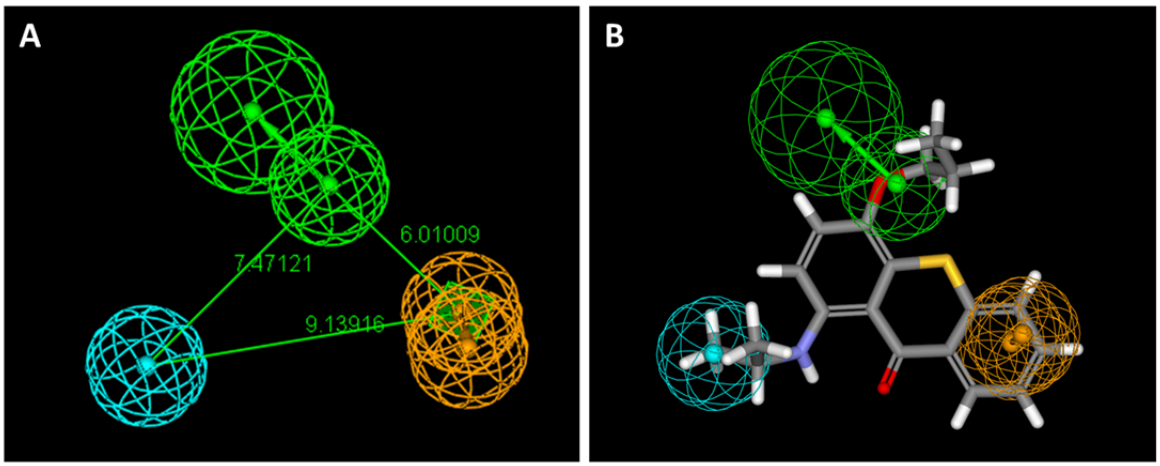

Figure 13. A) The top-ranked chemical feature-based pharmacophore model for P-gp activators developed using the HipHop module in Catalyst. The pharmacophore includes one hydrophobic group, one hydrogen bond acceptor feature, and one aromatic ring. Interfeature distances are depicted with green lines. B) TX **5** aligned with the pharmacophore (as an example). Distances are given in Angstrom. Blue = hydrophobic, orange = aromatic, green = hydrogen bond acceptor.

Table 6. Pharmacophore validation using a test set of known P-gp activators (Sterz et al. 2009).

P-gp activators	Fit value
4-(5,6,7,8-Tetrahydroimidazo[2,1-*b*][1,3]benzothiazol-2-yl)benzonitrile	2.985
2-(4-Nitrophenyl)-5,6,7,8-tetrahydroimidazo[2,1-*b*][1,3]benzothiazole	2.991
4-(9-Methyl-5,7,8,9-tetrahydro-6*H*-imidazo[1,2-*a*]benzimidazol-2-yl)benzonitrile	2.846
9-Methyl-2-(4-nitrophenyl)-5,7,8,9-tetrahydro-6*H*-imidazo[1,2-*a*]benzimidazole	2.846
9-Methyl-2-(3-nitrophenyl)-5,7,8,9-tetrahydro-6*H*-imidazo[1,2-*a*]benzimidazole	2.856
2-(4-Chlorophenyl)-9-methyl-5,7,8,9-tetrahydro-6*H*-imidazo[1,2-*a*]benzimidazole	2.898
3-(9-Methyl-5,7,8,9-tetrahydro-6*H*-imidazo[1,2-*a*]benzimidazol-2-yl)aniline	2.987
4-(4-((6-Chloro-4H-benzo[d][1,3]dioxin-8-yl)methyl)-5,6,7,8-tetrahydro-4*H*-benzo[d]imidazo[1,2-a]imidazol-2-yl)benzonitrile	2.976

4. DISCUSSION

The present data clearly demonstrate that four of the tested thioxanthones (TX **2-5**), by inducing both P-gp expression and activity, significantly protected Caco-2 cells against PQ-induced toxicity.

Caco-2 cells are a widely accepted *in vitro* model for predicting drug intestinal absorption and excretion in humans (Balimane et al. 2006; Barta et al. 2008; Biganzoli et al. 1999; Huynh-Delerme et al. 2005; Watanabe et al. 2005; Yamashita et al. 2000) and express P-gp at levels similar to those found in normal human jejunum (Taipalensuu et al. 2001). Moreover, they were already validated as a suitable *in vitro* model for the screening of P-gp inducers (Silva et al. 2011; Silva et al. 2013b).

Growing interests in the synthesis and potential applications of TXs, dibenzo- γ - thiopyrones, has been noted since the beginning of the 20th century (Paiva et al. 2013). However, in what concerns to their ability to modulate P-gp expression and activity little is known. In fact, only a few studies reported their ability to inhibit this important efflux pump (Palmeira et al. 2012b), suggesting a potential use in reducing multidrug resistance. Recently, Palmeira and co-workers have demonstrated that several aminated TXs were highly effective at inhibiting P-gp in a chronic myelogenous leukemia cell line, K562 cells (Palmeira et al. 2012b). Furthermore, twelve of the tested derivatives, caused a significant decrease in the RHO 123 accumulation ratio (Palmeira et al. 2012b), an effect compatible with increased P-gp activity. However, no further studies were conducted to clarify their mode of action. To the best of our knowledge, this is the first report on the ability of TXs to act as P-gp inducers, demonstrating also that they can effectively increase the pump activity. Additionally, for all the tested compounds, a good correlation between the observed increases in P-gp expression and activity was demonstrated. In fact, it is known that increases in protein expression may not necessarily result in proportional increases in pump activity (Silva et al. 2011; Silva et al. 2013a; Takara et al. 2009; Vilas-Boas et al. 2011). Using the same *in vitro* model, we have previously shown that the remarkable increase in P-gp expression caused by doxorubicin, a potent P-gp inducer, was not accompanied by a proportional increase in P-gp transport activity (Silva et al. 2011). However, as can be seen in Figures 3 and 5, all tested TXs **1-5** simultaneously increased P-gp expression and activity, being TX **5** the thioxanthonic derivative that caused the highest increase in the protein expression and in the pump activity. It is noteworthy that the observed increases in P-gp expression reveal a higher level of expression and incorporation in the cell membrane, since the monoclonal UIC2 antibody recognizes an external P-gp epitope (Vilas-Boas et al. 2011). Curiously, TX **4** and **5** are homologues varying by a single methylene unit and yet display rather large differences in P-gp

induction; this effect could be related to a steric influence of the substituent in position 1 of the thioxanthone scaffold. Additionally, all the tested TXs **1-5** fitted on a previously validated pharmacophore for P-gp induction (Silva et al. 2013a) and, therefore, it can be hypothesized that thioxanthones are P-gp inducers by a mechanism similar to that of compounds (such as carbamazepine) used to build the represented pharmacophore. In fact, all the tested compounds fitted the three-feature P-gp induction pharmacophore *in silico* and significantly increased the protein expression *in vitro*, demonstrating a good match between *in vitro* and *in silico* studies, and validating the use of such pharmacophores in the screening of new P-gp inducers.

P-gp ATPase activity assays have been long used to evaluate possible interactions with P-gp function. Compounds that act as P-gp substrates typically stimulate its ATPase activity (Ambudkar et al. 1999). Accordingly, our results showed that the tested compounds caused a notable increase in P-gp vanadate-sensitive ATPase activity (although not significant for TX **3**), demonstrating that these TXs derivatives are actively transported by the pump.

Another important aspect to note among the obtained data was the ability of all the tested compounds **(TX 1-5)** to rapidly and significantly increase the pump activity, as assessed by the RHO 123 efflux assay performed in the presence of the TXs during a short 45 min efflux phase (Figure 4). The RHO 123 efflux evaluated using this protocol does not reflect a possible contribution of increased P-gp expression in the increased activity due to the short duration of the contact between the TXs and the cells during the RHO 123 efflux phase. Nevertheless, compound TX **1**, which presented the highest increase in ATP consumption in the ATPase activity assay, showed an efflux ratio of RHO 123 similar to TX **5**. This difference in the results obtained from both assays could be related to the different permeability of the TXs (logP TX**1**=3.1 *vs*. logP TX **5**=4.1), since the ATPase assay uses membrane fractions, and, therefore, is not influenced by drug permeability in contrast with the cell-based RHO123 efflux assay (Eytan et al. 1996).

Considering the observed effects of the tested compounds on P-gp expression and activity, we further evaluated the impact of those effects on the toxicity induced by a toxic P-gp substrate, the herbicide paraquat. For four of the tested compounds (TX **2-5**), the observed inducing effects on both P-gp expression and activity resulted in a significant protection against PQ toxicity (with significant increases in the EC_{50} values of the PQ + TXs curves versus PQ only; Figure 7), meaning that they could have protective effects against PQ intoxications, by favouring its P-gp-induced efflux. In agreement, the observed reduction on the PQ-induced cell death was completely abolished in the presence of the potent P-gp inhibitor, GF120918 for TX **2**, TX **3**, and TX **4**. However, for TX **5**, in spite of the observed significant reduction of its protective effects in the presence GF120918, this

effect was incomplete, thus indicating that, for TX **5**, mechanisms other than P-gp induction may be involved in its protective effects against PQ toxicity.

Considering the typical PQ intoxication scenarios, the herbicide concentrations used in this study are within what is expected to be attained *in vivo.* PQ commercially available formulations generally contain 20 g herbicide/100 mL (Dinis-Oliveira et al. 2009). In most of the reported cases of human PQ intoxication, 25–50 mL of the PQ formulation are usually ingested (Dinis-Oliveira et al. 2009), suggesting an approximate intake of 5 to 10 g of PQ. Since only up to 5% of the ingested dose is absorbed at the intestinal level (Roberts 2011), under this intoxication scenarios, blood concentrations of PQ may easily reach a concentration of 0.1 g/L (0.4 mM). Additionally, post-mortem analysis have found PQ concentrations in the target organs, such as the lungs, up to 10 times higher than in the blood (Dinis-Oliveira et al. 2008). Moreover, the PQ concentrations that are found at autopsy are probably lower than the peak concentrations that may be reached after intake since, after intoxication, emergency-care treatments are administered, including hemodialysis, thus reducing the herbicide concentration in the organism.

Noteworthy, four of the assayed TXs were able to simultaneously increase RHO 123 efflux, ATP consumption, and PQ EC_{50} values in Caco-2 cells, indicating the existence of a mechanism involving P-gp activation. The ability of certain compounds to immediately increase P-gp activity without the need to increase its expression led to the recently used definition of P-gp activator (Sterz et al. 2009). In fact, it has long been known that there are compounds that bind to P-gp and stimulate the transport of a substrate on another binding site. For example, Hoechst-33342 and RHO 123 act by this cooperative mode of action (Shapiro and Ling 1998). This functional model of P-gp suggested that the efflux pump contained at least two positively cooperative sites (H site and R site, for Hoechst-33342 and RHO 123, respectively) for drug binding and transport (Shapiro and Ling 1997). This cooperative mechanism of action has also been suggested for prazosin and progesterone (Shapiro et al. 1999). Additionally, a four-P-gp-binding-sites model supports the presence of three transport sites and one regulatory site. This last site allosterically alters the conformation of the transport binding sites for substrates from low to high affinity, thus increasing the rate of translocation (Martin et al. 2000). It has been suggested that the adaption and survival mechanisms of living beings has allowed the binding of several xenobiotics at the same time to P-glycoprotein (Safa 1993; Safa 1998), increasing the transport of each other, not competing but activating the transportation cycle (Safa 2004). Hence, binding modes of TXs were further explored by docking studies. Thioxanthonic derivatives and PQ docked on two different binding sites in the cleft formed by the transmembrane alpha-helices of a P-gp model, based on homologous *S.aureus* ABC transporter, Sav1866 (Palmeira et al. 2012b). Furthermore, a simultaneous

docking of PQ and TX **1** or TX **5** revealed that a more stable complex with P-gp model was formed (lower free energy) than when those molecules were docked individually, suggesting that a co-transport may occur. The two mechanisms of activation by co-transport suggested by docking studies are: a) TXs dock on a different site than PQ, thus activating the efflux of the herbicide, and b) TXs and PQ bind to the same drug pocket, establishing stacking interactions between the dibenzo-γ-thiopyrone and the biphenyl group, and facilitate the transport to the extracellular medium. Additionally, from the tested TXs, TX **1** behaves as a strict competitive substrate, suggesting that this TX overlaps with PQ on the same site of P-gp. Therefore, in spite of the slight increases in P-gp expression, RHO 123 efflux, and P-gp ATPase activity, TX **1** apparently does not protect against PQ-induced toxicity. As docking scores reveal, TX **1** binds more tightly to the P-gp binding site than PQ (-6.5 versus -5.6 kJ/mol).

In conclusion, TX **5** was the thioxanthone derivative that demonstrated the highest potential in inducing P-gp, since, as a result of the highest P-gp expression and activation capacity, it elicited the highest protection against PQ-induced toxicity. Gathering all these *in vitro* data concerning P-gp activation, a pharmacophore was built, which can be used as a query to screen for new P-gp activators. Further *in vivo* demonstration of the protective effects of these TXs will confirm their potential use as effective antidotes against PQ intoxications.

5. ACKNOWLEDGMENTS

This work was supported by the Fundação para a Ciência e Tecnologia (FCT)-project PTDC/SAU-OSM/101437/2008 - QREN initiative with EU/FEDER funded through COMPETE - Operational Programme for Competitiveness Factors.

The work was also supported by FCT within the framework of Strategic Projects for Scientific Research Units of R&D (projects PEst-C/EQB/LA0006/2011 and Pest-OE/SAU/UI4040/2011).

Renata Silva and Daniel José Barbosa acknowledge FCT for their PhD grants [SFRH/BD/29559/2006] and [SFRH/BD/64939/2009], respectively.

Ana Paiva acknowledges to Liga Portuguesa Contra o Cancro/Pfizer for her grant.

6. CONFLICT OF INTEREST STATEMENT

The authors declare that there are no conflicts of interest.

7. REFERENCES

Ambudkar SV, Dey S, Hrycyna CA, Ramachandra M, Pastan I, Gottesman MM (1999) Biochemical, cellular, and pharmacological aspects of the multidrug transporter. Annu Rev Pharmacol Toxicol 39:361-398.

Balimane PV, Han YH, Chong S (2006) Current industrial practices of assessing permeability and P-glycoprotein interaction. AAPS J 8:1-13.

Barta CA, Sachs-Barrable K, Feng F, Wasan KM (2008) Effects of monoglycerides on p-glycoprotein: modulation of the activity and expression in caco-2 cell monolayers. Mol Pharm 5:863-875.

Biganzoli E, Cavenaghi LA, Rossi R, Brunati MC, Nolli ML (1999) Use of a Caco-2 cell culture model for the characterization of intestinal absorption of antibiotics. Farmaco 54:594-9.

Chang G (2003) Multidrug resistance ABC transporters. FEBS Lett 555:102-105.

Chen IJ, Foloppe N (2008) Conformational sampling of druglike molecules with MOE and catalyst: implications for pharmacophore modeling and virtual screening. J Chem Inf Model 48:1773-1791.

Cianchetta G, Singleton RW, Zhang M, et al. (2005) A pharmacophore hypothesis for P-glycoprotein substrate recognition using GRIND-based 3D-QSAR. J Med Chem 48:2927-2935.

Cordon-Cardo C, O'Brien JP, Boccia J, Casals D, Bertino JR, Melamed MR (1990) Expression of the multidrug resistance gene product (P-glycoprotein) in human normal and tumor tissues. J Histochem Cytochem 38:1277-1287.

Dinis-Oliveira RJ, de Pinho PG, Santos L, et al. (2009) Postmortem analyses unveil the poor efficacy of decontamination, anti-inflammatory and immunosuppressive therapies in paraquat human intoxications. PLoS One 4:e7149.

Dinis-Oliveira RJ, Duarte JA, Remiao F, Sanchez-Navarro A, Bastos ML, Carvalho F (2006) Single high dose dexamethasone treatment decreases the pathological score and increases the survival rate of paraquat-intoxicated rats. Toxicology 227:73-85.

Dinis-Oliveira RJ, Duarte JA, Sanchez-Navarro A, Remiao F, Bastos ML, Carvalho F (2008) Paraquat poisonings: mechanisms of lung toxicity, clinical features, and treatment. Crit Rev Toxicol 38:13-71.

Dorner B, Kuntner C, Bankstahl JP, et al. (2009) Synthesis and small-animal positron emission tomography evaluation of [11C]-elacridar as a radiotracer to assess the distribution of P-glycoprotein at the blood-brain barrier. J Med Chem 52:6073-6082.

Eytan GD, Regev R, Oren G, Assaraf YG (1996) The role of passive transbilayer drug movement in multidrug resistance and its modulation. J Biol Chem 271:12897-12902.

Froimowitz M (1993) HyperChem: a software package for computational chemistry and molecular modeling. Biotechniques 14:1010-1013.

Gottesman MM, Fojo T, Bates SE (2002) Multidrug resistance in cancer: role of ATP-dependent transporters. Nat Rev Cancer 2:48-58.

Guner O, Clement O, Kurogi Y (2004) Pharmacophore modeling and three dimensional database searching for drug design using catalyst: recent advances. Curr Med Chem 11:2991-3005.

Huynh-Delerme C, Huet H, Noel L, Frigieri A, Kolf-Clauw M (2005) Increased functional expression of P-glycoprotein in Caco-2 TC7 cells exposed long-term to cadmium. Toxicol In Vitro 19:439-447.

Jain S, Abraham I, Carvalho P, et al. (2009) Sipholane triterpenoids: chemistry, reversal of ABCB1/P-glycoprotein-mediated multidrug resistance, and pharmacophore modeling. J Nat Prod 72:1291-1298.

Juliano RL, Ling V (1976) A surface glycoprotein modulating drug permeability in Chinese hamster ovary cell mutants. Biochim Biophys Acta 455:152-162.

Kanaan M, Daali Y, Dayer P, Desmeules J (2009) Uptake/efflux transport of tramadol enantiomers and *O*-desmethyl-tramadol: focus on P-glycoprotein. Basic Clin Pharmacol Toxicol 105:199-206.

Klepsch F, Chiba P, Ecker GF (2011) Exhaustive sampling of docking poses reveals binding hypotheses for propafenone type inhibitors of P-glycoprotein. PLoS Comput Biol 7:e1002036.

Kothandan G, Gadhe CG, Madhavan T, Choi CH, Cho SJ (2011) Docking and 3D-QSAR (quantitative structure activity relationship) studies of flavones, the potent inhibitors of p-glycoprotein targeting the nucleotide binding domain. Eur J Med Chem 46:4078-4088.

Li WX, Li L, Eksterowicz J, Ling XB, Cardozo M (2007) Significance analysis and multiple pharmacophore models for differentiating P-glycoprotein substrates. J Chem Inf Model 47:2429-2438.

Lill MA, Danielson ML (2010) Computer-aided drug design platform using PyMOL. J Comput Aided Mol Des 25:13-19.

Loo TW, Bartlett MC, Clarke DM (2009) Identification of residues in the drug translocation pathway of the human multidrug resistance P-glycoprotein by arginine mutagenesis. J Biol Chem 284:24074-24087.

Loo TW, Clarke DM (1999) Identification of residues in the drug-binding domain of human P-glycoprotein. Analysis of transmembrane segment 11 by cysteine-scanning mutagenesis and inhibition by dibromobimane. J Biol Chem 274:35388-35392.

Martin C, Berridge G, Higgins CF, Mistry P, Charlton P, Callaghan R (2000) Communication between multiple drug binding sites on P-glycoprotein. Mol Pharmacol 58:624-632.

Meng XY, Zhang HX, Mezei M, Cui M (2011) Molecular docking: a powerful approach for structure-based drug discovery. Curr Comput Aided Drug Des 7:146-157.

Mohan V, Gibbs AC, Cummings MD, Jaeger EP, DesJarlais RL (2005) Docking: successes and challenges. Curr Pharm Des 11:323-333.

Paiva AM, Pinto MM, Sousa E (2013) A century of thioxanthones: through synthesis and biological applications. Curr Med Chem 20:2438-2457.

Pajeva IK, Wiese M (2002) Pharmacophore model of drugs involved in P-glycoprotein multidrug resistance: explanation of structural variety (hypothesis). J Med Chem 45:5671-5686.

Palmeira A, Rodrigues F, Sousa E, Pinto M, Vasconcelos MH, Fernandes MX (2011) New uses for old drugs: pharmacophore-based screening for the discovery of P-glycoprotein inhibitors. Chem Biol Drug Des 78:57-72.

Palmeira A, Sousa E, Vasconcelos MH, Pinto MM, Fernandes MX (2012a) Structure and ligand-based design of P-glycoprotein inhibitors: a historical perspective. Curr Pharm Design 18:4197-4214.

Palmeira A, Vasconcelos MH, Paiva A, Fernandes MX, Pinto M, Sousa E (2012b) Dual inhibitors of P-glycoprotein and tumor cell growth: (re)discovering thioxanthones. Biochem Pharmacol 83:57-68.

Patel Y, Gillet VJ, Bravi G, Leach AR (2002) A comparison of the pharmacophore identification programs: Catalyst, DISCO and GASP. J Comput Aided Mol Des 16:653-681.

Roberts DM (2011) Herbicides. In: Nelson LS, Lewin NA, Howland MA, Hoffman RS, Goldfrank LR, Flomenbaum NE (eds) Goldfrank's Toxicologic Emergencies, Ninth Edition McGraw-Hill Companies, Inc., p 1494-1515.

Safa AR (1993) Photoaffinity labeling of P-glycoprotein in multidrug-resistant cells. Cancer Invest 11:46-56.

Safa AR (1998) Photoaffinity labels for characterizing drug interaction sites of P-glycoprotein. Methods Enzymol 292:289-307.

Safa AR (2004) Identification and characterization of the binding sites of P-glycoprotein for multidrug resistance-related drugs and modulators. Curr Med Chem Anticancer Agents 4:1-17.

Seeliger D, de Groot BL (2010) Ligand docking and binding site analysis with PyMOL and Autodock/Vina. J Comput Aided Mol Des 24:417-422.

Shapiro AB, Fox K, Lam P, Ling V (1999) Stimulation of P-glycoprotein-mediated drug transport by prazosin and progesterone. Evidence for a third drug-binding site. Eur J Biochem 259:841-850.

Shapiro AB, Ling V (1997) Positively cooperative sites for drug transport by P-glycoprotein with distinct drug specificities. Eur J Biochem 250:130-137.

Shapiro AB, Ling V (1998) The mechanism of ATP-dependent multidrug transport by P-glycoprotein. Acta Physiol Scand Suppl 643:227-234.

Silva R, Carmo H, Dinis-Oliveira R, et al. (2011) In vitro study of P-glycoprotein induction as an antidotal pathway to prevent cytotoxicity in Caco-2 cells. Arch Toxicol 85:315-326.

Silva R, Carmo H, Vilas-Boas V, et al. (2013a) Colchicine effect on P-glycoprotein expression and activity: in silico and in vitro studies. Submitted for publication.

Silva R, Carmo H, Vilas-Boas V, et al. (2013b) Doxorubicin decreases paraquat accumulation and toxicity in Caco-2 cells. Toxicol Lett 217:34-41.

Silverman JA (1999) Multidrug-resistance transporters. Pharm Biotechnol 12:353-386.

Sousa E, Palmeira A, Cordeiro A, et al. (2013) Bioactive xanthones with effect on P-glycoprotein and prediction of intestinal absorption. Med Chem Res 22:2115-2123.

Sterz K, Mollmann L, Jacobs A, Baumert D, Wiese M (2009) Activators of P-glycoprotein: Structure-activity relationships and investigation of their mode of action. Chem Med Chem 4:1897-1911.

Storm J, O'Mara ML, Crowley EH, et al. (2007) Residue G346 in transmembrane segment six is involved in inter-domain communication in P-glycoprotein. Biochemistry 46:9899-9910.

Taipalensuu J, Tornblom H, Lindberg G, et al. (2001) Correlation of gene expression of ten drug efflux proteins of the ATP-binding cassette transporter family in normal human jejunum and in human intestinal epithelial Caco-2 cell monolayers. J Pharmacol Exp Ther 299:164-170.

Takara K, Hayashi R, Kokufu M, et al. (2009) Effects of nonsteroidal anti-inflammatory drugs on the expression and function of P-glycoprotein/MDR1 in Caco-2 cells. Drug Chem Toxicol 32:332-337.

Thiebaut F, Tsuruo T, Hamada H, Gottesman MM, Pastan I, Willingham MC (1987) Cellular localization of the multidrug-resistance gene product P-glycoprotein in normal human tissues. Proc Natl Acad Sci U S A 84:7735-7738.

Trott O, Olson AJ (2009) AutoDock Vina: improving the speed and accuracy of docking with a new scoring function, efficient optimization, and multithreading. J Comput Chem 31:455-461.

Vilas-Boas V, Silva R, Gaio AR, et al. (2011) P-glycoprotein activity in human Caucasian male lymphocytes does not follow its increased expression during aging. Cytometry A 79:912-919.

Watanabe T, Onuki R, Yamashita S, Taira K, Sugiyama Y (2005) Construction of a functional transporter analysis system using MDR1 knockdown Caco-2 cells. Pharm Res 22:1287-1293.

Yamashita S, Furubayashi T, Kataoka M, Sakane T, Sezaki H, Tokuda H (2000) Optimized conditions for prediction of intestinal drug permeability using Caco-2 cells. Eur J Pharm Sci 10:195-204.

Zhang L, Zhou W, Li D-H (2006) A descent modified Polak-Ribière-Polyak conjugate gradient method and its global convergence. IMA J Numer Anal 26:629-640.

Zhou SF (2008) Structure, function and regulation of P-glycoprotein and its clinical relevance in drug disposition. Xenobiotica 38:802-832.

III.8. MANUSCRIPT VII

Induction and activation of P-glycoprotein by dihydroxylated xanthones protect against the cytotoxicity of the P-glycoprotein substrate paraquat

Submitted for publication

TITLE

Induction and activation of P-glycoprotein by dihydroxylated xanthones protect against the cytotoxicity of the P-glycoprotein substrate paraquat

AUTHORS

Renata Silva[a*], Emília Sousa[b], Helena Carmo[a], Andreia Palmeira[b], Daniel José Barbosa[a], Mariline Gameiro[a], Madalena Pinto[b], Maria de Lourdes Bastos[a] and Fernando Remião[a*]

AFFILIATIONS

[a]REQUI*M*TE, Laboratório de Toxicologia, Departamento de Ciências Biológicas, Faculdade de Farmácia, Universidade do Porto, Rua de Jorge Viterbo Ferreira, 228, 4050-313 Porto, Portugal.

[b]Centro de Química Medicinal (CEQUIMED-UP), Laboratório de Química Orgânica e Farmacêutica, Departamento de Ciências Químicas, Faculdade de Farmácia, Universidade do Porto, Rua Jorge Viterbo Ferreira 228, 4050-313, Porto, Portugal

*CORRESPONDING AUTHORS

Renata Silva (e-mail: rsilva@ff.up.pt) and Fernando Remião (e-mail: remiao@ff.up.pt)

REQUI*M*TE - Laboratório de Toxicologia, Departamento de Ciências Biológicas, Faculdade de Farmácia, Universidade do Porto, Rua de Jorge Viterbo Ferreira, 228, 4050-313 Porto, Portugal.

Tel: 00351220428596

Fax: 00351226093390

RUNNING TITLE

New dihydroxylated xanthones induced P-glycoprotein

ABSTRACT

Xanthones are a family of compounds with several known biological activities and therapeutic potential for which information on their interaction with membrane transporters is lacking. Knowing that P-glycoprotein (P-gp) acts as a cellular defence mechanism by effluxing its toxic substrates, the aim of this study was to investigate the potential of five dihydroxylated xanthones as inducers of P-gp expression and/or activity, and to evaluate whether they could protect Caco-2 cells against the cytotoxicity induced by the toxic P-gp substrate paraquat.

After 24 h of incubation, all tested xanthones caused a significant increase in both P-gp expression and activity, as evaluated by flow cytometry using the UIC2 antibody and rhodamine 123, respectively. Additionally, after a short 45 min incubation all the tested xanthones induced a rapid increase in P-gp activity indicating direct pump activation without increased P-gp protein expression. The tested compounds also increased P-gp ATPase activity in MDR1-Sf9 membrane vesicles, demonstrating to be P-gp substrates. Moreover, when simultaneously incubated with paraquat, all xanthones significantly reduced the cytotoxicity of the herbicide, and these protective effects were completely reversed upon incubation with a specific P-gp inhibitor.

In silico studies evaluating the interactions between xanthones and P-gp in the presence of paraquat suggested that a co-transport mechanism may be operating. A QSAR model was developed and validated, and the maximal partial charge for an oxygen atom was the descriptor predicted as being implicated in P-gp activation by the dihydroxylated xanthones. These results disclose new perspectives in preventing paraquat and other P-gp substrates-induced poisonings.

KEYWORDS

P-glycoprotein; Induction; Activation; Xanthones; Paraquat; Caco-2 cells.

ABBREVIATIONS

DMEM - Dulbecco's modified Eagle's medium
EC_{50} - half-maximum-effect concentration
EDTA - Ethylenediamine tetraacetic acid
FBS - Fetal bovine serum
FITC - Fluorescein isothiocyanate
GeoMean - Geometric mean of fluorescence intensity
HBSS - Hanks balanced salt solution
IA - Inhibited rhodamine 123 accumulation
IAE - Inhibited rhodamine 123 accumulation followed by efflux in the absence of P-gp inhibitor
IAIE - Inhibited rhodamine 123 accumulation followed by efflux in the presence of P-gp inhibitor
MFI - Mean fluorescence intensity
MTT - (4,5-Dimethylthiazol-2-yl)-2,5-diphenyl tetrazolium bromide
MRP1- Multidrug resistance protein 1
NR - Neutral red
NEAA - Nonessential amino acids
PBS - Phosphate buffered saline solution
P-gp - P-glycoprotein
RHO 123 - Rhodamine 123
Xs - Xanthones

1. INTRODUCTION

P-glycoprotein (P-gp) is a 170 kDa ATP-dependent efflux pump, which promotes the outward transport of a wide spectrum of structurally unrelated compounds (Hennessy and Spiers 2007; Kim 2002; Seelig 1998; Sharom 2011; Ueda et al. 1997; Varma et al. 2003; Zhou 2008). In fact, this broad substrate specificity allied to its cellular polarized expression in many excretory and barrier tissues, and to its efflux capacity attribute to P-gp a crucial defense role against its toxic substrates (Dinis-Oliveira et al. 2006a; Huynh-Delerme et al. 2005; Silva et al. 2011; Silva et al. 2013c; Silva et al. 2013d; Vilas-Boas et al. 2013c; Watanabe et al. 2005). Therefore, strategies to increase P-gp expression and/or activity may be viewed as potential antidotal pathways to prevent the toxicity mediated by P-gp toxic substrates by decreasing their intracellular accumulation.

P-gp is inducible by many drugs, including dexamethasone, rifampicin, the herbal antidepressant St John's wort (hyperforin and hypericin) and several antineoplasic drugs (doxorubicin, daunorubicin and vinblastine) that increase the expression of the transporter (Chaudhary and Roninson 1993; Chin et al. 1990; Fardel et al. 1997; Harmsen et al. 2009; Hu et al. 1999; Kageyama et al. 2006; Kim et al. 2008; Nielsen et al. 1998; Tian et al. 2005; Zhou 2008). Also, P-gp activity can be directly increased by compounds that bind to P-gp and promote a conformational alteration that stimulates the transport of a substrate bound on another binding site (Sterz et al. 2009; Vilas-Boas et al. 2013c), suggesting that the efflux pump contains at least two positively cooperative sites for drug binding and transport (Shapiro and Ling 1997). For example, Hoechst-33342 and rhodamine 123 (RHO 123) have been shown to act by this cooperative mode of action (Shapiro and Ling 1997). This activation mechanism increases P-gp transport function without interfering with the protein expression levels, which makes it a more rapid process than P-gp induction.

Xanthones, dibenzo-γ-pyrones, are a family of compounds appealing to medicinal chemists due to their pronounced biological activity within a notably broad spectrum of disease states, resulting from their interaction with a correspondingly diverse range of target biomolecules (Masters and Bräse 2012). This has led to the description of xanthones as "privileged structures" (Pinto et al. 2005). Although several studies have addressed the biological activities of xanthone derivatives, information regarding their interaction with drug transporters is sparse. Some prenylated xanthones have shown affinity to bind to P-gp recombinant domain (Tchamo et al. 2000) and more recently, simple oxygenated xanthones were identified as selective killers of cancer cells overexpressing the MRP1 ABC transporter (Genoux-Bastide et al. 2011). Also, in P-gp overexpressing leukemia cells (K562Dox) a prenylated and a lignoid xanthone derivatives

inhibited P-gp activity, whereas two simple oxygenated xanthones increased the transporter activity (Sousa et al. 2013).

To better understand the impact of simple oxygenated xanthones on P-gp modulation and to establish a structure-activity relationship, in the present study, we aimed to evaluate the effect of a series of dihydroxylated xanthones (**1-5**, Figure 1) on the pump's expression and activity, and their potential to protect Caco-2 cells against the cytotoxicity of the herbicide paraquat (PQ), a known and highly toxic P-gp substrate (Dinis-Oliveira et al. 2006b; Silva et al. 2011; Silva et al. 2013c; Vilas-Boas et al. 2013c). Additionally, a simple QSAR model was established and the binding modes of the tested xanthones to the P-gp transporter were predicted by docking studies.

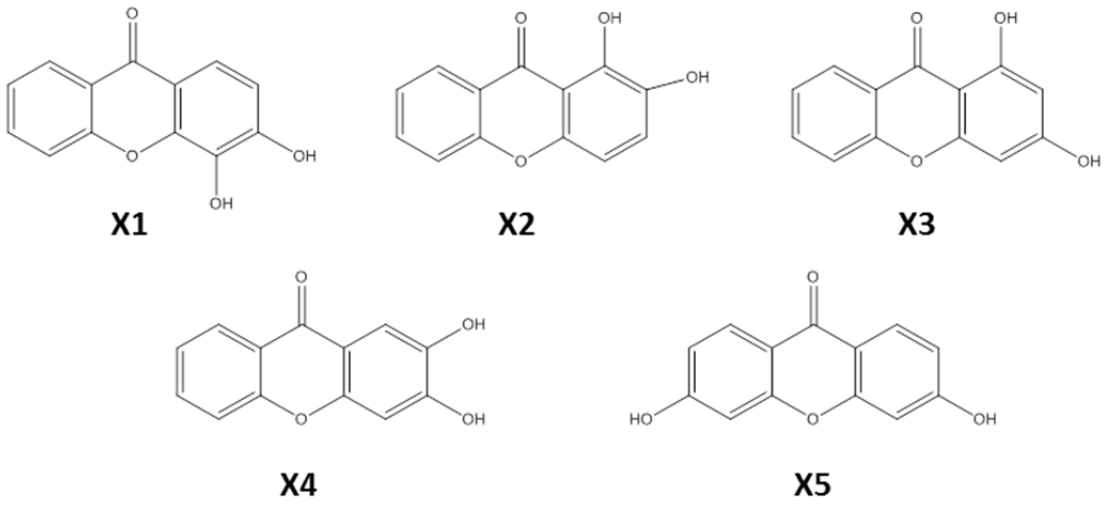

Figure 1. Xanthones **1-5** investigated in this study**.**

2. MATERIALS AND METHODS

2.1. Materials

Rhodamine 123 (RHO 123), cyclosporine A, (4,5-dimethylthiazol-2-yl)-2,5-diphenyl tetrazolium (MTT) bromide and neutral red (NR) solution were obtained from Sigma (St. Louis, MO, USA). Reagents used in cell culture, including Dulbecco's modified Eagle's medium (DMEM) with 4.5 g/L glucose and GlutaMAX™, nonessential amino acids (NEAA), heat inactivated fetal bovine serum (FBS), 0.25% trypsin/1 mM EDTA, antibiotic (10000 U/mL penicillin, 10000 µg/mL streptomycin), fungizone (250 µg/mL amphotericin B), human transferrin (4 mg/mL), phosphate-buffered saline solution (PBS) and Hank's balanced salt solution (HBSS) were purchased from Gibco Laboratories (Lenexa, KS). P-glycoprotein monoclonal antibody (clone UIC2), conjugated with fluorescein isothiocyanate (FITC), was purchased from Abcam (Cambridge, United Kingdom). IgG2a (negative mAb control to UIC2), conjugated with FITC, was obtained from ImmunoTools GmbH (Friesoythe, Germany). Flow cytometry reagents (BD FacsFlow™ and Facs Clean™) were purchased from Becton, Dickinson and Company (San Jose, CA, USA). MDR1 Predeasy ATPase assay kit was purchased from Solvo Biotechnology (Szeged, Hungary). GF120918 [9,10-dihydro - 5 - methoxy - 9 – oxo - N - [4 - [2 - (1,2,3,4 - tetrahydro - 6,7 - dimethoxy - 2-isoquinolinyl)ethyl]phenyl] - 4 - acridinecarboxamide] was a generous gift from GlaxoSmithKline (Hertfordshire, United Kingdom). All the reagents used were of analytical grade or of the highest grade available.

2.2. Synthesis of xanthones

Dihydroxylated xanthones **1-5** were synthesized by classical methods via benzophenone or a biphenyl ether intermediates and Grover, Shah, and Shah reaction and their syntheses are described elsewhere (Castanheiro et al. 2007; Costa et al. 2010; Pedro et al. 2002). 3,4-Dihydroxy-9*H*-xanthen-9-one (**X1**) and 3,6-dihydroxy-9*H*-xanthen-9-one (**X5**) were obtained by the cyclization of 2,2'-dioxygenated benzophenones through a nucleophilic substitution for **X1** (in 70% yield) (Pedro et al. 2002) or a dehydrative process for **X5** (in 90% yield) (Costa et al. 2010). 1,2-Dihydroxy-9*H*-xanthen-9-one (**X2**) and 2,3-dihydroxy-9*H*-xanthen-9-one (**X4**) were obtained via diaryl ether 2-(3',4'-dimethoxy)-phenoxybenzoic acid with the ring formation in lithium diisopropylamide for **X2** (in 50% yield) or acetyl chloride for **X4** (in 85% yield). 1,3-Dihydroxy-9*H*-xanthen-9-one (**X3**) was synthesized by condensation between an condensation of salicylic acid and phloroglucinol, in phosphorous oxychloride and zinc chloride (in 40% yield) (Castanheiro et al. 2007). Xanthones **1-5** were characterized by spectroscopic methods and HRMS according to described procedures (Castanheiro et al. 2007; Costa et al. 2010; Pedro et

al. 2002). The purity of each compound was determined by HPLC-DAD and all tested xanthones possessed a purity of at least 95%. Briefly, the HPLC analysis was performed in a Finnigan Surveyor -Autosampler Plus and LC Pump Plus (Thermo Electron Corporation, Waltham, MA, USA), equipped with a diode array detector TSP UV6000LP, and using a C-18 column (5 μm, 250 mm × 4.6 mm I.D.), from Macherey-Nagel (Deuren, Germany). Xcalibur2.0 SUR 1 software (Thermo Electron Corporation, Waltham, MA, USA) managed chromatographic data. Methanol was of HPLC grade from Merck. HPLC ultrapure water was generated by a Milli-Q system (Millipore, Bedford, MA, USA). The mobile phases were degassed for 15 min in an ultrasonic bath before use. It was used an isocratic elution of MeOH:H_2O acidified with CH_3COOH (1%), at a constant flow rate of 1.0 $mL.min^{-1}$ (several proportions).

2.3. Caco-2 cell culture

Caco-2 cells were routinely cultured in 75 cm^2 flasks using DMEM medium supplemented with 10% heat inactivated FBS, 1% NEAA, 1% antibiotic, 1% fungizone and 6 μg/mL transferrin. Cells were maintained in a 5% CO_2-95% air atmosphere, at 37 ºC, and the medium was changed every 2 days. Cultures were passaged weekly by trypsinization (0.25% trypsin/1 mM EDTA). The cells used for all the experiments were taken between the 59^{th} and 65^{th} passages. In all experiments, the cells were seeded at a density of 60,000 cells/cm^2, and used 4 days after seeding, when confluence was reached.

2.4. Compounds cytotoxicity assays

Xanthones **1-5** (0 – 50.0 μM) cytotoxicity was evaluated 24 h after exposure by the MTT reduction and NR uptake assays.

2.4.1. MTT reduction assay

Xanthones **1-5** cytotoxicity was evaluated by the MTT assay as previously described (Silva et al. 2013a). Briefly, the cells were seeded onto 96-well plates and exposed, after reaching confluence, to the tested compounds **X1-5** (0 - 50.0 μM) in fresh cell culture medium. Twenty-four hours after exposure, the cell culture medium was removed, followed by the addition of fresh cell culture medium containing 0.5 mg/mL MTT and incubation at 37 °C in a humidified, 5% CO_2-95% air atmosphere for 1 h. After this incubation period, the cell culture medium was removed and the formed formazan crystals dissolved in 100% DMSO. The absorbance was measured at 550 nm in a multi-well plate reader (PowerWave X, Bio-Tek Instruments, Vermont, US). The percentage of MTT

reduction relative to that of the control cells was used as the cytotoxicity measure. Results are presented as mean ± SEM from 5 independent experiments (run in triplicate).

2.4.2. Neutral red uptake assay

The neutral red (NR) uptake assay is based on the ability of viable cells to incorporate and bind the supravital dye neutral red in the lysosomes, thus providing a quantitative estimation of the number of viable cells in a culture. The assay was performed as previously described (Vilas-Boas et al. 2013b). The cells were seeded onto 96-well plates at a density of 60,000 cells/cm^2, and exposed, after reaching confluence, to the tested **X1-5** (0 - 50.0 μM) in fresh cell culture medium for 24 h. The cells were then incubated with NR (50 μg/ml in cell culture medium) at 37 °C in a humidified, 5% CO_2-95% air atmosphere for 90 min. After this incubation period, the cell culture medium was removed, the dye absorbed only by viable cells extracted [ethyl alcohol absolute/distilled water (1:1) with 5% acetic acid] and the absorbance measured at 540 nm in a multi-well plate reader (PowerWave X, Bio-Tek Instruments, Vermont, US). The percentage of NR uptake relative to that of the control cells was used as the cytotoxicity measure. Results are presented as mean ± SEM from 5 independent experiments (run in triplicate).

2.5. Evaluation of P-glycoprotein expression

The effect of the tested **X1-5** on P-gp expression was evaluated by flow cytometry as previously described (Palmeira et al. 2011; Silva et al. 2011; Silva et al. 2013b; Vilas-Boas et al. 2011; Vilas-Boas et al. 2013a; Vilas-Boas et al. 2013b). The cells were seeded onto 48-well plates, at a density of 60,000 cells/cm^2 and exposed, 4 days after seeding, to a non-cytotoxic (20.0 μM) concentration of the tested **X1-5** in fresh cell culture medium. Twenty-four hours after exposure, the cells were washed twice with PBS and harvested by trypsinization (0.25% trypsin /1mM EDTA) to obtain a cell suspension. The cells were then centrifuged (300 *g* for 10 min) and suspended in PBS buffer (pH 7.4) containing 10% FBS and P-gp antibody [UIC2] conjugated with FITC. The antibody dilution used in this experiment was applied according to the manufacturer's instructions for flow cytometry. Mouse IgG2a_FITC was used as an isotype-matched negative control to estimate non-specific binding of the FITC-labelled anti-P-glycoprotein antibody [UIC2]. The cells were then incubated for 30 min, at 37 °C, in the dark. After this incubation period, the cells were washed twice with PBS buffer (pH 7.4) containing 10% heat inactivated FBS, centrifuged (300 *g* for 10 min), suspended in ice-cold PBS, and kept on ice until analysis. Fluorescence measurements of isolated cells were performed with a flow cytometer (FACSCalibur, Becton-Dickinson Biosciences). The green fluorescence of FITC-UIC2

antibody was measured by a 530 ± 15 nm band-pass filter (FL1). Acquisition of data for 15,000 cells was gated to include viable cells on the basis of their forward and side light scatters and the propidium iodide (4 µg/mL) incorporation (propidium iodide interlaces with a nucleic acid helix with a resultant increase in fluorescence intensity emission at 615 nm). Logarithmic fluorescence was recorded and displayed as a single parameter histogram. The geometric mean of fluorescence intensity (GeoMean) for 15,000 cells was the parameter used for comparison (calculated as percentage of control). Non labelled cells (with or without the tested xanthones) were also analysed in each experiment by a 530 ± 15 nm band-pass filter (FL1) in order to detect a possible contribution from cells autofluorescence to the analysed fluorescence signals. Results are presented as mean ± SEM from 3 independent experiments (run in triplicate).

2.6. Evaluation of P-glycoprotein transport activity

P-gp transport activity was evaluated by flow cytometry, with 1.0 µM RHO 123 as a P-gp fluorescent substrate using two different protocols. In the first protocol, RHO 123 efflux was measured in cells pre-exposed to **X1-5** for 24 h. In this protocol the xanthones are removed from the incubation medium prior to the cell trypsinization. Therefore the measured RHO 123 fluorescence reflects the P-gp activity due to increased expression. In the second protocol, the xanthones are only added immediately prior to the 45 min-RHO 123 efflux phase. In this case, the measured RHO 123 fluorescence reflects a direct activation of the P-gp pump, without the contribution of protein expression increases.

2.6.1. RHO 123 efflux assay in Caco-2 cells pre-exposed to xanthones for 24 h

Caco-2 cells were seeded onto 24-well plates, at a density of 60,000 cells/cm^2, to obtain confluent monolayers at the day of the experiment. After reaching confluence, the cells were exposed to the tested **X1-5** (20.0 µM) in fresh cell culture medium for 24 h. After the incubation period, the cells were washed twice with PBS and harvested by trypsinization (0.25% trypsin /1mM EDTA) to obtain a cell suspension. The cells were then centrifuged (300 g for 10 min), suspended in PBS buffer (pH 7.4) containing 1.0 µM RHO 123 and a known P-gp inhibitor (10.0 µM cyclosporine A), and incubated at 37ºC for 30 min in order to allow maximum RHO 123 accumulation [inhibited accumulation (IA) phase]. After this incubation period, the cells were washed twice with ice-cold PBS with 10% FBS, centrifuged (300 *g* for 10 min) at 4°C, and divided into two aliquots. The first aliquot was submitted to an efflux phase performed under inhibited conditions (inhibited rhodamine accumulation followed by inhibited rhodamine efflux in the presence of P-gp inhibitor – IAIE) and the second aliquot was submitted to

an efflux phase performed under normal conditions (inhibited rhodamine accumulation followed by non-inhibited rhodamine efflux in the absence of P-gp inhibitor – IAE). For the efflux phase the cells were suspended in DMEM medium containing 4.5 g/L glucose, with or without 10.0 μM cyclosporine A, and incubated for 45 min at 37°C. After this efflux period, the cells were washed twice with ice-cold PBS with 10% FBS and suspended in ice-cold PBS immediately before analysis. The fluorescence measurements of isolated cells were performed as described in section 2.4. The green intracellular fluorescence of RHO 123 was measured by a 530 ± 15 nm band-pass filter (FL1). The ratio between the mean fluorescence intensity (MFI) after inhibited RHO 123 efflux (IAIE) and the MFI of non-inhibited RHO 123 efflux (IAE) was the parameter used for comparison and the results expressed as percentage of control. Results are presented as mean ± SEM from 4 independent experiments (run in triplicate).

2.6.2. RHO 123 efflux assay in the presence of xanthones

Ca**c**o-2 cells were seeded onto 75 cm^2 flasks and, after reaching confluence, washed twice with PBS and harvested by trypsinization (0.25% trypsin /1mM EDTA) to obtain a cellular suspension. This cell suspension was then divided into aliquots of 500,000 cells/mL. The cells were then centrifuged (300 *g* for 10 min) and submitted to an IA phase as described in section 2.5.1. After the RHO 123 accumulation, the cells were submitted to an efflux phase where the energy-dependent P-gp function was re-established by removing the P-gp inhibitor (cyclosporine A) and adding an energy source (DMEM supplemented with 4.5 g/mol glucose). Therefore, after the IA phase, the cells were washed twice with ice-cold PBS with 10% FBS, centrifuged (300 *g* for 10 min) at 4°C, and suspended in DMEM medium containing 4.5 g/L glucose, with or without the **X1-5** (20.0 μM), and incubated for 45 min at 37 °C. After this efflux period, the cells were washed twice with ice-cold PBS with 10% FBS and suspended in ice-cold PBS immediately before analysis. The fluorescence measurements of isolated cells were performed as described in section 2.4. The green intracellular fluorescence of RHO 123 was measured by a 530 ± 15 nm band-pass filter (FL1). When P-gp activity increases, the amount of RHO 123 effluxed from the cells is higher and accompanied by a decrease in the fluorescence intensity due to the corresponding decrease in intracellular RHO 123. As P-gp activity is inversely proportional to the intracellular fluorescence intensity, the inverse of mean fluorescence intensity (1/MFI) was the parameter used for comparison and the results expressed as percentage of control. Results are presented as mean ± SEM from 5 independent experiments (run in triplicate).

2.7. Evaluation of P-glycoprotein ATPase activity

P-gp ATPase activity was evaluated using the MDR1 Predeasy ATPase assay kit according to the manufacturer's instructions. Briefly, MDR1-Sf9 membrane vesicles (4 µg/well) were incubated in 50 µL ATPase assay buffer with 2 mM ATP and **X1-5** (20.0 µM) for 10 min at 37 °C, with or without simultaneous incubation with 1.2 mM sodium orthovanadate (Na_3VO_4).

The reaction was stopped by adding 100 µL of developer solution to each well, followed by 100 µL of blocker solution and an additional 30 min incubation at 37 ºC. The absorbance was measured at 590 nm, in a multi-well plate reader (BioTek Instruments, Vermont, USA), reflecting the amount of inorganic phosphate (Pi) liberated by the transporter, which is proportional to its activity. The MDR1-Sf9 membrane vesicles used, apart from P-gp, contain other ATPases. As P-gp is effectively inhibited by Na_3VO_4, P-gp ATPase activity was measured as the vanadate sensitive portion of the total ATPase activity. Thus, ATPase activities were determined as the difference of Pi liberation measured with and without 1.2 mM sodium orthovanadate (vanadate-sensitive ATPase activity) and expressed as nmol Pi liberated/mg protein/min. Results are presented as mean ± SEM from 3 independent experiments (run in duplicate). Control incubations were also performed in the absence of xanthones and the corresponding vanadate-sensitive ATPase activity referred to as basal vanadate-sensitive ATPase activity.

2.8. Paraquat cytotoxicity assays

Paraquat cytotoxicity was evaluated in Caco-2 cells by the NR uptake assay, with and without simultaneous incubation with the tested xanthones. Briefly, the cells were seeded onto 96 well plates to obtain confluent monolayers at the day of the experiment. After reaching confluence, the cells were exposed to PQ (0–7500 µM) for 24 h in the presence or absence of **X1-5** (20.0 µM) and cytotoxicity was evaluated as previously described in section 2.4.2. Results are presented as mean ± SEM from 6 independent experiments (run in triplicate).

To confirm P-gp involvement in the **X1-5** protective effects, these incubations were repeated in the presence of a well-known and potent P-gp inhibitor, GF120918 (10.0 µM) (Dorner et al. 2009; Kanaan et al. 2009; Silva et al. 2013d; Vilas-Boas et al. 2013c). Results are presented as mean ± SEM from 4 independent experiments (run in triplicate).

2.9. Statistical analysis

All statistical calculations were performed with the GraphPad Prism version 6.00 for Windows (GraphPad Software, San Diego California, USA). Normality of the data

distribution was assessed by three different tests, KS normality test, D'Agostino & Pearson omnibus normality test and Shapiro-Wilk normality test. For data with a parametric distribution, statistical comparisons were made using the parametric method of One-way ANOVA on ranks followed by the Bonferroni's multiple comparisons *post hoc* test. For data with a nonparametric distribution, statistical comparisons were estimated using the nonparametric method of Kruskal-Wallis [one-way analysis of variance (ANOVA) on ranks] followed by Dunn's *post hoc* test. In experiments with two variables, statistical comparisons between groups were made using Two-way ANOVA, followed by the Sidak's multiple comparisons *post hoc* test.

In the PQ cytotoxicity assays, concentration-response curves were fitted using least squares as the fitting method and the comparisons between curves (EC_{50}, TOP, BOTTOM and Hill slope) were made using the extra sum-of-squares F test.

Details of the performed statistical analysis are described in each figure legend. In all cases, *p* values lower than 0.05 were considered significant.

2.10. Quantitative structure activity relationships (QSAR) model

CODESSA (version 2.7.10, Semichem, University of Florida) software was used to calculate the molecular descriptors for each compound (Coi et al. 2006; Katritzky et al. 2001). The CODESSA software calculates more than 500 constitutional, topological, geometrical, electrostatic, quantum-chemical and thermodynamical molecular descriptors and performs the statistical analyses linear regression such as the heuristic method (Lü et al. 2008). Following the calculation of the molecular descriptors, the heuristic method was used in CODESSA to correlate the EC_{50} values of xanthonic compounds **1-5** (Table 1) with those descriptors. This method can also provide a good estimation concerning the quality of correlation to be expected from the data, or to derive several best regression models. The squared correlation coefficient (R2), the Fisher criteria (F), and the standard error (s) were used as criteria for stability and robustness of the models (Kubinyi 2008). The final model was further tested with an external validation method using two thioxanthones previously described as P-gp activators (Palmeira et al. 2012; Silva et al. 2013d), and assayed using the same *in vitro* method (paraquat cytotoxicity assay), in the same conditions, as the compounds described in the present paper (Supplementary data, Figure S4).

2.11. Docking of xanthones on a P-gp model

The 3D structures of the small molecules were drawn using HyperChem 7.5 (Froimowitz 1993) being minimized by the semi-empirical Polak-Ribiere conjugate

gradient method (RMS<0.1 kcal.Å-1. mol-1) (Zhang et al. 2006). Docking simulations between the P-gp model built based on Sav1866 [previously described in (Palmeira et al. 2012)] and the five dihydroxylated xanthones **1-5**, PQ, and pairs of small molecules (PQ together with a xanthone) were undertaken in AutoDock Vina (Scripps Research Institute, USA) (Seeliger and de Groot 2010; Trott and Olson 2009). AutoDock Vina considered the target conformation as a rigid unit while the ligands were allowed to be flexible and adaptable to the target. Vina searched for the lowest binding affinity conformations and returned nine different conformations for each ligand. AutoDock Vina was run using an exhaustiveness of 8 and a grid box with the dimensions 37.0, 30.0, 40.0, engulfing the channel formed by the transmembrane domains. Conformations and interactions were visualized using PyMOL version 1.3 (Lill and Danielson 2010).

3. RESULTS

3.1. Xanthones cytotoxicity assays

Xanthones **1-5** cytotoxicity was evaluated by the MTT reduction and by the NR uptake assays to select non-cytotoxic working concentrations (Supplementary data, Figures S1 and S2, respectively). No significant cytotoxicity was observed within the tested concentration range (0 - 50.0 μM) after 24 h of incubation.

3.2. P-glycoprotein expression

The effect of the tested **X1-5** on P-gp expression was evaluated by flow cytometry, using a P-gp monoclonal antibody [UIC2] conjugated with FITC. Nonspecific binding of the FITC-labelled-anti-P-glycoprotein antibody [UIC2] was not observed as estimated by the fluorescence obtained with the isotype-matched negative control (data not shown). As shown in Figure 2, a significant increase in P-gp expression was observed for all the tested xanthones (20.0 μM). In fact, **X1-5** significantly increased the protein expression to 134.30, 144.25, 133.05, 141.90, and 142.74 %, respectively, when compared to control cells. However, no significant differences were found between the tested compounds.

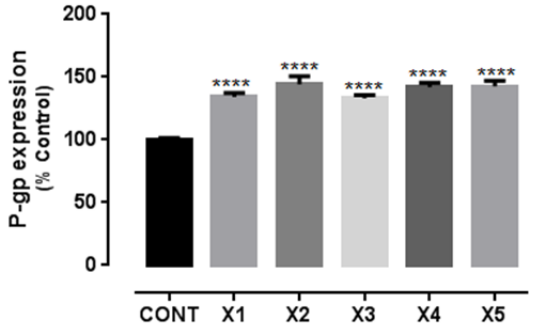

Figure 2. P-glycoprotein expression levels in Caco-2 cells exposed to **X1-5** (20 μM) for 24 h. Results are presented as mean ± SEM from 3 independent experiments performed in triplicate. Statistical comparisons were made using the parametric method of One-way ANOVA, followed by the Bonferroni's multiple comparisons *post hoc* test (****p<0.0001 *vs.* control).

3.3. P-glycoprotein transport activity

RHO 123 is widely used as a P-gp fluorescent substrate in the evaluation of P-gp function in many cell types. RHO 123 efflux was evaluated in cells pre-exposed to the tested **X1-5** (20.0 μM) for 24 h, to evaluate if P-gp activity reflected the observed increases in its expression, since P-gp activity is not always correlated with its protein content (Silva et al. 2013b; Takara et al. 2009; Vilas-Boas et al. 2011). As shown in Figure 3A, for all the tested xanthones, a significant increase in RHO 123 efflux was observed, demonstrating increased pump activity (123.71, 128.24, 114.88, 122.11 and 127.04 % for **X1-5**, respectively, when compared to control cells).

RHO 123 efflux was also evaluated using a different experimental design. As sown in Figure 3B, the presence of the tested **X1-5** during only the 45 min RHO 123 efflux phase resulted in a significant increase in the efflux of the dye, when compared to control cells. In fact, **X1-5** significantly increased RHO 123 efflux to 124.09, 112.25, 113.46, 114.06, and 124.02, respectively, indicating a slight, though significant, ability to directly activate the pump. Among the tested compounds, **X1** and **X5** were the most effective as P-gp activators.

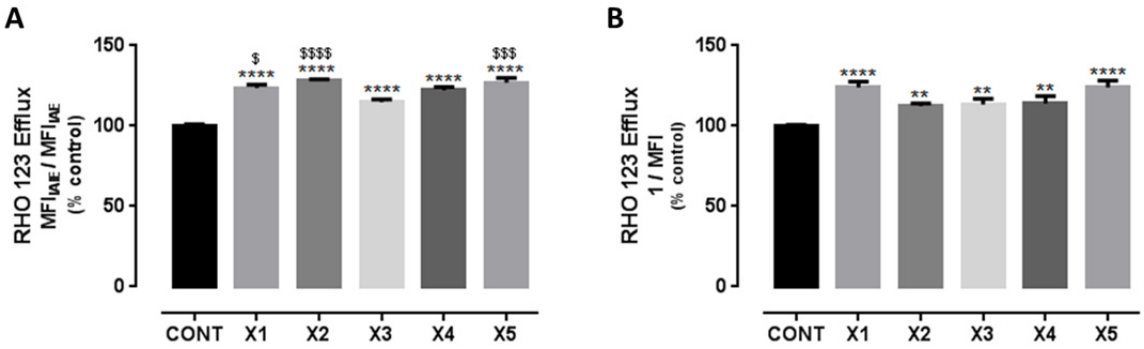

Figure 3. (A) P-glycoprotein activity evaluated through the RHO 123 efflux in Caco-2 cells pre-incubated with **X1-5** (20 μM) for 24 h. Results are presented as mean ± SEM from 4 independent experiments performed in triplicate. Statistical comparisons were made using the parametric method of One-way ANOVA, followed by the Bonferroni's multiple comparisons *post hoc* test (****p<0.0001 *vs.* control; ($^{\$}p$<0.05, $^{\$\$\$}p$<0.001; $^{\$\$\$\$}p$<0.0001*vs.* **X3**). **(B)** P-glycoprotein activity evaluated through the RHO 123 efflux in the presence of **X1-5** (20 μM) during the 45 min RHO 123 efflux phase. Results are presented as mean ± SEM from 5 independent experiments performed in triplicate. Statistical comparisons were estimated using the nonparametric method of Kruskal–Wallis (one-way ANOVA on ranks), followed by the Dunn's *post hoc* test (**p<0.01; ****p<0.0001 *vs.* control).

3.4. P-glycoprotein ATPase activity

As shown in Figure 4, all the tested xanthones (20.0 μM) significantly increased the amount of Pi released by the transporter, thus reflecting an increased P-gp activity. In comparison to the basal P-gp vanadate sensitive ATPase activity (11.37 nmol Pi liberated/mg protein/min) X**1-5** significantly increased P-gp vanadate sensitive ATPase activity to 15.81, 20.76, 19.39, 19.76, and 20.44 nmol Pi liberated/mg protein/min, respectively. The observed increases in vanadate sensitive ATPase activity suggested that the tested **X1-5** are P-gp substrates, being actively transported by the pump, thus resulting in an increased ATP consumption.

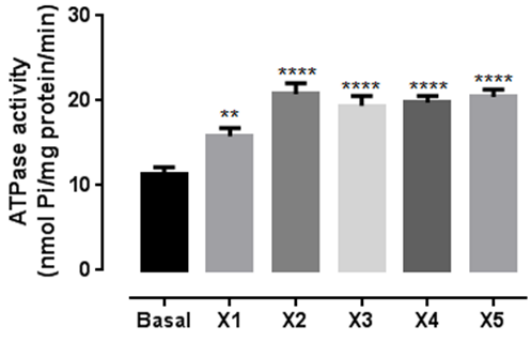

Figure 4. Vanadate sensitive ATPase activity (nmol Pi/mg protein/min) in MDR1-Sf9 membrane vesicles (4 µg/well) incubated with **X1-5** (20 µM). Results are presented as mean ± SEM from 3 independent experiments (performed in duplicate). Statistical comparisons were made using the parametric method of One-way ANOVA, followed by the Bonferroni's multiple comparisons *post hoc* test (*p<0.05; ****p<0.0001 vs. control).

3.5. Xanthones effect on PQ-induced cytotoxicity

Paraquat is a known P-gp substrate (Dinis-Oliveira et al. 2006b; Silva et al. 2011; Silva et al. 2013c; Vilas-Boas et al. 2013c). Therefore, the modulation of the pump may result in significant differences in the efflux and, consequently, in the cytotoxicity of the herbicide. To evaluate if the observed increases in both P-gp expression and activity could result in an effective protection against PQ-induced toxicity, the herbicide cytotoxicity (0 - 7,500 µM) was evaluated with and without simultaneous exposure to the tested **X1-5** (20.0 µM). The corresponding concentration–response curves obtained with only paraquat (PQ) and with simultaneous exposure with xanthones (PQ + Xs) are presented in Figure 5. In fact, a significant reduction in the cell death was observed for the 500 - 5000 µM PQ concentration range, resulting in significant rightwards shifts of all the PQ + Xs curves, when compared to the PQ curve. No significant differences were observed neither in the maximal cell death (TOP), nor in baseline (BOTTOM) of the fitted curves obtained for all the tested compounds (Table 1). Therefore, the EC_{50} values, which represent the half-maximum-effect concentrations from the fitted curves, were used for comparison. As shown in Table 1, a significant increase in the EC_{50} value of the fitted curves was observed for all the tested compounds, except for xanthone **X2**. In fact, for compounds **X1**, **X3**, **X4**, and **X5** the EC_{50} value significantly increased from 1260 µM for the PQ curve to 1620, 1509, 1520, and 1714 µM, respectively.

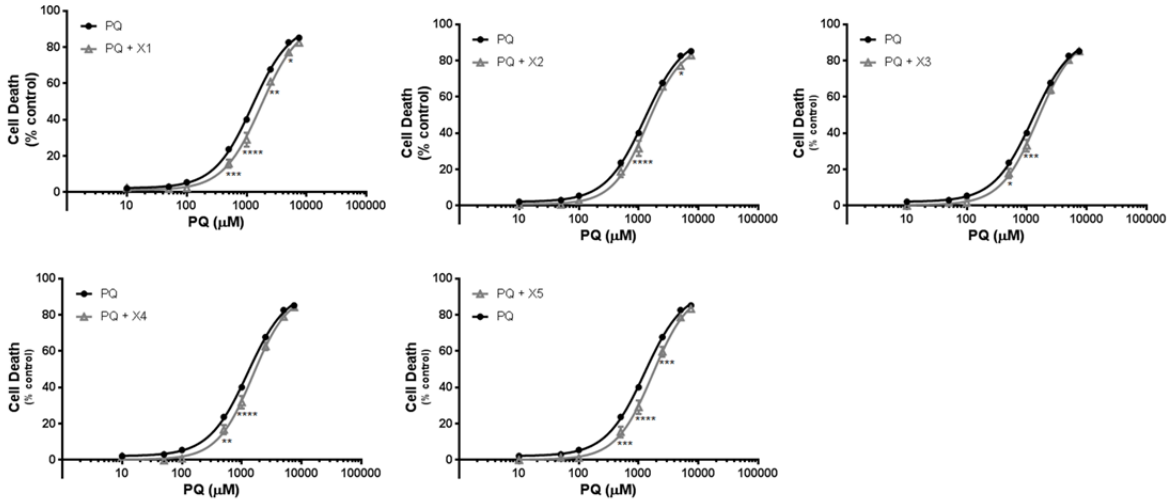

Figure 5. Paraquat concentration-response (cell death) curves in the absence (PQ) or in the presence of 20 μM of **X1-5** (PQ + Xs). Results are presented as mean ± SEM from 6 independent experiments (performed in triplicate). Concentration–response curves were fitted using least squares as the fitting method and the comparisons between PQ and PQ + Xs curves (LOG EC_{50}, TOP, BOTTOM and Hill slope) were made using the extra sum-of-squares F test. Statistical comparisons were made using Two-way ANOVA, followed by the Sidak's multiple comparisons *post hoc* test (**p*<0.05; ***p*<0.01; ****p*<0.001; *****p*<0.0001 *vs.* PQ alone).

Table 1. EC_{50} (half-maximum-effect concentration), TOP (maximal effect), BOTTOM (baseline) and Hill slope values of the paraquat concentration-response curves, with (PQ + Xs) or without (PQ) simultaneous exposure to **X1-5** (20 μM).

	PQ	PQ + X1	PQ + X2	PQ + X3	PQ + X4	PQ + X5
EC_{50} (half-maximum-effect concentration, μM)	**1260**	**1620**	**1392**	**1509**	**1520**	**1714**
TOP (maximal cell death, % control)	94.00	90.32	89.49	94.51	92.52	94.46
BOTTOM (baseline, % control)	2.137	1.819	0.7618	0.3466	0.2038	0.1541
Hill slope	1.330	1.534	1.491	1.412	1.460	1.416
LOG EC_{50} *p* value (comparison between LOG EC_{50} values)	-	**0.0022**	0.2474	**0.0385**	**0.0248**	**0.0007**
TOP *p* value (comparison between TOP values)	-	0.3831	0.2861	0.9059	0.7174	0.9247
BOTTOM *p* value (comparison between BOTTOM values)	-	0.7936	0.3003	0.1667	0.1086	0.1253
Hill slope *p* value (comparison between Hill slope values)	-	0.1856	0.3263	0.5840	0.3657	0.5772
Curve *p* value (Comparison between the Fitted Curves)	-	**< 0.0001**	**< 0.0001**	**< 0.0001**	**< 0.0001**	**< 0.0001**

Concentration-response curves were fitted using least squares as the fitting method and the comparisons between PQ and PQ + Xs curves were made using extra sum-of-squares F test. In all cases, *p* values <0.05 were considered significant.

To evaluate if the observed protective effects against PQ-induced toxicity were mediated by P-gp, the herbicide toxicity was further evaluated in the presence of a specific P-gp inhibitor, GF120918 (10 μM). The PQ cytotoxicity significantly increased in the presence of GF120918, resulting in a significant leftwards shift of the PQ + GF curve, when compared to the PQ curve (Supplementary data, Figure S3). Consequently, a significant decrease in the EC_{50} value of the PQ + GF curve was observed (906.0 μM *vs.* 1260 μM for the PQ curve), demonstrating the significant impact of P-gp inhibition on PQ toxicity (Supplementary data, Table S1). Moreover, under P-gp inhibition, a complete abolishment of **X1-5** protective effect against PQ-induced toxicity was observed (Figure 6). In fact, for **X1**, **X2**, **X4** and **X5** a leftwards shift of the PQ + GF + Xs curves was observed, when compared to the PQ + GF curve, resulting in significant differences in the overall comparison of the fitted curves (Table 2). Additionally, for compounds **X1** and **X2**, a significant increase in the cell death was observed with P-gp inhibition (PQ + GF + **X1**/**X2**) for the 500 - 1,000 μM PQ concentration range when compared to P-gp inhibition alone (PQ + GF) (Figure 6). However, no significant differences were obtained in the corresponding EC_{50} values (Table 2). For compound **X3**, no significant differences were observed neither in the overall comparison of the fitted curves, nor in the comparison of individual parameters (EC_{50}, TOP, BOTTOM and Hill slope).

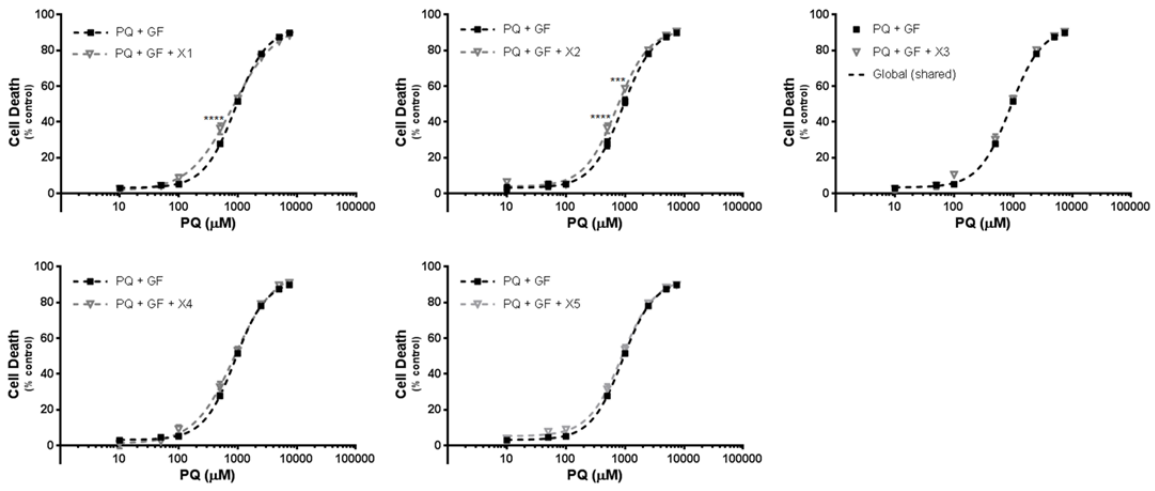

Figure 6. Paraquat concentration–response (cell death) curves in the presence of a potent P-gp inhibitor (10 μM GF120918), with (PQ + GF + Xs) and without (PQ + GF) exposure to **X1-5** (20 μM). Results are presented as mean ± SEM from 4 independent experiments (performed in triplicate). Concentration–response curves were fitted using least squares as the fitting method and the comparisons between PQ and PQ + Xs curves (LOG EC_{50}, TOP, BOTTOM and Hill slope) were made using the extra sum-of-squares F test. Statistical comparisons were made using Two-way ANOVA, followed by the Sidak's multiple comparisons *post hoc* test (***p<0.001; ****p<0.0001 *vs.* PQ + GF curve).

Table 2. EC_{50} (half-maximum-effect concentration), TOP (maximal effect), BOTTOM (baseline) and Hill slope values of the paraquat concentration-response curves, in the presence of a P-gp inhibitor (10 μM GF120918), with (PQ + GF + Xs) or without (PQ + GF) simultaneous exposure to **X1-5** (20 μM).

	PQ + GF	PQ + GF + X1	PQ + GF + X2	PQ + GF + X3	PQ + GF + X4	PQ + GF + X5
EC_{50} (half-maximum-effect concentration, μM)	**906.0**	**805.9**	**726.9**	**890.3**	**876.7**	**877.5**
TOP (maximal cell death, % control)	92.58	94.63	91.97	94.32	98.08	93.65
BOTTOM (baseline, % control)	3.118	1.530	3.884	4.067	1.113	5.198
Hill Slope	1.629	1.188	1.578	1.516	1.281	1.578
LOG EC_{50} *p* value (comparison between LOG EC_{50} values)	-	0.1506	**0.0002**	0.7741	0.6533	0.6036
TOP *p* value (comparison between TOP values)	-	0.4846	0.7676	0.4780	0.0551	0,6554
BOTTOM *p* value (comparison between BOTTOM values)	-	0.2899	0.5356	0.4798	0.1767	0.1078
Hill Slope *p* value (comparison between Hill slope values)	-	**0.0024**	0.7378	0.5058	**0.0264**	0.5559
Curve *p* value (Comparison between the Fitted Curves)	-	**< 0.0001**	**< 0.0001**	0.2493	**0.0232**	**0.0243**

Concentration-response curves were fitted using least squares as the fitting method and the comparisons between PQ + GF and PQ + GF + Xs curves were made using extra sum-of-squares F test. In all cases, *p* values <0.05 were considered significant.

3.6. *In silico* studies

In this work, one 2D QSAR model was elaborated at the beginning with Comprehensive Descriptors for Structural and Statistical Analysis (CODESSA) software package [CODESSA software version 2.7.2, University of Florida, USA]. A large number of molecular descriptors divided into five categories (constitutional, topological, geometrical, electrostatic, and quantum-chemical) were generated. Only some of them were significantly correlated with the effect of activating the P-gp transporter. The used heuristic method is a very useful tool for searching the best pool of descriptors. It is a quick method and presents no restrictions on the size of the data set (Dunn and Hopfinger 2002). The best regression model with the optimum values of statistical criteria (the square correlation R2, the F-test and the standard error s values) was determined (Walczac et al. 2010). The final model was validated using previously described P-gp activators (Supplementary data, Figure S4) (Palmeira et al. 2012; Silva et al. 2013d). A major concern in developing QSAR models is the number of descriptors used to elaborate the equation. Laws of QSAR establish that it should be one descriptor for each five

molecules (Kubinyi 2008), precisely the number of compounds assayed in the present work.

The multilinear regression analysis using Heuristic method for **X1-5** in the one-parameter model is given in Figure 7. The best training morel had a quality (R2) of 0.7100, Fisher value of 7.34, and s of 75.7, which demonstrate that the proposed model has satisfactory statistical stability and validity in spite of the small group of molecules used to build the model. The F-test reflects the ratio of the variance explained by the model and the variance due to the error in the regression; a high value of the F-test indicates that the model is significant. The QSAR model is significant at 95% level as shown by their Fischer ratio values which exceed the tabulated values (6.61) as desired for a meaningful correlation. The squared correlation coefficient R2 is a relative measure of quality of fit by regression equation; correspondingly, it represents more than 70% of the total variance (R2=0.710) in the P-gp activation effect exhibited by xanthone derivatives **1-5**; its value is close to 1.0 which represents the better fit to the regression line. Standard deviation s expresses the variation of the residuals or the variation about the regression line, being an absolute measure of quality of fit and should have a low value for the regression to be significant.

The maximal partial charge for an oxygen atom (Zefirov) was the descriptor predicted as being implicated in the P-gp activation ability of all dihydroxylated xanthones (Figure 7). This electrostatic parameter is associated with the electronegativity of the oxygen that is higher than the electronegativity of carbon, causing electrons to spend more time around the oxygen atom, giving it a partially negative charge while the carbon will become partially positive. This parameter indicates the importance of the presence of the O atom in specific positions in the molecule.

As P-gp activators bind in the drug-binding pocket formed by the transmembrane domain interface, docking simulations were performed in this binding pocket of P-glycoprotein. As dihydroxylated xanthones **1-5** revealed an effect compatible with P-gp activation in the *in vitro* studies, a visual inspection of these molecules in the transmembrane domain interface of P-gp was performed (Figure 8). Dihydroxylated xanthones **1-5** bind in one particular binding site, engulfed by TM 4, 5, 8-10, and 12 (Figure 8). Stable complexes between **X1-5** and P-gp binding-pocket are formed, with docking scores as low as -7.2 kJ/mol for **X5** (Table 3A). All the xanthones in study bind in a similar and almost superimposable conformation (Figure 8). Dihydroxylated xanthones have shape, size, and stereoelectronic complementarity to P-gp binding pocket, establishing hydrogen interactions with Ile-235, Arg-832, and Glu-875 (Loo and Clarke 2002; Wang et al. 2007), described as being important members of the drug-binding pocket, contributing also to the correct folding of the transporter; and stacking interactions

with Phe-77, described as being part of P-glycoprotein binding pocket and important to P-gp biosynthesis (Loo and Clarke 1993).

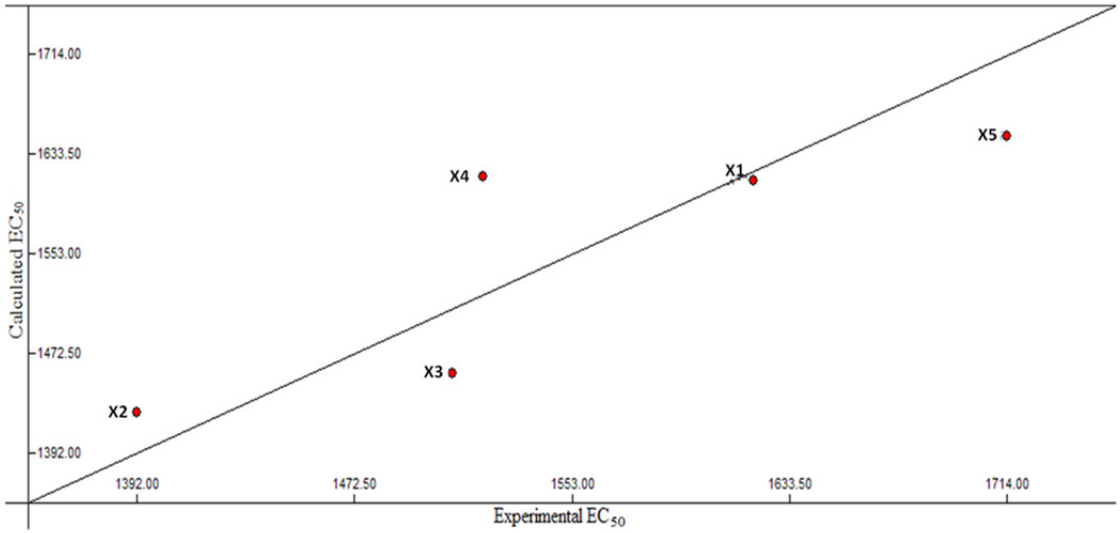

No	X	ΔX	t-test	Name of the descriptor
0	-11777	4918.3	-2.3944	Intercept
1	-115270	42538	-2.7098	Maximal partial charge of O atom

Figure 7. QSAR model obtained with the heuristic method for **X1-5** with the CODESSA software (R2 = 0.7100, F = 7.34, and s = 75.74). X, ΔX, and t-test are the regression coefficient of the linear model, standard errors of the regression coefficient, and the t significance coefficient of the determination, respectively.

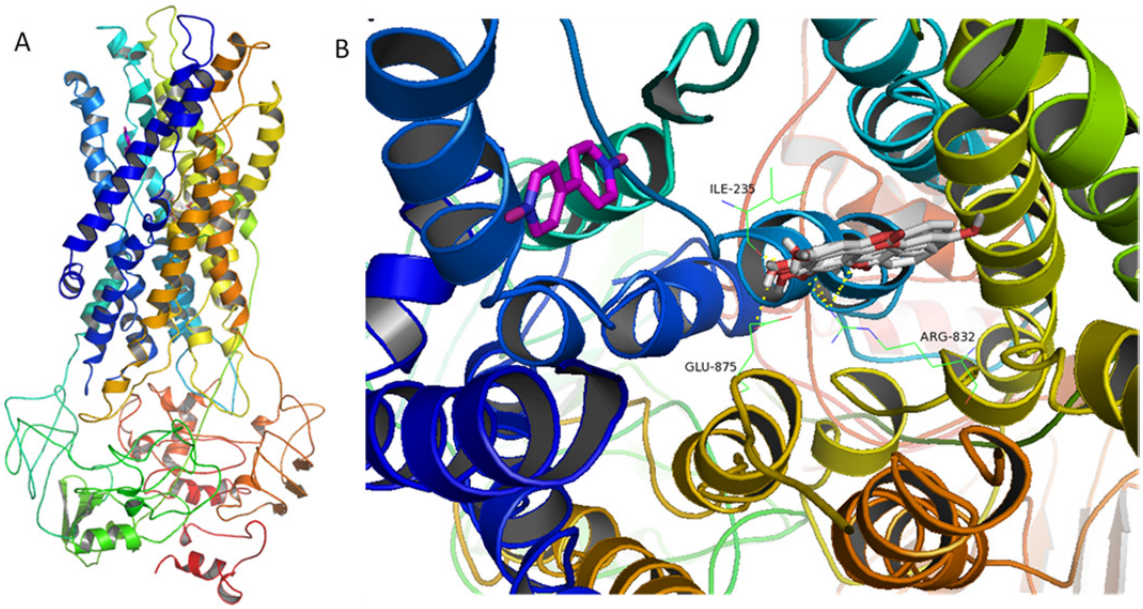

Figure 8. Docking of the dihydroxylated **X1-5** (grey) and paraquat (pink) individually to the P-gp model. Side (A) and top (B) view. Polar interactions are represented with the yellow broken line.

The top rank PQ docking pose presented a score of -5.6 kJ/mol (Table 3A), in a binding pocket distant from the place where **X1-5** were predicted to dock (Figure 8); other less stable PQ conformations are found in the xanthone binding site (data not shown). A simultaneous and cooperative transport may be hypothesized, as the binding of a xanthone at one binding site may stimulate the transport of PQ trough another binding site (Litman et al. 1997). Therefore, xanthone derivatives and PQ may bind simultaneously in P-gp in two different binding sites. Moreover, xanthones and PQ may establish stacking interactions while being co-transported; this noncovalent complex binds to P-gp with higher affinity than xanthone derivative and PQ individually (Figure 9, Table 3B). The two-ligand complex establishes polar interactions with P-gp residues, such as Gln347 and Val345, and stacking interactions with P-gp residues, such as Phe343 and Trp232 (Figure 9).

Table 3. Docking scores of **X1-5** alone **(A)** and **X1-5** + PQ **(B)** into the P-gp docking pocket.

(A)	Docking scores (kJ/mol)	(B)	Docking scores (kJ/mol)
X1	-7.1	**X1** + PQ	-9.9
X2	-6.7	**X2** + PQ	-9.6
X3	-6.8	**X3** + PQ	-9.8
X4	-7.0	**X4** + PQ	-9.8
X5	-7.2	**X5** + PQ	-10.0
PQ	-5.6	-	-

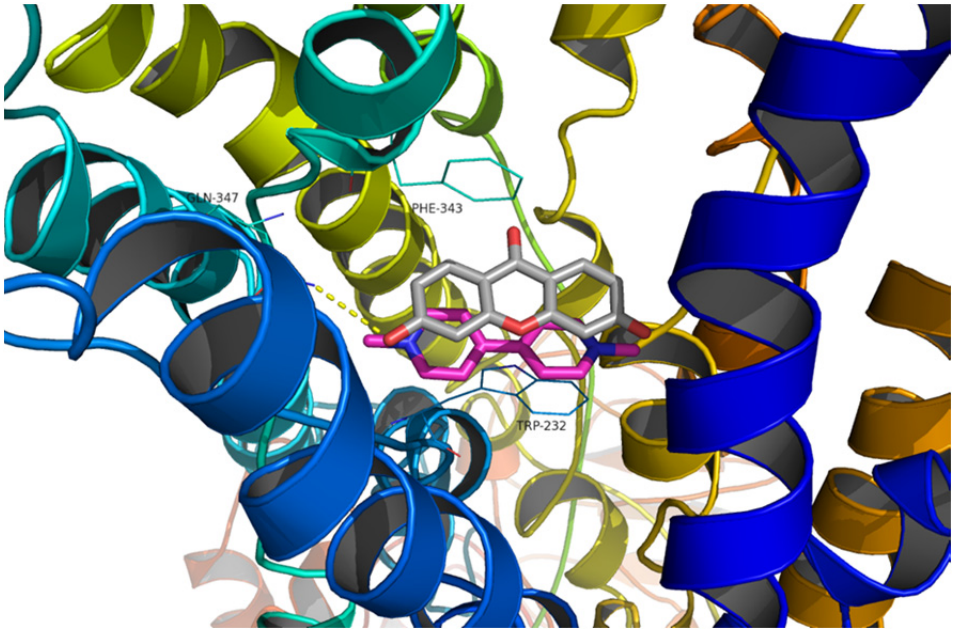

Figure 9. Docking of **X5**: paraquat complex into P-gp model. Polar interactions are represented with the yellow broken line.

4. DISCUSSION

The present data clearly demonstrate that all the tested dihydroxylated xanthones (**X1-5**, Figure 1) significantly increased both P-gp expression and activity, resulting in a significant protection of Caco-2 cells against PQ-induced toxicity.

Xanthones, dibenzo-γ-pyrones, comprise an important class of oxygenated heterocycles, with both natural and synthetic origin, and growing interest in this class of compounds has been associated with the pharmacological properties demonstrated by these derivatives (Pinto et al. 2005). The biological activities of this class of compounds are associated with their tricyclic scaffold, but vary depending on the nature and/or position of the different substituents (Pinto et al. 2005). Several xanthonic derivatives were already reported to modulate diverse enzymatic systems, as well as other cellular systems such as calcium channels, 5-HT 2A receptors, and β-adrenergic receptors [for review see (Pinto et al. 2005)]. However, in what concerns to modulation of drug transporters the available information is scarce. In fact, some prenylated xanthones have shown binding affinity to the P-gp recombinant domain (Tchamo et al. 2000). Moreover, in a study performed with P-gp overexpressing leukemia cells (K562Dox cells), a prenylated and a lignoid xanthonic derivative acted as noncompetitive P-gp inhibitors, blocking P-gp ATPase activity (Sousa et al. 2013). However, in the same study, two other simple oxygenated xanthone derivatives significantly decreased the intracellular accumulation of RHO 123, an effect compatible with increased P-gp activity, but no further studies were conducted to clarify their mode of action. To the best of our knowledge, this is the first report on the ability of xanthonic derivatives to act as P-gp inducers, demonstrating that they significantly increase the pump expression (Figure 2). The observed *in vitro* P-gp induction effect was not dependent on the position of the hydroxyl substituents at the xanthonic scaffold, since no significant differences were observed among the tested compounds. Moreover, the significant increase in the pump expression resulted in significant increases in its activity (Figure 3A). It is well known that increases in protein expression may not necessarily result in proportional increases in pump activity (Silva et al. 2011; Silva et al. 2013b; Takara et al. 2009; Vilas-Boas et al. 2011), since the increased expression does not mean that the protein is yet fully functional. However, as can be seen in Figures 2 and 3A, all tested dihydroxylated xanthones **1-5** simultaneously increased P-gp expression and activity, and the observed increases in the protein expression reveal a higher incorporation in the cell membrane, since the monoclonal UIC2 antibody recognizes an external P-gp epitope (Vilas-Boas et al. 2011). Noteworthy, a direct activation of the pump was observed when the compounds were in contact with the cells during a short 45 min RHO 123 efflux phase (Figure 3B), suggesting an increased P-

gp activity that does not reflect increased protein expression, given the short incubation period with the tested xanthones. Therefore, these compounds acted as P-gp activators, compounds with the ability to immediately increase P-gp activity without the need to increase its expression (Sterz et al. 2009; Vilas-Boas et al. 2013c). From the obtained results, **X1** and **X5** were the most effective P-gp activators.

P-gp ATPase activity assays have been widely used to evaluate possible interactions with P-gp function and compounds that act as P-gp substrates typically stimulate its ATPase activity (Ambudkar et al. 1999). Accordingly, our results showed that all the tested xanthones caused a significant increase in P-gp vanadate-sensitive ATPase activity, demonstrating to be actively transported by the pump (Figure 4).

To evaluate whether the observed effects of the tested **X1-5** on P-gp expression and activity could afford protection of Caco-2 cells against the toxicity of P-gp substrates, PQ was used as a model of a toxic substrate and its toxicity was evaluated in the presence or absence of the tested compounds. The suitability of this study model using PQ as the P-gp toxic substrate was already demonstrated with previous studies on the P-gp inducer doxorubicin in Caco-2 cells (Silva et al. 2011; Silva et al. 2013c) and a reduced rifampicin derivative (RedRif) in RBE4 cells (Vilas-Boas et al. 2013c). Upon simultaneous incubation with the five tested xanthonic derivatives, PQ cytotoxicity was significantly decreased, with significant increases in the EC_{50} values of the PQ + Xs curves, being **X1** and **X5** the most protecting derivatives (Figure 5; Table 1), the same compounds that demonstrated the highest effectiveness in activating the pump (Figure 3B). Moreover, when in presence of the potent P-gp inhibitor, GF120918, the observed protective effects were completely abolished (Figure 6), demonstrating that the tested **X1-5** can effectively reduce PQ-induced cell death through a P-gp-mediated mechanism.

Noteworthy, as all the five tested **X1-5** were able to simultaneously increase RHO 123 efflux, ATP consumption, and PQ EC_{50} values in Caco-2 cells, confirming an effective protection against PQ-induced toxicity, the existence of a mechanism involving P-gp activation was proposed. P-glycoprotein activators have been recently defined as compounds with the ability to immediately increase P-gp activity without increasing its expression (Sterz et al. 2009; Vilas-Boas et al. 2013c) although it has long been known that there are compounds that bind to P-gp and stimulate the transport of a substrate on another binding site. For example, Hoechst-33342 and RHO 123 act through this cooperative mode of action (Shapiro and Ling 1998). This functional model of P-gp suggested that the efflux pump contained at least two positively cooperative sites (H site and R site, for Hoechst-33342 and RHO 123, respectively) for drug binding and transport (Shapiro and Ling 1997). This cooperative mechanism of action has also been suggested for prazosin and progesterone (Shapiro and Ling 1998). A four-P-gp-binding-sites model

supports the presence of three transport sites and one regulatory site. This last site allostericaly alters the conformation of the transport binding sites from low to high affinity for substrates, increasing the rate of translocation (Martin et al. 2000). In fact, the adaption and survival mechanisms of living beings has allowed the binding of several xenobiotics at the same time to P-gp (Safa 1993; Safa 1998), increasing the transport of each other, not competing but activating the transportation cycle (Safa 2004). Hence, binding modes of xanthonic derivatives **1-5** and paraquat were further explored by a docking study. Xanthonic derivatives **1-5** and PQ docked on two different binding sites in the cleft formed by the transmembrane α-helices of a P-gp model based on homologous *S.aureus* ABC transporter, Sav1866 (Palmeira et al. 2012). Furthermore, a simultaneous docking of PQ and **X1-5** revealed that a more stable complex with P-gp model was formed (with lower free energy) than when those molecules were docked individually, suggesting that a co-transport may be occurring for PQ and the tested xanthonic derivatives. The docking studies suggest that two mechanisms of activation by co-transport may be occurring: a) xanthones dock on a different site than PQ, thus activating the efflux of the herbicide; b) xanthonic derivative and PQ bind to the same drug pocket, establishing stacking interactions between the xanthone scaffold and the biphenyl group, and facilitating the transport to the extracellular medium. In the future, mutation studies could be performed in order to determine whether PQ and xanthones bind to the same or to different binding sites on P-gp.

Maximal partial charge for oxygen atoms (Supplementary data, Figure S5), an electrostatic parameter associated with electronegativity of oxygen, and consequently, with the strength of the intermolecular polar interactions such as hydrogen interactions, was predicted as being related with the P-gp activation ability of dihydroxylated xanthonic derivatives **1-5**.

Both docking studies and QSAR model are in accordance with the biological data presented, with 3,6-dihydroxyxanthone (**X5**) being the most active and the 1,2-dihydroxyxanthone (**X2**) the least active xanthone in activating P-gp transport activity. Overall, position 3 of the xanthonic scaffold seems to be the most favourable for a hydroxyl substituent in P-gp activation, in contrast to position 1. Nevertheless, in the future, other simple oxygenated xanthonic derivatives will be investigated in order to improve the significance and predictability of the QSAR model, and to discover other descriptors involved in the P-gp activation capacity of xanthones.

In conclusion, adding to their known pharmacological actions, dihydroxylated xanthonic derivatives were shown to efficiently induce and activate P-gp, affording protection against its toxic substrates. These data disclose new perspectives in preventing paraquat and other P-gp substrates-induced poisonings.

5. ACKNOWLEDGMENTS

This work was supported by the Fundação para a Ciência e Tecnologia (FCT)-project PTDC/SAU-OSM/101437/2008 - QREN initiative with EU/FEDER funded through COMPETE - Operational Programme for Competitiveness Factors.

The work was also supported by FCT within the framework of Strategic Projects for Scientific Research Units of R&D (projects PEst-C/EQB/LA0006/2011 and Pest-OE/SAU/UI4040/2011).

Renata Silva and Daniel José Barbosa acknowledge FCT for their PhD grants [SFRH/BD/29559/2006] and [SFRH/BD/64939/2009], respectively.

6. CONFLICT OF INTEREST STATEMENT

The authors declare that there are no conflicts of interest.

7. REFERENCES

Ambudkar SV, Dey S, Hrycyna CA, Ramachandra M, Pastan I, Gottesman MM (1999) Biochemical, cellular, and pharmacological aspects of the multidrug transporter. Annu Rev Pharmacol Toxicol 39:361-398.

Castanheiro RAP, Pinto MMM, Silva AMS, et al. (2007) Dihydroxyxanthones prenylated derivatives: Synthesis, structure elucidation, and growth inhibitory activity on human tumor cell lines with improvement of selectivity for MCF-7. Bioorg Med Chem 15:6080-6088.

Chaudhary PM, Roninson IB (1993) Induction of multidrug resistance in human cells by transient exposure to different chemotherapeutic drugs. J Natl Cancer Inst 85:632-639.

Chin K, Chauhan S, Pastan I, Gottesman M (1990) Regulation of mdr RNA levels in response to cytotoxic drugs in rodent cells. Cell Growth Differ 1:361-365.

Coi A, Massarelli I, Murgia L, Saraceno M, Calderone V, Bianucci AM (2006) Prediction of hERG potassium channel affinity by the CODESSA approach. Bioorg Med Chem 14:3153-3159.

Costa E, Sousa E, Nazareth N, S.J. Nascimento M, M.M. Pinto M (2010) Synthesis of xanthones and benzophenones as inhibitors of tumor cell growth. Letters in Drug Design & Discovery 7:487-493.

Dinis-Oliveira RJ, Duarte JA, Remiao F, Sanchez-Navarro A, Bastos ML, Carvalho F (2006a) Single high dose dexamethasone treatment decreases the pathological score and increases the survival rate of paraquat-intoxicated rats. Toxicology 227:73-85.

Dinis-Oliveira RJ, Remiao F, Duarte JA, et al. (2006b) P-glycoprotein induction: an antidotal pathway for paraquat-induced lung toxicity. Free Radic Biol Med 41:1213-1224.

Dorner B, Kuntner C, Bankstahl JP, et al. (2009) Synthesis and small-animal positron emission tomography evaluation of [11C]-elacridar as a radiotracer to assess the distribution of P-glycoprotein at the blood-brain barrier. J Med Chem 52:6073-6082.

Dunn WJ, Hopfinger AJ (2002) 3D QSAR of flexible molecules using tensor representation. In: Kubinyi H, Folkers G, Martin YC (eds) 3D QSAR in drug design: Volume 3: Recent advances. Kluwer Academic Publishers, NewYork, USA, p 167-182.

Fardel O, Lecureur V, Daval S, Corlu A, Guillouzo A (1997) Up-regulation of P-glycoprotein expression in rat liver cells by acute doxorubicin treatment. Eur J Biochem 246:186-192.

Froimowitz M (1993) HyperChem: a software package for computational chemistry and molecular modeling. Biotechniques 14:1010-1013.

Genoux-Bastide E, Lorendeau D, Nicolle E, et al. (2011) Identification of xanthones as selective killers of cancer cells overexpressing the ABC transporter MRP1. ChemMedChem 6:1478-1484.

Harmsen S, Meijerman I, Febus CL, Maas-Bakker RF, Beijnen JH, Schellens JH (2009) PXR-mediated induction of P-glycoprotein by anticancer drugs in a human colon adenocarcinoma-derived cell line. Cancer Chemother Pharmacol 66:765-771.

Hennessy M, Spiers JP (2007) A primer on the mechanics of P-glycoprotein the multidrug transporter. Pharmacol Res 55:1-15.

Hu XF, Slater A, Rischin D, Kantharidis P, Parkin JD, Zalcberg J (1999) Induction of MDR1 gene expression by anthracycline analogues in a human drug resistant leukaemia cell line. Br J Cancer 79:831-837.

Huynh-Delerme C, Huet H, Noel L, Frigieri A, Kolf-Clauw M (2005) Increased functional expression of P-glycoprotein in Caco-2 TC7 cells exposed long-term to cadmium. Toxicol In Vitro 19:439-447.

Kageyama M, Fukushima K, Togawa T, et al. (2006) Relationship between excretion clearance of rhodamine 123 and P-glycoprotein (Pgp) expression induced by representative Pgp inducers. Biol Pharm Bull 29:779-784.

Kanaan M, Daali Y, Dayer P, Desmeules J (2009) Uptake/efflux transport of tramadol enantiomers and O-desmethyl-tramadol: focus on P-glycoprotein. Basic Clin Pharmacol Toxicol 105:199-206.

Katritzky AR, Perumal S, Petrukhin R, Kleinpeter E (2001) CODESSA-based theoretical QSPR model for hydantoin HPLC-RT lipophilicities. J Chem Inf Comput Sci 41:569-574.

Kim KA, Park PW, Liu KH, et al. (2008) Effect of rifampin, an inducer of CYP3A and P-glycoprotein, on the pharmacokinetics of risperidone. J Clin Pharmacol 48:66-72.

Kim RB (2002) Drugs as P-glycoprotein substrates, inhibitors, and inducers. Drug Metab Rev 34:47-54.

Kubinyi H (2008) Statistical Methods. In: Mannhold R, Krogsgaard-Larsen P, Timmerman H (eds) QSAR: Hansch Analysis and Related Approaches. Wiley-VCH Verlag GmbH, Weinheim, p 91-107.

Lill MA, Danielson ML (2010) Computer-aided drug design platform using PyMOL. J Comput Aided Mol Des 25:13-19.

Litman T, Zeuthen T, Skovsgaard T, Stein WD (1997) Competitive, non-competitive and cooperative interactions between substrates of P-glycoprotein as measured by its ATPase activity. Biochim Biophys Acta 1361:169-176.

Loo TW, Clarke DM (1993) Functional consequences of phenylalanine mutations in the predicted transmembrane domain of P-glycoprotein. J Biol Chem 268:19965-19972.

Loo TW, Clarke DM (2002) Location of the rhodamine-binding site in the human multidrug resistance P-glycoprotein. J Biol Chem 277:44332-44338.

Lü WJ, Chen YL, Ma WP, et al. (2008) QSAR study of neuraminidase inhibitors based on heuristic method and radial basis function network. Eur J Med Chem 43:569-576.

Martin C, Berridge G, Higgins CF, Mistry P, Charlton P, Callaghan R (2000) Communication between multiple drug binding sites on P-glycoprotein. Mol Pharmacol 58:624-632.

Masters K-S, Bräse S (2012) Xanthones from Fungi, Lichens, and Bacteria: The natural products and their synthesis. Chem Rev 112:3717-3776.

Nielsen D, Eriksen J, Maare C, Jakobsen A, Skovsgaard T (1998) P-glycoprotein expression in Ehrlich ascites tumour cells after in vitro and in vivo selection with daunorubicin. Br J Cancer 78:1175-1180.

Palmeira A, Rodrigues F, Sousa E, Pinto M, Vasconcelos MH, Fernandes MX (2011) New uses for old drugs: pharmacophore-based screening for the discovery of P-glycoprotein inhibitors. Chem Biol Drug Des 78:57-72.

Palmeira A, Vasconcelos MH, Paiva A, Fernandes MX, Pinto M, Sousa E (2012) Dual inhibitors of P-glycoprotein and tumor cell growth: (re)discovering thioxanthones. Biochem Pharmacol 83:57-68.

Pedro M, Cerqueira F, Sousa MEI, Nascimento MSJ, Pinto M (2002) Xanthones as inhibitors of growth of human cancer cell lines and their effects on the proliferation of human lymphocytes in vitro. Bioorg Med Chem 10:3725-3730.

Pinto MMM, Sousa ME, Nascimento MSJ (2005) Xanthone derivatives: New insights in biological activities Curr Med Chem 12:2517-2538

Safa AR (1993) Photoaffinity labeling of P-glycoprotein in multidrug-resistant cells. Cancer Invest 11:46-56.

Safa AR (1998) Photoaffinity labels for characterizing drug interaction sites of P-glycoprotein. Methods Enzymol 292:289-307.

Safa AR (2004) Identification and characterization of the binding sites of P-glycoprotein for multidrug resistance-related drugs and modulators. Curr Med Chem Anticancer Agents 4:1-17.

Seelig A (1998) A general pattern for substrate recognition by P-glycoprotein. Eur J Biochem 251:252-261.

Seeliger D, de Groot BL (2010) Ligand docking and binding site analysis with PyMOL and Autodock/Vina. J Comput Aided Mol Des 24:417-422.

Shapiro AB, Ling V (1997) Positively cooperative sites for drug transport by P-glycoprotein with distinct drug specificities. Eur J Biochem 250:130-137.

Shapiro AB, Ling V (1998) The mechanism of ATP-dependent multidrug transport by P-glycoprotein. Acta Physiol Scand Suppl 643:227-234.

Sharom FJ (2011) The P-glycoprotein multidrug transporter. Essays Biochem 50:161-178.

Silva R, Carmo H, Dinis-Oliveira R, et al. (2011) In vitro study of P-glycoprotein induction as an antidotal pathway to prevent cytotoxicity in Caco-2 cells. Arch Toxicol 85:315-326.

Silva R, Carmo H, Vilas-Boas V, et al. (2013a) Several transport systems contribute to the intestinal uptake of Paraquat, modulating its cytotoxic effects. Submitted for publication.

Silva R, Carmo H, Vilas-Boas V, et al. (2013b) Colchicine effect on P-glycoprotein expression and activity: in silico and in vitro studies. Submitted for publication.

Silva R, Carmo H, Vilas-Boas V, et al. (2013c) Doxorubicin decreases paraquat accumulation and toxicity in Caco-2 cells. Toxicol Lett 217:34-41.

Silva R, Palmeira A, Carmo H, et al. (2013d) P-glycoprotein induction in Caco-2 cells by newly synthetized thioxanthones prevents Paraquat cytotoxicity. Submitted for publication.

Sousa E, Palmeira A, Cordeiro A, et al. (2013) Bioactive xanthones with effect on P-glycoprotein and prediction of intestinal absorption. Med Chem Res 22:2115-2123.

Sterz K, Mollmann L, Jacobs A, Baumert D, Wiese M (2009) Activators of P-glycoprotein: Structure-activity relationships and investigation of their mode of action. ChemMedChem 4:1897-1911.

Takara K, Hayashi R, Kokufu M, et al. (2009) Effects of nonsteroidal anti-inflammatory drugs on the expression and function of P-glycoprotein/MDR1 in Caco-2 cells. Drug Chem Toxicol 32:332-337.

Tchamo DN, Dijoux-Franca MG, Mariotte AM, et al. (2000) Prenylated xanthones as potential P-glycoprotein modulators. Bioorg Med Chem Lett 10:1343-1345.

Tian R, Koyabu N, Morimoto S, Shoyama Y, Ohtani H, Sawada Y (2005) Functional induction and de-induction of P-glycoprotein by St. John's wort and its ingredients in a human colon adenocarcinoma cell line. Drug Metab Dispos 33:547-554.

Trott O, Olson AJ (2009) AutoDock Vina: improving the speed and accuracy of docking with a new scoring function, efficient optimization, and multithreading. J Comput Chem 31:455-461.

Ueda K, Taguchi Y, Morishima M (1997) How does P-glycoprotein recognize its substrates? Semin Cancer Biol 8:151-159.

Varma MV, Ashokraj Y, Dey CS, Panchagnula R (2003) P-glycoprotein inhibitors and their screening: a perspective from bioavailability enhancement. Pharmacol Res 48:347-359.

Vilas-Boas V, Silva R, Gaio AR, et al. (2011) P-glycoprotein activity in human Caucasian male lymphocytes does not follow its increased expression during aging. Cytometry A 79:912-919.

Vilas-Boas V, Silva R, Guedes-de-Pinho P, Carvalho F, Bastos ML, Remião F (2013a) RBE4 cells are highly resistant to paraquat-induced cytotoxicity: studies on uptake and efflux mechanisms. Journal of Applied Toxicology Epub ahead of print.

Vilas-Boas V, Silva R, Nunes C, et al. (2013b) Mechanisms of P-gp inhibition and effects on membrane fluidity of a new rifampicin derivative, 1,8-dibenzoyl-rifampicin. Toxicol Lett 220:259-266.

Vilas-Boas V, Silva R, Palmeira A, et al. (2013c) Development of novel rifampicin-derived P-glycoprotein activators/inducers. Synthesis, in silico analysis and application in the RBE4 cell model, using paraquat as substrate. PLoS One 8:e74425.

Walczac B, Daszykowski M, Stanimirova I (2010) Recent advances in QSAR studies: Methods and applications. In: Puzyn T, Leszczyński J, Cronin MTD (eds) Challenges and advances in computational chemistry and physics. vol 8. Springer, New York, USA, p 177-205.

Wang Y, Loo TW, Bartlett MC, Clarke DM (2007) Modulating the folding of P-glycoprotein and cystic fibrosis transmembrane conductance regulator truncation mutants with pharmacological chaperones. Mol Pharmacol 71:751-758.

Watanabe T, Onuki R, Yamashita S, Taira K, Sugiyama Y (2005) Construction of a functional transporter analysis system using MDR1 knockdown Caco-2 cells. Pharm Res 22:1287-293.

Zhang L, Zhou W, Li D-H (2006) A descent modified Polak-Ribière-Polyak conjugate gradient method and its global convergence. IMA Journal of Numerical Analysis 26:629-640.

Zhou SF (2008) Structure, function and regulation of P-glycoprotein and its clinical relevance in drug disposition. Xenobiotica 38:802-832.

SUPPLEMENTARY DATA

Supplementary Figures

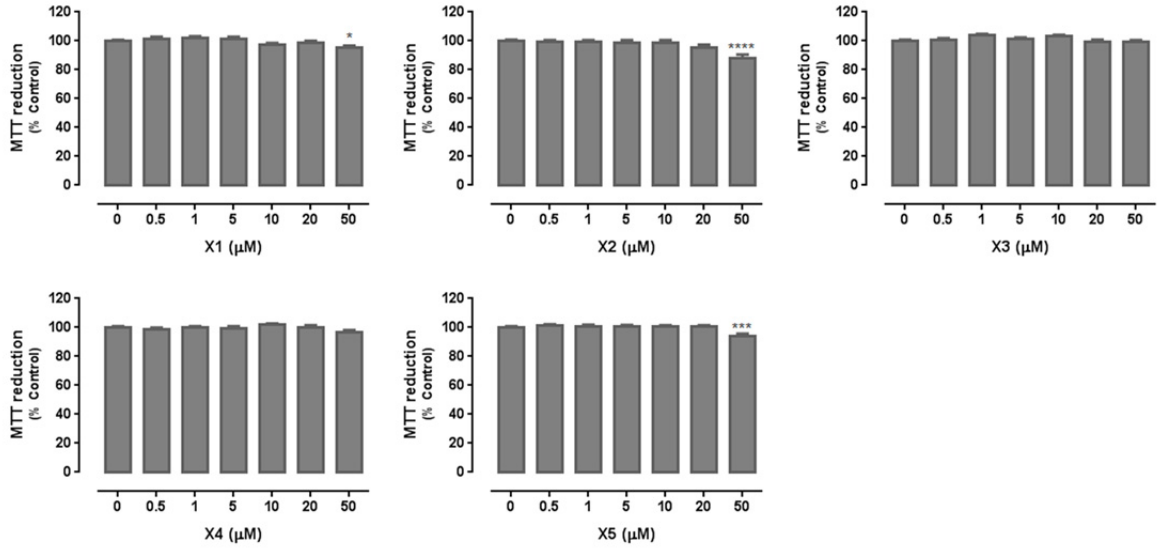

Figure S1. Xanthones **1-5** (0 - 50 μM) cytotoxicity in Caco-2 cells 24 h after incubation, evaluated by the MTT reduction assay. Results are presented as mean ± SEM from 5 independent experiments performed in triplicate. Statistical comparisons were made using the parametric method of One-way ANOVA, followed by the Bonferroni's multiple comparisons *post hoc* test (*p<0.05; ***p<0.001; ****p<0.0001 *vs.* control).

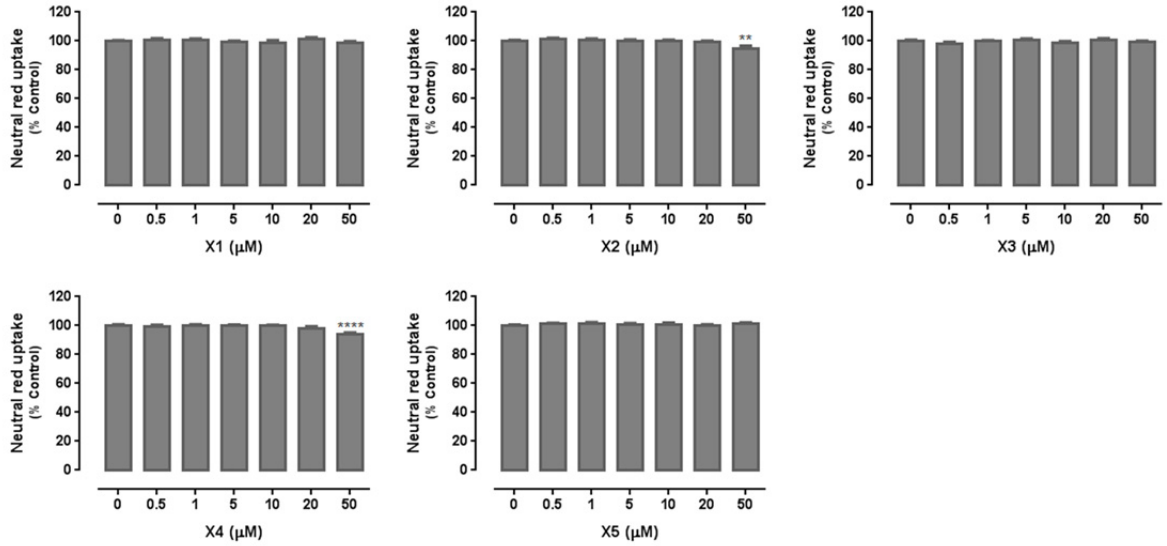

Figure S2. Xanthones **1-5** (0 - 50 μM) cytotoxicity in Caco-2 cells 24 h after incubation, evaluated by the NR uptake assay. Results are presented as mean ± SEM from 5 independent experiments performed in triplicate. Statistical comparisons were made using the parametric method of One-way ANOVA, followed by the Bonferroni's multiple comparisons *post hoc* test (**p<0.01; ****p<0.0001 *vs.* control).

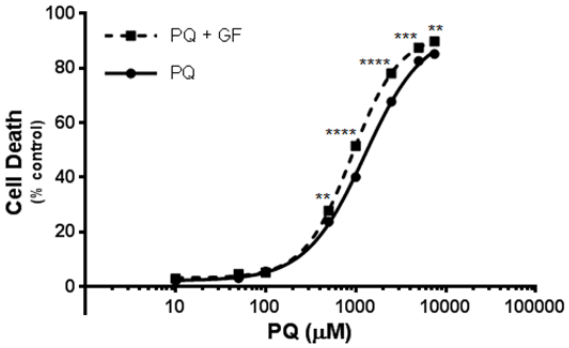

Figure S3. Paraquat concentration–response (cell death) curves in the absence (PQ) or in the presence (PQ + GF) of the P-gp inhibitor GF120918, confirming the P-gp involvement in PQ toxicity. Results are presented as mean ± SEM from at least 4 independent experiments (performed in triplicate). Concentration–response curves were fitted using least squares as the fitting method and the comparisons between the fitted curves (LOG EC_{50}, TOP, BOTTOM and Hill slope) were made using the extra sum-of-squares F test. Statistical comparisons were made using Two-way ANOVA, followed by the Sidak's multiple comparisons *post hoc* test (***p*<0.01; ****p*<0.001; *****p*<0.0001 *vs.* PQ alone). In all cases, *p* values <0.05 were considered significant.

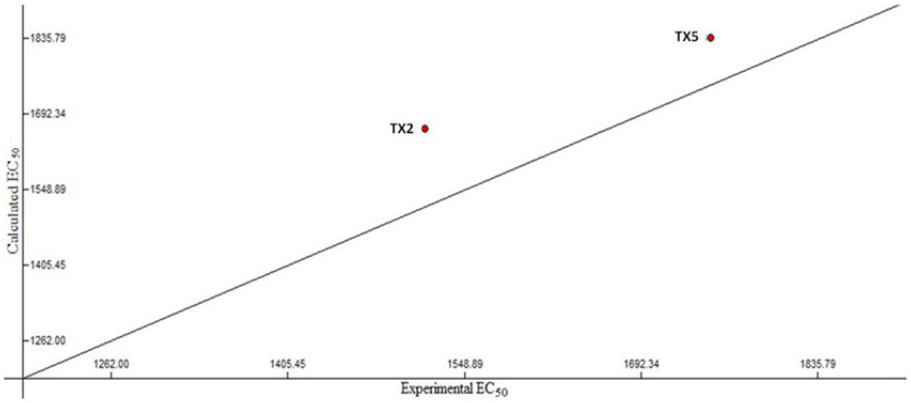

Molecules	Calculated EC_{50}	Experimental EC_{50}	Differential	Reference
1-chloro-4-hydroxy-9H-thioxanthen-9-one (TX2)	1664	1517	147	(Silva et al. 2013d)
1-(Propan-2-ylamino)-4-propoxy-9H-thioxanthen-9-one (TX5)	1835	1749	86	(Silva et al. 2013d)

Figure S4. External validation results of QSAR model using two thioxanthones described as P-gp activators (Palmeira et al. 2012; Silva et al. 2013d).

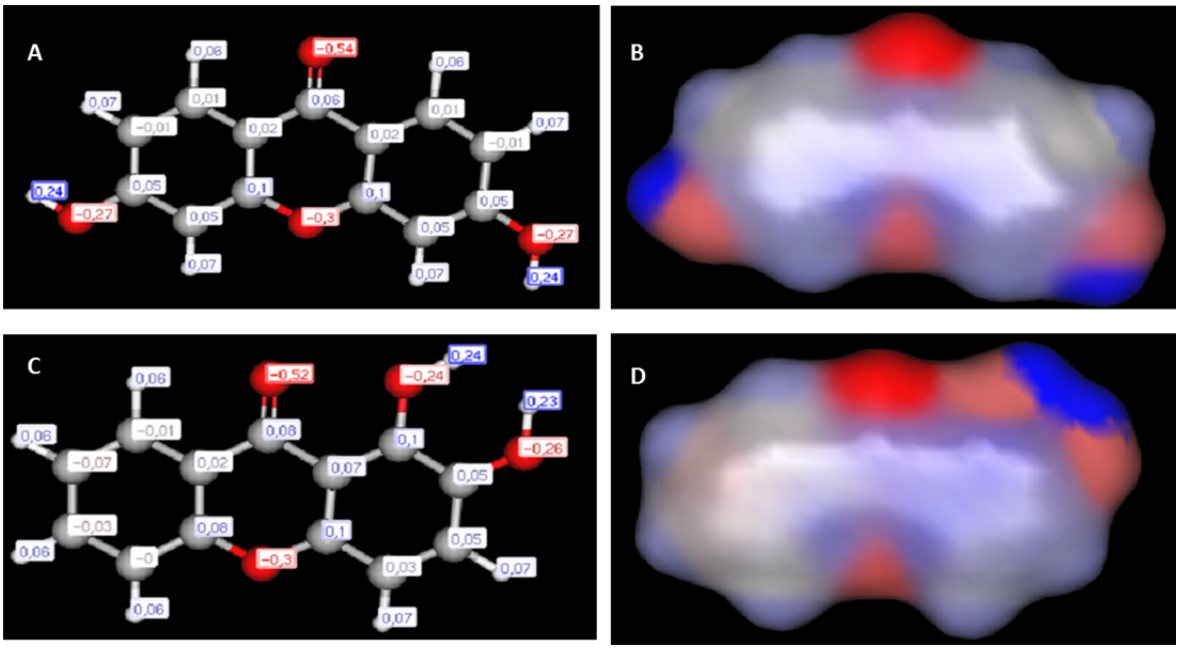

Figure S5. Partial charges of **X5** (A, B) and **X2** (C,D). B and D represent partial charges colour gradient (from negative – red – to positive – blue) mapped onto the **X5** and **X2** molecular surfaces, respectively.

Supplementary Tables

Table S1. EC_{50} (half-maximum-effect concentration), TOP (maximal effect), BOTTOM (baseline) and Hill slope values of the paraquat concentration-response fitted curves, with (PQ + GF) or without (PQ) simultaneous exposure to a P-gp inhibitor, GF120918 (10 μM).

	PQ + GF	PQ
EC_{50} (half-maximum-effect concentration, μM)	**906.0**	**1260**
TOP (maximal cell death, % control)	92.58	94.00
BOTTOM (baseline, % control)	3.118	2.137
Hill Slope	1.629	1.330
LOG EC_{50} *p* value (comparison between LOG EC_{50} values)	-	**< 0.0001**
TOP *p* value (comparison between TOP values)	-	0.4712
BOTTOM *p* value (comparison between BOTTOM values)	-	0.2466
Hill Slope *p* value (comparison between Hill slope values)	-	**0.0033**
Curve *p* value (Comparison between the Fitted Curves)	-	**< 0.0001**

Concentration-response curves were fitted using least squares as the fitting method and the comparisons between PQ and PQ + GF curves were made using extra sum-of-squares F test. In all cases, *p* values <0.05 were considered significant.

PART III

IV. INTEGRATED DISCUSSION

IV.1. Validation of Caco-2 cells as a suitable *in vitro* model for the study of P-gp induction

The first aim of the present work was the validation of Caco-2 cells as a suitable *in vitro* model to be used in the screening and selection of potent, safe and specific P-gp inducers. These human intestinal epithelial cells were chosen to evaluate changes in intestinal P-gp, since most of the intoxications by P-gp substrates result from accidental or intentional ingestion, thus resulting in their absorption at the intestinal level. Moreover, these cells are widely used for predicting drug intestinal absorption and excretion in humans (Barta et al. 2008; Huynh-Delerme et al. 2005; Watanabe et al. 2005; Yamashita et al. 2000; Yamashita et al. 2002a; Yamashita et al. 2002b). For this purpose, doxorubicin was initially used as a reference compound, in order to validate our experimental procedure (Manuscript I), given its known ability to activate the transcription of the *MDR1* gene and, therefore, increase P-gp levels (Boháčová et al. 2006; Chaudhary and Roninson 1993; Chin et al. 1990a; Fardel et al. 1997; Hu et al. 1995; Kohno et al. 1989; Liu et al. 2002b; Wongwanakul et al. 2013). According to the obtained results, a significant increase in P-gp expression in Caco-2 cells was observed as soon as 6 h after exposure to doxorubicin concentrations higher than 5 µM (147%, 186%, 312% and 365% for 5, 10, 50 and 100 µM doxorubicin, as compared to control, respectively). Moreover, doxorubicin-induced increase in P-gp expression was accompanied by significant increases in the pump activity, and both parameters were time- and concentration-dependent (Manuscript I). Noteworthy, the observed increases in P-gp protein expression revealed a higher incorporation in the cell membrane, since the used monoclonal UIC2 antibody recognizes an external P-gp epitope (Vilas-Boas et al. 2011).

This rapid activation of *MDR1* expression by chemotherapics has been demonstrated both *in vitro* and *in vivo*. In fact, several studies have shown that the *MDR1* gene can be transiently and rapidly induced in cultured cells following exposure to chemotherapeutic agents, such as doxorubicin (Asakuno et al. 1994; Boháčová et al. 2006; Brugger et al. 2002; Chaudhary and Roninson 1993; Chin et al. 1990a; Fardel et al. 1997; Gekeler et al. 1988; Hu et al. 1995; Kohno et al. 1989; Liu et al. 2002b; Ohga et al. 1996; Schuetz et al. 1996a; Wongwanakul et al. 2013). In a very recent study performed by Wongwanakul et al., using the same monoclonal antibody and the same *in vitro* model, it was observed, also by flow cytometry, a significant increase in cell surface P-gp after exposure of Caco-2 cells to doxorubicin for 24 h (2.15 fold over control for 3 µM doxorubicin). Moreover, the effect on P-gp expression was even more pronounced 7 days

after exposure to this anticancer drug (3.76 fold over control for 3 μM doxorubicin) (Wongwanakul et al. 2013), demonstrating also a time-dependent P-gp induction. Additionally, in accordance with our results, a concentration-dependent increase in the protein expression was also observed (Wongwanakul et al. 2013).

Noteworthy, similar rapid induction of *MDR1* gene expression was observed, *in vivo*, in tumours of patients during the course of chemotherapy with doxorubicin (Abolhoda et al. 1999). Metastatic sarcoma tumours isolated from patients undergoing chemotherapy with doxorubicin exhibited a very rapid induction of *MDR1* expression, with no induction observed in adjacent (lung) tissue. Indeed, in four out of five patients, a 3-15-fold (median, 6.8) increase in *MDR1* RNA levels was detected in tumours, at 50 min after administration of doxorubicin (Abolhoda et al. 1999). The rapidity of this response excludes gene rearrangement or mutations and supports transcriptional activation as the underlying mechanism. These results suggest a greater and heretofore unconsidered role of *MDR1* in the induction of solid tumour drug resistance. Moreover, these findings demonstrated that *MDR1* gene expression can be rapidly activated in human tumours after transient *in vivo* exposure to cytotoxic chemotherapy, as occurs with doxorubicin.

A rapid increase in *MDR1* gene expression was also reported for other drugs using the same *in vitro* model, the Caco-2 cells. For example, venlafaxine significantly increased the expression of *MDR1* and *MRP* genes in these cells during an acute treatment period (1.5, 3, and 6 h), as detected by RT-PCR (Ehret et al. 2007). However, the effects of the tested compound on P-gp activity and on P-gp protein levels were not evaluated. Anderle et al. also reported that verapamil, celiprolol, and vinblastine significantly induced P-gp protein expression, as evaluated by flow cytometry, although their effects on P-gp activity were not evaluated (Anderle et al. 1998). To note that in this study increased cell surface P-gp expression was detected, since the antibody used, MRK 16, also recognizes an external epitope of human P-gp.

It was also demonstrated that digoxin up-regulates *MDR1* mRNA in Caco-2 cells, as evaluated by RT-PCR (Takara et al. 2003a). Indeed, *MDR1* mRNA expression was increased after exposure to 1 μM digoxin for 24 h, in a concentration-dependent manner, although the effects on P-gp protein level and transport activity were not evaluated. However, in a previous study performed by the same authors, it was demonstrated that, besides the increase in *MDR1* mRNA levels, pre-treatment with 1 μM digoxin for 48 h significantly reduced the uptake of RHO 123 by Caco-2 cells, as well as significantly increased its efflux, an effect compatible with increased P-gp activity. Furthermore, according to the obtained results, the effect of digoxin on *MDR1* mRNA was concentration-dependent. In fact, the expression of *MDR1* mRNA was not significantly affected by treatment with 1 nM digoxin, but a significant increase of about 4-fold was

observed in Caco-2 cells, when digoxin concentration was increased to 1 μM. In accordance, at 1 nM digoxin, no significant differences were observed neither in RHO 123 intracellular accumulation nor in the efflux of the dye (Takara et al. 2002). Therefore, although digoxin effect on P-gp expression was not evaluated at the protein level, the similar results obtained in *MDR1* mRNA levels and P-gp activity suggest increased protein expression. Furthermore, as a result of digoxin-mediated up-regulation of *MDR1* in Caco-2 cells, the sensitivity of these cells to paclitaxel, an MDR1 substrate, was lower than that in the absence of digoxin (Takara et al. 2002). In accordance, in a recent study performed by Naruhashi et al., although P-gp protein content was not evaluated, a good correlation was also obtained between *MDR1* mRNA levels and P-gp transport function upon exposure to digoxin (Naruhashi et al. 2011). Indeed, 24 h after exposure to 1 μM digoxin significantly increased to ~150% the *MDR1* mRNA levels in Caco-2 cells, as well as significantly increased the efflux of RHO 123 (130%) (Naruhashi et al. 2011).

In another study performed in Caco-2 cells, the authors aimed to develop a highly sensitive assay system for P-gp-mediated drug transport by combining induction of P-gp with a short-term culture of Caco-2 cells (Shirasaka et al. 2006). To induce P-gp, the cells were cultured in vinblastine-containing medium (10 nM) and the *MDR1* mRNA level was approximately 7-fold higher than in control cells. In accordance, P-gp protein levels were also increased, as demonstrated by western blot analysis. Furthermore, the polarized transport of P-gp substrates was higher in P-gp induced cells than in control cells, thus demonstrating an increased P-gp activity (Shirasaka et al. 2006).

Interestingly, a stereoselective regulation of *MDR1* expression was demonstrated in Caco-2 cells by cetirizine enantiomers (Shen et al. 2007). R-Cetirizine (100 μM) significantly increased *MDR1* mRNA and P-gp levels, as compared to control cells, whereas these parameters were significantly decreased by S-cetirizine (100 μM). In accordance, RHO 123 and doxorubicin efflux was significantly enhanced after pre-treatment of Caco-2 monolayers with R-cetirizine, but was reduced by S-cetirizine. Also, the sensitivity of these cells to paclitaxel significantly decreased after cells pre-treatment with R-cetirizine and increased upon treatment with S-cetirizine. Therefore, in this study, a complete evaluation of the effect of the tested compounds on P-gp was performed (*MDR1* mRNA, protein and activity levels), suggesting that cetirizine enantiomers can regulate MDR1 expression in Caco-2 cells, and that these regulatory effects were opposite according to the enantiomer tested (R-cetirizine up-regulates, while S-cetirizine down-regulates *MDR1* expression) (Shen et al. 2007).

The expression of *MDR1* mRNA in Caco-2 cells was demonstrated to be also significantly increased by treatment with some NSAIDs, although P-gp transport function remained unchanged (Takara et al. 2009). In that study, the effect of the tested

compounds was not evaluated at the protein level, and the lack of correlation between *MDR1* mRNA levels and P-gp transport function may be due to a lack of increased translation (see IV.2).

In addition, several inhaled corticosteroids, such as fluticasone propionate, beclomethasone dipropionate, ciclesonide and budesonide, were also able to induce P-gp expression in Caco-2 cells, 72 h after exposure, while methylprednisolone was the only systemic corticosteroid able to increase the pump expression (Crowe and Tan 2012). Although this study demonstrated an increased protein expression, as determined by western blot, the effect was only evaluated 72 h after exposure. Thus, the rapid responsiveness of Caco-2 cells to these compounds could not be assessed. Furthermore, since the total amount of P-gp protein was evaluated, the observed effect does not discriminate the amount of protein already incorporated in the cell membrane. Although in this study the P-gp-mediated efflux of the tested corticosteroids across Caco-2 cells monolayers was evaluated, the effect of the observed increase in P-gp expression on the efflux of other P-gp substrates was not performed. Therefore, their effect on P-gp activity was not further explored.

In conclusion, in several studies performed in Caco-2 cells, the P-gp induction effect of several compounds was evaluated only at the *MDR1* mRNA level, and many of them did not evaluate the effects on the pump activity. As will be further discussed in the following section, increased levels of *MDR1* mRNA levels are not always associated with increased protein expression and, consequently, with an increased P-gp activity. In the scope of this dissertation, the P-gp induction effects of the tested compounds were always evaluated at the level of cell surface protein expression (using the UIC2 antibody) and transport activity (using RHO 123 as a P-gp fluorescent substrate). Noteworthy, our results clearly demonstrated that doxorubicin is highly effective in increasing both P-gp protein expression and activity, in a time- and concentration-dependent manner, and the significant increases obtained as soon as 6 h indicate that Caco-2 cells are highly responsive to an exogenous stimulus, thus representing a good *in vitro* model to accomplish the aims of the present work.

IV.2. P-gp expression and activity may not be proportionally increased

The analysis of the effect of DOX on P-gp expression and activity (Manuscript I) highlights that increases in P-gp protein levels are not always directly correlated with corresponding increases in pump functionality. Indeed, it was possible to verify that the observed remarkable increases in P-gp expression levels upon exposure to doxorubicin were not accompanied by proportional increases in RHO 123 efflux, and, consequently, in

P-gp transport activity. For example, the exposure of Caco-2 cells to 50 µM doxorubicin for 6 h significantly increased P-gp expression levels to approximately 312 % of control values, although P-gp transport activity increased only by 126 % (Manuscript I). This suggests that, although P-gp was highly expressed and incorporated in the cell membrane (since, as mentioned, the monoclonal antibody recognizes an external P-gp epitope), this transport efflux pump may not be yet fully functional. In accordance with these results, in the previously referred study reported by Wongwanakul et al., although treatment of Caco-2 cells with 3 µM doxorubicin for 1 and 7 days significantly increased P-gp expression up to 2.15 and 3.76 fold over control, respectively, the P-gp activity of these cells did not increase correspondingly (Wongwanakul et al. 2013). No significant differences were observed in P-gp activity at any tested doxorubicin concentration and up to 7 days of incubation, as evaluated by the calcein-AM uptake assay (Wongwanakul et al. 2013). In accordance, Vilas-Boas et al. also found that P-gp activity in human lymphocytes did not follow the significant increase observed in its expression during aging (Vilas-Boas et al. 2011). P-gp activity and expression were evaluated in lymphocytes isolated from whole blood samples of 65 healthy caucasian male donors, divided into two groups according to age (group 1: under 30-years old; group 2: above 60-years old). A significant age-dependent increase in P-gp expression was observed, which was not reflected in the transporter's activity, thus reinforcing the need for P-gp activity assessment, rather than P-gp expression determination alone, when starting new therapeutic regimens with P-gp substrates, especially in individuals over 60 years of age (Vilas-Boas et al. 2011).

Similarly, and as previously mentioned, Takara et al. also reported that P-gp transport function remained unchanged in Caco-2 cells exposed to several NSAIDs, in spite of the observed increases in *MDR1* mRNA levels (Takara et al. 2009). In fact, the expression of *MDR1* mRNA in these cells was significantly increased by diclofenac, fenbufen, indomethacin, and nimesulide. However, pre-treatment for 48 h with diclofenac, indomethacin, or nimesulide, but not fenbufen, resulted in a significant increase in cellular RHO 123 accumulation, an apparently contradictory effect with the observed increase in *MDR1* mRNA expression (Takara et al. 2009). Furthermore, the NSAIDs-elicited increases in the *MDR1* mRNA expression were not accompanied by changes in P-gp function given that no significant changes in RHO 123 efflux occurred (Takara et al. 2009). Therefore, since the observed increase in RHO 123 accumulation was inconsistent with the upregulation of *MDR1* mRNA expression, it was proposed that some carriers participating in the incorporation of the fluorescent substrate may be activated by pre-treatment with the NSAIDs. Thus, it was proposed that the increased *MDR1* mRNA was not translated into increased P-gp expression. In accordance, Giessmann et al. also reported that carbamazepine significantly increased the expression of *MDR1* mRNA in the

lower duodenum of healthy humans (biopsy of tissue specimens), but did not affect the level of MDR1 protein (Giessmann et al. 2004). This later study suggested that carbamazepine affected: 1) the translation from *MDR1* mRNA to MDR1 protein, 2) the post-translational protein synthesis, or 3) the movement to the cell-membrane surface of the MDR1 protein (Giessmann et al. 2004). Therefore, it was proposed that similar phenomena might occur in the case of NSAIDs (Takara et al. 2009). However, from the analysis of our data on the effect of DOX on P-gp expression and activity (Manuscript I), this explanation is not applicable, as the protein is indeed in the cell surface, and this poor correlation between the extent of P-gp expression and its activity was probably related to the lack of function of the newly expressed P-gp on the surface of the Caco-2 cells. According to a previous report on this *in vitro* model, although P-gp appears to be continuously expressed in Caco-2 monolayers, it may not be fully functional at an early stage in culture (Hosoya et al. 1996).

Another compound tested, in the scope of the present thesis, for its ability to increase P-gp expression and/or activity was colchicine (Manuscript III), an alkaloid with a narrow therapeutic index used to treat gout, pseudogout and familial Mediterranean fever (Ben-Chetrit and Levy 1991; Famaey 1988; Niel and Scherrmann 2006). This compound is a known P-gp substrate (Ambudkar et al. 1999; Decleves et al. 1998; El Hafny et al. 1997a; Niel and Scherrmann 2006) and was also previously reported to have P-gp inducing properties, both *in vitro* and *in vivo* (Decleves et al., 1998; Licht et al., 2000; Vollrath et al., 1994). In fact, colchicine was shown to increase the *mdr* mRNA levels in rat liver *in vivo,* as early as 3 h after a single injection (2 mg/kg, i.p.), peaking after 24 h (Vollrath et al. 1994). Additionally, Declèves et al. (1998) also demonstrated that colchicine (25 nM) was able to significantly increase P-gp expression in the promyelocytic HL-60 cell line after 24 h of exposure (Decleves et al. 1998). However, the ability of colchicine to modulate the activity of this important efflux transporter was not evaluated in these previous studies. According to our results, colchicine was able to significantly induce P-gp expression, in a concentration-dependent manner, up to 183%, as compared to control, for the highest colchicine concentration tested (100 μM) and for an incubation period of 24 h (at 0.5, 1, 5, 10, 50 and 100 μM colchicine, P-gp expression significantly increased by 129, 135, 145, 150, 154 and 183%, respectively, as compared to control cells) (Manuscript III). However, in what concerns to the pump´s activity, no significant differences were observed neither in the RHO 123 accumulation nor in the efflux of the dye, for all the tested colchicine concentrations and 24 h after exposure. Therefore, these results suggest that, although P-gp is being expressed at higher levels and incorporated in the cell membrane, the pump may not be yet fully functional. Periods longer than 24 h were not tested for this compound, given its significant toxicity towards Caco-2 cells.

Indeed, colchicine exposure resulted in a concentration-dependent cytotoxicity that was significant after 48 h of incubation and increased over time. Furthermore, since colchicine is a known P-gp substrate, which was also confirmed by the significant increase observed in P-gp ATPase activity (23 nmol Pi liberated/mg protein/min for 100 μM colchicine, when compared to 15 nmol Pi liberated/mg protein/min for basal P-gp vanadate-sensitive ATPase activity), it was proposed that this compound may compete with RHO 123 for P-gp-mediated transport. To better understand the colchicine mode of action, pharmacophores for competitive and noncompetitive P-gp inhibitors were created, based on previously reported data obtained from the ATPase assay for twenty three noncompetitive and for nineteen competitive inhibitors, including newly synthetized thioxanthonic derivatives and commercial drugs (Palmeira et al. 2011; Palmeira et al. 2012c) (Manuscript III). In spite of all the pharmacophore models for P-gp inhibition described in the literature (Chen et al. 2012a; Palmeira et al. 2012a; Palmeira et al. 2012b), a clear distinction between pharmacophores for competitive and noncompetitive inhibitors has never been accomplished before, being described herein for the first time (Manuscript III). In accordance with the *in vitro* results, colchicine was fit onto the pharmacophore for competitive P-gp inhibitors, but was not able to align to the noncompetitive P-gp inhibitors pharmacophore. Therefore, these data suggest that colchicine is not only a P-gp inducer (demonstrated by computational and biochemical results), but it may also be transported by P-gp, acting as a competitive P-gp inhibitor. However, the present results are in disagreement with the model proposed by Shapiro et al., which suggested two different P-gp functional binding sites (H site and R site) that interact in a positive cooperative manner. Being colchicine part of the H-type of P-gp substrates, according to the proposed model, it should activate the efflux of specific substrates of the R site, such as RHO 123 (Shapiro and Ling 1997c). Indeed, and in disagreement with our findings, it was demonstrated that colchicine stimulated RHO 123 transport and inhibited the transport of Hoechst 33342, an H-type substrate, in plasma membrane vesicles prepared from CH(R)B30 cells (Shapiro and Ling 1997c), but a different *in vitro* model was used in this study.

Finally, another compound tested for its induction ability was hypericin (HYP), one of the major components of St. John's wort, a flower extract that was reported to be responsible for several pharmacokinetic interactions, partially mediated by its effects on P-gp expression (Perloff et al. 2001b). However, its ability to modulate the pump's expression has been mainly attributed to hyperforin (Tian et al. 2005). Our results demonstrated that HYP significantly increased both P-gp expression and activity, according to the concentration and time of exposure tested (Manuscript IV). Moreover, a good correlation was observed between the HYP-elicited increases in P-gp expression

and activity. For example, exposure of Caco-2 cells to 10 μM HYP for 48 h significantly increased P-gp expression and activity by 147% and 142 %, respectively. In comparison, 48 h after exposure to 10 μM doxorubicin, P-gp expression and activity increased by 513% and 136 %, respectively. Additionally, newly synthetized (thio)xanthonic derivatives were also tested for their effects on both P-gp expression and activity, showing a good correlation between both effects, which will be further discussed in section IV.5.

In conclusion, our data demonstrated three different scenarios of P-gp induction: 1) increased cell surface P-gp expression followed by increases in pump activity, but to a different magnitude (as shown with doxorubicin); 2) increased P-gp protein expression with no changes in its activity (colchicine); and 3) proportional increases in both P-gp expression and activity [HYP and (thio)xanthonic derivatives]. Therefore, these results emphasize the importance of the simultaneous evaluation of both P-gp expression and activity in the screening of P-gp inducers, since an increase in the former may not be reflected in an increase in the later. Consequently, for the evaluation of potential protective effects mediated by P-gp inducers, it is of utmost importance to evaluate if the inducer is able not only to increase P-gp protein expression, but specially if it is able to promote the cellular efflux of toxic xenobiotics actively transported by the pump, which will eventually lead to decreased intracellular accumulation and, consequently, decreased toxicity. Also, it is important to note that, as previously mentioned, the evaluation of P-gp expression should be performed at the protein level, since an increase in *MDR1* RNA may not necessarily be translated into increased protein expression.

IV.3. P-gp induction as a potential therapeutic pathway in real life intoxication scenarios

Considering the observed effects of the tested compounds on both P-gp expression and activity, we further aimed to validate the mechanistic approach of P-gp induction as an effective way to reduce the intracellular accumulation of harmful compounds actively transported by this efflux pump and, consequently, to significantly reduce their cytotoxicity, using paraquat (PQ) as a model substrate. Indeed, this antidotal pathway has already been proposed, *in vivo,* as a new therapeutic approach for PQ poisonings, due to the decreased intestinal absorption and, consequently, increased intestinal excretion of the herbicide as a result of dexamethasone-mediated induction of *de novo* synthesis of P-gp (Dinis-Oliveira et al. 2006a; Dinis-Oliveira et al. 2006c). However, in these *in vivo* studies, mechanisms other that P-gp induction, such as dexamethasone anti-inflammatory effects, may also be involved in the observed protection of intoxicated rats (dexamethasone increased the survival rate by 50%). Therefore, to specifically address the contribution of

P-gp induction, PQ cytotoxicity was initially evaluated *in vitro* with and without pre-incubation with the tested inducer for 24, 48 or 72 h. In these studies, cells do not simultaneously contact with both PQ and the inducer in the incubation medium, and the observed effects can be more accurately correlated with the observed P-gp induction. The results showed that pre-exposure of Caco-2 cells to doxorubicin (DOX) for 24 h resulted in a significant decrease in PQ cytotoxicity, as shown by the PQ + DOX concentration-response curves shift to the right, and by the corresponding significant increases in EC_{50} values of the fitted curves (1825, 1899, 1853, and 1806 µM when the cells were pre-exposed to 5, 10, 50 and 100 µM DOX, respectively, when compared to 1047 µM for the PQ curve) (Manuscript I). However, the increases in the EC_{50} values were not concentration-dependent, which can be explained by the small differences observed in P-gp transport activity, in spite of the significant differences observed in P-gp expression levels at these DOX concentrations. Therefore, although the P-gp expression levels increased in a concentration-dependent manner upon exposure to DOX, the P-gp activity did not increase proportionally and, thus, the magnitude of the expected protective effect against PQ did not increase in a similar trend.

In what concerns to HYP, pre-exposure of Caco-2 cells to this inducer (1, 5 and 10 µM) for 24 h also significantly reduced PQ cytotoxicity, resulting in significant differences in the cell death observed for the higher PQ concentrations (1000 - 5000 µM) (Manuscript IV). Moreover, it was also possible to observe a significant rightwards shift of all the PQ + HYP curves, when compared to the PQ curve, as previously observed for all the PQ+DOX curves. However, for the 5 and 10 µM HYP concentration, a significant reduction in the maximal cell death (TOP value) was observed and, consequently, the EC_{50} value of the fitted curves could not be used for comparison. Indeed, pre-exposure to 5 and 10 µM HYP for 24 h resulted in a significant decrease in the TOP value by 67.49 and 63.80 %, respectively, when compared to the TOP value of the PQ curve (92.46 %). Additionally, given the technical interference of HYP in the MTT reduction assay (similar blue color to the formed formazan crystals) that was used for the DOX studies, the evaluation of PQ's cytotoxicity profile was performed by using the neutral red uptake assay. Therefore, two different methods were used for the estimation of cell viability and, consequently, the comparison between the protective effects of these inducers is limited.

As observed for DOX, the HYP protective effect after 24 h of pre-exposure was not concentration-dependent, as no significant differences were observed between the PQ + HYP curves. Once again, this result is in accordance with the small differences in P-gp activity observed 24 h after exposure to HYP (116, 118 and 129 % for 1, 5 and 10 µM HYP, respectively). The HYP protective effects against PQ-induced cytotoxicity were also evaluated with higher pre-exposure HYP incubation times, namely 48 and 72 h

(Manuscript IV). For both these pre-exposure incubation times, a significant protection against PQ cytotoxicity was also observed, resulting in significant rightwards shift of all the PQ + HYP curves, when compared to the PQ curve. Moreover, 48 and 72 h after pre-exposure to HYP no significant differences were observed neither in the TOP value, nor in the in baseline (BOTTOM) of the fitted curves and, therefore, the EC_{50} values were used for comparison. Pre-exposure of Caco-2 cells to HYP for 48 h resulted in significant increases in the EC_{50} values of all PQ + HYP curves (3243, 4490 and 4493 μM for 1, 5 and 10 μM HYP, respectively, *vs*. 1692 μM for the PQ curve), and significant differences were observed between the PQ + HYP 1 curve and the PQ + HYP 5 or 10 curves (Manuscript IV). When increasing HYP pre-exposure time to 72 h, the EC_{50} value of all the PQ + HYP curves significantly increased to 3843, 4518 and 4609 μM for 1, 5 and 10 μM HYP, respectively, when compared to 1783 μM for the PQ curve. Moreover, significant differences between all the fitted PQ + HYP curves were observed for this last pre-exposure incubation time. Additionally, the overall comparison of all the PQ + HYP curves obtained for all the pre-exposure times (24, 48 and 72 h) highlighted significant differences in the observed decreases in cell death, according to the HYP concentration and time of pre-exposure, which is correlated with the observed effects of HYP on both P-gp expression and activity. However, the main differences were found between 1 μM HYP and 5 or 10 μM HYP, and between 24 h and 48 or 72 h of pre-exposure. For example, by comparing HYP pre-exposure incubation times, at each tested HYP concentration, only small differences were detected in the protective effects observed with pre-exposure to HYP for 48 and 72 h. In accordance with these results, small differences were also observed in P-gp transport activity after exposure of Caco-2 cells to HYP for these incubation times (120, 122 and 142 % after 48 h of exposure to 1, 5 and 10 μM HYP, respectively, when compared to 119, 129 and 150 % after of 72 h exposure to 1, 5 and 10 μM HYP, respectively). Therefore, these results highlight that the inducer protective effects against PQ cytotoxicity are highly dependent on its effects on P-gp activity.

Furthermore, to clarify if the observed protective effects on the toxicity of the herbicide are only dependent on the P-gp induction effects, PQ cytotoxicity was also evaluated in the presence of a specific P-gp inhibitor, the UIC2 antibody. In all cases, the previously observed protective effects afforded by both DOX and HYP (in the pre-exposure experimental design) were completely abolished under P-gp inhibition, demonstrating that the observed protective effects are exclusively mediated by P-gp (Manuscript I and Manuscript IV).

For the validation of P-gp induction as an effective way to significantly reduce the toxicity of P-gp substrates other experimental designs were also tested. Therefore, we further aimed to reflect a real-life intoxication scenario, in which the potential antidote

exerts its protective effects well after the intoxicant contacts with the target tissues. Consequently, PQ exposure of Caco-2 cells was evaluated with and without incubation with DOX or HYP 6 h after the beginning of PQ exposure, taking into account, thus, the estimated average arrival time of the patient to the hospital after PQ intoxication (Dinis-Oliveira et al. 2008).

Exposure of Caco-2 cells to DOX (5, 10, 50 and 100 µM) 6 h after the beginning of PQ incubation also resulted in significant rightwards shifts of all PQ+DOX curves, when compared to the PQ curve, thus reflecting a protective effect against the herbicide cytotoxicity (Manuscript II). However, surprisingly, it was demonstrated that exposure of these cells to DOX only 6 h after PQ, over a 24 h period of incubation (with a total incubation time of 18 h for DOX), resulted in a more pronounced protection against PQ cytotoxicity, when compared to the results obtained with the pre-exposure to DOX for 24 h before PQ incubation. Indeed, this higher protection can be observed by the astonishing decreases in the observed maximal cell death (TOP value) and by the more pronounced rightwards shifts of all the PQ+DOX curves obtained with this experimental design developed to mimic a real-life intoxication scenario. Moreover, the observed decreases in the TOP values of the fitted curves were concentration-dependent, down to 88.1, 81.5, 48.4 and 38.9% maximal cell death, for 5, 10, 50 and 100 DOX, respectively, when compared to 93.7 % for the PQ curve. However, contrarily to what was observed in the pre-exposure assay, under P-gp inhibition, the protective effects of DOX, when incubated 6 h after the PQ insult, were not completely prevented by the UIC2 antibody. The comparison between the PQ + DOX and PQ + DOX + UIC2 curves demonstrated that the DOX protective effects were partially due to P-gp, given the leftwards shift and increased maximal cell observed in the presence of UIC2. However, the comparison between the PQ + UIC2 and the PQ + DOX + UIC2 curves demonstrated that, even under P-gp inhibition, DOX was still able to protect Caco-2 cells against PQ-induced toxicity. Thus, these results suggest that mechanisms other than P-gp induction were involved in DOX protective effects. Furthermore, these results were supported by the PQ intracellular levels that were significantly reduced by DOX (for the PQ exposure concentrations of 2500 and 5000 µM, intracellular levels were reduced to 35.03 and 46.25 nmol PQ/mg protein for PQ+DOX 50, compared to 51.81 and 97.71 nmol PQ/mg protein for PQ only, respectively), even in the presence of the UIC2 antibody (49.19 and 73.13 nmol PQ/mg protein for PQ+DOX 50+UIC2 *vs.* 78.41 and 106.59 nmol PQ/mg protein for PQ+UIC2) (Manuscript II). Knowing that the carrier-mediated transport system for choline is involved in PQ intestinal absorption (Nagao et al. 1993) (see IV.4) and that, in Caco-2 cells, this transport system is inhibited by P-gp substrates, such as daunomycin and verapamil, it was hypothesized that the DOX protective effects observed when the inducer was added

6 h after PQ could also be a result of the inhibition of this transport system. According to our results, and as expected given its structural similarity with daunomycin, DOX significantly inhibited choline intracellular accumulation in Caco-2 cells (incubation with 5, 10, 50 and 100 μM DOX, significantly reduced intracellular ^{3}H-choline to 42.9, 31.3, 19.9 and 16.9% of the control value, respectively). Consequently, its protective effects against PQ cytotoxicity result from a concerted action via two distinct mechanisms, the choline transport inhibition and the increased P-gp expression/activity in Caco-2 cells, which result in decreased intracellular PQ accumulation and, thereby, decreased toxicity.

In what concerns to HYP, the incubation of this inducer 6 h after the beginning of PQ insult also resulted in a significant protection of Caco-2 cells against the herbicide cytotoxicity, as observed by the significant increases in the EC_{50} values of the PQ + HYP curves, when compared to the PQ curve (2408 and 2437 μM for PQ + HYP 5 and PQ + HYP 10, respectively, *vs.* 1268 μM for the PQ curve) (Manuscript IV). However, the astonishing protection observed for DOX was not observed with HYP. The observed protection was dependent on HYP concentration, with significant differences between the PQ + HYP 1 curve and the PQ + HYP 5 or 10 curves. Additionally, contrarily to DOX, the observed protective effects were completely abolished under P-gp inhibition, demonstrating that P-gp induction is the major mechanism involved in HYP-mediated protection. Moreover, the huge differences in DOX protective effects observed according to the adopted experimental design of inducer incubation were not evident in the case of HYP.

Using a third experimental design, HYP protective effects were also evaluated after simultaneous incubation of Caco-2 cells with PQ for 24 h to mimic the presence of the potential antidote in the PQ formulation to prevent the intoxication upon ingestion. It is noteworthy that the incorporation of an inducer in the PQ formulation will overcome the disadvantage of the critical time between intoxication and treatment, with an expected increase in survival rate and decrease in morbidity. Indeed, such strategy of adding the antidote to the toxic formulation was already tested *in vivo* (Baltazar et al. 2013; Wilks et al. 2008). For example, in 2004, a new PQ formulation designed to reduce its toxicity was introduced by Syngenta in Sri Lanka, under the trade name Inteon® (Wilks et al. 2008). This new formulation included three components designed to reduce PQ absorption: (i) an alginate to thicken the formulation in the acidic environment of the stomach; (ii) an increase in the amount of emetic to induce vomiting more quickly; (ii) a purgative to speed its elimination from the small intestine, which is the main site of PQ absorption (Wilks et al. 2008). This study has shown that Inteon® reduces the mortality of patients following PQ ingestion and increases survival time. Additionally, in a very recent study, other authors aimed to develop a safe PQ formulation with the incorporation of lysine acetylsalicylate

(LAS) and to evaluate, *in vivo*, its potential applicability as an effective antidote (Baltazar et al. 2013). Indeed, it had been previously demonstrated by the same research group that sodium salicylate (NaSAL) has a great potential to be used as an antidote against PQ-induced lung toxicity, through an effective inhibition of pro-inflammatory factors such as NF-κB, scavenging of ROS, inhibition of myeloperoxidase activity, inhibition of platelet aggregation and by preventing death of pulmonary cells through apoptotic pathways (Dinis-Oliveira et al. 2007a; Dinis-Oliveira et al. 2007b). Importantly, this treatment was associated with full survival of PQ-intoxicated rats (Dinis-Oliveira et al. 2007a; Dinis-Oliveira et al. 2007b). Subsequently, since LAS releases salicylate *in vivo* and is available in hospitals for parenteral administration, in that previously mentioned study, the rats were intoxicated with a mix of the commercial PQ formulation (Gramoxone®) with increasing concentrations of LAS. This new formulation was administered to Wistar rats by gavage at 125 mg kg^{-1} body weight of PQ and 79, 158 or 316 mg kg^{-1} body weight of LAS, and the survival rate was observed for 30 days (Baltazar et al. 2013). According to the reported data, the survival rate of the PQ group was only 40%, while LAS provided and effective protection, with full survival observed in the groups that received 125 mg kg^{-1} of PQ and 316 mg kg^{-1} of LAS (Baltazar et al. 2013).

According to our results, simultaneous incubation of Caco-2 cells with both PQ and HYP also resulted in a significant protection against PQ-induced cytotoxicity, as observed by the significant reduction in the cell death for the higher PQ concentrations (500 - 5000 μM), resulting in a significant rightwards shift of all the PQ + HYP curves, when compared to the PQ curve (Manuscript IV). Moreover, for 5 and 10 μM HYP, a significant increase in the EC_{50} values of the fitted curves was observed (2400 and 2469 μM, for 5 and 10 μM HYP, respectively, *vs*. 1240 μM for the PQ curve). Again, significant differences were observed between the PQ + HYP 1 curve and the PQ + HYP 5 or PQ + HYP 10 curves, demonstrating that HYP protective effects depend on its concentration. Additionally, and as observed for the other experimental designs of HYP incubation, the protective effects were completely abolished under P-gp inhibition with the UIC2 antibody. However, no significant differences in the observed protection against PQ-induced cytotoxicity exist between these last two different experimental designs of HYP incubation (simultaneous exposure and exposure 6 h after PQ insult), which could be explained by the slow PQ absorption rate reported in humans, which occurs over 1-6 h (Dinis-Oliveira et al. 2008). In the case of rapidly absorbed P-gp toxic substrates, the presence of the potential inducer in the toxic formulation could be faced as the first therapeutic measure employed to limit their absorption, but may not prove as efficient in slowly absorbed substrates. Additionally, since HYP protective effects against PQ cytotoxicity, observed under the several experimental designs used, were completely prevented by UIC2-mediated P-gp inhibition,

this compound is an excellent candidate for drug design of new, potent and specific P-gp inducers, and for the study of potential protective effects against toxic P-gp substrates mediated only by P-gp induction.

Furthermore, the comparison between the PQ and PQ + UIC2 curves obtained in each experiment demonstrated a significant increase in PQ cytotoxicity under P-gp inhibition, further supporting that P-gp modulation has an important impact on the herbicide cytotoxicity. In accordance, GF120918, another P-gp inhibitor, significantly enhanced PQ-induced cytotoxicity in a cellular model of the rat blood-brain barrier (BBB), the RBE4 cells, as a result of increased intracellular accumulation of the herbicide 48 h after simultaneous exposure to both inhibitor and herbicide (Vilas-Boas et al. 2013a). Therefore, these observations reinforce the fact that PQ is a substrate for P-gp also at the BBB, which may limit its access to the brain and, therefore, reduce its neurotoxic effects that have been recently a matter of debate and ultimately led to the withdrawal of the herbicide from the EU market (Dinis-Oliveira et al. 2006b).

In the case of colchicine, given the lack of significant increases in P-gp transport activity, the effects of this compound on PQ cytotoxicity were not further evaluated.

In accordance with our results, other *in vitro* studies have demonstrated that P-gp induction represents an interesting antidotal pathway against PQ toxicity. It was reported that metilprednisolone significantly reduced PQ cytotoxicity in the alveolar A549 cell line, an effect attributed to the P-gp induction caused by this synthetic corticosteroid (Zerin et al. 2012). Indeed, metilprednisolone (200 μg/mL) significantly increased both *MDR1* mRNA and P-gp protein levels as soon as 3 h after incubation, which was accompanied by a significant decrease in the calcein fluorescence, thus reflecting increased pump activity (Zerin et al. 2012). Therefore, these results suggest that metilprednisolone activates P-gp expression, which leads to increased levels in the efflux pump activity and, consequently, to detoxification in the PQ-treated A549 cells. However, no further studies were performed to elucidate if mechanisms other than P-gp induction could also contribute to the observed results, since the metilprednisolone protective effects were not evaluated under P-gp inhibition. In fact, although P-gp expression level increased upon exposure to metilprednisolone, the magnitude of the expected protective effect against PQ-induced cytotoxicity did not increase to a similar extent. Therefore, it is highly probable that the anti-inflammatory effect of the corticosteroid might also contribute to lowering the PQ deleterious effects on lung toxicity.

Recently, a reduced rifampicin derivative, RedRif, was also able to significantly protect RBE4 cells against PQ-induced cytotoxicity, by significantly increasing both P-gp expression and activity (Vilas-Boas et al. 2013b). In fact, in that study, the protective effects were observed with pre-treatment of RBE4 cells with 10 μM RedRif for 24 or 72 h

before a 48h-PQ exposure (0.5-50 mM). Protection also occured after simultaneous exposure to 10 µM RedRif and PQ (0.5-50 mM) for 48 h, and these protective effects were completely reverted in the presence of GF120918 (Vilas-Boas et al. 2013b). Therefore, these results demonstrate that, for this rifampicin derivative, mechanisms other than P-gp induction are not likely to be involved in the observed protective effects.

In conclusion, our *in vitro* data validate the strategy of P-gp induction as an effective antidotal pathway against the cytotoxicity of P-gp substrates, such as PQ, by significantly increasing their cellular efflux, thus reducing their intracellular accumulation and, consequently, their toxicity. More importantly, in the case of PQ, systemic access of the herbicide to the target organs of toxicity, namely the lung, kidney, and brain, can be significantly limited. Additionally, these results highlight that this mechanistic approach could be efficiently used in real-life intoxication scenarios, demonstrating that it is possible to significantly reduce the toxicity of these toxic substrates even when the P-gp inducer contacts with the cells well after the toxic xenobiotic. Moreover, compounds that have the ability of both inhibiting the xenobiotics entrance and increasing their excretion, such as DOX in the specific case of PQ, are promising new sources of antidotal pathways to be explored. The inclusion of a P-gp inducer in the toxic substrate formulation may also greatly contribute to limiting toxicity, especially if the substrates are readily absorbed at the gastrointestinal tract.

IV.4. Paraquat uptake into Caco-2 cells - Involvement of multiple transport systems

The previously reported effect of DOX on the choline uptake shifted our attention towards better understanding the mechanisms involved in the PQ intestinal absorption. Noteworthy, although PQ is responsible for thousands of deaths due to accidental or intentional ingestion, little is known on the mechanisms of its intestinal uptake, namely about the transporters specifically involved. Therefore, we further aimed to clarify the herbicide uptake in Caco-2 cells, based on previous results on PQ uptake in other organs, such as the lung and the brain, where specifically the polyamines and the neutral amino acid transport systems, respectively, were implicated (Rose et al. 1974; Shimizu et al. 2001; Smith 1982; Wyatt et al. 1988).

Based on the observed DOX effect on choline uptake, the first transport system investigated was the choline uptake system (Manuscript V). Indeed, this transport system was, as previously mentioned, already implicated in the intestinal transport of PQ, using rat's brush-border membrane vesicles as the *in vitro* model (Nagao et al. 1993). In that study, PQ (0.5 mM) uptake was significantly reduced in the presence of choline (10 mM),

a structurally-related organic cation (Nagao et al. 1993). However, a single PQ concentration, that was much lower than the choline concentration, was tested.

According to our results, a significant reduction of PQ toxicity was observed in the presence of both choline and hemicolinium-3 (HC-3), a natural substrate and a competitive inhibitor for this transport system, respectively (Manuscript V). Moreover, two different experimental designs were performed, namely simultaneous exposure and exposure to choline or HC-3 6 h after PQ insult. As previously observed for HYP, no significant differences were found in the observed protection against PQ cytotoxicity between both experimental designs, which may also be explained by a slow PQ uptake in these cells. Additionally, the observed protective effects of both choline and HC-3 on PQ cytotoxicity were not concentration-dependent, which may occur due to the saturable activity of this transport system in Caco-2 cells (Kamath et al. 2003). Furthermore, in accordance with the significant reduction in cell death observed in the presence of both choline and HC-3, a significant decrease in PQ intracellular levels was observed (after exposure to 1000, 2500 and 5000 µM PQ alone, the intracellular PQ levels were 56.21, 150.07 and 189.98 nmol PQ/mg protein, respectively; with simultaneous exposure to 500 µM choline and PQ for 24 h, PQ intracellular levels were significantly reduced to 90.89 and 109.32 nmol PQ/mg protein, for 2500 and 5000 µM PQ + CHO, respectively; with simultaneous exposure to 500 µM HC-3 and PQ for 24 h, PQ intracellular levels were significantly reduced to 25.88, 94.50 and 118.86 nmol PQ/mg protein, for 1000, 2500 and 5000 µM PQ + HC-3, respectively) (Manuscript V). Therefore, the choline transport system is clearly involved on PQ uptake in Caco-2 cells, and choline or HC-3, by competing with PQ for the transport, significantly reduced the intracellular levels of the herbicide and, consequently, its cytotoxicity.

In accordance with our results in Caco-2 cells, it was reported that the choline uptake system is also involved in PQ uptake in RBE4 cells (Vilas-Boas et al. 2013a). Indeed, PQ's cytotoxic profile was assessed in the presence of HC-3, and a significant increase in cell viability was observed (significant increase in PQ's EC_{50} value), and such an effect was accompanied by a significant decrease in PQ intracellular levels observed in the presence of the competitive inhibitor of the choline-uptake system (Vilas-Boas et al. 2013a). Therefore, these results suggest that the choline uptake system seems to be also involved in the PQ uptake at the BBB and may potentially modulate the neurotoxic effects of this herbicide.

The mechanisms of PQ uptake were also studied by assessing the influence of other transporters previously described as uptake pathways for PQ, such as the large neutral amino acid transport system [using L-Valine (VAL) as substrate], the basic amino acid transport system [using arginine (ARG) and lysine (LYS) as substrates, and N-

ethylmalemide (NEM) as inhibitor], and the polyamine uptake system [using putrescine (PUT) as substrate, and trifluoperazine (TFP) as inhibitor] (Manuscript V).

The polyamine uptake system was the first transporter implicated in PQ uptake, and has long been considered responsible for its high accumulation rate in its main target organ, the lung (Rose et al. 1974; Smith 1982; Wyatt et al. 1988). According to our results, the polyamine uptake system may also be involved in PQ accumulation in Caco-2 cells, since the simultaneous exposure to PQ and PUT (substrate) for 24 h caused a significant reduction in PQ intracellular levels (100.16 and 130.94 nmol PQ/mg protein for 2500 and 5000 μM PQ + PUT 250, respectively, when compared to 150.07 and 189.98 nmol PQ/mg protein for PQ alone), resulting in a significant reduction in its cytotoxicity (Manuscript V). In accordance with our results, in the IEC-6 rat small intestine epithelial cell line, this transport system was also implicated in PQ uptake (Grabie et al. 1993). Indeed, PQ absorption was greatly inhibited by PUT and the herbicide acted as a competitive inhibitor of PUT uptake (Grabie et al. 1993). However, the slower rate of PQ uptake, when compared to the rate of PUT uptake, suggested that PQ has a lower affinity for the transporter (Grabie et al. 1993). Furthermore, in IEC-6 cells, this polyamine uptake system was characterized as being energy-dependent, saturable, and modulated by a calcium/calmodulin (Ca^{2+}/CaM) complex-dependent mechanism (Grabie et al. 1993; Groblewski et al. 1992). In accordance, our results also suggest that, in Caco-2 cells, PQ uptake is also regulated by a Ca^{2+}/CaM complex-dependent mechanism, as observed by the significant reduction in the herbicide intracellular content and, consequently, in its toxicity, after simultaneous exposure to the potent competitive inhibitor of the Ca^{2+}/CaM complex, TFP (Manuscript V). Additionally, other studies had also reported this Ca^{2+}/CaM sensitiveness of the polyamine transport in cultured gastrointestinal epithelial cells (Groblewski et al. 1992; Scemama et al. 1993; Sharpe and Seidel 2005). Moreover, our results highlight that only small differences exist in PQ cytotoxicity in the presence of the different PUT concentrations tested (PQ EC_{50} value of 1786, 1840 and 1863 μM obtained in the presence of 50, 100 and 250 μM PUT, respectively, *vs.* 1088 μM for PQ alone), which can be explained by the previously referred saturable activity of this transporter (Grabie et al. 1993).

Additionally, since in IEC-6 cells polyamines and basic amino acids, such as LYS and ARG (both positively charged at neutral pH) are, given their structural similarity, absorbed through a common carrier, the y^+ amino acid transport system (Sharpe and Seidel 2005), we hypothesized that mechanisms other than the polyamine uptake system may also contribute to the marked effect of PUT on PQ uptake into Caco-2 cells. Indeed, we verified that both LYS and ARG significantly reduced PQ accumulation in Caco-2 cells, resulting in a significant reduction in the herbicide toxicity. Moreover, in accordance with

the results in IEC-6 cells, where PUT inhibited approximately 75 % of LYS transport (Sharpe and Seidel 2005), our results also clearly demonstrated that LYS uptake, in Caco-2 cells, was significantly inhibited by PUT, thus also confirming that a significant fraction of the LYS transport is polyamine sensitive (Manuscript V). Therefore, these results indicate the presence of a common transporter in Caco-2 cells for polyamines and basic amino acids, as observed in the IEC-6 cells, which seems to be the y^+ amino acid transport system, since LYS uptake in Caco-2 cells was sensitive to NEM, an inhibitor of this transport system (Pan et al. 1995; Sharpe and Seidel 2005). Accordingly, NEM was also previously reported to significantly reduce LYS and ARG uptake in IEC-6 cells (Pan et al. 1995; Sharpe and Seidel 2005). Moreover, in our study, PQ cytotoxicity in Caco-2 cells was also significantly reduced in the presence of NEM, as a result of a significant decrease in its intracellular accumulation, further supporting the involvement of the y^+ amino acid transport system in PQ uptake in Caco-2 cells. Additionally, and as observed by Sharpe and Seidel using the IEC-6 cells (Sharpe and Seidel 2005), in our study, LYS uptake into Caco-2 cells was also Ca^{2+}/CaM sensitive, resulting in the observed significant reduction in LYS uptake in the presence of TFP. Thus, the protective effect against PQ induced toxicity observed under simultaneous exposure of Caco-2 cells to PUT, ARG, LYS, NEM or TFP, which is a consequence of a decreased PQ uptake, seems to be partially mediated by the y^+ transport system. Furthermore, knowing that the y^+ system is selective for cationic amino acids (interacting weakly with neutral amino acids) (Deves and Boyd 1998), our results indicate that basic amino acids uptake systems other than the y^+ transport system seem to be also involved in PQ and LYS uptake, since a significant reduction on both PQ and LYS accumulation was observed in the presence VAL, a neutral amino acid. Moreover, the observed reduction in PQ intracellular accumulation in the presence of VAL also resulted in a significant decrease in PQ-mediated cytotoxicity.

Three other transport systems for cationic amino acids have already been characterized namely, the $b^{0,+}$, y^+L, and $B^{0,+}$ systems, which, contrarily to the y^+ system, accept a wider range of substrates, including both cationic and neutral amino acids (Deves and Boyd 1998). Moreover, the cationic amino acids transport systems differ in their interactions with inorganic monovalent ions (Deves and Boyd 1998). According to the Na^+ dependency, the y^+ and $b^{0,+}$ systems are Na^+-independent, while the $B^{0,+}$ system is Na^+-dependent (Deves and Boyd 1998). On the other hand, the y^+L system exhibits a more complex pattern in its cation interaction, being the transport of basic amino acids, such as LYS, unaffected by Na^+ replacement, whereas its affinity towards neutral amino acids is dramatically decreased if Na^+ in the medium is replaced by K^+ (Deves and Boyd 1998).

In Caco-2 cells, the transporters involved in the LYS uptake were already characterized (Ferruzza et al. 1995; Thwaites et al. 1996). It was demonstrated that the uptake of LYS across monolayers of differentiated Caco-2 cells occurs via one or more Na^+-independent carriers, which were able to transport cationic amino acids but also shared by large neutral amino acids (Ferruzza et al. 1995). Moreover, it was also demonstrated that, in these cells, the $b^{0,+}$, y^+ and a nonsaturable component represented 47%, 27%, and 26%, respectively, of the total apical LYS uptake (Thwaites et al. 1996). The uptake of ARG, another basic amino acid, in the apical membranes of Caco-2 cells was also evaluated and equally characterized as mediated predominantly by Na^+-independent mechanisms (Pan et al. 1995; Pan et al. 2002). Moreover, the major pathways involved were y^+ (70%) and y^+L or $b^{0,+}$ (30%) systems (Pan et al. 2002). In accordance, given the significant reduction in LYS and PQ uptake caused by VAL, and the significant reduction observed on PQ toxicity in the presence of this neutral amino acid, our results suggest that PQ, LYS (and ARG) and VAL may be sharing a common carrier, namely the y^+L or $b^{0,+}$ systems.

However, contrarily to what was demonstrated in our studies performed in Caco-2 cells, at the BBB, the basic amino acid transporter was not involved in PQ uptake (Shimizu et al. 2001). According to the study reported by Shimizu et al., using the brain microdialysis technique with HPLC/UV detection, it was clearly demonstrated that PQ penetrates the BBB in a dose-dependent manner (Shimizu et al. 2001). Indeed, the obtained data indicated that the penetration of PQ into the brain would be mediated by a specific carrier process, not resulting from the destruction of BBB function by PQ itself or by a PQ radical. Moreover, although lung damage induced by PQ was initially suggested to be initiated, at least in part, by an energy-dependent accumulation through an uptake system shared by polyamines (Smith 1982), the polyamine transporters are not expressed in the BBB structure, since the BBB penetration of the polyamines is restricted (Shin et al. 1985). Therefore, from the chemical structure of PQ, it was assumed that the possible carrier involved in the BBB penetration would be one of the amino acid transporters, which are highly expressed in the BBB (Shimizu et al. 2001). In fact, the BBB penetration of PQ was significantly inhibited in rats pre-treated with VAL, but not with LYS, which are high affinity substrates for neutral and basic amino acid transporters, respectively (Shimizu et al. 2001). Moreover, the evidence that the ratio of brain extracellular to blood concentrations of PQ in VAL-treated rats was lower, also strongly supported the conclusion that both substances shared the same transport system. Although VAL is a high affinity substrate for both neutral and basic amino acid transporter, since LYS had no effect in PQ BBB penetration, this finding indicated that PQ was possibly taken up into the

brain by the neutral amino acid transport system expressed in the brain capillaries (Shimizu et al. 2001).

In the previous reported study using RBE4 cells (Vilas-Boas et al. 2013a), contrarily to what was previously suggested *in vivo* by Shimizu et al., it was demonstrated that it is unlikely that PQ accesses these cells through the basic amino acid and through the neutral amino acid transport systems. Indeed, no significant differences were observed in PQ's cytotoxic profile in the presence of 500 μM ARG or 500 μM VAL. Moreover, it was claimed that, in the presence of such high-affinity substrates, a decrease in PQ's cytotoxicity would be expected if both compounds were substrates for the same transporter, in spite of the difference in each compounds' concentrations (Vilas-Boas et al. 2013a). In these cells, the polyamine uptake system was also not involved in PQ uptake, given the lack of significant differences in PQ cytotoxicity observed in the presence of 500 μM PUT (Vilas-Boas et al. 2013a). Furthermore, these last results are in accordance with the previous reported absence of the polyamine uptake system at the BBB, resulting in limited access of polyamines to the brain (Shin et al. 1985). Therefore, the basic and the neutral amino acid transporters, as well as the polyamine-uptake system do not seem to mediate PQ's uptake in this cellular model of the rat BBB, which possibly contributes to the observed outstanding cell resistance to PQ-induced toxicity.

In conclusion, to the best of our knowledge, this was the first study investigating, *in vitro,* different mechanisms involved in the PQ absorption through the human intestinal epithelium. PQ uptake into intestinal epithelial Caco-2 cells is Ca^{2+}/CaM and NEM sensitive, and several transport systems seem to be involved. Therefore, the development of potent inhibitors of these transporters should be the first approach to reduce PQ toxic effects, since they will limit its intestinal absorption and, consequently, its access to the target tissues, such as the lung. These inhibitors may, thus, constitute a promising new source of antidotes against PQ intoxications.

IV.5. Screening of newly synthetized xanthone and thioxanthone derivatives – new potential therapeutic agents against Paraquat-induced intoxications

Xanthones (dibenzo-γ-pyrones, Xs) and thioxanthones (dibenzo-γ-thiopyrones, TXs) are promising compounds in the field of medicinal chemistry. Xanthones were reported to have pronounced biological activity within a notably broad spectrum of disease states, resulting from their interaction with a corresponding diverse range of target biomolecules (Masters and Bräse 2012), which led to their description as "privileged structures" (Pinto et al. 2005). In what concerns to TXs, these compounds were proven to have interesting biological properties, namely antitumor activity and P-gp modulation (Paiva et al. 2013;

Palmeira et al. 2012c). However, although several studies have addressed the biological activities of xanthonic and thioxanthonic derivatives, information regarding their interaction with drug transporters is sparse.

In what concerns to TXs, previous studies have reported the ability of aminated thioxanthones to act as dual inhibitors of both P-gp and tumour cell growth in the K562 chronic myelogenous leukemia cell line (Palmeira et al. 2012c). However, in those studies, some of the tested TXs demonstrated an opposite effect in P-gp activity, causing a significant decrease in the RHO 123 accumulation ratio, an effect compatible with an increased P-gp function (Palmeira et al. 2012c). In what concerns to Xs, some prenylated xanthones have shown affinity to bind to the P-gp recombinant domain (Tchamo et al. 2000) and more recently, simple oxygenated xanthones were identified as selective killers of cancer cells overexpressing the MRP1 ABC transporter (Genoux-Bastide et al. 2011). Also, in P-gp overexpressing leukemia cells (K562Dox) a prenylated and a lignoid xanthone derivatives inhibited P-gp activity, whereas two simple oxygenated xanthones increased the transporter activity (Sousa et al. 2013). However, no further studies were conducted to better clarify the mode of action of these xanthonic and thioxanthonic derivatives, specifically in what concerns to how they increase P-gp activity. Therefore, accordingly to the previously reported studies we aimed to:

- Screen five newly synthetized thioxanthonic derivatives as possible inducers of P-gp expression and/or activity, given the previously reported ability of certain TXs to increase P-gp activity (Palmeira et al. 2012c) (Manuscript VI).
- Understand the impact of simple oxygenated xanthones on P-gp activity/expression, given the previously reported ability of simple oxygenated xanthones to increase the pump's function (Sousa et al. 2013). Therefore, by evaluating the effect of a series of dihydroxylated xanthones on the pump's expression and activity, and knowing that the tested Xs only differ in the position of the hydroxyl substituents at the xanthonic scaffold, we also sought to establish a structure-activity relationship (Manuscript VII).

According to our results, all the tested Xs and TXs significantly increased both P-gp expression and activity in Caco-2 cells, being this the first report on the ability of such compounds to act as P-gp inducers. Moreover, although it is known that increases in protein expression may not necessarily result in proportional increases in pump activity (see IV.2), for these compounds, the detected increases in the cell surface P-gp expression were accompanied by similar increases in its transport activity. Among the tested TXs, TX**5** [1-(Propan-2-ylamino)-4-propoxy-9H-thioxanthen-9-one] was the thioxanthonic derivative that caused the highest increase in the protein expression and in

the pump's activity (208% and 198% for P-gp expression and activity, respectively, as compared to control cells). In the case of the tested Xs, which are positional isomers, the observed P-gp induction was not dependent on the position of the hydroxyl substituents at the xanthonic scaffold, since no significant differences were observed among the tested compounds, in what concerns to cell surface P-gp expression levels (134, 144, 133, 142, and 143 % for Xs **1-5**, respectively, when compared to control cells).

An important aspect to note among the obtained data was the ability of all the tested xanthonic and thioxanthonic compounds to rapidly and significantly increase P-gp activity, as assessed by the RHO 123 efflux assay performed in Caco-2 cells in the presence of such compounds during a short 45 min RHO 123 efflux phase. Moreover, this experimental design of RHO 123 efflux evaluation does not reflect a possible contribution of increased P-gp expression in the observed increased activity, given the short duration of contact between the tested compounds and the cells during the RHO 123 efflux phase. This experimental design for the evaluation of P-gp activity was only performed for these compounds, and not for the other compounds previously tested during this work, such as DOX, HYP and colchicine. Indeed, this experimental protocol of RHO 123 efflux was only adopted later, since it was based on the recently emerging concept of a new class of compounds, known as P-gp activators, which represent compounds that interact with P-gp increasing its transport activity without increasing its protein expression (Sterz et al. 2009; Vilas-Boas et al. 2013b). From the obtained results, X**1** and X**5** were the most effective P-gp activators among the tested Xs, whereas TX**1** and TX**5** were, among the tested TXs, the most effective P-gp activators.

Considering the previously described effects of the tested xanthonic and thioxanthonic derivatives on P-gp expression and activity, we further sough to elucidate if they could afford protection of Caco-2 cells against the toxicity of P-gp substrates, using again PQ as a model of a toxic substrate. The herbicide cytotoxicity was, thus, evaluated, by the neutral red uptake assay, with and without simultaneous exposure to the herbicide and the tested compounds for 24 h. The suitability of this study model, using PQ as the P-gp toxic substrate, was already demonstrated with the previously described studies on the P-gp inducers DOX and HYP in Caco-2 cells (see IV.3), as well as with the studies reported for the reduced rifampicin derivative, RedRif, in RBE4 cells (Vilas-Boas et al. 2013b). Except for TX**1** and X**2**, the simultaneous incubation with the tested (thio)xanthonic derivatives resulted in a significant reduction in PQ cytotoxicity, which was demonstrated by the significant rightwards shifts of all the fitted curves, and by the significant increases in the PQ's EC_{50} values obtained in the presence of these derivatives (Manuscript VI and Manuscript VII). For X**2**, although no significant differences were obtained in the EC_{50} value, a significant rightwards shift of the fitted curve was observed

as a consequence of a significant reduction in cell death detected for some of the tested PQ concentrations (Manuscript VII). For TX**1** no significant differences were observed in the overall comparison of the fitted curves (TOP, BOTTOM and EC50 value) (Manuscript VI). From the tested Xs, X**1** and X**5** derivatives afforded the highest protection (for X**1**, X**3**, X**4**, and X**5** the EC_{50} value significantly increased from 1260 μM for the PQ curve to 1620, 1509, 1520, and 1714 μM, respectively), the same compounds that demonstrated the highest effectiveness in activating the pump (Manuscript VII). From the tested TXs, TX**5** was the most effective compound in protecting Caco-2 cells against PQ-induced cytotoxicity (for TX**2**, TX**3**, TX**4**, and TX**5**, the EC_{50} value significantly increased to 1517, 1359, 1378, and 1749 μM, respectively, when compared to the 1204 μM EC_{50} value of the PQ curve), being this derivative the one that increased both P-gp expression and activity to the highest extent (Manuscript VI).

To evaluate if the observed protective effects against PQ-induced cell death were mediated by P-gp, the herbicide cytotoxicity was further evaluated in the presence of the specific P-gp inhibitor, GF120918. For all the tested Xs, the previously described protective effects were completely abolished under P-gp inhibition, demonstrating that these compounds can effectively reduce PQ-induced cell death through a P-gp-mediated mechanism. For the tested TXs, except for TX**5**, in the presence of GF120918, a complete abolishment of the observed TXs protective effects was also demonstrated, suggesting, again, a P-gp-mediated protection against PQ cytotoxicity. However, for TX**5**, even with an increased inhibitor concentration (since this derivative was, as previously mentioned, responsible for the highest observed P-gp induction), a small rightwards shift at the top of the fitted curve was still observed, and accompanied by a minor, although significant, increase in the EC_{50} value of the fitted curve. Nonetheless, since the TX**5** protection was almost completely abolished under P-gp inhibition, it may be concluded that P-gp was mainly involved on the protective effects mediated by TX**5** in PQ cytotoxicity. Furthermore, as observed after P-gp inhibition with the UIC2 antibody, using GF120918, it was again demonstrated that P-gp modulation has an important impact on PQ toxicity. This inhibitor proved to be also suitable for elucidating if the protective effects of the studied compounds are mediated by P-gp, and is a less expensive alternative when compared to the UIC2 antibody.

In accordance with these results, it was recently reported that a synthetic derivative of rifampicin, RedRif, which modulated P-gp expression and activity, could increase P-gp activity even at time points at which no increase in protein expression occurred, thus also acting as a P-gp activator in RBE4 cells (Vilas-Boas et al. 2013b). Indeed, RedRif (10 μM) was able to significantly increase P-gp expression 48 h after exposure, although the pump's activity increased as soon as 24 h after exposure. Moreover, and as mentioned,

this increased P-gp activity significantly protected RBE4 cell against PQ-induced cytotoxicity, since pre-exposing cells to the derivative for 24 h significantly increased the herbicide EC_{50} value. Furthermore, RedRif protection against PQ cytotoxicity was much more significant when simultaneous exposure to both derivative and PQ was performed, when compared to the pre-exposure assay, suggesting that P-gp activation by RedRif may be a more efficient way to prevent P-gp substrates' toxicity (Vilas-Boas et al. 2013b).

Additionally, although the definition of P-gp activators has been recently created (Sterz et al. 2009; Vilas-Boas et al. 2013b), it has long been known that there are compounds that bind to P-gp and stimulate the transport of a substrate on another binding site. As previously mentioned, according to the model proposed by Shapiro et al., P-gp possesses at least three positively cooperating drug binding sites, an H site selective for Hoechst 33342 and colchicine, an R site selective for RHO 123 and anthracyclines, and a third binding site for progesterone (an allosteric binding site exhibiting a regulatory function) (Shapiro et al. 1999). Moreover, it was demonstrated that drug binding to one site stimulates transport by the other binding site (Shapiro et al. 1999) (see I.3.1 and I.6.3). A four P-gp-binding sites' model was also proposed, which supports the presence of three transport sites and one regulatory site. This last site allostericaly alters the conformation of the transport binding sites from low to high affinity for substrates, increasing the rate of translocation (Martin et al. 2000). Furthermore, accordingly with the recently reported high-resolution X-ray crystal structure of mouse P-gp, rather than one or a few discrete drug-binding sites, a large, flexible drug-binding region exists, which permits the creation of numerous sub-sites where drugs can bind, thus allowing the accommodation of at least two substrate molecules simultaneously (Aller et al. 2009) (see I.3.1 and I.6.3).

In accordance with our data, other compounds were also reported to increase P-gp activity, without changing its protein expression. For example, some of the NSAIDs reported by Takara et al. demonstrated no remarkable effect on the expression of *MDR1* mRNA, although significantly altered the intracellular accumulation of RHO 123 (Takara et al. 2009). Indeed, the exposure of Caco-2 cells to mefenamic acid, sulindac, naproxen, and meloxicam, significantly reduced the amount of RHO 123 accumulated inside the cells, without changing the *MDR1* mRNA levels (Takara et al. 2009). However, no further studies were performed to explain the obtained results.

Furthermore, several substances, such as flavonoids and some hydrophobic peptides, have also been described to activate substrate transport by P-gp (Sharom et al. 1996; Wang et al. 2002). Indeed, some catechins were reported to facilitate the P-gp-mediated transport of LDS, a fluorescent P-gp marker substrate, without affecting daunorubicin or RHO 123 transport. Moreover, (-)epicatechin, in spite of being an inhibitor

of RHO 123 transport, significantly enhanced the active net transport of LDS. This result indicates that (-)epicatechin may bind to P-gp and activate an allosteric site that enhances P-gp overall function or efficiency (Wang et al. 2002). Additionally, Kondratov et al. identified several small molecules, first designed as p53 inhibitors, with different effects on the cellular accumulation of distinct P-gp substrates (Kondratov et al. 2001). The most potent compounds, QB102 and QB11, stimulated the transport of anthracyclines and RHO 123, whereas the efflux of Vinca alkaloids and Hoechst 33342 was inhibited, being the effect of these modulators dependent, at least partially, on the substrate-binding site postulated by Shapiro et al. (Kondratov et al. 2001). A series of 27 imidazobenzimidazoles and imidazobenzothiazoles structurally related to QB102 and QB11 were later synthesized, and their influence on the cellular accumulation of RHO 123 and daunorubicin was investigated (Sterz et al. 2009). These novel derivatives showed a similar effect to that of the substances described by Kondratov et al., and the most potent compounds yielded half-maximal P-gp activation in a high nanomolar concentration range. Most of the tested compounds were able to stimulate P-gp-mediated efflux of daunorubicin and RHO 123 in a concentration-dependent manner, and the P-gp-mediated efflux of vinblastine and colchicine was inhibited by several of the tested compounds. Therefore, it was proposed that these novel compounds bind to the P-gp H site and activate the efflux of specific substrates of the R site in a positive cooperative manner, whereas binding of H-type substrates is inhibited competitively. This hypothesis was further confirmed by the observation that these modulators do not influence hydrolysis of ATP or its affinity towards P-gp (Sterz et al. 2009).

Therefore, all these compounds seem to act as P-gp activators, having the ability to immediately increase P-gp activity without the need to increase its expression. Such compounds act by binding to a specific ligand-binding site, inducing a conformational change in P-gp that stimulates the efflux of a substrate bound on another ligand-binding site (Vilas-Boas et al. 2013b). In fact, adaption and survival mechanisms of living beings has allowed the binding of several xenobiotics at the same time to P-gp (Safa 1993; Safa 1998), increasing the transport of each other, not competing, but activating the transportation cycle (Safa 2004). Hence, as P-gp activators bind in the drug-binding pocket formed by the TMD interface, binding modes of the tested xanthonic and thioxanthonic derivatives, alone or with PQ, as well as of PQ alone, were further explored by a docking study, using a model built based on Sav1866, an ABC transporter from *S. aureus* (Palmeira et al. 2012c). Docking simulations between the P-gp drug-binding pocket and other known P-gp activators (Palmeira et al. 2012c; Sousa et al. 2013; Sterz et al. 2009) were also performed. Dihydroxylated xanthones bound in one particular P-gp binding site, engulfed by TMH 4, 5, 8-10, and 12, forming stable complexes between Xs

and the P-gp binding pocket. Furthermore, all the tested Xs bound in a similar and almost superimposable conformation, and all these compounds have shape, size, and stereoelectronic complementarity to the P-gp binding pocket, establishing hydrogen interactions with Ile235, Arg832, and Glu875 (Loo and Clarke 2002; Wang et al. 2007), described as being important members of the drug-binding pocket, contributing also to the correct folding of the transporter; and stacking interactions with Phe77, described as being part of P-gp binding pocket and important to P-gp biosynthesis (Loo and Clarke 1993).

In what concerns to the thioxanthonic derivatives, as TX**1** and TX**5** were the most active P-gp activators in the *in vitro* studies, a visual inspection of these molecules in the TMD interface of P-gp was performed, using the previously mentioned model built based on Sav1866. Both TX**1** and TX**5**, contrarily to the tested Xs, have two preferential binding sites, engulfed by TMH 4, 5, 8-10 and 12, or by TMH 1-3, 6, 7, and 11. TX**5** forms a stable complex with P-gp, and has also shape, size, and stereoelectronic complementarity to the P-gp binding pocket, establishing hydrogen interactions with Ala80, and stacking interactions with Phe201, described as being part of P-gp binding pocket (Loo et al. 2009). TX**1** established hydrogen interactions with Gly346, known as being involved in inter-domain communication, causing an helical movement required to ATP hydrolysis and multidrug transport (Storm et al. 2007); as well as with Ser228, also described as being an important residue in the P-gp drug binding pocket (Loo and Clarke 1999a); and stacking interactions with Phe201.

According to our data, PQ, similarly to the TXs, has two preferential binding sites in P-gp. Moreover, TXs and PQ may establish stacking interactions, and this noncovalent complex binds to P-gp with higher affinity than TXs and PQ individually. The two-ligand complex established polar interactions with P-gp residues, such as Asn839 and Val345, and stacking interactions with P-gp residues, such as Phe201, Phe239, and Phe777. On the other hand, the top rank PQ docking pose occurred in a binding site distant from the place where Xs were predicted to dock, although other less stable PQ conformations are found in the Xs binding site. Therefore, Xs and PQ may bind simultaneously in P-gp in two different binding sites. Consequently, a simultaneous and cooperative transport may be hypothesized for PQ and Xs, since the binding of a xanthone at one binding site may stimulate the transport of PQ through another binding site (Litman et al. 1997a). Moreover, Xs and PQ may also establish stacking interactions while being co-transported and, as for TXs, this noncovalent complex binds to P-gp with higher affinity than the xanthone derivative and PQ individually. In this case, the two-ligand complex established polar interactions with P-gp residues, such as Gln347 and Val345, and stacking interactions with P-gp residues, such as Phe343 and Trp232.

Therefore, the hypothesis of an activation mechanism of action for (thio)xanthonic derivatives was supported by this docking study, being these compounds and PQ docked on two different binding sites in the cleft formed by the P-gp transmembrane α-helices. Furthermore, a simultaneous docking of PQ and (thio)xanthones revealed, as mentioned, that a more stable complex with P-gp model was formed (with lower free energy) than when those molecules were docked individually, suggesting that a co-transport may be occurring. Furthermore, the docking studies suggested two alternative mechanisms of activation by co-transport: a) (thio)xanthones dock on a different site than PQ, thus activating the efflux of the herbicide; b) (thio)xanthonic derivative and PQ bind to the same drug pocket, establishing stacking interactions between the (thio)xanthone scaffold and the biphenyl group, thus facilitating the transport to the extracellular medium. In the future, mutation studies could be performed in order to determine whether PQ and (thio)xanthones bind to the same or to different binding sites on P-gp. Additionally, from the tested TXs, TX**1** was not able to afford protection against PQ-induced cytotoxicity in Caco-2 cells, in spite of the significant increases in both P-gp expression and activity. This indicates that this derivative acts as a strict competitive substrate, suggesting that this TX overlaps with PQ on the same site of P-gp. Furthermore, as docking scores revealed, TX**1** binds more tightly to the P-gp binding site than PQ.

In accordance with these docking studies, the previously referred rifampicin derivative, RedRif, which acted as P-gp activator in RBE4 cells, demonstrated to also have shape, size and stereoelectronic complementarity to P-gp drug-binding pocket, using the same P-gp Sav1866 model (Vilas-Boas et al. 2013b). Furthermore, this activator formed a more stable complex with P-gp than other known P-gp activators (Palmeira et al. 2011; Palmeira et al. 2012c; Sterz et al. 2009), also docked in this study, thus suggesting that RedRif may have higher affinity to the P-gp binding site than these compounds. Moreover, as RedRif established hydrogen interactions with Ser349 and Gln990, and this last residue has already been described as being part of the translocation pathway and being involved in the transport cycle (Loo et al. 2009), it was suggested that this compound has a high probability of interacting with the P-gp translocation channel, which supports the obtained experimental data (Vilas-Boas et al. 2013b).

In conclusion, (thio)xanthonic derivatives are a promising new source of antidotes against the cytotoxicity of harmful P-gp substrates, such as PQ, which act by simultaneously increasing both P-gp expression and activity. The proposed protection mechanisms of these derivatives, as well as of doxorubicin and hypericin, are illustrated in Figure 22. Furthermore, given their ability to immediately activate the pump function, even more pronounced protection can be potentially afforded for substrates that are rapidly absorbed upon ingestion.

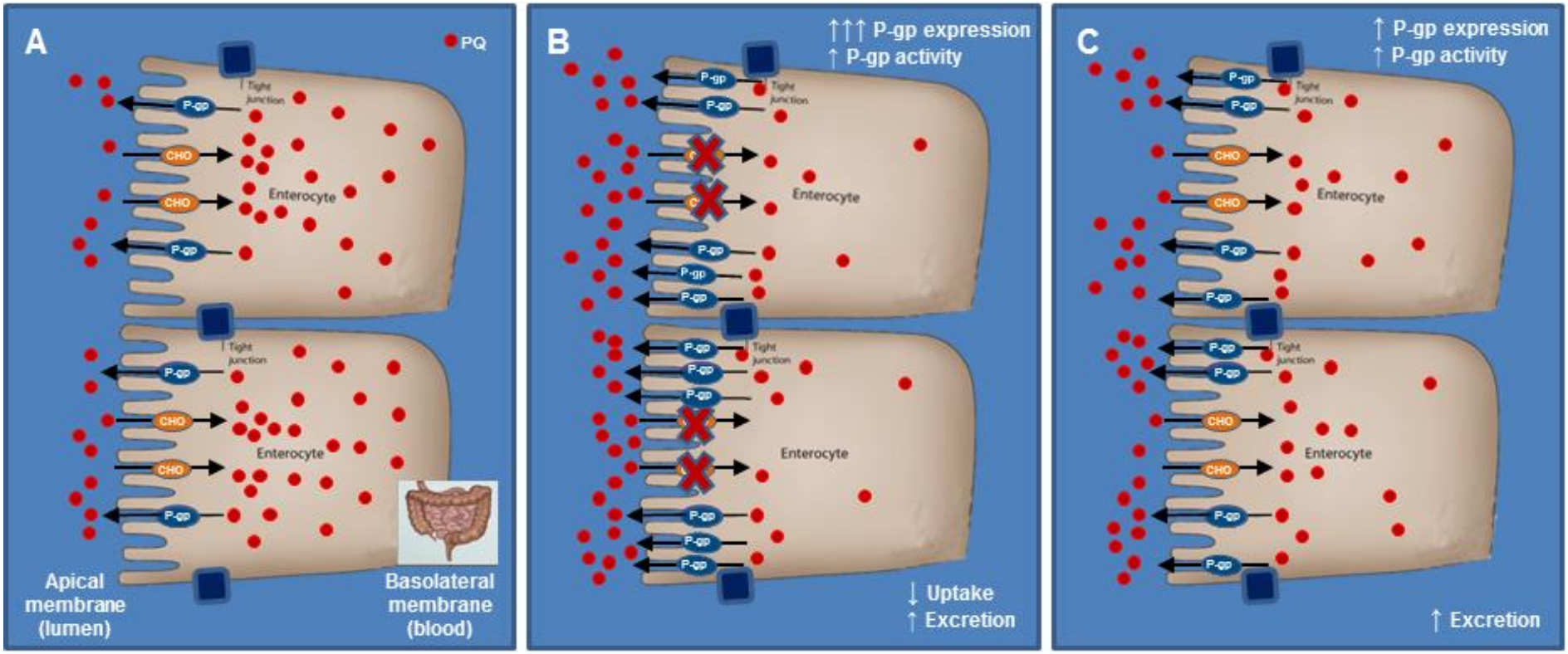

Figure 22. Proposed protection mechanism against PQ-induced cytotoxicity afforded by the tested compounds.

A. Untreated cells; B. Doxorubicin – exposure of Caco-2 cells to DOX results in a significant reduction in PQ intracellular accumulation, and consequently, in a significant reduction in its cytotoxicity, as a result of a double and unique feature in what concerns PQ poisonings: inhibition of PQ uptake (through the inhibition of choline uptake system, CHO), and increased PQ excretion (through increased P-gp expression and activity). **C. Hypericin, and xanthonic and thioxanthonic derivatives** – through the significant increase in both P-gp expression and activity, these compounds afforded a significant protection of Caco-2 cells against PQ-induced cytotoxicity, by increasing the herbicide's efflux, thus reducing its intracellular levels.

IV.6. In silico studies for P-gp inducers and activators – a new strategy

Knowing that the experimental *in vitro* assays used to assess the interactions and transport of new chemical entities with P-gp are expensive, laborious and time-consuming, several *in silico* models, that provide rapid and inexpensive screening platforms, have been developed for identifying P-gp substrates or inhibitors, and have been recognized to be valuable tools for these purposes (Ekins et al. 2007; Hou and Xu 2004). Indeed, numerous computational models, based on QSAR analyses (2D-QSAR and 3D-QSAR), pharmacophore modelling and molecular docking techniques, have been developed to predict P-gp substrates, as well as inhibitors (Chen et al. 2012a). However, in what concerns to P-gp inducers and activators, the search for new compounds with these properties has been mainly performed by random screening.

In an attempt to address this gap and based on 34 P-gp inducers reported in the scientific literature, we further aimed to build pharmacophores for P-gp induction (Manuscript III). Given the distinct and non-overlapping scaffolds of those compounds, prior to building a pharmacophore for P-gp induction, a ligand clustering analysis was performed, and the output clusters composed of more than 2 molecules were used on the pharmacophore construction. Accordingly, four different pharmacophores were built:

- Pharmacophore I, with a score of 52.9, and composed of six features: 3 hydrophobic features, and 3 hydrogen bond (Hb)-acceptor groups, having this pharmacophore the highest number of features found.
- Pharmacophore II, with a score of 64.3, and composed of 3 features: 2 Hb donor groups, and 1 Hb acceptor group.
- Pharmacophore III, with a score of 61.4, and composed of 5 features: 3 Hb acceptor groups and 2 hydrophobic groups.
- Pharmacophore IV, with a score of 40.9, and composed of 3 features: 1 Hb donor group and 2 hydrophobic groups.

Furthermore, these pharmacophores for predicting P-gp induction were validated using a test set formed by 4 known P-gp inducers, amprenavir (Huang et al. 2001), nelfinavir (Huang et al. 2001), puromycin (Male 2009), and yohimbine (Bhat et al. 1995), being these compounds detected as P-gp inducers when using pharmacophores I-IV as query. These pharmacophores were then used to map and align the thioxanthonic derivatives tested in our study, given the demonstrated ability of such compounds to increase, *in vitro,* the P-gp expression in Caco-2 cells (Manuscript VI). TX**3** was able to fit three of the four pharmacophores (pharmacophores I, III and IV). The other four screened TXs were able to fit a three-feature P-gp induction pharmacophore consisting of one

hydrogen-bond donor and two hydrophobic groups (pharmacophore IV). Pharmacophore IV was also the best fitting pharmacophore for colchicine (Manuscript III). Therefore, the fitting of these thioxanthonic derivatives onto these pharmacophores further reinforces their usefulness in the efficient prediction of new ligands (Manuscript VI).

The creation of such pharmacophores for P-gp induction can seem reductionist or even conflicting with the reported existence of various signalling pathways regulating P-gp expression, each involving different molecular targets and transcription factors (Figure 12 and Figure 21, section I.6.2.2). However, we aim in the future to greatly improve those pharmacophores, by firstly increasing the number of reported P-gp substrates used in the pharmacophore construction, including, for example, the compounds present in Table 7 (> 150 different compounds), thus increasing the representativeness of such pharmacophores. Consequently, more pharmacophores will be certainly created, and if, among the compounds mapped and aligned in a particular pharmacophore, common transcription activation pathways are identified, according to the data reported in the literature, it will be possible to predict how a new ligand mapped in that pharmacophore will regulate P-gp expression. Even when more than one pathway is involved in the P-gp induction effect mediated by the compounds used for the construction of that pharmacophore, it will help to guide the research on the new ligand towards a more restricted group of pathways, rather than the huge amount of pathways described to be involved in P-gp induction (see Figure 12 and Figure 21, section I.6.2.2). For example, one of the possible pathways involved in the transcriptional activation of *MDR1* expression is mediated by the activation of PXR (Maglich et al. 2002; Rosenfeld et al. 2003), a nuclear receptor with a wide range of reported ligands (Chen et al. 2012b). Among these ligands are anticancer compounds, plant extracts, cholesterol-lowering statins, rifampicin and HIV protease inhibitors (Chen et al. 2012b). If a new compound is mapped in the rifampicin's pharmacophore, a high probability exists for its ability to increase P-gp expression through a PXR-mediated mechanism.

In addition, based on the TXs *in vitro* P-gp activation ability, as well as on a set of known P-gp activators previously described in the literature (Palmeira et al. 2011; Palmeira et al. 2012c; Sousa et al. 2013; Sterz et al. 2009), common feature pharmacophore models for P-gp activation were created. The best ranked pharmacophore found (score of 110.3 kcal/mol) is composed of three features: one hydrophobic feature, one aromatic ring, and one hydrogen bond acceptor group (Manuscript VI). Moreover, this pharmacophore was validated by its alignment with a test set of 8 known P-gp activators with a benzimidazol scaffold, which were reported by Sterz et al. (Sterz et al. 2009). As with the new pharmacophores for P-gp induction, this

pharmacophore for P-gp activators can be faced as a very useful tool in the future, as it can be used to efficient and rapidly predict new ligands with the ability to activate P-gp.

Additionally, based on the obtained results for the xanthonic derivatives in what concerns to their ability for P-gp activation and, consequently, for protection against PQ-induced cytotoxicity, a 2D QSAR model was created (Manuscript VII). The developed model was in agreement with the laws of QSAR, which establish that one descriptor should be used for each five molecules (Kubinyi 2008), precisely the number of xanthonic compounds assayed. Moreover, the final model was validated using previously described P-gp activators, 1-chloro-4-hydroxy-9H-thioxanthen-9-one (TX**2**) and 1-(Propan-2-ylamino)-4-propoxy-9H-thioxanthen-9-one (TX**5**). The maximal partial charge for an oxygen atom was the descriptor predicted as being implicated in the P-gp activation ability of all dihydroxylated xanthones. This electrostatic parameter is associated with the electronegativity of the oxygen that is higher than the electronegativity of carbon, causing electrons to spend more time around the oxygen atom, giving it a partially negative charge, while the carbon will become partially positive. Therefore, this parameter highlights the importance of the presence of the oxygen atom in specific positions in the molecule. Noteworthy, for the tested xanthonic derivatives, both docking studies previously described (see IV.5) and the QSAR model are in accordance with the biological data presented, with 3,6-dihydroxyxanthone (X**5**) being the most active, and the 1,2-dihydroxyxanthone (X**2**) the least active xanthone derivative in activating P-gp transport activity. Overall, position 3 of the xanthonic scaffold seems to be the most favourable for a hydroxyl substituent in P-gp activation, in contrast to position 1. Nevertheless, in the future, other simple oxygenated xanthonic derivatives will be investigated in order to improve the significance and predictability of the developed QSAR model, and to discover other descriptors involved in the P-gp activation ability of xanthones.

In conclusion, to the best of our knowledge, this was the first time that pharmacophores were developed for P-gp inducers and activators, which can be of utmost importance, in the future, for predicting and disclosing new ligands. Furthermore, a 2D QSAR model was created, for the first time, for P-gp activators, which revealed that the maximal partial charge for oxygen atoms is related with the P-gp activation ability of dihydroxylated xanthones, thus opening a new window of opportunities in the drug design of more specific and potent P-gp activators.

.

V. GENERAL CONCLUSIONS

Since numerous intoxications with P-gp substrates result from accidental or intentional ingestion, limiting their intestinal absorption should constitute the first therapeutic measure to be adopted, thus significantly reducing their access to the target organs. In line with this, the overall conclusion of the present work is that effective antidotal pathways can be achieved by efficiently promoting the P-gp-mediated efflux of deleterious xenobiotics, such as the herbicide paraquat, resulting in a significant reduction in the intracellular levels of such compounds and, consequently, in a significant reduction in their toxicity. As such, appropriate *in vitro* models addressing P-gp induction that enable the selection of specific, safe and potent P-gp inducers, are needed. The studies described in this thesis contributed to a better understanding of the molecular basis of the regulation of P-gp expression and activity, and to the discovery of new compounds acting as P-gp inducers and activators. Thus, from these studies, the following major conclusions may be drawn (Figure 23):

- Caco-2 cells, representing the human intestinal epithelium, are a suitable *in vitro* model to study and select safe, potent, and specific P-gp inducers to be used as a cell protection tool against toxic P-gp substrates. Indeed, significant increases in P-gp expression were observed as soon as 6 h after exposure to the inducing agent (doxorubicin), demonstrating the rapid responsiveness of these cells. Furthermore, this *in vitro* model is also suitable for the study of P-gp induction as an antidotal pathway against substrates of this transporter system.
- Doxorubicin significantly increased both P-gp expression and activity in Caco-2 cells, in a time- and concentration-dependent manner, with significant increases observed as soon as 6 h after incubation. However, the observed remarkable increases in P-gp expression levels were not accompanied by proportional increases in P-gp transport activity. The observed DOX-mediated P-gp induction resulted in a significant reduction in PQ cytotoxicity, which was more pronounced when DOX was added 6 h after the beginning of PQ exposure. Under this experimental design, DOX demonstrated a double and unique feature in what concerns to PQ poisonings, having the ability of both inhibiting PQ entrance (through the inhibition of choline uptake system), and increasing its excretion (through increased P-gp expression and activity), thus resulting in a significant reduction in its intracellular accumulation and, consequently, in its toxicity. The study and development of compounds combining these two features are promising new sources of antidotal pathways to be explored.

- Hypericin, by significantly increasing both P-gp expression and activity, afforded a proportional and significant protection of Caco-2 cells against PQ-induced cytotoxicity. Furthermore, HYP protective effects against PQ cytotoxicity, observed under the several experimental designs used, were completely prevented under P-gp inhibition. Therefore, this compound is an excellent candidate for drug design of new potent and specific P-gp inducers, and for the study of potential protective effects against toxic P-gp substrates mediated only through P-gp induction.
- Colchicine significantly induced P-gp expression in Caco-2 cells without a concomitant increase in the protein activity. Therefore, although colchicine is a P-gp inducer it also acts as a P-gp competitive inhibitor, which could contribute to a great unpredictability of potential drug-drug interactions with other P-gp substrates.
- Both computational and biological data obtained for colchicine, HYP and DOX emphasize the importance of the simultaneous evaluation of P-gp expression and activity in the screening of P-gp inducers, since these parameters may be differently regulated. For a P-gp inducer to afford cellular protection against harmful xenobiotics, it is of utmost importance that it is especially able to increase the pump's function, and thus decrease the intracellular accumulation of toxic P-gp substrates. In fact, the protective effects of both DOX and HYP against PQ cytotoxicity were highly dependent on their effects on P-gp transport function.
- Different uptake mechanisms are involved in the PQ absorption through the human intestinal epithelium. PQ uptake into Caco-2 cells is a Ca^{2+}/CaM- and NEM-sensitive process and more than one transport system appear to be involved, such as the choline uptake and the basic amino acid y^+ transport systems. Knowing that limiting PQ intestinal absorption should be the first approach to reduce its toxic effects, the development of potent inhibitors of these transporters may constitute a potential new source of antidotes to be used in PQ intoxications. As noted with PQ, several uptake/efflux systems may determine the intracellular concentrations achieved by any given xenobiotic. Therefore, the multiplicity and redundance of transport systems must always be addressed.
- (Thio)xanthonic derivatives were, for the first time, reported to significantly increase P-gp expression, thus acting as P-gp inducers. The observed increases in the protein expression were accompanied by similar increases in its transport function. Furthermore, they demonstrated the ability to immediately increase P-gp activity after a short incubation period, an effect compatible with P-gp activation. The possibility of a co-transport mechanism between (thio)xanthones and PQ was further supported by docking studies. In addition, the observed effects on both P-

gp expression and activity resulted in a significant protection of Caco-2 cells against PQ cytotoxicity, thus representing a promising new source of antidotes against intoxications by harmful P-gp substrates, such as PQ. Thus, these data disclose new perspectives in preventing PQ and other P-gp substrates-induced poisonings.

- TX**5** was the thioxanthonic derivative that demonstrated the highest potential in inducing P-gp and, as a result of the highest P-gp expression and activation capacity, it elicited the highest protection against PQ-induced toxicity in Caco-2 cells.
- X**1** and X**5** were, among the tested xanthonic derivatives, the most effective in activating P-gp transport activity, which was demonstrated by both *in vitro* and *in silico* studies. As a consequence, these compounds afforded the highest protection of Caco-2 cells against PQ cytotoxicity.
- For the first time, pharmacophores for P-gp inducers and activators were developed, which can be of utmost importance, in the future, in predicting new ligands. Furthermore, a perfect match between *in silico* and *in vitro* studies was observed. These results indicate that the use of such *in silico* strategies can help to predict the P-gp modulatory effects of new drugs that can be initially screened through these newly developed pharmacophores. Furthermore, also for the first time, a 2D QSAR model was created for P-gp activators, demonstrating that the maximal partial charge for oxygen atoms is related with the P-gp activation ability of dihydroxylated xanthones.

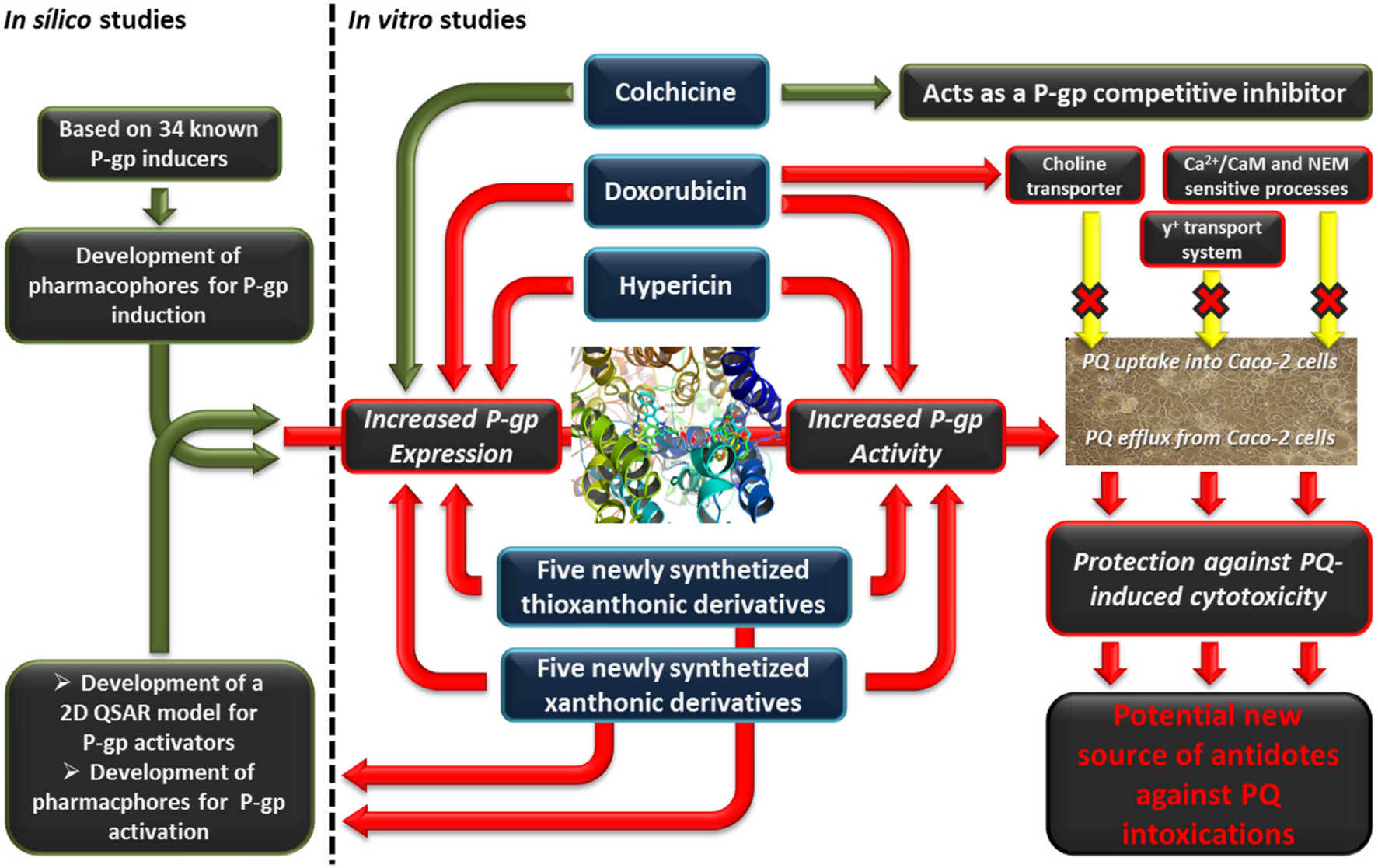

Figure 23. Graphical conclusions.

PART IV

VI. REFERENCES

Aanismaa P, Gatlik-Landwojtowicz E, Seelig A (2008) P-glycoprotein senses its substrates and the lateral membrane packing density: consequences for the catalytic cycle. Biochemistry 47:10197-10207.

Abate C, Patel L, Rauscher FJ, 3rd, Curran T (1990) Redox regulation of fos and jun DNA-binding activity in vitro. Science 249:1157-1161.

Abolhoda A, Wilson AE, Ross H, Danenberg PV, Burt M, Scotto KW (1999) Rapid activation of MDR1 gene expression in human metastatic sarcoma after in vivo exposure to doxorubicin. Clin Cancer Res 5:3352-3356.

Abraham I, Chin KV, Gottesman MM, Mayo JK, Sampson KE (1990) Transfection of a mutant regulatory subunit gene of cAMP-dependent protein kinase causes increased drug sensitivity and decreased expression of P-glycoprotein. Exp Cell Res 189:133-141.

Abulrob AG, Gumbleton M (1999) Transport of phosphatidylcholine in MDR3-negative epithelial cell lines via drug-induced MDR1 P-glycoprotein. Biochem Biophys Res Commun 262:121-126.

Abuznait AH, Patrick SG, Kaddoumi A (2011a) Exposure of LS-180 cells to drugs of diverse physicochemical and therapeutic properties up-regulates P-glycoprotein expression and activity. J Pharm Pharm Sci 14:236-248.

Abuznait AH, Qosa H, O'Connell ND, et al. (2011b) Induction of expression and functional activity of P-glycoprotein efflux transporter by bioactive plant natural products. Food and Chemical Toxicology 49:2765-2772.

Ackerman SL, Minden AG, Williams GT, Bobonis C, Yeung CY (1991) Functional significance of an overlapping consensus binding motif for Sp1 and Zif268 in the murine adenosine deaminase gene promoter. Proc Natl Acad Sci U S A 88:7523-7527.

Advani R, Fisher GA, Lum BL, et al. (2001) A Phase I Trial of Doxorubicin, Paclitaxel, and Valspodar (PSC 833), a Modulator of Multidrug Resistance. Clinical Cancer Research 7:1221-1229.

Akhtar N, Ahad A, Khar RK, et al. (2011) The emerging role of P-glycoprotein inhibitors in drug delivery: a patent review. Expert Opinion on Therapeutic Patents 21:561-576.

Akira S, Kishimoto T (1992) IL-6 and NF-IL6 in acute-phase response and viral infection. Immunol Rev 127:25-50.

Akiyama TE, Gonzalez FJ (2003) Regulation of P450 genes by liver-enriched transcription factors and nuclear receptors. Biochim Biophys Acta 1619:223-234.

Al-Shawi MK (2011) Catalytic and transport cycles of ABC exporters. Essays Biochem 50:63-83.

Al-Shawi MK, Polar MK, Omote H, Figler RA (2003) Transition state analysis of the coupling of drug transport to ATP hydrolysis by P-glycoprotein. J Biol Chem 278:52629-52640.

Allen JD, Van Dort SC, Buitelaar M, van Tellingen O, Schinkel AH (2003) Mouse breast cancer resistance protein (Bcrp1/Abcg2) mediates etoposide resistance and transport, but etoposide oral availability is limited primarily by P-glycoprotein. Cancer Res 63:1339-1344.

Allenspach K, Bergman PJ, Sauter S, Grone A, Doherr MG, Gaschen F (2006) P-glycoprotein expression in lamina propria lymphocytes of duodenal biopsy samples in dogs with chronic idiopathic enteropathies. J Comp Pathol 134:1-7.

Aller SG, Yu J, Ward A, et al. (2009) Structure of P-Glycoprotein Reveals a Molecular Basis for Poly-Specific Drug Binding. Science 323:1718-1722.

Alvarez M, Paull K, Monks A, et al. (1995) Generation of a drug resistance profile by quantitation of mdr-1/P-glycoprotein in the cell lines of the National Cancer Institute Anticancer Drug Screen. J Clin Invest 95:2205–2214.

Ambudkar SV, Dey S, Hrycyna CA, Ramachandra M, Pastan I, Gottesman MM (1999) Biochemical, cellular, and pharmacological aspects of the multidrug transporter. Annu Rev Pharmacol Toxicol 39:361-398.

Ambudkar SV, Kim IW, Sauna ZE (2006) The power of the pump: mechanisms of action of P-glycoprotein (ABCB1). Eur J Pharm Sci 27:392-400.

Ambudkar SV, Lelong IH, Zhang J, Cardarelli CO, Gottesman MM, Pastan I (1992) Partial purification and reconstitution of the human multidrug-resistance pump: characterization of the drug-stimulatable ATP hydrolysis. Proc Natl Acad Sci U S A 89:8472-8476.

Anderle P, Niederer E, Rubas W, et al. (1998) P-Glycoprotein (P-gp) mediated efflux in Caco-2 cell monolayers: the influence of culturing conditions and drug exposure on P-gp expression levels. J Pharm Sci 87:757-762.

Angel P, Imagawa M, Chiu R, et al. (1987) Phorbol ester-inducible genes contain a common cis element recognized by a TPA-modulated trans-acting factor. Cell 49:729-739.

Angel P, Karin M (1991) The role of Jun, Fos and the AP-1 complex in cell-proliferation and transformation. Biochim Biophys Acta 1072:129-157.

Angelova A, Tenev T, Varadinova T (2004) Expression of cellular proteins Bcl-X(L), XIAP and Bax involved in apoptosis in cells infected with herpes simplex virus 1 and effect of pavine alkaloid (-)-thalimonine on virus-induced suppression of apoptosis. Acta Virol 48:193-196.

Aquilante CL, Letrent SP, Pollack GM, Brouwer KL (2000) Increased brain P-glycoprotein in morphine tolerant rats. Life Sci 66:PL47-51.

Arceci RJ, Baas F, Raponi R, Horwitz SB, Housman D, Croop JM (1990) Multidrug resistance gene expression is controlled by steroid hormones in the secretory epithelium of the uterus. Mol Reprod Dev 25:101-109.

Arceci RJ, Croop JM, Horwitz SB, Housman D (1988) The gene encoding multidrug resistance is induced and expressed at high levels during pregnancy in the secretory epithelium of the uterus. Proc Natl Acad Sci U S A 85:4350-4354.

Asakuno K, Kohno K, Uchiumi T, et al. (1994) Involvement of a DNA binding protein, MDR-NF1/YB-1, in human MDR1 gene expression by actinomycin D. Biochem Biophys Res Commun 199:1428-1435.

Ayesh S, Shao YM, Stein WD (1996) Co-operative, competitive and non-competitive interactions between modulators of P-glycoprotein. Biochim Biophys Acta 1316:8-18.

Bachmeier C, Levin GM, Beaulieu-Abdelahad D, Reed J, Mullan M (2013) Effect of Venlafaxine and Desvenlafaxine on Drug Efflux Protein Expression and Biodistribution In Vivo. J Pharm Sci 102:3838-3843.

Bachmeier CJ, Beaulieu-Abdelahad D, Ganey NJ, Mullan MJ, Levin GM (2011) Induction of drug efflux protein expression by venlafaxine but not desvenlafaxine. Biopharm Drug Dispos 32:233-244.

Baekelandt M, Lehne G, Trope CG, et al. (2001) Phase I/II trial of the multidrug-resistance modulator valspodar combined with cisplatin and doxorubicin in refractory ovarian cancer. J Clin Oncol 19:2983-2993.

Baer MR, George SL, Dodge RK, et al. (2002) Phase 3 study of the multidrug resistance modulator PSC-833 in previously untreated patients 60 years of age and older with acute myeloid leukemia: Cancer and Leukemia Group B Study 9720. Blood 100:1224-1232.

Baes M, Gulick T, Choi HS, Martinoli MG, Simha D, Moore DD (1994) A new orphan member of the nuclear hormone receptor superfamily that interacts with a subset of retinoic acid response elements. Mol Cell Biol 14:1544-1552.

Baguley BC (2002) Novel strategies for overcoming multidrug resistance in cancer. BioDrugs 16:97-103.

Bahr O, Wick W, Weller M (2001) Modulation of MDR/MRP by wild-type and mutant p53. J Clin Invest 107:643-646.

Bain LJ, McLachlan JB, LeBlanc GA (1997) Structure-activity relationships for xenobiotic transport substrates and inhibitory ligands of P-glycoprotein. Environ Health Perspect 105:812-818.

Baltazar MT, Dinis-Oliveira RJ, Guilhermino L, de Lourdes Bastos M, Duarte JA, Carvalho F (2013) New formulation of paraquat with lysine acetylsalicylate with low mammalian toxicity and effective herbicidal activity. Pest Management Science 69:553-558.

Barancik M, Bohacova V, Kvackajova J, Hudecova S, Krizanova O, Breier A (2001) SB203580, a specific inhibitor of p38-MAPK pathway, is a new reversal agent of P-glycoprotein-mediated multidrug resistance. Eur J Pharm Sci 14:29-36.

Barancik M, Bohacova V, Sedlak J, Sulova Z, Breier A (2006) LY294,002, a specific inhibitor of PI3K/Akt kinase pathway, antagonizes P-glycoprotein-mediated multidrug resistance. Eur J Pharm Sci 29:426-434.

Bardelmeijer HA, Beijnen JH, Brouwer KR, et al. (2000) Increased Oral Bioavailability of Paclitaxel by GF120918 in Mice through Selective Modulation of P-glycoprotein. Clinical Cancer Research 6:4416-4421.

Bardelmeijer HA, Ouwehand M, Beijnen JH, Schellens JH, van Tellingen O (2004) Efficacy of novel P-glycoprotein inhibitors to increase the oral uptake of paclitaxel in mice. Invest New Drugs 22:219-229.

Bargou RC, Emmerich F, Krappmann D, et al. (1997a) Constitutive nuclear factor-kappaB-RelA activation is required for proliferation and survival of Hodgkin's disease tumor cells. J Clin Invest 100:2961-2969.

Bargou RC, Jurchott K, Wagener C, et al. (1997b) Nuclear localization and increased levels of transcription factor YB-1 in primary human breast cancers are associated with intrinsic MDR1 gene expression. Nat Med 3:447-450.

Bark H, Choi CH (2010) PSC833, cyclosporine analogue, downregulates MDR1 expression by activating JNK/c-Jun/AP-1 and suppressing NF-kappaB. Cancer Chemother Pharmacol 65:1131-1136.

Barnes KM, Dickstein B, Cutler GB, Jr., Fojo T, Bates SE (1996) Steroid treatment, accumulation, and antagonism of P-glycoprotein in multidrug-resistant cells. Biochemistry 35:4820-4827.

Barta CA, Sachs-Barrable K, Feng F, Wasan KM (2008) Effects of monoglycerides on p-glycoprotein: modulation of the activity and expression in caco-2 cell monolayers. Mol Pharm 5:863-875.

Bates S, Kang M, Meadows B, et al. (2001) A Phase I study of infusional vinblastine in combination with the P-glycoprotein antagonist PSC 833 (valspodar). Cancer 92:1577-1590.

Bates SE, Bakke S, Kang M, et al. (2004) A phase I/II study of infusional vinblastine with the P-glycoprotein antagonist valspodar (PSC 833) in renal cell carcinoma. Clin Cancer Res 10:4724-4733.

Bates SE, Mickley LA, Chen YN, et al. (1989) Expression of a drug resistance gene in human neuroblastoma cell lines: modulation by retinoic acid-induced differentiation. Mol Cell Biol 9:4337-4344.

Bauer B, Hartz AM, Fricker G, Miller DS (2004) Pregnane X receptor up-regulation of P-glycoprotein expression and transport function at the blood-brain barrier. Mol Pharmacol 66:413-419.

Bauer B, Hartz AM, Miller DS (2007) Tumor necrosis factor alpha and endothelin-1 increase P-glycoprotein expression and transport activity at the blood-brain barrier. Mol Pharmacol 71:667-675.

Bauer B, Yang X, Hartz AMS, et al. (2006) In Vivo Activation of Human Pregnane X Receptor Tightens the Blood-Brain Barrier to Methadone through P-Glycoprotein Up-Regulation. Molecular Pharmacology 70:1212-1219.

Bauer KS, Karp JE, Garimella TS, Wu S, Tan M, Ross DD (2005) A phase I and pharmacologic study of idarubicin, cytarabine, etoposide, and the multidrug resistance protein (MDR1/Pgp) inhibitor PSC-833 in patients with refractory leukemia. Leuk Res 29:263-271.

Becker J-P, Depret G, Van Bambeke F, Tulkens P, Prevost M (2009) Molecular models of human P-glycoprotein in two different catalytic states. BMC Structural Biology 9:3.

Ben-Chetrit E, Levy M (1991) Colchicine prophylaxis in familial Mediterranean fever: reappraisal after 15 years. Semin Arthritis Rheum 20:241-246.

Benet LZ, Cummins CL (2001) The drug efflux-metabolism alliance: biochemical aspects. Adv Drug Deliv Rev 50 Suppl 1:S3-11.

Bentires-Alj M, Barbu V, Fillet M, et al. (2003) NF-kappaB transcription factor induces drug resistance through MDR1 expression in cancer cells. Oncogene 22:90-97.

Bercovich D, Friedlander Y, Korem S, et al. (2006) The association of common SNPs and haplotypes in the CETP and MDR1 genes with lipids response to fluvastatin in familial hypercholesterolemia. Atherosclerosis 185:97-107.

Bergman PJ, Gravitt KR, Ward NE, Beltran P, Gupta KP, O'Brian CA (1997) Potent induction of human colon cancer cell uptake of chemotherapeutic drugs by N-myristoylated protein kinase C-alpha (PKC-alpha) pseudosubstrate peptides through a P-glycoprotein-independent mechanism. Invest New Drugs 15:311-318.

Bernards R, Weinberg RA (2002) A progression puzzle. Nature 418:823.

Bertz RJ, Granneman GR (1997) Use of in vitro and in vivo data to estimate the likelihood of metabolic pharmacokinetic interactions. Clin Pharmacokinet 32:210-258.

Bhat UG, Winter MA, Pearce HL, Beck WT (1995) A structure-function relationship among reserpine and yohimbine analogues in their ability to increase expression of mdr1 and P-glycoprotein in a human colon carcinoma cell line. Mol Pharmacol 48:682-689.

Bieker JJ (2001) Kruppel-like factors: three fingers in many pies. J Biol Chem 276:34355-34358.

Blobe GC, Sachs CW, Khan WA, et al. (1993) Selective regulation of expression of protein kinase C (PKC) isoenzymes in multidrug-resistant MCF-7 cells. Functional significance of enhanced expression of PKC alpha. J Biol Chem 268:658-664.

Boháčová V, Sulová Z, Dovinová I, et al. (2006) L1210 cells cultivated under the selection pressure of doxorubicin or vincristine express common mechanisms of multidrug resistance based on the overexpression of P-glycoprotein. Toxicology in Vitro 20:1560-1568.

Bond TD, Valverde MA, Higgins CF (1998) Protein kinase C phosphorylation disengages human and mouse-1a P-glycoproteins from influencing the rate of activation of swelling-activated chloride currents. J Physiol 508 (Pt 2):333-340.

Borgnia MJ, Eytan GD, Assaraf YG (1996) Competition of hydrophobic peptides, cytotoxic drugs, and chemosensitizers on a common P-glycoprotein pharmacophore as revealed by its ATPase activity. J Biol Chem 271:3163-3171.

Borrelli F, Izzo AA (2009) Herb-drug interactions with St John's wort (Hypericum perforatum): an update on clinical observations. AAPS J 11:710-727.

Borst P, Elferink RO (2002) Mammalian ABC transporters in health and disease. Annu Rev Biochem 71:537-592.

Bosch I, Dunussi-Joannopoulos K, Wu RL, Furlong ST, Croop J (1997) Phosphatidylcholine and phosphatidylethanolamine behave as substrates of the human MDR1 P-glycoprotein. Biochemistry 36:5685-5694.

Bourguignon LY, Xia W, Wong G (2009) Hyaluronan-mediated CD44 interaction with p300 and SIRT1 regulates beta-catenin signaling and NFkappaB-specific transcription activity leading to MDR1 and Bcl-xL gene expression and chemoresistance in breast tumor cells. J Biol Chem 284:2657-2671.

Brand C, Cipok M, Attali V, Bak A, Sampson SR (2006) Protein kinase Cdelta participates in insulin-induced activation of PKB via PDK1. Biochem Biophys Res Commun 349:954-962.

Brant SR, Panhuysen CI, Nicolae D, et al. (2003) MDR1 Ala893 polymorphism is associated with inflammatory bowel disease. Am J Hum Genet 73:1282-1292.

Breier A, Gibalova L, Seres M, Barancik M, Sulova Z (2013) New insight into p-glycoprotein as a drug target. Anticancer Agents Med Chem 13:159-170.

Brembeck FH, Rosário M, Birchmeier W (2006) Balancing cell adhesion and Wnt signaling, the key role of β-catenin. Current Opinion in Genetics & Development 16:51-59.

Bright-Thomas RM, Hargest R (2003) APC, beta-Catenin and hTCF-4; an unholy trinity in the genesis of colorectal cancer. Eur J Surg Oncol 29:107-117.

Brown JM, Giaccia AJ (1998) The unique physiology of solid tumors: opportunities (and problems) for cancer therapy. Cancer Res 58:1408-1416.

Brown NS, Bicknell R (2001) Hypoxia and oxidative stress in breast cancer. Oxidative stress: its effects on the growth, metastatic potential and response to therapy of breast cancer. Breast Cancer Res 3:323-327.

Brown NS, Jones A, Fujiyama C, Harris AL, Bicknell R (2000) Thymidine phosphorylase induces carcinoma cell oxidative stress and promotes secretion of angiogenic factors. Cancer Res 60:6298-6302.

Brtko J, Thalhamer J (2003) Renaissance of the biologically active vitamin A derivatives: established and novel directed therapies for cancer and chemoprevention. Curr Pharm Des 9:2067-2077.

Bruder JT, Heidecker G, Rapp UR (1992) Serum-, TPA-, and Ras-induced expression from Ap-1/Ets-driven promoters requires Raf-1 kinase. Genes Dev 6:545-556.

Bruggemann EP, Currier SJ, Gottesman MM, Pastan I (1992) Characterization of the azidopine and vinblastine binding site of P-glycoprotein. J Biol Chem 267:21020-21026.

Brugger D, Brischwein K, Liu C, et al. (2002) Induction of drug resistance and protein kinase C genes in A2780 ovarian cancer cells after incubation with antineoplastic agents at sublethal concentrations. Anticancer Res 22:4229-4232.

Bunting KD (2002) ABC Transporters as Phenotypic Markers and Functional Regulators of Stem Cells. STEM CELLS 20:274-274.

Burk O, Arnold KA, Geick A, Tegude H, Eichelbaum M (2005) A role for constitutive androstane receptor in the regulation of human intestinal MDR1 expression. Biol Chem 386:503-513.

Burt RK, Thorgeirsson SS (1988) Coinduction of MDR-1 Multidrug-Resistance and Cytochrome P-450 Genes in Rat Liver by Xenobiotics. Journal of the National Cancer Institute 80:1383-1386.

Bush JA, Li G (2002) Regulation of the Mdr1 isoforms in a p53-deficient mouse model. Carcinogenesis 23:1603-1607.

Cabrera MA, González I, Fernández C, Navarro C, Bermejo M (2006) A topological substructural approach for the prediction of P-glycoprotein substrates. J Pharm Sci 95:589-606.

Callaghan R, Crowley E, Potter S, Kerr ID (2008) P-glycoprotein: so many ways to turn it on. J Clin Pharmacol 48:365-378.

Callaghan R, Ford RC, Kerr ID (2006) The translocation mechanism of P-glycoprotein. FEBS Lett 580:1056-1063.

Callaghan R, Stafford A, Epand RM (1993) Increased accumulation of drugs in a multidrug resistant cell line by alteration of membrane biophysical properties. Biochim Biophys Acta 1175:277-282.

Callen DF, Baker E, Simmers RN, Seshadri R, Roninson IB (1987) Localization of the human multiple drug resistance gene, MDR1, to 7q21.1. Hum Genet 77:142-144.

Callies S, de Alwis DP, Wright JG, Sandler A, Burgess M, Aarons L (2003) A population pharmacokinetic model for doxorubicin and doxorubicinol in the presence of a novel MDR modulator, zosuquidar trihydrochloride (LY335979). Cancer Chemother Pharmacol 51:107-118.

Cao Z, Liu LZ, Dixon DA, Zheng JZ, Chandran B, Jiang BH (2007) Insulin-like growth factor-I induces cyclooxygenase-2 expression via PI3K, MAPK and PKC signaling pathways in human ovarian cancer cells. Cell Signal 19:1542-1553.

Carlson RW, O'Neill AM, Goldstein LJ, et al. (2006) A pilot phase II trial of valspodar modulation of multidrug resistance to paclitaxel in the treatment of metastatic carcinoma of the breast (E1195): a trial of the Eastern Cooperative Oncology Group. Cancer Invest 24:677-681.

Cascorbi I (2006) Role of pharmacogenetics of ATP-binding cassette transporters in the pharmacokinetics of drugs. Pharmacol Ther 112:457-473.

Cermanova J, Fuksa L, Brcakova E, et al. (2009) Up-regulation of renal Mdr1 and Mrp2 transporters during amiodarone pretreatment in rats. Pharmacol Res 61:129-135.

Chan GNY, Patel R, Cummins CL, Bendayan R (2013a) Induction of P-glycoprotein by Antiretroviral Drugs in Human Brain Microvessel Endothelial Cells. Antimicrobial Agents and Chemotherapy 57:4481-4488.

Chan GNY, Saldivia V, Yang Y, Pang H, de Lannoy I, Bendayan R (2013b) In Vivo Induction of P-Glycoprotein Expression at the Mouse Blood-Brain Barrier: An Intracerebral Microdialysis Study. Journal of Neurochemistry 127:342-352.

Chang G (2003) Multidrug resistance ABC transporters. FEBS Lett 555:102-105.

Chaudhary PM, Roninson IB (1993) Induction of Multidrug Resistance in Human Cells by Transient Exposure to Different Chemotherapeutic Drugs. Journal of the National Cancer Institute 85:632-639.

Chauncey TR, Rankin C, Anderson JE, et al. (2000) A phase I study of induction chemotherapy for older patients with newly diagnosed acute myeloid leukemia (AML) using mitoxantrone, etoposide, and the MDR modulator PSC 833: a southwest oncology group study 9617. Leuk Res 24:567-574.

Chelule PK, Gordon M, Palanee T, et al. (2003) MDR1 and CYP3A4 polymorphisms among African, Indian, and white populations in KwaZulu-Natal, South Africa. Clin Pharmacol Ther 74:195-196.

Chen C-j, Chin JE, Ueda K, et al. (1986) Internal duplication and homology with bacterial transport proteins in the mdr1 (P-glycoprotein) gene from multidrug-resistant human cells. Cell 47:381-389.

Chen G, Goeddel DV (2002) TNF-R1 Signaling: A Beautiful Pathway. Science 296:1634-1635.

Chen L, Li Y, Yu H, Zhang L, Hou T (2012a) Computational models for predicting substrates or inhibitors of P-glycoprotein. Drug Discovery Today 17:343-351.

Chen Q, Bian Y, Zeng S (2013) Involvement of AP-1 and NF-kappaB in the Up-regulation of P-gp in Vinblastine Resistant Caco-2 Cells. Drug Metab Pharmacokinet Epub ahead of print.

Chen Q, Zhou J, Jiang C, Chen J (2010a) Reversal of P-glycoprotein-mediated multidrug resistance in SGC7901/VCR cells by PPARgamma activation by troglitazone. J Huazhong Univ Sci Technolog Med Sci 30:326-331.

Chen W, Chen M, Barak LS (2010b) Development of small molecules targeting the Wnt pathway for the treatment of colon cancer: a high-throughput screening approach. Am J Physiol Gastrointest Liver Physiol 299:G293-300.

Chen Y, Tang Y, Chen S, Nie D (2009) Regulation of drug resistance by human pregnane X receptor in breast cancer. Cancer Biol Ther 8:1265-1272.

Chen Y, Tang Y, Guo C, Wang J, Boral D, Nie D (2012b) Nuclear receptors in the multidrug resistance through the regulation of drug-metabolizing enzymes and drug transporters. Biochemical Pharmacology 83:1112-1126.

Chen Y, Tang Y, Wang MT, Zeng S, Nie D (2007) Human pregnane X receptor and resistance to chemotherapy in prostate cancer. Cancer Res 67:10361-10367.

Chiarini F, Del Sole M, Mongiorgi S, et al. (2008) The novel Akt inhibitor, perifosine, induces caspase-dependent apoptosis and downregulates P-glycoprotein expression in multidrug-resistant human T-acute leukemia cells by a JNK-dependent mechanism. Leukemia 22:1106-1116.

Chico I, Kang MH, Bergan R, et al. (2001) Phase I study of infusional paclitaxel in combination with the P-glycoprotein antagonist PSC 833. J Clin Oncol 19:832-842.

Chieli E, Romiti N, Rodeiro I, Garrido G (2010) In vitro modulation of ABCB1/P-glycoprotein expression by polyphenols from Mangifera indica. Chemico-Biological Interactions 186:287-294.

Chin JE, Soffir R, Noonan KE, Choi K, Roninson IB (1989) Structure and expression of the human MDR (P-glycoprotein) gene family. Mol Cell Biol 9:3808-3820.

Chin K, Chauhan S, Pastan I, Gottesman M (1990a) Regulation of mdr RNA levels in response to cytotoxic drugs in rodent cells. Cell Growth Differ 1:361-365.

Chin KV, Tanaka S, Darlington G, Pastan I, Gottesman MM (1990b) Heat shock and arsenite increase expression of the multidrug resistance (MDR1) gene in human renal carcinoma cells. Journal of Biological Chemistry 265:221-226.

Chin KV, Ueda K, Pastan I, Gottesman MM (1992) Modulation of activity of the promoter of the human MDR1 gene by Ras and p53. Science 255:459-462.

Choudhuri S, Klaassen CD (2006) Structure, function, expression, genomic organization, and single nucleotide polymorphisms of human ABCB1 (MDR1), ABCC (MRP), and ABCG2 (BCRP) efflux transporters. Int J Toxicol 25:231-259.

Chow EC, Durk MR, Cummins CL, Pang KS (2011) 1Alpha,25-dihydroxyvitamin D3 up-regulates P-glycoprotein via the vitamin D receptor and not farnesoid X receptor in both fxr(-/-) and fxr(+/+) mice and increased renal and brain efflux of digoxin in mice in vivo. J Pharmacol Exp Ther 337:846-859.

Chowbay B, Li H, David M, Cheung YB, Lee EJ (2005) Meta-analysis of the influence of MDR1 C3435T polymorphism on digoxin pharmacokinetics and MDR1 gene expression. Br J Clin Pharmacol 60:159-171.

Cianchetta G, Singleton RW, Zhang M, et al. (2005) A pharmacophore hypothesis for P-glycoprotein substrate recognition using GRIND-based 3D-QSAR. J Med Chem 48:2927-2935.

Clay AT, Sharom FJ (2013) Lipid bilayer properties control membrane partitioning, binding, and transport of p-glycoprotein substrates. Biochemistry 52:343-354.

Coley H (2010a) Overcoming Multidrug Resistance in Cancer: Clinical Studies of P-Glycoprotein Inhibitors. In: Zhou J (ed) Multi-Drug Resistance in Cancer. Methods in Molecular Biology, vol 596. Humana Press, p 341-358.

Coley HM (2010b) Overcoming multidrug resistance in cancer: clinical studies of p-glycoprotein inhibitors. Methods Mol Biol 596:341-358.

Combates NJ, Kwon PO, Rzepka RW, Cohen D (1997) Involvement of the transcription factor NF-IL6 in phorbol ester induction of P-glycoprotein in U937 cells. Cell Growth Differ 8:213-219.

Combates NJ, Rzepka RW, Chen YN, Cohen D (1994) NF-IL6, a member of the C/EBP family of transcription factors, binds and trans-activates the human MDR1 gene promoter. Journal of Biological Chemistry 269:29715-29719.

Comerford KM, Cummins EP, Taylor CT (2004) c-Jun NH2-terminal kinase activation contributes to hypoxia-inducible factor 1alpha-dependent P-glycoprotein expression in hypoxia. Cancer Res 64:9057-9061.

Comerford KM, Wallace TJ, Karhausen J, Louis NA, Montalto MC, Colgan SP (2002) Hypoxia-inducible factor-1-dependent regulation of the multidrug resistance (MDR1) gene. Cancer Res 62:3387-3394.

Cordo Russo RI, Garcia MG, Alaniz L, Blanco G, Alvarez E, Hajos SE (2008) Hyaluronan oligosaccharides sensitize lymphoma resistant cell lines to vincristine by modulating P-glycoprotein activity and PI3K/Akt pathway. Int J Cancer 122:1012-1018.

Cordon-Cardo C, O'Brien JP, Boccia J, Casals D, Bertino JR, Melamed MR (1990) Expression of the multidrug resistance gene product (P-glycoprotein) in human normal and tumor tissues. J Histochem Cytochem 38:1277-1287.

Cordon-Cardo C, O'Brien JP, Casals D, et al. (1989) Multidrug-resistance gene (P-glycoprotein) is expressed by endothelial cells at blood-brain barrier sites. Proc Natl Acad Sci U S A 86:695-698.

Corna G, Santambrogio P, Minotti G, Cairo G (2004) Doxorubicin paradoxically protects cardiomyocytes against iron-mediated toxicity: role of reactive oxygen species and ferritin. J Biol Chem 279:13738-13745.

Cornwell MM, Smith DE (1993a) A signal transduction pathway for activation of the mdr1 promoter involves the proto-oncogene c-raf kinase. J Biol Chem 268:15347-15350.

Cornwell MM, Smith DE (1993b) SP1 activates the MDR1 promoter through one of two distinct G-rich regions that modulate promoter activity. Journal of Biological Chemistry 268:19505-19511.

Correa S, Binato R, Du Rocher B, Castelo-Branco MT, Pizzatti L, Abdelhay E (2012) Wnt/beta-catenin pathway regulates ABCB1 transcription in chronic myeloid leukemia. BMC Cancer 12:303.

Couture L, Nash JA, Turgeon J (2006) The ATP-binding cassette transporters and their implication in drug disposition: a special look at the heart. Pharmacol Rev 58:244-258.

Crivori P, Reinach B, Pezzetta D, Poggesi I (2006) Computational models for identifying potential P-glycoprotein substrates and inhibitors. Mol Pharm 3:33-44.

Croop JM, Raymond M, Haber D, et al. (1989) The three mouse multidrug resistance (mdr) genes are expressed in a tissue-specific manner in normal mouse tissues. Mol Cell Biol 9:1346-1350.

Crowe A, Tan AM (2012) Oral and inhaled corticosteroids: Differences in P-glycoprotein (ABCB1) mediated efflux. Toxicology and Applied Pharmacology 260:294-302.

Cummins CL, Jacobsen W, Benet LZ (2002) Unmasking the Dynamic Interplay between Intestinal P-Glycoprotein and CYP3A4. Journal of Pharmacology and Experimental Therapeutics 300:1036-1045.

Daleke DL (2007) Phospholipid flippases. J Biol Chem 282:821-825.

Dalton TP, Shertzer HG, Puga A (1999) Regulation of gene expression by reactive oxygen. Annu Rev Pharmacol Toxicol 39:67-101.

Dantzig AH, Law KL, Cao J, Starling JJ (2001) Reversal of multidrug resistance by the P-glycoprotein modulator, LY335979, from the bench to the clinic. Curr Med Chem 8:39-50.

Dantzig AH, Shepard RL, Cao J, et al. (1996) Reversal of P-glycoprotein-mediated multidrug resistance by a potent cyclopropyldibenzosuberane modulator, LY335979. Cancer Res 56:4171-4179.

Dantzig AH, Shepard RL, Law KL, et al. (1999) Selectivity of the Multidrug Resistance Modulator, LY335979, for P-Glycoprotein and Effect on Cytochrome P-450 Activities. Journal of Pharmacology and Experimental Therapeutics 290:854-862.

Das KC, White CW (1997) Activation of NF-kappaB by antineoplastic agents. Role of protein kinase C. J Biol Chem 272:14914-14920.

Daschner PJ, Ciolino HP, Plouzek CA, Yeh GC (1999) Increased AP-1 activity in drug resistant human breast cancer MCF-7 cells. Breast Cancer Res Treat 53:229-240.

Davis RJ (1993) The mitogen-activated protein kinase signal transduction pathway. J Biol Chem 268:14553-14556.

Davis W, Ronai Ze, Tew KD (2001) Cellular Thiols and Reactive Oxygen Species in Drug-Induced Apoptosis. Journal of Pharmacology and Experimental Therapeutics 296:1-6.

Dawson RJ, Locher KP (2006) Structure of a bacterial multidrug ABC transporter. Nature 443:180-185.

de Boer AG, Gaillard PJ (2007a) Drug targeting to the brain. Annu Rev Pharmacol Toxicol 47:323-355.

de Boer AG, Gaillard PJ (2007b) Strategies to improve drug delivery across the blood-brain barrier. Clin Pharmacokinet 46:553-576.

de Boer AG, van der Sandt IC, Gaillard PJ (2003) The role of drug transporters at the blood-brain barrier. Annu Rev Pharmacol Toxicol 43:629-656.

de Bruijn MH, Van der Bliek AM, Biedler JL, Borst P (1986) Differential amplification and disproportionate expression of five genes in three multidrug-resistant Chinese hamster lung cell lines. Mol Cell Biol 6:4717-4722.

de Bruin M, Miyake K, Litman T, Robey R, Bates SE (1999) Reversal of resistance by GF120918 in cell lines expressing the ABC half-transporter, MXR. Cancer Lett 146:117-126.

de Graaf D, Sharma RC, Mechetner EB, Schimke RT, Roninson IB (1996) P-glycoprotein confers methotrexate resistance in 3T6 cells with deficient carrier-mediated methotrexate uptake. Proc Natl Acad Sci U S A 93:1238-1242.

Dean M, Hamon Y, Chimini G (2001) The human ATP-binding cassette (ABC) transporter superfamily. Journal of Lipid Research 42:1007-1017.

Debry P, Nash EA, Neklason DW, Metherall JE (1997) Role of multidrug resistance P-glycoproteins in cholesterol esterification. J Biol Chem 272:1026-1031.

Decleves X, Chappey O, Boval B, Niel E, Scherrmann JM (1998) P-glycoprotein is more efficient at limiting uptake than inducing efflux of colchicine and vinblastine in HL-60 cells. Pharm Res 15:712-718.

DeGorter MK, Xia CQ, Yang JJ, Kim RB (2012) Drug transporters in drug efficacy and toxicity. Annu Rev Pharmacol Toxicol 52:249-273.

del Moral RG, Andujar M, Ramirez C, et al. (1997) Chronic cyclosporin A nephrotoxicity, P-glycoprotein overexpression, and relationships with intrarenal angiotensin II deposits. Am J Pathol 151:1705-1714.

Delannoy S, Urbatsch IL, Tombline G, Senior AE, Vogel PD (2005) Nucleotide binding to the multidrug resistance P-glycoprotein as studied by ESR spectroscopy. Biochemistry 44:14010-14019.

Demeule M, Brossard M, Beliveau R (1999) Cisplatin induces renal expression of P-glycoprotein and canalicular multispecific organic anion transporter. Am J Physiol 277:F832-840.

Demeule M, Laplante A, Murphy GF, Wenger RM, Beliveau R (1998) Identification of the cyclosporin-binding site in P-glycoprotein. Biochemistry 37:18110-18118.

Demmer A, Thole H, Kubesch P, et al. (1997) Localization of the iodomycin binding site in hamster P-glycoprotein. J Biol Chem 272:20913-20919.

Deng L, Lin-Lee YC, Claret FX, Kuo MT (2001) 2-acetylaminofluorene up-regulates rat mdr1b expression through generating reactive oxygen species that activate NF-kappa B pathway. J Biol Chem 276:413-420.

Denson LA, Auld KL, Schiek DS, McClure MH, Mangelsdorf DJ, Karpen SJ (2000) Interleukin-1beta suppresses retinoid transactivation of two hepatic transporter genes involved in bile formation. J Biol Chem 275:8835-8843.

Deves R, Boyd CA (1998) Transporters for cationic amino acids in animal cells: discovery, structure, and function. Physiol Rev 78:487-545.

Dey S, Ramachandra M, Pastan I, Gottesman MM, Ambudkar SV (1997) Evidence for two nonidentical drug-interaction sites in the human P-glycoprotein. Proc Natl Acad Sci U S A 94:10594-10599.

Diéras V, Bonneterre J, Laurence V, et al. (2005) Phase I Combining a P-Glycoprotein Inhibitor, MS209, in Combination with Docetaxel in Patients with Advanced Malignancies. Clinical Cancer Research 11:6256-6260.

Dinis-Oliveira RJ, de Pinho PG, Santos L, et al. (2009) Postmortem analyses unveil the poor efficacy of decontamination, anti-inflammatory and immunosuppressive therapies in paraquat human intoxications. PLoS One 4:e7149.

Dinis-Oliveira RJ, Duarte JA, Remiao F, Sanchez-Navarro A, Bastos ML, Carvalho F (2006a) Single high dose dexamethasone treatment decreases the pathological score and increases the survival rate of paraquat-intoxicated rats. Toxicology 227:73-85.

Dinis-Oliveira RJ, Duarte JA, Sanchez-Navarro A, Remiao F, Bastos ML, Carvalho F (2008) Paraquat poisonings: mechanisms of lung toxicity, clinical features, and treatment. Crit Rev Toxicol 38:13-71.

Dinis-Oliveira RJ, Remiao F, Carmo H, et al. (2006b) Paraquat exposure as an etiological factor of Parkinson's disease. Neurotoxicology 27:1110-22.

Dinis-Oliveira RJ, Remiao F, Duarte JA, et al. (2006c) P-glycoprotein induction: an antidotal pathway for paraquat-induced lung toxicity. Free Radic Biol Med 41:1213-1224.

Dinis-Oliveira RJ, Sousa C, Remiao F, et al. (2007a) Sodium salicylate prevents paraquat-induced apoptosis in the rat lung. Free Radic Biol Med 43:48-61.

Dinis-Oliveira RJ, Sousa C, Remiao F, et al. (2007b) Full survival of paraquat-exposed rats after treatment with sodium salicylate. Free Radic Biol Med 42:1017-28.

Dittmer D, Pati S, Zambetti G, et al. (1993) Gain of function mutations in p53. Nat Genet 4:42-46.

Doige CA, Yu X, Sharom FJ (1993) The effects of lipids and detergents on ATPase-active P-glycoprotein. Biochim Biophys Acta 1146:65-72.

Doran A, Obach RS, Smith BJ, et al. (2005) The impact of P-glycoprotein on the disposition of drugs targeted for indications of the central nervous system: evaluation using the MDR1A/1B knockout mouse model. Drug Metab Dispos 33:165-174.

Dorr R, Karanes C, Spier C, et al. (2001) Phase I/II study of the P-glycoprotein modulator PSC 833 in patients with acute myeloid leukemia. J Clin Oncol 19:1589-1599.

Doublier S, Riganti C, Voena C, et al. (2008) RhoA silencing reverts the resistance to doxorubicin in human colon cancer cells. Mol Cancer Res 6:1607-1620.

Drach J, Gsur A, Hamilton G, et al. (1996) Involvement of P-glycoprotein in the transmembrane transport of interleukin-2 (IL-2), IL-4, and interferon-gamma in normal human T lymphocytes. Blood 88:1747-1754.

Drori S, Eytan GD, Assaraf YG (1995) Potentiation of anticancer-drug cytotoxicity by multidrug-resistance chemosensitizers involves alterations in membrane fluidity leading to increased membrane permeability. Eur J Biochem 228:1020-1029.

Drozdzik M, Bialecka M, Mysliwiec K, Honczarenko K, Stankiewicz J, Sych Z (2003) Polymorphism in the P-glycoprotein drug transporter MDR1 gene: a possible link between environmental and genetic factors in Parkinson's disease. Pharmacogenetics 13:259-263.

Druley TE, Stein WD, Roninson IB (2001) Analysis of MDR1 P-glycoprotein conformational changes in permeabilized cells using differential immunoreactivity. Biochemistry 40:4312-4322.

Duraj J, Zazrivcova K, Bodo J, Sulikova M, Sedlak J (2005) Flavonoid quercetin, but not apigenin or luteolin, induced apoptosis in human myeloid leukemia cells and their resistant variants. Neoplasma 52:273-279.

Durk MR, Chan GNY, Campos CR, et al. (2012) 1α,25-Dihydroxyvitamin D3-liganded vitamin D receptor increases expression and transport activity of P-glycoprotein in isolated rat brain capillaries and human and rat brain microvessel endothelial cells. Journal of Neurochemistry 123:944-953.

Dussault I, Lin M, Hollister K, Wang EH, Synold TW, Forman BM (2001) Peptide mimetic HIV protease inhibitors are ligands for the orphan receptor SXR. J Biol Chem 276:33309-33312.

Ecker GF, Csaszar E, Kopp S, et al. (2002) Identification of ligand-binding regions of P-glycoprotein by activated-pharmacophore photoaffinity labeling and matrix-assisted laser desorption/ionization-time-of-flight mass spectrometry. Mol Pharmacol 61:637-648.

Eckford PD, Sharom FJ (2005) The reconstituted P-glycoprotein multidrug transporter is a flippase for glucosylceramide and other simple glycosphingolipids. Biochem J 389:517-526.

Eckford PD, Sharom FJ (2006) P-glycoprotein (ABCB1) interacts directly with lipid-based anti-cancer drugs and platelet-activating factors. Biochem Cell Biol 84:1022-1033.

Eckford PD, Sharom FJ (2008) Interaction of the P-glycoprotein multidrug efflux pump with cholesterol: effects on ATPase activity, drug binding and transport. Biochemistry 47:13686-13698.

Eckford PDW, Sharom FJ (2009) ABC Efflux Pump-Based Resistance to Chemotherapy Drugs. Chemical Reviews 109:2989-3011.

Eedara BB, Veerareddy PR, Jukanti R, Bandari S (2013) Improved oral bioavailability of fexofenadine hydrochloride using lipid surfactants: ex vivo, in situ and in vivo studies. Drug Dev Ind Pharm Epub ahead of print.

Ehret MJ, Levin GM, Narasimhan M, Rathinavelu A (2007) Venlafaxine induces P-glycoprotein in human Caco-2 cells. Hum Psychopharmacol 22:49-53.

Ekins S, Ecker GF, Chiba P, Swaan PW (2007) Future directions for drug transporter modelling. Xenobiotica 37:1152-1170.

Ekins S, Kim RB, Leake BF, et al. (2002) Application of three-dimensional quantitative structure-activity relationships of P-glycoprotein inhibitors and substrates. Mol Pharmacol 61:974-981.

El-Osta A, Kantharidis P, Zalcberg JR, Wolffe AP (2002) Precipitous release of methyl-CpG binding protein 2 and histone deacetylase 1 from the methylated human multidrug resistance gene (MDR1) on activation. Mol Cell Biol 22:1844-1857.

El Hafny B, Cano N, Piciotti M, Regina A, Scherrmann JM, Roux F (1997a) Role of P-glycoprotein in colchicine and vinblastine cellular kinetics in an immortalized rat brain microvessel endothelial cell line. Biochem Pharmacol 53:1735-1742.

El Hafny B, Chappey O, Piciotti M, Debray M, Boval B, Roux F (1997b) Modulation of P-glycoprotein activity by glial factors and retinoic acid in an immortalized rat brain microvessel endothelial cell line. Neurosci Lett 236:107-111.

Erlichman C, Moore M, Thiessen JJ, et al. (1993) Phase I pharmacokinetic study of cyclosporin A combined with doxorubicin. Cancer Res 53:4837-4842.

Ernest S, Bello-Reuss E (1999) Secretion of platelet-activating factor is mediated by MDR1 P-glycoprotein in cultured human mesangial cells. J Am Soc Nephrol 10:2306-2313.

Eytan GD, Regev R, Oren G, Assaraf YG (1996) The role of passive transbilayer drug movement in multidrug resistance and its modulation. J Biol Chem 271:12897-12902.

Famaey JP (1988) Colchicine in therapy. State of the art and new perspectives for an old drug. Clin Exp Rheumatol 6:305-317.

Fang M, Li J, Blauwkamp T, Bhambhani C, Campbell N, Cadigan KM (2006) C-terminal-binding protein directly activates and represses Wnt transcriptional targets in Drosophila. EMBO J 25:2735-2745.

Fardel O, Lecureur V, Daval S, Corlu A, Guillouzo A (1997) Up-regulation of P-glycoprotein expression in rat liver cells by acute doxorubicin treatment. Eur J Biochem 246:186-192.

Ferruzza S, Ranaldi G, Di Girolamo M, Sambuy Y (1995) The transport of lysine across monolayers of human cultured intestinal cells (Caco-2) depends on Na(+)-dependent and Na(+)-independent mechanisms on different plasma membrane domains. J Nutr 125:2577-2585.

Ferry DR, Malkhandi PJ, Russell MA, Kerr DJ (1995) Allosteric regulation of [3H]vinblastine binding to P-glycoprotein of MCF-7 ADR cells by dexniguldipine. Biochem Pharmacol 49:1851-1861.

Fine RL, Chambers TC, Sachs CW (1996) P-Glycoprotein, Multidrug Resistance and Protein Kinase C. Oncologist 1:261-268.

Fine RL, Patel J, Chabner BA (1988) Phorbol esters induce multidrug resistance in human breast cancer cells. Proc Natl Acad Sci U S A 85:582-586.

Fischer V, Rodriguez-Gascon A, Heitz F, et al. (1998) The multidrug resistance modulator valspodar (PSC 833) is metabolized by human cytochrome P450 3A. Implications for drug-drug interactions and pharmacological activity of the main metabolite. Drug Metab Dispos 26:802-811.

Flahaut M, Meier R, Coulon A, et al. (2009) The Wnt receptor FZD1 mediates chemoresistance in neuroblastoma through activation of the Wnt/beta-catenin pathway. Oncogene 28:2245-2256.

Fojo AT, Ueda K, Slamon DJ, Poplack DG, Gottesman MM, Pastan I (1987) Expression of a multidrug-resistance gene in human tumors and tissues. Proc Natl Acad Sci U S A 84:265–269.

Fojo AT, Whang-Peng J, Gottesman MM, Pastan I (1985) Amplification of DNA sequences in human multidrug-resistant KB carcinoma cells. Proc Natl Acad Sci U S A 82:7661-7665.

Ford JM, Hait WN (1990) Pharmacology of drugs that alter multidrug resistance in cancer. Pharmacol Rev 42:155-199.

Fox E, Bates SE (2007) Tariquidar (XR9576): a P-glycoprotein drug efflux pump inhibitor. Expert Rev Anticancer Ther 7:447-459.

Fracasso PM, Blum KA, Ma MK, et al. (2005) Phase I study of pegylated liposomal doxorubicin and the multidrug-resistance modulator, valspodar. Br J Cancer 93:46-53.

Fracasso PM, Brady MF, Moore DH, et al. (2001) Phase II study of paclitaxel and valspodar (PSC 833) in refractory ovarian carcinoma: a gynecologic oncology group study. J Clin Oncol 19:2975-2982.

Freedman LP (1999) Strategies for transcriptional activation by steroid/nuclear receptors. J Cell Biochem Suppl 32-33:103-109.

Frelet A, Klein M (2006) Insight in eukaryotic ABC transporter function by mutation analysis. FEBS Lett 580:1064-1084.

Fromm MF (2002) The influence of MDR1 polymorphisms on P-glycoprotein expression and function in humans. Adv Drug Deliv Rev 54:1295-1310.

Frommel TO, Coon JS, Tsuruo T, Roninson IB (1993) Variable effects of sodium butyrate on the expression and function of the MDR1 (P-glycoprotein) gene in colon carcinoma cell lines. Int J Cancer 55:297-302.

Fujita-Hamabe W, Nishida M, Nawa A, et al. (2012) Etoposide modulates the effects of oral morphine analgesia by targeting the intestinal P-glycoprotein. J Pharm Pharmacol 64:496-504.

Furuno T, Landi MT, Ceroni M, et al. (2002) Expression polymorphism of the blood-brain barrier component P-glycoprotein (MDR1) in relation to Parkinson's disease. Pharmacogenetics 12:529-534.

Furuya KN, Thottassery JV, Schuetz EG, Sharif M, Schuetz JD (1997) Bromocriptine transcriptionally activates the multidrug resistance gene (pgp2/mdr1b) by a novel pathway. J Biol Chem 272:11518-11525.

Gant TW, Oconnor CK, Corbitt R, Thorgeirsson U, Thorgeirsson SS (1995) In Vivo Induction of Liver P-Glycoprotein Expression by Xenobiotics in Monkeys. Toxicology and Applied Pharmacology 133:269-276.

Gant TW, Silverman JA, Thorgeirsson SS (1992) Regulation of P-glycoprotein gene expression in hepatocyte cultures and liver cell lines by a trans-acting transcriptional repressor. Nucleic Acids Res 20:2841-2846.

Garcia-Martin E, Pizarro RM, Martinez C, et al. (2006) Acquired resistance to the anticancer drug paclitaxel is associated with induction of cytochrome P450 2C8. Pharmacogenomics 7:575-585.

Garcia MG, Alaniz L, Lopes EC, Blanco G, Hajos SE, Alvarez E (2005) Inhibition of NF-kappaB activity by BAY 11-7082 increases apoptosis in multidrug resistant leukemic T-cell lines. Leuk Res 29:1425-1434.

Garcia MG, Alaniz LD, Cordo Russo RI, Alvarez E, Hajos SE (2009) PI3K/Akt inhibition modulates multidrug resistance and activates NF-kappaB in murine lymphoma cell lines. Leuk Res 33:288-296.

Garrigos M, Mir LM, Orlowski S (1997) Competitive and non-competitive inhibition of the multidrug-resistance-associated P-glycoprotein ATPase--further experimental evidence for a multisite model. Eur J Biochem 244:664-673.

Gayet L, Dayan G, Barakat S, et al. (2005) Control of P-glycoprotein activity by membrane cholesterol amounts and their relation to multidrug resistance in human CEM leukemia cells. Biochemistry 44:4499-4509.

Geick A, Eichelbaum M, Burk O (2001) Nuclear Receptor Response Elements Mediate Induction of Intestinal MDR1 by Rifampin. Journal of Biological Chemistry 276:14581-14587.

Gekeler V, Boer R, Ise W, Sanders KH, Schachtele C, Beck J (1995) The specific bisindolylmaleimide PKC-inhibitor GF 109203X efficiently modulates MRP-associated multiple drug resistance. Biochem Biophys Res Commun 206:119-126.

Gekeler V, Frese G, Diddens H, Probst H (1988) Expression of a P-glycoprotein gene is inducible in a multidrug-resistant human leukemia cell line. Biochem Biophys Res Commun 155:754-760.

Genoux-Bastide E, Lorendeau D, Nicolle E, et al. (2011) Identification of Xanthones as Selective Killers of Cancer Cells Overexpressing the ABC Transporter MRP1. ChemMedChem 6:1478-1484.

Gerbal-Chaloin S, Daujat M, Pascussi JM, Pichard-Garcia L, Vilarem MJ, Maurel P (2002) Transcriptional regulation of CYP2C9 gene. Role of glucocorticoid receptor and constitutive androstane receptor. J Biol Chem 277:209-217.

Germann UA (1996) P-glycoprotein--a mediator of multidrug resistance in tumour cells. Eur J Cancer 32A:927-944.

Germann UA, Chambers TC, Ambudkar SV, Pastan I, Gottesman MM (1995) Effects of phosphorylation of P-glycoprotein on multidrug resistance. J Bioenerg Biomembr 27:53-61.

Germann UA, Ford PJ, Shlyakhter D, Mason VS, Harding MW (1997a) Chemosensitization and drug accumulation effects of VX-710, verapamil, cyclosporin A, MS-209 and GF120918 in multidrug resistant HL60/ADR cells expressing the multidrug resistance-associated protein MRP. Anticancer Drugs 8:141-155.

Germann UA, Shlyakhter D, Mason VS, et al. (1997b) Cellular and biochemical characterization of VX-710 as a chemosensitizer: reversal of P-glycoprotein-mediated multidrug resistance in vitro. Anticancer Drugs 8:125-140.

Ghanem CI, Gómez PC, Arana MC, et al. (2006) Induction of Rat Intestinal P-glycoprotein by Spironolactone and Its Effect on Absorption of Orally Administered Digoxin. Journal of Pharmacology and Experimental Therapeutics 318:1146-1152.

Giaccone G, Linn SC, Welink J, et al. (1997) A dose-finding and pharmacokinetic study of reversal of multidrug resistance with SDZ PSC 833 in combination with doxorubicin in patients with solid tumors. Clin Cancer Res 3:2005-2015.

Giacomini KM, Huang SM, Tweedie DJ, et al. (2010) Membrane transporters in drug development. Nat Rev Drug Discov 9:215-236.

Giessmann T, May K, Modess C, et al. (2004) Carbamazepine regulates intestinal P-glycoprotein and multidrug resistance protein MRP2 and influences disposition of talinolol in humans. Clin Pharmacol Ther 76:192-200.

Gil S, Saura R, Forestier F, Farinotti R (2005) P-glycoprotein expression of the human placenta during pregnancy. Placenta 26:268-270.

Gill DR, Hyde SC, Higgins CF, Valverde MA, Mintenig GM, Sepulveda FV (1992) Separation of drug transport and chloride channel functions of the human multidrug resistance P-glycoprotein. Cell 71:23-32.

Gill PK, Gescher A, Gant TW (2001) Regulation of MDR1 promoter activity in human breast carcinoma cells by protein kinase C isozymes alpha and theta. Eur J Biochem 268:4151-4157.

Gille H, Sharrocks AD, Shaw PE (1992) Phosphorylation of transcription factor p62TCF by MAP kinase stimulates ternary complex formation at c-fos promoter. Nature 358:414-417.

Goldsmith ME, Gudas JM, Schneider E, Cowan KH (1995) Wild type p53 stimulates expression from the human multidrug resistance promoter in a p53-negative cell line. J Biol Chem 270:1894-1898.

Goldsmith ME, Madden MJ, Morrow CS, Cowan KH (1993) A Y-box consensus sequence is required for basal expression of the human multidrug resistance (mdr1) gene. J Biol Chem 268:5856-5860.

Gottesman MM, Ambudkar SV (2001) Overview: ABC transporters and human disease. J Bioenerg Biomembr 33:453-458.

Gottesman MM, Fojo T, Bates SE (2002) Multidrug resistance in cancer: role of ATP-dependent transporters. Nat Rev Cancer 2:48-58.

Gottesman MM, Pastan I (1993) Biochemistry of multidrug resistance mediated by the multidrug transporter. Annu Rev Biochem 62:385-427.

Gottesman MM, Pastan I, Ambudkar SV (1996) P-glycoprotein and multidrug resistance. Curr Opin Genet Dev 6:610-617.

Grabie V, Scemama JL, Robertson JB, Seidel ER (1993) Paraquat uptake in the cultured gastrointestinal epithelial cell line, IEC-6. Toxicol Appl Pharmacol 122:95-100.

Green LJ, Marder P, Slapak CA (2001) Modulation by LY335979 of P-glycoprotein function in multidrug-resistant cell lines and human natural killer cells. Biochem Pharmacol 61:1393-1399.

Greenberger LM (1993) Major photoaffinity drug labeling sites for iodoaryl azidoprazosin in P-glycoprotein are within, or immediately C-terminal to, transmembrane domains 6 and 12. J Biol Chem 268:11417-11425.

Greiner B, Eichelbaum M, Fritz P, et al. (1999) The role of intestinal P-glycoprotein in the interaction of digoxin and rifampin. J Clin Invest 104:147-153.

Groblewski GE, Hargittai PT, Seidel ER (1992) Ca2+/calmodulin regulation of putrescine uptake in cultured gastrointestinal epithelial cells. Am J Physiol 262:C1356-1363.

Gromnicova R, Romero I, Male D (2012) Transcriptional control of the multi-drug transporter ABCB1 by transcription factor Sp3 in different human tissues. PLoS One 7:e48189.

Gruber A, Bjorkholm M, Brinch L, et al. (2003) A phase I/II study of the MDR modulator Valspodar (PSC 833) combined with daunorubicin and cytarabine in patients with relapsed and primary refractory acute myeloid leukemia. Leuk Res 27:323-328.

Grunicke H, Hofmann J, Utz I, Uberall F (1994) Role of protein kinases in antitumor drug resistance. Ann Hematol 69 Suppl 1:S1-6.

Gruol DJ, Vo QD, Zee MC (1999) Profound differences in the transport of steroids by two mouse P-glycoproteins. Biochem Pharmacol 58:1191-1199.

Gumbiner BM (2005) Coordinate Gene Regulation by Two Different Catenins. Developmental Cell 8:795-796.

Guns ES, Denyssevych T, Dixon R, Bally MB, Mayer L (2002) Drug interaction studies between paclitaxel (Taxol) and OC144-093--a new modulator of MDR in cancer chemotherapy. Eur J Drug Metab Pharmacokinet 27:119-126.

Guo X, Ma N, Wang J, et al. (2008) Increased p38-MAPK is responsible for chemotherapy resistance in human gastric cancer cells. BMC Cancer 8:375.

Haber M, Smith J, Bordow SB, et al. (2006) Association of high-level MRP1 expression with poor clinical outcome in a large prospective study of primary neuroblastoma. J Clin Oncol 24:1546-1553.

Han Y, Chin Tan TM, Lim L-Y (2008) In vitro and in vivo evaluation of the effects of piperine on P-gp function and expression. Toxicology and Applied Pharmacology 230:283-289.

Han Y, Tan TM, Lim LY (2006) Effects of capsaicin on P-gp function and expression in Caco-2 cells. Biochem Pharmacol 71:1727-1734.

Hanekop N, Zaitseva J, Jenewein S, Holland IB, Schmitt L (2006) Molecular insights into the mechanism of ATP-hydrolysis by the NBD of the ABC-transporter HlyB. FEBS Lett 580:1036-1041.

Hardy SP, Goodfellow HR, Valverde MA, Gill DR, Sepulveda V, Higgins CF (1995) Protein kinase C-mediated phosphorylation of the human multidrug resistance P-glycoprotein regulates cell volume-activated chloride channels. EMBO J 14:68-75.

Harmsen S, Meijerman I, Febus CL, Maas-Bakker RF, Beijnen JH, Schellens JH (2009) PXR-mediated induction of P-glycoprotein by anticancer drugs in a human colon adenocarcinoma-derived cell line. Cancer Chemother Pharmacol 66:765-771.

Harmsen S, Meijerman I, Maas-Bakker RF, Beijnen JH, Schellens JHM (2013) PXR-mediated P-glycoprotein induction by small molecule tyrosine kinase inhibitors. European Journal of Pharmaceutical Sciences 48:644-649.

Hartz AM, Bauer B, Block ML, Hong JS, Miller DS (2008) Diesel exhaust particles induce oxidative stress, proinflammatory signaling, and P-glycoprotein up-regulation at the blood-brain barrier. FASEB J 22:2723-2733.

Haslam IS, Jones K, Coleman T, Simmons NL (2008a) Induction of P-glycoprotein expression and function in human intestinal epithelial cells (T84). Biochem Pharmacol 76:850-861.

Haslam IS, Jones K, Coleman T, Simmons NL (2008b) Rifampin and digoxin induction of MDR1 expression and function in human intestinal (T84) epithelial cells. Br J Pharmacol 154:246-255.

Hassan HE, Myers AL, Lee IJ, Coop A, Eddington ND (2007) Oxycodone induces overexpression of P-glycoprotein (ABCB1) and affects paclitaxel's tissue distribution in Sprague Dawley rats. J Pharm Sci 96:2494-2506.

Helmlinger G, Yuan F, Dellian M, Jain RK (1997) Interstitial pH and pO2 gradients in solid tumors in vivo: high-resolution measurements reveal a lack of correlation. Nat Med 3:177-182.

Hennessy M, Kelleher D, Spiers JP, et al. (2002) St Johns wort increases expression of P-glycoprotein: implications for drug interactions. Br J Clin Pharmacol 53:75-82.

Hennessy M, Spiers JP (2007) A primer on the mechanics of P-glycoprotein the multidrug transporter. Pharmacological Research 55:1-15.

Herzog CE, Tsokos M, Bates SE, Fojo AT (1993) Increased mdr-1/P-glycoprotein expression after treatment of human colon carcinoma cells with P-glycoprotein antagonists. Journal of Biological Chemistry 268:2946-2952.

Hidalgo IJ, Jibin L (1996) Carrier-mediated transport and efflux mechanisms in Caco-2 cells Advanced Drug Delivery Reviews 22:53-66.

Hien TT, Kim HG, Han EH, Kang KW, Jeong HG (2010) Molecular mechanism of suppression of MDR1 by puerarin from Pueraria lobata via NF-kappaB pathway and cAMP-responsive element transcriptional activity-dependent up-regulation of AMP-activated protein kinase in breast cancer MCF-7/adr cells. Mol Nutr Food Res 54:918-928.

Higgins CF (1992) ABC transporters: from microorganisms to man. Annu Rev Cell Biol 8:67-113.

Higgins CF (2007) Multiple molecular mechanisms for multidrug resistance transporters. Nature 446:749-757.

Higgins CF, Callaghan R, Linton KJ, Rosenberg MF, Ford RC (1997) Structure of the multidrug resistance P-glycoprotein. Seminars in Cancer Biology 8:135-142.

Higgins CF, Gottesman MM (1992) Is the multidrug transporter a flippase? Trends Biochem Sci 17:18-21.

Higgins CF, Linton KJ (2004) The ATP switch model for ABC transporters. Nat Struct Mol Biol 11:918-926.

Hill BT, Whelan RD, Hurst HC, McClean S (1994) Identification of a distinctive P-glycoprotein-mediated resistance phenotype in human ovarian carcinoma cells after their in vitro exposure to fractionated X-irradiation. Cancer 73:2990-2999.

Hill CS, Treisman R (1995) Transcriptional regulation by extracellular signals: mechanisms and specificity. Cell 80:199-211.

Hirao M, Sato N, Kondo T, et al. (1996) Regulation mechanism of ERM (ezrin/radixin/moesin) protein/plasma membrane association: possible involvement of phosphatidylinositol turnover and Rho-dependent signaling pathway. J Cell Biol 135:37-51.

Hirohashi T, Suzuki H, Chu X-Y, Tamai I, Tsuji A, Sugiyama Y (2000) Function and Expression of Multidrug Resistance-Associated Protein Family in Human Colon Adenocarcinoma Cells (Caco-2). The Journal of Pharmacology and Experimental Therapeutics 292:265-270.

Ho GT, Soranzo N, Nimmo ER, Tenesa A, Goldstein DB, Satsangi J (2006) ABCB1/MDR1 gene determines susceptibility and phenotype in ulcerative colitis: discrimination of critical variants using a gene-wide haplotype tagging approach. Hum Mol Genet 15:797-805.

Hoffmeyer S, Burk O, von Richter O, et al. (2000) Functional polymorphisms of the human multidrug-resistance gene: multiple sequence variations and correlation of one allele with P-glycoprotein expression and activity in vivo. Proc Natl Acad Sci U S A 97:3473-3478.

Hollenstein K, Frei DC, Locher KP (2007) Structure of an ABC transporter in complex with its binding protein. Nature 446:213-216.

Hollo Z, Homolya L, Davis CW, Sarkadi B (1994) Calcein accumulation as a fluorometric functional assay of the multidrug transporter. Biochim Biophys Acta 1191:384-388.

Homolya L, Hollo Z, Germann UA, Pastan I, Gottesman MM, Sarkadi B (1993) Fluorescent cellular indicators are extruded by the multidrug resistance protein. J Biol Chem 268:21493-21496.

Hosokawa N, Hirayoshi K, Kudo H, et al. (1992) Inhibition of the activation of heat shock factor in vivo and in vitro by flavonoids. Mol Cell Biol 12:3490-3498.

Hosoya KI, Kim KJ, Lee VH (1996) Age-dependent expression of P-glycoprotein gp170 in Caco-2 cell monolayers. Pharm Res 13:885-890.

Hou T, Xu X (2004) Recent development and application of virtual screening in drug discovery: an overview. Curr Pharm Des 10:1011-1033.

Hou X-L, Takahashi K, Tanaka K, et al. (2008) Curcuma drugs and curcumin regulate the expression and function of P-gp in Caco-2 cells in completely opposite ways. International Journal of Pharmaceutics 358:224-229.

Howe LR, Leevers SJ, Gomez N, Nakielny S, Cohen P, Marshall CJ (1992) Activation of the MAP kinase pathway by the protein kinase raf. Cell 71:335-342.

Hu XF, Slater A, Rischin D, Kantharidis P, Parkin JD, Zalcberg J (1999) Induction of MDR1 gene expression by anthracycline analogues in a human drug resistant leukaemia cell line. Br J Cancer 79:831-837.

Hu XF, Slater A, Wall DM, et al. (1995) Rapid up-regulation of mdr1 expression by anthracyclines in a classical multidrug-resistant cell line. Br J Cancer 71:931-936.

Hu Z, Jin S, Scotto KW (2000) Transcriptional Activation of the MDR1 Gene by UV Irradiation: ROLE OF NF-Y AND Sp1. Journal of Biological Chemistry 275:2979-2985.

Huang J, Ma G, Muhammad I, Cheng Y (2007) Identifying P-Glycoprotein Substrates Using a Support Vector Machine Optimized by a Particle Swarm. Journal of Chemical Information and Modeling 47:1638-1647.

Huang L, Wring SA, Woolley JL, Brouwer KR, Serabjit-Singh C, Polli JW (2001) Induction of P-glycoprotein and cytochrome P450 3A by HIV protease inhibitors. Drug Metab Dispos 29:754-760.

Huang R, Murry DJ, Kolwankar D, Hall SD, Foster DR (2006) Vincristine transcriptional regulation of efflux drug transporters in carcinoma cell lines. Biochem Pharmacol 71:1695-1704.

Hugger ED, Audus KL, Borchardt RT (2002a) Effects of poly(ethylene glycol) on efflux transporter activity in Caco-2 cell monolayers. J Pharm Sci 91:1980-1990.

Hugger ED, Novak BL, Burton PS, Audus KL, Borchardt RT (2002b) A comparison of commonly used polyethoxylated pharmaceutical excipients on their ability to inhibit P-glycoprotein activity in vitro. J Pharm Sci 91:1991-2002.

Humeny A, Rodel F, Rodel C, et al. (2003) MDR1 single nucleotide polymorphism C3435T in normal colorectal tissue and colorectal carcinomas detected by MALDI-TOF mass spectrometry. Anticancer Res 23:2735-2740.

Hunter J, Jepson MA, Tsuruo T, Simmons NL, Hirst BH (1993) Functional expression of P-glycoprotein in apical membranes of human intestinal Caco-2 cells. Kinetics of vinblastine secretion and interaction with modulators. J Biol Chem 268:14991-14997.

Hunter T, Karin M (1992) The regulation of transcription by phosphorylation. Cell 70:375-387.

Huynh-Delerme C, Huet H, Noel L, Frigieri A, Kolf-Clauw M (2005) Increased functional expression of P-glycoprotein in Caco-2 TC7 cells exposed long-term to cadmium. Toxicol In Vitro 19:439-447.

Hyafil F, Vergely C, Du Vignaud P, Grand-Perret T (1993) In vitro and in vivo reversal of multidrug resistance by GF120918, an acridonecarboxamide derivative. Cancer Res 53:4595-4602.

Hyde SC, Emsley P, Hartshorn MJ, et al. (1990) Structural model of ATP-binding proteing associated with cystic fibrosis, multidrug resistance and bacterial transport. Nature 346:362-365.

Ichihashi N, Kitajima Y (2001) Chemotherapy induces or increases expression of multidrug resistance-associated protein in malignant melanoma cells. Br J Dermatol 144:745-750.

Ihnat MA, Lariviere JP, Warren AJ, et al. (1997) Suppression of P-glycoprotein expression and multidrug resistance by DNA cross-linking agents. Clin Cancer Res 3:1339-1346.

IJpenberg A, Tan NS, Gelman L, et al. (2004) In vivo activation of PPAR target genes by RXR homodimers. EMBO J 23:2083-2091.

Ikeguchi M, Teeter LD, Eckersberg T, Ganapathi R, Kuo MT (1991) Structural and functional analyses of the promoter of the murine multidrug resistance gene mdr3/mdr1a reveal a negative element containing the AP-1 binding site. DNA Cell Biol 10:639-649.

Isenberg B, Thole H, Tummler B, Demmer A (2001) Identification and localization of three photobinding sites of iodoarylazidoprazosin in hamster P-glycoprotein. Eur J Biochem 268:2629-2634.

Ishii K, Tanaka S, Kagami K, et al. (2010) Effects of naturally occurring polymethyoxyflavonoids on cell growth, p-glycoprotein function, cell cycle, and apoptosis of daunorubicin-resistant T lymphoblastoid leukemia cells. Cancer Invest 28:220-229.

Ishri RK, Menzies S, Halliday GM (2006) Verapamil induces upregulation of P-glycoprotein expression on human monocyte derived dendritic cells. Immunol Invest 35:1-18.

Ivetac A, Campbell JD, Sansom MS (2007) Dynamics and function in a bacterial ABC transporter: simulation studies of the BtuCDF system and its components. Biochemistry 46:2767-2778.

Jacobs MN, Nolan GT, Hood SR (2005) Lignans, bacteriocides and organochlorine compounds activate the human pregnane X receptor (PXR). Toxicol Appl Pharmacol 209:123-133.

Janas E, Hofacker M, Chen M, Gompf S, van der Does C, Tampe R (2003) The ATP hydrolysis cycle of the nucleotide-binding domain of the mitochondrial ATP-binding cassette transporter Mdl1p. J Biol Chem 278:26862-26869.

Janknecht R, Ernst WH, Pingoud V, Nordheim A (1993) Activation of ternary complex factor Elk-1 by MAP kinases. EMBO J 12:5097-5104.

Janssen YM, Heintz NH, Mossman BT (1995) Induction of c-fos and c-jun proto-oncogene expression by asbestos is ameliorated by N-acetyl-L-cysteine in mesothelial cells. Cancer Res 55:2085-2089.

Jette L, Beaulieu E, Leclerc JM, Beliveau R (1996) Cyclosporin A treatment induces overexpression of P-glycoprotein in the kidney and other tissues. Am J Physiol 270:F756-765.

Jette L, Pouliot JF, Murphy GF, Beliveau R (1995) Isoform I (mdr3) is the major form of P-glycoprotein expressed in mouse brain capillaries. Evidence for cross-reactivity of antibody C219 with an unrelated protein. Biochem J 305 (Pt 3):761-766.

Ji D, Deeds SL, Weinstein EJ (2007) A screen of shRNAs targeting tumor suppressor genes to identify factors involved in A549 paclitaxel sensitivity. Oncol Rep 18:1499-1505.

Ji Z, Long H, Hu Y, et al. (2010) Expression of MDR1, HIF-1α and MRP1 in sacral chordoma and chordoma cell line CM-319. Journal of Experimental & Clinical Cancer Research 29:158.

Jin MS, Oldham ML, Zhang Q, Chen J (2012) Crystal structure of the multidrug transporter P-glycoprotein from Caenorhabditis elegans. Nature 490:566-569.

Jin S, Scotto KW (1998) Transcriptional regulation of the MDR1 gene by histone acetyltransferase and deacetylase is mediated by NF-Y. Mol Cell Biol 18:4377-4384.

Jin W, Scotto KW, Hait WN, Yang J-M (2007) Involvement of CtBP1 in the transcriptional activation of the MDR1 gene in human multidrug resistant cancer cells. Biochemical Pharmacology 74:851-859.

Johnson DR, Finch RA, Lin ZP, Zeiss CJ, Sartorelli AC (2001a) The pharmacological phenotype of combined multidrug-resistance mdr1a/1b- and mrp1-deficient mice. Cancer Res 61:1469-1476.

Johnson RA, Ince TA, Scotto KW (2001b) Transcriptional repression by p53 through direct binding to a novel DNA element. J Biol Chem 276:27716-27720.

Johnstone RW, Cretney E, Smyth MJ (1999) P-glycoprotein protects leukemia cells against caspase-dependent, but not caspase-independent, cell death. Blood 93:1075-1085.

Johnstone RW, Ruefli AA, Smyth MJ (2000) Multiple physiological functions for multidrug transporter P-glycoprotein? Trends Biochem Sci 25:1-6.

Jones PM, George AM (1998) A new structural model for P-glycoprotein. J Membr Biol 166:133-147.

Jones PM, George AM (1999) Subunit interactions in ABC transporters: towards a functional architecture. FEMS Microbiol Lett 179:187-202.

Jones PM, George AM (2000) Symmetry and structure in P-glycoprotein and ABC transporters what goes around comes around. Eur J Biochem 267:5298-5305.

Jonker JW, Wagenaar E, van Deemter L, et al. (1999) Role of blood-brain barrier P-glycoprotein in limiting brain accumulation and sedative side-effects of asimadoline, a peripherally acting analgaesic drug. Br J Pharmacol 127:43-50.

Juliano RL, Ling V (1976) A surface glycoprotein modulating drug permeability in Chinese hamster ovary cell mutants. Biochim Biophys Acta 455:152-162.

Julien M, Gros P (2000) Nucleotide-induced conformational changes in P-glycoprotein and in nucleotide binding site mutants monitored by trypsin sensitivity. Biochemistry 39:4559-4568.

Kageyama M, Fukushima K, Togawa T, et al. (2006) Relationship between excretion clearance of rhodamine 123 and P-glycoprotein (Pgp) expression induced by representative Pgp inducers. Biol Pharm Bull 29:779-784.

Kajiji S, Talbot F, Grizzuti K, et al. (1993) Functional analysis of P-glycoprotein mutants identifies predicted transmembrane domain 11 as a putative drug binding site. Biochemistry 32:4185-4194.

Kajinami K, Brousseau ME, Ordovas JM, Schaefer EJ (2004) Polymorphisms in the multidrug resistance-1 (MDR1) gene influence the response to atorvastatin treatment in a gender-specific manner. Am J Cardiol 93:1046-1050.

Kalabis GM, Kostaki A, Andrews MH, Petropoulos S, Gibb W, Matthews SG (2005) Multidrug resistance phosphoglycoprotein (ABCB1) in the mouse placenta: fetal protection. Biol Reprod 73:591-597.

Kalin N, Fernandes J, Hrafnsdottir S, van Meer G (2004) Natural phosphatidylcholine is actively translocated across the plasma membrane to the surface of mammalian cells. J Biol Chem 279:33228-33236.

Kamath AV, Darling IM, Morris ME (2003) Choline uptake in human intestinal Caco-2 cells is carrier-mediated. J Nutr 133:2607-2611.

Kamau SW, Kramer SD, Gunthert M, Wunderli-Allenspach H (2005) Effect of the modulation of the membrane lipid composition on the localization and function of P-glycoprotein in MDR1-MDCK cells. In Vitro Cell Dev Biol Anim 41:207-216.

Kang C-D, Ahn B-K, Jeong C-S, et al. (2000) Downregulation of JNK/SAPK Activity Is Associated with the Cross-Resistance to P-Glycoprotein-Unrelated Drugs in Multidrug-Resistant FM3A/M Cells Overexpressing P-Glycoprotein. Experimental Cell Research 256:300-307.

Kang MH, Figg WD, Ando Y, et al. (2001) The P-glycoprotein antagonist PSC 833 increases the plasma concentrations of 6alpha-hydroxypaclitaxel, a major metabolite of paclitaxel. Clin Cancer Res 7:1610-1617.

Karin M (1999) How NF-kappaB is activated: the role of the IkappaB kinase (IKK) complex. Oncogene 18:6867-6874.

Kast C, Canfield V, Levenson R, Gros P (1996) Transmembrane Organization of Mouse P-glycoprotein Determined by Epitope Insertion and Immunofluorescence. Journal of Biological Chemistry 271:9240-9248.

Kast HR, Goodwin B, Tarr PT, et al. (2002) Regulation of multidrug resistance-associated protein 2 (ABCC2) by the nuclear receptors pregnane X receptor, farnesoid X-activated receptor, and constitutive androstane receptor. J Biol Chem 277:2908-2915.

Katayama K, Yoshioka S, Tsukahara S, Mitsuhashi J, Sugimoto Y (2007) Inhibition of the mitogen-activated protein kinase pathway results in the down-regulation of P-glycoprotein. Mol Cancer Ther 6:2092-2102.

Kato T, Duffey DC, Ondrey FG, et al. (2000) Cisplatin and radiation sensitivity in human head and neck squamous carcinomas are independently modulated by glutathione and transcription factor NF-kappaB. Head Neck 22:748-759.

Kelly RJ, Draper D, Chen CC, et al. (2011) A Pharmacodynamic Study of Docetaxel in Combination with the P-glycoprotein Antagonist Tariquidar (XR9576) in Patients with Lung, Ovarian, and Cervical Cancer. Clinical Cancer Research 17:569-580.

Keniry M, Parsons R (2008) The role of PTEN signaling perturbations in cancer and in targeted therapy. Oncogene 27:5477-5485.

Kikuchi S, Hata M, Fukumoto K, et al. (2002) Radixin deficiency causes conjugated hyperbilirubinemia with loss of Mrp2 from bile canalicular membranes. Nat Genet 31:320-325.

Kim KA, Park PW, Liu KH, et al. (2008) Effect of rifampin, an inducer of CYP3A and P-glycoprotein, on the pharmacokinetics of risperidone. J Clin Pharmacol 48:66-72.

Kim R, Beck WT (1994) Differences between drug-sensitive and -resistant human leukemic CEM cells in c-jun expression, AP-1 DNA-binding activity, and formation of Jun/Fos family dimers, and their association with internucleosomal DNA ladders after treatment with VM-26. Cancer Res 54:4958-4966.

Kim RB (2002) Drugs as P-glycoprotein substrates, inhibitors, and inducers. Drug Metab Rev 34:47-54.

Kim RB, Leake BF, Choo EF, et al. (2001) Identification of functionally variant MDR1 alleles among European Americans and African Americans. Clin Pharmacol Ther 70:189-199.

Kim RB, Wandel C, Leake B, et al. (1999) Interrelationship between substrates and inhibitors of human CYP3A and P-glycoprotein. Pharm Res 16:408-414.

Kim S-H, Lee S-H, Kwak N-H, Kang C-D, Chung B-S (1996) Effect of the activated Raf protein kinase on the human multidrug resistance 1 (MDR1) gene promoter. Cancer letters 98:199-205.

Kim SH, Hur WY, Kang CD, Lim YS, Kim DW, Chung BS (1997) Involvement of heat shock factor in regulating transcriptional activation of MDR1 gene in multidrug-resistant cells. Cancer Lett 115:9-14.

Kim SH, Park JI, Chung BS, Kang CD, Hidaka H (1993) Inhibition of MDR1 gene expression by H-87, a selective inhibitor of cAMP-dependent protein kinase. Cancer Lett 74:37-41.

Kim SH, Yeo GS, Lim YS, Kang CD, Kim CM, Chung BS (1998) Suppression of multidrug resistance via inhibition of heat shock factor by quercetin in MDR cells. Exp Mol Med 30:87-92.

Kimchi-Sarfaty C, Oh JM, Kim IW, et al. (2007) A "silent" polymorphism in the MDR1 gene changes substrate specificity. Science 315:525-528.

Kimura Y, Aoki J, Kohno M, Ooka H, Tsuruo T, Nakanishi O (2002) P-glycoprotein inhibition by the multidrug resistance-reversing agent MS-209 enhances bioavailability and antitumor efficacy of orally administered paclitaxel. Cancer Chemother Pharmacol 49:322-328.

Kioka N, Hosokawa N, Komano T, Hirayoshi K, Nagata K, Ueda K (1992a) Quercetin, a bioflavonoid, inhibits the increase of human multidrug resistance gene (MDR1) expression caused by arsenite. FEBS Lett 301:307-309.

Kioka N, Yamano Y, Komano T, Ueda K (1992b) Heat-shock responsive elements in the induction of the multidrug resistance gene (MDR1). FEBS Letters 301:37-40.

Kisucka J, Barancik M, Bohacova V, Breier A (2001) Reversal effect of specific inhibitors of extracellular-signal regulated protein kinase pathway on P-glycoprotein mediated vincristine resistance of L1210 cells. Gen Physiol Biophys 20:439-444.

Klaunig JE, Kamendulis LM (2004) The role of oxidative stress in carcinogenesis. Annu Rev Pharmacol Toxicol 44:239-267.

Klepsch F, Ecker GF (2010) Impact of the Recent Mouse P-Glycoprotein Structure for Structure-Based Ligand Design. Molecular Informatics 29:276-286.

Kliewer SA, Goodwin B, Willson TM (2002) The nuclear pregnane X receptor: a key regulator of xenobiotic metabolism. Endocr Rev 23:687-702.

Klimecki WT, Futscher BW, Grogan TM, Dalton WS (1994) P-glycoprotein expression and function in circulating blood cells from normal volunteers. Blood 83:2451-2458.

Kobori T, Harada S, Nakamoto K, Tokuyama S (2013a) Activation of ERM-family proteins via RhoA-ROCK signaling increases intestinal P-gp expression and leads to attenuation of oral morphine analgesia. J Pharm Sci 102:1095-1105.

Kobori T, Harada S, Nakamoto K, Tokuyama S (2013b) Time-dependent changes in the activation of RhoA/ROCK and ERM/p-ERM in the increased expression of intestinal P-glycoprotein by repeated oral treatment with etoposide. J Pharm Sci 102:1670-1682.

Kobori T, Kobayashi M, Harada S, Nakamoto K, Fujita-Hamabe W, Tokuyama S (2012) RhoA affects oral morphine analgesia depending on functional variation in intestinal P-glycoprotein induced by repeated etoposide treatment. Eur J Pharm Sci 47:934-940.

Kohno K, Sato S, Takano H, Matsuo K, Kuwano M (1989) The direct activation of human multidrug resistance gene (MDR1) by anticancer agents. Biochem Biophys Res Commun 165:1415-1421.

Kondratov RV, Komarov PG, Becker Y, Ewenson A, Gudkov AV (2001) Small molecules that dramatically alter multidrug resistance phenotype by modulating the substrate specificity of P-glycoprotein. Proc Natl Acad Sci U S A 98:14078-14083.

Krishnamurthy K, Vedam K, Kanagasabai R, Druhan LJ, Ilangovan G (2012) Heat shock factor-1 knockout induces multidrug resistance gene, MDR1b, and enhances P-glycoprotein (ABCB1)-based drug extrusion in the heart. Proc Natl Acad Sci U S A 109:9023-9028.

Kruijtzer CM, Beijnen JH, Rosing H, et al. (2002) Increased oral bioavailability of topotecan in combination with the breast cancer resistance protein and P-glycoprotein inhibitor GF120918. J Clin Oncol 20:2943-2950.

Kubinyi H (2008) Statistical Methods. In: Mannhold R, Krogsgaard-Larsen P, Timmerman H (eds) QSAR: Hansch Analysis and Related Approaches. Wiley-VCH Verlag GmbH, Weinheim, p 91-107.

Kuo MT, Liu Z, Wei Y, et al. (2002) Induction of human MDR1 gene expression by 2-acetylaminofluorene is mediated by effectors of the phosphoinositide 3-kinase pathway that activate NF-kappaB signaling. Oncogene 21:1945-1954.

Kuppens IELM, Bosch TM, Maanen MJ, et al. (2005) Oral bioavailability of docetaxel in combination with OC144-093 (ONT-093). Cancer Chemotherapy and Pharmacology 55:72-78.

Kurzawski M, Drozdzik M, Suchy J, et al. (2005) Polymorphism in the P-glycoprotein drug transporter MDR1 gene in colon cancer patients. Eur J Clin Pharmacol 61:389-394.

Kusaba H, Nakayama M, Harada T, et al. (1999) Association of 5' CpG demethylation and altered chromatin structure in the promoter region with transcriptional activation of the multidrug resistance 1 gene in human cancer cells. Eur J Biochem 262:924-932.

Kusunoki N, Takara K, Tanigawara Y, et al. (1998) Inhibitory effects of a cyclosporin derivative, SDZ PSC 833, on transport of doxorubicin and vinblastine via human P-glycoprotein. Jpn J Cancer Res 89:1220-1228.

Labialle S, Gayet L, Marthinet E, Rigal D, Baggetto LG (2002a) Transcriptional Regulation of the Human MDR1 Gene at the Level of the Inverted MED-1 Promoter Region. Annals of the New York Academy of Sciences 973:468-471.

Labialle S, Gayet L, Marthinet E, Rigal D, Baggetto LG (2002b) Transcriptional regulators of the human multidrug resistance 1 gene: recent views. Biochemical Pharmacology 64:943-948.

Lagadinou ED, Ziros PG, Tsopra OA, et al. (2008) c-Jun N-terminal kinase activation failure is a new mechanism of anthracycline resistance in acute myeloid leukemia. Leukemia 22:1899-1908.

Lage H (2008) An overview of cancer multidrug resistance: a still unsolved problem. Cell Mol Life Sci 65:3145-3167.

Lala P, Ito S, Lingwood CA (2000) Retroviral transfection of Madin-Darby canine kidney cells with human MDR1 results in a major increase in globotriaosylceramide and 10(5)- to 10(6)-fold

increased cell sensitivity to verocytotoxin. Role of p-glycoprotein in glycolipid synthesis. J Biol Chem 275:6246-6251.

Lamba JK, Adachi M, Sun D, et al. (2003) Nonsense mediated decay downregulates conserved alternatively spliced ABCC4 transcripts bearing nonsense codons. Hum Mol Genet 12:99-109.

Lan LB, Dalton JT, Schuetz EG (2000) Mdr1 limits CYP3A metabolism in vivo. Mol Pharmacol 58:863-869.

Lankas GR, Wise LD, Cartwright ME, Pippert T, Umbenhauer DR (1998) Placental P-glycoprotein deficiency enhances susceptibility to chemically induced birth defects in mice. Reprod Toxicol 12:457-463.

Ledoux S, Yang R, Friedlander G, Laouari D (2003) Glucose depletion enhances P-glycoprotein expression in hepatoma cells: role of endoplasmic reticulum stress response. Cancer Res 63:7284-7290.

Lee J-Y, Urbatsch IL, Senior AE, Wilkens S (2002) Projection Structure of P-glycoprotein by Electron Microscopy: EVIDENCE FOR A CLOSED CONFORMATION OF THE NUCLEOTIDE BINDING DOMAINS. Journal of Biological Chemistry 277:40125-40131.

Lee JT, Jr., Steelman LS, McCubrey JA (2004) Phosphatidylinositol 3'-kinase activation leads to multidrug resistance protein-1 expression and subsequent chemoresistance in advanced prostate cancer cells. Cancer Res 64:8397-8404.

Lee JY, Urbatsch IL, Senior AE, Wilkens S (2008) Nucleotide-induced structural changes in P-glycoprotein observed by electron microscopy. J Biol Chem 283:5769-5779.

Lee S, Choi EJ, Jin C, Kim DH (2005) Activation of PI3K/Akt pathway by PTEN reduction and PIK3CA mRNA amplification contributes to cisplatin resistance in an ovarian cancer cell line. Gynecol Oncol 97:26-34.

Lee YJ, Galoforo SS, Berns CM, et al. (1998) Glucose Deprivation-induced Cytotoxicity and Alterations in Mitogen-activated Protein Kinase Activation Are Mediated by Oxidative Stress in Multidrug-resistant Human Breast Carcinoma Cells. Journal of Biological Chemistry 273:5294-5299.

Leevers SJ, Paterson HF, Marshall CJ (1994) Requirement for Ras in Raf activation is overcome by targeting Raf to the plasma membrane. Nature 369:411-414.

Lehnert M (1996) Clinical multidrug resistance in cancer: a multifactorial problem. Eur J Cancer 32A:912-920.

Leone V, di Palma A, Ricchi P, et al. (2007) PGE2 inhibits apoptosis in human adenocarcinoma Caco-2 cell line through Ras-PI3K association and cAMP-dependent kinase A activation. Am J Physiol Gastrointest Liver Physiol 293:G673-681.

Leonessa F, Clarke R (2003) ATP binding cassette transporters and drug resistance in breast cancer. Endocr Relat Cancer 10:43-73.

Leschziner G, Zabaneh D, Pirmohamed M, et al. (2006) Exon sequencing and high resolution haplotype analysis of ABC transporter genes implicated in drug resistance. Pharmacogenet Genomics 16:439-450.

Leschziner GD, Andrew T, Pirmohamed M, Johnson MR (2007) ABCB1 genotype and PGP expression, function and therapeutic drug response: a critical review and recommendations for future research. Pharmacogenomics J 7:154-179.

Li-Blatter X, Nervi P, Seelig A (2009) Detergents as intrinsic P-glycoprotein substrates and inhibitors. Biochim Biophys Acta 1788:2335-2344.

Li Z-H, Zhu Y-J, Lit X-T (1997) Wild-type p53 gene increases MDR1 gene expression but decreases drug resistance in an MDR cell line KBV200. Cancer letters 119:177-184.

Lin HL, Liu TY, Lui WY, Chi CW (1999a) Up-regulation of multidrug resistance transporter expression by berberine in human and murine hepatoma cells. Cancer 85:1937-1942.

Lin JH (2003) Drug-drug interaction mediated by inhibition and induction of P-glycoprotein. Adv Drug Deliv Rev 55:53-81.

Lin JH, Chiba M, Chen I-W, et al. (1999b) Effect of Dexamethasone on the Intestinal First-Pass Metabolism of Indinavir in Rats: Evidence of Cytochrome P-450 A and p-Glycoprotein Induction. Drug Metabolism and Disposition 27:1187-1193.

Lin JH, Yamazaki M (2003a) Clinical relevance of P-glycoprotein in drug therapy. Drug Metab Rev 35:417-454.

Lin JH, Yamazaki M (2003b) Role of P-glycoprotein in pharmacokinetics: clinical implications. Clin Pharmacokinet 42:59-98.

Linhoff MW, Wright KL, Ting JP (1997) CCAAT-binding factor NF-Y and RFX are required for in vivo assembly of a nucleoprotein complex that spans 250 base pairs: the invariant chain promoter as a model. Mol Cell Biol 17:4589-4596.

Linton KJ, Higgins CF (2002) P-glycoprotein misfolds in Escherichia coli : evidence against alternating-topology models of the transport cycle. Molecular Membrane Biology 19:51-58.

List AF, Spier C, Greer J, et al. (1993) Phase I/II trial of cyclosporine as a chemotherapy-resistance modifier in acute leukemia. Journal of Clinical Oncology 11:1652-1660.

Litman T, Zeuthen T, Skovsgaard T, Stein WD (1997a) Competitive, non-competitive and cooperative interactions between substrates of P-glycoprotein as measured by its ATPase activity. Biochimica et Biophysica Acta (BBA) - Molecular Basis of Disease 1361:169-176.

Litman T, Zeuthen T, Skovsgaard T, Stein WD (1997b) Structure-activity relationships of P-glycoprotein interacting drugs: kinetic characterization of their effects on ATPase activity. Biochim Biophys Acta 1361:159-168.

Liu H, Liu X, Jia L, et al. (2008) Insulin therapy restores impaired function and expression of P-glycoprotein in blood-brain barrier of experimental diabetes. Biochem Pharmacol 75:1649-1658.

Liu H, Yang H, Wang D, et al. (2009) Insulin regulates P-glycoprotein in rat brain microvessel endothelial cells via an insulin receptor-mediated PKC/NF-kappaB pathway but not a PI3K/Akt pathway. Eur J Pharmacol 602:277-282.

Liu J, Chen H, Miller DS, et al. (2001) Overexpression of Glutathione S-Transferase II and Multidrug Resistance Transport Proteins Is Associated with Acquired Tolerance to Inorganic Arsenic. Molecular Pharmacology 60:302-309.

Liu J, Liu Y, Powell DA, Waalkes MP, Klaassen CD (2002a) Multidrug-resistance mdr1a/1b double knockout mice are more sensitive than wild type mice to acute arsenic toxicity, with higher arsenic accumulation in tissues. Toxicology 170:55-62.

Liu M, Li D, Aneja R, et al. (2007) PO(2)-dependent differential regulation of multidrug resistance 1 gene expression by the c-Jun NH2-terminal kinase pathway. J Biol Chem 282:17581-17586.

Liu R, Sharom FJ (1996) Site-directed fluorescence labeling of P-glycoprotein on cysteine residues in the nucleotide binding domains. Biochemistry 35:11865-11873.

Liu R, Sharom FJ (1997) Fluorescence studies on the nucleotide binding domains of the P-glycoprotein multidrug transporter. Biochemistry 36:2836-2843.

Liu ZL, Onda K, Tanaka S, Toma T, Hirano T, Oka K (2002b) Induction of multidrug resistance in MOLT-4 cells by anticancer agents is closely related to increased expression of functional P-glycoprotein and MDR1 mRNA. Cancer Chemother Pharmacol 49:391-397.

Lohner K, Schnabele K, Daniel H, et al. (2007) Flavonoids alter P-gp expression in intestinal epithelial cells in vitro and in vivo. Mol Nutr Food Res 51:293-300.

Loo TW, Bartlett MC, Clarke DM (2002) The "LSGGQ" motif in each nucleotide-binding domain of human P-glycoprotein is adjacent to the opposing walker A sequence. J Biol Chem 277:41303-41306.

Loo TW, Bartlett MC, Clarke DM (2003a) Drug binding in human P-glycoprotein causes conformational changes in both nucleotide-binding domains. J Biol Chem 278:1575-1578.

Loo TW, Bartlett MC, Clarke DM (2003b) Methanethiosulfonate derivatives of rhodamine and verapamil activate human P-glycoprotein at different sites. J Biol Chem 278:50136-50141.

Loo TW, Bartlett MC, Clarke DM (2003c) Simultaneous binding of two different drugs in the binding pocket of the human multidrug resistance P-glycoprotein. J Biol Chem 278:39706-39710.

Loo TW, Bartlett MC, Clarke DM (2003d) Substrate-induced Conformational Changes in the Transmembrane Segments of Human P-glycoprotein: DIRECT EVIDENCE FOR THE SUBSTRATE-INDUCED FIT MECHANISM FOR DRUG BINDING. Journal of Biological Chemistry 278:13603-13606.

Loo TW, Bartlett MC, Clarke DM (2004a) Disulfide Cross-linking Analysis Shows That Transmembrane Segments 5 and 8 of Human P-glycoprotein Are Close Together on the Cytoplasmic Side of the Membrane. Journal of Biological Chemistry 279:7692-7697.

Loo TW, Bartlett MC, Clarke DM (2004b) The drug-binding pocket of the human multidrug resistance P-glycoprotein is accessible to the aqueous medium. Biochemistry 43:12081-12089.

Loo TW, Bartlett MC, Clarke DM (2004c) Val133 and Cys137 in Transmembrane Segment 2 Are Close to Arg935 and Gly939 in Transmembrane Segment 11 of Human P-glycoprotein. Journal of Biological Chemistry 279:18232-18238.

Loo TW, Bartlett MC, Clarke DM (2005) ATP hydrolysis promotes interactions between the extracellular ends of transmembrane segments 1 and 11 of human multidrug resistance P-glycoprotein. Biochemistry 44:10250-10258.

Loo TW, Bartlett MC, Clarke DM (2006a) Transmembrane segment 1 of human P-glycoprotein contributes to the drug-binding pocket. Biochem J 396:537-545.

Loo TW, Bartlett MC, Clarke DM (2006b) Transmembrane segment 7 of human P-glycoprotein forms part of the drug-binding pocket. Biochem J 399:351-359.

Loo TW, Bartlett MC, Clarke DM (2009) Identification of residues in the drug translocation pathway of the human multidrug resistance P-glycoprotein by arginine mutagenesis. J Biol Chem 284:24074-24087.

Loo TW, Clarke DM (1993) Functional consequences of phenylalanine mutations in the predicted transmembrane domain of P-glycoprotein. Journal of Biological Chemistry 268:19965-19972.

Loo TW, Clarke DM (1995a) Covalent modification of human P-glycoprotein mutants containing a single cysteine in either nucleotide-binding fold abolishes drug-stimulated ATPase activity. J Biol Chem 270:22957-22961.

Loo TW, Clarke DM (1995b) Membrane Topology of a Cysteine-less Mutant of Human P-glycoprotein. Journal of Biological Chemistry 270:843-848.

Loo TW, Clarke DM (1997) Identification of residues in the drug-binding site of human P-glycoprotein using a thiol-reactive substrate. J Biol Chem 272:31945-31948.

Loo TW, Clarke DM (1999a) Identification of residues in the drug-binding domain of human P-glycoprotein. Analysis of transmembrane segment 11 by cysteine-scanning mutagenesis and inhibition by dibromobimane. J Biol Chem 274:35388-35392.

Loo TW, Clarke DM (1999b) Merck Frosst Award Lecture 1998. Molecular dissection of the human multidrug resistance P-glycoprotein. Biochem Cell Biol 77:11-23.

Loo TW, Clarke DM (1999c) The Transmembrane Domains of the Human Multidrug Resistance P-glycoprotein Are Sufficient to Mediate Drug Binding and Trafficking to the Cell Surface. Journal of Biological Chemistry 274:24759-24765.

Loo TW, Clarke DM (2000) The Packing of the Transmembrane Segments of Human Multidrug Resistance P-glycoprotein Is Revealed by Disulfide Cross-linking Analysis. Journal of Biological Chemistry 275:5253-5256.

Loo TW, Clarke DM (2001a) Cross-linking of human multidrug resistance P-glycoprotein by the substrate, tris-(2-maleimidoethyl)amine, is altered by ATP hydrolysis. Evidence for rotation of a transmembrane helix. J Biol Chem 276:31800-31805.

Loo TW, Clarke DM (2001b) Defining the drug-binding site in the human multidrug resistance P-glycoprotein using a methanethiosulfonate analog of verapamil, MTS-verapamil. J Biol Chem 276:14972-14979.

Loo TW, Clarke DM (2001c) Determining the dimensions of the drug-binding domain of human P-glycoprotein using thiol cross-linking compounds as molecular rulers. J Biol Chem 276:36877-36880.

Loo TW, Clarke DM (2002) Location of the Rhodamine-binding Site in the Human Multidrug Resistance P-glycoprotein. Journal of Biological Chemistry 277:44332-44338.

Loo TW, Clarke DM (2005a) Do drug substrates enter the common drug-binding pocket of P-glycoprotein through “gates”? Biochemical and Biophysical Research Communications 329:419-422.

Loo TW, Clarke DM (2005b) Recent progress in understanding the mechanism of P-glycoprotein-mediated drug efflux. J Membr Biol 206:173-185.

Luciani F, Molinari A, Lozupone F, et al. (2002) P-glycoprotein-actin association through ERM family proteins: a role in P-glycoprotein function in human cells of lymphoid origin. Blood 99:641-648.

Lugo MR, Sharom FJ (2005a) Interaction of LDS-751 and rhodamine 123 with P-glycoprotein: evidence for simultaneous binding of both drugs. Biochemistry 44:14020-14029.

Lugo MR, Sharom FJ (2005b) Interaction of LDS-751 with P-glycoprotein and mapping of the location of the R drug binding site. Biochemistry 44:643-655.

Luker GD, Nilsson KR, Covey DF, Piwnica-Worms D (1999) Multidrug resistance (MDR1) P-glycoprotein enhances esterification of plasma membrane cholesterol. J Biol Chem 274:6979-6991.

Lum BL, Kaubisch S, Yahanda AM, et al. (1992) Alteration of etoposide pharmacokinetics and pharmacodynamics by cyclosporine in a phase I trial to modulate multidrug resistance. Journal of Clinical Oncology 10:1635-1642.

Luo L, Sun Y-J, Yang L, Huang S, Wu Y-J (2013) Avermectin induces P-glycoprotein expression in S2 cells via the calcium/calmodulin/NF-κB pathway. Chemico-Biological Interactions 203:430-439.

MacFarland A, Abramovich DR, Ewen SW, Pearson CK (1994) Stage-specific distribution of P-glycoprotein in first-trimester and full-term human placenta. Histochem J 26:417-423.

Maehama T, Dixon JE (1998) The tumor suppressor, PTEN/MMAC1, dephosphorylates the lipid second messenger, phosphatidylinositol 3,4,5-trisphosphate. J Biol Chem 273:13375-13378.

Maggio-Price L, Bielefeldt-Ohmann H, Treuting P, et al. (2005) Dual infection with Helicobacter bilis and Helicobacter hepaticus in p-glycoprotein-deficient mdr1a-/- mice results in colitis that progresses to dysplasia. Am J Pathol 166:1793-1806.

Maglich JM, Stoltz CM, Goodwin B, Hawkins-Brown D, Moore JT, Kliewer SA (2002) Nuclear pregnane x receptor and constitutive androstane receptor regulate overlapping but distinct sets of genes involved in xenobiotic detoxification. Mol Pharmacol 62:638-646.

Maier A, Zimmermann C, Beglinger C, Drewe J, Gutmann H (2007) Effects of budesonide on P-glycoprotein expression in intestinal cell lines. Br J Pharmacol 150:361-368.

Maitra R, Halpin PA, Karlson KH, et al. (2001) Differential effects of mitomycin C and doxorubicin on P-glycoprotein expression. Biochem J 355:617-624.

Male DK (2009) Expression and induction of p-glycoprotein-1 on cultured human brain endothelium. J Cereb Blood Flow Metab 29:1760-1763.

Manceau S, Giraud C, Declèves X, et al. (2012) ABC drug transporter and nuclear receptor expression in human cytotrophoblasts: Influence of spontaneous syncytialization and induction by glucocorticoids. Placenta 33:927-932.

Mani S, Huang H, Sundarababu S, et al. (2005) Activation of the steroid and xenobiotic receptor (human pregnane X receptor) by nontaxane microtubule-stabilizing agents. Clin Cancer Res 11:6359-6369.

Mansat-de Mas V, Bezombes C, Quillet-Mary A, et al. (1999) Implication of radical oxygen species in ceramide generation, c-Jun N-terminal kinase activation and apoptosis induced by daunorubicin. Mol Pharmacol 56:867-874.

Mantovani R (1998) A survey of 178 NF-Y binding CCAAT boxes. Nucleic Acids Res 26:1135-1143.

Martin C, Berridge G, Higgins CF, Callaghan R (1997) The multi-drug resistance reversal agent SR33557 and modulation of vinca alkaloid binding to P-glycoprotein by an allosteric interaction. Br J Pharmacol 122:765-771.

Martin C, Berridge G, Higgins CF, Mistry P, Charlton P, Callaghan R (2000) Communication between multiple drug binding sites on P-glycoprotein. Mol Pharmacol 58:624-632.

Martin C, Berridge G, Mistry P, Higgins C, Charlton P, Callaghan R (1999) The molecular interaction of the high affinity reversal agent XR9576 with P-glycoprotein. Br J Pharmacol 128:403-411.

Martin C, Higgins CF, Callaghan R (2001) The vinblastine binding site adopts high- and low-affinity conformations during a transport cycle of P-glycoprotein. Biochemistry 40:15733-15742.

Marzolini C, Paus E, Buclin T, Kim RB (2004) Polymorphisms in human MDR1 (P-glycoprotein): recent advances and clinical relevance. Clin Pharmacol Ther 75:13-33.

Masuyama H, Suwaki N, Tateishi Y, Nakatsukasa H, Segawa T, Hiramatsu Y (2005) The pregnane X receptor regulates gene expression in a ligand- and promoter-selective fashion. Mol Endocrinol 19:1170-1180.

Matheny CJ, Lamb MW, Brouwer KLR, Pollack GM (2001) Pharmacokinetic and Pharmacodynamic Implications of P-glycoprotein Modulation. Pharmacotherapy: The Journal of Human Pharmacology and Drug Therapy 21:778-796.

Mathieu MC, Lapierre I, Brault K, Raymond M (2001) Aromatic hydrocarbon receptor (AhR).AhR nuclear translocator- and p53-mediated induction of the murine multidrug resistance mdr1 gene by 3-methylcholanthrene and benzo(a)pyrene in hepatoma cells. J Biol Chem 276:4819-4827.

Matsui T, Maeda M, Doi Y, et al. (1998) Rho-kinase phosphorylates COOH-terminal threonines of ezrin/radixin/moesin (ERM) proteins and regulates their head-to-tail association. J Cell Biol 140:647-657.

May P, May E (1999) Twenty years of p53 research: structural and functional aspects of the p53 protein. Oncogene 18:7621-7636.

McClean S, Whelan RD, Hosking LK, et al. (1993) Characterization of the P-glycoprotein over-expressing drug resistance phenotype exhibited by Chinese hamster ovary cells following their in-vitro exposure to fractionated X-irradiation. Biochim Biophys Acta 1177:117-126.

McCoy C, McGee SB, Cornwell MM (1999) The Wilms' tumor suppressor, WT1, inhibits 12-O-tetradecanoylphorbol-13-acetate activation of the multidrug resistance-1 promoter. Cell Growth Differ 10:377-386.

McCoy C, Smith DE, Cornwell MM (1995) 12-O-tetradecanoylphorbol-13-acetate activation of the MDR1 promoter is mediated by EGR1. Molecular and Cellular Biology 15:6100-6108.

McCubrey JA, Steelman LS, Abrams SL, et al. (2006) Roles of the RAF/MEK/ERK and PI3K/PTEN/AKT pathways in malignant transformation and drug resistance. Adv Enzyme Regul 46:249-279.

Mealey KL (2004) Therapeutic implications of the MDR-1 gene. Journal of Veterinary Pharmacology and Therapeutics 27:257-264.

Mealey KL, Barhoumi R, Burghardt RC, Safe S, Kochevar DT (2002) Doxycycline induces expression of P glycoprotein in MCF-7 breast carcinoma cells. Antimicrob Agents Chemother 46:755-761.

Mechetner EB, Schott B, Morse BS, et al. (1997) P-glycoprotein function involves conformational transitions detectable by differential immunoreactivity. Proc Natl Acad Sci U S A 94:12908-12913.

Melisi D, Chiao PJ (2007) NF-kappa B as a target for cancer therapy. Expert Opin Ther Targets 11:133-144.

Ménez C, Mselli-Lakhal L, Foucaud-Vignault M, Balaguer P, Alvinerie M, Lespine A (2012) Ivermectin induces P-glycoprotein expression and function through mRNA stabilization in murine hepatocyte cell line. Biochemical Pharmacology 83:269-278.

Merino V, Jimenez-Torres NV, Merino-Sanjuan M (2004) Relevance of multidrug resistance proteins on the clinical efficacy of cancer therapy. Curr Drug Deliv 1:203-212.

Merkle D, Hoffmann R (2011) Roles of cAMP and cAMP-dependent protein kinase in the progression of prostate cancer: cross-talk with the androgen receptor. Cell Signal 23:507-515.

Merlin JL, Guerci A, Marchal S, et al. (1994) Comparative evaluation of S9788, verapamil, and cyclosporine A in K562 human leukemia cell lines and in P-glycoprotein-expressing samples from patients with hematologic malignancies. Blood 84:262-269.

Merlin JL, Marchal S, Ramacci C, et al. (1995) Influence of S9788, a new modulator of multidrug resistance, on the cellular accumulation and subcellular distribution of daunorubicin in P-glycoprotein-expressing MCF7 human breast adenocarcinoma cells. Cytometry 20:315-323.

Miao ZH, Ding J (2003) Transcription factor c-Jun activation represses mdr-1 gene expression. Cancer Res 63:4527-4532.

Mickley LA, Bates SE, Richert ND, et al. (1989) Modulation of the expression of a multidrug resistance gene (mdr-1/P-glycoprotein) by differentiating agents. Journal of Biological Chemistry 264:18031-18040.

Miller TP, Grogan TM, Dalton WS, Spier CM, Scheper RJ, Salmon SE (1991) P-glycoprotein expression in malignant lymphoma and reversal of clinical drug resistance with chemotherapy plus high-dose verapamil. J Clin Oncol 9:17-24.

Miltenberger RJ, Cortner J, Farnham PJ (1993) An inhibitory Raf-1 mutant suppresses expression of a subset of v-raf-activated genes. J Biol Chem 268:15674-15680.

Miltenberger RJ, Farnham PJ, Smith DE, Stommel JM, Cornwell MM (1995) v-Raf activates transcription of growth-responsive promoters via GC-rich sequences that bind the transcription factor Sp1. Cell Growth Differ 6:549-556.

Misra UK, Pizzo SV (2009) Epac1-induced cellular proliferation in prostate cancer cells is mediated by B-Raf/ERK and mTOR signaling cascades. J Cell Biochem 108:998-1011.

Mistry P, Stewart AJ, Dangerfield W, et al. (2001) In Vitro and in Vivo Reversal of P-Glycoprotein-mediated Multidrug Resistance by a Novel Potent Modulator, XR9576. Cancer Research 61:749-758.

Miyazaki M, Kohno K, Uchiumi T, et al. (1992) Activation of human multidrug resistance-1 gene promoter in response to heat shock stress. Biochem Biophys Res Commun 187:677-684.

Mizutani T, Masuda M, Nakai E, et al. (2008) Genuine Functions of P-Glycoprotein (ABCB1). Current Drug Metabolism 9:167-174.

Modok S, Mellor HR, Callaghan R (2006) Modulation of multidrug resistance efflux pump activity to overcome chemoresistance in cancer. Curr Opin Pharmacol 6:350-354.

Moreira PN, de Pinho PG, Baltazar MT, Bastos ML, Carvalho F, Dinis-Oliveira RJ (2012) Quantification of paraquat in postmortem samples by gas chromatography-ion trap mass spectrometry and review of the literature. Biomed Chromatogr 26:338-349.

Morita N, Yasumori T, Nakayama K (2003) Human MDR1 polymorphism: G2677T/A and C3435T have no effect on MDR1 transport activities. Biochem Pharmacol 65:1843-1852.

Morphy R, Rankovic Z (2009) Designing multiple ligands - medicinal chemistry strategies and challenges. Curr Pharm Des 15:587-600.

Morris DI, Greenberger LM, Bruggemann EP, et al. (1994) Localization of the forskolin labeling sites to both halves of P-glycoprotein: similarity of the sites labeled by forskolin and prazosin. Mol Pharmacol 46:329-337.

Morrow CS, Nakagawa M, Goldsmith ME, Madden MJ, Cowan KH (1994) Reversible transcriptional activation of mdr1 by sodium butyrate treatment of human colon cancer cells. Journal of Biological Chemistry 269:10739-10746.

Murshid A, Chou SD, Prince T, Zhang Y, Bharti A, Calderwood SK (2010) Protein kinase A binds and activates heat shock factor 1. PLoS One 5:e13830.

Nagai N, Nakai A, Nagata K (1995a) Quercetin Suppresses Heat Shock Response by Down-Regulation of HSF1. Biochemical and Biophysical Research Communications 208:1099-1105.

Nagai N, Nakai A, Nagata K (1995b) Quercetin suppresses heat shock response by down regulation of HSF1. Biochem Biophys Res Commun 208:1099-1105.

Nagao M, Saitoh H, Zhang WD, et al. (1993) Transport characteristics of paraquat across rat intestinal brush-border membrane. Arch Toxicol 67:262-267.

Nakano H (2005) [Signaling crosstalk between NF-kappaB and JNK]. Seikagaku 77:29-32.

Nakatsukasa H, Silverman JA, Gant TW, Evarts RP, Thorgeirsson SS (1993) Expression of multidrug resistance genes in rat liver during regeneration and after carbon tetrachloride intoxication. Hepatology 18:1202-1207.

Narang VS, Fraga C, Kumar N, et al. (2008) Dexamethasone increases expression and activity of multidrug resistance transporters at the rat blood-brain barrier. American Journal of Physiology - Cell Physiology 295:C440-C450.

Naruhashi K, Kurahashi Y, Fujita Y, et al. (2011) Comparison of the expression and function of ATP binding cassette transporters in Caco-2 and T84 cells on stimulation by selected endogenous compounds and xenobiotics. Drug Metab Pharmacokinet 26:145-153.

Nelson DR, Koymans L, Kamataki T, et al. (1996) P450 superfamily: update on new sequences, gene mapping, accession numbers and nomenclature. Pharmacogenetics 6:1-42.

Nguyen KT, Liu B, Ueda K, Gottesman MM, Pastan I, Chin KV (1994) Transactivation of the human multidrug resistance (MDR1) gene promoter by p53 mutants. Oncol Res 6:71-77.

Niel E, Scherrmann JM (2006) Colchicine today. Joint Bone Spine 73:672-678.

Nielsen D, Eriksen J, Maare C, Jakobsen A, Skovsgaard T (1998) P-glycoprotein expression in Ehrlich ascites tumour cells after in vitro and in vivo selection with daunorubicin. Br J Cancer 78:1175-1180.

Nieto-Sotelo J, Wiederrecht G, Okuda A, Parker CS (1990) The yeast heat shock transcription factor contains a transcriptional activation domain whose activity is repressed under nonshock conditions. Cell 62:807-817.

Nwaozuzu OM, Sellers LA, Barrand MA (2003) Signalling pathways influencing basal and H(2)O(2)-induced P-glycoprotein expression in endothelial cells derived from the blood-brain barrier. J Neurochem 87:1043-1051.

O'Brien MM, Lacayo NJ, Lum BL, et al. (2010) Phase I study of valspodar (PSC-833) with mitoxantrone and etoposide in refractory and relapsed pediatric acute leukemia: a report from the Children's Oncology Group. Pediatr Blood Cancer 54:694-702.

Oda Y, Ohishi Y, Saito T, et al. (2003) Nuclear expression of Y-box-binding protein-1 correlates with P-glycoprotein and topoisomerase II alpha expression, and with poor prognosis in synovial sarcoma. J Pathol 199:251-258.

Ogretmen B, Safa AR (1999a) Identification and Characterization of the MDR1 Promoter-Enhancing Factor 1 (MEF1) in the Multidrug Resistant HL60/VCR Human Acute Myeloid Leukemia Cell Line†. Biochemistry 39:194-204.

Ogretmen B, Safa AR (1999b) Negative regulation of MDR1 promoter activity in MCF-7, but not in multidrug resistant MCF-7/Adr, cells by cross-coupled NF-kappa B/p65 and c-Fos transcription factors and their interaction with the CAAT region. Biochemistry 38:2189-2199.

Ogura M, Takatori T, Tsuruo T (1992) Purification and characterization of NF-R1 that regulates the expression of the human multidrug resistance (MDR1) gene. Nucleic Acids Res 20:5811-5817.

Ohga T, Koike K, Ono M, et al. (1996) Role of the human Y box-binding protein YB-1 in cellular sensitivity to the DNA-damaging agents cisplatin, mitomycin C, and ultraviolet light. Cancer Res 56:4224-4228.

Ohga T, Uchiumi T, Makino Y, et al. (1998) Direct Involvement of the Y-box Binding Protein YB-1 in Genotoxic Stress-induced Activation of the Human Multidrug Resistance 1 Gene. Journal of Biological Chemistry 273:5997-6000.

Oldham ML, Khare D, Quiocho FA, Davidson AL, Chen J (2007) Crystal structure of a catalytic intermediate of the maltose transporter. Nature 450:515-521.

Omote H, Al-Shawi MK (2002) A novel electron paramagnetic resonance approach to determine the mechanism of drug transport by P-glycoprotein. J Biol Chem 277:45688-45694.

Omote H, Al-Shawi MK (2006) Interaction of transported drugs with the lipid bilayer and P-glycoprotein through a solvation exchange mechanism. Biophys J 90:4046-4059.

Osborn MT, Chambers TC (1996) Role of the Stress-activated/c-Jun NH2-terminal Protein Kinase Pathway in the Cellular Response to Adriamycin and Other Chemotherapeutic Drugs. Journal of Biological Chemistry 271:30950-30955.

Oswald C, Holland IB, Schmitt L (2006) The motor domains of ABC-transporters. What can structures tell us? Naunyn Schmiedebergs Arch Pharmacol 372:385-399.

Owen A, Goldring C, Morgan P, Park BK, Pirmohamed M (2006) Induction of P-glycoprotein in lymphocytes by carbamazepine and rifampicin: the role of nuclear hormone response elements. Br J Clin Pharmacol 62:237-242.

Pahl HL (1999) Activators and target genes of Rel/NF-kappaB transcription factors. Oncogene 18:6853-6866.

Paiva AM, Pinto MM, Sousa E (2013) A century of thioxanthones: through synthesis and biological applications. Curr Med Chem 20:2438-2457.

Pajeva IK, Globisch C, Wiese M (2009) Combined pharmacophore modeling, docking, and 3D QSAR studies of ABCB1 and ABCC1 transporter inhibitors. ChemMedChem 4:1883-1896.

Palmeira A, Rodrigues F, Sousa E, Pinto M, Vasconcelos MH, Fernandes MX (2011) New uses for old drugs: pharmacophore-based screening for the discovery of P-glycoprotein inhibitors. Chem Biol Drug Des 78:57-72.

Palmeira A, Sousa E, Vasconcelos MH, Pinto MM (2012a) Three Decades of P-gp Inhibitors: Skimming Through Several Generations and Scaffolds. Current Medicinal Chemistry 19:1946-2025.

Palmeira A, Sousa E, Vasconcelos MH, Pinto MM, Fernandes MX (2012b) Structure and ligand-based design of P-glycoprotein inhibitors: a historical perspective. Curr Pharm Design 18:4197-4214.

Palmeira A, Vasconcelos MH, Paiva A, Fernandes MX, Pinto M, Sousa E (2012c) Dual inhibitors of P-glycoprotein and tumor cell growth: (re)discovering thioxanthones. Biochem Pharmacol 83:57-68.

Pan M, Malandro M, Stevens BR (1995) Regulation of system y+ arginine transport capacity in differentiating human intestinal Caco-2 cells. Am J Physiol 268:G578-585.

Pan M, Souba WW, Karinch AM, Lin CM, Stevens BR (2002) Specific reversible stimulation of system y(+) L-arginine transport activity in human intestinal cells. J Gastrointest Surg 6:379-386.

Patel NR, Rathi A, Mongayt D, Torchilin VP (2011) Reversal of multidrug resistance by co-delivery of tariquidar (XR9576) and paclitaxel using long-circulating liposomes. Int J Pharm 416:296-299.

Patil Y, Sadhukha T, Ma L, Panyam J (2009) Nanoparticle-mediated simultaneous and targeted delivery of paclitaxel and tariquidar overcomes tumor drug resistance. J Control Release 136:21-29.

Pauwels EK, Erba P, Mariani G, Gomes CM (2007) Multidrug resistance in cancer: its mechanism and its modulation. Drug News Perspect 20:371-377.

Pearce HL, Safa AR, Bach NJ, Winter MA, Cirtain MC, Beck WT (1989) Essential features of the P-glycoprotein pharmacophore as defined by a series of reserpine analogs that modulate multidrug resistance. Proc Natl Acad Sci U S A 86:5128-5132.

Peer M, Csaszar E, Vorlaufer E, Kopp S, Chiba P (2005) Photoaffinity labeling of P-glycoprotein. Mini Rev Med Chem 5:165-172.

Penzotti JE, Lamb ML, Evensen E, Grootenhuis PDJ (2002) A Computational Ensemble Pharmacophore Model for Identifying Substrates of P-Glycoprotein. Journal of Medicinal Chemistry 45:1737-1740.

Perez-Tomas R (2006) Multidrug resistance: retrospect and prospects in anti-cancer drug treatment. Curr Med Chem 13:1859-1876.

Perloff MD, Moltke LLV, Greenblatt DJ (2004) Ritonavir and dexamethasone induce expression of CYP3A and P-glycoprotein in rats. Xenobiotica 34:133-150.

Perloff MD, von Moltke LL, Fahey JM, Daily JP, Greenblatt DJ (2000) Induction of P-glycoprotein expression by HIV protease inhibitors in cell culture. AIDS 14:1287-1289.

Perloff MD, von Moltke LL, Fahey JM, Greenblatt DJ (2007) Induction of P-glycoprotein expression and activity by ritonavir in bovine brain microvessel endothelial cells. Journal of Pharmacy and Pharmacology 59:947-953.

Perloff MD, Von Moltke LL, Marchand JE, Greenblatt DJ (2001a) Ritonavir induces P-glycoprotein expression, multidrug resistance-associated protein (MRP1) expression, and drug transporter-mediated activity in a human intestinal cell line. J Pharm Sci 90:1829-1837.

Perloff MD, von Moltke LL, Stormer E, Shader RI, Greenblatt DJ (2001b) Saint John's wort: an in vitro analysis of P-glycoprotein induction due to extended exposure. Br J Pharmacol 134:1601-1608.

Petropoulos S, Gibb W, Matthews SG (2010) Effect of glucocorticoids on regulation of placental multidrug resistance phosphoglycoprotein (P-gp) in the mouse. Placenta 31:803-810.

Pinkett HW, Lee AT, Lum P, Locher KP, Rees DC (2007) An inward-facing conformation of a putative metal-chelate-type ABC transporter. Science 315:373-277.

Pleban K, Kopp S, Csaszar E, et al. (2005) P-glycoprotein substrate binding domains are located at the transmembrane domain/transmembrane domain interfaces: a combined photoaffinity labeling-protein homology modeling approach. Mol Pharmacol 67:365-374.

Polgar O, Bates SE (2005) ABC transporters in the balance: is there a role in multidrug resistance? Biochem Soc Trans 33:241-245.

Polli JW, Wring SA, Humphreys JE, et al. (2001) Rational Use of in Vitro P-glycoprotein Assays in Drug Discovery. Journal of Pharmacology and Experimental Therapeutics 299:620-628.

Prakash AS (2010) Selecting surfactants for the maximum inhibition of the activity of the multidrug resistance efflux pump transporter, P-glycoprotein: conceptual development. J Excipients and Food Chem 1: 51-59.

Prenkert M, Uggla B, Tina E, Tidefelt U, Strid H (2009) Rapid induction of P-glycoprotein mRNA and protein expression by cytarabine in HL-60 cells. Anticancer Res 29:4071-4076.

Qu Q, Russell PL, Sharom FJ (2003) Stoichiometry and affinity of nucleotide binding to P-glycoprotein during the catalytic cycle. Biochemistry 42:1170-1177.

Qu Q, Sharom FJ (2001) FRET Analysis Indicates That the Two ATPase Active Sites of the P-Glycoprotein Multidrug Transporter Are Closely Associated†. Biochemistry 40:1413-1422.

Qu Q, Sharom FJ (2002) Proximity of Bound Hoechst 33342 to the ATPase Catalytic Sites Places the Drug Binding Site of P-glycoprotein within the Cytoplasmic Membrane Leaflet†. Biochemistry 41:4744-4752.

Raggers RJ, Vogels I, van Meer G (2001) Multidrug-resistance P-glycoprotein (MDR1) secretes platelet-activating factor. Biochem J 357:859-865.

Raghu G, Park SW, Roninson IB, Mechetner EB (1996) Monoclonal antibodies against P-glycoprotein, an MDR1 gene product, inhibit interleukin-2 release from PHA-activated lymphocytes. Exp Hematol 24:1258-1264.

Ramji DP, Foka P (2002) CCAAT/enhancer-binding proteins: structure, function and regulation. Biochem J 365:561-575.

Randolph GJ, Beaulieu S, Pope M, et al. (1998) A physiologic function for p-glycoprotein (MDR-1) during the migration of dendritic cells from skin via afferent lymphatic vessels. Proc Natl Acad Sci U S A 95:6924-6929.

Rao VV, Dahlheimer JL, Bardgett ME, et al. (1999) Choroid plexus epithelial expression of MDR1 P glycoprotein and multidrug resistance-associated protein contribute to the blood-cerebrospinal-fluid drug-permeability barrier. Proc Natl Acad Sci U S A 96:3900-3905.

Raviv Y, Pollard HB, Bruggemann EP, Pastan I, Gottesman MM (1990) Photosensitized labeling of a functional multidrug transporter in living drug-resistant tumor cells. Journal of Biological Chemistry 265:3975-3980.

Rege BD, Kao JPY, Polli JE (2002) Effects of nonionic surfactants on membrane transporters in Caco-2 cell monolayers. European Journal of Pharmaceutical Sciences 16:237-246.

Regev R, Assaraf YG, Eytan GD (1999) Membrane fluidization by ether, other anesthetics, and certain agents abolishes P-glycoprotein ATPase activity and modulates efflux from multidrug-resistant cells. Eur J Biochem 259:18-24.

Regev R, Katzir H, Yeheskely-Hayon D, Eytan GD (2007) Modulation of P-glycoprotein-mediated multidrug resistance by acceleration of passive drug permeation across the plasma membrane. FEBS J 274:6204-6214.

Rigalli JP, Ruiz ML, Perdomo VG, Villanueva SS, Mottino AD, Catania VA (2011) Pregnane X receptor mediates the induction of P-glycoprotein by spironolactone in HepG2 cells. Toxicology 285:18-24.

Riganti C, Campia I, Polimeni M, Pescarmona G, Ghigo D, Bosia A (2009a) Digoxin and ouabain induce P-glycoprotein by activating calmodulin kinase II and hypoxia-inducible factor-1α in human colon cancer cells. Toxicology and Applied Pharmacology 240:385-392.

Riganti C, Doublier S, Viarisio D, et al. (2009b) Artemisinin induces doxorubicin resistance in human colon cancer cells via calcium-dependent activation of HIF-1α and P-glycoprotein overexpression. Br J Pharmacol 156:1054-1066.

Riganti C, Miraglia E, Viarisio D, et al. (2005) Nitric Oxide Reverts the Resistance to Doxorubicin in Human Colon Cancer Cells by Inhibiting the Drug Efflux. Cancer Research 65:516-525.

Riganti C, Orecchia S, Pescarmona G, Betta PG, Ghigo D, Bosia A (2006) Statins revert doxorubicin resistance via nitric oxide in malignant mesothelioma. Int J Cancer 119:17-27.

Riley J, Styles J, Verschoyle RD, Stanley LA, White INH, Gant TW (2000) Association of tamoxifen biliary excretion rate with prior tamoxifen exposure and increased mdr1b expression. Biochemical Pharmacology 60:233-239.

Rimler A, Jockers R, Lupowitz Z, Sampson SR, Zisapel N (2006) Differential effects of melatonin and its downstream effector PKCalpha on subcellular localization of RGS proteins. J Pineal Res 40:144-152.

Roberts DM (2011) Herbicides. In: Nelson LS, Lewin NA, Howland MA, Hoffman RS, Goldfrank LR, Flomenbaum NE (eds) Goldfrank's Toxicologic Emergencies, Ninth Edition McGraw-Hill Companies, Inc., p 1494-1515.

Robey RW, Steadman K, Polgar O, et al. (2004) Pheophorbide a Is a Specific Probe for ABCG2 Function and Inhibition. Cancer Research 64:1242-1246.

Robey RW, Zhan Z, Piekarz RL, Kayastha GL, Fojo T, Bates SE (2006) Increased MDR1 Expression in Normal and Malignant Peripheral Blood Mononuclear Cells Obtained from Patients Receiving Depsipeptide (FR901228, FK228, NSC630176). Clinical Cancer Research 12:1547-1555.

Robinson LJ, Roberts WK, Ling TT, Lamming D, Sternberg SS, Roepe PD (1997) Human MDR 1 protein overexpression delays the apoptotic cascade in Chinese hamster ovary fibroblasts. Biochemistry 36:11169-11178.

Rohlff C, Glazer RI (1995) Regulation of multidrug resistance through the cAMP and EGF signalling pathways. Cell Signal 7:431-443.

Rohlff C, Glazer RI (1998) Regulation of the MDR1 promoter by cyclic AMP-dependent protein kinase and transcription factor Sp1. Int J Oncol 12:383-386.

Romiti N, Tramonti G, Chieli E (2002) Influence of Different Chemicals on MDR-1 P-Glycoprotein Expression and Activity in the HK-2 Proximal Tubular Cell Line. Toxicology and Applied Pharmacology 183:83-91.

Romsicki Y, Sharom FJ (1999) The membrane lipid environment modulates drug interactions with the P-glycoprotein multidrug transporter. Biochemistry 38:6887-6896.

Romsicki Y, Sharom FJ (2001) Phospholipid flippase activity of the reconstituted P-glycoprotein multidrug transporter. Biochemistry 40:6937-69347.

Roninson IB (1992) From amplification to function: the case of the MDR1 gene. Mutat Res 276:151-161.

Roose J, Clevers H (1999) TCF transcription factors: molecular switches in carcinogenesis. Biochim Biophys Acta 1424:M23-37.

Ros JE, Schuetz JD, Geuken M, et al. (2001) Induction of Mdr1b expression by tumor necrosis factor-α in rat liver cells is independent of p53 but requires NF-κB signaling. Hepatology 33:1425-1431.

Rose MS, Smith LL, Wyatt I (1974) Evidence for energy-dependent accumulation of paraquat into rat lung. Nature 252:314-315.

Rosenberg MF, Callaghan R, Ford RC, Higgins CF (1997) Structure of the multidrug resistance P-glycoprotein to 2.5 nm resolution determined by electron microscopy and image analysis. J Biol Chem 272:10685-10694.

Rosenberg MF, Callaghan R, Modok S, Higgins CF, Ford RC (2005) Three-dimensional Structure of P-glycoprotein: the transmembrane regions adopt an asymmetric configuration in the nucleotide-bound state. Journal of Biological Chemistry 280:2857-2862.

Rosenberg MF, Kamis AB, Callaghan R, Higgins CF, Ford RC (2003) Three-dimensional structures of the mammalian multidrug resistance P-glycoprotein demonstrate major conformational changes in the transmembrane domains upon nucleotide binding. J Biol Chem 278:8294-8299.

Rosenberg MF, Velarde G, Ford RC, et al. (2001) Repacking of the transmembrane domains of P-glycoprotein during the transport ATPase cycle. EMBO J 20:5615-5625.

Rosenfeld JM, Vargas R, Xie W, Evans RM (2003) Genetic Profiling Defines the Xenobiotic Gene Network Controlled by the Nuclear Receptor Pregnane X Receptor. Molecular Endocrinology 17:1268-1282.

Roth BL, Sheffler DJ, Kroeze WK (2004) Magic shotguns versus magic bullets: selectively non-selective drugs for mood disorders and schizophrenia. Nat Rev Drug Discov 3:353-359.

Rothnie A, Storm J, McMahon R, Taylor A, Kerr ID, Callaghan R (2005) The coupling mechanism of P-glycoprotein involves residue L339 in the sixth membrane spanning segment. FEBS Lett 579:3984-3990.

Rowinsky EK, Smith L, Wang YM, et al. (1998) Phase I and pharmacokinetic study of paclitaxel in combination with biricodar, a novel agent that reverses multidrug resistance conferred by overexpression of both MDR1 and MRP. Journal of Clinical Oncology 16:2964-2976.

Ruetz S, Gros P (1994) Phosphatidylcholine translocase: a physiological role for the mdr2 gene. Cell 77:1071-1081.

Ruth A, Stein WD, Rose E, Roninson IB (2001) Coordinate changes in drug resistance and drug-induced conformational transitions in altered-function mutants of the multidrug transporter P-glycoprotein. Biochemistry 40:4332-4339.

Sababi M, Borga O, Hultkvist-Bengtsson U (2001) The role of P-glycoprotein in limiting intestinal regional absorption of digoxin in rats. Eur J Pharm Sci 14:21-27.

Saeki M, Kurose K, Hasegawa R, Tohkin M (2011) Functional analysis of genetic variations in the 5'-flanking region of the human MDR1 gene. Mol Genet Metab 102:91-98.

Safa AR (1993) Photoaffinity labeling of P-glycoprotein in multidrug-resistant cells. Cancer Invest 11:46-56.

Safa AR (1998) Photoaffinity labels for characterizing drug interaction sites of P-glycoprotein. Methods Enzymol 292:289-307.

Safa AR (2004) Identification and characterization of the binding sites of P-glycoprotein for multidrug resistance-related drugs and modulators. Curr Med Chem Anticancer Agents 4:1-17.

Safa AR, Agresti M, Bryk D, Tamai I (1994) N-(p-azido-3-[125I]iodophenethyl)spiperone binds to specific regions of P-glycoprotein and another multidrug binding protein, spiperophilin, in human neuroblastoma cells. Biochemistry 33:256-265.

Safe S, Abdelrahim M (2005) Sp transcription factor family and its role in cancer. Eur J Cancer 41:2438-2448.

Saito T, Zhang ZJ, Tsuzuki H, et al. (1997) Expression of P-glycoprotein in inner ear capillary endothelial cells of the guinea pig with special reference to blood-inner ear barrier. Brain Res 767:388-392.

Saji H, Toi M, Saji S, Koike M, Kohno K, Kuwano M (2003) Nuclear expression of YB-1 protein correlates with P-glycoprotein expression in human breast carcinoma. Cancer Lett 190:191-197.

Sakurai A, Onishi Y, Hirano H, et al. (2007) Quantitative structure--activity relationship analysis and molecular dynamics simulation to functionally validate nonsynonymous polymorphisms of human ABC transporter ABCB1 (P-glycoprotein/MDR1). Biochemistry 46:7678-7693.

Salphati L, Benet LZ (1998) Modulation of P-glycoprotein expression by cytochrome P450 3A inducers in male and female rat livers. Biochemical Pharmacology 55:387-395.

Sambuy Y, De Angelis I, Ranaldi G, Scarino ML, Stammati A, Zucco F (2005) The Caco-2 cell line as a model of the intestinal barrier: influence of cell and culture-related factors on Caco-2 cell functional characteristics. Cell Biol Toxicol 21:1-26.

Sampath J, Sun D, Kidd VJ, et al. (2001) Mutant p53 cooperates with ETS and selectively up-regulates human MDR1 not MRP1. J Biol Chem 276:39359-39367.

Satsu H, Hiura Y, Mochizuki K, Hamada M, Shimizu M (2008) Activation of Pregnane X Receptor and Induction of MDR1 by Dietary Phytochemicals. J Agric Food Chem 56:5366-5373.

Sauna ZE, Ambudkar SV (2001) Characterization of the catalytic cycle of ATP hydrolysis by human P-glycoprotein. The two ATP hydrolysis events in a single catalytic cycle are kinetically similar but affect different functional outcomes. J Biol Chem 276:11653-11661.

Sauna ZE, Kim IW, Nandigama K, Kopp S, Chiba P, Ambudkar SV (2007) Catalytic cycle of ATP hydrolysis by P-glycoprotein: evidence for formation of the E.S reaction intermediate with ATP-gamma-S, a nonhydrolyzable analogue of ATP. Biochemistry 46:13787-13799.

Scemama JL, Grabie V, Seidel ER (1993) Characterization of univectorial polyamine transport in duodenal crypt cell line. Am J Physiol 265:G851-856.

Schinkel AH (1999) P-Glycoprotein, a gatekeeper in the blood-brain barrier. Adv Drug Deliv Rev 36:179-194.

Schinkel AH, Kemp S, Dolle M, Rudenko G, Wagenaar E (1993) N-glycosylation and deletion mutants of the human MDR1 P-glycoprotein. J Biol Chem 268:7474-7481.

Schinkel AH, Mayer U, Wagenaar E, et al. (1997) Normal viability and altered pharmacokinetics in mice lacking mdr1-type (drug-transporting) P-glycoproteins. Proc Natl Acad Sci U S A 94:4028-4033.

Schinkel AH, Smit JJ, van Tellingen O, et al. (1994) Disruption of the mouse mdr1a P-glycoprotein gene leads to a deficiency in the blood-brain barrier and to increased sensitivity to drugs. Cell 77:491-502.

Schinkel AH, Wagenaar E, Mol CA, van Deemter L (1996) P-glycoprotein in the blood-brain barrier of mice influences the brain penetration and pharmacological activity of many drugs. J Clin Invest 97:2517-2524.

Schinkel AH, Wagenaar E, van Deemter L, Mol CA, Borst P (1995) Absence of the mdr1a P-Glycoprotein in mice affects tissue distribution and pharmacokinetics of dexamethasone, digoxin, and cyclosporin A. J Clin Invest 96:1698-1705.

Schrenk D, Michalke A, Gant TW, Brown PC, Silverman JA, Thorgeirsson SS (1996) Multidrug resistance gene expression in rodents and rodent hepatocytes treated with mitoxantrone. Biochem Pharmacol 52:1453-1460.

Schuetz EG, Beck WT, Schuetz JD (1996a) Modulators and substrates of P-glycoprotein and cytochrome P4503A coordinately up-regulate these proteins in human colon carcinoma cells. Molecular Pharmacology 49:311-318.

Schuetz EG, Schinkel AH, Relling MV, Schuetz JD (1996b) P-glycoprotein: a major determinant of rifampicin-inducible expression of cytochrome P4503A in mice and humans. Proc Natl Acad Sci U S A 93:4001-4005.

Schwab M, Eichelbaum M, Fromm MF (2003a) Genetic polymorphisms of the human MDR1 drug transporter. Annu Rev Pharmacol Toxicol 43:285-307.

Schwab M, Schaeffeler E, Marx C, et al. (2003b) Association between the C3435T MDR1 gene polymorphism and susceptibility for ulcerative colitis. Gastroenterology 124:26-33.

Schweyer S, Soruri A, Heintze A, Radzun HJ, Fayyazi A (2004) The role of reactive oxygen species in cisplatin-induced apoptosis in human malignant testicular germ cell lines. Int J Oncol 25:1671-1676.

Scotto KW (2003) Transcriptional regulation of ABC drug transporters. Oncogene 22:7496-7511.

Scotto KW, Biedler JL, Melera PW (1986) Amplification and expression of genes associated with multidrug resistance in mammalian cells. Science 232:751-755.

Scotto KW, Egan DA (1998) Transcriptional regulation of MDR genes. Cytotechnology 27:257-269.

Seelig A (1998) A general pattern for substrate recognition by P-glycoprotein. European Journal of Biochemistry 251:252-261.

Seelig A, Gottschlich R, Devant RM (1994) A method to determine the ability of drugs to diffuse through the blood-brain barrier. Proc Natl Acad Sci U S A 91:68-72.

Seelig A, Landwojtowicz E (2000) Structure–activity relationship of P-glycoprotein substrates and modifiers. European Journal of Pharmaceutical Sciences 12:31-40.

Semenza GL (1998) Hypoxia-inducible factor 1: master regulator of O2 homeostasis. Curr Opin Genet Dev 8:588-594.

Semenza GL (2002) Signal transduction to hypoxia-inducible factor 1. Biochemical Pharmacology 64:993-998.

Senior AE, al-Shawi MK, Urbatsch IL (1995) The catalytic cycle of P-glycoprotein. FEBS Lett 377:285-289.

Seo SB, Hur JG, Kim MJ, et al. (2010) TRAIL sensitize MDR cells to MDR-related drugs by down-regulation of P-glycoprotein through inhibition of DNA-PKcs/Akt/GSK-3beta pathway and activation of caspases. Mol Cancer 9:199.

Sérée E, Villard PH, Hevér A, et al. (1998) Modulation of MDR1 and CYP3A Expression by Dexamethasone: Evidence for an Inverse Regulation in Adrenals. Biochemical and Biophysical Research Communications 252:392-395.

Shapiro AB, Corder AB, Ling V (1997) P-glycoprotein-mediated Hoechst 33342 transport out of the lipid bilayer. Eur J Biochem 250:115-121.

Shapiro AB, Fox K, Lam P, Ling V (1999) Stimulation of P-glycoprotein-mediated drug transport by prazosin and progesterone. Evidence for a third drug-binding site. Eur J Biochem 259:841-850.

Shapiro AB, Ling V (1994) ATPase activity of purified and reconstituted P-glycoprotein from Chinese hamster ovary cells. J Biol Chem 269:3745-3754.

Shapiro AB, Ling V (1997a) Effect of quercetin on Hoechst 33342 transport by purified and reconstituted P-glycoprotein. Biochem Pharmacol 53:587-596.

Shapiro AB, Ling V (1997b) Extraction of Hoechst 33342 from the cytoplasmic leaflet of the plasma membrane by P-glycoprotein. Eur J Biochem 250:122-129.

Shapiro AB, Ling V (1997c) Positively cooperative sites for drug transport by P-glycoprotein with distinct drug specificities. Eur J Biochem 250:130-137.

Shapiro AB, Ling V (1998a) The mechanism of ATP-dependent multidrug transport by P-glycoprotein. Acta Physiol Scand Suppl 643:227-234.

Shapiro AB, Ling V (1998b) Transport of LDS-751 from the cytoplasmic leaflet of the plasma membrane by the rhodamine-123-selective site of P-glycoprotein. Eur J Biochem 254:181-188.

Shareef MM, Brown B, Shajahan S, et al. (2008) Lack of P-Glycoprotein Expression by Low-Dose Fractionated Radiation Results from Loss of Nuclear Factor-κB and NF-Y Activation in Oral Carcinoma Cells. Molecular Cancer Research 6:89-98.

Sharma R, Awasthi YC, Yang Y, Sharma A, Singhal SS, Awasthi S (2003) Energy dependent transport of xenobiotics and its relevance to multidrug resistance. Curr Cancer Drug Targets 3:89-107.

Sharom FJ (1997) The P-glycoprotein efflux pump: how does it transport drugs? J Membr Biol 160:161-175.

Sharom FJ (2007) Multidrug resistance protein: P-glycoprotein. In: You G, Morris ME (eds) Drug Transporters: Molecular Characterization and Role in Drug Disposition. John Wiley & Sons, Hoboken, p 223–262.

Sharom FJ (2008) ABC multidrug transporters: structure, function and role in chemoresistance. Pharmacogenomics 9:105-127.

Sharom FJ (2011) The P-glycoprotein multidrug transporter. Essays Biochem 50:161-178.

Sharom FJ, Yu X, Chu JW, Doige CA (1995) Characterization of the ATPase activity of P-glycoprotein from multidrug-resistant Chinese hamster ovary cells. Biochem J 308 (Pt 2):381-390.

Sharom FJ, Yu X, DiDiodato G, Chu JW (1996) Synthetic hydrophobic peptides are substrates for P-glycoprotein and stimulate drug transport. Biochem J 320 (Pt 2):421-428.

Sharpe JG, Seidel ER (2005) Polyamines are absorbed through a y+ amino acid carrier in rat intestinal epithelial cells. Amino Acids 29:245-253.

Shaulian E, Karin M (2001) AP-1 in cell proliferation and survival. Oncogene 20:2390-2400.

Shen DW, Fojo A, Chin JE, et al. (1986) Human multidrug-resistant cell lines: increased mdr1 expression can precede gene amplification. Science 232:643-645.

Shen H, Xu W, Luo W, et al. (2011) Upregulation of mdr1 gene is related to activation of the MAPK/ERK signal transduction pathway and YB-1 nuclear translocation in B-cell lymphoma. Experimental hematology 39:558-569.

Shen S, He Y, Zeng S (2007) Stereoselective regulation of MDR1 expression in Caco-2 cells by cetirizine enantiomers. Chirality 19:485-490.

Shilling RA, Venter H, Velamakanni S, et al. (2006) New light on multidrug binding by an ATP-binding-cassette transporter. Trends in Pharmacological Sciences 27:195-203.

Shimizu K, Ohtaki K, Matsubara K, et al. (2001) Carrier-mediated processes in blood--brain barrier penetration and neural uptake of paraquat. Brain Res 906:135-142.

Shin WW, Fong WF, Pang SF, Wong PC (1985) Limited blood-brain barrier transport of polyamines. J Neurochem 44:1056-1059.

Shirasaka Y, Kawasaki M, Sakane T, et al. (2006) Induction of human P-glycoprotein in Caco-2 cells: development of a highly sensitive assay system for P-glycoprotein-mediated drug transport. Drug Metab Pharmacokinet 21:414-423.

Shtil AA, Azare J (2005) Redundancy of biological regulation as the basis of emergence of multidrug resistance. Int Rev Cytol 246:1-29.

Siarheyeva A, Liu R, Sharom FJ (2010) Characterization of an asymmetric occluded state of P-glycoprotein with two bound nucleotides: implications for catalysis. J Biol Chem 285:7575-7586.

Siarheyeva A, Lopez JJ, Glaubitz C (2006) Localization of multidrug transporter substrates within model membranes. Biochemistry 45:6203-6211.

Siddiqui A, Kerb R, Weale ME, et al. (2003) Association of multidrug resistance in epilepsy with a polymorphism in the drug-transporter gene ABCB1. N Engl J Med 348:1442-1448.

Siegsmund M, Brinkmann U, Schaffeler E, et al. (2002) Association of the P-glycoprotein transporter MDR1(C3435T) polymorphism with the susceptibility to renal epithelial tumors. J Am Soc Nephrol 13:1847-1854.

Sies H (1997) Oxidative stress: oxidants and antioxidants. Exp Physiol 82:291-295.

Sinicrope FA, Dudeja PK, Bissonnette BM, Safa AR, Brasitus TA (1992) Modulation of P-glycoprotein-mediated drug transport by alterations in lipid fluidity of rat liver canalicular membrane vesicles. J Biol Chem 267:24995-25002.

Slater LM, Sweet P, Stupecky M, Gupta S (1986) Cyclosporin A reverses vincristine and daunorubicin resistance in acute lymphatic leukemia in vitro. J Clin Invest 77:1405-1408.

Slotte JP, Bierman EL (1988) Depletion of plasma-membrane sphingomyelin rapidly alters the distribution of cholesterol between plasma membranes and intracellular cholesterol pools in cultured fibroblasts. Biochem J 250:653-658.

Smale ST, Baltimore D (1989) The "initiator" as a transcription control element. Cell 57:103-113.

Smeal T, Binetruy B, Mercola DA, Birrer M, Karin M (1991) Oncogenic and transcriptional cooperation with Ha-Ras requires phosphorylation of c-Jun on serines 63 and 73. Nature 354:494-496.

Smit JJ, Schinkel AH, Mol CA, et al. (1994) Tissue distribution of the human MDR3 P-glycoprotein. Lab Invest 71:638-649.

Smit JW, Schinkel AH, Weert B, Meijer DK (1998) Hepatobiliary and intestinal clearance of amphiphilic cationic drugs in mice in which both mdr1a and mdr1b genes have been disrupted. Br J Pharmacol 124:416-424.

Smith AJ, Timmermans-Hereijgers JL, Roelofsen B, et al. (1994) The human MDR3 P-glycoprotein promotes translocation of phosphatidylcholine through the plasma membrane of fibroblasts from transgenic mice. FEBS Lett 354:263-266.

Smith AJ, van Helvoort A, van Meer G, et al. (2000) MDR3 P-glycoprotein, a phosphatidylcholine translocase, transports several cytotoxic drugs and directly interacts with drugs as judged by interference with nucleotide trapping. J Biol Chem 275:23530-23539.

Smith CA, Rayment I (1996) X-ray structure of the magnesium(II).ADP.vanadate complex of the Dictyostelium discoideum myosin motor domain to 1.9 A resolution. Biochemistry 35:5404-5417.

Smith LL (1982) Young Scientists Award lecture 1981: The identification of an accumulation system for diamines and polyamines into the lung and its relevance to paraquat toxicity. Arch Toxicol Suppl 5:1-14.

Smith PC, Karpowich N, Millen L, et al. (2002) ATP binding to the motor domain from an ABC transporter drives formation of a nucleotide sandwich dimer. Mol Cell 10:139-149.

Smyth MJ, Krasovskis E, Sutton VR, Johnstone RW (1998) The drug efflux protein, P-glycoprotein, additionally protects drug-resistant tumor cells from multiple forms of caspase-dependent apoptosis. Proc Natl Acad Sci U S A 95:7024-7029.

Soler C, Grangeasse C, Baggetto LG, Damour O (1999) Dermal fibroblast proliferation is improved by beta-catenin overexpression and inhibited by E-cadherin expression. FEBS Lett 442:178-182.

Song X, Liu X, Chi W, et al. (2006) Hypoxia-induced resistance to cisplatin and doxorubicin in non-small cell lung cancer is inhibited by silencing of HIF-1alpha gene. Cancer Chemother Pharmacol 58:776-784.

Sonneveld P, Burnett A, Vossebeld P, et al. (2000) Dose-finding study of valspodar (PSC 833) with daunorubicin and cytarabine to reverse multidrug resistance in elderly patients with previously untreated acute myeloid leukemia. Hematol J 1:411-421.

Sonveaux N, Vigano C, Shapiro AB, Ling V, Ruysschaert JM (1999) Ligand-mediated tertiary structure changes of reconstituted P-glycoprotein. A tryptophan fluorescence quenching analysis. J Biol Chem 274:17649-17654.

Sousa E, Palmeira A, Cordeiro A, et al. (2013) Bioactive xanthones with effect on P-glycoprotein and prediction of intestinal absorption. Med Chem Res 22:2115-2123.

Sovak MA, Bellas RE, Kim DW, et al. (1997) Aberrant nuclear factor-kappaB/Rel expression and the pathogenesis of breast cancer. J Clin Invest 100:2952-2960.

Spitz DR, Azzam EI, Li JJ, Gius D (2004) Metabolic oxidation/reduction reactions and cellular responses to ionizing radiation: a unifying concept in stress response biology. Cancer Metastasis Rev 23:311-322.

Spitz DR, Sim JE, Ridnour LA, Galoforo SS, Lee YJ (2000) Glucose Deprivation-Induced Oxidative Stress in Human Tumor Cells: A Fundamental Defect in Metabolism? Annals of the New York Academy of Sciences 899:349-362.

Stadler P, Putnik K, Kreimeyer T, Sprague LD, Koelbl O, Schafer C (2006) Split course hyperfractionated accelerated radio-chemotherapy (SCHARC) for patients with advanced head and neck cancer: influence of protocol deviations and hemoglobin on overall survival, a retrospective analysis. BMC Cancer 6:279.

Staud F, Ceckova M, Micuda S, Pavek P (2010) Expression and function of p-glycoprotein in normal tissues: effect on pharmacokinetics. Methods Mol Biol 596:199-222.

Stein U, Walther W, Shoemaker RH (1996) Reversal of Multidrug Resistance by Transduction of Cytokine Genes Into Human Colon Carcinoma Cells. Journal of the National Cancer Institute 88:1383-1392.

Stein WD, Cardarelli C, Pastan I, Gottesman MM (1994) Kinetic evidence suggesting that the multidrug transporter differentially handles influx and efflux of its substrates. Mol Pharmacol 45:763-772.

Steinbach D, Legrand O (2007) ABC transporters and drug resistance in leukemia: was P-gp nothing but the first head of the Hydra? Leukemia 21:1172-1176.

Sterz K, Mollmann L, Jacobs A, Baumert D, Wiese M (2009) Activators of P-glycoprotein: Structure-activity relationships and investigation of their mode of action. ChemMedChem 4:1897-1911.

Stewart A, Steiner J, Mellows G, Laguda B, Norris D, Bevan P (2000) Phase I trial of XR9576 in healthy volunteers demonstrates modulation of P-glycoprotein in CD56+ lymphocytes after oral and intravenous administration. Clin Cancer Res 6:4186-4191.

Storm J, O'Mara ML, Crowley EH, et al. (2007) Residue G346 in transmembrane segment six is involved in inter-domain communication in P-glycoprotein. Biochemistry 46:9899-9910.

Störmer E, von Moltke LL, Perloff MD, Greenblatt DJ (2001) P-glycoprotein Interactions of Nefazodone and Trazodone in Cell Culture. The Journal of Clinical Pharmacology 41:708-714.

Subarsky P, Hill RP (2003) The hypoxic tumour microenvironment and metastatic progression. Clin Exp Metastasis 20:237-250.

Sueyoshi T, Negishi M (2001) Phenobarbital response elements of cytochrome P450 genes and nuclear receptors. Annu Rev Pharmacol Toxicol 41:123-143.

Sugawara S, Hosono M, Ogawa Y, Takayanagi M, Nitta K (2005) Catfish Egg Lectin Causes Rapid Activation of Multidrug Resistance 1 P-Glycoprotein as a Lipid Translocase. Biol Pharm Bull 28:434-441.

Sugihara N, Toyama K, Okamoto T, Kadowaki M, Terao K, Furuno K (2007) Effects of benzo(e)pyrene and benzo(a)pyrene on P-glycoprotein-mediated transport in Caco-2 cell monolayer: a comparative approach. Toxicol In Vitro 21:827-834.

Sui H, Fan ZZ, Li Q (2012) Signal transduction pathways and transcriptional mechanisms of ABCB1/Pgp-mediated multiple drug resistance in human cancer cells. J Int Med Res 40:426-435.

Sui H, Zhou S, Wang Y, et al. (2011) COX-2 contributes to P-glycoprotein-mediated multidrug resistance via phosphorylation of c-Jun at Ser63/73 in colorectal cancer. Carcinogenesis 32:667-675.

Sukhai M, Piquette-Miller M (2000) Regulation of the multidrug resistance genes by stress signals. J Pharm Pharm Sci 3:268-280.

Sulova Z, Macejova D, Seres M, Sedlak J, Brtko J, Breier A (2008) Combined treatment of P-gp-positive L1210/VCR cells by verapamil and all-trans retinoic acid induces down-regulation of P-glycoprotein expression and transport activity. Toxicol In Vitro 22:96-105.

Sundseth R, Macdonald G, Ting J, King AC (1997) DNA Elements Recognizing NF-Y and Sp1 Regulate the Human Multidrug-Resistance Gene Promoter. Molecular Pharmacology 51:963-971.

Suzuki H, Sugiyama Y (2000) Role of metabolic enzymes and efflux transporters in the absorption of drugs from the small intestine. Eur J Pharm Sci 12:3-12.

Synold TW, Dussault I, Forman BM (2001) The orphan nuclear receptor SXR coordinately regulates drug metabolism and efflux. Nat Med 7:584-590.

Szakacs G, Paterson JK, Ludwig JA, Booth-Genthe C, Gottesman MM (2006) Targeting multidrug resistance in cancer. Nat Rev Drug Discov 5:219-234.

Szlosarek PW, Balkwill FR (2003) Tumour necrosis factor alpha: a potential target for the therapy of solid tumours. Lancet Oncol 4:565-573.

Taipalensuu J, Tornblom H, Lindberg G, et al. (2001) Correlation of gene expression of ten drug efflux proteins of the ATP-binding cassette transporter family in normal human jejunum and in human intestinal epithelial Caco-2 cell monolayers. J Pharmacol Exp Ther 299:164-170.

Takanaga H, Ohnishi A, Yamada S, et al. (2000) Polymethoxylated flavones in orange juice are inhibitors of P-glycoprotein but not cytochrome P450 3A4. J Pharmacol Exp Ther 293:230-236.

Takara K, Hayashi R, Kokufu M, et al. (2009) Effects of nonsteroidal anti-inflammatory drugs on the expression and function of P-glycoprotein/MDR1 in Caco-2 cells. Drug Chem Toxicol 32:332-337.

Takara K, Sakaeda T, Okumura K (2006) An update on overcoming MDR1-mediated multidrug resistance in cancer chemotherapy. Curr Pharm Des 12:273-286.

Takara K, Takagi K, Tsujimoto M, Ohnishi N, Yokoyama T (2003a) Digoxin up-regulates multidrug resistance transporter (MDR1) mRNA and simultaneously down-regulates steroid xenobiotic receptor mRNA. Biochemical and Biophysical Research Communications 306:116-120.

Takara K, Tsujimoto M, Kokufu M, Ohnishi N, Yokoyama T (2003b) Up-regulation of MDR1 function and expression by cisplatin in LLC-PK1 cells. Biol Pharm Bull 26:205-209.

Takara K, Tsujimoto M, Ohnishi N, Yokoyama T (2002) Digoxin Up-Regulates MDR1 in Human Colon Carcinoma Caco-2 Cells. Biochemical and Biophysical Research Communications 292:190-194.

Takatori T, Ogura M, Tsuruo T (1993) Purification and characterization of NF-R2 that regulates the expression of the human multidrug resistance (MDR1) gene. Jpn J Cancer Res 84:298-303.

Tan EK, Chan DK, Ng PW, et al. (2005) Effect of MDR1 haplotype on risk of Parkinson disease. Arch Neurol 62:460-464.

Tang PM, Zhang DM, Xuan NH, et al. (2009) Photodynamic therapy inhibits P-glycoprotein mediated multidrug resistance via JNK activation in human hepatocellular carcinoma using the photosensitizer pheophorbide a. Mol Cancer 8:56.

Tateishi T, Nakura H, Asoh M, et al. (1999) Multiple cytochrome P-450 subfamilies are co-induced with P-glycoprotein by both phenothiazine and 2-acetylaminofluorene in rats. Cancer Lett 138:73-79.

Tchamo DN, Dijoux-Franca MG, Mariotte AM, et al. (2000) Prenylated xanthones as potential P-glycoprotein modulators. Bioorg Med Chem Lett 10:1343-1345.

te Boekhorst PA, van Kapel J, Schoester M, Sonneveld P (1992) Reversal of typical multidrug resistance by cyclosporin and its non-immunosuppressive analogue SDZ PSC 833 in Chinese hamster ovary cells expressing the mdr1 phenotype. Cancer Chemother Pharmacol 30:238-242.

Teeter LD, Eckersberg T, Tsai Y, Kuo MT (1991a) Analysis of the Chinese hamster P-glycoprotein/multidrug resistance gene pgp1 reveals that the AP-1 site is essential for full promoter activity. Cell Growth Differ 2:429-437.

Teeter LD, Petersen DD, Nebert DW, Kuo MT (1991b) Murine mdr-1, mdr-2, and mdr-3 gene expression: no coinduction with the Cyp1a-1 and Nmo-1 genes in liver by 2,3,7,8-tetrachlorodibenzo-p-dioxin. DNA Cell Biol 10:433-441.

Terasaki T, Ohtsuki S (2005) Brain-to-blood transporters for endogenous substrates and xenobiotics at the blood-brain barrier: an overview of biology and methodology. NeuroRx 2:63-72.

Thevenod F, Friedmann JM, Katsen AD, Hauser IA (2000) Up-regulation of multidrug resistance P-glycoprotein via nuclear factor-kappaB activation protects kidney proximal tubule cells from cadmium- and reactive oxygen species-induced apoptosis. J Biol Chem 275:1887-1896.

Thews O, Gassner B, Kelleher DK, Schwerdt G, Gekle M (2006) Impact of extracellular acidity on the activity of P-glycoprotein and the cytotoxicity of chemotherapeutic drugs. Neoplasia 8:143-152.

Thiebaut F, Tsuruo T, Hamada H, Gottesman MM, Pastan I, Willingham MC (1987) Cellular localization of the multidrug-resistance gene product P-glycoprotein in normal human tissues. Proc Natl Acad Sci U S A 84:7735-7738.

Thomas H, Coley HM (2003) Overcoming Multidrug Resistance in Cancer: An Update on the Clinical Strategy of Inhibiting P-Glycoprotein. Cancer Control 10:159-165.

Thottassery JV, Zambetti GP, Arimori K, Schuetz EG, Schuetz JD (1997) p53-dependent regulation of MDR1 gene expression causes selective resistance to chemotherapeutic agents. Proc Natl Acad Sci U S A 94:11037-11042.

Thwaites DT, Markovich D, Murer H, Simmons NL (1996) Na+-independent lysine transport in human intestinal Caco-2 cells. J Membr Biol 151:215-224.

Tian R, Koyabu N, Morimoto S, Shoyama Y, Ohtani H, Sawada Y (2005) Functional induction and de-induction of P-glycoprotein by St. John's wort and its ingredients in a human colon adenocarcinoma cell line. Drug Metab Dispos 33:547-554.

Tolcher AW, Cowan KH, Solomon D, et al. (1996) Phase I crossover study of paclitaxel with r-verapamil in patients with metastatic breast cancer. J Clin Oncol 14:1173-1184.

Tombline G, Bartholomew LA, Urbatsch IL, Senior AE (2004) Combined mutation of catalytic glutamate residues in the two nucleotide binding domains of P-glycoprotein generates a conformation that binds ATP and ADP tightly. J Biol Chem 279:31212-31220.

Tombline G, Muharemagic A, White LB, Senior AE (2005) Involvement of the "occluded nucleotide conformation" of P-glycoprotein in the catalytic pathway. Biochemistry 44:12879-12886.

Tsuruo T, Iida H, Tsukagoshi S, Sakurai Y (1981) Overcoming of vincristine resistance in P388 leukemia in vivo and in vitro through enhanced cytotoxicity of vincristine and vinblastine by verapamil. Cancer Res 41:1967-1972.

Tsuruoka S, Sugimoto KI, Fujimura A, Imai M, Asano Y, Muto S (2001) P-glycoprotein-mediated drug secretion in mouse proximal tubule perfused in vitro. J Am Soc Nephrol 12:177-181.

Twentyman PR, Bleehen NM (1991) Resistance modification by PSC-833, a novel non-immunosuppressive cyclosporin [corrected]. Eur J Cancer 27:1639-1642.

Uchiumi T, Kohno K, Tanimura H, et al. (1993) Enhanced expression of the human multidrug resistance 1 gene in response to UV light irradiation. Cell Growth Differ 4:147-157.

Ueda K, Okamura N, Hirai M, et al. (1992) Human P-glycoprotein transports cortisol, aldosterone, and dexamethasone, but not progesterone. J Biol Chem 267:24248-24252.

Ueda K, Pastan I, Gottesman MM (1987) Isolation and sequence of the promoter region of the human multidrug-resistance (P-glycoprotein) gene. J Biol Chem 262:17432-17436.

Ueda K, Taguchi Y, Morishima M (1997) How does P-glycoprotein recognize its substrates? Seminars in Cancer Biology 8:151-159.

Um JH, Kang CD, Lee BG, Kim DW, Chung BS, Kim SH (2001) Increased and correlated nuclear factor-kappa B and Ku autoantigen activities are associated with development of multidrug resistance. Oncogene 20:6048-6056.

Urbatsch IL, al-Shawi MK, Senior AE (1994) Characterization of the ATPase activity of purified Chinese hamster P-glycoprotein. Biochemistry 33:7069-7076.

Urbatsch IL, Gimi K, Wilke-Mounts S, et al. (2001) Cysteines 431 and 1074 Are Responsible for Inhibitory Disulfide Cross-linking between the Two Nucleotide-binding Sites in Human P-glycoprotein. Journal of Biological Chemistry 276:26980-26987.

Urbatsch IL, Sankaran B, Bhagat S, Senior AE (1995a) Both P-glycoprotein nucleotide-binding sites are catalytically active. J Biol Chem 270:26956-26961.

Urbatsch IL, Sankaran B, Weber J, Senior AE (1995b) P-glycoprotein is stably inhibited by vanadate-induced trapping of nucleotide at a single catalytic site. J Biol Chem 270:19383-19390.

Urbatsch IL, Senior AE (1995) Effects of lipids on ATPase activity of purified Chinese hamster P-glycoprotein. Arch Biochem Biophys 316:135-140.

Valverde MA, Bond TD, Hardy SP, et al. (1996) The multidrug resistance P-glycoprotein modulates cell regulatory volume decrease. EMBO J 15:4460-4468.

Valverde MA, Diaz M, Sepulveda FV, Gill DR, Hyde SC, Higgins CF (1992) Volume-regulated chloride channels associated with the human multidrug-resistance P-glycoprotein. Nature 355:830-833.

van Groenigen M, Valentijn LJ, Baas F (1993) Identification of a functional initiator sequence in the human MDR1 promoter. Biochimica et Biophysica Acta (BBA) - Gene Structure and Expression 1172:138-146.

van Helvoort A, Smith AJ, Sprong H, et al. (1996) MDR1 P-glycoprotein is a lipid translocase of broad specificity, while MDR3 P-glycoprotein specifically translocates phosphatidylcholine. Cell 87:507-517.

van Kalken CK, Giaccone G, van der Valk P, et al. (1992) Multidrug resistance gene (P-glycoprotein) expression in the human fetus. Am J Pathol 141:1063-1072.

van Meer G (2005) Cellular lipidomics. EMBO J 24:3159-3165.

van Meer G, Halter D, Sprong H, Somerharju P, Egmond MR (2006) ABC lipid transporters: extruders, flippases, or flopless activators? FEBS Lett 580:1171-1177.

van Tellingen O, Buckle T, Jonker JW, van der Valk MA, Beijnen JH (2003) P-glycoprotein and Mrp1 collectively protect the bone marrow from vincristine-induced toxicity in vivo. Br J Cancer 89:1776-1782.

van Veen HW, Callaghan R, Soceneantu L, Sardini A, Konings WN, Higgins CF (1998) A bacterial antibiotic-resistance gene that complements the human multidrug-resistance P-glycoprotein gene. Nature 391:291-295.

van Zuylen L, Sparreboom A, van der Gaast A, et al. (2002) Disposition of docetaxel in the presence of P-glycoprotein inhibition by intravenous administration of R101933. Eur J Cancer 38:1090-1099.

Vanoye CG, Castro AF, Pourcher T, Reuss L, Altenberg GA (1999) Phosphorylation of P-glycoprotein by PKA and PKC modulates swelling-activated Cl- currents. Am J Physiol 276:C370-378.

Vara JÁF, Casado E, de Castro J, Cejas P, Belda-Iniesta C, González-Barón M (2004) PI3K/Akt signalling pathway and cancer. Cancer Treatment Reviews 30:193-204.

Varma MV, Ashokraj Y, Dey CS, Panchagnula R (2003) P-glycoprotein inhibitors and their screening: a perspective from bioavailability enhancement. Pharmacol Res 48:347-359.

Vasiliou V, Vasiliou K, Nebert DW (2009) Human ATP-binding cassette (ABC) transporter family. Hum Genomics 3:281-290.

Verhalen B, Ernst S, Borsch M, Wilkens S (2012) Dynamic ligand-induced conformational rearrangements in P-glycoprotein as probed by fluorescence resonance energy transfer spectroscopy. J Biol Chem 287:1112-1127.

Vertegaal AC, Kuiperij HB, Yamaoka S, Courtois G, van der Eb AJ, Zantema A (2000) Protein kinase C-alpha is an upstream activator of the IkappaB kinase complex in the TPA signal transduction pathway to NF-kappaB in U2OS cells. Cell Signal 12:759-68.

Vilaboa NE, Galan A, Troyano A, de Blas E, Aller P (2000) Regulation of multidrug resistance 1 (MDR1)/P-glycoprotein gene expression and activity by heat-shock transcription factor 1 (HSF1). J Biol Chem 275:24970-24976.

Vilas-Boas V, Silva R, Gaio AR, et al. (2011) P-glycoprotein activity in human Caucasian male lymphocytes does not follow its increased expression during aging. Cytometry A 79:912-919.

Vilas-Boas V, Silva R, Guedes-de-Pinho P, Carvalho F, Bastos ML, Remião F (2013a) RBE4 cells are highly resistant to paraquat-induced cytotoxicity: studies on uptake and efflux mechanisms. Journal of Applied Toxicology Epub ahead of print.

Vilas-Boas V, Silva R, Palmeira A, et al. (2013b) Development of Novel Rifampicin-Derived P-Glycoprotein Activators/Inducers. Synthesis, In Silico Analysis and Application in the RBE4 Cell Model, Using Paraquat as Substrate. PLoS One 8:e74425.

Vivanco I, Sawyers CL (2002) The phosphatidylinositol 3-Kinase AKT pathway in human cancer. Nat Rev Cancer 2:489-501.

Vlahos CJ, Matter WF, Hui KY, Brown RF (1994) A specific inhibitor of phosphatidylinositol 3-kinase, 2-(4-morpholinyl)-8-phenyl-4H-1-benzopyran-4-one (LY294002). J Biol Chem 269:5241-5248.

Vollrath V, Wielandt AM, Acuna C, Duarte I, Andrade L, Chianale J (1994) Effect of colchicine and heat shock on multidrug resistance gene and P-glycoprotein expression in rat liver. Journal of hepatology 21:754-763.

Wacher VJ, Wu CY, Benet LZ (1995) Overlapping substrate specificities and tissue distribution of cytochrome P450 3A and P-glycoprotein: implications for drug delivery and activity in cancer chemotherapy. Mol Carcinog 13:129-134.

Walker JE, Saraste M, Runswick MJ, Gay NJ (1982) Distantly related sequences in the alpha- and beta-subunits of ATP synthase, myosin, kinases and other ATP-requiring enzymes and a common nucleotide binding fold. EMBO J 1:945-951.

Walker LG, Eremin JM, Aloysius MM, et al. (2011) Effects on quality of life, anti-cancer responses, breast conserving surgery and survival with neoadjuvant docetaxel: a randomised study of sequential weekly versus three-weekly docetaxel following neoadjuvant doxorubicin and cyclophosphamide in women with primary breast cancer. BMC Cancer 11:179.

Wandel C, Kim RB, Kajiji S, Guengerich P, Wilkinson GR, Wood AJ (1999) P-glycoprotein and cytochrome P-450 3A inhibition: dissociation of inhibitory potencies. Cancer Res 59:3944-3948.

Wang E-j, Barecki-Roach M, Johnson WW (2002) Elevation of P-glycoprotein function by a catechin in green tea. Biochemical and Biophysical Research Communications 297:412-418.

Wang E, Casciano CN, Clement RP, Johnson WW (2000) Cholesterol interaction with the daunorubicin binding site of P-glycoprotein. Biochem Biophys Res Commun 276:909-916.

Wang G, Pincheira R, Zhang JT (1998a) Dissection of drug-binding-induced conformational changes in P-glycoprotein. Eur J Biochem 255:383-390.

Wang RB, Kuo CL, Lien LL, Lien EJ (2003) Structure–activity relationship: analyses of p-glycoprotein substrates and inhibitors. Journal of Clinical Pharmacy and Therapeutics 28:203-228.

Wang X, Martindale JL, Liu Y, Holbrook NJ (1998b) The cellular response to oxidative stress: influences of mitogen-activated protein kinase signalling pathways on cell survival. Biochem J 333 (Pt 2):291-300.

Wang Y, Loo TW, Bartlett MC, Clarke DM (2007) Modulating the Folding of P-Glycoprotein and Cystic Fibrosis Transmembrane Conductance Regulator Truncation Mutants with Pharmacological Chaperones. Molecular Pharmacology 71:751-758.

Wang Y, Qu Y, Niu XL, Sun WJ, Zhang XL, Li LZ (2011) Autocrine production of interleukin-8 confers cisplatin and paclitaxel resistance in ovarian cancer cells. Cytokine 56:365-375.

Ward A, Reyes CL, Yu J, Roth CB, Chang G (2007) Flexibility in the ABC transporter MsbA: Alternating access with a twist. Proceedings of the National Academy of Sciences 104:19005-19010.

Wartenberg M, Hoffmann E, Schwindt H, et al. (2005) Reactive oxygen species-linked regulation of the multidrug resistance transporter P-glycoprotein in Nox-1 overexpressing prostate tumor spheroids. FEBS Letters 579:4541-4549.

Wartenberg M, Ling FC, Muschen M, et al. (2003) Regulation of the multidrug resistance transporter P-glycoprotein in multicellular tumor spheroids by hypoxia-inducible factor (HIF-1) and reactive oxygen species. FASEB J 17:503-505.

Wartenberg M, Ling FC, Schallenberg M, et al. (2001a) Down-regulation of intrinsic P-glycoprotein expression in multicellular prostate tumor spheroids by reactive oxygen species. J Biol Chem 276:17420-17428.

Wartenberg M, Ling FC, Schallenberg M, et al. (2001b) Down-regulation of Intrinsic P-glycoprotein Expression in Multicellular Prostate Tumor Spheroids by Reactive Oxygen Species. Journal of Biological Chemistry 276:17420-17428.

Watanabe T, Onuki R, Yamashita S, Taira K, Sugiyama Y (2005) Construction of a functional transporter analysis system using MDR1 knockdown Caco-2 cells. Pharm Res 22:1287-1293.

Watanabe T, Suzuki H, Sawada Y, et al. (1995) Induction of hepatic P-glycoprotein enhances biliary excretion of vincristine in rats. Journal of hepatology 23:440-448.

Watkins RE, Maglich JM, Moore LB, et al. (2003) 2.1 A crystal structure of human PXR in complex with the St. John's wort compound hyperforin. Biochemistry 42:1430-1438.

Wattel, Solary, Hecquet, et al. (1998) Quinine improves the results of intensive chemotherapy in myelodysplastic syndromes expressing P glycoprotein: results of a randomized study. British Journal of Haematology 102:1015-1024.

Weiss J, Haefeli WE (2013) Potential of the novel antiretroviral drug rilpivirine to modulate the expression and function of drug transporters and drug-metabolising enzymes in vitro. International Journal of Antimicrobial Agents 41:484-487.

Weiss J, Theile D, Spalwisz A, Burhenne J, Riedel K-D, Haefeli WE (2013) Influence of sildenafil and tadalafil on the enzyme- and transporter-inducing effects of bosentan and ambrisentan in LS180 cells. Biochemical Pharmacology 85:265-273.

Wempe MF, Wright C, Little JL, et al. (2009) Inhibiting efflux with novel non-ionic surfactants: Rational design based on vitamin E TPGS. International Journal of Pharmaceutics 370:93-102.

Wen T, Liu Y-C, Yang H-W, et al. (2008) Effect of 21-day exposure of phenobarbital, carbamazepine and phenytoin on P-glycoprotein expression and activity in the rat brain. Journal of the Neurological Sciences 270:99-106.

Wessler JD, Grip LT, Mendell J, Giugliano RP (2013) The P-glycoprotein transport system and cardiovascular drugs. J Am Coll Cardiol 61:2495-2502.

Weston CR, Davis RJ (2002) The JNK signal transduction pathway. Curr Opin Genet Dev 12:14-21.

Westphal K, Weinbrenner A, Zschiesche M, et al. (2000) Induction of P-glycoprotein by rifampin increases intestinal secretion of talinolol in human beings: A new type of drug/drug interaction[ast]. Clin Pharmacol Ther 68:345-355.

Wilks MF, Fernando R, Ariyananda PL, et al. (2008) Improvement in survival after paraquat ingestion following introduction of a new formulation in Sri Lanka. PLoS Med 5:e49.

Wong KK, Engelman JA, Cantley LC (2010) Targeting the PI3K signaling pathway in cancer. Curr Opin Genet Dev 20:87-90.

Wongwanakul R, Vardhanabhuti N, Siripong P, Jianmongkol S (2013) Effects of rhinacanthin-C on function and expression of drug efflux transporters in Caco-2 cells. Fitoterapia 89:80-85.

Woodcock DM, Linsenmeyer ME, Chojnowski G, et al. (1992) Reversal of multidrug resistance by surfactants. Br J Cancer 66:62-68.

Wu CP, Calcagno AM, Ambudkar SV (2008) Reversal of ABC drug transporter-mediated multidrug resistance in cancer cells: evaluation of current strategies. Curr Mol Pharmacol 1:93-105.

Wu M, Lee H, Bellas RE, et al. (1996) Inhibition of NF-kappaB/Rel induces apoptosis of murine B cells. EMBO J 15:4682-4690.

Wyatt I, Soames AR, Clay MF, Smith LL (1988) The accumulation and localisation of putrescine, spermidine, spermine and paraquat in the rat lung. In vitro and in vivo studies. Biochem Pharmacol 37:1909-1918.

Xie J, Li DW, Chen XW, Wang F, Dong P (2013) Expression and significance of hypoxia-inducible factor-1alpha and MDR1/P-glycoprotein in laryngeal carcinoma tissue and hypoxic Hep-2 cells. Oncol Lett 6:232-238.

Xie W, Barwick JL, Simon CM, et al. (2000) Reciprocal activation of xenobiotic response genes by nuclear receptors SXR/PXR and CAR. Genes Dev 14:3014-3023.

Xu C, Li CY, Kong AN (2005) Induction of phase I, II and III drug metabolism/transport by xenobiotics. Arch Pharm Res 28:249-268.

Yague E, Armesilla AL, Harrison G, et al. (2003) P-glycoprotein (MDR1) expression in leukemic cells is regulated at two distinct steps, mRNA stabilization and translational initiation. J Biol Chem 278:10344-10352.

Yamada T, Takaoka AS, Naishiro Y, et al. (2000) Transactivation of the multidrug resistance 1 gene by T-cell factor 4/beta-catenin complex in early colorectal carcinogenesis. Cancer Res 60:4761-4766.

Yamashita S, Furubayashi T, Kataoka M, Sakane T, Sezaki H, Tokuda H (2000) Optimized conditions for prediction of intestinal drug permeability using Caco-2 cells. Eur J Pharm Sci 10:195-204.

Yamashita S, Hattori E, Shimada A, et al. (2002a) New methods to evaluate intestinal drug absorption mediated by oligopeptide transporter from in vitro study using Caco-2 cells. Drug Metab Pharmacokinet 17:408-415.

Yamashita S, Konishi K, Yamazaki Y, et al. (2002b) New and better protocols for a short-term Caco-2 cell culture system. J Pharm Sci 91:669-679.

Yanagisawa T, Newman A, Coley H, Renshaw J, Pinkerton CR, Pritchard-Jones K (1999) BIRICODAR (VX-710; Incel): an effective chemosensitizer in neuroblastoma. Br J Cancer 80:1190-1196.

Yang JM, Vassil AD, Hait WN (2001) Activation of phospholipase C induces the expression of the multidrug resistance (MDR1) gene through the Raf-MAPK pathway. Mol Pharmacol 60:674-680.

Yang Q, Onuki R, Nakai C, Sugiyama Y (2007) Ezrin and radixin both regulate the apical membrane localization of ABCC2 (MRP2) in human intestinal epithelial Caco-2 cells. Exp Cell Res 313:3517-3525.

Yokomizo A, Ono M, Nanri H, et al. (1995) Cellular levels of thioredoxin associated with drug sensitivity to cisplatin, mitomycin C, doxorubicin, and etoposide. Cancer Res 55:4293-4296.

Yousif S, Chaves C, Potin S, Margaill I, Scherrmann J-M, Declèves X (2012) Induction of P-glycoprotein and Bcrp at the rat blood–brain barrier following a subchronic morphine treatment is mediated through NMDA/COX-2 activation. Journal of Neurochemistry 123:491-503.

Yu L, Wu Q, Yang CP, Horwitz SB (1995) Coordination of transcription factors, NF-Y and C/EBP beta, in the regulation of the mdr1b promoter. Cell Growth Differ 6:1505-1512.

Zamora JM, Pearce HL, Beck WT (1988) Physical-chemical properties shared by compounds that modulate multidrug resistance in human leukemic cells. Mol Pharmacol 33:454-462.

Zastawny RL, Salvino R, Chen J, Benchimol S, Ling V (1993) The core promoter region of the P-glycoprotein gene is sufficient to confer differential responsiveness to wild-type and mutant p53. Oncogene 8:1529-1535.

Zastre JA, Chan GNY, Ronaldson PT, et al. (2009) Up-regulation of P-glycoprotein by HIV protease inhibitors in a human brain microvessel endothelial cell line. Journal of Neuroscience Research 87:1023-1036.

Zerin T, Kim Y-S, Hong S-Y, Song H-Y (2012) Protective effect of methylprednisolone on paraquat-induced A549 cell cytotoxicity via induction of efflux transporter, P-glycoprotein expression. Toxicology Letters 208:101-107.

Zhang XF, Settleman J, Kyriakis JM, et al. (1993) Normal and oncogenic p21ras proteins bind to the amino-terminal regulatory domain of c-Raf-1. Nature 364:308-313.

Zhang Y, Chen F (2004) Reactive oxygen species (ROS), troublemakers between nuclear factor-kappaB (NF-kappaB) and c-Jun NH(2)-terminal kinase (JNK). Cancer Res 64:1902-1905.

Zhang Y, Lu M, Sun X, Li C, Kuang X, Ruan X (2012) Expression and Activity of p-Glycoprotein Elevated by Dexamethasone in Cultured Retinal Pigment Epithelium Involve Glucocorticoid Receptor and Pregnane X Receptor. Investigative Ophthalmology & Visual Science 53:3508-3515.

Zhang Y, Zhou J, Xu W, Li A, Xu S (2009) JWA sensitizes P-glycoprotein-mediated drug-resistant choriocarcinoma cells to etoposide via JNK and mitochondrial-associated signal pathway. J Toxicol Environ Health A 72:774-781.

Zhao JY, Ikeguchi M, Eckersberg T, Kuo MT (1993) Modulation of multidrug resistance gene expression by dexamethasone in cultured hepatoma cells. Endocrinology 133:521-528.

Zhong Y, Hennig B, Toborek M (2010) Intact lipid rafts regulate HIV-1 Tat protein-induced activation of the Rho signaling and upregulation of P-glycoprotein in brain endothelial cells. J Cereb Blood Flow Metab 30:522-533.

Zhou-Pan XR, Seree E, Zhou XJ, et al. (1993) Involvement of human liver cytochrome P450 3A in vinblastine metabolism: drug interactions. Cancer Res 53:5121-5126.

Zhou G, Kuo MT (1997) NF-κB-mediated Induction of mdr1b Expression by Insulin in Rat Hepatoma Cells. Journal of Biological Chemistry 272:15174-15183.

Zhou J, Liu M, Aneja R, Chandra R, Lage H, Joshi HC (2006) Reversal of P-glycoprotein-mediated multidrug resistance in cancer cells by the c-Jun NH2-terminal kinase. Cancer Res 66:445-452.

Zhou SF (2008) Structure, function and regulation of P-glycoprotein and its clinical relevance in drug disposition. Xenobiotica 38:802-832.

Ziemann C, Burkle A, Kahl GF, Hirsch-Ernst KI (1999) Reactive oxygen species participate in mdr1b mRNA and P-glycoprotein overexpression in primary rat hepatocyte cultures. Carcinogenesis 20:407-414.

Ziemann C, Riecke A, Rudell G, et al. (2006) The role of prostaglandin E receptor-dependent signaling via cAMP in Mdr1b gene activation in primary rat hepatocyte cultures. J Pharmacol Exp Ther 317:378-386.

Zolnerciks JK, Andress EJ, Nicolaou M, Linton KJ (2011) Structure of ABC transporters. Essays Biochem 50:43-61.